

Power System Dynamics and Stability

Power System Dynamics and Stability

With Synchrophasor Measurement and Power System Toolbox

Second Edition

Peter W. Sauer and M. A. Pai

*Department of Electrical and Computer Engineering
The University of Illinois at Urbana-Champaign*

Joe H. Chow

*Department of Electrical, Computer, and Systems Engineering
Rensselaer Polytechnic Institute*



WILEY

This edition first published 2018
© 2018 John Wiley & Sons Ltd

Edition History

Prentice Hall (1st Edition, 1997), Stipes (1st Edition Revised, 2007)

All rights reserved. No part of this publication may be reproduced, stored in a retrieval system, or transmitted, in any form or by any means, electronic, mechanical, photocopying, recording or otherwise, except as permitted by law. Advice on how to obtain permission to reuse material from this title is available at <http://www.wiley.com/go/permissions>.

The right of Peter W. Sauer, M. A. Pai and Joe H. Chow to be identified as the authors of this work has been asserted in accordance with law.

Registered Offices

John Wiley & Sons, Inc., 111 River Street, Hoboken, NJ 07030, USA

John Wiley & Sons Ltd, The Atrium, Southern Gate, Chichester, West Sussex, PO19 8SQ, UK

Editorial Office

The Atrium, Southern Gate, Chichester, West Sussex, PO19 8SQ, UK

For details of our global editorial offices, customer services, and more information about Wiley products visit us at www.wiley.com.

Wiley also publishes its books in a variety of electronic formats and by print-on-demand. Some content that appears in standard print versions of this book may not be available in other formats.

Limit of Liability/Disclaimer of Warranty

MATLAB® is a trademark of The MathWorks, Inc. and is used with permission. The MathWorks does not warrant the accuracy of the text or exercises in this book. This work's use or discussion of MATLAB® software or related products does not constitute endorsement or sponsorship by The MathWorks of a particular pedagogical approach or particular use of the MATLAB® software. While the publisher and authors have used their best efforts in preparing this work, they make no representations or warranties with respect to the accuracy or completeness of the contents of this work and specifically disclaim all warranties, including without limitation any implied warranties of merchantability or fitness for a particular purpose. No warranty may be created or extended by sales representatives, written sales materials or promotional statements for this work. The fact that an organization, website, or product is referred to in this work as a citation and/or potential source of further information does not mean that the publisher and authors endorse the information or services the organization, website, or product may provide or recommendations it may make. This work is sold with the understanding that the publisher is not engaged in rendering professional services. The advice and strategies contained herein may not be suitable for your situation. You should consult with a specialist where appropriate. Further, readers should be aware that websites listed in this work may have changed or disappeared between when this work was written and when it is read. Neither the publisher nor authors shall be liable for any loss of profit or any other commercial damages, including but not limited to special, incidental, consequential, or other damages.

Library of Congress Cataloging-in-Publication Data

Names: Sauer, Peter W., author. | Pai, M. A., 1931– author. | Chow, J. H. (Joe H.), 1951– author.

Title: Power system dynamics and stability : with synchrophasor measurement and power system toolbox / Peter W Sauer, M. A Pai, University of Illinois at Urbana-Champaign, United States, Joe H. Chow, Rensselaer Polytechnic Institute, Troy, New York, United States.

Description: Second edition. | Hoboken, NJ, USA : Wiley, [2017] | Includes bibliographical references and index. |

Identifiers: LCCN 2017012512 (print) | LCCN 2017014476 (ebook) | ISBN 9781119355793 (pdf) | ISBN 9781119355748 (epub) | ISBN 9781119355779 (cloth)

Subjects: LCSH: Electric power system stability. | Electric machinery, Synchronous—Mathematical models. | Electric power systems—Control.

Classification: LCC TK1010 (ebook) | LCC TK1010 .S38 2017 (print) | DDC 621.31—dc23
LC record available at <https://lccn.loc.gov/2017012512>

Cover Images: (Background) © troyek/Gettyimages; (Foreground) MATLAB®

Cover design by Wiley

Set in 10/12pt WarnockPro by Aptara Inc., New Delhi, India

To

Sylvia, Nandini, and Doris

Contents

Preface *xiii*

About the Companion Website *xv*

1	Introduction	<i>1</i>
1.1	Background	<i>1</i>
1.2	Physical Structures	<i>2</i>
1.3	Time-Scale Structures	<i>3</i>
1.4	Political Structures	<i>4</i>
1.5	The Phenomena of Interest	<i>5</i>
1.6	New Chapters Added to this Edition	<i>5</i>
2	Electromagnetic Transients	<i>7</i>
2.1	The Fastest Transients	<i>7</i>
2.2	Transmission Line Models	<i>7</i>
2.3	Solution Methods	<i>12</i>
2.4	Problems	<i>17</i>
3	Synchronous Machine Modeling	<i>19</i>
3.1	Conventions and Notation	<i>19</i>
3.2	Three-Damper-Winding Model	<i>20</i>
3.3	Transformations and Scaling	<i>21</i>
3.4	The Linear Magnetic Circuit	<i>29</i>
3.5	The Nonlinear Magnetic Circuit	<i>35</i>
3.6	Single-Machine Steady State	<i>40</i>
3.7	Operational Impedances and Test Data	<i>44</i>
3.8	Problems	<i>49</i>
4	Synchronous Machine Control Models	<i>53</i>
4.1	Voltage and Speed Control Overview	<i>53</i>
4.2	Exciter Models	<i>53</i>
4.3	Voltage Regulator Models	<i>58</i>
4.4	Turbine Models	<i>62</i>
4.4.1	Hydroturbines	<i>62</i>
4.4.2	Steam Turbines	<i>64</i>
4.5	Speed Governor Models	<i>67</i>
4.6	Problems	<i>70</i>

5	Single-Machine Dynamic Models	71
5.1	Terminal Constraints	71
5.2	The Multi-Time-Scale Model	74
5.3	Elimination of Stator/Network Transients	76
5.4	The Two-Axis Model	81
5.5	The One-Axis (Flux-Decay) Model	83
5.6	The Classical Model	84
5.7	Damping Torques	86
5.8	Single-Machine Infinite-Bus System	90
5.9	Synchronous Machine Saturation	94
5.10	Problems	100
6	Multimachine Dynamic Models	101
6.1	The Synchronously Rotating Reference Frame	101
6.2	Network and R-L Load Constraints	103
6.3	Elimination of Stator/Network Transients	105
6.3.1	Generalization of Network and Load Dynamic Models	110
6.3.2	The Special Case of “Impedance Loads”	112
6.4	Multimachine Two-Axis Model	113
6.4.1	The Special Case of “Impedance Loads”	115
6.5	Multimachine Flux-Decay Model	116
6.5.1	The Special Case of “Impedance Loads”	117
6.6	Multimachine Classical Model	118
6.6.1	The Special Case of “Impedance Loads”	119
6.7	Multimachine Damping Torques	120
6.8	Multimachine Models with Saturation	121
6.8.1	The Multimachine Two-Axis Model with Synchronous Machine Saturation	123
6.8.2	The Multimachine Flux-Decay Model with Synchronous Machine Saturation	124
6.9	Frequency During Transients	126
6.10	Angle References and an Infinite Bus	127
6.11	Automatic Generation Control (AGC)	129
7	Multimachine Simulation	135
7.1	Differential-Algebraic Model	135
7.1.1	Generator Buses	136
7.1.2	Load Buses	137
7.2	Stator Algebraic Equations	138
7.2.1	Polar Form	138
7.2.2	Rectangular Form	138
7.2.3	Alternate Form of Stator Algebraic Equations	139
7.3	Network Equations	140
7.3.1	Power-Balance Form	140
7.3.2	Real Power Equations	141
7.3.3	Reactive Power Equations	141
7.3.4	Current-Balance Form	142

7.4	Industry Model	149
7.5	Simplification of the Two-Axis Model	153
7.5.1	Simplification #1 (Neglecting Transient Saliency in the Synchronous Machine)	153
7.5.2	Simplification #2 (Constant Impedance Load in the Transmission System)	154
7.6	Initial Conditions (Full Model)	158
7.6.1	Load-Flow Formulation	158
7.6.2	Standard Load Flow	159
7.6.3	Initial Conditions for Dynamic Analysis	160
7.6.4	Angle Reference, Infinite Bus, and COI Reference	165
7.7	Numerical Solution: Power-Balance Form	165
7.7.1	SI Method	165
7.7.2	Review of Newton's Method	165
7.7.3	Numerical Solution Using SI Method	166
7.7.4	Disturbance Simulation	167
7.7.5	PE Method	168
7.8	Numerical Solution: Current-Balance Form	168
7.8.1	Some Practical Details	170
7.8.2	Prediction	171
7.9	Reduced-Order Multimachine Models	171
7.9.1	Flux-Decay Model	171
7.9.2	Generator Equations	172
7.9.3	Stator Equations	172
7.9.4	Network Equations	172
7.9.5	Initial Conditions	172
7.9.6	Structure-Preserving Classical Model	173
7.9.7	Internal-Node Model	177
7.10	Initial Conditions	179
7.11	Conclusion	180
7.12	Problems	180
8	Small-Signal Stability	183
8.1	Background	183
8.2	Basic Linearization Technique	184
8.2.1	Linearization of Model A	185
8.2.2	Differential Equations	185
8.2.3	Stator Algebraic Equations	186
8.2.4	Network Equations	186
8.2.5	Linearization of Model B	193
8.2.6	Differential Equations	194
8.2.7	Stator Algebraic Equations	194
8.2.8	Network Equations	194
8.3	Participation Factors	194
8.4	Studies on Parametric Effects	198
8.4.1	Effect of Loading	198
8.4.2	Effect of K_A	200

8.4.3	Effect of Type of Load	201
8.4.4	Hopf Bifurcation	203
8.5	Electromechanical Oscillatory Modes	205
8.5.1	Eigenvalues of A and A_ω	207
8.6	Power System Stabilizers	209
8.6.1	Basic Approach	209
8.6.2	Derivation of $K1 - K6$ Constants	209
8.6.3	Linearization	211
8.6.4	Synchronizing and Damping Torques	215
8.6.5	Damping of Electromechanical Modes	215
8.6.6	Torque-Angle Loop	219
8.6.7	Synchronizing Torque	221
8.6.8	Damping Torque	221
8.6.9	Power System Stabilizer Design	221
8.6.10	Frequency-Domain Approach	222
8.6.11	Design Procedure Using the Frequency-Domain Method	223
8.7	Conclusion	227
8.8	Problems	227
9	Energy Function Methods	233
9.1	Background	233
9.2	Physical and Mathematical Aspects of the Problem	233
9.3	Lyapunov's Method	236
9.4	Modeling Issues	237
9.5	Energy Function Formulation	238
9.6	Potential Energy Boundary Surface (PEBS)	241
9.6.1	Single-Machine Infinite-Bus System	241
9.6.2	Energy Function for a Single-Machine Infinite-Bus System	244
9.6.3	Equal-Area Criterion and the Energy Function	247
9.6.4	Multimachine PEBS	249
9.6.5	Initialization of $V_{PE}(\theta)$ and its Use in PEBS Method	252
9.7	The Boundary Controlling u.e.p (BCU) Method	254
9.7.1	Algorithm	256
9.8	Structure-Preserving Energy Functions	259
9.9	Conclusion	260
9.10	Problems	260
10	Synchronized Phasor Measurement	263
10.1	Background	263
10.2	Phasor Computation	264
10.2.1	Nominal Frequency Phasors	264
10.2.2	Off-Nominal Frequency Phasors	265
10.2.3	Post Processing	269
10.2.4	Positive-Sequence Signals	271
10.2.5	Frequency Estimation	272
10.2.6	Phasor Data Accuracy	274
10.2.7	PMU Simulator	275

10.3	Phasor Data Communication	276
10.4	Power System Frequency Response	277
10.5	Power System Disturbance Propagation	280
10.5.1	Disturbance Triggering	285
10.6	Power System Disturbance Signatures	285
10.6.1	Generator or Load Trip	286
10.6.2	Oscillations	287
10.6.3	Fault and Line Switching	288
10.6.4	Shunt Capacitor or Reactor Switching	289
10.6.5	Voltage Collapse	289
10.7	Phasor State Estimation	289
10.8	Modal Analyses of Oscillations	293
10.9	Energy Function Analysis	296
10.10	Control Design Using PMU Data	299
10.11	Conclusions and Remarks	301
10.12	Problems	302
11	Power System Toolbox	305
11.1	Background	305
11.2	Power Flow Computation	306
11.2.1	Data Requirement	306
11.2.2	Power Flow Formulation and Solution	308
11.2.3	Nonconvergent Power Flow	311
11.3	Dynamic Simulation	311
11.3.1	Dynamic Models and Per-Unit Parameter Values	312
11.3.2	Initialization	313
11.3.3	Network Solution	314
11.3.4	Integration Methods	316
11.3.5	Disturbance Specifications	317
11.4	Linear Analysis	321
11.5	Conclusions and Remarks	324
11.6	Problems	324
A	Integral Manifolds for Model Reduction	327
A.1	Manifolds and Integral Manifolds	327
A.2	Integral Manifolds for Linear Systems	328
A.3	Integral Manifolds for Nonlinear Systems	336
Bibliography 341		
Index 353		

Preface

The need for power system dynamic analysis has grown significantly in recent years. This is due largely to the desire to utilize transmission networks for more flexible interchange transactions. While dynamics and stability have been studied for years in a long-term planning and design environment, there is a recognized need to perform this analysis in a weekly or even daily operation environment. This book is devoted to dynamic modeling and simulation as it relates to such a need, combining theoretical as well as practical information for use as a text for formal instruction or for reference by working engineers.

The investigation of power system dynamics has taken on a new urgency since the August 14, 2003 US Northeast Blackout, resulting in power disruption to 40 million people, some for up to a week. This event led to the installation of large number of time-synchronized high-sampling-rate phasor measurement units (PMUs) in the US, China, and many other countries, to monitor power system dynamic response to disturbances in real time. In this second edition, a new chapter on synchrophasor measurement has been added, showing several traces of actual PMU data. It is envisioned that the materials will reinforce the power system dynamic aspects treated more analytically in the earlier chapters.

As a text for formal instruction, this book assumes a background in electromechanics, machines, and power system analysis. As such, the text would normally be used in a graduate course in electrical engineering. It has been designed for use in a one-semester (15-week), 3-hour course. The notation follows that of most traditional machine and power system analysis books and attempts to follow the industry standards so that a transition to more detail and practical application is easy.

The text is divided into two parts. Chapters 1 to 6 give an introduction to electromagnetic transient analysis and a systematic derivation of synchronous machine dynamic models together with speed and voltage control subsystems. They include a rigorous explanation of model origins, development, and simplification. Particular emphasis is given to the concept of reduced-order modeling using integral manifolds as a firm basis for understanding the derivations and limitations of lower-order dynamic models. An appendix on integral manifolds gives a mathematical introduction to this technique of model reduction.

In the second part, Chapters 6 to 9 utilize these dynamic models for simulation and stability analysis. Particular care is given to the calculation of initial conditions and the alternative computational methods for simulation. Small-signal stability analysis is presented in a sequential manner, concluding with the design of power system stabilizers.

Transient stability analysis is formulated using energy function methods with an emphasis on the essentials of the potential energy boundary surface and the controlling unstable equilibrium point approaches. The new Chapter 10 describes synchrophasor technology and PMU data applications. In addition, a new Chapter 11 describes the Power System Toolbox, a MATLABTM-based free software. This simulation tool can be used for many examples throughout the book. Thus this chapter can be used as a reference as well as a primer on building a practical power system simulator. The Power System Toolbox, the PMU Simulator, and data and MATLABTM code for selected examples and problems can be downloaded from the website <https://ecse.rpi.edu/~chowj/>.

The book does not claim to be a complete collection of all models and simulation techniques, but seeks to provide a basic understanding of power system dynamics. While many more detailed and accurate models exist in the literature, a major goal of this book is to explain how individual component models are interfaced for a system study. Our objective is to provide a firm theoretical foundation for power system dynamic analysis to serve as a starting point for deeper exploration of complex phenomena and applications in electric power engineering.

We have so many people to acknowledge for their assistance in our careers and lives that we will limit our list to six people who have had a direct impact on the University of Illinois power program and the preparation of this book: Stan Helm, for his devotion to the power area of electrical engineering for over 60 years; George Swenson, for his leadership in strengthening the power area in the department; Mac VanValkenburg, for his fatherly wisdom and guidance; David Grainger, for his financial support of the power program; Petar Kokotovic, for his inspiration and energetic discussions; and Karen Chitwood, for preparing the manuscript. We have also benefited from our interactions with many power system experts from General Electric Company, including William Price, Richard Schulz, Einar Larsen, Dale Swann, and Thomas Younkins. The opportunity to work with Jay Murphy (Macrodyne) and Jim Ingleson (NYISO) on PMUs has greatly helped us. A special thank is due to Dr. Daniel Dotta (State University of Campinas (UNICAMP), Brazil) for writing the first part of Chapter 10.

Throughout our many years of collaboration at the University of Illinois and Rensselaer Polytechnic Institute, we have strived to maintain a healthy balance between education and research. We thank the University administration and the funding support of the National Science Foundation, the Department of Energy, and the Grainger Foundation for making this possible.

Peter W. Sauer and M. A. Pai

Urbana, Illinois

Joe H. Chow

Troy, New York

About the Companion Website

This book is accompanied by a companion website:

www.wiley.com/go/sauer/powersystemdynamics

The website hosts a variety of supplementary resources for students and instructors.

For Instructors:

- PowerPoint files of the illustrations presented within this text
- MATLAB codes and data for Examples and Problems
- Solutions to Problems at the end of each chapter
- Example Folders
- Sample lecture slides

For Students:

- Example Folders
- Data for Problems

1

Introduction

1.1 Background

The modern power grid has become more complex with the addition of many devices both in terms of transmission and generating sources. But the central generating systems station concept supported by a highly interconnected system remains the major part of power delivery network. The techniques for analysis and operation of the grid have been influenced both by advanced computational techniques and GPS-based communication such as synchronized phasor measurements for monitoring and control purposes.

Compared to other disciplines within electrical engineering, the analytical techniques of power systems were often based on experience and heuristic assumptions. The impact of control, system theory, and in recent years, communication and signal processing techniques has been significant. It is necessary to develop a sound theoretical basis for the area of power system dynamics, stability, and control. The purpose of this book is to achieve these objectives.

The subject of power system dynamics, stability, and control is an extremely broad topic with a long history and volumes of published literature. There are many ways to divide and categorize this subject for both education and research. While a substantial amount of information about the dynamic behavior of power systems can be gained through experience, working with and testing individual pieces of equipment, the complex problems and operating practices of large interconnected systems can be better understood if this experience is coupled with a mathematical model. There are several main divisions in the study of power system dynamics and stability [1].

F. P. deMello classified dynamic processes into three categories:

1. Electrical machine and system dynamics
2. System governing and generation control
3. Prime-mover energy supply dynamics and control

In the same reference, C. Concordia and R. P. Schulz classify dynamic studies according to four concepts:

1. The time of the system condition: past, present, or future
2. The time range of the study: microsecond through hourly response

3. The nature of the system under study: new station, new line, etc.
4. The technical scope of the study: fault analysis, load shedding, sub-synchronous resonance, etc.

All of these classifications share a common thread: They emphasize that the system is not in steady state and that many models for various components must be used in varying degrees of detail to allow efficient and practical analysis. The first six chapters of this book are thus devoted to the subject of modeling. The next three chapters discuss the use of the interconnected models for common dynamic studies. Finally we discuss the use of synchro phasor measurements for monitoring the system in real time. It forms the foundation for modern control techniques optimization and security analysis of the grid.

1.2 Physical Structures

The major components of a power system can be represented in a block-diagram format, as shown in Figure 1.1. While this block-diagram representation does not show all of the complex dynamic interaction between components and their controls, it serves to broadly describe the dynamic structures involved. Historically, there has been a major division into the mechanical and electrical subsystems as shown. This division is not absolute, however, since the electrical side clearly contains components with mechanical

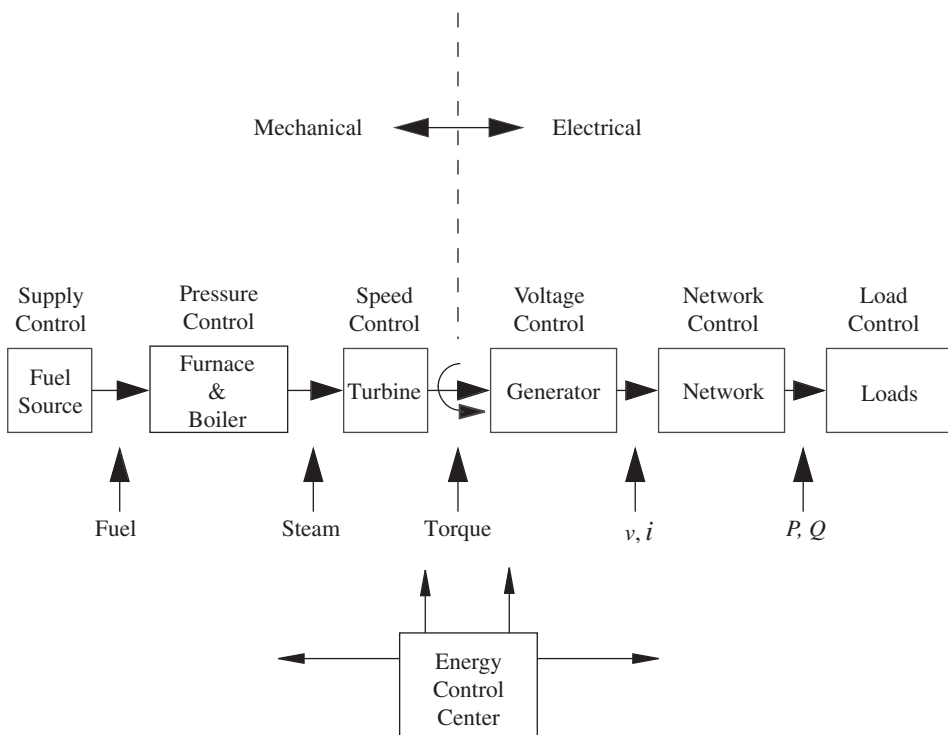


Figure 1.1 System dynamic structure.

dynamics (tap-changing-under-load (TCUL) transformers, motor loads, etc.) and the mechanical side clearly contains components with electrical dynamics (auxiliary motor drives, process controls, etc.). Furthermore, both sides are coupled through the monitoring and control functions of the energy control center. The energy control center gets information about the states of the system, that is, voltages and phase angles at various buses, through the phasor measurement units (PMUs) positioned all over the network.

1.3 Time-Scale Structures

Perhaps the most important classification of dynamic phenomena is their natural time range of response. A typical classification is shown in Figure 1.2. A similar concept is presented in [6]. This time-range classification is important because of its impact on component modeling. It should be intuitively obvious that it is not necessary to solve the complex transmission line wave equations to investigate the impact of a change in boiler control set points. This confirms a statement made earlier that “the system is not in steady state.” Evidently, depending on the nature of the dynamic disturbance, portions of the power system can be considered in “quasi-steady state.” This rather ambiguous term will be explained fully in the context of time-scale modeling [2].

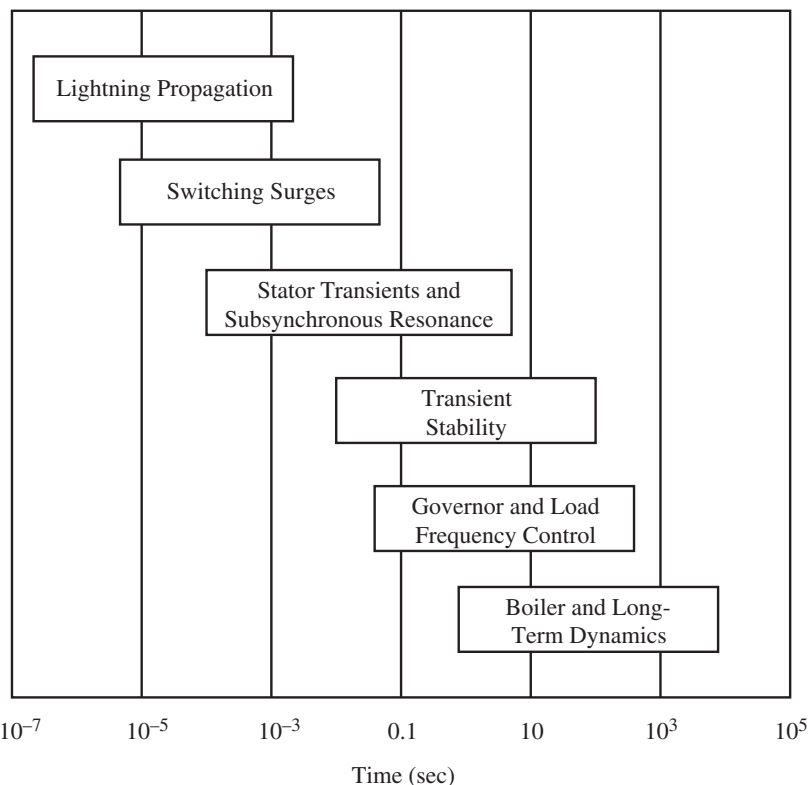
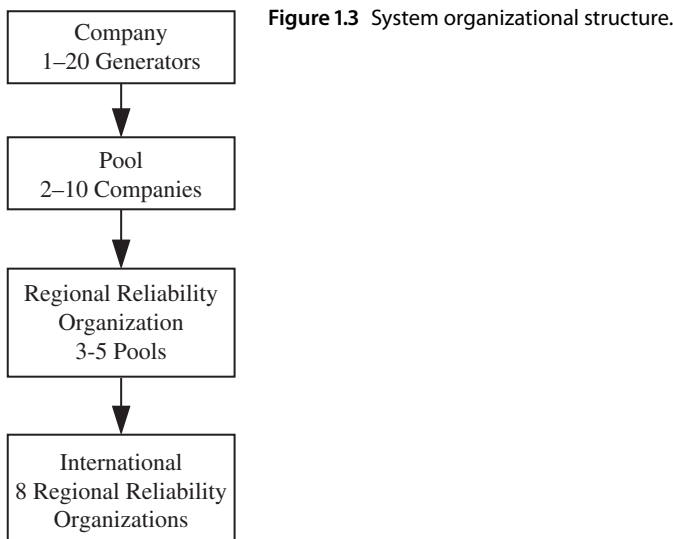


Figure 1.2 Time ranges of dynamic phenomena.

**Figure 1.3** System organizational structure.

1.4 Political Structures

The dynamic structure and time-range classifications of dynamic phenomena illustrate the potential complexity of even small or moderate-sized problems. The problems of power system dynamics and stability are compounded immensely by the current size of interconnected systems. A general system structure is shown in Figure 1.3. While this structure is not necessarily common to interconnected systems throughout the world, it represents a typical North American system and serves to illustrate the concept of a “large-scale system.” If we speculate about the possible size of a single interconnected system containing 8 regional reliability organizations, 4 pools per regional reliability organization, 6 companies per pool, and 10 generators per company, the total possible number of generating stations can exceed 2000. The bulk power transmission network (138–765 kV) then typically consists of over 10,000 buses. Indeed, the current demand in the 8 regional reliability organizations within the North American Electric Reliability Corporation (NERC) exceeds 500,000 MW [3]. At an average 250 MW per generator, this roughly confirms the estimate of over 2000 generators in the interconnected North American grid.

Dynamic studies are routinely performed on systems ranging in size from the smallest company to the largest regional reliability organization. These are made at both the planning/design and operating stages. These studies provide information about local capabilities as well as regional power interchange capabilities. In view of the potential size, dynamic studies must be capable of sufficiently accurate representation without prohibitive computational cost. The nature of system engineering problems inherent in such a complex task was emphasized in two benchmark reports by the Department of Energy (DOE) and the Electric Power Research Institute (EPRI) [4, 5]. These reports resulted in a meeting of international leaders to identify directions for the future of this technology. These reports set the stage for a whole new era of power system planning and operation. The volume of follow-on research and industry application has been

tremendous. Perhaps the most significant impact of these reports was the stimulation of new ideas that grew into student interest and eventual manpower.

1.5 The Phenomena of Interest

The dynamic performance of power systems is important to both the system organizations, from an economic viewpoint, and society in general, from a reliability viewpoint. The analysis of power system dynamics and stability is increasing daily in terms of number and frequency of studies, as well as in complexity and size. Dynamic phenomena have been discussed according to basic function, time-scale properties, and problem size. These three fundamental concepts are very closely related and represent the essence of the challenges of effective simulation of power system dynamics. When properly performed, modeling and simulation capture the phenomena of interest at minimal cost. The first step in this process is understanding the phenomena of interest. Only with a solid physical *and* mathematical understanding can the modeling and simulation properly reflect the critical system behavior. This means that the origin of mathematical models must be understood, and their purpose must be well defined. Once this is accomplished, the minimal cost is achieved by model reduction and simplification without significant loss in accuracy.

1.6 New Chapters Added to this Edition

Two new chapters have been added in this edition of the book to reaffirm learning from the existing chapters. For generations, most power students had to take “faith” in the generator swing equations and excitation system control to determine power system dynamics. However, with high-sampling-rate digital recording of power system signals using the phasor measurement technology and the ability to precisely time tag the measurements over wide geographical areas using a timing signal from the Global Positioning System (GPS), the propagation of a disturbance can be observed as it travels through a power grid. This observation can be used to corroborate the dynamic models of power systems. Synchrophasor measurement is covered in Chapter 10.

Chapter 11 on the Power System Toolbox (PST) is a timely addition to this edition, as the first edition was published before PST was developed. Although limited in the availability of exciter and governor models, the PST program structure is in many aspects similar to those of several commercial power system simulation tools. In addition to a description on the fundamentals of power system computer simulation, Chapter 11 also provides useful pointers for the proper use of such simulation programs. An ambitious reader may even try to incorporate additional models into PST.

The Power System Toolbox, the PMU Simulator, and the data and MATLABTM code for selected examples and problems can be downloaded from the website <https://ecse.rpi.edu/~chowj/>.

2

Electromagnetic Transients

2.1 The Fastest Transients

In the time-scale classification of power system dynamics, the fastest transients are generally considered to be those associated with lightning propagation and switching surges. Since this text is oriented toward system analysis rather than component design, these transients are discussed in the context of their propagation into other areas of an interconnected system. While quantities such as conductor temperature, motion, and chemical reaction are important aspects of such high-speed transients, we focus mainly on a circuit view, where voltage and current are of primary importance. While the theories of insulation breakdown, arcing, and lightning propagation rarely lend themselves to incorporation into standard circuit analysis [7], some simulation software does include a portion of these transients [8, 9]. From a system viewpoint, the transmission line is the main component that provides the interconnection to form large complex models. While the electromagnetic transients programs (EMTP) described in [8] and [9] are unique for their treatment of switching phenomena of value to designers, they include the capability to study the propagation of transients through transmission lines. This feature makes the EMTP program a system analyst's tool as well as a designer's tool. The transmission line models and basic network solution methods used in these programs are discussed in the following sections.

2.2 Transmission Line Models

Models for transmission lines for use in network analysis are usually categorized by line lengths (long, medium, short) [10–12]. This line length concept is interesting, and presents a major challenge in the systematic formulation of line models for dynamic analysis. For example, most students and engineers have been introduced to the argument that shunt capacitance need not be included in short-line models because it has a negligible effect on “the accuracy.” Thus, a short line can be modeled using only series resistance and inductance, resulting in a single (for a single line) differential equation in the current state variable. With capacitance, there would also be a differential equation involving the voltage state variable.

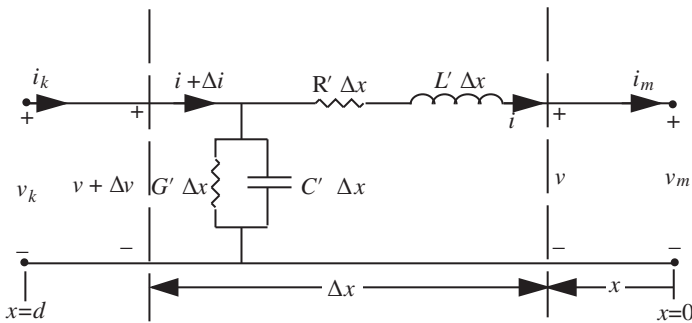


Figure 2.1 Transmission line segment.

Reducing a model from two or three differential equations to only one is a process that has to be justified mathematically as well as physically. As will be shown, the “long-line” model involves partial differential equations, which in some sense represent an infinite number of ordinary differential equations. The reduction from infinity to one is, indeed, a major reduction and deserves further attention.

Since this text deals with dynamics, it is important to be careful with familiar models and concepts. Lumped-parameter models are normally valid for transient analysis unless they are the result of a reduction technique such as Thevenin equivalencing. Investigation of the various traditional transmission line models illustrates this point very well. The traditional derivation of the “long-line” model begins with the construction of an infinitesimal segment of length Δx in Figure 2.1. This length is assumed to be small enough that magnetic and electric field effects can be considered separately, resulting in per-unit length line parameters R' , L' , G' , C' . These distributed parameters have the units of ohms/mi, henries/mi, etc., and are calculated from the line configuration. This incremental lumped-parameter model is, in itself, an approximation of the exact interaction of the electric and magnetic fields. The hope, of course, is that as the incremental segment approaches zero length, the resulting model gives a good approximation of Maxwell's equations. For certain special cases, it can be shown that such an approach is indeed valid ([13], pp. 393–397).

The line has voltages and currents at its sending end (k) and receiving end (m). The voltage and current anywhere along the line are simply

$$v = v(x, t) \quad (2.1)$$

$$i = i(x, t) \quad (2.2)$$

so that

$$v_m = v(0, t) \quad (2.3)$$

$$i_m = i(0, t) \quad (2.4)$$

$$v_k = v(d, t) \quad (2.5)$$

$$i_k = i(d, t) \quad (2.6)$$

where d is the line length. The dynamic equation for the voltage drop across the infinitesimal segment is

$$\Delta v = R' \Delta x i + L' \Delta x \frac{\partial i}{\partial t} \quad (2.7)$$

and the current through the shunt is

$$\Delta i = G' \Delta x (\nu + \Delta v) + C' \Delta x \frac{\partial}{\partial t} (\nu + \Delta v). \quad (2.8)$$

Substituting (2.7) into (2.8),

$$\Delta i = G' \Delta x \nu + G' \Delta x \left[R' \Delta x i + L' \Delta x \frac{\partial i}{\partial t} \right] + C' \Delta x \frac{\partial \nu}{\partial t} + C' \Delta x \left[R' \Delta x \frac{\partial i}{\partial t} + L' \Delta x \frac{\partial^2 i}{\partial t^2} \right]. \quad (2.9)$$

Dividing by Δx ,

$$\frac{\Delta \nu}{\Delta x} = R' i + L' \frac{\partial i}{\partial t} \quad (2.10)$$

$$\frac{\Delta i}{\Delta x} = G' \nu + G' \left[R' \Delta x i + L' \Delta x \frac{\partial i}{\partial t} \right] + C' \frac{\partial \nu}{\partial t} + C' \left[R' \Delta x \frac{\partial i}{\partial t} + L' \Delta x \frac{\partial^2 i}{\partial t^2} \right]. \quad (2.11)$$

Now, the original assumption that the magnetic and electric fields may be analyzed separately to obtain the distributed parameters has more credibility when the length under consideration is zero. Thus, the final step is to evaluate (2.10) and (2.11) in the limit as Δx approaches zero, which gives

$$\lim_{\Delta x \rightarrow 0} \frac{\Delta \nu}{\Delta x} = \frac{\partial \nu}{\partial x} = R' i + L' \frac{\partial i}{\partial t} \quad (2.12)$$

$$\lim_{\Delta x \rightarrow 0} \frac{\Delta i}{\Delta x} = \frac{\partial i}{\partial x} = G' \nu + C' \frac{\partial \nu}{\partial t}. \quad (2.13)$$

Equations (2.12) and (2.13) are the final distributed-parameter models of a lossy transmission line.

There are two special cases when these partial differential equations have very nice known solutions. The first is the special case of no shunt elements ($C' = G' = 0$). From (2.13), the line current is independent of x so that (2.12) simplifies to

$$\nu(x, t) = \nu(o, t) + R' x i + L' x \frac{di}{dt} \quad (2.14)$$

which has a simple series lumped R-L circuit representation. This special case essentially neglects all electric field effects.

The second special case is the lossless line ($R' = G' = 0$), which has the general solution [13, 14]

$$i(x, t) = -f_1(x - v_p t) - f_2(x + v_p t) \quad (2.15)$$

$$\nu(x, t) = z_c f_1(x - v_p t) - z_c f_2(x + v_p t) \quad (2.16)$$

where f_1 and f_2 are unknown functions that depend on the boundary conditions, and the phase velocity and the characteristic impedance

$$v_p = \frac{1}{\sqrt{L' C'}} \quad z_c = \sqrt{L'/C'}. \quad (2.17)$$

If only the terminal response (v_k, i_k, v_m, i_m) is of interest, the following method, often referred to as Bergeron's method, has a significant value in practical implementations. The receiving end current is

$$i_m(t) = i(o, t) = -f_1(-v_p t) - f_2(v_p t). \quad (2.18)$$

Now, $f_1(-v_p t)$ can be expressed as a function of $v(o, t)$ and $f_2(v_p t)$ from (2.16) to obtain

$$i_m(t) = -\frac{1}{z_c} v(o, t) - 2f_2(v_p t) \quad (2.19)$$

$$= -\frac{1}{z_c} v_m(t) - 2f_2(v_p t). \quad (2.20)$$

To determine $f_2(v_p t)$, it is necessary to evaluate the sending end current at time d/v_p seconds before t as

$$i_k \left(t - \frac{d}{v_p} \right) = -f_1(d - v_p t + d) - f_2(d + v_p t - d). \quad (2.21)$$

Using (2.16) at $x = d$ and at time d/v_p before t ,

$$v_k \left(t - \frac{d}{v_p} \right) = z_c f_1(d - v_p t + d) - z_c f_2(d + v_p t - d) \quad (2.22)$$

so that (2.21) can be evaluated as

$$i_k \left(t - \frac{d}{v_p} \right) = -\frac{1}{z_c} v_k \left(t - \frac{d}{v_p} \right) - 2f_2(v_p t). \quad (2.23)$$

This solves for $f_2(v_p t)$ to obtain the expression for the current $i_m(t)$:

$$i_m(t) = -\frac{1}{z_c} v_m(t) + i_k \left(t - \frac{d}{v_p} \right) + \frac{1}{z_c} v_k \left(t - \frac{d}{v_p} \right). \quad (2.24)$$

This expression has a circuit model as shown in Figure 2.2, where

$$I_m = i_k \left(t - \frac{d}{v_p} \right) + \frac{1}{z_c} v_k \left(t - \frac{d}{v_p} \right). \quad (2.25)$$

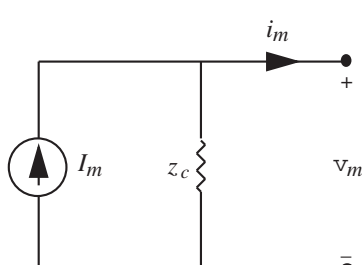
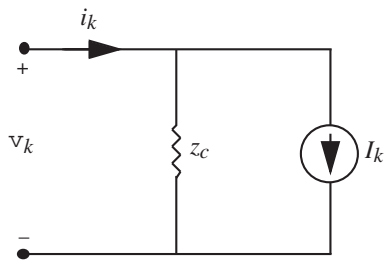


Figure 2.2 Transmission line model receiving end.

Figure 2.3 Transmission line model sending end.

A similar derivation (see Problem 2.1) can be made to determine the sending-end model shown in Figure 2.3, where

$$I_k = i_m \left(t - \frac{d}{v_p} \right) - \frac{1}{z_c} v_m \left(t - \frac{d}{v_p} \right). \quad (2.26)$$

These circuit models are illustrated with other components in the next section.

Before leaving this topic, we consider the special case in which the voltages and currents are sinusoidal functions of the form

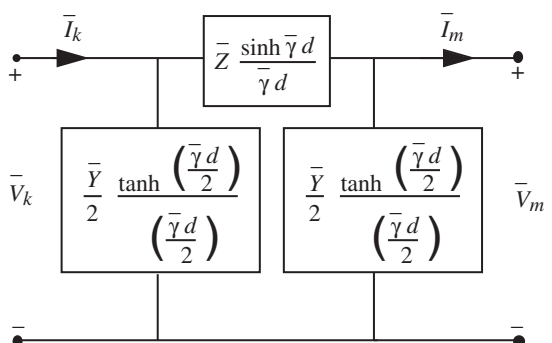
$$v(x, t) = V(x) \cos(\omega_s t + \theta_v(x)) \quad (2.27)$$

$$i(x, t) = I(x) \cos(\omega_s t + \phi_i(x)) \quad (2.28)$$

where ω_s is a constant. Substitution of these functions into the partial differential equations yields the model of Figure 2.4, with phasors [10]

$$\bar{V}(x) = \frac{1}{\sqrt{2}} V(x) \angle \theta_v(x) \quad (2.29)$$

$$\bar{I}(x) = \frac{1}{\sqrt{2}} I(x) \angle \theta_i(x) \quad (2.30)$$

Figure 2.4 PI lumped-parameter circuit for sinusoidal voltages/currents.

where

$$\begin{aligned}\bar{Z} &= R'd + j\omega_s L'd, \\ \bar{Y} &= G'd + j\omega_s C'd, \\ \bar{\gamma} &= \sqrt{\frac{\bar{Z}\bar{Y}}{d^2}}.\end{aligned}\tag{2.31}$$

There is always a great temptation to convert Figure 2.4 into a lumped-parameter time-domain $R - L - C$ circuit for transient analysis. While such a circuit would clearly be without mathematical justification, it would be some approximation of the more exact partial differential equation representation. The accuracy of such an approximation would depend on the phenomena of interest and on the relative sizes of the line parameters. In later chapters, we will discuss the concept of “network transients” in the context of fast and slow dynamics.

2.3 Solution Methods

Since most power system models contain nonlinearities, transient analysis usually involves some form of numerical integration. Such numerical methods are well documented for general networks and for power systems [15–19]. The trapezoidal rule is a common method used in EMTP and other transient analysis programs. For a dynamic system of the form

$$\frac{dy}{dt} = f(y, t)\tag{2.32}$$

the trapezoidal rule approximates the change of state y over a change of time Δt as

$$y(t_i + \Delta t) \approx y(t_i) + \frac{\Delta t}{2}[f(y(t_i + \Delta t), t_i + \Delta t) + f(y(t_i), t_i)].\tag{2.33}$$

This is an implicit integration scheme, since $y(t_i + \Delta t)$ appears on the right-hand side of (2.33). To illustrate the method, consider the pure inductive branch of Figure 2.5. The state representation is

$$\frac{di}{dt} = \frac{1}{L}v \quad i(t_o) = i_o\tag{2.34}$$

This approximation can be written as the circuit constraint of Figure 2.6. The circuit is linear for given values of $i(t_i)$, $v(t_i)$, and Δt . A similar circuit can be constructed for a pure linear capacitor (see Problem 2.2). Since these are linear elements, there is really no need to employ such an approximation, but recall the lossless-line circuit representation

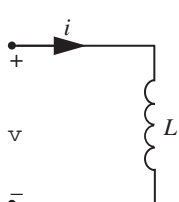
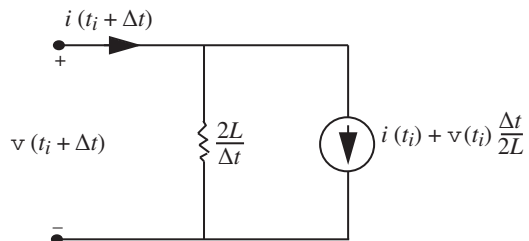


Figure 2.5 Pure linear inductive branch.

Figure 2.6 Circuit representation of trapezoidal rule (linear L).



of Figures 2.2 and 2.3. The combination of the Bergeron lossless-line model and the trapezoidal rule for lumped parameters is appealing. There are two difficulties. First, it may be necessary to consider transmission line losses. Second, the lossless-line terminal constraints require knowledge of voltages and currents at a previous time $(t - \frac{d}{v_p})$, which may not coincide with a multiple of the integration step size Δt . The first problem is usually overcome by simply lumping a series or shunt resistance at either end of the transmission line terminal model. It is common to break the line into several segments, each using the circuits of Figures 2.2 and 2.3 together with a corresponding fraction of the line losses. The second problem is usually overcome either by rounding off the time d/v_p to the nearest multiple of Δt , or by linear interpolation over one time step Δt (see discussion published with [14]). This is illustrated in the following example.

Example 2.1 Consider a single-phase lossless transmission line connected to an $R - L$ load, as shown in Figure 2.7:

$$v_s = \frac{230,000\sqrt{2}}{\sqrt{3}} \cos(2\pi 60t).$$

Find i_1 , i_2 , and v_2 if the switch is closed at $t = 0.0001$ sec using the trapezoidal rule with a time step $\Delta t = 0.0001$ sec. Initial conditions are $i_1(0) = i_2(0) = v_1(0) = v_2(0) = 0$.

Solution:

For the parameters given,

$$z_c = 274 \text{ ohm}, \frac{2L}{\Delta t} = 5000 \text{ ohm}, \frac{d}{v_p} = 0.00055 \text{ sec}, v_p = 182,574 \text{ mi/sec}.$$

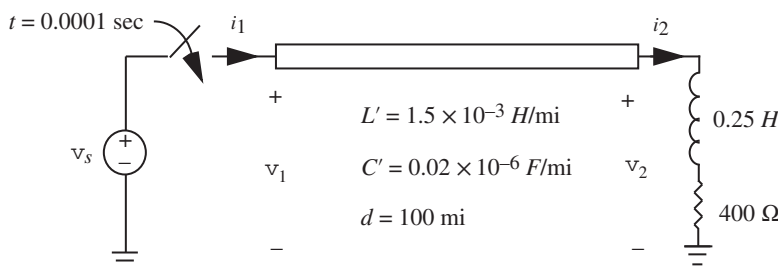


Figure 2.7 Single lossless line and R-L load diagram.

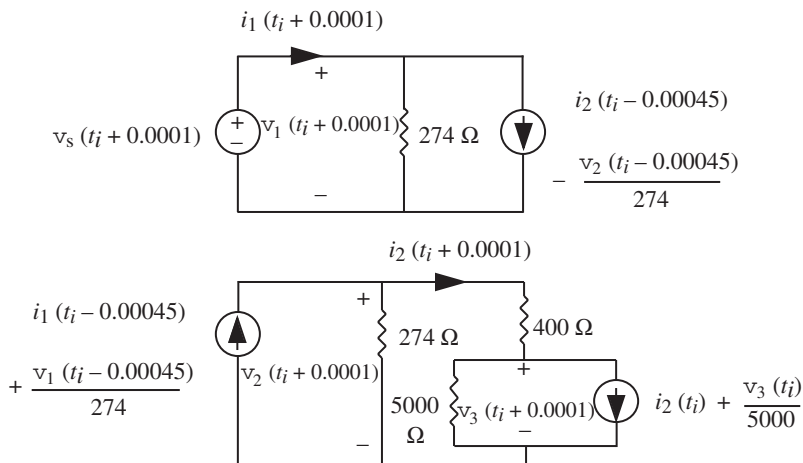


Figure 2.8 Single line and $R-L$ load circuit at $t = t_i + 0.0001$.

The circuit connection when the switch is closed is found using $t = t_i + 0.0001$ as shown in Figure 2.8

For $t_i = 0$ ($t = 0.0001$ sec)

From the initial conditions,

$$\begin{aligned} i_1(-0.00045) &= 0 \\ v_1(-0.00045) &= 0 \\ i_2(-0.00045) &= 0 \\ v_2(-0.00045) &= 0 \\ i_2(0) &= 0 \\ v_3(0) &= 0 \\ v_s(0.0001) &= 187,661 \text{ V.} \end{aligned}$$

The circuit to be solved at $t = 0.0001$ sec is shown in Figure 2.9. Solving the circuits gives

$$\begin{aligned} i_1(0.0001) &= 685 \text{ A} \\ v_1(0.0001) &= 187,661 \text{ V} \\ i_2(0.0001) &= 0 \\ v_2(0.0001) &= 0 \\ v_3(0.0001) &= 0. \end{aligned}$$

The sending-end current has changed instantaneously from zero to 685 A as the switch is closed.

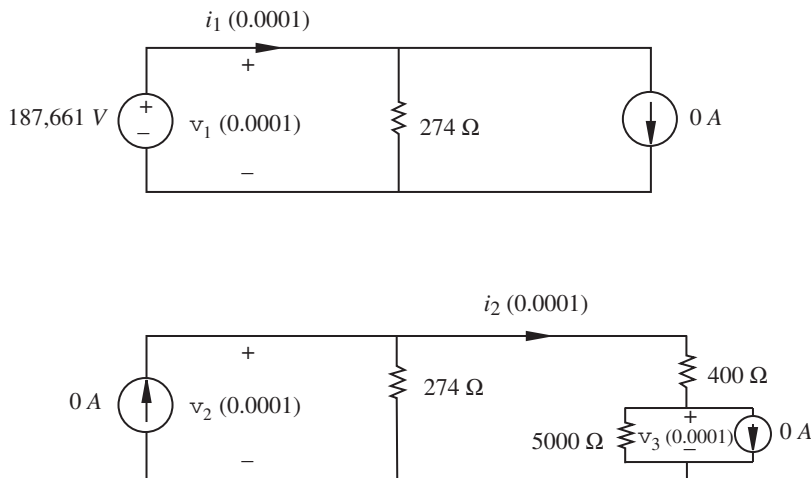


Figure 2.9 Single line and $R - L$ load circuit at $t = 0.0001$ sec.

For $t_i = 0.0001$ ($t = 0.0002$ sec)

From the initial conditions and the solution at time $t = 0.0001$ sec,

$$\begin{aligned}i_1(-0.00035) &= 0 \\v_1(-0.00035) &= 0 \\i_2(-0.00035) &= 0 \\v_2(-0.00035) &= 0 \\i_2(0.0001) &= 0 \\v_3(0.0001) &= 0 \\v_s(0.0002) &= 187,261 \text{ V}.\end{aligned}$$

The circuit for this time is the same as before, except that the source has changed. Solving the circuit gives

$$\begin{aligned}i_1(0.0002) &= 683 \text{ A} \\v_1(0.0002) &= 187,261 \text{ V} \\i_2(0.0002) &= 0 \\v_2(0.0002) &= 0 \\v_3(0.0002) &= 0.\end{aligned}$$

This will continue until the traveling wave reaches the receiving end at $t_i = 0.00055$ sec. Since we are using a time step of 0.0001 sec, it will first appear at $t_i = 0.0006$ sec.

For $t_i = 0.0006$ ($t = 0.0007$ sec)

Need:

$$\begin{aligned}i_1(0.00015), v_1(0.00015), i_2(0.00015), \\v_2(0.00015), i_2(0.0006), v_3(0.0006), v_s(0.0007)\end{aligned}$$

There is now a problem, since i_1 , i_2 , and v_2 are not known at $t = 0.00015$. The voltage $v_1(0.00015)$ can be found exactly, since it is equal to the source v_s . The other “sources”

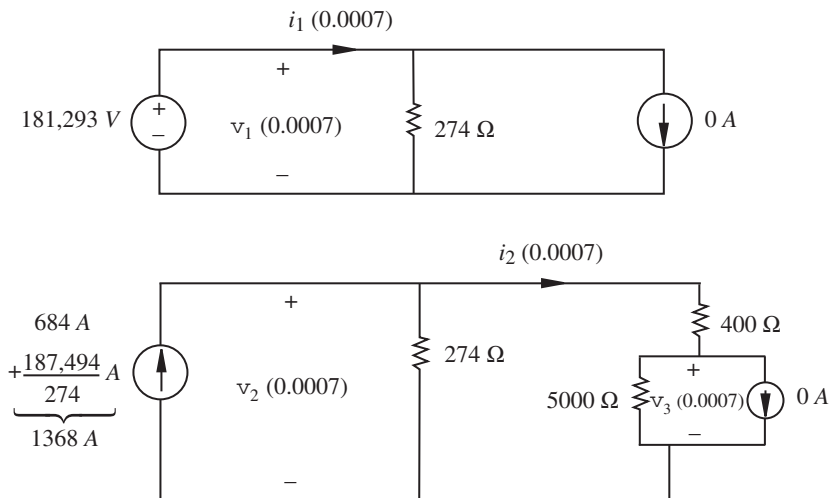


Figure 2.10 Single line and $R - L$ load at $t = 0.0007$ sec.

in the circuits must be approximated. There are at least two approximations that can be used. The first approximation is to use

$$i_1(0.00015) \approx i_1(0.0002) = 683 \text{ A}.$$

The second approximation uses linear interpolation as

$$\begin{aligned} i_1(0.00015) &\approx i_1(0.0001) + \frac{0.00015 - 0.0001}{0.0002 - 0.0001} (i_1(0.0002) - i_1(0.0001)) \\ &= 685 + 0.5 \times (683 - 685) \\ &= 684 \text{ A}. \end{aligned}$$

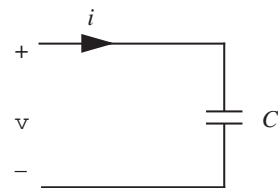
Using this approximation for $i_1(0.00015)$, the circuits to be solved at $t_i = 0.0006$ ($t = 0.0007$ sec) are shown in Figure 2.10. Solving these circuits,

$$\begin{aligned} i_1(0.0007) &= 662 \text{ A} \\ v_1(0.0007) &= 181,293 \text{ V} \\ i_2(0.0007) &= 66 \text{ A} \\ v_2(0.0007) &= 356,731 \text{ V}. \end{aligned}$$

The traveling wave has reached the receiving end and has resulted in nearly a doubling of voltage, because the receiving end is initially nearly an open circuit. The analysis continues with linear interpolation as needed. When a study contains only one line (like this example), the interface problem between Δt and d/v_p can be avoided by choosing Δt to be an integer fraction of d/v_p :

$$\Delta t = \frac{1}{N} \frac{d}{v_p}.$$

Typical values of N range between 5 and 10,000. □

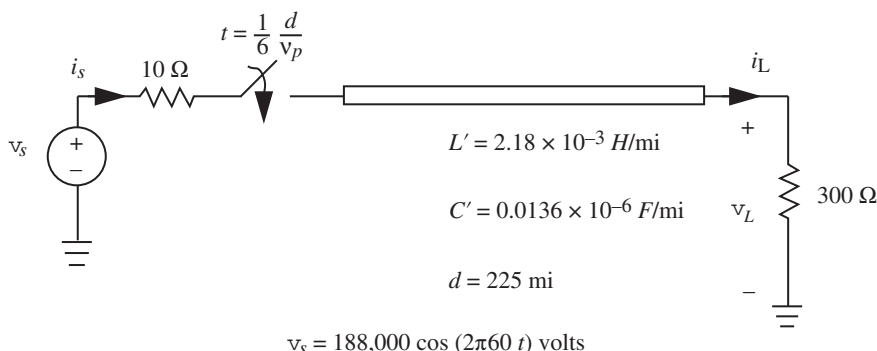
Figure 2.11 Figure for Problem 2.2.

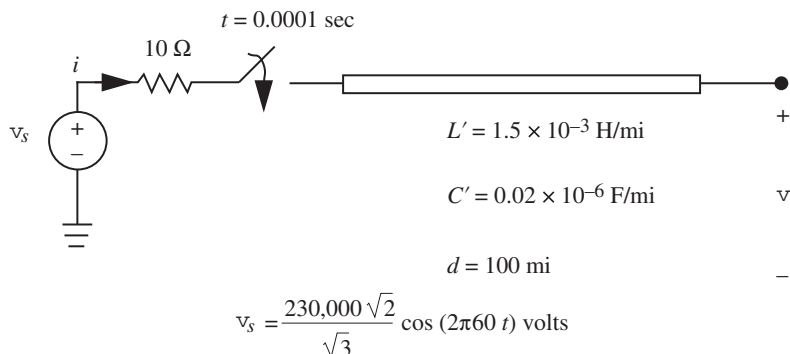
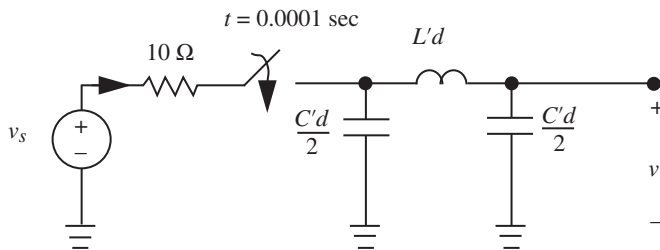
The unique feature of the combination of Bergeron circuits with trapezoidal rule circuits is the heart of most EMTP programs. This enables transmission line plus load transients to be solved using simple “dc” circuits. Most EMTP programs contain many other features, including three-phase representations and other devices. Its use is normally limited to small-sized systems in which the very fast transients of switching are the phenomena of interest.

The purpose of this chapter was to present the basic concepts for dealing with the fastest transients from a systems viewpoint. In most studies, these dynamics are approximated further as attention shifts to electromechanical dynamics and subsystems with slower response times.

2.4 Problems

- 2.1** Starting with (2.15) and (2.16), derive the circuit representation of Figure 2.3 for the sending-end terminals of a lossless transmission line.
- 2.2** Given the continuous time-domain circuit shown in Figure 2.11, use the trapezoidal rule approximation to find an algebraic “dc” circuit representation of the relationship between $v(t_i + \Delta t)$ and $i(t_i + \Delta t)$.
- 2.3** Given the sinusoidal source and de-energized lossless transmission line shown in Figure 2.12, draw the “Bergeron” algebraic “dc” circuit and find v_L , i_L , i_s for $0 \leq t \leq 0.04$ sec using a time step of $\Delta t = \frac{1}{6} \frac{d}{v_p}$. Plot v_L .

**Figure 2.12** Figure for Problem 2.3.

**Figure 2.13** Figure for Problem 2.4.**Figure 2.14** Figure for Problem 2.5.

- 2.4** Given the sinusoidal source and de-energized lossless transmission line shown in Figure 2.13, use Bergeron's method with linear interpolation to find v and i using a time step of $\Delta t = 0.0001$ sec. Solve for a total time of 0.02 sec. Plot the results.
- 2.5** Repeat Problem 2.4 using the lumped-parameter model shown in Figure 2.14 using the trapezoidal rule approximation with a time step of 10^{-6} sec.
- 2.6** Euler's forward integration scheme solves ordinary differential equations ($dx/dt = f(x)$) using a time step h as

$$x(t_i + h) = x(t_i) + (dx/dt)h$$

where dx/dt is evaluated at time t_i . Use this solution scheme to derive an algebraic "dc" circuit to solve for the current through a lumped-parameter R-L series circuit at each time step for any given applied voltage.

3

Synchronous Machine Modeling

3.1 Conventions and Notation

There is probably more literature on synchronous machines than on any other device in electrical engineering. Unfortunately, this vast amount of material often makes the subject complex and confusing. In addition, most of the work on reduced-order modeling is based primarily on physical intuition, practical experience, and years of experimentation. The evolution of dynamic analysis has caused some problems in notation as it relates to common symbols that eventually require data from manufacturers. This text uses the conventions and notations of [20], which essentially follows those of many publications on synchronous machines [21–27]. When the notation differs significantly from these and other conventions, notes are given to clarify any possible misunderstanding. The topics of time constants and machine inductances are examples of such notations. While some documents define time constants and inductances in terms of physical experiments, this text uses fixed expressions in terms of model parameters. Since there can be a considerable difference in numerical values, it is important to always verify the meaning of symbols when obtaining data. This is most effectively done by comparing the model in which a parameter appears with the test or calculation that was performed to produce the data. In many cases, the parameter values are provided from design data based on the same expressions given in this text. In some cases, the parameter values are provided from standard tests that may not precisely relate to the expressions given in this text. In this case, there is normally a procedure to convert the values into consistent data [20].

The original Park's transformation is used together with the " x_{ad} " per-unit system [28,29]. This results in a reciprocal transformed per-unit model where 1.0 per-unit excitation results in rated open-circuit voltage for a linear magnetic system. Even with this standard choice, there is enough freedom in scaling to produce various model structures that appear different [30]. These issues are discussed further in later sections.

In this chapter, the machine transformation and scaling were separated from the topic of the magnetic circuit representation. This is done so that it is clear which equations and parameters are independent of the magnetic circuit representation.

3.2 Three-Damper-Winding Model

This section presents the basic dynamic equations for a balanced, symmetrical, three-phase synchronous machine with a field winding and three damper windings on the rotor. The simplified schematic of Figure 3.1 shows the coil orientation, assumed polarities, and rotor position reference. The stator windings have axes 120 electrical degrees apart and are assumed to have an equivalent sinusoidal distribution [20]. While a two-pole machine is shown, all equations will be written for a P -pole machine with $\omega = \frac{p}{2}\omega_{\text{shaft}}$ expressed in electrical radians per second. The circles with dots and x 's indicate the windings. Current flow is assumed to be into the “ x ” and out of the “dot.” The voltage polarity of the coils is assumed to be plus to minus from the “ x ” to the “dots.”

This notation uses “motor” current notation for all the windings at this point. The transformed stator currents will be changed to “generator” current notation at the point of per-unit scaling. The fundamental Kirchhoff's, Faraday's and Newton's laws give

$$v_a = i_a r_s + \frac{d\lambda_a}{dt} \quad (3.1)$$

$$v_b = i_b r_s + \frac{d\lambda_b}{dt} \quad (3.2)$$

$$v_c = i_c r_s + \frac{d\lambda_c}{dt} \quad (3.3)$$

$$v_{fd} = i_{fd} r_{fd} + \frac{d\lambda_{fd}}{dt} \quad (3.4)$$

$$v_{1d} = i_{1d} r_{1d} + \frac{d\lambda_{1d}}{dt} \quad (3.5)$$

$$v_{1q} = i_{1q} r_{1q} + \frac{d\lambda_{1q}}{dt} \quad (3.6)$$

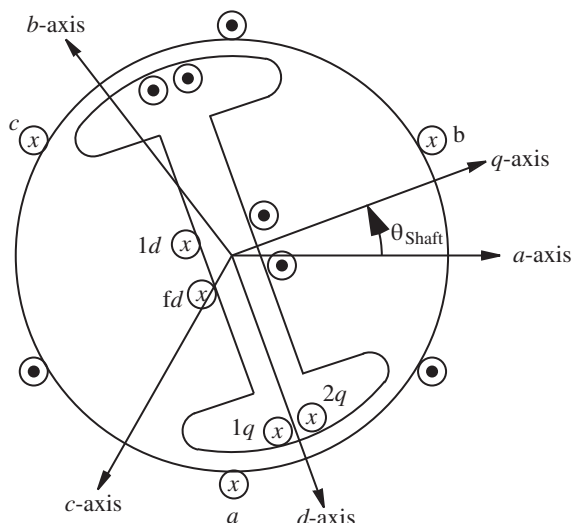


Figure 3.1 Synchronous machine schematic.

$$v_{2q} = i_{2q}r_{2q} + \frac{d\lambda_{2q}}{dt} \quad (3.7)$$

$$\frac{d\theta_{\text{shaft}}}{dt} = \frac{2}{P}\omega \quad (3.8)$$

$$J \frac{2}{P} \frac{d\omega}{dt} = T_m - T_e - T_{fw} \quad (3.9)$$

where λ is flux linkage, r is winding resistance, J is the inertia constant, P is the number of magnetic poles per phase, T_m is the mechanical torque applied to the shaft, $-T_e$ is the torque of electrical origin, and T_{fw} is a friction windage torque. A major modeling challenge is to obtain the relationship between flux linkage and current. These relationships will be presented in later sections.

3.3 Transformations and Scaling

The sinusoidal steady state of balanced symmetrical machines can be transformed to produce constant states. The general form of the transformation that accomplishes this is Park's transformation [20],

$$v_{dqo} \stackrel{\Delta}{=} T_{dqo}v_{abc}, \quad i_{dqo} \stackrel{\Delta}{=} T_{dqo}i_{abc}, \quad \lambda_{dqo} \stackrel{\Delta}{=} T_{dqo}\lambda_{abc} \quad (3.10)$$

where

$$v_{abc} \stackrel{\Delta}{=} [v_a v_b v_c]^t, \quad i_{abc} \stackrel{\Delta}{=} [i_a i_b i_c]^t, \quad \lambda_{abc} \stackrel{\Delta}{=} [\lambda_a \lambda_b \lambda_c]^t \quad (3.11)$$

$$v_{dqo} \stackrel{\Delta}{=} [v_d v_q v_o]^t, \quad i_{dqo} \stackrel{\Delta}{=} [i_d i_q i_o]^t, \quad \lambda_{dqo} \stackrel{\Delta}{=} [\lambda_d \lambda_q \lambda_o]^t \quad (3.12)$$

and

$$T_{dqo} \stackrel{\Delta}{=} \frac{2}{3} \begin{bmatrix} \sin \frac{P}{2}\theta_{\text{shaft}} & \sin \left(\frac{P}{2}\theta_{\text{shaft}} - \frac{2\pi}{3} \right) & \sin \left(\frac{P}{2}\theta_{\text{shaft}} + \frac{2\pi}{3} \right) \\ \cos \frac{P}{2}\theta_{\text{shaft}} & \cos \left(\frac{P}{2}\theta_{\text{shaft}} - \frac{2\pi}{3} \right) & \cos \left(\frac{P}{2}\theta_{\text{shaft}} + \frac{2\pi}{3} \right) \\ \frac{1}{2} & \frac{1}{2} & \frac{1}{2} \end{bmatrix} \quad (3.13)$$

with the inverse

$$T_{dqo}^{-1} = \begin{bmatrix} \sin \frac{P}{2}\theta_{\text{shaft}} & \cos \frac{P}{2}\theta_{\text{shaft}} & 1 \\ \sin \left(\frac{P}{2}\theta_{\text{shaft}} - \frac{2\pi}{3} \right) & \cos \left(\frac{P}{2}\theta_{\text{shaft}} - \frac{2\pi}{3} \right) & 1 \\ \sin \left(\frac{P}{2}\theta_{\text{shaft}} + \frac{2\pi}{3} \right) & \cos \left(\frac{P}{2}\theta_{\text{shaft}} + \frac{2\pi}{3} \right) & 1 \end{bmatrix}. \quad (3.14)$$

From (3.1)–(3.9), Kirchhoff's and Faraday's laws are

$$v_{abc} = r_s i_{abc} + \frac{d}{dt}(\lambda_{abc}) \quad (3.15)$$

which, when transformed using (3.13) and (3.14), are

$$v_{dqo} = r_s i_{dqo} + T_{dqo} \frac{d}{dt} \left(T_{dqo}^{-1} \lambda_{dqo} \right). \quad (3.16)$$

After evaluation, the system in dqo coordinates has the forms

$$\nu_d = r_s i_d - \omega \lambda_q + \frac{d\lambda_d}{dt} \quad (3.17)$$

$$\nu_q = r_s i_q + \omega \lambda_d + \frac{d\lambda_q}{dt} \quad (3.18)$$

$$\nu_o = r_s i_o + \frac{d\lambda_o}{dt} \quad (3.19)$$

$$\nu_{fd} = r_{fd} i_{fd} + \frac{d\lambda_{fd}}{dt} \quad (3.20)$$

$$\nu_{1d} = r_{1d} i_{1d} + \frac{d\lambda_{1d}}{dt} \quad (3.21)$$

$$\nu_{1q} = r_{1q} i_{1q} + \frac{d\lambda_{1q}}{dt} \quad (3.22)$$

$$\nu_{2q} = r_{2q} i_{2q} + \frac{d\lambda_{2q}}{dt} \quad (3.23)$$

$$\frac{d\theta_{\text{shaft}}}{dt} = \frac{2}{P}\omega \quad (3.24)$$

$$J \frac{2}{P} \frac{d\omega}{dt} = T_m - T_e - T_{fw}. \quad (3.25)$$

To derive an expression for T_e , it is necessary to look at the overall energy or power balance for the machine. This is an electromechanical system that can be divided into an electrical system, a mechanical system, and a coupling field [31]. In such a system, resistance causes real power losses in the electrical system, friction causes heat losses in the mechanical system, and hysteresis causes losses in the coupling field. Energy is stored in inductances in the electrical system, the rotating mass of the mechanical system, and the magnetic field that couples the two. Any energy that is not lost or stored must be transferred. In this text we make two assumptions about this energy balance. First, all energy stored in the electrical system inside the machine terminals is included in the energy stored in the coupling field. Second, the coupling field is lossless. The first assumption is arbitrary, and the second assumption neglects phenomena such as hysteresis (but not saturation). A diagram that shows such a power balance for a single machine using the above notation is given in Figure 3.2, with input powers for both the electrical and mechanical systems.

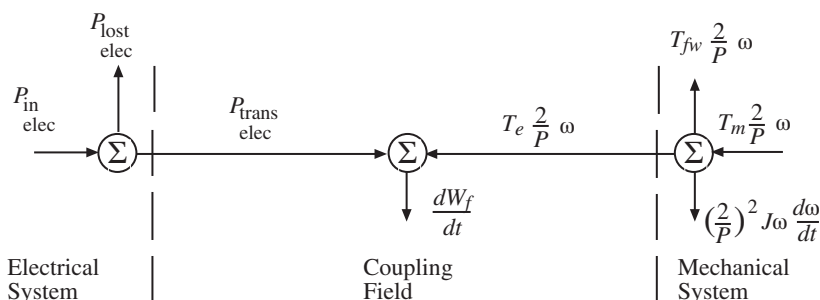


Figure 3.2 Synchronous machine power balance.

The electrical powers are

$$\begin{aligned} P_{\text{in}} &= v_a i_a + v_b i_b + v_c i_c + v_{fd} i_{fd} + v_{1d} i_{1d} + v_{1q} i_{1q} + v_{2q} i_{2q} \\ &\quad \text{elec} \end{aligned} \quad (3.26)$$

$$P_{\text{lost}} = r_s (i_a^2 + i_b^2 + i_c^2) + r_{fd} i_{fd}^2 + r_{1d} i_{1d}^2 + r_{1q} i_{1q}^2 + r_{2q} i_{2q}^2 \quad (3.27)$$

$$P_{\text{trans}} = i_a \frac{d\lambda_a}{dt} + i_b \frac{d\lambda_b}{dt} + i_c \frac{d\lambda_c}{dt} + i_{fd} \frac{d\lambda_{fd}}{dt} + i_{1d} \frac{d\lambda_{1d}}{dt} + i_{1q} \frac{d\lambda_{1q}}{dt} + i_{2q} \frac{d\lambda_{2q}}{dt}. \quad (3.28)$$

The summation of the electrical system is simply Kirchhoff's plus Faraday's laws, and the summation of the mechanical system is Newton's second law. In terms of the transformed variables, since

$$v_a i_a + v_b i_b + v_c i_c = \frac{3}{2} v_d i_d + \frac{3}{2} v_q i_q + 3 v_o i_o \quad (3.29)$$

$$\begin{aligned} P_{\text{in}} &= \frac{3}{2} v_d i_d + \frac{3}{2} v_q i_q + 3 v_o i_o + v_{fd} i_{fd} + v_{1d} i_{1d} + v_{1q} i_{1q} + v_{2q} i_{2q} \\ &\quad \text{elec} \end{aligned} \quad (3.30)$$

$$P_{\text{lost}} = \frac{3}{2} r_s i_d^2 + \frac{3}{2} r_s i_q^2 + 3 r_s i_o^2 + r_{fd} i_{fd}^2 + r_{1d} i_{1d}^2 + r_{1q} i_{1q}^2 + r_{2q} i_{2q}^2 \quad (3.31)$$

$$\begin{aligned} P_{\text{trans}} &= -\frac{3}{2} \frac{P}{2} \frac{d\theta_{\text{shaft}}}{dt} \lambda_q i_d + \frac{3}{2} \frac{P}{2} \frac{d\theta_{\text{shaft}}}{dt} \lambda_d i_q \\ &\quad + \frac{3}{2} i_d \frac{d\lambda_d}{dt} + \frac{3}{2} i_q \frac{d\lambda_q}{dt} + 3 i_o \frac{d\lambda_o}{dt} \\ &\quad + i_{fd} \frac{d\lambda_{fd}}{dt} + i_{1d} \frac{d\lambda_{1d}}{dt} + i_{1q} \frac{d\lambda_{1q}}{dt} + i_{2q} \frac{d\lambda_{2q}}{dt}. \end{aligned} \quad (3.32)$$

The power balance equation in the coupling field in these *dqo* coordinates gives the time derivative of the energy stored in the coupling field as

$$\begin{aligned} \frac{dW_f}{dt} &= \left[\frac{3}{2} \frac{P}{2} (\lambda_d i_q - \lambda_q i_d) + T_e \right] \frac{d\theta_{\text{shaft}}}{dt} + \frac{3}{2} i_d \frac{d\lambda_d}{dt} + \frac{3}{2} i_q \frac{d\lambda_q}{dt} + 3 i_o \frac{d\lambda_o}{dt} \\ &\quad + i_{fd} \frac{d\lambda_{fd}}{dt} + i_{1d} \frac{d\lambda_{1d}}{dt} + i_{1q} \frac{d\lambda_{1q}}{dt} + i_{2q} \frac{d\lambda_{2q}}{dt}. \end{aligned} \quad (3.33)$$

For independent states $\theta_{\text{shaft}}, \lambda_d, \lambda_q, \lambda_o, \lambda_{fd}, \lambda_{1d}, \lambda_{1q}, \lambda_{2q}$ the total derivative of W_f is

$$\begin{aligned} \frac{dW_f}{dt} &= \frac{\partial W_f}{\partial \theta_{\text{shaft}}} \frac{d\theta_{\text{shaft}}}{dt} + \frac{\partial W_f}{\partial \lambda_d} \frac{d\lambda_d}{dt} + \frac{\partial W_f}{\partial \lambda_q} \frac{d\lambda_q}{dt} + \frac{\partial W_f}{\partial \lambda_o} \frac{d\lambda_o}{dt} + \frac{\partial W_f}{\partial \lambda_{fd}} \frac{d\lambda_{fd}}{dt} \\ &\quad + \frac{\partial W_f}{\partial \lambda_{1d}} \frac{d\lambda_{1d}}{dt} + \frac{\partial W_f}{\partial \lambda_{1q}} \frac{d\lambda_{1q}}{dt} + \frac{\partial W_f}{\partial \lambda_{2q}} \frac{d\lambda_{2q}}{dt}. \end{aligned} \quad (3.34)$$

For this total derivative to be exact [32], the following identities must hold:

$$\frac{\partial W_f}{\partial \theta_{\text{shaft}}} = \frac{3}{2} \frac{P}{2} (\lambda_d i_q - \lambda_q i_d) + T_e, \quad \frac{\partial W_f}{\partial \lambda_d} = \frac{3}{2} i_d \quad \text{etc.} \quad (3.35)$$

With appropriate continuity assumptions [33], the coupling field energy can be obtained from (3.33) as a path integral

$$\begin{aligned} W_f = W_f^o + \int \left[\frac{3}{2} \frac{P}{2} (\lambda_d i_q - \lambda_q i_d) + T_e \right] d\theta_{\text{shaft}} + \int \frac{3}{2} i_d d\lambda_d \\ + \int \frac{3}{2} i_q d\lambda_q + \int 3 i_o d\lambda_o + \int i_{fd} d\lambda_{fd} + \int i_{1d} d\lambda_{1d} \\ + \int i_{1q} d\lambda_{1q} + \int i_{2q} d\lambda_{2q}. \end{aligned} \quad (3.36)$$

For this integral to be path independent, the partial derivatives of all integrands with respect to other states must be equal [34], i.e.,

$$\frac{3}{2} \frac{\partial i_d}{\partial \lambda_{fd}} = \frac{\partial i_{fd}}{\partial \lambda_d} \quad \text{etc.} \quad (3.37)$$

These constraints can also be obtained from those of (3.35) by taking the second partials of W_f with respect to states. The assumption that the coupling field is conservative is sufficient to guarantee that these constraints are satisfied. Nevertheless, these constraints should always be kept in mind when deriving the magnetic circuit relationships between flux linkage and current.

Assuming that these constraints are satisfied, the following arbitrary path is chosen from the de-energized ($W_f^o = 0$) condition to the energized condition:

1. Integrate rotor position to some arbitrary θ_{shaft} while all sources are de-energized.
This adds zero to W_f since λ_d, λ_q , and T_e must be zero.
2. Integrate each source in sequence while maintaining θ_{shaft} at its arbitrary position.

With this chosen path, W_f will be the sum of seven integrals for the seven independent sources $\lambda_d, \lambda_q, \lambda_o, \lambda_{fd}, \lambda_{1d}, \lambda_{1q}, \lambda_{2q}$. Each integrand is the respective source current that must be given as a function of the states. Since this is not done until later sections, we make the following assumption. Assume that the relationships between $\lambda_d, \lambda_q, \lambda_o, \lambda_{fd}, \lambda_{1d}, \lambda_{1q}, \lambda_{2q}$ and $i_d, i_q, i_o, i_{fd}, i_{1d}, i_{1q}, i_{2q}$ are independent of θ_{shaft} . For this assumption, W_f will be independent of θ_{shaft} so that, from (3.35),

$$T_e = - \left(\frac{3}{2} \right) \left(\frac{P}{2} \right) (\lambda_d i_q - \lambda_q i_d). \quad (3.38)$$

To complete the dynamic model in the transformed variables, it is desirable to define an angle that is constant for constant shaft speed. We define this angle as follows:

$$\delta \stackrel{\Delta}{=} \frac{P}{2} \theta_{\text{shaft}} - \omega_s t \quad (3.39)$$

where ω_s is a constant normally called rated synchronous speed in electrical radians per second, giving

$$\frac{d\delta}{dt} = \omega - \omega_s. \quad (3.40)$$

The final unscaled model in the new variables is

$$\frac{d\lambda_d}{dt} = -r_s i_d + \omega \lambda_q + v_d \quad (3.41)$$

$$\frac{d\lambda_q}{dt} = -r_s i_q - \omega \lambda_d + v_q \quad (3.42)$$

$$\frac{d\lambda_o}{dt} = -r_s i_o + v_o \quad (3.43)$$

$$\frac{d\lambda_{fd}}{dt} = -r_{fd} i_{fd} + v_{fd} \quad (3.44)$$

$$\frac{d\lambda_{1d}}{dt} = -r_{1d} i_{1d} + v_{1d} \quad (3.45)$$

$$\frac{d\lambda_{1q}}{dt} = -r_{1q} i_{1q} + v_{1q} \quad (3.46)$$

$$\frac{d\lambda_{2q}}{dt} = -r_{2q} i_{2q} + v_{2q} \quad (3.47)$$

$$\frac{d\delta}{dt} = \omega - \omega_s \quad (3.48)$$

$$J \frac{2}{p} \frac{d\omega}{dt} = T_m + \left(\frac{3}{2} \right) \left(\frac{P}{2} \right) (\lambda_d i_q - \lambda_q i_d) - T_{fw}. \quad (3.49)$$

It is customary to scale the synchronous machine equations using the traditional concept of per-unit [28, 29]. This scaling process is presented here as a change of variables and a change of parameters. We begin by defining new *abc* variables as

$$\begin{aligned} V_a &\stackrel{\Delta}{=} \frac{v_a}{V_{BABC}}, & V_b &\stackrel{\Delta}{=} \frac{v_b}{V_{BABC}}, & V_c &\stackrel{\Delta}{=} \frac{v_c}{V_{BABC}}, \\ I_a &\stackrel{\Delta}{=} \frac{-i_a}{I_{BABC}}, & I_b &\stackrel{\Delta}{=} \frac{-i_b}{I_{BABC}}, & I_c &\stackrel{\Delta}{=} \frac{-i_c}{I_{BABC}}, \\ \psi_a &\stackrel{\Delta}{=} \frac{\lambda_a}{\lambda_{BABC}}, & \psi_b &\stackrel{\Delta}{=} \frac{\lambda_b}{\lambda_{BABC}}, & \psi_c &\stackrel{\Delta}{=} \frac{\lambda_c}{\lambda_{BABC}} \end{aligned} \quad (3.50)$$

where V_{BABC} is a rated RMS line to neutral stator voltage and

$$I_{BABC} \stackrel{\Delta}{=} \frac{S_B}{3V_{BABC}}, \quad \lambda_{BABC} \stackrel{\Delta}{=} \frac{V_{BABC}}{\omega_B} \quad (3.51)$$

with S_B equal to the rated three-phase voltamperes and ω_B equal to rated speed in electrical radians per second (ω_s). This scaling also converts the model to “generator” notation. The new *dqo* variables are defined as

$$\begin{aligned} V_d &\stackrel{\Delta}{=} \frac{v_d}{V_{BDQ}}, & V_q &\stackrel{\Delta}{=} \frac{v_q}{V_{BDQ}}, & V_o &\stackrel{\Delta}{=} \frac{v_o}{V_{BDQ}}, \\ I_d &\stackrel{\Delta}{=} \frac{-i_d}{I_{BDQ}}, & I_q &\stackrel{\Delta}{=} \frac{-i_q}{I_{BDQ}}, & I_o &\stackrel{\Delta}{=} \frac{-i_o}{I_{BDQ}}, \\ \psi_d &\stackrel{\Delta}{=} \frac{\lambda_d}{\lambda_{BDQ}}, & \psi_q &\stackrel{\Delta}{=} \frac{\lambda_q}{\lambda_{BDQ}}, & \psi_o &\stackrel{\Delta}{=} \frac{\lambda_o}{\lambda_{BDQ}} \end{aligned} \quad (3.52)$$

where V_{BDQ} is rated peak line to neutral voltage, and

$$I_{BDQ} \stackrel{\Delta}{=} \frac{2S_B}{3V_{BDQ}}, \quad \lambda_{BDQ} \stackrel{\Delta}{=} \frac{V_{BDQ}}{\omega_B} \quad (3.53)$$

with S_B and ω_B defined as above, and again the scaling has converted to generator notation. The new rotor variables are defined as

$$\begin{aligned} V_{fd} &\stackrel{\Delta}{=} \frac{v_{fd}}{V_{BFD}}, & V_{1d} &\stackrel{\Delta}{=} \frac{v_{1d}}{V_{B1D}}, & V_{1q} &\stackrel{\Delta}{=} \frac{v_{1q}}{V_{B1Q}}, & V_{2q} &\stackrel{\Delta}{=} \frac{v_{2q}}{V_{B2Q}}, \\ I_{fd} &\stackrel{\Delta}{=} \frac{i_{fd}}{I_{BFD}}, & I_{1d} &\stackrel{\Delta}{=} \frac{i_{1d}}{I_{B1D}}, & I_{1q} &\stackrel{\Delta}{=} \frac{i_{1q}}{I_{B1Q}}, & I_{2q} &\stackrel{\Delta}{=} \frac{i_{2q}}{I_{B2Q}}, \\ \psi_{fd} &\stackrel{\Delta}{=} \frac{\lambda_{fd}}{\lambda_{BFD}}, & \psi_{1d} &\stackrel{\Delta}{=} \frac{\lambda_{1d}}{\lambda_{B1D}}, & \psi_{1q} &\stackrel{\Delta}{=} \frac{\lambda_{1q}}{\lambda_{B1Q}}, & \psi_{2q} &\stackrel{\Delta}{=} \frac{\lambda_{2q}}{\lambda_{B2Q}} \end{aligned} \quad (3.54)$$

where the rotor circuit base voltages are

$$V_{BFD} \stackrel{\Delta}{=} \frac{S_B}{I_{BFD}}, \quad V_{B1D} \stackrel{\Delta}{=} \frac{S_B}{I_{B1D}}, \quad V_{B1Q} \stackrel{\Delta}{=} \frac{S_B}{I_{B1Q}}, \quad V_{B2Q} \stackrel{\Delta}{=} \frac{S_B}{I_{B2Q}} \quad (3.55)$$

and the rotor circuit base flux linkages are

$$\lambda_{BFD} \stackrel{\Delta}{=} \frac{V_{BFD}}{\omega_B}, \quad \lambda_{B1D} \stackrel{\Delta}{=} \frac{V_{B1D}}{\omega_B}, \quad \lambda_{B1Q} \stackrel{\Delta}{=} \frac{V_{B1Q}}{\omega_B}, \quad \lambda_{B2Q} \stackrel{\Delta}{=} \frac{V_{B2Q}}{\omega_B} \quad (3.56)$$

with S_B and ω_B defined as above. The definitions of the rotor circuit base currents will be given later, when the flux linkage/current relationships are presented. In some models, it is convenient to define a scaled per-unit speed as

$$\nu \stackrel{\Delta}{=} \frac{\omega}{\omega_B} \quad (3.57)$$

where ω_B is as defined above.

This completes the scaling of the model variables. The model parameters are scaled as follows. Define new resistances

$$\begin{aligned} R_s &\stackrel{\Delta}{=} \frac{r_s}{Z_{BDQ}}, & R_{fd} &\stackrel{\Delta}{=} \frac{r_{fd}}{Z_{BFD}}, & R_{1d} &\stackrel{\Delta}{=} \frac{r_{1d}}{Z_{B1D}}, \\ R_{1q} &\stackrel{\Delta}{=} \frac{r_{1q}}{Z_{B1Q}}, & R_{2q} &\stackrel{\Delta}{=} \frac{r_{2q}}{Z_{B2Q}} \end{aligned} \quad (3.58)$$

where

$$\begin{aligned} Z_{BDQ} &\stackrel{\Delta}{=} \frac{V_{BDQ}}{I_{BDQ}}, & Z_{BFD} &\stackrel{\Delta}{=} \frac{V_{BFD}}{I_{BFD}}, & Z_{B1D} &\stackrel{\Delta}{=} \frac{V_{B1D}}{I_{B1D}}, \\ Z_{B1Q} &\stackrel{\Delta}{=} \frac{V_{B1Q}}{I_{B1Q}}, & Z_{B2Q} &\stackrel{\Delta}{=} \frac{V_{B2Q}}{I_{B2Q}}. \end{aligned} \quad (3.59)$$

The shaft inertia constant is scaled by defining

$$H \stackrel{\Delta}{=} \frac{\frac{1}{2}J \left(\omega_B \frac{2}{P} \right)^2}{S_B} \quad (3.60)$$

It is also common to define other inertia constants as

$$M \stackrel{\Delta}{=} \frac{2H}{\omega_s}, \quad M' \stackrel{\Delta}{=} 2H \quad (3.61)$$

where the constants H and M' have the units of seconds, while M has the units of seconds squared. The shaft torques are scaled by defining

$$T_M \stackrel{\Delta}{=} \frac{T_m}{T_B}, \quad T_{ELEC} \stackrel{\Delta}{=} \frac{T_e}{T_B}, \quad T_{FW} \stackrel{\Delta}{=} \frac{T_{fw}}{T_B} \quad (3.62)$$

where

$$T_B \stackrel{\Delta}{=} \frac{S_B}{\omega_B^2 P}. \quad (3.63)$$

Using these scaled variables and parameters, the synchronous machine dynamic equations at this stage of development with $\omega_B = \omega_s$ are

$$\frac{1}{\omega_s} \frac{d\psi_d}{dt} = R_s I_d + \frac{\omega}{\omega_s} \psi_q + V_d \quad (3.64)$$

$$\frac{1}{\omega_s} \frac{d\psi_q}{dt} = R_s I_q - \frac{\omega}{\omega_s} \psi_d + V_q \quad (3.65)$$

$$\frac{1}{\omega_s} \frac{d\psi_o}{dt} = R_s I_o + V_o \quad (3.66)$$

$$\frac{1}{\omega_s} \frac{d\psi_{fd}}{dt} = -R_{fd} I_{fd} + V_{fd} \quad (3.67)$$

$$\frac{1}{\omega_s} \frac{d\psi_{1d}}{dt} = -R_{1d} I_{1d} + V_{1d} \quad (3.68)$$

$$\frac{1}{\omega_s} \frac{d\psi_{1q}}{dt} = -R_{1q} I_{1q} + V_{1q} \quad (3.69)$$

$$\frac{1}{\omega_s} \frac{d\psi_{2q}}{dt} = -R_{2q} I_{2q} + V_{2q} \quad (3.70)$$

$$\frac{d\delta}{dt} = \omega - \omega_s \quad (3.71)$$

$$\frac{2H}{\omega_s} \frac{d\omega}{dt} = T_M - (\psi_d I_q - \psi_q I_d) - T_{FW}. \quad (3.72)$$

It is important to pause at this point to consider the scaling of variables. Consider a balanced set of scaled sinusoidal voltages and currents of the form:

$$V_a = \sqrt{2} V_s \cos(\omega_s t + \theta_s) \quad (3.73)$$

$$V_b = \sqrt{2} V_s \cos\left(\omega_s t + \theta_s - \frac{2\pi}{3}\right) \quad (3.74)$$

$$V_c = \sqrt{2} V_s \cos\left(\omega_s t + \theta_s + \frac{2\pi}{3}\right) \quad (3.75)$$

$$I_a = \sqrt{2} I_s \cos(\omega_s t + \phi_s) \quad (3.76)$$

$$I_b = \sqrt{2}I_s \cos\left(\omega_s t + \phi_s - \frac{2\pi}{3}\right) \quad (3.77)$$

$$I_c = \sqrt{2}I_s \cos\left(\omega_s t + \phi_s + \frac{2\pi}{3}\right). \quad (3.78)$$

Using the transformation (3.13),

$$V_d = \left(\frac{\sqrt{2}V_s V_{BABC}}{V_{BDQ}} \right) \sin\left(\frac{P}{2}\theta_{\text{shaft}} - \omega_s t - \theta_s\right) \quad (3.79)$$

$$V_q = \left(\frac{\sqrt{2}V_s V_{BABC}}{V_{BDQ}} \right) \cos\left(\frac{P}{2}\theta_{\text{shaft}} - \omega_s t - \theta_s\right) \quad (3.80)$$

$$V_o = 0 \quad (3.81)$$

$$I_d = \left(\frac{\sqrt{2}I_s I_{BABC}}{I_{BDQ}} \right) \sin\left(\frac{P}{2}\theta_{\text{shaft}} - \omega_s t - \phi_s\right) \quad (3.82)$$

$$I_q = \left(\frac{\sqrt{2}I_s I_{BABC}}{I_{BDQ}} \right) \cos\left(\frac{P}{2}\theta_{\text{shaft}} - \omega_s t - \phi_s\right) \quad (3.83)$$

$$I_o = 0. \quad (3.84)$$

By the definitions of V_{BABC} , V_{BDQ} , I_{BABC} , and I_{BDQ} ,

$$\frac{\sqrt{2}V_s V_{BABC}}{V_{BDQ}} = V_s, \quad \frac{\sqrt{2}I_s I_{BABC}}{I_{BDQ}} = I_s. \quad (3.85)$$

Using the definition of δ from (3.39),

$$V_d = V_s \sin(\delta - \theta_s) \quad (3.86)$$

$$V_q = V_s \cos(\delta - \theta_s) \quad (3.87)$$

$$I_d = I_s \sin(\delta - \phi_s) \quad (3.88)$$

$$I_q = I_s \cos(\delta - \phi_s). \quad (3.89)$$

These algebraic equations can be written as complex equations

$$(V_d + jV_q)e^{j(\delta - \pi/2)} = V_s e^{j\theta_s} \quad (3.90)$$

$$(I_d + jI_q)e^{j(\delta - \pi/2)} = I_s e^{j\phi_s}. \quad (3.91)$$

These are recognized as the per-unit RMS phasors of (3.73) and (3.76).

It is also important, at this point, to note that the model of (3.64)–(3.72) was derived using essentially four general assumptions. These assumptions are summarized as follows.

1. Stator has three coils in a balanced symmetrical configuration centered 120 electrical degrees apart.
2. Rotor has four coils in a balanced symmetrical configuration located in pairs 90 electrical degrees apart.
3. The relationship between the flux linkages and currents must reflect a conservative coupling field.

4. The relationships between the flux linkages and currents must be independent of θ_{shaft} when expressed in the dqo coordinate system.

The following sections give the flux linkage/current relationships that satisfy these four assumptions and thus complete the dynamic model.

3.4 The Linear Magnetic Circuit

This section presents the special case in which the machine flux linkages are assumed to be linear functions of currents:

$$\lambda_{abc} = L_{ss}(\theta_{\text{shaft}})i_{abc} + L_{sr}(\theta_{\text{shaft}})i_{\text{rotor}} \quad (3.92)$$

$$\lambda_{\text{rotor}} = L_{rs}(\theta_{\text{shaft}})i_{abc} + L_{rr}(\theta_{\text{shaft}})i_{\text{rotor}} \quad (3.93)$$

where

$$i_{\text{rotor}} \stackrel{\Delta}{=} [i_{fd} i_{1d} i_{1q} i_{2q}]^t, \quad \lambda_{\text{rotor}} \stackrel{\Delta}{=} [\lambda_{fd} \lambda_{1d} \lambda_{1q} \lambda_{2q}]^t. \quad (3.94)$$

If space harmonics are neglected, the entries of these inductance matrices can be written in a form that satisfies assumptions (3) and (4) of the last section. Reference [20] discusses this formulation and gives the following standard first approximation of the inductances for a P -pole machine.

$$L_{ss}(\theta_{\text{shaft}}) \stackrel{\Delta}{=} \begin{bmatrix} L_{\ell s} + L_A - L_B \cos P\theta_{\text{shaft}} & -\frac{1}{2}L_A - L_B \cos \left(P\theta_{\text{shaft}} - \frac{2\pi}{3}\right) \\ -\frac{1}{2}L_A - L_B \cos \left(P\theta_{\text{shaft}} - \frac{2\pi}{3}\right) & L_{\ell s} + L_A - L_B \cos \left(P\theta_{\text{shaft}} + \frac{2\pi}{3}\right) \\ -\frac{1}{2}L_A - L_B \cos \left(P\theta_{\text{shaft}} + \frac{2\pi}{3}\right) & -\frac{1}{2}L_A - L_B \cos P\theta_{\text{shaft}} \\ -\frac{1}{2}L_A - L_B \cos \left(P\theta_{\text{shaft}} + \frac{2\pi}{3}\right) & -\frac{1}{2}L_A - L_B \cos P\theta_{\text{shaft}} \\ L_{\ell s} + L_A - L_B \cos \left(P\theta_{\text{shaft}} - \frac{2\pi}{3}\right) \end{bmatrix} \quad (3.95)$$

$$L_{sr}(\theta_{\text{shaft}}) = L_{rs}^t(\theta_{\text{shaft}}) \stackrel{\Delta}{=} \begin{bmatrix} L_{sfld} \sin \frac{P}{2}\theta_{\text{shaft}} & L_{s1d} \sin \frac{P}{2}\theta_{\text{shaft}} \\ L_{sfld} \sin \left(\frac{P}{2}\theta_{\text{shaft}} - \frac{2\pi}{3}\right) & L_{s1d} \sin \left(\frac{P}{2}\theta_{\text{shaft}} - \frac{2\pi}{3}\right) \\ L_{sfld} \sin \left(\frac{P}{2}\theta_{\text{shaft}} + \frac{2\pi}{3}\right) & L_{s1d} \sin \left(\frac{P}{2}\theta_{\text{shaft}} + \frac{2\pi}{3}\right) \\ L_{s1q} \cos \frac{P}{2}\theta_{\text{shaft}} & L_{s2q} \cos \frac{P}{2}\theta_{\text{shaft}} \\ L_{s1q} \cos \left(\frac{P}{2}\theta_{\text{shaft}} - \frac{2\pi}{3}\right) & L_{s2q} \cos \left(\frac{P}{2}\theta_{\text{shaft}} - \frac{2\pi}{3}\right) \\ L_{s1q} \cos \left(\frac{P}{2}\theta_{\text{shaft}} + \frac{2\pi}{3}\right) & L_{s2q} \cos \left(\frac{P}{2}\theta_{\text{shaft}} + \frac{2\pi}{3}\right) \end{bmatrix} \quad (3.96)$$

$$L_{rr}(\theta_{\text{shaft}}) \stackrel{\Delta}{=} \begin{bmatrix} L_{fd fd} & L_{fd 1d} & 0 & 0 \\ L_{fd 1d} & L_{1d 1d} & 0 & 0 \\ 0 & 0 & L_{1q 1q} & L_{1q 2q} \\ 0 & 0 & L_{1q 2q} & L_{2q 2q} \end{bmatrix} \quad (3.97)$$

The rotor self-inductance matrix $L_{rr}(\theta_{\text{shaft}})$ is independent of θ_{shaft} . Using the transformation of (3.10),

$$\lambda_d = (L_{\ell s} + L_{md})i_d + L_{sf d}i_{fd} + L_{s1d}i_{1d} \quad (3.98)$$

$$\lambda_{fd} = \frac{3}{2}L_{sf d}i_d + L_{fd fd}i_{fd} + L_{fd 1d}i_{1d} \quad (3.99)$$

$$\lambda_{1d} = \frac{3}{2}L_{s1d}i_d + L_{fd 1d}i_{fd} + L_{1d 1d}i_{1d} \quad (3.100)$$

and

$$\lambda_q = (L_{\ell s} + L_{mq})i_q + L_{s1q}i_{1q} + L_{s2q}i_{2q} \quad (3.101)$$

$$\lambda_{1q} = \frac{3}{2}L_{s1q}i_q + L_{1q 1q}i_{1q} + L_{1q 2q}i_{2q} \quad (3.102)$$

$$\lambda_{2q} = \frac{3}{2}L_{s2q}i_q + L_{1q 2q}i_{1q} + L_{2q 2q}i_{2q} \quad (3.103)$$

and

$$\lambda_o = L_{\ell s}i_o \quad (3.104)$$

where

$$L_{md} \stackrel{\Delta}{=} \frac{3}{2}(L_A + L_B), \quad L_{mq} \stackrel{\Delta}{=} \frac{3}{2}(L_A - L_B). \quad (3.105)$$

This set of flux linkage/current relationships does reflect a conservative coupling field, since the original matrices of (3.95)–(3.97) are symmetric, and the partial derivatives of (3.37) are satisfied by (3.98)–(3.104). This can be easily verified using Cramer's rule to find entries of the inverses of the inductance matrices.

In terms of the scaled quantities of the last section,

$$\psi_d = \frac{\omega_s(L_{\ell s} + L_{md})(-I_d I_{BDQ})}{V_{BDQ}} + \frac{\omega_s L_{sf d} I_{fd} I_{BFD}}{V_{BDQ}} + \frac{\omega_s L_{s1d} I_{1d} I_{B1D}}{V_{BDQ}} \quad (3.106)$$

$$\psi_{fd} = \frac{\omega_s \frac{3}{2}L_{sf d}(-I_d I_{BDQ})}{V_{BFD}} + \frac{\omega_s L_{fd fd} I_{fd} I_{BFD}}{V_{BFD}} + \frac{\omega_s L_{fd 1d} I_{1d} I_{B1D}}{V_{BFD}} \quad (3.107)$$

$$\psi_{1d} = \frac{\omega_s \frac{3}{2}L_{s1d}(-I_d I_{BDQ})}{V_{B1D}} + \frac{\omega_s L_{fd 1d} I_{fd} I_{BFD}}{V_{B1D}} + \frac{\omega_s L_{1d 1d} I_{1d} I_{B1D}}{V_{B1D}} \quad (3.108)$$

$$\psi_q = \frac{\omega_s(L_{\ell s} + L_{mq})(-I_q I_{BDQ})}{V_{BDQ}} + \frac{\omega_s L_{s1q} I_{1q} I_{B1Q}}{V_{BDQ}} + \frac{\omega_s L_{s2q} I_{2q} I_{B2Q}}{V_{BDQ}} \quad (3.109)$$

$$\psi_{1q} = \frac{\omega_s \frac{3}{2}L_{s1q}(-I_q I_{BDQ})}{V_{B1Q}} + \frac{\omega_s L_{1q 1q} I_{1q} I_{B1Q}}{V_{B1Q}} + \frac{\omega_s L_{1q 2q} I_{2q} I_{B2Q}}{V_{B1Q}} \quad (3.110)$$

$$\psi_{2q} = \frac{\omega_s \frac{3}{2} L_{s2q} (-I_q I_{BDQ})}{V_{B2Q}} + \frac{\omega_s L_{1q2q} I_{1q} I_{B1Q}}{V_{B2Q}} + \frac{\omega_s L_{2q2q} I_{2q} I_{B2Q}}{V_{B2Q}} \quad (3.111)$$

$$\psi_o = \frac{\omega_s L_{\ell s} (-I_o I_{BDQ})}{V_{BDQ}}. \quad (3.112)$$

Although the values of I_{BFD} , I_{B1D} , I_{B1Q} , I_{B2Q} have not yet been specified, their relationship to their respective voltage bases assures that the scaled transformed system (3.106)–(3.112) is reciprocal (symmetric inductance matrices). The rotor current bases are chosen at this point to make as many off-diagonal terms equal as possible. To do this, define

$$I_{BFD} \stackrel{\Delta}{=} \frac{L_{md}}{L_{sfld}} I_{BDQ}, \quad I_{B1D} \stackrel{\Delta}{=} \frac{L_{md}}{L_{s1d}} I_{BDQ} \quad (3.113)$$

$$I_{B1Q} \stackrel{\Delta}{=} \frac{L_{mq}}{L_{s1q}} I_{BDQ}, \quad I_{B2Q} \stackrel{\Delta}{=} \frac{L_{mq}}{L_{s2q}} I_{BDQ} \quad (3.114)$$

and the following scaled parameters:

$$X_{\ell s} \stackrel{\Delta}{=} \frac{\omega_s L_{\ell s}}{Z_{BDQ}}, \quad X_{md} \stackrel{\Delta}{=} \frac{\omega_s L_{md}}{Z_{BDQ}}, \quad X_{mq} \stackrel{\Delta}{=} \frac{\omega_s L_{mq}}{Z_{BDQ}} \quad (3.115)$$

$$X_{fd} \stackrel{\Delta}{=} \frac{\omega_s L_{fd} I_{fd}}{Z_{BFD}}, \quad X_{1d} \stackrel{\Delta}{=} \frac{\omega_s L_{1d} I_{1d}}{Z_{B1D}}, \quad X_{fd1d} \stackrel{\Delta}{=} \frac{\omega_s L_{fd} I_{fd} L_{sfld}}{Z_{BFD} L_{s1d}} \quad (3.116)$$

$$X_{1q} \stackrel{\Delta}{=} \frac{\omega_s L_{1q} I_{1q}}{Z_{B1Q}}, \quad X_{2q} \stackrel{\Delta}{=} \frac{\omega_s L_{2q} I_{2q}}{Z_{B2Q}}, \quad X_{1q2q} \stackrel{\Delta}{=} \frac{\omega_s L_{1q} I_{1q} L_{s1q}}{Z_{B1Q} L_{s2q}}. \quad (3.117)$$

It is convenient also to define the scaled leakage reactances of the rotor windings as

$$X_{\ell fd} \stackrel{\Delta}{=} X_{fd} - X_{md}, \quad X_{\ell 1d} \stackrel{\Delta}{=} X_{1d} - X_{md} \quad (3.118)$$

$$X_{\ell 1q} \stackrel{\Delta}{=} X_{1q} - X_{mq}, \quad X_{\ell 2q} \stackrel{\Delta}{=} X_{2q} - X_{mq}. \quad (3.119)$$

Similarly, we also define

$$X_d \stackrel{\Delta}{=} X_{\ell s} + X_{md}, \quad X_q \stackrel{\Delta}{=} X_{\ell s} + X_{mq} \quad (3.120)$$

$$c_d \stackrel{\Delta}{=} \frac{X_{fd1d}}{X_{md}}, \quad c_q \stackrel{\Delta}{=} \frac{X_{1q2q}}{X_{mq}}. \quad (3.121)$$

The resulting scaled $\psi - I$ relationship is

$$\psi_d = X_d (-I_d) + X_{md} I_{fd} + X_{md} I_{1d} \quad (3.122)$$

$$\psi_{fd} = X_{md} (-I_d) + X_{fd} I_{fd} + c_d X_{md} I_{1d} \quad (3.123)$$

$$\psi_{1d} = X_{md} (-I_d) + c_d X_{md} I_{fd} + X_{1d} I_{1d} \quad (3.124)$$

and

$$\psi_q = X_q (-I_q) + X_{mq} I_{1q} + X_{mq} I_{2q} \quad (3.125)$$

$$\psi_{1q} = X_{mq} (-I_q) + X_{1q} I_{1q} + c_q X_{mq} I_{2q} \quad (3.126)$$

$$\psi_{2q} = X_{mq} (-I_q) + c_q X_{mq} I_{1q} + X_{2q} I_{2q} \quad (3.127)$$

and

$$\psi_o = X_{\ell s}(-I_o). \quad (3.128)$$

While several examples [30] have shown that the terms c_d and c_q are important in some simulations, it is customary to make the following simplification [20]:

$$c_d \approx 1, \quad c_q \approx 1. \quad (3.129)$$

This assumption makes all of the off-diagonal entries of the decoupled inductance matrices equal. An alternative way to obtain the same structure without the above simplification would require a different choice of scaling and different definitions of leakage reactances [30]: Using the previously defined parameters and the simplification (3.129), it is common to define the following parameters [20]

$$X'_d \stackrel{\Delta}{=} X_{\ell s} + \frac{1}{\frac{1}{X_{md}} + \frac{1}{X_{\ell fd}}} = X_{\ell s} + \frac{X_{md}X_{\ell fd}}{X_{fd}} = X_d - \frac{X_{md}^2}{X_{fd}} \quad (3.130)$$

$$X'_q \stackrel{\Delta}{=} X_{\ell s} + \frac{1}{\frac{1}{X_{mq}} + \frac{1}{X_{\ell 1q}}} = X_{\ell s} + \frac{X_{mq}X_{\ell 1q}}{X_{1q}} = X_q - \frac{X_{mq}^2}{X_{1q}} \quad (3.131)$$

$$X''_d \stackrel{\Delta}{=} X_{\ell s} + \frac{1}{\frac{1}{X_{md}} + \frac{1}{X_{\ell fd}} + \frac{1}{X_{\ell 1d}}} \quad (3.132)$$

$$X''_q \stackrel{\Delta}{=} X_{\ell s} + \frac{1}{\frac{1}{X_{mq}} + \frac{1}{X_{\ell 1q}} + \frac{1}{X_{\ell 2q}}} \quad (3.133)$$

$$T'_{do} \stackrel{\Delta}{=} \frac{X_{fd}}{\omega_s R_{fd}} \quad (3.134)$$

$$T'_{qo} \stackrel{\Delta}{=} \frac{X_{1q}}{\omega_s R_{1q}} \quad (3.135)$$

$$T''_{do} \stackrel{\Delta}{=} \frac{1}{\omega_s R_{1d}} \left(X_{\ell 1d} + \frac{1}{\frac{1}{X_{md}} + \frac{1}{X_{\ell fd}}} \right) \quad (3.136)$$

$$T''_{qo} \stackrel{\Delta}{=} \frac{1}{\omega_s R_{2q}} \left(X_{\ell 2q} + \frac{1}{\frac{1}{X_{mq}} + \frac{1}{X_{\ell 1q}}} \right) \quad (3.137)$$

and the following variables

$$E'_q \stackrel{\Delta}{=} \frac{X_{md}}{X_{fd}} \psi_{fd} \quad (3.138)$$

$$E_{fd} \stackrel{\Delta}{=} \frac{X_{md}}{R_{fd}} V_{fd} \quad (3.139)$$

$$E'_d \stackrel{\Delta}{=} -\frac{X_{mq}}{X_{1q}} \psi_{1q}. \quad (3.140)$$

Adkins [23] and several earlier references define X''_q as in (3.131) and T''_{qo} as in (3.135). This practice is based on the convention that single primes refer to the so-called “transient” period, while the double primes refer to the supposedly faster “subtransient” period. Thus, when a single damper winding is modeled on the rotor, this is interpreted as a “subtransient” effect and denoted as such with a double prime. Some published models use the notation of Young [35], which uses an E'_d definition that is the same as (3.140) but with a positive sign. In several publications, the terminology X_{fd} is used to define leakage reactance rather than self-reactance. The symbols X_{ad} and X_{aq} are common alternatives for the magnetizing reactances X_{md} and X_{mq} .

The dynamic model can contain at most only seven of the fourteen flux linkages and currents as independent state variables. The natural form of the state equations invites the elimination of currents by solving (3.122)–(3.128). Since the terminal constraints have not yet been specified, it is unwise to eliminate I_d , I_q , or I_o at this time. Since the terminal constraints do not affect I_{fd} , I_{1d} , I_{1q} , I_{2q} , these currents can be eliminated from the dynamic model now. This is done by rearranging (3.122)–(3.128) using the newly defined variables and parameters to obtain

$$\psi_d = -X''_d I_d + \frac{(X''_d - X'_{\ell s})}{(X'_d - X'_{\ell s})} E'_q + \frac{(X'_d - X''_d)}{(X'_d - X'_{\ell s})} \psi_{1d} \quad (3.141)$$

$$I_{fd} = \frac{1}{X_{md}} [E'_q + (X_d - X'_d)(I_d - I_{1d})] \quad (3.142)$$

$$I_{1d} = \frac{X'_d - X''_d}{(X'_d - X'_{\ell s})^2} [\psi_{1d} + (X'_d - X'_{\ell s}) I_d - E'_q] \quad (3.143)$$

and

$$\psi_q = -X''_q I_q - \frac{(X''_q - X'_{\ell s})}{(X'_q - X'_{\ell s})} E'_d + \frac{(X'_q - X''_q)}{(X'_q - X'_{\ell s})} \psi_{2q} \quad (3.144)$$

$$I_{1q} = \frac{1}{X_{mq}} [-E'_d + (X_q - X'_q)(I_q - I_{2q})] \quad (3.145)$$

$$I_{2q} = \frac{X'_q - X''_q}{(X'_q - X'_{\ell s})^2} [\psi_{2q} + (X'_q - X'_{\ell s}) I_q + E'_d] \quad (3.146)$$

and

$$\psi_o = -X'_{\ell s} I_o. \quad (3.147)$$

Substitution into (3.64)–(3.72) gives the dynamic model for a linear magnetic circuit with the terminal constraints (relationship between V_d , I_d , V_q , I_q , V_o , I_o) not yet specified. Since these terminal constraints are not specified, it is necessary to keep the three flux linkage/current algebraic equations involving I_d , I_q , and I_o . In addition, the variables E_{fd} , T_M , and T_{FW} are also as yet unspecified. It would be reasonable, if desired at this point, to make E_{fd} and T_M constant inputs, and T_{FW} equal to zero. We will continue to carry them along as variables. With these clarifications, the linear magnetic circuit model is shown in the following boxed set.

$$\frac{1}{\omega_s} \frac{d\psi_d}{dt} = R_s I_d + \frac{\omega}{\omega_s} \psi_q + V_d \quad (3.148)$$

$$\frac{1}{\omega_s} \frac{d\psi_q}{dt} = R_s I_q - \frac{\omega}{\omega_s} \psi_d + V_q \quad (3.149)$$

$$\frac{1}{\omega_s} \frac{d\psi_o}{dt} = R_s I_o + V_o \quad (3.150)$$

$$T'_{do} \frac{dE'_q}{dt} = -E'_q - (X_d - X'_d) \left[I_d - \frac{X'_d - X''_d}{(X'_d - X_{\ell s})^2} (\psi_{1d} \right. \\ \left. + (X'_d - X_{\ell s}) I_d - E'_q) \right] + E_{fd} \quad (3.151)$$

$$T''_{do} \frac{d\psi_{1d}}{dt} = -\psi_{1d} + E'_q - (X'_d - X_{\ell s}) I_d \quad (3.152)$$

$$T'_{qo} \frac{dE'_d}{dt} = -E'_d + (X_q - X'_q) \left[I_q - \frac{X'_q - X''_q}{(X'_q - X_{\ell s})^2} (\psi_{2q} \right. \\ \left. + (X'_q - X_{\ell s}) I_q + E'_d) \right] \quad (3.153)$$

$$T''_{qo} \frac{d\psi_{2q}}{dt} = -\psi_{2q} - E'_d - (X'_q - X_{\ell s}) I_q \quad (3.154)$$

$$\frac{d\delta}{dt} = \omega - \omega_s \quad (3.155)$$

$$\frac{2H}{\omega_s} \frac{d\omega}{dt} = T_M - (\psi_d I_q - \psi_q I_d) - T_{FW} \quad (3.156)$$

$$\psi_d = -X''_d I_d + \frac{(X''_d - X_{\ell s})}{(X'_d - X_{\ell s})} E'_q + \frac{(X'_d - X''_d)}{(X'_d - X_{\ell s})} \psi_{1d} \quad (3.157)$$

$$\psi_q = -X''_q I_q - \frac{(X''_q - X_{\ell s})}{(X'_q - X_{\ell s})} E'_d + \frac{(X'_q - X''_q)}{(X'_q - X_{\ell s})} \psi_{2q} \quad (3.158)$$

$$\psi_o = -X_{\ell s} I_o \quad (3.159)$$

Although there are time constants that appear on all of the flux linkage derivatives, the right-hand sides contain flux linkages multiplied by constants. Furthermore, the addition of the terminal constraints could add more terms when I_d , I_q , and I_o are eliminated. Thus, the time constants shown are not true time constants in the traditional sense,

where the respective states appear on the right-hand side multiplied only by - 1. It is also possible to define a mechanical time constant T_s as

$$T_s \stackrel{\Delta}{=} \sqrt{\frac{2H}{\omega_s}} \quad (3.160)$$

and a scaled transient speed as

$$\omega_t \stackrel{\Delta}{=} T_s(\omega - \omega_s) \quad (3.161)$$

to produce the following angle/speed state pair

$$T_s \frac{d\delta}{dt} = \omega_t \quad (3.162)$$

$$T_s \frac{d\omega_t}{dt} = T_M - (\psi_d I_q - \psi_q I_d) - T_{FW}. \quad (3.163)$$

While this will prove useful later, in the analysis of the time-scale properties of synchronous machines, the model normally will be used in the form of (3.148)–(3.159). This concludes the basic dynamic modeling of synchronous machines if saturation of the magnetic circuit is not considered. The next section presents a fairly general method for including such nonlinearities in the flux linkage/current relationships.

3.5 The Nonlinear Magnetic Circuit

In this section, we propose a fairly generalized treatment of nonlinearities in the magnetic circuit. The generalization is motivated by the multitude of various representations of saturation that have appeared in the literature. Virtually all methods proposed to date involve the addition of one or more nonlinear terms to the model of (3.148)–(3.159). The following treatment returns to the original *abc* variables so that any assumptions or added terms can be traced through the transformation and scaling processes of the last section. It is clear that, as in the last section, the flux linkage/current relationships must satisfy assumptions (3) and (4) at the end of Section 3.3 if the results here are to be valid for the general model of (3.64)–(3.72). Toward this end, we propose a flux linkage/current relationship of the following form:

$$\lambda_{abc} = L_{ss}(\theta_{\text{shaft}})i_{abc} + L_{sr}(\theta_{\text{shaft}})i_{\text{rotor}} - S_{abc}(i_{abc}, \lambda_{\text{rotor}}, \theta_{\text{shaft}}) \quad (3.164)$$

$$\lambda_{\text{rotor}} = L_{sr}^t(\theta_{\text{shaft}})i_{abc} + L_{rr}(\theta_{\text{shaft}})i_{\text{rotor}} - S_{\text{rotor}}(i_{abc}, \lambda_{\text{rotor}}, \theta_{\text{shaft}}) \quad (3.165)$$

where all quantities are as previously defined, and S_{abc} and S_{rotor} satisfy assumptions (3) and (4) at the end of Section 3.3. The choice of stator currents and rotor flux linkages for the nonlinearity dependence was made to allow comparison with traditional choices of functions. With these two assumptions, S_{abc} and S_{rotor} must be such that when (3.164) and (3.165) are transformed using (3.10), the following nonlinear flux linkage/current relationship is obtained

$$\lambda_d = (L_{\ell s} + L_{md})i_d + L_{sf d}i_{fd} + L_{s1d}i_{1d} - S_d(i_{dqo}, \lambda_{\text{rotor}}) \quad (3.166)$$

$$\lambda_{fd} = \frac{3}{2}L_{sf d}i_d + L_{fd}i_{fd} + L_{fd1d}i_{1d} - S_{fd}(i_{dqo}, \lambda_{\text{rotor}}) \quad (3.167)$$

$$\lambda_{1d} = \frac{3}{2}L_{s1d}i_d + L_{fd1d}i_{fd} + L_{1d1d}i_{1d} - S_{1d}(i_{dqo}, \lambda_{\text{rotor}}) \quad (3.168)$$

$$\lambda_q = (L_{\ell s} + L_{mq})i_q + L_{s1q}i_{1q} + L_{s2q}i_{2q} - S_q(i_{dqo}, \lambda_{\text{rotor}}) \quad (3.169)$$

$$\lambda_{1q} = \frac{3}{2}L_{s1q}i_q + L_{1q1q}i_{1q} + L_{1q2q}i_{2q} - S_{1q}(i_{dqo}, \lambda_{\text{rotor}}) \quad (3.170)$$

$$\lambda_{2q} = \frac{3}{2}L_{s2q}i_q + L_{1q2q}i_{1q} + L_{2q2q}i_{2q} - S_{2q}(i_{dqo}, \lambda_{\text{rotor}}) \quad (3.171)$$

and

$$\lambda_o = L_{\ell s}i_o - S_o(i_{dqo}, \lambda_{\text{rotor}}). \quad (3.172)$$

This system includes the possibility of coupling between all of the d , q , and o subsystems. Saturation functions that satisfy these two assumptions normally have a balanced symmetrical three-phase dependence on shaft position.

In terms of the scaled variables of the last two sections, and using (3.129) ($c_d = c_q = 1$),

$$\psi_d = X_d(-I_d) + X_{md}I_{fd} + X_{md}I_{1d} - S_d^{(1)}(Y_1) \quad (3.173)$$

$$\psi_{fd} = X_{md}(-I_d) + X_{fd}I_{fd} + X_{md}I_{1d} - S_{fd}^{(1)}(Y_1) \quad (3.174)$$

$$\psi_{1d} = X_{md}(-I_d) + X_{md}I_{fd} + X_{1d}I_{1d} - S_{1d}^{(1)}(Y_1) \quad (3.175)$$

and

$$\psi_q = X_q(-I_q) + X_{mq}I_{1q} + X_{mq}I_{2q} - S_q^{(1)}(Y_1) \quad (3.176)$$

$$\psi_{1q} = X_{mq}(-I_q) + X_{1q}I_{1q} + X_{mq}I_{2q} - S_{1q}^{(1)}(Y_1) \quad (3.177)$$

$$\psi_{2q} = X_{mq}(-I_q) + X_{mq}I_{1q} + X_{2q}I_{2q} - S_{2q}^{(1)}(Y_1) \quad (3.178)$$

and

$$\psi_o = X_{\ell s}(-I_o) - S_o^{(1)}(Y_1) \quad (3.179)$$

where

$$Y_1 \stackrel{\Delta}{=} [I_d \quad \psi_{fd} \quad \psi_{1d} \quad I_q \quad \psi_{1q} \quad \psi_{2q} \quad I_o]^t \quad (3.180)$$

$$S_d^{(1)} \stackrel{\Delta}{=} S_d/\Lambda_{BDQ}, \quad S_{fd}^{(1)} \stackrel{\Delta}{=} S_{fd}/\Lambda_{BFD}, \quad S_{1d}^{(1)} \stackrel{\Delta}{=} S_{1d}/\Lambda_{B1D}$$

$$S_q^{(1)} \stackrel{\Delta}{=} S_q/\Lambda_{BDQ}, \quad S_{1q}^{(1)} \stackrel{\Delta}{=} S_{1q}/\Lambda_{B1Q}, \quad S_{2q}^{(1)} \stackrel{\Delta}{=} S_{2q}/\Lambda_{B2Q}$$

$$S_o^{(1)} \stackrel{\Delta}{=} S_o/\Lambda_{BDQ} \quad (3.181)$$

with each S evaluated using λ_{dqo} , λ_{rotor} written as a function of Y_1 . Using new variables E'_d and E'_q , and rearranging so that rotor currents can be eliminated, gives

$$\psi_d = -X''_d I_d + \frac{(X''_d - X'_{\ell s})}{(X'_d - X'_{\ell s})} E'_q + \frac{(X'_d - X''_d)}{(X'_d - X'_{\ell s})} \psi_{1d} - S_d^{(2)}(Y_2) \quad (3.182)$$

$$I_{fd} = \frac{1}{X_{md}} \left[E'_q + (X_d - X'_d)(I_d - I_{1d}) + S_{fd}^{(2)}(Y_2) \right] \quad (3.183)$$

$$I_{1d} = \frac{X'_d - X''_d}{(X'_d - X'_{\ell s})^2} \left[\psi_{1d} + (X'_d - X'_{\ell s}) I_d - E'_q + S_{1d}^{(2)}(Y_2) \right] \quad (3.184)$$

and

$$\psi_q = -X''_q I_q - \frac{(X''_q - X'_{\ell s})}{(X'_q - X'_{\ell s})} E'_d + \frac{(X'_q - X''_q)}{(X'_q - X'_{\ell s})} \psi_{2q} - S_q^{(2)}(Y_2) \quad (3.185)$$

$$I_{1q} = \frac{1}{X_{mq}} \left[-E'_d + (X_q - X'_q)(I_q - I_{2q}) + S_{1q}^{(2)}(Y_2) \right] \quad (3.186)$$

$$I_{2q} = \frac{X'_q - X''_q}{(X'_q - X'_{\ell s})^2} \left[\psi_{2q} + (X'_q - X'_{\ell s}) I_q + E'_d + S_{2q}^{(2)}(Y_2) \right] \quad (3.187)$$

and

$$\psi_o = -X'_{\ell s} I_o - S_o^{(2)}(Y_2) \quad (3.188)$$

where

$$Y_2 \stackrel{\Delta}{=} [I_d \quad E'_q \quad \psi_{1d} \quad I_q \quad E'_d \quad \psi_{2q} \quad I_o]^t \quad (3.189)$$

and

$$\begin{aligned} S_d^{(2)} &\stackrel{\Delta}{=} S_d^{(1)} - S_{fd}^{(2)} - \frac{(X'_d - X''_d)}{(X'_d - X'_{\ell s})} S_{1d}^{(2)}, \\ S_{fd}^{(2)} &\stackrel{\Delta}{=} \frac{X_{md}}{X_{fd}} S_{fd}^{(1)}, \quad S_{1d}^{(2)} \stackrel{\Delta}{=} S_{1d}^{(1)} - S_{fd}^{(2)}, \\ S_q^{(2)} &\stackrel{\Delta}{=} S_q^{(1)} - S_{1q}^{(2)} - \frac{(X'_q - X''_q)}{(X'_q - X'_{\ell s})} S_{2q}^{(2)}, \\ S_{1q}^{(2)} &\stackrel{\Delta}{=} \frac{X_{mq}}{X_{1q}} S_{1q}^{(1)}, \quad S_{2q}^{(2)} \stackrel{\Delta}{=} S_{2q}^{(1)} - S_{1q}^{(2)}, \\ S_o^{(2)} &\stackrel{\Delta}{=} S_o^{(1)} \end{aligned} \quad (3.190)$$

with each $S^{(1)}$ evaluated using Y_1 , written as a function of Y_2 .

Elimination of rotor currents from (3.64)–(3.72) gives the final dynamic model with general nonlinearities.

$$\frac{1}{\omega_s} \frac{d\psi_d}{dt} = R_s I_d + \frac{\omega}{\omega_s} \psi_q + V_d \quad (3.191)$$

$$\frac{1}{\omega_s} \frac{d\psi_q}{dt} = R_s I_q - \frac{\omega}{\omega_s} \psi_d + V_q \quad (3.192)$$

$$\frac{1}{\omega_s} \frac{d\psi_o}{dt} = R_s I_o + V_o \quad (3.193)$$

$$T'_{do} \frac{dE'_q}{dt} = -E'_q - (X_d - X'_d) \left[I_d - \frac{X'_d - X''_d}{(X'_d - X_{\ell s})^2} (\psi_{1d} + (X'_d - X_{\ell s}) I_d - E'_q + S_{1d}^{(2)}(Y_2)) \right] - S_{fd}^{(2)}(Y_2) + E_{fd} \quad (3.194)$$

$$T''_{do} \frac{d\psi_{1d}}{dt} = -\psi_{1d} + E'_q - (X'_d - X_{\ell s}) I_d - S_{1d}^{(2)}(Y_2) \quad (3.195)$$

$$T'_{qo} \frac{dE'_d}{dt} = -E'_d + (X_q - X'_q) \left[I_q - \frac{X'_q - X''_q}{(X'_q - X_{\ell s})^2} (\psi_{2q} + (X'_q - X_{\ell s}) I_q + E'_d + S_{2q}^{(2)}(Y_2)) \right] + S_{1q}^{(2)}(Y_2) \quad (3.196)$$

$$T''_{qo} \frac{d\psi_{2q}}{dt} = -\psi_{2q} - E'_d - (X'_q - X_{\ell s}) I_q - S_{2q}^{(2)}(Y_2) \quad (3.197)$$

$$\frac{d\delta}{dt} = \omega - \omega_s \quad (3.198)$$

$$\frac{2H}{\omega_s} \frac{d\omega}{dt} = T_M - (\psi_d I_q - \psi_q I_d) - T_{FW} \quad (3.199)$$

with the three algebraic equations,

$$\begin{aligned} \psi_d &= -X''_d I_d + \frac{(X''_d - X_{\ell s})}{(X'_d - X_{\ell s})} E'_q + \frac{(X'_d - X''_d)}{(X'_d - X_{\ell s})} \psi_{1d} \\ &\quad - S_d^{(2)}(Y_2) \end{aligned} \quad (3.200)$$

$$\begin{aligned} \psi_q &= -X''_q I_q - \frac{(X''_q - X_{\ell s})}{(X'_q - X_{\ell s})} E'_d + \frac{(X'_q - X''_q)}{(X'_q - X_{\ell s})} \psi_{2q} \\ &\quad - S_q^{(2)}(Y_2) \end{aligned} \quad (3.201)$$

$$\psi_o = -X_{\ell s} I_o - S_o^{(2)}(Y_2) \quad (3.202)$$

$$Y_2 = [I_d \ E'_q \ \psi_{1d} \ I_q \ E'_d \ \psi_{2q} \ I_o]^t \quad (3.203)$$

As in the last section, new speeds could be defined so that each dynamic state includes a time constant. It is important to note, however, that, as in the last section, terms on the right-hand side of the dynamic state model imply that these time constants do not necessarily completely identify the speed of response of each variable. This is even more evident with the addition of nonlinearities.

One purpose for beginning this section by returning to the *abc* variables was to trace the nonlinearities through the transformation and scaling process. This ensures that the resulting model with nonlinearities is, in some sense, consistent. This was partly motivated by the proliferation of different methods to account for saturation in the literature. For example, the literature talks about “ X_{md} ” saturating, or X_{md} being a function of the dynamic states. This could imply that many constants we have defined would change when saturation is considered. With the presentation given above, it is clear that all constants can be left unchanged, while the nonlinearities are included in a set of functions to be specified based on some design calculation or test procedure.

It is interesting to compare these general nonlinearity functions with other methods that have appeared in the literature [20, 22, 23, 26, 27, 35]–[50]. Reference [37] discusses a typical representation that uses:

$$S_d^{(2)} = 0, \quad S_{1d}^{(2)} = 0, \quad S_q^{(2)} = 0, \quad S_{2q}^{(2)} = 0, \quad S_o^{(2)} = 0 \quad (3.204)$$

and keeps $S_{fd}^{(2)}$ and $S_{1q}^{(2)}$ expressed as

$$S_{fd}^{(2)} = \frac{\psi_d''}{|\psi''|} S_G(|\psi''|) \quad (3.205)$$

$$S_{1q}^{(2)} = \frac{\psi_q''(X_q - X_{\ell s})}{|\psi''|(X_d - X_{\ell s})} S_G(|\psi''|) \quad (3.206)$$

where

$$|\psi''| \stackrel{\Delta}{=} \left(\psi_d''^2 + \psi_q''^2 \right)^{1/2} \quad (3.207)$$

and

$$\psi_d'' \stackrel{\Delta}{=} \left(\frac{X_d'' - X_{\ell s}}{X_d' - X_{\ell s}} \right) E'_q + \left(\frac{X_d' - X_d''}{X_d' - X_{\ell s}} \right) \psi_{1d} \quad (3.208)$$

$$\psi_q'' \stackrel{\Delta}{=} - \left(\frac{X_q'' - X_{\ell s}}{X_q' - X_{\ell s}} \right) E'_d + \left(\frac{X_q' - X_q''}{X_q' - X_{\ell s}} \right) \psi_{2q}. \quad (3.209)$$

The saturation function S_G should be correct under open-circuit conditions. For steady state with

$$\begin{aligned} I_d &= I_q = I_o = I_{1d} = I_{1q} = I_{2q} = 0 \\ \psi_q &= -E'_d = \psi_q'' = -V_d = \psi_{1q} = \psi_{2q} = 0 \\ \psi_d &= E'_q = \psi_d'' = V_q = \psi_{1d} = E_{fd} - S_{fd}^{(2)} \end{aligned} \quad (3.210)$$

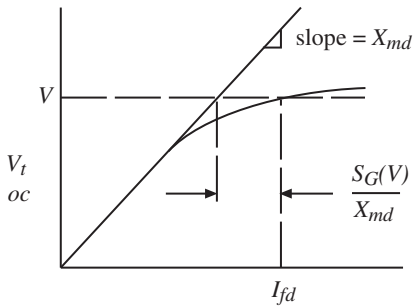


Figure 3.3 Synchronous machine open-circuit characteristic.

the open-circuit terminal voltage is

$$V_{t_{oc}} = \sqrt{V_d^2 + V_q^2} = E'_q \quad (3.211)$$

and the field current is

$$I_{fd} = \frac{E'_q + S_{fd}^{(2)}}{X_{md}}. \quad (3.212)$$

From the saturation representation of (3.205),

$$S_{fd}^{(2)} = S_G(V_{t_{oc}}) \quad (3.213)$$

$$X_{md}I_{fd} = V_{t_{oc}} + S_G(V_{t_{oc}}). \quad (3.214)$$

The function S_G can then be obtained from an open-circuit characteristic, as shown in Figure 3.3. While this illustrates the validity of the saturation function under open-circuit conditions, it does not totally support its use under load. In addition, it has been shown that this representation does not satisfy the assumption of a conservative coupling field [51].

3.6 Single-Machine Steady State

To introduce steady state, we assume constant states and look at the algebraic equations resulting from the dynamic model. We will analyze the system under the condition of a linear magnetic circuit. Thus, beginning with (3.148)–(3.159), we observe that, for constant states, we must have constant speed ω and constant angle δ , thus requiring $\omega = \omega_s$ and, therefore,

$$V_d = -R_s I_d - \psi_q \quad (3.215)$$

$$V_q = -R_s I_q + \psi_d. \quad (3.216)$$

Assuming a balanced three-phase operation, all of the “zero” variables and damper winding currents are zero. The fact that damper-winding currents are zero can be seen by recalling that the right-hand sides of (3.152)–(3.154) are actually scaled damper-winding currents. Using these to simplify (3.151), (3.153), (3.157), and (3.158), the other

algebraic equations to be solved are

$$0 = -E'_q - (X_d - X'_d)I_d + E_{fd} \quad (3.217)$$

$$0 = -\psi_{1d} + E'_q - (X'_d - X_{\ell s})I_d \quad (3.218)$$

$$0 = -E'_d + (X_q - X'_q)I_q \quad (3.219)$$

$$0 = -\psi_{2q} - E'_d - (X'_q - X_{\ell s})I_q \quad (3.220)$$

$$0 = T_M - (\psi_d I_q - \psi_q I_d) - T_{FW} \quad (3.221)$$

$$\psi_d = E'_q - X'_d I_d \quad (3.222)$$

$$\psi_q = -E'_d - X'_q I_q. \quad (3.223)$$

Except for (3.221), these are all linear equations that can easily be solved for various steady-state representations. Substituting for ψ_d and ψ_q in (3.215) and (3.216) gives

$$V_d = -R_s I_d + E'_d + X'_q I_q \quad (3.224)$$

$$V_q = -R_s I_q + E'_q - X'_d I_d. \quad (3.225)$$

These two real algebraic equations can be written as one complex equation of the form

$$(V_d + jV_q)e^{j(\delta-\pi/2)} = -(R_s + jX_q)(I_d + jI_q)e^{j(\delta-\pi/2)} + \bar{E} \quad (3.226)$$

where

$$\begin{aligned} \bar{E} &= [(E'_d - (X_q - X'_q)I_q) + j(E'_q + (X_q - X'_d)I_d)]e^{j(\delta-\pi/2)} \\ &= j[(X_q - X'_d)I_d + E'_q]e^{j(\delta-\pi/2)}. \end{aligned} \quad (3.227)$$

Clearly, many alternative complex equations can be written from (3.224) and (3.225), depending on what is included in the “internal” voltage \bar{E} . For balanced symmetrical sinusoidal steady-state *abc* voltages and currents, the quantities $(V_d + jV_q)e^{j(\delta-\pi/2)}$ and $(I_d + jI_q)e^{j(\delta-\pi/2)}$ are the per-unit RMS phasors for *a* phase voltage and current (see (3.73)–(3.91)). This gives considerable physical significance to the circuit form of (3.226) shown in Figure 3.4. The internal voltage \bar{E} can be further simplified, using (3.217), as

$$\begin{aligned} \bar{E} &= j[(X_q - X_d)I_d + E_{fd}]e^{j(\delta-\pi/2)} \\ &= [(X_q - X_d)I_d + E_{fd}]e^{j\delta}. \end{aligned} \quad (3.228)$$

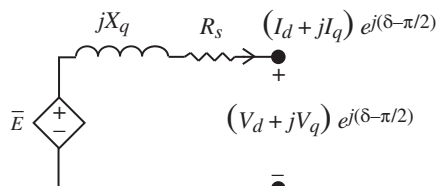
An important observation is

$$\delta = \text{angle on } \bar{E}. \quad (3.229)$$

Also from (3.142) and (3.143),

$$I_{fd} = E_{fd}/X_{md}. \quad (3.230)$$

Figure 3.4 Synchronous machine circuit representation in steady state.



Several other points are worth noting. First, the open-circuit (or zero stator current) terminal voltage is

$$(V_d + jV_q)e^{j(\delta - \pi/2)}|_{I_d=I_q=0} = E_{fd}e^{j\delta}. \quad (3.231)$$

Therefore, for $E_{fd} = 1$, the open-circuit terminal voltage is 1, and field current is $1/X_{md}$. Also,

$$V_d|_{I_d=I_q=0} = E'_d|_{I_d=I_q=0} = -\psi_q|_{I_d=I_q=0} = 0 \quad (3.232)$$

$$V_q|_{I_d=I_q=0} = E'_q|_{I_d=I_q=0} = \psi_d|_{I_d=I_q=0} = E_{fa}. \quad (3.233)$$

The electrical torque is

$$T_{ELEC} = \psi_d I_q - \psi_q I_d = V_d I_d + V_q I_q + R_s(I_d^2 + I_q^2) \quad (3.234)$$

This torque is precisely the “real power” delivered by the controlled source of Figure 3.4. That is, for $\bar{I} = (I_d + jI_q)e^{j(\delta - \pi/2)}$,

$$T_{ELEC} = T_M = \text{Real}[\bar{E}\bar{I}^*]. \quad (3.235)$$

We can then conclude that the electrical torque from the shaft is equal to the power delivered by the controlled source. In steady state, the electrical torque from the shaft equals T_M when $T_{FW} = 0$. From the circuit with $\bar{V} = (V_d + jV_q)e^{j(\delta - \pi/2)}$,

$$T_{ELEC} = \text{Real} \left[\bar{E} \left(\frac{\bar{E} - \bar{V}}{R_s + jX_q} \right)^* \right]. \quad (3.236)$$

For zero stator resistance and round rotor,

$$T_{ELEC} \Big|_{\substack{R_s=0 \\ X_d=X_q}} = \text{Real} \left[E_{fd} e^{j\delta} \left(\frac{E_{fd} e^{-j\delta} - \bar{V}^*}{-jX_d} \right) \right] \quad (3.237)$$

or

$$T_{ELEC} \Big|_{\substack{R_s=0 \\ X_d=X_q}} = \frac{E_{fd} V}{X_d} \sin \delta_T \quad (3.238)$$

where the angle δ_T is called the torque angle,

$$\delta_T \stackrel{\Delta}{=} \delta - \theta \quad (3.239)$$

with

$$\bar{V} = V e^{j\theta}. \quad (3.240)$$

Under these conditions, and this definition of the torque angle, $\delta_T < 0$ for a motor and $\delta_T > 0$ for a generator.

Example 3.1 Consider a synchronous machine (without saturation) serving a load with

$$\bar{V} = 1 \angle 10^\circ \text{pu} \quad \bar{I} = 0.5 \angle -20^\circ \text{pu}.$$

It has $X_d = 1.2$, $X_q = 1.0$, $X_{md} = 1.1$, $X'_d = 0.232$, $R_s = 0$ (all in pu). Find δ , δ_T , I_d , I_q , V_d , V_q , ψ_d , ψ_q , E'_q , E_{fd} , I_{fd} (all in pu except angles in degrees).

Solution:

$$(0.768I_d + E'_q)\angle\delta = 1\angle90^\circ \times 0.5\angle - 20^\circ + 1\angle10^\circ \\ = 1.323\angle29.1^\circ$$

so

$$\begin{aligned}\delta &= 29.1^\circ \quad \delta_T = 29.1^\circ - 10^\circ = 19.1^\circ \\ I_d + jI_q &= 0.5\angle - 20^\circ - 29.1^\circ + 90^\circ = 0.5\angle40.9^\circ \\ I_d &= 0.378 \quad I_q = 0.327 \\ V_d + jV_q &= 1\angle10^\circ - 29.1^\circ + 90^\circ = 1\angle70.9^\circ \\ V_d &= 0.327 \quad V_q = 0.945 \\ \psi_d &= V_q + 0I_q = 0.945 \\ \psi_q &= -V_d - 0I_d = -0.327.\end{aligned}$$

To find E'_q and E_{fd} , return to $|\bar{E}|$

$$\begin{aligned}0.768 \times 0.378 + E'_q &= 1.323 \\ E'_q &= 1.033 \\ 1.033 &= -(1.2 - 0.232) \times 0.378 + E_{fd} \\ E_{fd} &= 1.399.\end{aligned}$$

To find I_{fd} , it is easy to show that

$$I_{fd} = \frac{E_{fd}}{X_{md}} = \frac{1.399}{1.1} = 1.27.$$

These solutions can be checked by noting that, in scaled per unit, T_{ELEC} is equal to P_{OUT} .

$$\begin{aligned}T_{ELEC} &= \psi_d I_q - \psi_q I_d = 0.4326 \\ P_{OUT} &= \text{Real}(\bar{V} \bar{I}^*) = \text{Real}(0.5\angle + 30^\circ) = 0.433.\end{aligned}$$

Also,

$$\begin{aligned}Q_{OUT} &= \text{Imag}(\bar{V} \bar{I}^*) = \text{Imag}(0.5\angle30^\circ) = 0.25 \\ &= \text{Imag}((V_d + jV_q)e^{-j(\delta-\pi/2)}(I_d - jI_q)e^{j(\delta-\pi/2)}) \\ &= \text{Imag}((V_d + jV_q)(I_d - jI_q)) \\ &= \psi_d I_d + \psi_q I_q = 0.25.\end{aligned}$$

□

The steady-state analysis of a given problem involves certain constraints. For example, depending on what is specified, the solution of the steady-state equations may be very difficult to solve. The solution of steady-state in multimachine power systems is usually called load flow (or power flow), and is discussed in later chapters. The extension of this steady-state analysis to include saturation is left as an exercise.

3.7 Operational Impedances and Test Data

The synchronous machine model derived in this chapter was based on the initial assumption of three stator windings, one field winding, and three damper windings ($1d$, $1q$, $2q$). In addition, the machine reactances and time constants were defined in terms of this machine structure. This is consistent with [20] and many other references. It was noted earlier, however, that many of the machine reactances and time constants have been defined through physical tests or design parameters rather than a presupposed physical structure and model. Regardless of the definition of constants, a given model contains quantities that must be replaced by numbers in a specific simulation. Since designers use considerably more detailed modeling, and physical tests are model independent, there could be at least three different ways to arrive at a value for a constant denoted by the symbols used in the model of this chapter. For example, a physical test can be used to compute a value of T''_{do} if T''_{do} is defined through the outcome of a test. A designer can compute a value of T''_{do} from physical parameters such that the value would approximate the test value. The definition of T''_{do} in this chapter was not based on any test and could, therefore, be different from that furnished by a manufacturer. For this reason, it is important to always verify the definitions of all constants to ensure that the numerical value is a good approximation of the constant used in the model.

The concept of operational impedance was introduced as a means for relating test data to model constants. The concept is based on the response of a machine to known test voltages. These test voltages may be either dc or sinusoidal ac of variable frequency. The stator equations in the transformed and scaled variables can be written in the Laplace domain from (3.64)–(3.72) with constant speed ($\omega = \omega_{ss}$) as

$$\bar{V}_d = -R_s \bar{I}_d - \frac{\omega_{ss}}{\omega_s} \bar{\psi}_q + \frac{s}{\omega_s} \bar{\psi}_d \quad (3.241)$$

$$\bar{V}_q = -R_s \bar{I}_q + \frac{\omega_{ss}}{\omega_s} \bar{\psi}_d + \frac{s}{\omega_s} \bar{\psi}_q \quad (3.242)$$

$$\bar{V}_o = -R_s \bar{I}_o + \frac{s}{\omega_s} \bar{\psi}_o \quad (3.243)$$

where s is the Laplace domain operator, which, in sinusoidal steady state with frequency ω_0 in radians/sec, is

$$s = j\omega_0 \quad (3.244)$$

If we make the assumption that the magnetic circuit has a linear flux linkage/current relationship that satisfies assumptions (3) and (4) of Section 3.3, we can propose that we have the Laplace domain relationship for any number of rotor-windings (or equivalent windings that represent solid iron rotor effects). When scaled, these relationships could be solved for $\bar{\psi}_d$, $\bar{\psi}_q$, and $\bar{\psi}_o$ as functions of \bar{I}_d , \bar{I}_q , \bar{I}_o , all rotor winding voltages and the operator s . For balanced, symmetric windings and all-rotor winding voltages zero except for V_{fd} , the result would be

$$\bar{\psi}_d = -X_{dop}(s) \bar{I}_d + \bar{G}_{op}(s) \bar{V}_{fd} \quad (3.245)$$

$$\bar{\psi}_q = -X_{qop}(s) \bar{I}_q \quad (3.246)$$

$$\bar{\psi}_o = -X_{oop} \bar{I}_o \quad (3.247)$$

To see how this could be done for a specific model, consider the three-damper-winding model of the previous sections. The scaled Kirchhoff equations are given as (3.67)–(3.70), and the scaled linear magnetic circuit equations are given as (3.122)–(3.128). From these equations in the Laplace domain with operator s and $V_{1d} = V_{1q} = V_{2q} = 0$,

$$\frac{s}{\omega_s}[X_{md}(-\bar{I}_d) + X_{fd}\bar{I}_{fd} + c_d X_{md}\bar{I}_{1d}] = -R_{fd}\bar{I}_{fd} + \bar{V}_{fd} \quad (3.248)$$

$$\frac{s}{\omega_s}[X_{md}(-\bar{I}_d) + c_d X_{md}\bar{I}_{fd} + X_{1d}\bar{I}_{1d}] = -R_{1d}\bar{I}_{1d} \quad (3.249)$$

$$\frac{s}{\omega_s}[X_{mq}(-\bar{I}_q) + X_{1q}\bar{I}_q + c_q X_{mq}\bar{I}_{2q}] = -R_{1q}\bar{I}_{1q} \quad (3.250)$$

$$\frac{s}{\omega_s}[X_{mq}(-\bar{I}_q) + c_q X_{mq}\bar{I}_{1q} + X_{2q}\bar{I}_{2q}] = -R_{2q}\bar{I}_{2q} \quad (3.251)$$

$$\bar{\psi}_o = X_{\ell s}(-\bar{I}_o). \quad (3.252)$$

The two d equations can be solved for \bar{I}_{fd} and \bar{I}_{1d} as functions of s times \bar{I}_d and \bar{V}_{fd} . The two q axis equations can be solved for \bar{I}_{1q} and \bar{I}_{2q} as functions of s times \bar{I}_q . When substituted into (3.122) and (3.125), this would produce the following operational functions for this given model:

$$\bar{X}_{dop}(s) = X_d - \left[\frac{\frac{s}{\omega_s}X_{md}^2 \left(R_{1d} + \frac{s}{\omega_s}X_{1d} - 2\frac{s}{\omega_s}c_d X_{md} + R_{fd} + \frac{s}{\omega_s}X_{fd} \right)}{\left(R_{fd} + \frac{s}{\omega_s}X_{fd} \right) \left(R_{1d} + \frac{s}{\omega_s}X_{1d} \right) - \left(\frac{s}{\omega_s}c_d X_{md} \right)^2} \right] \quad (3.253)$$

$$\bar{G}_{op}(s) = \left[\frac{X_{md} \left(R_{1d} + \frac{s}{\omega_s}X_{1d} - \frac{s}{\omega_s}c_d X_{md} \right)}{\left(R_{fd} + \frac{s}{\omega_s}X_{fd} \right) \left(R_{1d} + \frac{s}{\omega_s}X_{1d} \right) - \left(\frac{s}{\omega_s}c_d X_{md} \right)^2} \right] \quad (3.254)$$

$$\bar{X}_{qop}(s) = X_q - \frac{\frac{s}{\omega_s}X_{mq}^2 \left(R_{2q} + \frac{s}{\omega_s}X_{2q} - 2\frac{s}{\omega_s}c_q X_{mq} + R_{1q} + \frac{s}{\omega_s}X_{1q} \right)}{\left(R_{2q} + \frac{s}{\omega_s}X_{2q} \right) \left(R_{1q} + \frac{s}{\omega_s}X_{1q} \right) - \left(\frac{s}{\omega_s}c_q X_{mq} \right)^2} \quad (3.255)$$

$$\bar{X}_{oop}(s) = X_{\ell s}. \quad (3.256)$$

Note that for $s = 0$ in this model

$$\bar{X}_{dop}(0) = X_d \quad (3.257)$$

$$\bar{G}_{op}(0) = \frac{X_{md}}{R_{fd}} \quad (3.258)$$

$$\bar{X}_{qop}(0) = X_q \quad (3.259)$$

and for $s = \infty$ in this model with $c_d = c_q = 1$

$$\bar{X}_{dop}(\infty) = X_d'' \quad (3.260)$$

$$\bar{X}_{qop}(\infty) = X_q''. \quad (3.261)$$

For this model, it is also possible to rewrite (3.253)–(3.256) as a ratio of polynomials in s that can be factored to give a time constant representation. The purpose for introducing this concept of operational functions is to show one possible way in which a set of parameters may be obtained from a machine test. At standstill, the Laplace domain equations (3.241)–(3.243) and (3.245)–(3.247) are

$$\bar{V}_d = - \left(R_s + \frac{s}{\omega_s} X_{dop}(s) \right) \bar{I}_d + \frac{s}{\omega_s} \bar{G}_{op}(s) \bar{V}_{fd} \quad (3.262)$$

$$\bar{V}_q = - \left(R_s + \frac{s}{\omega_s} X_{qop}(s) \right) \bar{I}_q \quad (3.263)$$

$$\bar{V}_o = - \left(R_s + \frac{s}{\omega_s} X_{oop}(s) \right) \bar{I}_o. \quad (3.264)$$

To see how these can be used with a test, consider the schematic of Figure 3.1 introduced earlier. With all the abc dot ends connected together to form a neutral point, the three abc x ends form the stator terminals. If a scaled voltage V_{test} is applied across bc , with the a terminal open, the scaled series $I_c(-I_b)$ current establishes an axis that is 90° ahead of the original a -axis, as shown in Figure 3.5. With this symmetry and $\theta_{\text{shaft}} = \frac{2\pi}{p}$ mech. rad (found by observing the field voltage as the rotor is turned), the scaled voltage V_a will be zero even for nonzero $I_c = -I_b$ and I_{fd} , since its axis is perpendicular to both the b - and c -axis and the field winding d -axis. Also, the unscaled test voltage is

$$v_{\text{test}} = v_b - v_c \quad (3.265)$$

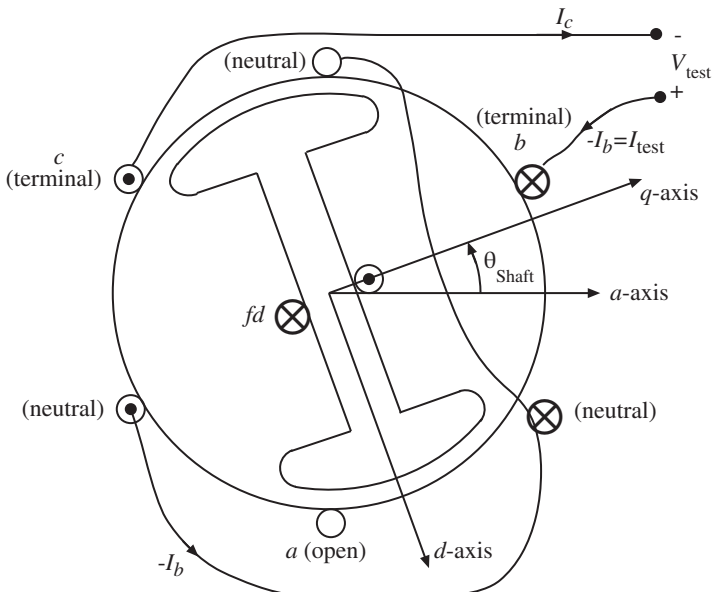


Figure 3.5 Standstill test schematic.

and, by symmetry with $\theta_{\text{shaft}} = \frac{2\pi}{p}$ mechanical radians,

$$\nu_b = -\nu_c. \quad (3.266)$$

The unscaled transformed voltages are

$$\nu_d = \frac{\sqrt{3}}{2}\nu_b - \frac{\sqrt{3}}{2}\nu_c = \frac{\sqrt{3}}{2}\nu_{\text{test}} \quad (3.267)$$

$$\nu_q = \nu_o = 0 \quad (3.268)$$

and the unscaled transformed currents are

$$i_d = \frac{\sqrt{3}}{2}i_b - \frac{\sqrt{3}}{2}i_c = \sqrt{3}i_b = \sqrt{3}i_{\text{test}} \quad (3.269)$$

$$i_q = i_o = 0. \quad (3.270)$$

For a test set of voltage and current,

$$\nu_{\text{test}} = \sqrt{3}\sqrt{2}V_{to} \cos(\omega_o t + \theta_o) \quad (3.271)$$

$$i_{\text{test}} = \sqrt{2}I_{to} \cos(\omega_o t + \phi_o) \quad (3.272)$$

with scaled RMS cosine reference phasors defined as

$$\bar{V}_{\text{test}}_{pu} \stackrel{\Delta}{=} \frac{\sqrt{3}V_{to}}{V_{BABC}} e^{j\theta_o} \quad (3.273)$$

$$\bar{I}_{\text{test}}_{pu} \stackrel{\Delta}{=} \frac{I_{to}}{I_{BABC}} e^{j\phi_o} \quad (3.274)$$

the scaled quantities V_d and I_d are

$$V_d = \frac{\nu_d}{V_{BDQ}} = \frac{1}{\sqrt{2}V_{BABC}} \frac{\sqrt{3}}{2} \sqrt{3}\sqrt{2}V_{to} \cos(\omega_o t + \theta_o) \quad (3.275)$$

$$I_d = \frac{-i_d}{I_{BDQ}} = \frac{-1}{\sqrt{2}I_{BABC}} \sqrt{3}\sqrt{2}I_{to} \cos(\omega_o t + \phi_o) \quad (3.276)$$

or

$$V_d = \frac{\sqrt{3}}{2} |\bar{V}_{\text{test}}_{pu}| \cos(\omega_o t + \theta_o) \quad (3.277)$$

$$I_d = -\sqrt{3} |\bar{I}_{\text{test}}_{pu}| \cos(\omega_o t + \phi_o) \quad (3.278)$$

$$\left(\bar{V}_d = \frac{\sqrt{3}}{2} |\bar{V}_{\text{test}}_{pu}| e^{j\theta_o}, \bar{I}_d = -\sqrt{3} |\bar{I}_{\text{test}}_{pu}| e^{j\phi_o} \right).$$

For $s = j\omega_o$, the ratio of test voltage to current is

$$\bar{Z}_o(j\omega_o) \stackrel{\Delta}{=} \frac{\bar{V}_{\text{test}}_{pu}}{\bar{I}_{\text{test}}_{pu}} = -2 \frac{\bar{V}_d}{\bar{I}_d} \quad (3.279)$$

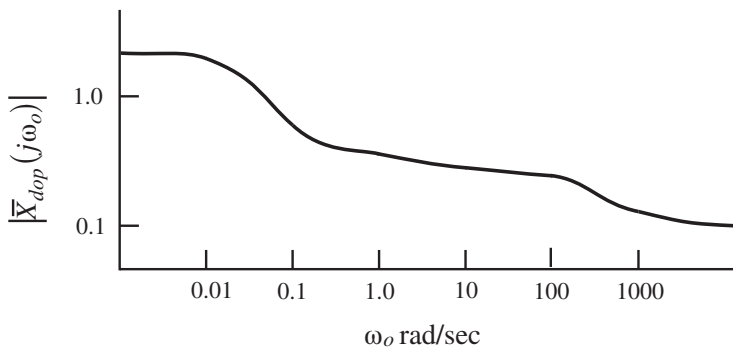


Figure 3.6 Salient-pole machine.

which can be written as a real plus imaginary function

$$\bar{Z}_o(j\omega_o) = R_o(\omega_o) + jX_o(\omega_o). \quad (3.280)$$

Therefore, from (3.262), with $\bar{V}_{fd} = 0$ and $s = j\omega_o$,

$$\left(R_s + j\frac{\omega_o}{\omega_s} \bar{X}_{dop}(j\omega_o) \right) = \frac{1}{2} \bar{Z}_o(j\omega_o). \quad (3.281)$$

Clearly R_s is one-half the ratio of a set of dc test voltage and current. After R_s is determined, the operational impedance for any frequency ω_o is

$$\bar{X}_{dop}(j\omega_o) = -j \frac{\omega_s}{\omega_o} \left(\frac{\bar{V}_{test}}{2\bar{I}_{test}} - R_s \right). \quad (3.282)$$

A typical test result for a salient pole machine is shown in Figure 3.6 [20, 52] ($\bar{X}_{dop}(j\omega_o)$ is a complex quantity). The plot typically has three levels with two somewhat distinct breakpoints, as shown. For round rotor machines, the plot is more uniform, decreasing with a major breakpoint at 0.01 Hz. A similar test with different rotor positions could be used to compute $\bar{X}_{qop}(j\omega_o)$. These tests, as well as others, are described in considerable detail in [20, 52, 53]. Reference [53] also includes a discussion on curve-fitting procedures to compute “best-fit” model parameters from the frequency response test data. For example, the operational impedance $\bar{X}_{dop}(s)$ for the model used earlier is given by (3.253). If a plot similar to Figure 3.6 (together with a plot of the angle on $\bar{X}_{dop}(s)$) is available, the model parameters can be computed so that (3.253) is some “best-fit” to Figure 3.6. It is possible to make the fit better for different frequency ranges. Thus, the data to be used for a given model can be adjusted to make the model more accurate in certain frequency ranges. The only way to make the model more accurate in all frequency ranges is to increase the dynamic order of the model by adding more “damper” windings in an attempt to reach a better overall fit of $\bar{X}_{dop}(s)$ to the standstill frequency response. Similarly it is clear that the key to model reduction is to properly eliminate dynamic states while still preserving some phenomena (or frequency range response) of interest. This is discussed extensively in later chapters.

In summary, it is important to note several important points about synchronous machine dynamic modeling. First, the literature abounds with various notational conventions and definitions. The notations and conventions used in this text are as standard as possible given the proliferation of models. It basically follows that of [20–29]. Second, it is important to repeat that standard symbols have been defined through the model proposed in this text (and [20–29]) with a few noted exceptions. The procedures followed by the industry often define constants through well-defined tests. In some cases, these definitions do not coincide precisely with the model definitions in this text. Thus, when using data obtained from manufacturers, it is important to clarify which definition of symbols is being used. If frequency response data are given, the model parameters can be computed using curve-fitting techniques.

3.8 Problems

- 3.1** The text uses T_{qdo} to transform abc variables into dqo variables. Consider the following alternative transformation matrix:

$$P_{dqo} = \sqrt{\frac{2}{3}} \begin{bmatrix} \cos \frac{P}{2}\theta_{\text{shaft}} & \cos \left(\frac{P}{2}\theta_{\text{shaft}} - \frac{2\pi}{3} \right) & \cos \left(\frac{P}{2}\theta_{\text{shaft}} + \frac{2\pi}{3} \right) \\ \sin \frac{P}{2}\theta_{\text{shaft}} & \sin \left(\frac{P}{2}\theta_{\text{shaft}} - \frac{2\pi}{3} \right) & \sin \left(\frac{P}{2}\theta_{\text{shaft}} + \frac{2\pi}{3} \right) \\ \frac{1}{\sqrt{2}} & \frac{1}{\sqrt{2}} & \frac{1}{\sqrt{2}} \end{bmatrix}.$$

Show that $P_{dqo}^t = P_{dqo}^{-1}$ (P_{dqo} is orthogonal).

- 3.2** Given the following model

$$\nu = 10i + \frac{d\lambda}{dt}, \lambda = 0.05i$$

scale ν , i , and λ as follows:

$$V = \frac{\nu}{V_B}, I = \frac{i}{I_B}, \psi = \frac{\lambda}{\Lambda_B}$$

to get

$$V = RI + \frac{1}{\omega_B} \frac{d\psi}{dt}, \psi = XI.$$

Find R and X if $V_B = 10,000$ volts, $S_B = 5 \times 10^6$ VA, $\omega_B = 2\pi 60$ rad/sec, and $I_B = S_B/V_B$, $\Lambda_B = V_B/\omega_B$.

- 3.3** Using the P_{dqo} of Problem 3.1 with

$$\begin{aligned} \nu_a &= \sqrt{2}V \cos(\omega_s t + \theta) \\ \nu_b &= \sqrt{2}V \cos \left(\omega_s t + \theta - \frac{2\pi}{3} \right) \\ \nu_c &= \sqrt{2}V \cos \left(\omega_s t + \theta + \frac{2\pi}{3} \right) \end{aligned}$$

and $\hat{\delta} \stackrel{\Delta}{=} \frac{p}{2}\theta_{\text{shaft}} - \omega_s t - \frac{\pi}{2}$, express the phasor $\bar{V} = Ve^{j\theta}$ in terms of v_d , v_q , and δ that you get from using P_{dqo} to transform v_a , v_b , v_c into v_d , v_q , v_o .

- 3.4** Neglect saturation and derive an expression for \bar{E}' in the alternative steady-state equivalent circuit in Figure 3.7. Write \bar{E}' as a function of E'_q , I_d , I_q , δ .

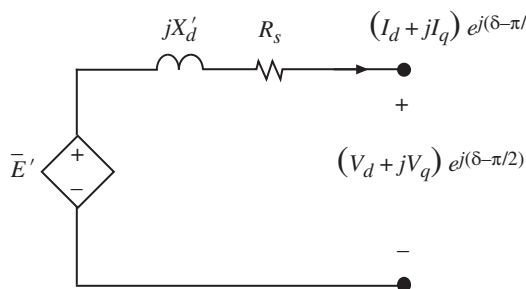


Figure 3.7 Figure for Problem 3.4.

- 3.5** Given the magnetization curve shown in pu in Figure 3.8, compute X_{md} and plot $S_G(\psi)$ for

$$\psi = X_{md}I - S_G(\psi).$$

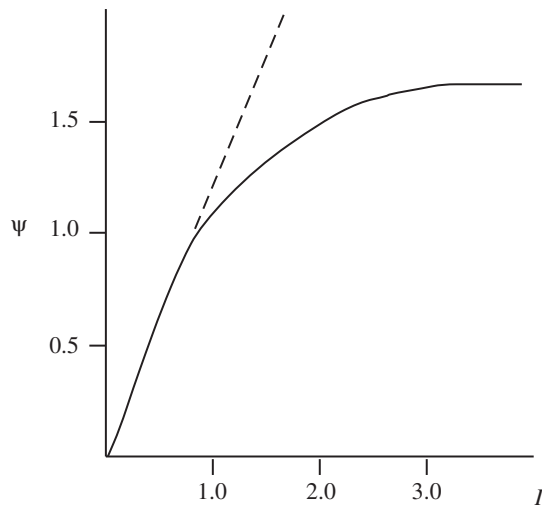


Figure 3.8 Figure for Problem 3.5.

- 3.6** Repeat the derivation of the single-machine steady-state equivalent circuit using the following saturation functions:

$$\begin{aligned} S_d^{(2)} &= S_{1d}^{(2)} = S_q^{(2)} = S_{1q}^{(2)} = S_{2q}^{(2)} = S_o^{(2)} = 0 \\ S_{fd}^{(2)} &= S_G(E'_q) \end{aligned}$$

where S_G is obtained from the open-circuit characteristic as given in the text.

- 3.7** From Ref. [51], show that the saturation model of Problem 3.6 does satisfy all conditions for a conservative coupling field.
- 3.8** Given (3.122)–(3.124) and (3.125)–(3.127), together with (3.64)–(3.70), find a circuit representation for these mathematical models. (Hint: Split X_d , X_{fd} , X_{1d} , etc. into leakage plus magnetizing.)
- 3.9** Given the following nonlinear magnetic circuit model for a synchronous machine:

$$\begin{aligned}\psi_d &= X_d(-I_d) + X_{md}I_{fd} - S_d(\psi_d, \psi_{fd}) \\ \psi_{fd} &= X_{md}(-I_d) + X_{fd}I_{fd} - S_{fd}(\psi_d, \psi_{fd}) \\ \psi_q &= X_q(-I_q) + X_{mq}I_{1q} - S_q(\psi_q, \psi_{1q}) \\ \psi_{1q} &= X_{mq}(-I_q) + X_{1q}I_{1q} - S_{1q}(\psi_q, \psi_{1q}).\end{aligned}$$

- (a)** Find the constraints on the saturation functions S_d , S_{fd} , S_q , S_{1q} such that the overall model does not violate the assumption of a conservative coupling field.
(b) If the other steady-state equations are

$$\begin{aligned}V_d &= -R_s I_d - \psi_q & V_{fd} &= R_{fd} I_{fd} \\ V_q &= -R_s I_q + \psi_d & 0 &= R_{1q} I_{1q}\end{aligned}$$

find an expression for \bar{E} , where \bar{E} is the voltage “behind” $R_s + jX_q$ in a circuit that has a terminal voltage

$$\bar{V} = (V_d + jV_q)e^{j(\delta - \pi/2)}.$$

4

Synchronous Machine Control Models

4.1 Voltage and Speed Control Overview

The primary objective of an electrical power system is to maintain balanced sinusoidal voltages with virtually constant magnitude and frequency. In the synchronous machine models of the last chapter, the terminal constraints (relationships between V_d , I_d , V_q , I_q , V_o , and I_o) were not specified. These will be discussed in the next chapter. In addition, the two quantities E_{fd} and T_M were left as inputs to be specified. E_{fd} is the scaled field voltage, which, if set equal to 1.0 pu, gives 1.0 pu open-circuit terminal voltage. T_M is the scaled mechanical torque to the shaft. If it is specified as a constant, the machine terminal constraints will determine the steady-state speed. Specifying E_{fd} and T_M to be constants in the model means that the machine does not have voltage or speed (and, hence, frequency) control. If a synchronous machine is to be useful for a wide range of operating conditions, it should be capable of participating in the attempt to maintain constant voltage and frequency. This means that E_{fd} and T_M should be systematically adjusted to accommodate any change in terminal constraints. The physical device that provides the value of E_{fd} is called the exciter. The physical device that provides the value of T_M is called the prime mover. This chapter is devoted to basic mathematical models of these components and their associated control systems.

4.2 Exciter Models

One primary reason for using three-phase generators is the constant electrical torque developed in steady state by the interaction of the magnetic fields produced by the armature ac currents with the field dc current. Furthermore, for balanced three-phase machines, a dc current can be produced in the field winding by a dc voltage source. In steady state, adjustment of the field voltage changes the field current and, therefore, the terminal voltage. Perhaps the simplest scheme for voltage control would be a battery with a rheostat adjusted voltage divider connected to the field winding through slip rings. Manual adjustment of the rheostat could be used to continuously react to changes in operating conditions to maintain a voltage magnitude at some point. Since large amounts of power are normally required for the field excitation, the control device is usually not a battery, and is referred to as the main exciter. This main exciter may be

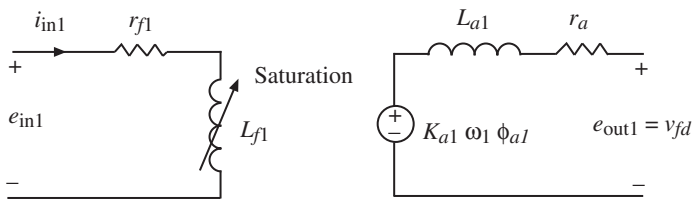


Figure 4.1 Separately excited dc machine circuit.

either a dc generator driven off the main shaft (with brushes and slip rings), an inverted ac generator driven off the main shaft (brushless with rotating diodes), or a static device such as an ac-to-dc converter fed from the synchronous machine terminals or auxiliary power (with slip rings). The main exciter may have a pilot exciter that provides the means for changing the output of the main exciter. In any case, E_{fd} normally is not manipulated directly, but is changed through the actuation of the exciter or pilot exciter.

Consider first the model for rotating dc excitors. One circuit for a separately excited dc generator is shown in Figure 4.1 [21].

Its output is the unscaled synchronous machine field voltage v_{fd} . For small r_{a1} and L_{a1} , this circuit has the dynamic model

$$e_{in1} = i_{in1}r_{f1} + \frac{d\lambda_{f1}}{dt} \quad (4.1)$$

$$v_{fd} = K_{a1}\omega_1\phi_{a1} \quad (4.2)$$

with the exciter field flux linkage related to field flux ϕ_{f1} by

$$\lambda_{f1} = N_{f1}\phi_{f1}. \quad (4.3)$$

Assuming a constant percent leakage (coefficient of dispersion σ_1), the armature flux is

$$\phi_{a1} = \frac{1}{\sigma_1}\phi_{f1}. \quad (4.4)$$

Assuming constant exciter shaft speed ω_1 ,

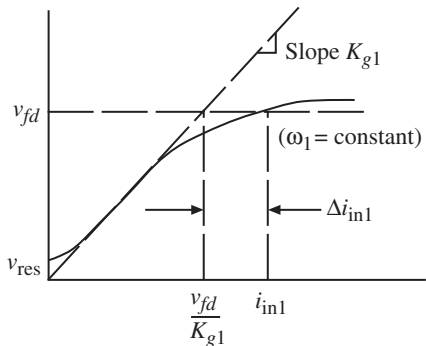
$$\lambda_{f1} = \frac{N_{f1}\sigma_1}{K_{a1}\omega_1}v_{fd}. \quad (4.5)$$

Now, the relationship between v_{fd} and i_{in1} is nonlinear due to saturation of the exciter iron, as shown in Figure 4.2. Without armature resistance or inductance, this curve is valid for open-circuit or loaded conditions. The slope of the unsaturated curve (air-gap line) is [54, 55]

$$K_{g1} = \frac{K_{a1}\omega_1}{N_{f1}\sigma_1}L_{f1us} \quad (4.6)$$

where L_{f1us} is referred to as the “unsaturated” field inductance. The saturation can be accounted for by a saturation function f_{sat} defined through Figure 4.2 as

$$f_{sat}(v_{fd}) = \Delta i_{in1}/v_{fa}. \quad (4.7)$$

Figure 4.2 Exciter saturation curve.

In terms of these quantities,

$$\lambda_{f1} = \frac{L_{f1us}}{K_{g1}} v_{fd} \quad (4.8)$$

and

$$i_{in1} = \frac{v_{fd}}{K_{g1}} + f_{sat}(v_{fd})v_{fd}. \quad (4.9)$$

With these assumptions, the unscaled exciter dynamic model is

$$e_{in1} = \frac{r_{f1}}{K_{g1}} v_{fd} + r_{f1} f_{sat}(v_{fd}) v_{fd} + \frac{L_{f1us}}{K_{g1}} \frac{dv_{fd}}{dt}. \quad (4.10)$$

This equation must now be scaled for use with the previously scaled synchronous model. Since the armature terminals of the exciter are connected directly to the terminals of the synchronous machine field winding, we must scale v_{fd} as before and use the same system power base. Thus, using (3.54), (3.59), (3.113), and (3.139), we define

$$V_R \stackrel{\Delta}{=} \frac{X_{md} e_{in1}}{R_{fd} V_{BFD}} \quad (4.11)$$

$$K_{E\text{sep}} \stackrel{\Delta}{=} \frac{r_{f1}}{K_{g1}} \quad (4.12)$$

$$T_E \stackrel{\Delta}{=} \frac{L_{f1us}}{K_{g1}} \quad (4.13)$$

$$S_E(E_{fd}) \stackrel{\Delta}{=} r_{f1} f_{sat} \left(\frac{V_{BFD} R_{fd}}{X_{md}} E_{fd} \right) \quad (4.14)$$

With these assumptions and definitions, the scaled model of a separately excited dc generator main exciter is

$$T_E \frac{dE_{fd}}{dt} = - \left(K_{E\text{sep}} + S_E(E_{fd}) \right) E_{fd} + V_R. \quad (4.15)$$

The input V_R is normally the scaled output of the amplifier (or pilot exciter), which is applied to the field of the separately excited main exciter.

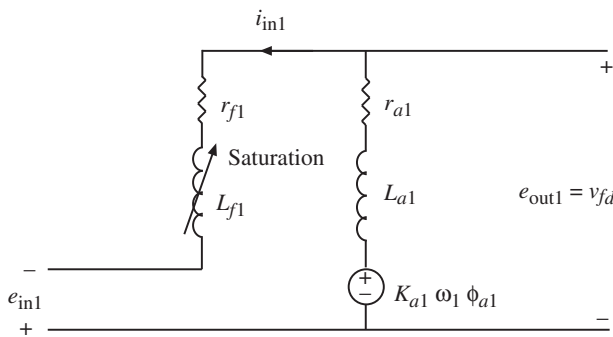


Figure 4.3 Self-excited dc generator circuit.

When the main dc generator is self-excited, this amplifier voltage appears in series with the exciter field, as shown in Figure 4.3. This field circuit has the dynamic equation

$$e_{in1} = r_{f1}i_{in1} + \frac{d\lambda_{f1}}{dt} - v_{fd} \quad (4.16)$$

with the same assumptions as above, and the new constant K_E_{self} defined as

$$K_E_{self} \stackrel{\Delta}{=} K_E_{sep} - 1. \quad (4.17)$$

The scaled model of a self-excited dc generator main exciter is, then,

$$T_E \frac{dE_{fd}}{dt} = - \left(K_E_{self} + S_E(E_{fd}) \right) E_{fd} + V_R. \quad (4.18)$$

For typical machines, K_E_{self} is a small negative number. To allow voltage buildup, it would be necessary to specify V_R to include the residual voltage that exists at zero i_{in1} , as shown in Figure 4.2. Also, if e_{in1} is replaced by a rheostat whose variable resistance is included in r_{f1} , K_E_{self} and S_E would be functions of both the actual field resistance and the rheostat resistance. This rheostat can be set to produce the required terminal voltage. In steady state with $V_R = V_{res}$ this requires

$$K_E_{self} = \left(\frac{V_{res}}{E_{fd}} \right) - S_E(E_{fd}). \quad (4.19)$$

That is, since r_{f1} includes the rheostat setting, it can be adjusted for a given steady-state condition. This would make r_{f1} , rather than V_R , a control variable.

In steady state, the exciter equation (written simply with K_E) is

$$0 = -(K_E + S_E(E_{fd}))E_{fd} + V_R. \quad (4.20)$$

The input V_R usually has a maximum $V_{R_{max}}$, which produces maximum (ceiling) excitation voltage $E_{fd_{max}}$. Since S_E is a function of this excitation level, these quantities must satisfy

$$0 = -(K_E + S_{E_{max}})E_{fd_{max}} + V_{R_{max}}. \quad (4.21)$$

When specifying exciter data, it is common to specify the saturation function through the number $S_{E_{\max}}$ and the number $S_{E_{0.75_{\max}}}$, which is the saturation level when E_{fd} is 0.75 $E_{fd_{\max}}$. A saturation function is then fitted to these two points. One typical function is

$$S_E(E_{fd}) = A_x e^{B_x E_{fd}}. \quad (4.22)$$

When evaluated at two points, this function gives

$$S_{E_{\max}} = A_x e^{B_x E_{fd_{\max}}} \quad (4.23)$$

$$S_{E_{0.75_{\max}}} = A_x e^{B_x \frac{3}{4} E_{fd_{\max}}}. \quad (4.24)$$

For given values of K_E , $V_{R_{\max}}$, $S_{E_{\max}}$, and $S_{E_{0.75_{\max}}}$, the constants A_x and B_x can be computed. This is illustrated in the following example.

Example 4.1 Given: $K_E = 1.0$, $V_{R_{\max}} = 7.3$, $S_{E_{\max}} = 0.86$, $S_{E_{0.75_{\max}}} = 0.50$ (all in pu)

Find: A_x and B_x

Solution:

From (4.20),

$$\begin{aligned} 0 &= -(1 + 0.86)E_{fd_{\max}} + 7.3 \\ 0.86 &= A_x e^{B_x E_{fd_{\max}}} \\ 0.50 &= A_x e^{B_x \frac{3}{4} E_{fd_{\max}}} \end{aligned}$$

Solving these three equations gives

$$\begin{aligned} E_{fd_{\max}} &= 3.925 \\ A_x &= 0.09826 \\ B_x &= 0.5527 \end{aligned}$$

□

Newer types of excitation systems do not use alternators. Instead, the field voltage is supplied directly from a rectifier. These are the static excitation (type ST) systems. The dynamics of the rectifier is assumed to be fast and thus neglected in the exciter model. There are two main groups of such excitors: the potential-source excitors using only the terminal bus voltage to drive the rectifiers, and the compound-source excitors using both the generator terminal bus voltage and current to drive the rectifiers. The latter system would have better performance for close-by faults, as the reduction of the bus voltage is compensated by the increase in the generator output current. These excitors typically can provide high field voltages during fault, which is beneficial for transient stability. Because of the fast response of the rectifiers, the exciter is modeled using only a first-order control loop to regulate the field voltage E_{fd} [56, 57].

References [55–57] and [78] give additional information on these and other exciter models.

4.3 Voltage Regulator Models

The exciter provides the mechanism for controlling the synchronous machine terminal voltage magnitude. In order to automatically control terminal voltage, a transducer signal must be compared to a reference voltage and amplified to produce the exciter input V_R . The amplifier can be a pilot exciter (another dc generator) or a solid-state amplifier. In either case, the amplifier is often modeled as in the last section with a limiter replacing the saturation function.

$$T_A \frac{dV_R}{dt} = -V_R + K_A V_{\text{in}} \quad (4.25)$$

$$V_R^{\min} \leq V_R \leq V_R^{\max} \quad (4.26)$$

where V_{in} is the amplifier input, T_A is the amplifier time constant, and K_A is the amplifier gain. The V_R limit can be multivalued to allow a higher limit during transients. The steady-state limit would be lower to reflect thermal constraints on the exciter and synchronous machine field winding. Recall that V_R is the scaled input to the main exciter. This voltage may be anything between zero and its limits if the main exciter is self-excited, but must be nonzero if the exciter is separately excited. We have assumed that the amplifier data have been scaled according to our given per-unit system.

If the voltage V_{in} is simply the error voltage produced by the difference between a reference voltage and a conditioned potential transformer connected to the synchronous machine terminals, the closed-loop control system can exhibit instabilities. This can be seen by noting that the self-excited dc exciter can have a negative K_E such that its open-loop eigenvalue is positive for small saturation S_E . Even without this potential instability, there is always a need to shape the regulator response to achieve desirable dynamic performance. In many standard excitation systems, this is accomplished through a stabilizing transformer whose input is connected to the output of the exciter and whose output voltage is subtracted from the amplifier input. A scaled circuit showing the transformer output as V_F is shown in Figure 4.4. If I_{t2} is initially zero and L_{t2} is very large, then I_{t2} must remain near zero.

With this assumption, an approximate dynamic model for this circuit is

$$E_{fd} = R_{t1} I_{t1} + (L_{t1} + L_{tm}) \frac{dI_{t1}}{dt} \quad (4.27)$$

$$V_F = \frac{N_2}{N_1} L_{tm} \frac{dI_{t1}}{dt} \quad (4.28)$$

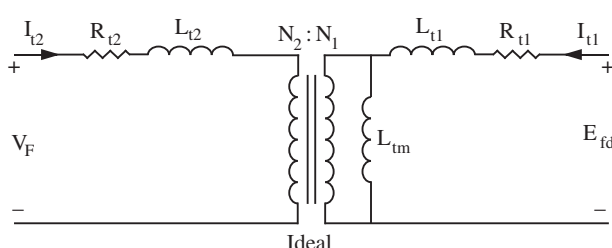


Figure 4.4 Stabilizing transformer circuit.

where V_F is a scaled output of the stabilizing transformer. Differentiating V_F and E_{fd} gives

$$\frac{dV_F}{dt} = \frac{N_2}{N_1} L_{tm} \left(\frac{1}{(L_{t1} + L_{tm})} \left(\frac{dE_{fd}}{dt} - \frac{R_{t1}}{L_{tm}} \frac{N_1}{N_2} V_F \right) \right). \quad (4.29)$$

Using (4.18) with general K_E and defining

$$T_F \triangleq \frac{L_{t1} + L_{tm}}{R_{t1}} \quad (4.30)$$

$$K_F \triangleq \frac{N_2}{N_1} \frac{L_{tm}}{R_{t1}} \quad (4.31)$$

the dynamic model of the stabilizing transformer can be written as

$$T_F \frac{dV_F}{dt} = -V_F + K_F \left(-\frac{K_E + S_E(E_{fd})}{T_E} E_{fd} + \frac{V_R}{T_E} \right). \quad (4.32)$$

Another form of this model is often used by defining

$$R_f \triangleq \frac{K_F}{T_F} E_{fd} - V_F. \quad (4.33)$$

With R_f (called rate feedback) as the dynamic state,

$$T_F \frac{dR_f}{dt} = -R_f + \frac{K_F}{T_F} E_{fd}. \quad (4.34)$$

This form will be used throughout the remainder of the text.

If the amplifier input V_{in} contained only the reference voltage minus the terminal voltage minus V_F , the voltage regulator could still have regulation and stability problems. There can be regulation problems when two or more synchronous machines are connected in parallel and each machine has an exciter plus voltage regulator. Since the synchronous machine field current has a major role in determining the reactive power output of the machine, parallel operation requires that the field currents be adjusted properly so that the machines share reactive power. This is accomplished through the addition of a load compensation circuit in the regulator, which makes the parallel operation appear as if there are two different terminal voltages even though both machines are paralleled to the same bus. This can be done by including stator current in the regulator input. To see how this can be modeled, consider the scaled terminal voltages V_a , V_b , and V_c found by transforming and rescaling V_d , V_q , and V_o . Using (3.14) with $V_o = 0$ and (3.39)

$$V_a = \sqrt{2}(V_d \sin(\omega_s t + \delta) + V_q \cos(\omega_s t + \delta)) \quad (4.35)$$

$$V_b = \sqrt{2} \left(V_d \sin \left(\omega_s t + \delta - \frac{2\pi}{3} \right) + V_q \cos \left(\omega_s t + \delta - \frac{2\pi}{3} \right) \right) \quad (4.36)$$

$$V_c = \sqrt{2} \left(V_d \sin \left(\omega_s t + \delta + \frac{2\pi}{3} \right) + V_q \cos \left(\omega_s t + \delta + \frac{2\pi}{3} \right) \right). \quad (4.37)$$

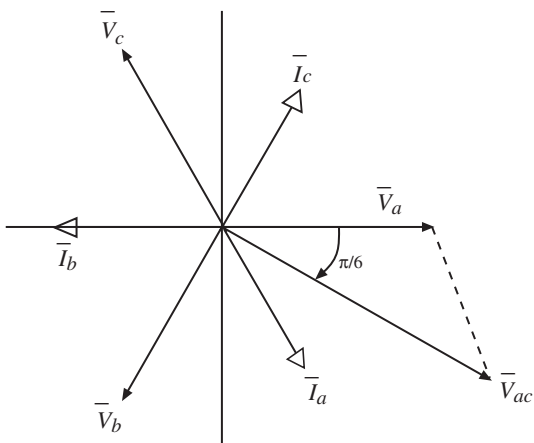


Figure 4.5 Steady-state overexcited phasor diagram.

The stator line currents I_a , I_b , and I_c are related in the same way with V_d and V_q replaced by I_d and I_q . These expressions are valid for transients as well as steady state, and can be written alternatively as

$$V_a = \sqrt{2} \sqrt{V_d^2 + V_q^2} \cos \left(\omega_s t + \delta - \frac{\pi}{2} + \tan^{-1} \frac{V_q}{V_d} \right) \quad (4.38)$$

$$V_b = \sqrt{2} \sqrt{V_d^2 + V_q^2} \cos \left(\omega_s t + \delta - \frac{\pi}{2} + \tan^{-1} \frac{V_q}{V_d} - \frac{2\pi}{3} \right) \quad (4.39)$$

$$V_c = \sqrt{2} \sqrt{V_d^2 + V_q^2} \cos \left(\omega_s t + \delta - \frac{\pi}{2} + \tan^{-1} \frac{V_q}{V_d} + \frac{2\pi}{3} \right) \quad (4.40)$$

and similarly for I_a , I_b , and I_c . To see how load compensation can be performed, consider the case of an overexcited synchronous machine (serving inductive load), with the steady-state phasor diagram of Figure 4.5. Suppose that the sensed voltage is line-to-line RMS voltage \bar{V}_{ac} ; then the uncompensated voltage is defined as

$$V_{t\text{uncomp}} \triangleq \frac{1}{\sqrt{3}} |\bar{V}_{ac}|. \quad (4.41)$$

Consider the compensated voltage defined as

$$V_{t\text{comp}} \triangleq \frac{1}{\sqrt{3}} |\bar{V}_{ac} - \alpha_{\text{comp}} \bar{I}_b| \quad (4.42)$$

where α_{comp} is some positive compensation constant. The compensated terminal voltage will differ from the uncompensated terminal voltage by an amount proportional to α_{comp} and the phase shift of \bar{I}_b . With \bar{I}_b in the position shown in the phasor diagram, and if the reference voltage is near the uncompensated value of V_t , the error signal from the compensated V_t will tell the regulator to lower the terminal voltage (the reverse of what you might expect!). When the machine is underexcited (serving capacitive load), the current \bar{I}_b will lead \bar{V}_b , and the compensated voltage will be less than the uncompensated voltage. This voltage, when compared to a reference voltage near the uncompensated voltage, will tell the regulator to raise the terminal voltage (again, the reverse of what you might expect). When two generators are operating in parallel, if the field

current on one generator becomes excessive and causes “circulating” reactive power, this reactive power will be an inductive load to the excessively excited machine and a capacitive load to the other. The compensation circuits then will cause the excessive excitation to be reduced and the other to be raised, thus balancing the reactive power loading. This type of load compensation is called parallel droop compensation. Additional types of compensation that do not result in a drop in voltage under inductive load are also available.

In terms of the dq components of \bar{V}_a , \bar{V}_c , and \bar{I}_b , we can define the compensated and uncompensated voltages as

$$V_{t\text{comp}} \triangleq \frac{1}{\sqrt{3}} \left[\left(\frac{3}{2}V_d + \frac{\sqrt{3}}{2}V_q - \alpha_{\text{comp}} I_d \right)^2 + \left(\frac{3}{2}V_q - \frac{\sqrt{3}}{2}V_d - \alpha_{\text{comp}} I_q \right)^2 \right]^{1/2}. \quad (4.43)$$

This gives

$$V_{t\text{uncomp}} = V_{t\text{comp}}|_{\alpha_{\text{comp}}=0} = \sqrt{V_d^2 + V_q^2}. \quad (4.44)$$

Example 4.2

$$\bar{V}_a = 1\angle 0^\circ, \bar{V}_b = 1\angle -120^\circ, \bar{V}_c = 1\angle 120^\circ$$

$$\bar{I}_b = 0.5\angle 180^\circ \text{ (all pu).}$$

This is a power factor $= \cos 60^\circ$ (lagging power factor load)

$$V_{t\text{uncomp}} = \frac{1}{\sqrt{3}}\sqrt{3} = 1.0$$

$$V_{t\text{comp}} = \frac{1}{\sqrt{3}} |\sqrt{3}\angle -30^\circ - \alpha_{\text{comp}} 0.5\angle 180^\circ|.$$

For $\alpha_{\text{comp}} = 0.1$

$$V_{t\text{comp}} = 1.025.$$

If the reference voltage is 1.0, the voltage regulator will attempt to *lower* the voltage by lowering E_{fd} . \square

Example 4.3 Let us use the same voltages, $\bar{I}_b = 0.5\angle -90^\circ$ (pu). This is the power factor $\cos 30^\circ$ (leading).

$$V_{t\text{uncomp}} = \frac{1}{\sqrt{3}}\sqrt{3} = 1.0$$

$$V_{t\text{comp}} = \frac{1}{\sqrt{3}} |\sqrt{3}\angle -30^\circ - 0.05\angle -90^\circ| \\ = 0.986.$$

If the reference voltage is 1.0, the voltage regulator will attempt to *raise* the voltage by raising E_{fd} . This compensation will make two parallel generators share the total reactive power output. \square

Realizing that the sensed voltage may be either compensated or uncompensated, we simply drop the subscript and write the final general expression for the amplifier input voltage using the stabilizer feedback variable R_f , rather than V_F , as

$$V_{\text{in}} = V_{\text{ref}} - V_t + R_f - \frac{K_F}{T_F} E_{fd}. \quad (4.45)$$

In this model, we have not included any dynamics for the transducer, which could be a potential transformer, filters, and smoothers. There are many other fine details about excitation systems that may be important for some simulations. In keeping with the philosophy of this text as one on fundamental dynamic modeling, we conclude this section with a summary of a fundamental model of an excitation system:

$$T_E \frac{dE_{fd}}{dt} = -(K_E + S_E(E_{fd}))E_{fd} + V_R \quad (4.46)$$

$$T_F \frac{dR_f}{dt} = -R_f + \frac{K_F}{T_F} E_{fd} \quad (4.47)$$

$$T_A \frac{dV_R}{dt} = -V_R + K_A R_f - \frac{K_A K_F}{T_F} E_{fd} + K_A (V_{\text{ref}} - V_t) \quad (4.48)$$

$$V_R^{\min} \leq V_R \leq V_R^{\max} \quad (4.49)$$

where K_E may be the previously defined separate or self-excited constant, and V_t may be either of the previously defined compensated or uncompensated terminal voltages. To be complete, the model should include an expression for S_E and an algebraic equation for V_t .

4.4 Turbine Models

The frequency of the ac voltage at the terminals of a synchronous machine is determined by its shaft speed and the number of magnetic poles of the machine. The steady-state speed of a synchronous machine is determined by the speed of the prime mover that drives its shaft. Typical prime movers are diesel engines, gasoline engines, steam turbines, hydroturbines (water wheels), and gas turbines. The prime mover output affects the input T_M in the model of the last chapter. This section presents basic models for the hydroturbine and steam turbine.

4.4.1 Hydroturbines

Hydropower plants have essentially five major components. These are the storage reservoir, intake tunnel, surge tank, penstock, and water (hydro) turbine. Precise nonlinear models of these components are not typically used in power system dynamic analysis. Alternatively, approximate linear models are used to capture the fundamental characteristics of the plant and its impact on the electrical system. Thus, the following models

should not be used for studies where large changes in turbine power are expected. Since the turbine torque is the primary variable of interest, most models are made as simple as possible while still preserving the turbine torque and speed control characteristics. The power to the water turbine depends on the position of the gate valve at the bottom of the penstock. The power is derived from the water pressure that arises due to the water head (elevation). The penstock is the water channel from the intake tunnel of the elevated reservoir down to the gate valves and turbine. The gate valve position then corresponds to a certain level of power P_{HV} at rated speed. Using scaled parameters consistent with the last chapter, a simplified model of hydroturbine small-change dynamics is [58]

$$\Delta FR = A_{11}\Delta TH + A_{12}\Delta\omega_{HT} + A_{13}\Delta P_{HV} \quad (4.50)$$

$$\Delta T_{HT} = A_{21}\Delta TH + A_{22}\Delta\omega_{HT} + A_{23}\Delta P_{HV} \quad (4.51)$$

where ΔFR is the change in water flow rate, ΔTH is the change in turbine head, $\Delta\omega_{HT}$ is the change in hydroturbine speed, and ΔT_{HT} is the change in hydroturbine output torque, all scaled consistently with the last chapter. One common model considers only two dynamic phenomena, the rate of change of flow deviation as [58]

$$\frac{d\Delta FR}{dt} = -\frac{\Delta TH}{T_w} \quad (4.52)$$

and Newton's law for the turbine mass with scaled inertia constant H_{HT}

$$\frac{d\Delta\delta_{HT}}{dt} = \Delta\omega_{HT} \quad (4.53)$$

$$\frac{2H_{HT}}{\omega_s} \frac{d\Delta\omega_{HT}}{dt} = \Delta T_{HT} - \Delta T_M \quad (4.54)$$

where T_w is the water starting time in seconds, and T_M is as previously defined for the synchronous machine shaft dynamics. The last equation allows for the case where the shaft connection between the hydroturbine output and the synchronous machine input is considered a stiff spring rather than a rigid connection. In this case, the change in torque into the synchronous machine would be

$$\Delta T_M = -K_{HM}(\Delta\delta - \Delta\delta_{HT}) \quad (4.55)$$

where K_{HM} represents the stiffness of the coupling between the turbine and the synchronous machine, and δ is the machine angle, as previously defined. While it is clearly possible to keep all terms, it is customary to assume that $A_{12}\Delta\omega_{HT}$ and $A_{22}\Delta\omega_{HT}$ are small compared to other terms.

For operation near an equilibrium point (denoted as superscript o) with

$$T_{HT}^o = A_{23}P_{HV}^o = T_M^o = -K_{HM}(\delta^o - \delta_{HT}^o) \quad (4.56)$$

and

$$\omega_{HT}^o = \omega_s \quad (4.57)$$

the actual variables are

$$T_{HT} = T_{HT}^o + \Delta T_{HT} \quad (4.58)$$

$$T_M = T_M^o + \Delta T_M \quad (4.59)$$

$$P_{HV} = P_{HV}^o + \Delta P_{HV} \quad (4.60)$$

$$\delta = \delta^o + \Delta\delta \quad (4.61)$$

$$\delta_{HT} = \delta_{HT}^o + \Delta\delta_{HT} \quad (4.62)$$

$$\omega_{HT} = \omega_{HT}^o + \Delta\omega_{HT}. \quad (4.63)$$

The hydroturbine model written in actual per-unit torques (but valid only for small changes about an equilibrium point) is written with T_{HT} as a state:

$$T_w \frac{dT_{HT}}{dt} = -\frac{1}{A_{11}} T_{HT} + \frac{A_{23}}{A_{11}} P_{HV} + T_w \left(A_{23} - \frac{A_{13}A_{21}}{A_{11}} \right) \frac{dP_{HV}}{dt} \quad (4.64)$$

$$\frac{d\delta_{HT}}{dt} = \omega_{HT} - \omega_s \quad (4.65)$$

$$\frac{2H_{HT}}{\omega_s} \frac{d\omega_{HT}}{dt} = T_{HT} - T_M \quad (4.66)$$

$$T_M = -K_{HM}(\delta - \delta_{HT}). \quad (4.67)$$

When used with the synchronous machine model, the above T_M expression must be used in the speed equation for the synchronous machine. Thus, the synchronous machine and turbine are coupled through the angles δ and δ_{HT} . The hydrovalve power P_{HV} will become a dynamic state when the hydro-governor is added. For a rigid connection, T_{HT} becomes T_M and the turbine inertia is simply added to the synchronous machine inertia H , giving only

$$T_w \frac{dT_M}{dt} = -\frac{1}{A_{11}} T_M + \frac{A_{23}}{A_{11}} P_{HV} + T_w \left(A_{23} - \frac{A_{13}A_{21}}{A_{11}} \right) \frac{dP_{HV}}{dt} \quad (4.68)$$

and T_M remains in the synchronous machine speed equation. For an ideal lossless hydro-turbine at full load [58]

$$A_{11} = 0.5, \quad A_{21} = 1.5, \quad A_{13} = 1.0, \quad A_{23} = 1.0 \quad (4.69)$$

and T_w ranges between 0.5 and 5 seconds. Additional hydroturbine models are discussed in references [58–61].

4.4.2 Steam Turbines

Steam plants consist of a fuel supply to a steam boiler that supplies a steam chest. The steam chest contains pressurized steam that enters a high-pressure (HP) turbine through a steam valve. As in the hydroturbine, the power into the high-pressure turbine is proportional to the valve opening. A nonreheat system would then terminate in the condenser and cooling systems, with the HP turbine shaft connected to the synchronous machine. It is common to include additional stages, such as the intermediate (IP) and low (LP) pressure turbines. The steam is reheated upon leaving the high-pressure turbine, and either reheated or simply crossed over between the IP and LP turbines. The dynamics that are normally represented are the steam chest delay, the reheat delay, or the crossover piping delay. In a tandem connection, all stages are on the same shaft. In a cross-compound system, the different stages may be connected on different shafts. These two shafts then supply the torque for two generators. In this analysis, we model the steam chest dynamics, the single reheat dynamics, and the mass dynamics for a two-stage (HP and LP) turbine tandem mounted. In this model, we are interested in the effect of the steam valve position (power P_{SV}) on the synchronous machine torque T_M . The

incremental steam chest dynamic model is a simple linear single time constant with unity gain, written in scaled variables consistent with the last chapter as

$$T_{CH} \frac{d\Delta P_{CH}}{dt} = -\Delta P_{CH} + \Delta P_{SV} \quad (4.70)$$

where ΔP_{CH} is the change in output power of the steam chest. This output is either converted into torque on the HP turbine or passed on to the reheat cycle. Let the fraction that is converted into torque be

$$\Delta T_{HP} = K_{HP} \Delta P_{CH} \quad (4.71)$$

and the fraction passed on to the reheater be $(1 - K_{HP})\Delta P_{CH}$. The dynamics of the HP turbine mass in incremental scaled variables are

$$\frac{d\Delta\delta_{HP}}{dt} = \Delta\omega_{HP} \quad (4.72)$$

$$\frac{2H_{HP}}{\omega_s} \frac{d\Delta\omega_{HP}}{dt} = \Delta T_{HP} - \Delta T_{HL} \quad (4.73)$$

where ΔT_{HL} is the incremental change in torque transmitted through the shaft to the LP turbine. This is modeled as a stiff spring:

$$\Delta T_{HL} = -K_{HL}(\Delta\delta_{LP} - \Delta\delta_{HP}). \quad (4.74)$$

The reheat process has a time delay that can be modeled similarly as

$$T_{RH} \frac{d\Delta P_{RH}}{dt} = -\Delta P_{RH} + (1 - K_{HP})\Delta P_{CH} \quad (4.75)$$

where ΔP_{RH} is the change in output power of the reheater. Assuming that this output is totally converted into torque on the LP turbine,

$$\Delta T_{LP} = \Delta P_{RH}. \quad (4.76)$$

The dynamics of the LP turbine mass in incremental scaled variables are

$$\frac{d\Delta\delta_{LP}}{dt} = \Delta\omega_{LP} \quad (4.77)$$

$$\frac{2H_{LP}}{\omega_s} \frac{d\Delta\omega_{LP}}{dt} = \Delta T_{HL} + \Delta T_{LP} - \Delta T_M \quad (4.78)$$

where the torque to the connection of the LP turbine to the synchronous machine is assumed to be transmitted through a stiff spring as

$$\Delta T_M = -K_{LM}(\Delta\delta - \Delta\delta_{LP}). \quad (4.79)$$

For operation near an equilibrium point (denoted by superscript o) with

$$\begin{aligned} P_{CH}^o &= P_{SV}^o, & T_{HP}^o &= T_{HL}^o = K_{HP}P_{CH}^o = -K_{HL}(\delta_{LP}^o - \delta_{HP}^o), \\ T_{LP}^o &= P_{RH}^o = (1 - K_{HP})P_{CH}^o, & \omega_{LP}^o &= \omega_s, & \omega_{HP}^o &= \omega_s, \\ T_M^o &= P_{CH}^o = -K_{LM}(\delta^o - \delta_{LP}^o) \end{aligned} \quad (4.80)$$

the actual variables are

$$P_{CH} = P_{CH}^o + \Delta P_{CH} \quad (4.81)$$

$$P_{SV} = P_{SV}^o + \Delta P_{SV} \quad (4.82)$$

$$\delta_{HP} = \delta_{HP}^o + \Delta \delta_{HP} \quad (4.83)$$

$$\omega_{HP} = \omega_{HP}^o + \Delta \omega_{HP} \quad (4.84)$$

$$P_{RH} = P_{RH}^o + \Delta P_{RH} \quad (4.85)$$

$$\delta_{LP} = \delta_{LP}^o + \Delta \delta_{LP} \quad (4.86)$$

$$\omega_{LP} = \omega_{LP}^o + \Delta \omega_{LP} \quad (4.87)$$

$$\delta = \delta^o + \Delta \delta \quad (4.88)$$

$$T_M = T_M^o + \Delta T_M. \quad (4.89)$$

The steam turbine model written in actual per-unit torques (but valid only for small changes about an equilibrium point) is written as

$$T_{CH} \frac{dP_{CH}}{dt} = -P_{CH} + P_{SV} \quad (4.90)$$

$$\frac{d\delta_{HP}}{dt} = \omega_{HP} - \omega_s \quad (4.91)$$

$$\frac{2H_{HP}}{\omega_s} \frac{d\omega_{HP}}{dt} = K_{HP}P_{CH} + K_{HL}(\delta_{LP} - \delta_{HP}) \quad (4.92)$$

$$T_{RH} \frac{dP_{RH}}{dt} = -P_{RH} + (1 - K_{HP})P_{CH} \quad (4.93)$$

$$\frac{d\delta_{LP}}{dt} = \omega_{LP} - \omega_s \quad (4.94)$$

$$\frac{2H_{LP}}{\omega_s} \frac{d\omega_{LP}}{dt} = -K_{HL}(\delta_{LP} - \delta_{HP}) + P_{RH} + K_{LM}(\delta - \delta_{LP}) \quad (4.95)$$

and T_M in the synchronous machine speed equation must be replaced by

$$T_M = -K_{LM}(\delta - \delta_{LP}). \quad (4.96)$$

The steam valve position P_{SV} will become a dynamic state when the steam-governor equations are added.

For rigid shaft couplings

$$K_{HP}P_{CH} = T_M - P_{RH} \quad (4.97)$$

and the two turbine masses are added into the synchronous machine inertia to give the following steam turbine model with T_M as a dynamic state:

$$T_{RH} \frac{dT_M}{dt} = -T_M + \left(1 - \frac{K_{HP}T_{RH}}{T_{CH}} \right) P_{CH} + \frac{K_{HP}T_{RH}}{T_{CH}} P_{SV} \quad (4.98)$$

$$T_{CH} \frac{dP_{CH}}{dt} = -P_{CH} + P_{SV} \quad (4.99)$$

and T_M remains as a state in the synchronous machine model. It is possible to add more reheat stages and additional details. It is also possible to further simplify.

For a nonreheat system, simply set $T_{RH} = 0$ in (4.98)–(4.99), and the following model is obtained:

$$T_{CH} \frac{dT_M}{dt} = -T_M + P_{SV} \quad (4.100)$$

where again T_M remains a state in the synchronous machine model and P_{SV} will become a state when the governor is added. The above non-reheat model is often referred to as a Type A steam turbine model [60, 62, 63].

4.5 Speed Governor Models

The prime mover provides the mechanism for controlling the synchronous machine speed and, hence, terminal voltage frequency. To automatically control speed (and therefore frequency), a device must sense either speed or frequency in such a way that comparison with a desired value can be used to create an error signal to take corrective action. In order to give a physical feeling to the governor process, we will derive the dynamics of what could be considered a crude (and yet practical) mechanical hydraulic governor. This illustration and the derivation were originally given by Elgerd in [64].

Figure 4.6 gives a simple schematic of a flyball speed sensor with ideal linkage to a hydraulic amplifier and piston for main valve control. Suppose that the distance of points a and e from a fixed higher horizontal reference are related to the per-unit values of a power change setting P_C and value power P_{SV} , respectively. To see how the flyball functions for some fixed P_C^0 , suppose that a load is removed from the generator such that an excess of power is being supplied to the turbine through the valve. This excess power will cause a change in generator speed $\Delta\omega$, which will increase the velocity of the flyballs and hence lower point b . Lowering point b results in a lowering of point c since they are assumed to be connected by a rigid rod. Lowering point c must either lower d (if e does not change) or raise e (if d does not change). If point d is lowered, the high-pressure fluid will enter the hydraulic servo through the lower channel and exert a force on the main piston to move up point e . Thus, in any case, lowering c results in a raising of e and a corresponding decrease in P_{SV} . The decrease in P_{SV} will eventually stop the increase in speed that initiated the movement of point b . To model this action, we analyze the linkages and note that any incremental change in the positions of points a , b , and c are related by

$$\Delta y_b = K_{ba}\Delta y_a + K_{bc}\Delta y_c. \quad (4.101)$$

Any incremental change in the position of points c , d , and e are related by

$$\Delta y_d = K_{dc}\Delta y_c + K_{de}\Delta y_e. \quad (4.102)$$

The position of point a is related to the scaled value of P_C so that

$$\Delta P_C = K_a\Delta y_a. \quad (4.103)$$

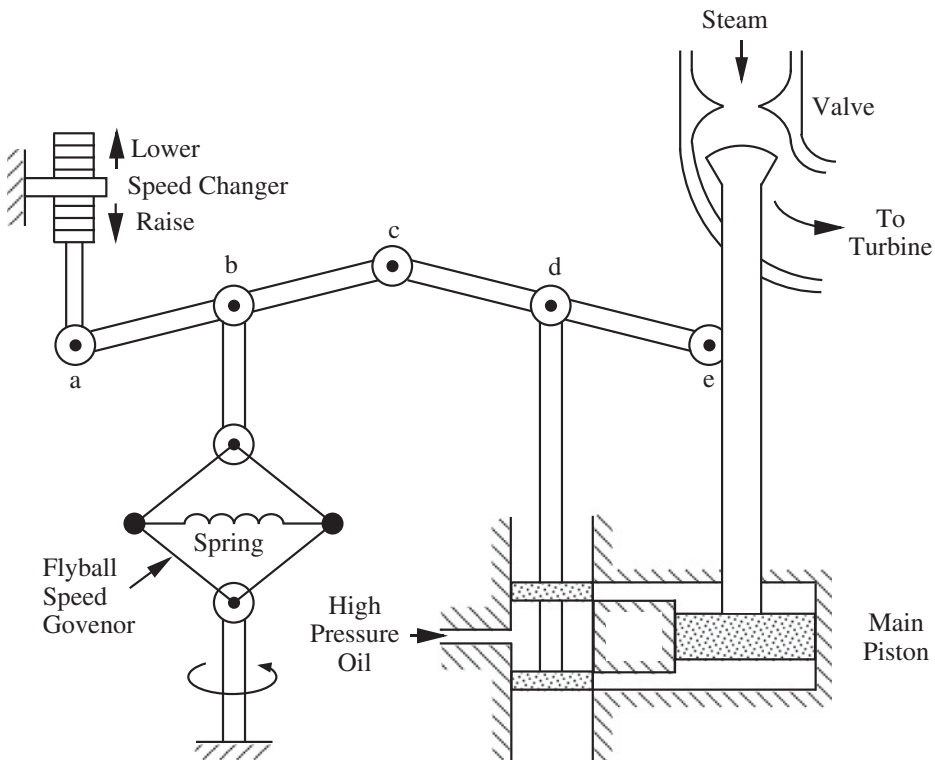


Figure 4.6 Mechanical-hydraulic speed governor [64, 65]. Source: Elgerd 1982 [64]. Reproduced with permission of McGraw Hill.

Neglecting the flyball dynamics, the position of point b changes in proportion to a change in electrical speed as

$$\Delta\omega = \omega_s K_b \Delta y_b. \quad (4.104)$$

A change in the position of point d affects the position of point e through the time delay associated with the fluid in the servo. We assume a linear dynamic response for this time delay:

$$\frac{d\Delta y_e}{dt} = -K_e \Delta y_d. \quad (4.105)$$

Substituting the linkage relations in terms of the power change setting and the speed change:

$$\begin{aligned} \frac{d\Delta y_e}{dt} &= -K_e(K_{dc}\Delta y_c + K_{de}\Delta y_e) \\ &= -K_e K_{dc} \left(\frac{\Delta y_b - K_{ba}\Delta y_a}{K_{bc}} \right) - K_e K_{de} \Delta y_e \\ &= -\frac{K_e K_{dc}}{K_{bc} K_b} \frac{\Delta\omega}{\omega_s} + \frac{K_e K_{dc} K_{ba}}{K_{bc} K_a} \Delta P_C - K_e K_{de} \Delta y_e. \end{aligned} \quad (4.106)$$

Using the proportionality between ΔP_{SV} and Δy_e as

$$\Delta y_e = \frac{K_{dc} K_{ba}}{K_{de} K_{bc} K_a} \Delta P_{SV} \quad (4.107)$$

and defining

$$\text{droop} \triangleq \frac{K_{ba} K_b}{K_a} \left(\frac{\omega_s}{2\pi} \right) \quad (4.108)$$

$$T_{SV} \triangleq \frac{1}{K_e K_{de}} \quad (4.109)$$

the incremental governor model is

$$T_{SV} \frac{d\Delta P_{SV}}{dt} = -\Delta P_{SV} + \Delta P_C - \left(\frac{\omega_s}{2\pi \text{droop}} \right) \frac{\Delta\omega}{\omega_s}. \quad (4.110)$$

The quantity “droop” is a speed droop expressed in Hz/per-unit megawatts. Alternatively, we define a speed regulation quantity R_D as

$$R_D \triangleq \frac{2\pi \text{droop}}{\omega_s} \quad (4.111)$$

For operation near an equilibrium point (denoted by superscript o) with

$$P_C^o = P_{SV}^o + \frac{1}{R_D} \left(\frac{\omega^o}{\omega_s} - 1 \right) \quad (4.112)$$

the actual per-unit variables are

$$P_{SV} = P_{SV}^o + \Delta P_{SV} \quad (4.113)$$

$$P_C = P_C^o + \Delta P_C \quad (4.114)$$

$$\omega = \omega^o + \Delta\omega. \quad (4.115)$$

In these variables, the governor model including limits on the value position is

$$T_{SV} \frac{dP_{SV}}{dt} = -P_{SV} + P_C - \frac{1}{R_D} \left(\frac{\omega}{\omega_s} - 1 \right) \quad (4.116)$$

$$0 \leq P_{SV} \leq P_{SV}^{\max} \quad (4.117)$$

In addition to the limit on the valve position P_{SV} , it may also be important to constrain the derivative of P_{SV} as rate limits. If this is done, the above model corresponds to a General Electric type EH [60].

This model is not valid for large changes, but to illustrate the significance of P_C and R_D , suppose that the machine is unloaded with $P_{SV} = P_c = 0$. If P_C is left at 0 and the machine is loaded to its rating ($P_{SV} = 1$), the full load speed would be $(1 - R_D)\omega_s$. So, if the speed regulation is set for 5% droop ($R_D = 0.05$), the change in speed between no load and full load would be 5% of the rated load. Thus, R_D can be written as

$$R_D = \frac{\% \text{ droop}}{100} \times \frac{(P_{\text{base}})_{\text{system}}}{(P_{\text{base}})_{\text{unit}}} \quad (4.118)$$

The quantity P_C is a control input that can be either a constant, or the output of an automatic generation control (AGC) scheme. To provide zero steady-state error in speed (and therefore frequency), an integral control is needed. In multimachine power systems, this load frequency control (LFC) is used together with economic dispatch to maintain frequency at minimum cost on an areawide and systemwide basis. In this case, P_C would be the output of a load reference motor, which is driven by an AGC signal based on a unit control error. While this control ideally would maintain rated frequency in steady state, the accumulated error during transients makes it necessary to have time corrections whenever the total accumulated time error passes a specified threshold [64]. These controls involve fuel and boiler dynamics that are often considered slow enough to be constants.

4.6 Problems

- 4.1** Using the steady-state exciter model of (4.20) and (4.22) with $K_E = 1.0$, $V_{R\max} = 8.0$, $S_{E\max} = 0.9$, $S_{E0.75\max} = 0.5$ (all pu), find $E_{fd\max}$, A_x , and B_x .
- 4.2** Using the exciter model of (4.46) with $K_E = 1.0$, $S_E = 0$, and $T_E = 0.5$ sec, compute the response of E_{fd} for a constant input of $V_R = 1.0$. Use an initial value of $E_{fd} = 0$ (all pu).
- 4.3** Using the exciter model of (4.18) and (4.22) with $V_R = V_{res} = 0.05$, find $K_{E\text{self}}$ so that $E_{fd} = 1.0$ when $A_x = 0.1$ and $B_x = 0.6$ (all pu).
- 4.4** Using the answer to Problem 4.3, compute the response of E_{fd} for $T_E = 0.5$ sec when it starts at zero. This requires the solution of a nonlinear differential equation.
- 4.5** Using the excitation system models of (4.46)–(4.49), construct a block diagram in the Laplace domain that shows the control system with inputs V_{ref} and V_t , and output E_{fd} .
- 4.6** Repeat Problem 4.5 using V_F as a dynamic state, rather than R_f .
- 4.7** Starting with the dynamic model of (4.46)–(4.49), derive the following dynamic model (a fast static exciter/regulator):

$$T \frac{dE_{fd}}{dt} = -E_{fd} + K(V_{ref} - V_t).$$

- 4.8** Using the turbine/governor model of (4.100) and (4.116), with

$$\begin{aligned} T_{SV} &= 0.2 \text{ sec} & P_C &= 0.7 \text{ pu} & R_D &= 0.05 \text{ pu} \\ T_{CH} &= 0.4 \text{ sec} & \omega_s &= 2\pi 60 \text{ r/s} \end{aligned}$$

- (a) Find the steady-state values of P_{SV} and T_M if $\omega = 376.9$ r/s.
- (b) Find the dynamic response of P_{SV} and T_M if ω changes at time zero to be 376.8 r/s.

5

Single-Machine Dynamic Models

5.1 Terminal Constraints

Throughout Chapters 3 and 4, the constraints on I_d , I_q , I_o and V_d , V_q , V_o have been left unspecified. Perhaps the simplest terminal constraint that could be specified is that of an ideal balanced three-phase resistive load (R_{load} in per unit). This terminal constraint is

$$V_d = I_d R_{\text{load}} \quad (R_{\text{load}} < \infty) \quad (5.1)$$

$$V_q = I_q R_{\text{load}} \quad (R_{\text{load}} < \infty) \quad (5.2)$$

$$V_o = I_o R_{\text{load}} \quad (R_{\text{load}} < \infty) \quad (5.3)$$

and

$$I_d = I_q = I_o = 0 \quad (R_{\text{load}} = \infty). \quad (5.4)$$

The most commonly used terminal constraint for a single machine is the notorious infinite bus. In most power engineering terminology, an infinite bus is an ideal sinusoidal voltage source with constant magnitude, frequency, and phase. In three-phase systems, this implies an ideal balanced symmetrical three-phase set such as

$$V_a = \sqrt{2} V_s \cos(\omega_s t + \theta_{vs}) \quad (5.5)$$

$$V_b = \sqrt{2} V_s \cos\left(\omega_s t + \theta_{vs} - \frac{2\pi}{3}\right) \quad (5.6)$$

$$V_c = \sqrt{2} V_s \cos\left(\omega_s t + \theta_{vs} + \frac{2\pi}{3}\right). \quad (5.7)$$

This is a positive phase sequence (*ABC*) set written in per-unit so that $V_s = 1.0$ for rated voltage and $\omega_s = 2\pi f_s$ for rated frequency f_s . In many studies, θ_{vs} is arbitrarily selected as zero. It is useful to know how a synchronous machine dynamic model can be made into an infinite bus. We begin by using the dynamic models of (3.148)–(3.159), (4.46)–(4.49), (4.100), and (4.116)–(4.117) with V_t defined through (4.43) and (4.44). As discussed

earlier, the “ a phase” voltage of the machine during transients and steady state is

$$V_a = \sqrt{2} \sqrt{V_d^2 + V_q^2} \cos \left(\omega_s t + \delta - \frac{\pi}{2} + \tan^{-1} \frac{V_q}{V_d} \right) \quad (5.8)$$

To qualify as an infinite bus, we must have

$$\sqrt{V_d^2 + V_q^2} = V_\infty \quad (\text{a constant}) \quad (5.9)$$

and

$$\delta - \frac{\pi}{2} + \tan^{-1} \frac{V_q}{V_d} = \theta_{v\infty} \quad (\text{a constant}) \quad (5.10)$$

Clearly, we must find parameter values that result in constants V_d , V_q , and δ .

Considering the voltage magnitude first, there are two ways in which $\sqrt{V_d^2 + V_q^2}$ can be made a constant. The first involves an infinitely high-gain voltage regulator with an infinitely fast amplifier and exciter. This makes the field winding flux linkage infinitely fast so that V_t is constant for all disturbances. This method, however, does not constrain V_d and V_q to be individually constant, and thus there is no way to force $\theta_{v\infty}$ to be constant. The second way to force the terminal voltage magnitude to be constant is actually the opposite of the high-gain regulator approach. Rather than force the field winding to be infinitely fast, we force it to be infinitely slow by letting T'_{do} equal infinity. In addition, we let T'_{qo} go to infinity as well as the machine inertia H . To complete the infinite bus specifications, we let R_s , X'_d , X'_q , T''_{do} , and T''_{qo} be zero. To see the result, we write the model (3.148) –(3.159) with these parameters:

$$\frac{1}{\omega_s} \frac{d\psi_{d\infty}}{dt} = \frac{\omega_\infty}{\omega_s} \psi_{q\infty} + V_{d\infty} \quad (5.11)$$

$$\frac{1}{\omega_s} \frac{d\psi_{q\infty}}{dt} = -\frac{\omega_\infty}{\omega_s} \psi_{d\infty} + V_{q\infty} \quad (5.12)$$

$$\frac{1}{\omega_s} \frac{d\psi_{o\infty}}{dt} = V_{o\infty} \quad (5.13)$$

$$\frac{dE'_{q\infty}}{dt} = 0 \quad (5.14)$$

$$\frac{dE'_{d\infty}}{dt} = 0 \quad (5.15)$$

$$\frac{d\delta_\infty}{dt} = \omega_\infty - \omega_s \quad (5.16)$$

$$\frac{d\omega_\infty}{dt} = 0 \quad (5.17)$$

$$\psi_{d\infty} = E'_{q\infty} \quad (5.18)$$

$$\psi_{q\infty} = -E'_{d\infty}. \quad (5.19)$$

For $\omega_\infty(o) = \omega_s$, this model requires

$$E'_{q\infty} = E'_{q\infty}(0) \quad (5.20)$$

$$E'_{d\infty} = E'_{d\infty}(0) \quad (5.21)$$

$$\delta_\infty = \delta_\infty(0) \quad (5.22)$$

$$\psi_{d\infty} = E'_{q\infty}(0) \quad (5.23)$$

$$\psi_{q\infty} = -E'_{d\infty}(0) \quad (5.24)$$

which then gives

$$V_{d\infty} = E'_{d\infty}(0) \quad (5.25)$$

$$V_{q\infty} = E'_{q\infty}(0) \quad (5.26)$$

which satisfies the requirements of an infinite bus.

Consider the model of a synchronous machine connected to an infinite bus through a balanced three-phase line in unscaled parameters:

$$v_a = -i_a r_e - \frac{d\lambda_{ea}}{dt} + \sqrt{2}v_s \cos(\omega_s t + \theta_{vs}) \quad (5.27)$$

$$v_b = -i_b r_e - \frac{d\lambda_{eb}}{dt} + \sqrt{2}v_s \cos\left(\omega_s t + \theta_{vs} - \frac{2\pi}{3}\right) \quad (5.28)$$

$$v_c = -i_c r_e - \frac{d\lambda_{ec}}{dt} + \sqrt{2}v_s \cos\left(\omega_s t + \theta_{vs} + \frac{2\pi}{3}\right) \quad (5.29)$$

with

$$\begin{bmatrix} \lambda_{ea} \\ \lambda_{eb} \\ \lambda_{ec} \end{bmatrix} = \begin{bmatrix} L_{es} & L_{em} & L_{em} \\ L_{em} & L_{es} & L_{em} \\ L_{em} & L_{em} & L_{es} \end{bmatrix} \begin{bmatrix} i_a \\ i_b \\ i_c \end{bmatrix}. \quad (5.30)$$

Transformation and scaling consistent with Chapter 3 give the following terminal constraints in per-unit:

$$V_d = R_e I_d + \frac{\omega}{\omega_s} \psi_{eq} - \frac{1}{\omega_s} \frac{d\psi_{ed}}{dt} + V_s \sin(\delta - \theta_{vs}) \quad (5.31)$$

$$V_q = R_e I_q - \frac{\omega}{\omega_s} \psi_{ed} - \frac{1}{\omega_s} \frac{d\psi_{eq}}{dt} + V_s \cos(\delta - \theta_{vs}) \quad (5.32)$$

$$V_o = R_e I_o - \frac{1}{\omega_s} \frac{d\psi_{eo}}{dt} \quad (5.33)$$

with

$$\psi_{ed} = X_{ep}(-I_d) \quad (5.34)$$

$$\psi_{eq} = X_{ep}(-I_q) \quad (5.35)$$

$$\psi_{eo} = X_{eo}(-I_o). \quad (5.36)$$

Note that V_s is the RMS per-unit infinite bus voltage, and all quantities are scaled on the machine ratings. It is customary to set θ_{vs} equal to zero, since one angle in any system can always be arbitrarily selected as a reference for all other angles. We will leave this angle as θ_{vs} for now.

While other terminal constraints can be specified, the infinite bus is the most widely used for single-machine analysis, partly because it has been traditional to study a single generator with the entire remaining network as a Thevenin equivalent impedance and voltage source. Such equivalents are clearly valid only for some steady-state conditions. Other uses of infinite bus models for machines have arisen recently as mechanisms for avoiding the problems associated with a reference angle and steady-state speed. Clearly, with an infinite bus in a system, the steady-state speed for synchronous machines must be ω_s , and the reference angle is conveniently specified. Because of their wide use, the remainder of this chapter is devoted to the analysis of single-machine infinite bus systems. It is also useful for illustrating several concepts of time scales in synchronous machines that will help in the extension to multimachine systems.

While the following sections are written to follow naturally, the Appendix gives an introduction to integral manifolds and singular perturbation, and provides the basic fundamentals used in the following sections to develop reduced-order models.

5.2 The Multi-Time-Scale Model

In this section, we study the special case of a single machine connected to an infinite bus. In particular, we use the synchronous machine model of (3.148)–(3.159), the exciter/AVR model of (4.46)–(4.49) without load compensation, the turbine/governor model of (4.100) and (4.116)–(4.117), and the terminal constraint of (5.31)–(5.33) and (5.34)–(5.36). Before combining these, we introduce the following scaled speed and time constant

$$\omega_t \stackrel{\Delta}{=} T_s(\omega - \omega_s) \quad (5.37)$$

$$T_s \stackrel{\Delta}{=} \sqrt{\frac{2H}{\omega_s}} \quad (5.38)$$

and the parameter

$$\epsilon \stackrel{\Delta}{=} \frac{1}{\omega_s} \quad (5.39)$$

where we assume that H is large enough so that

$$\epsilon \ll T_s. \quad (5.40)$$

We also combine the machine and line flux linkages and parameters as follows:

$$\begin{aligned} \psi_{de} &\stackrel{\Delta}{=} \psi_d + \psi_{ed}, \quad \psi_{qe} \stackrel{\Delta}{=} \psi_q + \psi_{eq}, \quad \psi_{oe} \stackrel{\Delta}{=} \psi_o + \psi_{eo}, \\ X_{de} &\stackrel{\Delta}{=} X_d + X_{ep}, \quad X_{qe} \stackrel{\Delta}{=} X_q + X_{ep}, \quad X'_{de} \stackrel{\Delta}{=} X'_d + X_{ep}, \\ X'_{qe} &\stackrel{\Delta}{=} X'_q + X_{ep}, \quad X''_{de} \stackrel{\Delta}{=} X''_d + X_{ep}, \quad X''_{qe} \stackrel{\Delta}{=} X''_q + X_{ep}, \\ R_{se} &\stackrel{\Delta}{=} R_s + R_e, \quad X_{\ell se} \stackrel{\Delta}{=} X_{\ell s} + X_{ep}. \end{aligned} \quad (5.41)$$

Substituting (5.31)–(5.33) into (3.148)–(3.159) and adding the other dynamic models give the following multi-time-scale model:

$$\epsilon \frac{d\psi_{de}}{dt} = R_{se} I_d + \left(1 + \frac{\epsilon}{T_s} \omega_t\right) \psi_{qe} + V_s \sin(\delta - \theta_{vs}) \quad (5.42)$$

$$\epsilon \frac{d\psi_{qe}}{dt} = R_{se} I_q - \left(1 + \frac{\epsilon}{T_s} \omega_t\right) \psi_{de} + V_s \cos(\delta - \theta_{vs}) \quad (5.43)$$

$$\epsilon \frac{d\psi_{oe}}{dt} = R_{se} I_o \quad (5.44)$$

$$T'_{do} \frac{dE'_q}{dt} = -E'_q - (X_d - X'_d) \left[I_d - \frac{X'_d - X''_d}{(X'_d - X'_{\ell s})^2} (\psi_{1d} + (X'_d - X'_{\ell s}) I_d - E'_q) \right] + E_{fd} \quad (5.45)$$

$$T''_{do} \frac{d\psi_{1d}}{dt} = -\psi_{1d} + E'_q - (X'_d - X'_{\ell s}) I_d \quad (5.46)$$

$$T'_{qo} \frac{dE'_d}{dt} = -E'_d + (X_q - X'_q) \left[I_q - \frac{X'_q - X''_q}{(X'_q - X'_{\ell s})^2} (\psi_{2q} + (X'_q - X'_{\ell s}) I_q + E'_d) \right] \quad (5.47)$$

$$T''_{qo} \frac{d\psi_{2q}}{dt} = -\psi_{2q} - E'_d - (X'_q - X'_{\ell s}) I_q \quad (5.48)$$

$$T_s \frac{d\delta}{dt} = \omega_t \quad (5.49)$$

$$T_s \frac{d\omega_t}{dt} = T_M - (\psi_{de} I_q - \psi_{qe} I_d) - T_{FW} \quad (5.50)$$

$$\psi_{de} = -X''_{de} I_d + \frac{(X''_d - X'_{\ell s})}{(X'_d - X'_{\ell s})} E'_q + \frac{(X'_d - X''_d)}{(X'_d - X'_{\ell s})} \psi_{1d} \quad (5.51)$$

$$\psi_{qe} = -X''_{qe} I_q - \frac{(X''_q - X'_{\ell s})}{(X'_q - X'_{\ell s})} E'_d + \frac{(X'_q - X''_q)}{(X'_q - X'_{\ell s})} \psi_{2q} \quad (5.52)$$

$$\psi_{oe} = -X_{oe} I_o \quad (5.53)$$

$$T_E \frac{dE_{fd}}{dt} = -(K_E + S_E(E_{fd})) E_{fd} + V_R \quad (5.54)$$

$$T_F \frac{dR_f}{dt} = -R_f + \frac{K_F}{T_F} E_{fd} \quad (5.55)$$

$$T_A \frac{dV_R}{dt} = -V_R + K_A R_f - \frac{K_A K_F}{T_F} E_{fd} + K_A (V_{ref} - V_t) \quad (5.56)$$

$$V_R^{\min} \leq V_R \leq V_R^{\max} \quad (5.57)$$

$$V_t = \sqrt{V_d^2 + V_q^2} \quad (5.58)$$

$$V_d = R_e I_d + \left(1 + \frac{\epsilon}{T_s} \omega_t\right) \psi_{eq} - \epsilon \frac{d\psi_{ed}}{dt} + V_s \sin(\delta - \theta_{vs}) \quad (5.59)$$

$$V_q = R_e I_q - \left(1 + \frac{\epsilon}{T_s} \omega_t\right) \psi_{ed} - \epsilon \frac{d\psi_{eq}}{dt} + V_s \cos(\delta - \theta_{vs}) \quad (5.60)$$

$$\psi_{ed} = -X_{ep}I_d \quad (5.61)$$

$$\psi_{eq} = -X_{ep}I_q \quad (5.62)$$

$$T_{CH} \frac{dT_M}{dt} = -T_M + P_{SV} \quad (5.63)$$

$$T_{SV} \frac{dP_{SV}}{dt} = -P_{SV} + P_C - \epsilon \frac{\omega_t}{R_D T_S} \quad (5.64)$$

$$0 \leq P_{SV} \leq P_{SV}^{\max}. \quad (5.65)$$

This model could be put in closed form without algebraic equations by solving (5.51)–(5.53) and (5.61)–(5.62) for I_d , I_q , I_o , ψ_{ed} , and ψ_{eq} and substituting into the remaining differential equations, and by replacing the derivative terms in (5.59) and (5.60) with their respective functions, and substitution into (5.58) and (5.56).

This single-machine/infinite bus model has several classifications of dynamic time scales. The stator transients of ψ_{de} and ψ_{qe} are very fast relative to other dynamics. This shows up in the model as a small “time constant” ϵ multiplying their derivatives. The damper flux linkages ψ_{1d} and ψ_{2q} are also quite fast, since T_{do}'' and T_{qo}'' typically are quite small. The voltage regulator states E_{fd} and V_R tend to be fast because T_E and T_A are typically small. The field winding and rate feedback states E'_q , R_f tend to be slow because T'_{do} and T_F can be relatively large. The turbine/governor states T_M , P_{SV} tend to be slow because T_{CH} and T_{SV} can be relatively large. This can be countered, however, by a small speed regulation R_D . The damper-winding flux linkage E'_d can be either fast or slow, depending on T'_{qo} . These classifications should be considered as general rule-of-thumb guidelines, and not absolute characteristics. The actual time-scale classification for a specific set of data can be quite different than that stated above, and can change between load levels.

The time-scale characteristics of a model are important since they determine the step size required in a time simulation. If a model contains fast dynamics, a small step size is needed. If the phenomenon of interest in a time simulation is known to be a predominantly average or slow response, it would be very helpful if the fast dynamics could be eliminated. They must be eliminated properly, so that their effect on the slower phenomena of interest is still preserved. Only in rare cases can fast dynamics be “eliminated” exactly. One such case is given in the next section.

5.3 Elimination of Stator/Network Transients

We begin this section by considering the special case of zero stator and network resistance. For this special (although common) assumption, (5.42)–(5.44) and (5.49) are

$$\epsilon \frac{d\psi_{de}}{dt} = \left(1 + \frac{\epsilon}{T_s} \omega_t\right) \psi_{qe} + V_s \sin(\delta - \theta_{vs}) \quad (5.66)$$

$$\epsilon \frac{d\psi_{qe}}{dt} = - \left(1 + \frac{\epsilon}{T_s} \omega_t\right) \psi_{de} + V_s \cos(\delta - \theta_{vs}) \quad (5.67)$$

$$\epsilon \frac{d\psi_{oe}}{dt} = 0 \quad (5.68)$$

$$T_s \frac{d\delta}{dt} = \omega_t. \quad (5.69)$$

The first three differential equations have an explicit solution in terms of δ :

$$\psi_{de} = V_s \cos(\delta - \theta_{vs}) \quad (5.70)$$

$$\psi_{qe} = -V_s \sin(\delta - \theta_{vs}) \quad (5.71)$$

$$\psi_{oe} = 0. \quad (5.72)$$

This can be verified by substituting (5.70)–(5.72) into (5.66)–(5.69) and observing an exact identity. If the initial conditions on ψ_{de} , ψ_{qe} , ψ_{oe} , and δ satisfy (5.70)–(5.72), then ψ_{de} , ψ_{qe} , and ψ_{oe} are related to δ through (5.70)–(5.72) for all time. This makes (5.70)–(5.72) an integral manifold for ψ_{de} , ψ_{qe} , and ψ_{oe} . If the initial conditions do not satisfy (5.70)–(5.72) (the system starts off the manifold), there is still an exact explicit solution for ψ_{de} , ψ_{qe} , and ψ_{oe} as a function of δ and time t . This interesting fact about synchronous machine stator transients has been explained in considerable detail in [66] through [68]. The result is as follows. For any initial conditions ψ_{de}^o , ψ_{qe}^o , ψ_{oe}^o , δ^o , t_o and for any ϵ , the exact solutions of the differential equations (5.66)–(5.68) are

$$\psi_{de} = c_1 \cos(\omega_s t + \delta - c_2) + V_s \cos(\delta - \theta_{vs}) \quad (5.73)$$

$$\psi_{qe} = -c_1 \sin(\omega_s t + \delta - c_2) - V_s \sin(\delta - \theta_{vs}) \quad (5.74)$$

$$\psi_{oe} = c_3 \quad (5.75)$$

with

$$c_1 = [(\psi_{de}^o - V_s \cos(\delta^o - \theta_{vs}))^2 + (\psi_{qe}^o + V_s \sin(\delta^o - \theta_{vs}))^2]^{\frac{1}{2}} \quad (5.76)$$

$$c_2 = \omega_s t_o + \delta^o + \tan^{-1} \left(\frac{\psi_{qe}^o + V_s \sin(\delta^o - \theta_{vs})}{\psi_{de}^o - V_s \cos(\delta^o - \theta_{vs})} \right) \quad (5.77)$$

$$c_3 = \psi_{oe}^o. \quad (5.78)$$

Clearly, if the initial conditions are on the manifold (satisfy (5.70)–(5.72)), this solution simplifies to the manifold itself ((5.70)–(5.72)). We emphasize that this interesting solution is valid for any ϵ , and requires only $R_{se} = 0$. This solution does, however, show the importance of R_{se} . If the initial condition is off the manifold, the exact solution of (5.73)–(5.75) reveals a sustained oscillation in ψ_{de} and ψ_{qe} , which means that the machine will never reach a constant speed equilibrium condition. Evidently, the resistance acts to damp out this oscillation in the actual model, keeping R_{se} .

When resistance R_{se} is not zero, an integral manifold for ψ_{de} , ψ_{qe} , and ψ_{oe} has been shown to exist only for the case in which ϵ is sufficiently small [66]–[68]. A first approximation of this integral manifold (keeping R_{se}) can be found by setting ϵ equal to zero on the left-hand side of (5.42)–(5.65) and solving the algebraic equations on the right-hand side for ψ_{de} , ψ_{qe} and ψ_{oe} as functions of all remaining dynamic states. As a matter of consistency, ϵ can also be set to zero on the right-hand side of (5.42)–(5.65). In either case, the resulting reduced-order model should approximate the exact model up to an “order ϵ ” error [69, 70]. If the ϵ in (5.64) is set to zero, the turbine/governor dynamics would no longer depend on shaft speed. It could be argued that since R_D is usually also

quite small, the ratio of ϵ/R_D should be kept and, thus, keep governor dynamics. For ϵ sufficiently small, this reduced-order model can be improved to virtually any order of accuracy (see Appendix).

It is customary to set ϵ equal to zero in (5.42)–(5.44) and (5.59)–(5.60) to give the following approximation of the exact stator transients integral manifold written together with the original algebraic equations for currents:

$$0 = R_{se}I_d + \psi_{qe} + V_s \sin(\delta - \theta_{vs}) \quad (5.79)$$

$$0 = R_{se}I_q - \psi_{de} + V_s \cos(\delta - \theta_{vs}) \quad (5.80)$$

$$0 = R_{se}I_o \quad (5.81)$$

$$\psi_{de} = -X''_{de}I_d + \frac{(X''_d - X'_{\ell s})}{(X'_d - X'_{\ell s})}E'_q + \frac{(X'_d - X''_d)}{(X'_d - X'_{\ell s})}\psi_{1d} \quad (5.82)$$

$$\psi_{qe} = -X''_{qe}I_q - \frac{(X''_q - X'_{\ell s})}{(X'_q - X'_{\ell s})}E'_d + \frac{(X'_q - X''_q)}{(X'_q - X'_{\ell s})}\psi_{2q} \quad (5.83)$$

$$\psi_{oe} = -X_{oe}I_o. \quad (5.84)$$

These six algebraic equations clearly can be solved for the six variables ψ_{de} , ψ_{qe} , ψ_{oe} , I_d , I_q , and I_o as functions of δ , E'_q , E'_d , ψ_{1d} , and ψ_{2q} . If R_{se} is equal to zero, this approximation of the integral manifold becomes exact (compare (5.70)–(5.72) and (5.79)–(5.84)).

With the above results, the dynamic model has been reduced from a 14th-order model to an 11th-order model. The solution of (5.79)–(5.84) for ψ_{oe} and I_o is trivial, and ψ_{de} , ψ_{qe} can be eliminated, leaving only two equations to be solved for I_d and I_q as functions of δ , E'_q , E'_d , ψ_{1d} , and ψ_{2q} :

$$0 = R_{se}I_d - X''_{qe}I_q - \frac{(X''_q - X'_{\ell s})}{(X'_q - X'_{\ell s})}E'_d + \frac{(X'_q - X''_q)}{(X'_q - X'_{\ell s})}\psi_{2q} + V_s \sin(\delta - \theta_{vs}) \quad (5.85)$$

$$0 = R_{se}I_q + X''_{de}I_d - \frac{(X''_d - X'_{\ell s})}{(X'_d - X'_{\ell s})}E'_q - \frac{(X'_d - X''_d)}{(X'_d - X'_{\ell s})}\psi_{1d} + V_s \cos(\delta - \theta_{vs}) \quad (5.86)$$

These two real equations can be used to solve for I_d and I_q . They can also be used to make one complex equation and an interesting “dynamic” circuit. Adding (5.85) plus j times (5.86) and multiplying by $e^{j(\delta-\pi/2)}$ give the following “circuit” equation:

$$\begin{aligned} & \left[\left[\frac{(X''_q - X'_{\ell s})}{(X'_q - X'_{\ell s})}E'_d - \frac{(X'_q - X''_q)}{(X'_q - X'_{\ell s})}\psi_{2q} + (X''_q - X''_d)I_q \right] \right. \\ & \quad \left. + j \left[\frac{(X''_d - X'_{\ell s})}{(X'_d - X'_{\ell s})}E'_q + \frac{(X'_d - X''_d)}{(X'_d - X'_{\ell s})}\psi_{1d} \right] \right] e^{j(\delta-\pi/2)} \\ & = (R_s + jX''_d)(I_d + jI_q)e^{j(\delta-\pi/2)} + (R_e + jX_{ep})(I_d + jI_q)e^{j(\delta-\pi/2)} + V_s e^{j\theta_{vs}} \end{aligned} \quad (5.87)$$

From (5.58)–(5.60) with $\epsilon = 0$,

$$V_t = \sqrt{V_d^2 + V_q^2} \quad (5.88)$$

$$V_d = R_e I_d - X_{ep} I_q + V_s \sin(\delta - \theta_{vs}) \quad (5.89)$$

$$V_q = R_e I_q + X_{ep} I_d + V_s \cos(\delta - \theta_{vs}) \quad (5.90)$$

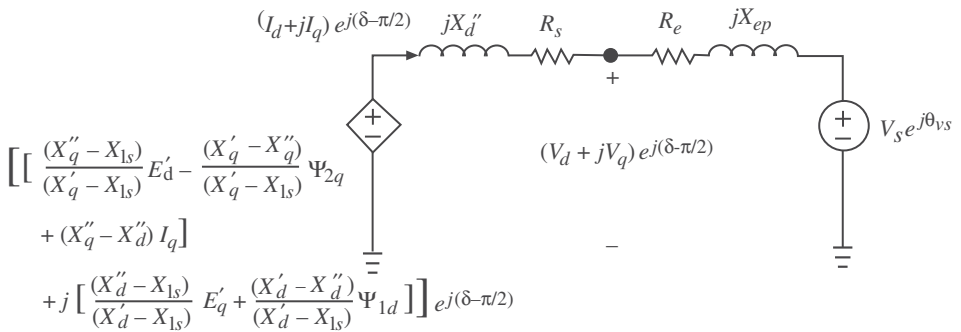


Figure 5.1 Synchronous machine sub-transient dynamic circuit.

These last two equations can be written as one complex equation.

$$(V_d + jV_q) e^{j(\delta - \pi/2)} = (R_e + jX_{ep})(I_d + jI_q) e^{j(\delta - \pi/2)} + V_s e^{j\theta_{vs}} \quad (5.91)$$

Equations (5.87) and (5.91) can be expressed as a “dynamic equivalent circuit” with a controlled source voltage behind X''_d , as shown in Figure 5.1. This circuit does not imply anything about steady state, but merely reflects the consequence of setting $\epsilon = 0$ in the original full dynamic model. Such a circuit is clearly not a unique representation of these algebraic equations. Many other similar circuits can be created by simply adding or subtracting reactances in the line and modifying the internal “source” accordingly [71].

An interesting and useful observation about this circuit is that the “real power from the internal source” is exactly equal to the electrical torque in the air gap (T_{ELEC}).

$$\begin{aligned}
 P_{\text{from source}} &= \left[\frac{(X''_q - X'_{ls})}{(X'_q - X'_{ls})} E'_d - \frac{(X'_q - X''_q)}{(X'_q - X'_{ls})} \Psi_{2q} + (X''_q - X''_d) I_q \right] I_d \\
 &\quad + \left[\frac{(X''_d - X'_{ls})}{(X'_d - X'_{ls})} E'_q + \frac{(X'_d - X''_d)}{(X'_d - X'_{ls})} \Psi_{1d} \right] I_q.
 \end{aligned}$$

From (5.44) and (5.82) to (5.83):

$$\begin{aligned}
 T_{ELEC} &= \left[-X''_{de} I_d + \frac{(X''_d - X'_{ls})}{(X'_d - X'_{ls})} E'_q + \frac{(X'_d - X''_d)}{(X'_d - X'_{ls})} \Psi_{1d} \right] I_q \\
 &\quad - \left[-X''_{qe} I_q - \frac{(X''_q - X'_{ls})}{(X'_q - X'_{ls})} E'_d + \frac{(X'_q - X''_q)}{(X'_q - X'_{ls})} \Psi_{2q} \right] I_d.
 \end{aligned}$$

These are clearly equal, since the reactances X''_{de} and X''_{qe} each contain X_{ep} .

The final form of this model that has eliminated the stator/network transients by setting $\epsilon = 0$ on the left and right sides of (5.42)–(5.65) (except for (5.64), where we have chosen to keep the governor by arguing that R_D can be small) can be written in terms of

the original variables as

$$T'_{do} \frac{dE'_q}{dt} = -E'_q - (X_d - X'_d) \left[I_d - \frac{X'_d - X''_d}{(X'_d - X'_{\ell s})^2} (\psi_{1d} + (X'_d - X'_{\ell s})I_d - E'_q) \right] + E_{fd} \quad (5.92)$$

$$T''_{do} \frac{d\psi_{1d}}{dt} = -\psi_{1d} + E'_q - (X'_d - X'_{\ell s})I_d \quad (5.93)$$

$$T'_{qo} \frac{dE'_d}{dt} = -E'_d + (X_q - X'_q) \left[I_q - \frac{X'_q - X''_q}{(X'_q - X'_{\ell s})^2} (\psi_{2q} + (X'_q - X'_{\ell s})I_q + E'_d) \right] \quad (5.94)$$

$$T''_{qo} \frac{d\psi_{2q}}{dt} = -\psi_{2q} - E'_d - (X'_q - X'_{\ell s})I_q \quad (5.95)$$

$$\frac{d\delta}{dt} = \omega - \omega_s \quad (5.96)$$

$$\begin{aligned} \frac{2H}{\omega_s} \frac{d\omega}{dt} &= T_M - \frac{(X''_d - X'_{\ell s})}{(X'_d - X'_{\ell s})} E'_q I_q - \frac{(X'_d - X''_d)}{(X'_d - X'_{\ell s})} \psi_{1d} I_q - \frac{(X''_q - X'_{\ell s})}{(X'_q - X'_{\ell s})} E'_d I_d \\ &\quad + \frac{(X'_q - X''_q)}{(X'_q - X'_{\ell s})} \psi_{2q} I_d - (X''_q - X''_d) I_d I_q - T_{FW} \end{aligned} \quad (5.97)$$

$$T_E \frac{dE_{fd}}{dt} = -(K_E + S_E(E_{fd}))E_{fd} + V_R \quad (5.98)$$

$$T_F \frac{dR_f}{dt} = -R_f + \frac{K_F}{T_F} E_{fd} \quad (5.99)$$

$$T_A \frac{dV_R}{dt} = -V_R + K_A R_f - \frac{K_A K_F}{T_F} E_{fd} + K_A (V_{ref} - V_t) \quad (5.100)$$

$$T_{CH} \frac{dT_M}{dt} = -T_M + P_{SV} \quad (5.101)$$

$$T_{SV} \frac{dP_{SV}}{dt} = -P_{SV} + P_C - \frac{1}{R_D} \left(\frac{\omega}{\omega_s} - 1 \right) \quad (5.102)$$

with the limit constraints

$$V_R^{\min} \leq V_R \leq V_R^{\max} \quad (5.103)$$

$$0 \leq P_{SV} \leq P_{SV}^{\max} \quad (5.104)$$

and the required algebraic equations, which come from the circuit of Figure 5.1, or the solution of the following for I_d , I_q :

$$\begin{aligned} 0 &= (R_s + R_e)I_d - (X''_q + X_{ep})I_q \\ &\quad - \frac{(X''_q - X'_{\ell s})}{(X'_q - X'_{\ell s})} E'_d + \frac{(X'_q - X''_q)}{(X'_q - X'_{\ell s})} \psi_{2q} + V_s \sin(\delta - \theta_{vs}) \end{aligned} \quad (5.105)$$

$$0 = (R_s + R_e)I_q + (X_d'' + X_{ep})I_d - \frac{(X_d'' - X_{\ell s})}{(X_d' - X_{\ell s})}E'_q - \frac{(X_d' - X_d'')}{(X_d' - X_{\ell s})}\psi_{1d} + V_s \cos(\delta - \theta_{vs}) \quad (5.106)$$

and then substitution into the following equations for V_d , V_q :

$$V_d = R_e I_d - X_{ep} I_q + V_s \sin(\delta - \theta_{vs}) \quad (5.107)$$

$$V_q = R_e I_q + X_{ep} I_d + V_s \cos(\delta - \theta_{vs}) \quad (5.108)$$

and finally

$$V_t = \sqrt{V_d^2 + V_q^2}. \quad (5.109)$$

The quantities V_{ref} and P_C remain as inputs.

5.4 The Two-Axis Model

The reduced-order model obtained in the last section still contains the damper-winding dynamics ψ_{1d} and ψ_{2q} . If T_{do}'' and T_{qo}'' are sufficiently small, there is an integral manifold for these dynamic states. A first approximation of the fast damper-winding integral manifold is found by setting T_{do}'' and T_{qo}'' equal to zero in (5.92)–(5.109) to obtain

$$0 = -\psi_{1d} + E'_q - (X_d' - X_{\ell s})I_d \quad (5.110)$$

$$0 = -\psi_{2q} - E'_d - (X_q' - X_{\ell s})I_q. \quad (5.111)$$

When used to eliminate ψ_{1d} and ψ_{2q} in (5.107), the equations for I_d and I_q become

$$0 = (R_s + R_e)I_d - (X_q' + X_{ep})I_q - E'_d + V_s \sin(\delta - \theta_{vs}) \quad (5.112)$$

$$0 = (R_s + R_e)I_q + (X_d' + X_{ep})I_d - E'_q + V_s \cos(\delta - \theta_{vs}). \quad (5.113)$$

As in the last section, these two real equations can be written as one complex equation:

$$\begin{aligned} & [E'_d + (X_q' - X_d')I_q + jE'_q]e^{j(\delta - \frac{\pi}{2})} \\ &= (R_s + jX_d')(I_d + jI_q)e^{j(\delta - \frac{\pi}{2})} + (R_e + jX_{ep})(I_d + jI_q)e^{j(\delta - \frac{\pi}{2})} + V_s e^{j\theta_{vs}} \end{aligned} \quad (5.114)$$

The equations for V_d and V_q remain the same as in the last section so that the circuit of Figure 5.2 can be constructed to reflect the algebraic constraints for this two-axis model. It is easy to verify that, as in the last section, the “real power from” the internal source is exactly equal to the electrical torque across the air gap (T_{ELEC}) for this model.

The final form of this two-axis model, which has eliminated the stator/network and fast damper winding dynamics, is obtained by substituting (5.110) and (5.111) into

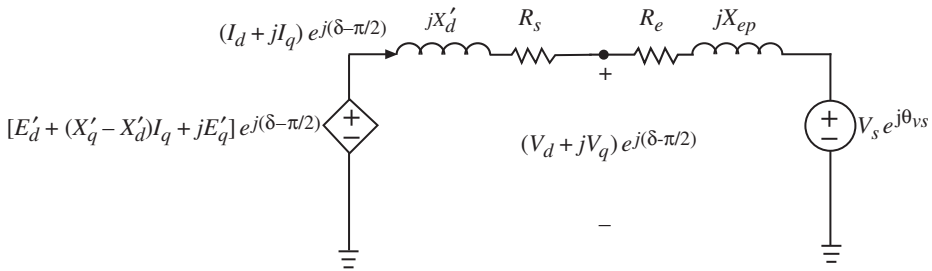


Figure 5.2 Synchronous machine two-axis dynamic circuit.

(5.92)–(5.109) to eliminate ψ_{1d} and ψ_{2q} :

$$T'_{do} \frac{dE'_q}{dt} = -E'_q - (X_d - X'_d)I_d + E_{fd} \quad (5.115)$$

$$T'_{qo} \frac{dE'_d}{dt} = -E'_d + (X_q - X'_q)I_q \quad (5.116)$$

$$\frac{d\delta}{dt} = \omega - \omega_s \quad (5.117)$$

$$\frac{2H}{\omega_s} \frac{d\omega}{dt} = T_M - E'_d I_d - E'_q I_q - (X'_q - X'_d) I_d I_q - T_{FW} \quad (5.118)$$

$$T_E \frac{dE_{fd}}{dt} = -(K_E + S_E(E_{fd}))E_{fd} + V_R \quad (5.119)$$

$$T_F \frac{dR_f}{dt} = -R_f + \frac{K_F}{T_F} E_{fd} \quad (5.120)$$

$$T_A \frac{dV_R}{dt} = -V_R + K_A R_f - \frac{K_A K_F}{T_F} E_{fd} + K_A (V_{ref} - V_t) \quad (5.121)$$

$$T_{CH} \frac{dT_M}{dt} = -T_M + P_{SV} \quad (5.122)$$

$$T_{SV} \frac{dP_{SV}}{dt} = -P_{SV} + P_C - \frac{1}{R_D} \left(\frac{\omega}{\omega_s} - 1 \right) \quad (5.123)$$

with the limit constraints

$$V_R^{\min} \leq V_R \leq V_R^{\max} \quad (5.124)$$

$$0 \leq P_{SV} \leq P_{SV}^{\max} \quad (5.125)$$

and the required algebraic equations, which come from the circuit of Figure 5.2, or the solution of the following for I_d , I_q :

$$0 = (R_s + R_e)I_d - (X'_q + X_{ep})I_q - E'_d + V_s \sin(\delta - \theta_{vs}) \quad (5.126)$$

$$0 = (R_s + R_e)I_q + (X'_d + X_{ep})I_d - E'_q + V_s \cos(\delta - \theta_{vs}) \quad (5.127)$$

and then substitution into the following equations for V_d and V_q :

$$V_d = R_e I_d - X_{ep} I_q + V_s \sin(\delta - \theta_{vs}) \quad (5.128)$$

$$V_q = R_e I_q + X_{ep} I_d + V_s \cos(\delta - \theta_{vs}) \quad (5.129)$$

and finally

$$V_t = \sqrt{V_d^2 + V_q^2}. \quad (5.130)$$

The quantities V_{ref} and P_C remain as inputs.

5.5 The One-Axis (Flux-Decay) Model

The reduced-order model obtained in the last section still contains the damper-winding dynamics E'_d . If T'_{qo} is sufficiently small, there is an integral manifold for this dynamic state also. A first approximation of this fast damper winding integral manifold is found by setting T'_{qo} equal to zero in (5.115)–(5.130) to obtain

$$0 = -E'_d + (X_q - X'_d)I_q. \quad (5.131)$$

When used to eliminate E'_d in (5.115)–(5.130), the equations for I_d and I_q then become

$$0 = (R_s + R_e)I_d - (X_q + X_{ep})I_q + V_s \sin(\delta - \theta_{vs}) \quad (5.132)$$

$$0 = (R_s + R_e)I_q + (X'_d + X_{ep})I_d - E'_q + V_s \cos(\delta - \theta_{vs}). \quad (5.133)$$

As in the last sections, these two real equations can be written as one complex equation:

$$\begin{aligned} & [(X_q - X'_d)I_q + jE'_q]e^{j(\delta-\pi/2)} \\ &= (R_s + jX'_d)(I_d + jI_q)e^{(\delta-\pi/2)} + (R_e + jX_{ep})(I_d + jI_q)e^{(\delta-\pi/2)} + V_s e^{j\theta_{vs}}. \end{aligned} \quad (5.134)$$

The equations for V_d and V_q remain the same as in the last sections, so that the circuit of Figure 5.3 can be constructed to reflect the algebraic constraints for this one-axis model. It is easy to verify that, as in the last two sections, the “real power from” the internal source is exactly equal to the electrical torque across the air gap (T_{ELEC}) for this model.

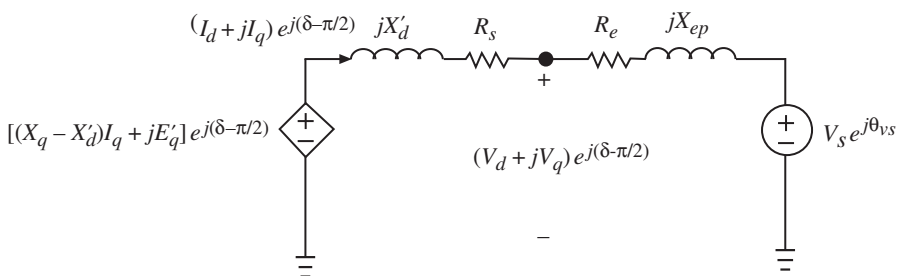


Figure 5.3 Synchronous machine one-axis dynamic circuit.

The final form of this one-axis model, which has eliminated the stator/network and all three fast damper-winding dynamics, is obtained by substituting (5.131) into (5.115)–(5.130) to eliminate E'_d :

$$T'_{do} \frac{dE'_q}{dt} = -E'_q - (X_d - X'_d)I_d + E_{fd} \quad (5.135)$$

$$\frac{d\delta}{dt} = \omega - \omega_s \quad (5.136)$$

$$\frac{2H}{\omega_s} \frac{d\omega}{dt} = T_M - E'_q I_q - (X_q - X'_d) I_d I_q - T_{FW} \quad (5.137)$$

$$T_E \frac{dE_{fd}}{dt} = -(K_E + S_E(E_{fd}))E_{fd} + V_R \quad (5.138)$$

$$T_F \frac{dR_f}{dt} = -R_f + \frac{K_F}{T_F} E_{fd} \quad (5.139)$$

$$T_A \frac{dV_R}{dt} = -V_R + K_A R_f - \frac{K_A K_F}{T_F} E_{fd} + K_A (V_{ref} - V_t) \quad (5.140)$$

$$T_{CH} \frac{dT_M}{dt} = -T_M + P_{SV} \quad (5.141)$$

$$T_{SV} \frac{dP_{SV}}{dt} = -P_{SV} + P_C - \frac{1}{R_D} \left(\frac{\omega}{\omega_s} - 1 \right) \quad (5.142)$$

with the limit constraints

$$V_R^{\min} \leq V_R \leq V_R^{\max} \quad (5.143)$$

$$0 \leq P_{SV} \leq P_{SV}^{\max} \quad (5.144)$$

and the required algebraic equations, which come from the circuit of Figure 5.3, or the solution of the following equations for I_d , I_q :

$$0 = (R_s + R_e)I_d - (X_q + X_{ep})I_q + V_s \sin(\delta - \theta_{vs}) \quad (5.145)$$

$$0 = (R_s + R_e)I_q + (X'_d + X_{ep})I_d - E'_q + V_s \cos(\delta - \theta_{vs}) \quad (5.146)$$

and then substitution into the following equations for V_d , V_q :

$$V_d = R_e I_d - X_{ep} I_q + V_s \sin(\delta - \theta_{vs}) \quad (5.147)$$

$$V_q = R_e I_q + X_{ep} I_d + V_s \cos(\delta - \theta_{vs}) \quad (5.148)$$

and finally

$$V_t = \sqrt{V_d^2 + V_q^2} \quad (5.149)$$

The quantities V_{ref} and P_C remain as inputs.

5.6 The Classical Model

The classical model is the simplest of all the synchronous machine models, but it is the hardest to justify. In an effort to derive its basis, we first state what it is. In reference to

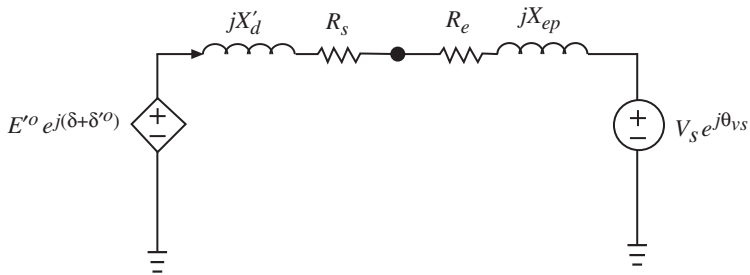


Figure 5.4 Synchronous machine classical model dynamic circuit.

all of the dynamic circuits of this chapter, the classical model is also called the constant voltage behind the transient reactance (X'_d) model. Return to the two-axis dynamic circuit Figure 5.2 and the dynamic model of (5.115)–(5.130). Rather than assuming $T'_{qo} = 0$, as in the last section, assume that an integral manifold exists for E'_d , E'_q , E_{fd} , R_f , and V_R , which, as a first approximation, gives E'_q equal to a constant and $(E'_d + (X'_q - X'_d)I_q)$ equal to a constant. For this constant based on the initial values E'^o_d , I^o_q , and E'^o_q , we define the constant voltage

$$E'^o \stackrel{\Delta}{=} \sqrt{(E'^o_d + (X'_q - X'_d)I^o_q)^2 + (E'^o_q)^2} \quad (5.150)$$

and the constant angle

$$\delta'^o \stackrel{\Delta}{=} \tan^{-1} \left(\frac{E'^o_q}{E'^o_d + (X'_q - X'_d)I^o_q} \right) - \frac{\pi}{2}. \quad (5.151)$$

The classical model dynamic circuit is shown in Figure 5.4. Because the classical model is usually used with the assumption of constant shaft torque (initial T_M^o) and zero resistance, we assume

$$T_{CH} = \infty, \quad R_s + R_e = 0 \quad (5.152)$$

and define

$$\delta_{\text{classical}} \stackrel{\Delta}{=} \delta + \delta'^o. \quad (5.153)$$

The classical model is then a second-order system:

$$\frac{d\delta_{\text{classical}}}{dt} = \omega - \omega_s \quad (5.154)$$

$$\frac{2H}{\omega_s} \frac{d\omega}{dt} = T_M^o - \frac{E'^o V_s}{(X'_d + X'_{ep})} \sin(\delta_{\text{classical}} - \theta_{vs}) - T_{FW}. \quad (5.155)$$

This classical model can also be obtained formally from the two-axis model by setting $X'_q = X'_d$ and $T_{CH} = T'_{qo} = T'_{do} = \infty$, or from the one-axis model by setting $X_q = X'_{d'}$, $T'_{qo} = 0$, and $T_{CH} = T'_{do} = \infty$. In the latter case, δ'^o is equal to zero, so that $\delta_{\text{classical}}$ is equal to δ and E'^o is equal to E'^o_q .

5.7 Damping Torques

The dynamic models proposed so far have all included a friction windage torque term T_{FW} . For opposition to rotation, such torque terms should have the form

$$T_{FW} = D_{FW}\omega \text{ or } D'_{FW}\omega^2. \quad (5.156)$$

The literature often includes damping torque terms of the form

$$T_D = D(\omega - \omega_s) \quad (5.157)$$

or

$$T_D = \frac{D'}{\omega_s}(\omega - \omega_s). \quad (5.158)$$

These damping torque terms can be positive or negative, depending on the machine speed. Values of $D' = 1$ or 2 pu have been cited as a reasonable method to account for the turbine windage damping [65]. Such terms look like induction motor slip torque terms, and have often been included to model the short circuited damper windings. Thus, if damper windings are modeled through their differential equations, then their effects need not be added in T_D . In this case, friction can be modeled through T_{FW} , if desired. If damper windings have been eliminated, as in the one-axis or classical models, all of the third damping effects have been lost. To account for their damping without including their differential equations, T_D can be added to the torque equation (added to T_{FW}), with D appropriately specified to approximate the damper-winding action. We now justify this damping torque term by returning to the two-axis model of (5.115)–(5.130), which included one damper-winding differential equation.

We would like to show that if E'_d is more accurately eliminated, a damping torque term proportional to slip speed should automatically appear in the swing equation. To show this, we propose that the integral manifold for E'_d should be found more accurately. To begin, we define the small parameter μ as

$$\mu \stackrel{\Delta}{=} T'_{qo} \quad (5.159)$$

and propose an integral manifold for E'_d of the form

$$E'_d = \phi_o + \mu\phi_1 + \mu^2\phi_2 + \dots \quad (5.160)$$

where each ϕ_i is a function of all remaining dynamic states. Substituting (5.160) into (5.116) gives

$$\begin{aligned} & \mu \left(\frac{\partial\phi_o}{\partial E'_q} + \mu \frac{\partial\phi_1}{\partial E'_q} + \mu^2 \frac{\partial\phi_2}{\partial E'_q} + \dots \right) (-E'_q - (X_d - X'_d)I_d + E_{fd})/T'_{do} \\ & + \mu \left(\frac{\partial\phi_o}{\partial \delta} + \mu \frac{\partial\phi_1}{\partial \delta} + \mu^2 \frac{\partial\phi_2}{\partial \delta} + \dots \right) (\omega - \omega_s) \\ & + \mu \left(\frac{\partial\phi_o}{\partial \omega} + \mu \frac{\partial\phi_1}{\partial \omega} + \mu^2 \frac{\partial\phi_2}{\partial \omega} + \dots \right) (T_M - (\phi_o + \mu\phi_1 + \mu^2\phi_2 + \dots)I_d \\ & - E'_q I_q - (X'_q - X'_d)I_d I_q - T_{FW}) / \left(\frac{2H}{\omega_s} \right) \end{aligned}$$

$$\begin{aligned}
& + \mu \left(\frac{\partial \phi_o}{\partial E_{fd}} + \mu \frac{\partial \phi_1}{\partial E_{fd}} + \mu^2 \frac{\partial \phi_2}{\partial E_{fd}} + \dots \right) (- (K_E + S_E) E_{fd} + V_R) / T_E \\
& + \mu \left(\frac{\partial \phi_o}{\partial R_f} + \mu \frac{\partial \phi_1}{\partial R_f} + \mu^2 \frac{\partial \phi_2}{\partial R_f} + \dots \right) \left(-R_f + \frac{K_F}{T_F} E_{fd} \right) / T_F \\
& + \mu \left(\frac{\partial \phi_o}{\partial V_R} + \mu \frac{\partial \phi_1}{\partial V_R} + \mu^2 \frac{\partial \phi_2}{\partial V_R} + \dots \right) \left(-V_R + K_A R_f - \frac{K_A K_F}{T_F} E_{fd} \right. \\
& \quad \left. + K_A (V_{ref} - V_t) \right) / T_A \\
& + \mu \left(\frac{\partial \phi_o}{\partial T_M} + \mu \frac{\partial \phi_1}{\partial T_M} + \mu^2 \frac{\partial \phi_2}{\partial T_M} + \dots \right) (-T_M + P_{SV}) / T_{CH} \\
& + \mu \left(\frac{\partial \phi_o}{\partial P_{SV}} + \mu \frac{\partial \phi_1}{\partial P_{SV}} + \mu^2 \frac{\partial \phi_2}{\partial P_{SV}} + \dots \right) \left(-P_{SV} + P_C - \frac{1}{R_D} \right. \\
& \quad \left. \left(\frac{\omega}{\omega_s} - 1 \right) \right) / T_{SV} = -(\phi_o + \mu \phi_1 + \mu^2 \phi_2 + \dots) + (X_q - X'_q) I_q \tag{5.161}
\end{aligned}$$

where I_d and I_q are

$$\begin{aligned}
I_d &= \frac{(R_s + R_e)(\phi_o + \mu \phi_1 + \mu^2 \phi_2 + \dots - V_s \sin(\delta - \theta_{vs}))}{\Delta_1} \\
&\quad + \frac{(X'_q + X_{ep})(E'_q - V_s \cos(\delta - \theta_{vs}))}{\Delta_1} \\
I_q &= \frac{-(X'_d + X_{ep})(\phi_o + \mu \phi_1 + \mu^2 \phi_2 + \dots - V_s \sin(\delta - \theta_{vs}))}{\Delta_1} \\
&\quad + \frac{(R_s + R_e)(E'_q - V_s \cos(\delta - \theta_{vs}))}{\Delta_1}
\end{aligned}$$

where

$$\Delta_1 = (R_s + R_e)^2 + (X'_d + X_{ep})(X'_q + X_{ep}) \tag{5.162}$$

and V_d , V_q , and V_t are as before. This partial differential equation may seem difficult to solve; on the contrary, it is actually very easy to solve for ϕ_o , ϕ_1 , ϕ_2 in sequence. To see how this is done systematically, suppose that we want the simplest possible approximation of the integral manifold. This is ϕ_o , and is found by neglecting all μ terms, giving

$$0 = -\phi_o + (X_q - X'_q) I_q \mid_{\mu=0}. \tag{5.163}$$

To find ϕ_o as a function of the states, we must solve (5.162) and (5.163) neglecting all μ terms, giving

$$\begin{aligned}
\phi_o &= \frac{(X_q - X'_q)(X'_d + X_{ep}) V_s \sin(\delta - \theta_{vs})}{\Delta_2} \\
&\quad + \frac{(X_q - X'_q)(R_s + R_e)(E'_q - V_s \cos(\delta - \theta_{vs}))}{\Delta_2} \tag{5.164}
\end{aligned}$$

where

$$\Delta_2 = (R_s + R_e)^2 + (X_q + X_{ep})(X'_d + X_{ep})$$

or

$$\phi_o = f_{oX}(\delta) + f_{oR}(E'_q, \delta). \quad (5.165)$$

This is the first term of the series for the integral manifold for E'_d , and is what would be obtained if T'_{qo} were simply set to zero. When substituted in the remaining equations, it would not reflect any of the damping due to this damper-winding (this is what was done in Sections 5.5 and 5.6). If we want to recover some of the damping due to this damper-winding without resorting to the two-axis model, we can compute ϕ_1 by returning to (5.161) and keeping μ terms, but neglecting μ^2 and higher powers of μ . Note that ϕ_o is only a function of E'_q and δ ; all the partials of ϕ_o are zero except for two, giving

$$\begin{aligned} & \frac{\partial \phi_o}{\partial E'_q} (-E'_q - (X_d - X'_d)I_d |_{\mu=0} + E_{fd}) / T'_{do} + \frac{\partial \phi_o}{\partial \delta} (\omega - \omega_s) \\ &= -\phi_1 - (X_q - X'_q) \left(\frac{(X'_d + X_{ep})\phi_1}{(R_s + R_e)^2 + (X'_d + X_{ep})(X'_q + X_{ep})} \right) \end{aligned}$$

where I_d is evaluated at $\mu = 0$. This makes ϕ_1 some function of E'_q , E_{fd} , δ , and ω , written here as

$$\phi_1 = -f_{1X}(\delta)(\omega - \omega_s) + f_{1R}(E'_q, E_{fd}, \delta). \quad (5.166)$$

Stopping with this level of accuracy, the integral manifold for E'_d is

$$E'_d = \phi_o + \mu\phi_1 + O(\mu^2) \quad (5.167)$$

where $O(\mu^2)$ is some error of “order” μ^2 . In terms of the above functions, an approximate expression for $E'_{d'}$, which will capture some of the damping of the damper-winding, is

$$E'_d = f_{oX}(\delta) + f_{oR}(E'_q, \delta) - T'_{qo}f_{1X}(\delta)(\omega - \omega_s) + T'_{qo}f_{1R}(E'_q, E_{fd}, \delta). \quad (5.168)$$

Note that f_{oR} and f_{1R} are zero if $R_s + R_e = 0$. Substitution of this approximation of the exact integral manifold for E'_d into the two-axis model gives the circuit of Figure 5.5

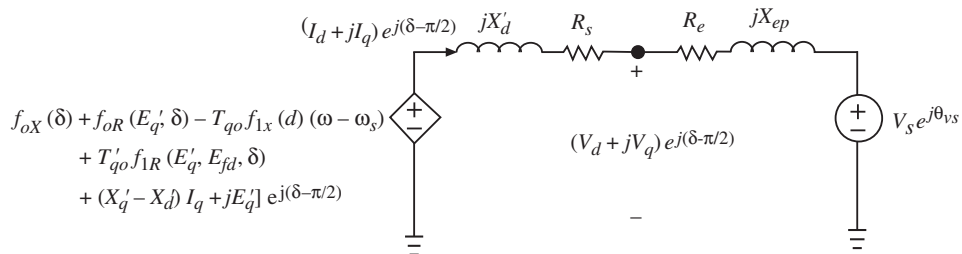


Figure 5.5 Synchronous machine one-axis dynamic circuit with damping term.

and the following differential equations.

$$T'_{do} \frac{dE'_q}{dt} = -E'_q - (X_d - X'_d)I_d + E_{fd} \quad (5.169)$$

$$\frac{d\delta}{dt} = \omega - \omega_s \quad (5.170)$$

$$\begin{aligned} \frac{2H}{\omega_s} \frac{d\omega}{dt} &= T_M - I_d(f_{oX}(\delta) + f_{oR}(E'_q, \delta) - T'_{qo}f_{1X}(\delta)(\omega - \omega_s) \\ &\quad + T'_{qo}f_{1R}(E'_q, E_{fd}, \delta)) - E'_q I_q - (X'_q - X'_d)I_d I_q - T_{FW} \end{aligned} \quad (5.171)$$

$$T_E \frac{dE_{fd}}{dt} = -(K_E + S_E)E_{fd} + V_R \quad (5.172)$$

$$T_F \frac{dR_f}{dt} = -R_f + \frac{K_F}{T_F}E_{fd} \quad (5.173)$$

$$T_A \frac{dV_R}{dt} = -V_R + K_A R_f - \frac{K_A K_F}{T_F}E_{fd} + K_A(V_{ref} - V_t) \quad (5.174)$$

$$T_{CH} \frac{dT_M}{dt} = -T_M + P_{SV} \quad (5.175)$$

$$T_{SV} \frac{dP_{SV}}{dt} = -P_{SV} + P_C - \frac{1}{R_D} \left(\frac{\omega}{\omega_s} - 1 \right) \quad (5.176)$$

with the limit constraints

$$V_R^{\min} \leq V_R \leq V_R^{\max} \quad (5.177)$$

$$0 \leq P_{SV} \leq P_{SV}^{\max} \quad (5.178)$$

and the required algebraic equations for I_d , I_q , V_t , which come from the circuit of Figure 5.5 or the solution of the following equations for I_d , I_q :

$$\begin{aligned} 0 &= (R_s + R_e)I_d - (X'_q + X_{ep})I_q - f_{oX}(\delta) - f_{oR}(E'_q, \delta) + T'_{qo}f_{1X}(\delta)(\omega - \omega_s) \\ &\quad - T'_{qo}f_{1R}(E'_q, E_{fd}, \delta) + V_s \sin(\delta - \theta_{vs}) \end{aligned} \quad (5.179)$$

$$0 = (R_s + R_e)I_q + (X'_d + X_{ep})I_d - E'_q + V_s \cos(\delta - \theta_{vs}) \quad (5.180)$$

and then substitution into the following for V_d , V_q :

$$V_d = R_e I_d - X_{ep} I_q + V_s \sin(\delta - \theta_{vs}) \quad (5.181)$$

$$V_q = R_e I_q + X_{ep} I_d + V_s \cos(\delta - \theta_{vs}) \quad (5.182)$$

and finally

$$V_t = \sqrt{V_d^2 + V_q^2} \quad (5.183)$$

When $R_s + R_e = 0$

$$E'_d = \frac{X_q - X'_q}{X_q + X_{ep}} V_s \sin(\delta - \theta_{vs}) - T'_{qo} \frac{(X'_q + X_{ep})(X_q - X'_q)}{(X_q + X_{ep})^2} V_s \cos(\delta - \theta_{vs})(\omega - \omega_s) \quad (5.184)$$

which gives an accelerating torque of

$$\begin{aligned} T_{\text{accel}}|_{R_s+R_e=0} &= T_M - \frac{E'_q V_s}{X'_d + X_{ep}} \sin(\delta - \theta_{vs}) \\ &+ \frac{1}{2} \left(\frac{1}{X'_d + X_{ep}} - \frac{1}{X_q + X_{ep}} \right) V_s^2 \sin 2(\delta - \theta_{vs}) \\ &- T'_{qo} \frac{(X_q - X'_q)}{(X_q + X_{ep})^2} V_s^2 \cos^2(\delta - \theta_{vs})(\omega - \omega_s) - T_{FW} \end{aligned} \quad (5.185)$$

The T'_{qo} term reflects the damping due to the damper-winding as a slip torque term

$$T_D = T'_{qo} \frac{(X_q - X'_q)}{(X_q + X_{ep})^2} V_s^2 \cos^2(\delta - \theta_{vs})(\omega - \omega_s). \quad (5.186)$$

This is often approximated as

$$T_D \approx D(\omega - \omega_s) \quad (5.187)$$

where D is a damping constant. The approximation of (5.187) is normally considered valid only for small deviations about an operating point, but it has been used for large changes as well.

5.8 Single-Machine Infinite-Bus System

It is constructive to pause at this point to consider the dynamics of a very simple model of a single machine connected to a very strong grid (infinite bus). The classical model of this chapter connected to an infinite bus through a lossless transmission line (without shunt capacitance) can be summarized as

$$\begin{aligned} \frac{d\delta_c}{dt} &= \omega_t \\ \frac{d\omega_t}{dt} &= K_1 - K_2 \sin \delta_c - K_3 \omega_t \end{aligned} \quad (5.188)$$

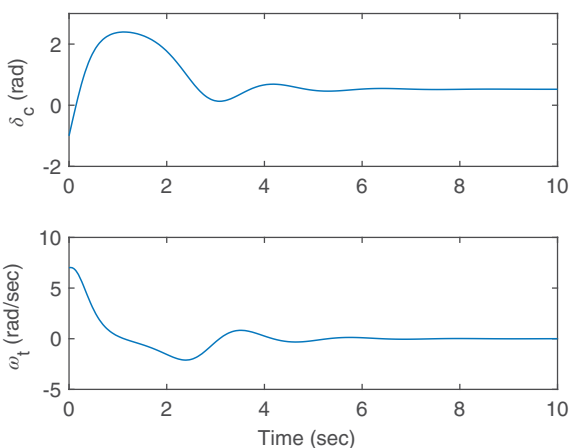
where δ_c is the machine internal voltage angle $\delta_{\text{classcial}}$ and $\omega_t = \omega - \omega_s$ (the transient speed) and

$$K_1 = \frac{\omega_s}{2H} T_M^o, \quad K_2 = \frac{\omega_s}{2H} \frac{E_c V}{X}, \quad K_3 = \frac{\omega_s}{2H} D \quad (5.189)$$

with E_c equal to the magnitude of the internal voltage of the machine (typically 1.0), V is equal to the magnitude of the infinite bus voltage (typically 1.0), X is the sum of the internal machine reactance (stator resistance is neglected) plus the reactance of the lossless line connecting to the infinite bus which has an angle of zero, and T_M^o is the constant mechanical torque from the prime mover. All quantities are in normal per unit notation and H and D are the machine inertia and damping constants, respectively.

This dynamic model is exactly the same as a classical pendulum model with constant force applied and the damping term is friction. It is fairly clear that this simple dynamic

Figure 5.6 Machine rotor angle δ_c and speed ω_t responses.



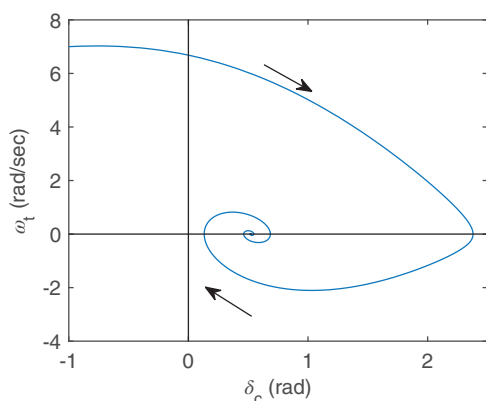
model has two equilibrium points that depend primarily on K_1 and K_2 . Thinking of a pendulum with no applied force ($K_1 = 0$), the “down” position ($\delta_c = 0^\circ$) is normally considered stable and the up position ($\delta_c = 180^\circ$) is normally considered unstable. As it turns out, this is the same for a synchronous machine connected to an infinite bus and operating at no load ($T_M^o = 0$).

The responses in Figure 5.6 were computed using Euler’s Forward method with a time step of 0.001 sec, an initial angle of $\delta_c(0) = -1$ rad, an initial transient speed $\omega_t(0) = 7.0$ rad/sec, and the constants $K_1 = 5$, $K_2 = 10$, and $K_3 = 1.7$ (all in appropriate per unit values).

The plot in Figure 5.7 showing the rotor angle (in rad) on the horizontal axis vs the transient speed ω_t (in rad/sec) on the vertical axis is called a “phase portrait.”

When the damping coefficient is lowered to $K_3 = 1.3$, the phase portrait in Figure 5.8 shows a very interesting result – the speed ω_t does not go directly to zero, but eventually converges to zero and the angle eventually converges to a constant (13.09 rad = $4\pi + 0.524$ rad = 30° plus two cycles). For a synchronous machine, this is called “pole slipping” which occurs until the transient speed can reach zero (machine reaches synchronous speed), at which point the angle equilibrium is reached from there.

Figure 5.7 Phase portrait showing machine rotor speed ω_t vs rotor angle δ_c .



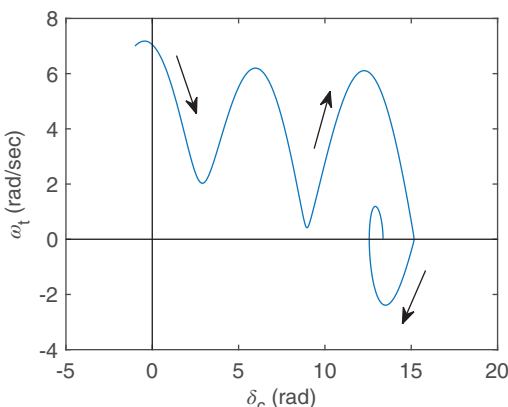


Figure 5.8 Phase portrait starting from a high rotor speed.

Another interesting observation shows the importance of step size in numerical integration. If the time step is increased from 0.001 to 0.003 sec, the phase portrait changes to the one shown in Figure 5.9. It seems that the larger time step produced an error in the solution which manifested itself as negative damping which counteracted the model damping and produced a response that appeared to be an undamped sustained oscillation [187]. We of course assume that the response with the smaller time step solution is closer to the real solutions than this one.

The topic of phase portraits leads directly to the notion of a separatrix. The separatrix of a dynamic model is a plot of the stable and unstable equilibrium points plus the stable and unstable manifolds associated with the unstable equilibrium points. It is also considered as a phase portrait that maps out all possible trajectories from all possible initial conditions, showing how some trajectories are attracted to the stable equilibrium points and some are not – so the separatrix shows the boundaries of regions of attraction. The separatrix for our example here with $K_3 = 1.3$ is shown in Figure 5.10.

In Figure 5.10, the region of attraction of the stable equilibrium point ($\delta_c = 13.09$ rad, $\omega_t = 0$ pu) is bounded by four trajectories that are on the stable manifolds of the adjacent

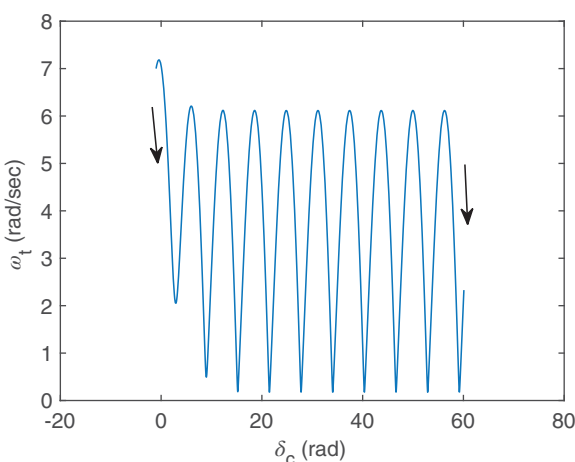
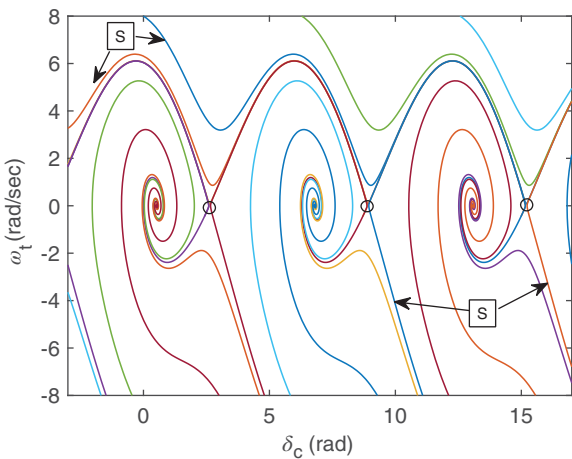


Figure 5.9 Phase portrait for dynamics using an increased time step of 0.003 sec.

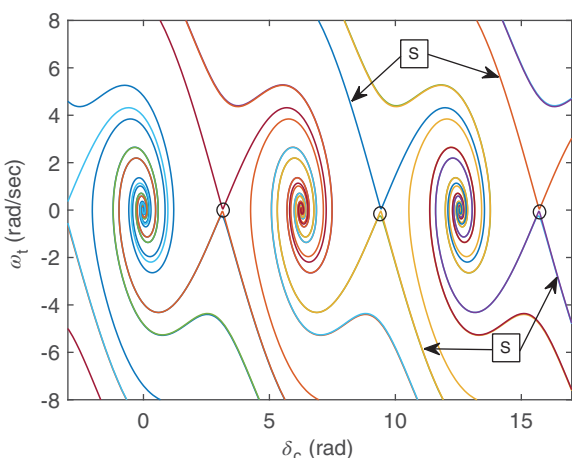
Figure 5.10 The separatrix of the region of attraction for a stable equilibrium point ($\delta_c = 13.09$ rad, $\omega_t = 0$ pu) as defined by 4 trajectories (indicated by "S") emanating from unstable equilibrium points (indicated by circles).



unstable equilibrium points (uep's) marked by circles. These 4 trajectories converge to the two adjacent uep's. At negative speed ω_t , the trajectories converge monotonically (when close to the uep's), thus allowing a wide region of attraction. For positive speed ω_t , the trajectories have to go through pole-slipping and as a result, there is one part of the region of attraction with positive speed which is quite narrow. This phenomenon is attributed to the non-zero forcing input K_1 .

If the forcing input K_1 is set to zero, then the regions of attraction above and below $\omega_t = 0$ are similar, as shown in Figure 5.11. While the basic shape of this plot is essentially the same as Figure 5.10, this plot clearly shows the stable equilibrium points with the solid circles (in this case $0, 2\pi, 4\pi, \dots$) and the unstable equilibrium points with the hollow circles (in this case $\pi, 3\pi, 5\pi, \dots$). The S labels the stable manifolds of the unstable equilibrium points which together create the region of attraction of the associated stable equilibrium point. Trajectories coming in from the upper part and lower part both converge directly into the solid circle stable equilibrium point.

Figure 5.11 The separatrix of the region of attraction for a stable equilibrium point ($\delta_c = 4\pi$ rad, $\omega_t = 0$ pu) for a system with no forcing input. The separatrix is defined by 4 trajectories (indicated by "S") emanating from unstable equilibrium points (indicated by circles).



5.9 Synchronous Machine Saturation

The dynamic models of (5.42)–(5.65), (5.92)–(5.109), (5.115)–(5.130), (5.135) –(5.149), and (5.154)–(5.155) began with the assumption of a linear magnetic circuit ((3.148)–(3.159)). To account for saturation, it is necessary to repeat this analysis starting with (3.191)–(3.203), rather than (3.148)–(3.159). Without explicit information about the saturation functions $S_d^{(2)}$, $S_q^{(2)}$, $S_o^{(2)}$, $S_{fd}^{(2)}$, $S_{1d}^{(2)}$, $S_{1q}^{(2)}$, and $S_{2q}^{(2)}$, it is not possible to rigorously show that these functions do not affect the fundamental assumptions about time-scale properties. We assume that the functions do not affect the time-scale property so that the stator plus line algebraic equations for this single-machine model become

$$0 = R_{se}I_d + \psi_{qe} + V_s \sin(\delta - \theta_{vs}) \quad (5.190)$$

$$0 = R_{se}I_q - \psi_{de} + V_s \cos(\delta - \theta_{vs}) \quad (5.191)$$

$$0 = R_{se}I_o \quad (5.192)$$

$$\psi_{de} = -X''_{de}I_d + \frac{(X''_d - X'_{\ell s})}{(X'_d - X'_{\ell s})}E'_q + \frac{(X'_d - X''_d)}{(X'_d - X'_{\ell s})}\psi_{1d} - S_d^{(2)}(Y_2) \quad (5.193)$$

$$\psi_{qe} = -X''_{qe}I_q - \frac{(X''_q - X'_{\ell s})}{(X'_q - X'_{\ell s})}E'_d + \frac{(X'_q - X''_q)}{(X'_q - X'_{\ell s})}\psi_{2q} - S_q^{(2)}(Y_2) \quad (5.194)$$

$$V_d = R_e I_d - X_{ep} I_q + V_s \sin(\delta - \theta_{vs}) \quad (5.195)$$

$$V_q = R_e I_q + X_{ep} I_d + V_s \cos(\delta - \theta_{vs}). \quad (5.196)$$

These equations can be written in circuit form as shown in Figure 5.12.

With this assumption, the dynamic model with saturation included but stator/network transients eliminated is

$$T'_{do} \frac{dE'_q}{dt} = -E'_q - (X_d - X'_d) \left[I_d - \frac{X'_d - X''_d}{(X'_d - X'_{\ell s})^2} (\psi_{1d} + (X'_d - X'_{\ell s})I_d - E'_q + S_{1d}^{(2)}(Y_2)) \right] - S_{fd}^{(2)}(Y_2) + E_{fd} \quad (5.197)$$

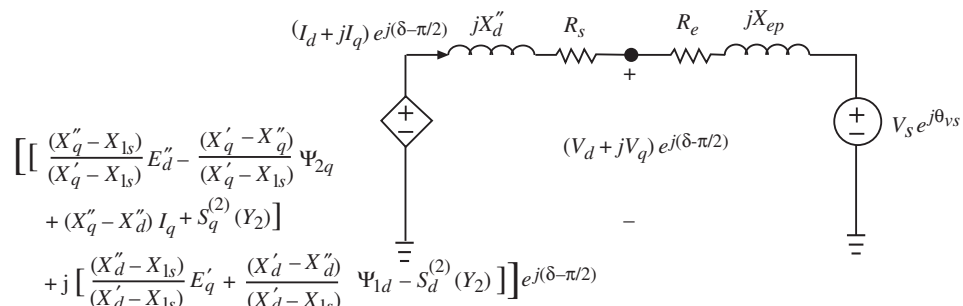


Figure 5.12 Synchronous machine subtransient dynamic circuit including saturation.

$$T''_{do} \frac{d\psi_{1d}}{dt} = -\psi_{1d} + E'_q - (X'_d - X'_{\ell s})I_d - S^{(2)}_{1d}(Y_2) \quad (5.198)$$

$$\begin{aligned} T'_{qo} \frac{dE'_d}{dt} = & -E'_d + (X_q - X'_q) \left[I_q - \frac{X'_q - X''_q}{(X'_q - X'_{\ell s})^2} (\psi_{2q} + (X'_q - X'_{\ell s})I_q \right. \\ & \left. + E'_d + S^{(2)}_{2q}(Y_2)) \right] + S^{(2)}_{1q}(Y_2) \end{aligned} \quad (5.199)$$

$$T''_{qo} \frac{d\psi_{2q}}{dt} = -\psi_{2q} - E'_d - (X'_q - X'_{\ell s})I_q - S^{(2)}_{2q}(Y_2) \quad (5.200)$$

$$\frac{d\delta}{dt} = \omega - \omega_s \quad (5.201)$$

$$\begin{aligned} \frac{2H}{\omega_s} \frac{d\omega}{dt} = & T_M - \frac{(X''_d - X'_{\ell s})}{(X'_d - X'_{\ell s})} E'_q I_q - \frac{(X'_d - X''_d)}{(X'_d - X'_{\ell s})} \psi_{1d} I_q \\ & - \frac{(X''_q - X'_{\ell s})}{(X'_q - X'_{\ell s})} E'_d I_d + \frac{(X'_q - X''_q)}{(X'_q - X'_{\ell s})} \psi_{2q} I_d - (X''_q - X''_d) I_d I_q \\ & + S^{(2)}_d(Y_2) I_q - S^{(2)}_q(Y_2) I_d - T_{FW} \end{aligned} \quad (5.202)$$

$$T_E \frac{dE_{fd}}{dt} = -(K_E + S_E(E_{fd}))E_{fd} + V_R \quad (5.203)$$

$$T_F \frac{dR_f}{dt} = -R_f + \frac{K_F}{T_F} E_{fd} \quad (5.204)$$

$$T_A \frac{dV_R}{dt} = -V_R + K_A R_f - \frac{K_A K_F}{T_F} E_{fd} + K_A (V_{ref} - V_t) \quad (5.205)$$

$$T_{CH} \frac{dT_M}{dt} = -T_M + P_{SV} \quad (5.206)$$

$$T_{SV} \frac{dP_{SV}}{dt} = -P_{SV} + P_C - \frac{1}{R_D} \left(\frac{\omega}{\omega_s} - 1 \right) \quad (5.207)$$

with the limit constraints

$$V_R^{\min} \leq V_R \leq V_R^{\max} \quad (5.208)$$

$$0 \leq P_{SV} \leq P_{SV}^{\max} \quad (5.209)$$

and the required algebraic equations for V_t , I_d , and I_q , which come from the circuit of Figure 5.12:

$$\begin{aligned} 0 = & (R_s + R_e)I_d - (X''_q + X_{ep})I_q - \frac{(X''_q - X'_{\ell s})}{(X'_q - X'_{\ell s})} E'_d \\ & + \frac{(X'_q - X''_q)}{(X'_q - X'_{\ell s})} \psi_{2q} - S^{(2)}_q(Y_2) + V_s \sin(\delta - \theta_{vs}) \end{aligned} \quad (5.210)$$

$$0 = (R_s + R_e)I_q + (X_d'' + X_{ep})I_d - \frac{(X_d'' - X_{\ell s})}{(X_d' - X_{\ell s})}E'_q \\ - \frac{(X_d' - X_d'')}{(X_d' - X_{\ell s})}\psi_{1d} + S_d^{(2)}(Y_2) + V_s \cos(\delta - \theta_{vs}) \quad (5.211)$$

the following equations for V_d , V_q , V_t :

$$V_d = R_e I_d - X_{ep} I_q + V_s \sin(\delta - \theta_{vs}) \quad (5.212)$$

$$V_q = R_e I_q + X_{ep} I_d + V_s \cos(\delta - \theta_{vs}) \quad (5.213)$$

$$V_t = \sqrt{V_d^2 + V_q^2} \quad (5.214)$$

and finally the saturation function relations, which must be specified.

The saturation functions, in general, may be functions of I_d , I_q , and I_o . From (5.192), these functions would be evaluated at $I_o = 0$. If the saturation functions include I_d and I_q , the nonlinear algebraic equations (5.210) and (5.211) must be solved for I_d and I_q as functions of E'_q , E'_d , ψ_{1d} , ψ_{2q} , and δ , and then substituted into (5.212)–(5.214) to obtain V_d , V_q , and V_t . If the saturation functions do not include I_d , I_q , then the currents I_d , I_q can easily be solved from (5.210) and (5.211).

To obtain a two-axis model with saturation included as above, we again assume that T_{do}'' and T_{qo}'' are sufficiently small so that an integral manifold exists for ψ_{1d} and ψ_{2q} . A first approximation of this integral manifold is found by setting T_{do}'' and T_{qo}'' equal to zero in (5.198) and (5.200) to obtain

$$0 = -\psi_{1d} + E'_q - (X_d' - X_{\ell s})I_d - S_{1d}^{(2)}(Y_2) \quad (5.215)$$

$$0 = -\psi_{2q} - E'_d - (X_q' - X_{\ell s})I_q - S_{2q}^{(2)}(Y_2) \quad (5.216)$$

We now assume that $S_{1d}^{(2)}(Y_2)$ and $S_{2q}^{(2)}(Y_2)$ are such that these two equations can be solved for ψ_{1d} and ψ_{2q} to obtain

$$\psi_{1d} = E'_q - (X_d' - X_{\ell s})I_d - S_{1d}^{(3)}(Y_3) \quad (5.217)$$

$$\psi_{2q} = -E'_d - (X_q' - X_{\ell s})I_q - S_{2q}^{(3)}(Y_3) \quad (5.218)$$

where

$$Y_3 \stackrel{\Delta}{=} [I_d \ E'_q \ I_q \ E'_d]^t. \quad (5.219)$$

When used to eliminate ψ_{1d} and ψ_{2q} in (5.197)–(5.214), the equations for I_d and I_q become

$$0 = (R_s + R_e)I_d - (X_q' + X_{ep})I_q - E'_d - S_q^{(3)}(Y_3) + V_s \sin(\delta - \theta_{vs}) \quad (5.220)$$

$$0 = (R_s + R_e)I_q + (X_d' + X_{ep})I_d - E'_q + S_d^{(3)}(Y_3)V_s \cos(\delta - \theta_{vs}). \quad (5.221)$$

The saturation functions $S_d^{(3)}(Y_3)$ and $S_q^{(3)}(Y_3)$ are a combination of $S_d^{(2)}$, $S_q^{(2)}$ and $S_{1d}^{(2)}$, $S_{2q}^{(2)}$ as found by substituting (5.217) and (5.218) into (5.210) and (5.211). These two equations can be represented by the circuit shown in Figure 5.13.

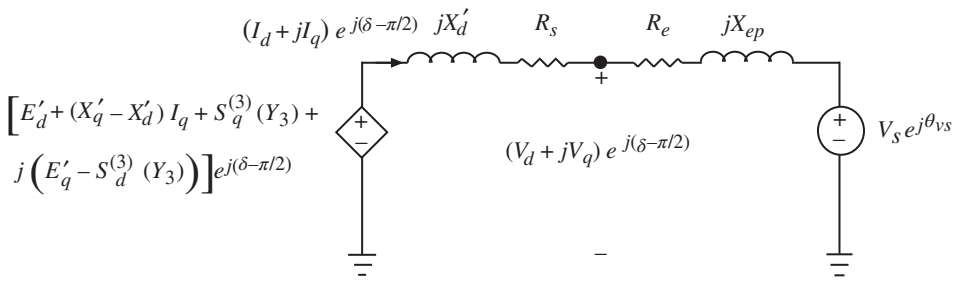


Figure 5.13 Synchronous machine two-axis dynamic circuit with saturation.

The two-axis dynamic model with synchronous machine saturation is

$$T'_{do} \frac{dE'_q}{dt} = -E'_q - (X_d - X'_d)I_d - S_{fd}^{(3)}(Y_3) + E_{fd} \quad (5.222)$$

$$T'_{qo} \frac{dE'_d}{dt} = -E'_d + (X_q - X'_q)I_q + S_{1q}^{(3)}(Y_3) \quad (5.223)$$

$$\frac{d\delta}{dt} = \omega - \omega_s \quad (5.224)$$

$$\frac{2H}{\omega_s} \frac{d\omega}{dt} = T_M - E'_d I_d - E'_q I_q - (X'_q - X'_d) I_d I_q + S_d^{(3)}(Y_3) I_q - S_q^{(3)}(Y_3) I_d - T_{FW} \quad (5.225)$$

$$T_E \frac{dE_{fd}}{dt} = -(K_E + S_E(E_{fd}))E_{fd} + V_R \quad (5.226)$$

$$T_F \frac{dR_f}{dt} = -R_f + \frac{K_F}{T_F} E_{fd} \quad (5.227)$$

$$T_A \frac{dV_R}{dt} = -V_R + K_A R_f - \frac{K_A K_F}{T_F} E_{fd} + K_A (V_{ref} - V_t) \quad (5.228)$$

$$T_{CH} \frac{dT_M}{dt} = -T_M + P_{SV} \quad (5.229)$$

$$T_{SV} \frac{dP_{SV}}{dt} = -P_{SV} + P_C - \frac{1}{R_D} \left(\frac{\omega}{\omega_s} - 1 \right) \quad (5.230)$$

with the limit constraints

$$V_R^{\min} \leq V_R \leq V_R^{\max} \quad (5.231)$$

$$0 \leq P_{SV} \leq P_{SV}^{\max} \quad (5.232)$$

and the required algebraic equations for I_d , I_q , which come from the circuit of Figure 5.13, or the solution of the following for I_d , I_q :

$$0 = (R_s + R_e)I_d - (X'_q + X_{ep})I_q - E'_d - S_q^{(3)}(Y_3) + V_s \sin(\delta - \theta_{vs}) \quad (5.233)$$

$$0 = (R_s + R_e)I_q + (X'_d + X_{ep})I_d - E'_q + S_d^{(3)}(Y_3) + V_s \cos(\delta - \theta_{vs}) \quad (5.234)$$

then substitution into the following for V_d , V_q , V_t :

$$V_d = R_e I_d - X_{ep} I_q + V_s \sin(\delta - \theta_{vs}) \quad (5.235)$$

$$V_q = R_e I_q + X_{ep} I_d + V_s \cos(\delta - \theta_{vs}) \quad (5.236)$$

$$V_t = \sqrt{V_d^2 + V_q^2} \quad (5.237)$$

If the saturation functions include a dependence on I_d and I_q , the nonlinear algebraic equations (5.233) and (5.234) must be solved for I_d and I_q as functions of E'_q , E'_d , and δ and then substituted into (5.235)–(5.237) to obtain V_d , V_q , and V_t . If the saturation functions do not include a dependence on I_d and I_q , then I_d and I_q can easily be found from (5.233) and (5.234).

To obtain a flux-decay model with saturation included, we again assume T'_{qo} is sufficiently small so that an integral manifold exists for E'_d . A first approximation of this integral manifold is found by setting T'_{qo} equal to zero in (5.223) to obtain

$$0 = -E'_d + (X_q - X'_q)I_q + S_{1q}^{(3)}(Y_3). \quad (5.238)$$

We now assume that $S_{1q}^{(3)}(Y_3)$ is such that this equation can be solved for E'_d to obtain

$$E'_d = (X_q - X'_q)I_q + S_{1q}^{(4)}(Y_4) \quad (5.239)$$

where

$$Y_4 \stackrel{\Delta}{=} [I_d \ E'_q \ I_q]^t \quad (5.240)$$

when used to eliminate E'_d in (5.222)–(5.237), the equations for I_d and I_q become

$$0 = (R_s + R_e)I_d - (X_q + X_{ep})I_q - S_q^{(4)}(Y_4)V_s \sin(\delta - \theta_{vs}) \quad (5.241)$$

$$0 = (R_s + R_e)I_q + (X'_d + X_{ep})I_d - E'_q + S_d^{(4)}(Y_4)V_s \cos(\delta - \theta_{vs}). \quad (5.242)$$

The saturation functions $S_d^{(4)}(Y_4)$ and $S_q^{(4)}(Y_4)$ are a combination of $S_d^{(3)}$, $S_q^{(3)}$, and $S_{1q}^{(4)}$ as found by substituting (5.239) into (5.220) and (5.221). These two equations can be represented by the circuit shown in Figure 5.14. The one-axis (flux-decay) dynamic model

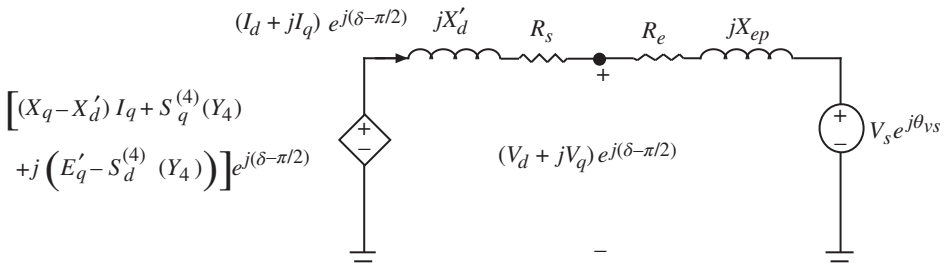


Figure 5.14 Synchronous machine one-axis (flux-decay) dynamic circuit with saturation.

with saturation is

$$T'_{do} \frac{dE'_q}{dt} = -E'_q - (X_d - X'_d)I_d - S_{fd}^{(4)}(Y_4) + E_{fd} \quad (5.243)$$

$$\frac{d\delta}{dt} = \omega - \omega_s \quad (5.244)$$

$$\frac{2H}{\omega_s} \frac{d\omega}{dt} = T_M - E'_q I_q - (X_q - X'_d)I_d I_q + S_d^{(4)}(Y_4)I_q - S_q^{(4)}(Y_4)I_d - T_{FW} - T_D \quad (5.245)$$

$$T_E \frac{dE_{fd}}{dt} = -(K_E + S_E(E_{fd}))E_{fd} + V_R \quad (5.246)$$

$$T_F \frac{dR_f}{dt} = -R_f + \frac{K_F}{T_F}E_{fd} \quad (5.247)$$

$$T_A \frac{dV_R}{dt} = -V_R + K_A R_f - \frac{K_A K_F}{T_F}E_{fd} + K_A(V_{ref} - V_t) \quad (5.248)$$

$$T_{CH} \frac{dT_M}{dt} = -T_M + P_{SV} \quad (5.249)$$

$$T_{SV} \frac{dP_{SV}}{dt} = -P_{SV} + P_C - \frac{1}{R_D} \left(\frac{\omega}{\omega_s} - 1 \right) \quad (5.250)$$

with the limit constraints

$$V_R^{\min} \leq V_R \leq V_R^{\max} \quad (5.251)$$

$$0 \leq P_{SV} \leq P_{SV}^{\max} \quad (5.252)$$

and the required algebraic equations, which come from the circuit of Figure 5.14:

$$0 = (R_s + R_e)I_d - (X_q + X_{ep})I_q - S_q^{(4)}(Y_4) + V_s \sin(\delta - \theta_{vs}) \quad (5.253)$$

$$0 = (R_s + R_e)I_q + (X'_d + X_{ep})I_d - E'_q + S_d^{(4)}(Y_4) + V_s \cos(\delta - \theta_{vs}) \quad (5.254)$$

then substitution into the following for V_d , V_q , V_t :

$$V_d = R_e I_d - X_{ep} I_q + V_s \sin(\delta - \theta_{vs}) \quad (5.255)$$

$$V_q = R_e I_q + X_{ep} I_d + V_s \cos(\delta - \theta_{vs}) \quad (5.256)$$

$$V_t = \sqrt{V_d^2 + V_q^2} \quad (5.257)$$

If the saturation functions include a dependence on I_d and I_q , the nonlinear algebraic equations (5.253) and (5.254) must be solved for I_d and I_q as functions of E'_q , δ and then substituted into (5.255)–(5.257) to obtain V_d , V_q , and V_t . If the saturation functions do not include a dependence on I_d and I_q , then I_d and I_q can easily be found from (5.253) and (5.254).

There is really no point in trying to incorporate saturation into the classical model, since it essentially assumes constant flux linkage.

5.10 Problems

- 5.1** Given the two-axis dynamic circuit of Figure 5.2, solve for I_d and I_q in terms of the circuit parameters plus δ , E'_q , E'_d and the source V_s , θ_{vs} .
- 5.2** Given the one-axis dynamic circuit of Figure 5.3, solve for I_d and I_q in terms of the circuit parameters plus δ , E'_q and the source V_s , θ_{vs} .
- 5.3** Using the two-axis dynamic model of Section 5.4, derive an expression for the voltage behind X_q that gives a circuit that is equally as valid as that of Figure 5.2.
- 5.4** Using the one-axis dynamic model of Section 5.5, derive an expression for the voltage behind X_q that gives a circuit that is equally as valid as that of Figure 5.3.
- 5.5** Given a synchronous generator with a two-axis model:
- $$(V_d + jV_q)e^{j(\delta - \pi/2)} = 1\angle 0 \text{ pu}$$
- $$(I_d + jI_q)e^{j(\delta - \pi/2)} = 0.5\angle 30^\circ \text{ pu}$$
- $R_s = 0 \text{ pu}$, $X_d = 1.2 \text{ pu}$, $X_q = 1.0 \text{ pu}$, $X'_d = 0.2 \text{ pu}$, $X'_q = 0.2 \text{ pu}$
- (a) Find the steady-state values of δ , E'_q , E'_d .
- (b) Find the inputs E_{fd} and T_m .
- (c) Find E'^o and δ'^o for the classical model.
- 5.6** Given the following two-axis dynamic model of a synchronous machine connected to an infinite bus, with the parameters shown (and $R_s = 0$):
- (a) If the machine is in a stable steady-state condition supplying zero real power and some reactive power Q , what can you say about the values of I_d and I_q ?
- (b) Find the values of T_M and E_{fd} in part (a) if $Q = 1 \text{ pu}$.
- (c) Describe, in as much detail as possible, the system response if E_{fd} is suddenly changed to be 2.0 pu .

$$T'_{do} \frac{dE'_q}{dt} = -E'_q - (X_d - X'_d)I_d + E_{fd}$$

$$T'_{qo} \frac{dE'_d}{dt} = -E'_d + (X_q - X'_q)I_q$$

$$\frac{d\delta}{dt} = \omega - \omega_s$$

$$\frac{2H}{\omega_s} \frac{d\omega}{dt} = T_M - E'_d I_d - E'_q I_q - (X'_q - X'_d) I_d I_q$$

$$[E'_d + (X'_q - X'_d)I_q + jE'_q]e^{j(\delta - \pi/2)} = jX'_d[I_d + jI_q]e^{j(\delta - \pi/2)} + Ve^{j\theta}$$

$$T'_{do} = 5.0 \text{ sec}, \quad X_d = 1.2 \text{ pu}, \quad X'_d = 0.3 \text{ pu}$$

$$T'_{qo} = 0.6 \text{ sec}, \quad X_q = 1.1 \text{ pu}, \quad X'_q = 0.7 \text{ pu}$$

$$\omega_s = 2\pi 60 \text{ rad/sec}, \quad H = 6.0 \text{ sec}, \quad V = 1.0 \text{ pu}, \quad \theta = 0 \text{ rad.}$$

6

Multimachine Dynamic Models

This chapter considers the dynamic model of many synchronous machines interconnected by transformers and transmission lines. For the initial analysis, loads will be considered balanced symmetrical $R-L$ elements. For notation, we adopt the following “number” symbols:

m = number of synchronous machines (if there is an infinite bus, it is machine number 1)

n = number of system three-phase buses (excluding the datum or reference bus)

b = total number of machines plus transformers plus lines plus loads (total branches).

6.1 The Synchronously Rotating Reference Frame

It is convenient to transform all synchronous machine stator and network variables into a reference frame that converts balanced three-phase sinusoidal variations into constants. Such a transformation is

$$T_{dqos} \triangleq \frac{2}{3} \begin{bmatrix} \cos \omega_s t & \cos \left(\omega_s t - \frac{2\pi}{3} \right) & \cos \left(\omega_s t + \frac{2\pi}{3} \right) \\ -\sin \omega_s t & -\sin \left(\omega_s t - \frac{2\pi}{3} \right) & -\sin \left(\omega_s t + \frac{2\pi}{3} \right) \\ \frac{1}{2} & \frac{1}{2} & \frac{1}{2} \end{bmatrix} \quad (6.1)$$

with

$$T_{dqos}^{-1} = \begin{bmatrix} \cos \omega_s t & -\sin \omega_s t & 1 \\ \cos \left(\omega_s t - \frac{2\pi}{3} \right) & -\sin \left(\omega_s t - \frac{2\pi}{3} \right) & 1 \\ \cos \left(\omega_s t + \frac{2\pi}{3} \right) & -\sin \left(\omega_s t + \frac{2\pi}{3} \right) & 1 \end{bmatrix} \quad (6.2)$$

Recalling the transformation and scaling of Section 3.3, we use the subscript i for all variables and parameters to denote machine i . We now define the scaled machine stator

voltages, currents, and flux linkages in the synchronously rotating reference frame as

$$\begin{bmatrix} V_{Di} \\ V_{Qi} \\ V_{O_i} \end{bmatrix} \stackrel{\Delta}{=} T_{dqos} T_{dqli}^{-1} \begin{bmatrix} V_{di} \\ V_{qi} \\ V_{oi} \end{bmatrix} = T_{dqos} \frac{V_{BABCi}}{V_{BDQi}} \begin{bmatrix} V_{ai} \\ V_{bi} \\ V_{ci} \end{bmatrix} = \frac{1}{\sqrt{2}} T_{dqos} \begin{bmatrix} V_{ai} \\ V_{bi} \\ V_{ci} \end{bmatrix} \quad i = 1, \dots, m \quad (6.3)$$

$$\begin{bmatrix} I_{Di} \\ I_{Qi} \\ I_{O_i} \end{bmatrix} \stackrel{\Delta}{=} T_{dqos} T_{dqli}^{-1} \begin{bmatrix} I_{di} \\ I_{qi} \\ I_{oi} \end{bmatrix} = T_{dqos} \frac{I_{BABCi}}{I_{BDQi}} \begin{bmatrix} I_{ai} \\ I_{bi} \\ I_{ci} \end{bmatrix} = \frac{1}{\sqrt{2}} T_{dqos} \begin{bmatrix} I_{ai} \\ I_{bi} \\ I_{ci} \end{bmatrix} \quad i = 1, \dots, m \quad (6.4)$$

$$\begin{bmatrix} \psi_{Di} \\ \psi_{Qi} \\ \psi_{O_i} \end{bmatrix} \stackrel{\Delta}{=} T_{dqos} T_{dqli}^{-1} \begin{bmatrix} \psi_{di} \\ \psi_{qi} \\ \psi_{oi} \end{bmatrix} = T_{dqos} \frac{\lambda_{BABCi}}{\lambda_{BDQi}} \begin{bmatrix} \psi_{ai} \\ \psi_{bi} \\ \psi_{ci} \end{bmatrix} = \frac{1}{\sqrt{2}} T_{dqos} \begin{bmatrix} \psi_{ai} \\ \psi_{bi} \\ \psi_{ci} \end{bmatrix} \quad i = 1, \dots, m \quad (6.5)$$

where T_{dqli} is the machine i transformation of Section 3.3, and all base scaling quantities are also as previously defined. For $\delta_i = \frac{P}{2}\theta_{\text{shaft}_i} - \omega_s t$, it is easy to show that

$$T_{dqos} T_{dqli}^{-1} = \begin{bmatrix} \sin \delta_i & \cos \delta_i & 0 \\ -\cos \delta_i & \sin \delta_i & 0 \\ 0 & 0 & 1 \end{bmatrix} \quad i = 1, \dots, m \quad (6.6)$$

and

$$T_{dqli} T_{dqos}^{-1} = \begin{bmatrix} \sin \delta_i & -\cos \delta_i & 0 \\ \cos \delta_i & \sin \delta_i & 0 \\ 0 & 0 & 1 \end{bmatrix} \quad i = 1, \dots, m. \quad (6.7)$$

This transformation gives

$$(V_{Di} + jV_{Qi}) = (V_{di} + jV_{qi}) e^{j(\delta_i - \frac{\pi}{2})} \quad i = 1, \dots, m \quad (6.8)$$

and

$$(I_{Di} + jI_{Qi}) = (I_{di} + jI_{qi}) e^{j(\delta_i - \frac{\pi}{2})} \quad i = 1, \dots, m. \quad (6.9)$$

We now assume that all of the m machine data sets and variables have been scaled by selecting a common system-wide power base and voltage bases that are related in accordance with the interconnecting nominal transformer ratings. Applying this transformation to the general model of (3.148)–(3.159) with the same scaling of (5.37)–(5.40) with $\epsilon = 1/\omega_s$, the multimachine model (without controls) in the synchronously rotating reference frame is

$$\epsilon \frac{d\psi_{Di}}{dt} = R_{si} I_{Di} + \psi_{Qi} + V_{Di} \quad i = 1, \dots, m \quad (6.10)$$

$$\epsilon \frac{d\psi_{Qi}}{dt} = R_{si} I_{Qi} - \psi_{Di} + V_{Qi} \quad i = 1, \dots, m \quad (6.11)$$

$$\epsilon \frac{d\psi_{O_i}}{dt} = R_{si} I_{O_i} + V_{O_i} \quad i = 1, \dots, m \quad (6.12)$$

$$T'_{doi} \frac{dE'_{qi}}{dt} = -E'_{qi} - (X_{di} - X'_{di}) \left[I_{di} - \frac{(X'_{di} - X''_{di})}{(X'_{di} - X'_{\ell si})^2} (\psi_{1di} + (X'_{di} - X'_{\ell si})I_{di} - E'_{qi}) \right] + E_{fdi} \quad i = 1, \dots, m \quad (6.13)$$

$$T''_{doi} \frac{d\psi_{1di}}{dt} = -\psi_{1di} + E'_{qi} - (X'_{di} - X'_{\ell si})I_{di} \quad i = 1, \dots, m \quad (6.14)$$

$$T'_{qoi} \frac{dE'_{di}}{dt} = -E'_{di} + (X_{qi} - X'_{qi}) \left[I_{qi} - \frac{(X'_{qi} - X''_{qi})}{(X'_{qi} - X'_{\ell si})^2} (\psi_{2qi} + (X'_{qi} - X'_{\ell si})I_{qi} + E'_{di}) \right] \quad i = 1, \dots, m \quad (6.15)$$

$$T''_{qoi} \frac{d\psi_{2qi}}{dt} = -\psi_{2qi} - E'_{di} - (X'_{qi} - X'_{\ell si})I_{qi} \quad i = 1, \dots, m \quad (6.16)$$

$$T_{si} \frac{d\delta_i}{dt} = \omega_{ti} \quad i = 1, \dots, m \quad (6.17)$$

$$T_{si} \frac{d\omega_{ti}}{dt} = T_{Mi} - (\psi_{di}I_{qi} - \psi_{qi}I_{di}) - T_{FWi} \quad i = 1, \dots, m \quad (6.18)$$

$$\psi_{di} = -X''_{di}I_{di} + \frac{(X''_{di} - X'_{\ell si})}{(X'_{di} - X'_{\ell si})} E'_{qi} + \frac{(X'_{di} - X''_{di})}{(X'_{di} - X'_{\ell si})} \psi_{1di} \quad i = 1, \dots, m \quad (6.19)$$

$$\psi_{qi} = -X''_{qi}I_{qi} - \frac{(X''_{qi} - X'_{\ell si})}{(X'_{qi} - X'_{\ell si})} E'_{di} + \frac{(X'_{qi} - X''_{qi})}{(X'_{qi} - X'_{\ell si})} \psi_{2qi} \quad i = 1, \dots, m \quad (6.20)$$

$$\psi_{oi} = -X'_{\ell si}I_{oi} \quad i = 1, \dots, m \quad (6.21)$$

where

$$(V_{Di} + jV_{Qi}) = (V_{di} + jV_{qi})e^{j(\delta_i - \frac{\pi}{2})} \quad i = 1, \dots, m \quad (6.22)$$

$$(I_{Di} + jI_{Qi}) = (I_{di} + jI_{qi})e^{j(\delta_i - \frac{\pi}{2})} \quad i = 1, \dots, m \quad (6.23)$$

$$(\psi_{Di} + j\psi_{Qi}) = (\psi_{di} + j\psi_{qi})e^{j(\delta_i - \frac{\pi}{2})} \quad i = 1, \dots, m. \quad (6.24)$$

The terminal constraints for each machine are still unspecified. The next section gives a multimachine set of terminal constraints, which can be analyzed in a manner similar to the last chapter.

6.2 Network and R-L Load Constraints

Rather than introduce an infinite bus as a terminal constraint, we propose that all m synchronous machine terminals be interconnected by balanced symmetrical three-phase R - L elements. These R - L elements are either transmission lines where capacitive effects have been neglected, or transformers. For now, we assume that all loads are balanced symmetrical three-phase R - L elements, so that the multimachine dynamic model can be written in a multi-time-scale form, as in Chapter 5. We assume that all line, transformer, and load variables have been scaled by selecting the same common power base

as the machines, and voltage buses that are related in accordance with the interconnecting nominal transformer ratings. The scaled voltage across the line, transformers, and loads is assumed to be related to the scaled current through them by

$$V_{ai} = -R_i I_{ai} + \frac{1}{\omega_s} \frac{d\psi_{ai}}{dt} \quad i = m + 1, \dots, b \quad (6.25)$$

$$V_{bi} = -R_i I_{bi} + \frac{1}{\omega_s} \frac{d\psi_{bi}}{dt} \quad i = m + 1, \dots, b \quad (6.26)$$

$$V_{ci} = -R_i I_{ci} + \frac{1}{\omega_s} \frac{d\psi_{ci}}{dt} \quad i = m + 1, \dots, b \quad (6.27)$$

with

$$\begin{bmatrix} \psi_{ai} \\ \psi_{bi} \\ \psi_{ci} \end{bmatrix} = \begin{bmatrix} X_{esi} & X_{emi} & X_{emi} \\ X_{emi} & X_{esi} & X_{emi} \\ X_{emi} & X_{emi} & X_{esi} \end{bmatrix} \begin{bmatrix} -I_{ai} \\ -I_{bi} \\ -I_{ci} \end{bmatrix} \quad i = m + 1, \dots, b. \quad (6.28)$$

To connect the machines, these constraints must also be transformed. The scaled line, transformer, and load variables in the synchronously rotating reference frame are defined as

$$\begin{bmatrix} V_{Di} \\ V_{Qi} \\ V_{Oi} \end{bmatrix} \stackrel{\Delta}{=} \frac{1}{\sqrt{2}} T_{dqos} \begin{bmatrix} V_{ai} \\ V_{bi} \\ V_{ci} \end{bmatrix} \quad i = m + 1, \dots, b \quad (6.29)$$

$$\begin{bmatrix} I_{Di} \\ I_{Qi} \\ I_{Oi} \end{bmatrix} \stackrel{\Delta}{=} \frac{1}{\sqrt{2}} T_{dqos} \begin{bmatrix} I_{ai} \\ I_{bi} \\ I_{ci} \end{bmatrix} \quad i = 1 + m, \dots, b \quad (6.30)$$

$$\begin{bmatrix} \psi_{Di} \\ \psi_{Qi} \\ \psi_{Oi} \end{bmatrix} \stackrel{\Delta}{=} \frac{1}{\sqrt{2}} T_{dqos} \begin{bmatrix} \psi_{ai} \\ \psi_{bi} \\ \psi_{ci} \end{bmatrix} \quad i = m + 1, \dots, b. \quad (6.31)$$

The $\sqrt{2}$ is needed because of (6.3)–(6.5). Applying this transformation to (6.25)–(6.28) gives the network and load constraints suitable for connecting the m machines:

$$\epsilon \frac{d\psi_{Di}}{dt} = R_i I_{Di} + \psi_{Qi} + V_{Di} \quad i = m + 1, \dots, b \quad (6.32)$$

$$\epsilon \frac{d\psi_{Qi}}{dt} = R_i I_{Qi} - \psi_{Di} + V_{Qi} \quad i = m + 1, \dots, b \quad (6.33)$$

$$\epsilon \frac{d\psi_{Oi}}{dt} = R_i I_{Oi} + V_{Oi} \quad i = m + 1, \dots, b \quad (6.34)$$

$$\psi_{Di} = -X_{epi} I_{Di} \quad i = m + 1, \dots, b \quad (6.35)$$

$$\psi_{Qi} = -X_{epi} I_{Qi} \quad i = m + 1, \dots, b \quad (6.36)$$

$$\psi_{Oi} = -X_{eo} I_{Oi} \quad i = m + 1, \dots, b. \quad (6.37)$$

with $X_{epi} = X_{esi} - X_{emi}$ and $X_{eo} = X_{esi} + 2X_{emi}$. The stator and network plus loads all have exactly the same form when expressed in this reference frame. The b sets of flux linkages and currents are not all independent.

6.3 Elimination of Stator/Network Transients

With this synchronous machine plus the $R-L$ element model, it is possible to formally extend the elimination of stator/network transients of Section 5.3 to the multimachine case. To be proper, we should reduce our dynamic states to an independent set. For inductive elements, this is normally done by writing the dynamics in terms of an independent set of loop currents. To do this, we use several concepts from basic graph theory. Consider the three-node, four-branch directed graph of Figure 6.1. It is a directed graph because each branch (labeled a, b, c, d) has an arrow associated with it. This arrow is the assumed direction of the branch current, as well as the assumed polarity of the voltage. For example, the four branch voltages (all written with the same rise/drop convention) must satisfy Kirchhoff's laws (the three loops shown in Figure 6.1):

$$v_a - v_b - v_c = 0 \quad (6.38)$$

$$v_c - v_d = 0 \quad (6.39)$$

$$v_a - v_b - v_d = 0 \quad (6.40)$$

or

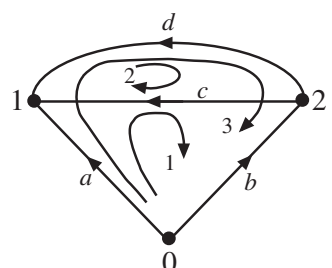
$$C_a^t v_{\text{branch}} = 0 \quad (6.41)$$

where C_a is the augmented branch-loop incidence matrix

$$C_a = \begin{matrix} & \begin{matrix} 1 & 2 & 3 \end{matrix} \\ \begin{matrix} a \\ b \\ c \\ d \end{matrix} & \left(\begin{matrix} 1 & 0 & 1 \\ -1 & 0 & -1 \\ -1 & 1 & 0 \\ 0 & -1 & -1 \end{matrix} \right) \end{matrix} \quad (6.42)$$

In general, the branch-loop incidence matrix is $b \times \ell$, where ℓ is the total number of loops in the graph (or circuit). Clearly, C_a is not unique, since we can define loops in any direction we choose. Furthermore, electrical engineers should recall that, for a given circuit (graph), there are at most $b-n$ independent loop currents. For planar circuits, these are the mesh currents. In the graph shown, $n = 2$, since n was defined previously as the number of nodes excluding the reference node. Thus, since one of the nodes in Figure 6.1 must be the reference node, there are only two independent columns in C_a (two independent rows of C_a^t). For assumed arrows of the b branches and assumed

Figure 6.1 Directed graph.



directions of the ℓ loops, the C_a matrix can be written by inspection using the following algorithm:

$$\begin{aligned} C_a(i,j) &= 1 && \text{if branch } i \text{ is in the same direction as loop } j, \text{ and branch } i \text{ is in} \\ &\quad \text{loop } j \\ C_a(i,j) &= -1 && \text{if branch } i \text{ is in the opposite direction of loop } j, \text{ and branch } i \text{ is} \\ &\quad \text{in loop } j \\ C_a(i,j) &= 0 && \text{if branch } i \text{ is not in loop } j \end{aligned}$$

Since the branch directions are the assumed branch current directions as well,

$$i_{\text{branch}} = C_a i_{\text{loop}} \quad (6.43)$$

which, for our example, gives

$$i_a = i_{\text{loop1}} + i_{\text{loop3}} \quad (6.44)$$

$$i_b = -i_{\text{loop1}} - i_{\text{loop3}} \quad (6.45)$$

$$i_c = -i_{\text{loop1}} + i_{\text{loop2}} \quad (6.46)$$

$$i_d = -i_{\text{loop2}} - i_{\text{loop3}} \quad (6.47)$$

which can be easily verified by inspection.

The $b-n$ independent loops can be determined by partitioning C_a in a special way. Begin with b branches all disconnected (as our multimachine model currently is). Connect n branches such that every node is connected, but no loops are formed. The resulting graph is called a tree. The remaining $b-n$ branches are called tree links, and are now added one at a time. Adding one tree link will create a loop. This loop should be oriented in the same direction as the tree link. Adding a second tree link will create a second loop. This loop should also be oriented in the same direction as the second tree link, and must not include the previously added tree link. When this process is completed, there will be $b-n$ loops, which correspond to the $b-n$ tree links. Thus, the incidence matrix created in this manner will have only $b-n$ columns and will be structured as

$$C_b = \begin{matrix} 1 \\ \vdots \\ n \\ n+1 \\ \vdots \\ b \end{matrix} \left[\begin{matrix} 1 \dots \ell' \\ \hline C_T \\ I \end{matrix} \right]. \quad (6.48)$$

This $b \times \ell'$ ($\ell' = b - n$) branch loop incidence matrix is called a basic loop matrix, and does not have the subscript a . The columns of C_a that do not appear in C_b are dependent. It should be clear that we still have the relations for Kirchhoff's laws:

$$i_{\text{branch}} = C_b i_{\text{indep. loop}} \quad (6.49)$$

$$C_b^t v_{\text{branch}} = 0. \quad (6.50)$$

This matrix will now be used with our b sets of stator/network/load equations. We define

$$\psi_{D\text{branch}} \stackrel{\Delta}{=} [\psi_{D1} \cdots \psi_{Db}]^t \quad (6.51)$$

$$I_{D\text{branch}} \stackrel{\Delta}{=} [I_{D1} \cdots I_{Db}]^t \quad (6.52)$$

$$V_{D\text{branch}} \stackrel{\Delta}{=} [V_{D1} \cdots V_{Db}]^t \quad (6.53)$$

and similarly for Q and O . For a system with a basic branch loop incidence matrix describing the interconnection of these b branches as C_b , we define loop flux linkages as

$$\psi_{D\text{loop}} \stackrel{\Delta}{=} C_b^t \psi_{D\text{branch}} \quad (6.54)$$

$$\psi_{Q\text{loop}} \stackrel{\Delta}{=} C_b^t \psi_{Q\text{branch}} \quad (6.55)$$

$$\psi_{O\text{loop}} \stackrel{\Delta}{=} C_b^t \psi_{O\text{branch}} \quad (6.56)$$

and write the corresponding branch currents in terms of independent loop currents as

$$I_{D\text{branch}} = C_b I_{D\text{loop}} \quad (6.57)$$

$$I_{Q\text{branch}} = C_b I_{Q\text{loop}} \quad (6.58)$$

$$I_{O\text{branch}} = C_b I_{O\text{loop}} \quad (6.59)$$

By our choice of numbering, the first m branches are synchronous machines, and the last $b-m$ branches are transformers, lines, and loads. It might appear that this numbering scheme would not allow us to have two synchronous machines connected to the same bus, since the first n branches must form a tree. This clearly is not a real limitation, since the ordering of C_a can be changed arbitrarily after it is formed to suit a particular preference.

We have not shown it formally, but the topology relationships between the abc branch voltages and branch currents are the same as for the dqo branch voltages and currents. We now write the stator/network/load transients of (6.10)–(6.24) and (6.32)–(6.37) in vector/matrix form:

$$\epsilon \frac{d\psi_{D\text{branch}}}{dt} = R_{\text{branch}} I_{D\text{branch}} + \psi_{Q\text{branch}} + V_{D\text{branch}} \quad (6.60)$$

$$\epsilon \frac{d\psi_{Q\text{branch}}}{dt} = R_{\text{branch}} I_{Q\text{branch}} - \psi_{D\text{branch}} + V_{Q\text{branch}} \quad (6.61)$$

$$\epsilon \frac{d\psi_{O\text{branch}}}{dt} = R_{\text{branch}} I_{O\text{branch}} + V_{O\text{branch}} \quad (6.62)$$

where additional algebraic equations relating the flux linkages and currents could be written using (6.19)–(6.24) and (6.35)–(6.37).

Multiplying these equations by C_b^t and using the properties of C_b from (6.50) and (6.57)–(6.59) gives the b - n independent sets of stator/network/load transients

$$\epsilon \frac{d\psi_{D\text{loop}}}{dt} = C_b^t R_{\text{branch}} C_b I_{D\text{loop}} + \psi_{Q\text{loop}} \quad (6.63)$$

$$\epsilon \frac{d\psi_{Q\text{loop}}}{dt} = C_b^t R_{\text{branch}} C_b I_{Q\text{loop}} - \psi_{D\text{loop}} \quad (6.64)$$

$$\epsilon \frac{d\psi_{O\text{loop}}}{dt} = C_b^t R_{\text{branch}} C_b I_{O\text{loop}}. \quad (6.65)$$

As in the single machine/infinite bus case of Chapter 5, the $R_{\text{branch}} = 0$ case has a very interesting result. When resistance is zero, (6.63)–(6.65) have an exact integral manifold for $\psi_{D\text{loop}}$, $\psi_{Q\text{loop}}$, and $\psi_{O\text{loop}}$, regardless of ϵ :

$$\psi_{D\text{loop}} \Big|_{R_{\text{branch}}=0} = \psi_{Q\text{loop}} \Big|_{R_{\text{branch}}=0} = \psi_{O\text{loop}} \Big|_{R_{\text{branch}}=0} = 0. \quad (6.66)$$

This means that if $\psi_{D\text{loop}}$, $\psi_{Q\text{loop}}$, and $\psi_{O\text{loop}}$ are initially zero and $R_{\text{branch}} = 0$, then $\psi_{D\text{loop}}$, $\psi_{Q\text{loop}}$, and $\psi_{O\text{loop}}$ remain at zero for all time t regardless of the size of ϵ . If $\psi_{D\text{loop}}$, $\psi_{Q\text{loop}}$, and $\psi_{O\text{loop}}$ are not initially zero and $R_{\text{branch}} = 0$, then $\psi_{D\text{loop}}$, $\psi_{Q\text{loop}}$ oscillate forever and $\psi_{O\text{loop}}$ remains at its initial value, according to (6.63)–(6.65). Unlike the single machine/infinite bus case, the $R_{\text{branch}} = 0$ condition is not practical, since this means that the only possible load could be one or more synchronous machines acting as motors.

For R_{branch} not equal to zero but ϵ sufficiently small, an integral manifold for $\psi_{D\text{loop}}$, $\psi_{Q\text{loop}}$, and $\psi_{O\text{loop}}$ still exists, but has not been found exactly. An approximation of this integral manifold can be found by setting ϵ to zero and solving all the algebraic equations for the stator/network/load flux linkages and currents. This requires the solution of the following equations:

$$0 = C_b^t R_{\text{branch}} C_b I_{D\text{loop}} + \psi_{Q\text{loop}} \quad (6.67)$$

$$0 = C_b^t R_{\text{branch}} C_b I_{Q\text{loop}} - \psi_{D\text{loop}} \quad (6.68)$$

$$0 = C_b^t R_{\text{branch}} C_b I_{O\text{loop}} \quad (6.69)$$

with

$$\psi_{D\text{loop}} = C_b^t \psi_{D\text{branch}} \quad (6.70)$$

$$\psi_{Q\text{loop}} = C_b^t \psi_{Q\text{branch}} \quad (6.71)$$

$$\psi_{O\text{loop}} = C_b^t \psi_{O\text{branch}} \quad (6.72)$$

$$I_{D\text{branch}} = C_b I_{D\text{loop}} \quad (6.73)$$

$$I_{Q\text{branch}} = C_b I_{Q\text{loop}} \quad (6.74)$$

$$I_{O\text{branch}} = C_b I_{O\text{loop}} \quad (6.75)$$

and (6.19)–(6.24) plus (6.35)–(6.37). Alternatively, we solve (6.10)–(6.12), (6.19)–(6.24), and (6.32)–(6.37) evaluated at $\epsilon = 0$. The “zero” variables are decoupled and will not be

$$\left[(X_{qi}'' - X_{di}'') I_{qi} + \frac{(X_{qi}'' - X_{\ell si})}{(X_{qi}' - X_{\ell si})} E_{di}' - \frac{(X_{qi}' - X_{qi}'')}{(X_{qi}' - X_{\ell si})} \psi_{2qi} + j \frac{(X_{di}'' - X_{\ell si})}{(X_{di}' - X_{\ell si})} E_{qi}' + j \frac{(X_{di}' - X_{di}'')}{(X_{di}' - X_{\ell si})} \psi_{1di} \right] e^{j(\delta_i - \pi/2)}$$

Figure 6.2 Multimachine subtransient dynamic circuit ($i = 1, \dots, m$).

carried further. Adding (6.10) plus j times (6.11) and using (6.22)–(6.24) gives

$$0 = R_{si}(I_{di} + jI_{qi})e^{j(\delta_i - \frac{\pi}{2})} - j(\psi_{di} + j\psi_{qi})e^{j(\delta_i - \frac{\pi}{2})} + (V_{di} + jV_{qi})e^{j(\delta_i - \frac{\pi}{2})} \quad i = 1, \dots, m. \quad (6.76)$$

Substituting (6.19) and (6.20) gives the following complex equation, which can be written as the circuit of Figure 6.2.

$$0 = (R_{si} + jX_{di}'') (I_{di} + jI_{qi}) e^{j(\delta_i - \frac{\pi}{2})} + (V_{di} + jV_{qi}) e^{j(\delta_i - \frac{\pi}{2})} - \left[(X_{qi}'' - X_{di}'') I_{qi} + \frac{(X_{qi}'' - X_{\ell si})}{(X_{qi}' - X_{\ell si})} E_{di}' - \frac{(X_{qi}' - X_{qi}'')}{(X_{qi}' - X_{\ell si})} \psi_{2qi} + j \frac{(X_{di}'' - X_{\ell si})}{(X_{di}' - X_{\ell si})} E_{qi}' + j \frac{(X_{di}' - X_{di}'')}{(X_{di}' - X_{\ell si})} \psi_{1di} \right] e^{j(\delta_i - \frac{\pi}{2})} \quad i = 1, \dots, m. \quad (6.77)$$

Adding (6.32) plus j times (6.33) and eliminating ψ_{Di} , ψ_{Qi} using (6.35) and (6.36) give the network/load equation, which can be written as the circuit of Figure 6.3.

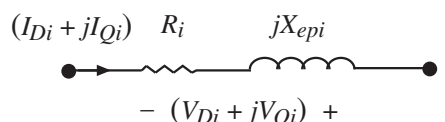
$$0 = (R_i + jX_{epi})(I_{Di} + jI_{Qi}) + (V_{Di} + jV_{Qi}) \quad i = m + 1, \dots, b. \quad (6.78)$$

To convert from branch subscript notation to bus subscript notation, we make the following notational numbering of branches. Assume that loads are present at all n buses, and connected to the reference bus. These n branch voltages are then bus voltages denoted as

$$V_i e^{j\theta_i} \stackrel{\Delta}{=} (V_{Di} + jV_{Qi}) \quad i = 1, \dots, n. \quad (6.79)$$

All branches in excess of these n have branch voltages that are either equal to bus voltages or equal to the difference between two bus voltages. With this bus notation, the multimachine dynamic model is any connection of the circuits of Figures 6.2 and 6.3 into a network resulting in m machines, b branches, and n buses.

Figure 6.3 Network plus R-L load dynamic circuit ($i = m + 1, \dots, b$).



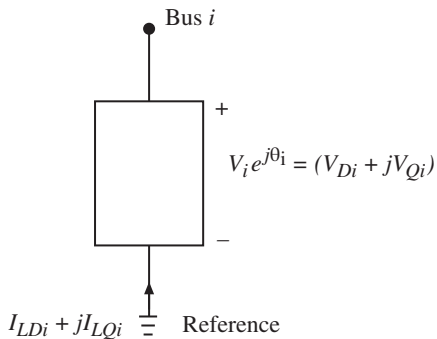


Figure 6.4 Generalized load electrical dynamic circuit.

6.3.1 Generalization of Network and Load Dynamic Models

Before stating the final model, we now make a major assumption about the actual network and loads. We assume that an integral manifold also exists for all dynamic states associated with networks and loads that are not simple $R-L$ elements. We assume that the integral manifold for the network dynamic states can be approximated by the same representation as above (Figure 6.3 allowing X_{ep} to be negative). We also assume that the integral manifold for the load electrical dynamic states can be approximated by sets of two algebraic equations that can be written as sets of complex equations of the following general form, using the convention of Figure 6.4.

$$(V_{Di} + jV_{Qi})(I_{LDi} - jI_{LQi}) = P_{Li}(V_i) + jQ_{Li}(V_i) \quad i = 1, \dots, n \quad (6.80)$$

where $P_{Li}(V_i)$ and $Q_{Li}(V_i)$ may be nonlinear functions of the bus voltage magnitude V_i . Commonly used load models are

$$P_{Li}(V_i) = P_{Loi} + k_{P1i}V_i + k_{P2i}V_i^2 + \dots \quad i = 1, \dots, n \quad (6.81)$$

$$Q_{Li}(V_i) = Q_{Loi} + k_{Q1i}V_i + k_{Q2i}V_i^2 + \dots \quad i = 1, \dots, n \quad (6.82)$$

or any combination of terms involving any power of V_i . The constants P_{Loi} and Q_{Loi} represent a “constant power” component, k_{P1i} and k_{Q1i} represent a “constant current magnitude at constant power factor” component, and k_{P2i} and k_{Q2i} represent a “constant impedance” component. Note that P_{Li} and Q_{Li} are given as “injected” powers, meaning that P_{Li} will normally be negative for a passive load.

With this generalized model for the network and loads, we write the algebraic equations for the interconnection of m machine circuits with all transformers, lines, and loads using the standard network bus admittance matrix defined through the bus voltages and net injected currents by

$$(I_{di} + jI_{qi})e^{j(\delta_i - \frac{\pi}{2})} + (I_{LDi} + jI_{LQi}) = \sum_{k=1}^n Y_{ik} e^{j\alpha_{ik}} V_k e^{j\theta_k} \quad i = 1, \dots, m \quad (6.83)$$

$$(I_{LDi} + jI_{LQi}) = \sum_{k=1}^n Y_{ik} e^{j\alpha_{ik}} V_k e^{j\theta_k} \quad i = m + 1, \dots, n \quad (6.84)$$

where all quantities are as previously defined, and $Y_{ik} e^{j\alpha_{ik}}$ is the ik^{th} entry of the network bus admittance matrix. This matrix is formed using all of the branches of the form of

Figure 6.3. It has the same formulation as the admittance matrix used for load–flow analysis.

This representation gives the following dynamic model for the m machine, n bus power system after stator/network and load electrical transients have been eliminated, and using the load model of Figure 6.4 and (6.80):

$$T'_{doi} \frac{dE'_{qi}}{dt} = -E'_{qi} - (X_{di} - X'_{di}) \left[I_{di} - \frac{(X'_{di} - X''_{di})}{(X'_{di} - X'_{\ell si})^2} (\psi_{1di} + (X'_{di} - X'_{\ell si})I_{di} - E'_{qi}) \right] + E_{fdi} \quad i = 1, \dots, m \quad (6.85)$$

$$T''_{doi} \frac{d\psi_{1di}}{dt} = -\psi_{1di} + E'_{qi} - (X'_{di} - X'_{\ell si})I_{di} \quad i = 1, \dots, m \quad (6.86)$$

$$T'_{qoi} \frac{dE'_{di}}{dt} = -E'_{di} + (X_{qi} - X'_{qi}) \left[I_{qi} - \frac{(X'_{qi} - X''_{qi})}{(X'_{qi} - X'_{\ell si})^2} (\psi_{2qi} + (X'_{qi} - X'_{\ell si})I_{qi} + E'_{di}) \right] \quad i = 1, \dots, m \quad (6.87)$$

$$T''_{qoi} \frac{d\psi_{2qi}}{dt} = -\psi_{2qi} - E'_{di} - (X'_{qi} - X'_{\ell si})I_{qi} \quad i = 1, \dots, m \quad (6.88)$$

$$\frac{d\delta_i}{dt} = \omega_i - \omega_s \quad i = 1, \dots, m \quad (6.89)$$

$$\begin{aligned} \frac{2H_i}{\omega_s} \frac{d\omega_i}{dt} &= T_{Mi} - \frac{(X''_{di} - X'_{\ell si})}{(X'_{di} - X'_{\ell si})} E'_{qi} I_{qi} - \frac{(X'_{di} - X''_{di})}{(X'_{di} - X'_{\ell si})} \psi_{1di} I_{qi} - \frac{(X''_{qi} - X'_{\ell si})}{(X'_{qi} - X'_{\ell si})} E'_{di} I_{di} \\ &\quad + \frac{(X'_{qi} - X''_{qi})}{(X'_{qi} - X'_{\ell si})} \psi_{2qi} I_{di} - (X''_{qi} - X''_{di}) I_{di} I_{qi} - T_{FWi} \quad i = 1, \dots, m \end{aligned} \quad (6.90)$$

$$T_{Ei} \frac{dE_{fdi}}{dt} = -(K_{Ei} + S_{Ei}(E_{fdi}))E_{fdi} + V_{Ri} \quad i = 1, \dots, m \quad (6.91)$$

$$T_{Fi} \frac{dR_{fi}}{dt} = -R_{fi} + \frac{K_{Fi}}{T_{Fi}} E_{fdi} \quad i = 1, \dots, m \quad (6.92)$$

$$T_{Ai} \frac{dV_{Ri}}{dt} = -V_{Ri} + K_{Ai} R_{fi} - \frac{K_{Ai} K_{Fi}}{T_{Fi}} E_{fdi} + K_{Ai} (V_{refi} - V_i) \quad i = 1, \dots, m \quad (6.93)$$

$$T_{CHi} \frac{dT_{Mi}}{dt} = -T_{Mi} + P_{SVi} \quad i = 1, \dots, m \quad (6.94)$$

$$T_{SVi} \frac{dP_{SVi}}{dt} = -P_{SVi} + P_{Ci} - \frac{1}{R_{Di}} \left(\frac{\omega_i}{\omega_s} - 1 \right) \quad i = 1, \dots, m \quad (6.95)$$

with the limit constraints

$$V_{Ri}^{\min} \leq V_{Ri} \leq V_{Ri}^{\max} \quad i = 1, \dots, m \quad (6.96)$$

$$0 \leq P_{SVi} \leq P_{SVi}^{\max} \quad i = 1, \dots, m \quad (6.97)$$

and the algebraic constraints

$$0 = V_i e^{j\theta_i} + (R_{si} + jX''_{di})(I_{di} + jI_{qi})e^{j(\delta_i - \frac{\pi}{2})} - \left[(X''_{qi} - X''_{di})I_{qi} + \frac{(X''_{qi} - X'_{\ell si})}{(X'_{qi} - X'_{\ell si})} E'_{di} \right. \\ \left. - \frac{(X'_{qi} - X''_{qi})}{(X'_{qi} - X'_{\ell si})} \psi_{2qi} + j \frac{(X''_{di} - X'_{\ell si})}{(X'_{di} - X'_{\ell si})} E'_{qi} + j \frac{(X'_{di} - X''_{di})}{(X'_{di} - X'_{\ell si})} \psi_{1di} \right] e^{j(\delta_i - \frac{\pi}{2})} \\ i = 1, \dots, m \quad (6.98)$$

$$V_i e^{j\theta_i} (I_{di} - jI_{qi}) e^{-j(\delta_i - \frac{\pi}{2})} + P_{Li}(V_i) + jQ_{Li}(V_i) = \sum_{k=1}^n V_i V_k Y_{ik} e^{j(\theta_i - \theta_k - \alpha_{ik})} \quad i = 1, \dots, m \quad (6.99)$$

$$P_{Li}(V_i) + jQ_{Li}(V_i) = \sum_{k=1}^n V_i V_k Y_{ik} e^{j(\theta_i - \theta_k - \alpha_{ik})} \quad i = m+1, \dots, n. \quad (6.100)$$

The voltage regulator input voltage is V_i , which is automatically defined through the network algebraic constraints. Also, for given functions $P_{Li}(V_i)$ and $Q_{Li}(V_i)$, the $n+m$ complex algebraic equations must be solved for V_i, θ_i ($i = 1, \dots, n$), I_{di}, I_{qi} ($i = 1, \dots, m$) in terms of the states $\delta_i, E'_{di}, \psi_{2qi}, E'_{qi}, \psi_{1di}$ ($i = 1, \dots, m$). The currents clearly can be explicitly eliminated by solving either (6.98) or (6.99) and substituting into the differential equations and remaining algebraic equations. This would leave only n complex algebraic equations to be solved for the n complex voltages $V_i e^{j\theta_i}$.

6.3.2 The Special Case of “Impedance Loads”

In some cases, the above dynamic model can be put in explicit closed form without algebraic equations. We make the special assumptions about the load representations:

$$P_{Li}(V_i) = k_{P2i} V_i^2 \quad i = 1, \dots, n \quad (6.101)$$

$$Q_{Li}(V_i) = k_{Q2i} V_i^2 \quad i = 1, \dots, n. \quad (6.102)$$

In this case, the loads and $R_{si} + jX''_{di}$ can be added into the bus admittance matrix diagonal entries to obtain the following algebraic equations:

$$(I_{di} + jI_{qi}) e^{j(\delta_i - \frac{\pi}{2})} = \frac{1}{(R_{si} + jX''_{di})} \left[(X''_{qi} - X''_{di})I_{qi} + \frac{(X''_{qi} - X'_{\ell si})}{(X'_{qi} - X'_{\ell si})} E'_{di} - \frac{(X'_{qi} - X''_{qi})}{(X'_{qi} - X'_{\ell si})} \psi_{2qi} \right. \\ \left. + j \frac{(X''_{di} - X'_{\ell si})}{(X'_{di} - X'_{\ell si})} E'_{qi} + j \frac{(X'_{di} - X''_{di})}{(X'_{di} - X'_{\ell si})} \psi_{1di} \right] e^{j(\delta_i - \frac{\pi}{2})} - \left(\frac{1}{R_{si} + jX''_{di}} \right) V_i e^{j\theta_i} \\ i = 1, \dots, m \quad (6.103)$$

$$0 = - \left(\frac{1}{R_{si} + jX''_{di}} \right) \left[(X''_{qi} - X''_{di})I_{qi} + \frac{(X''_{qi} - X'_{\ell si})}{(X'_{qi} - X'_{\ell si})} E'_{di} - \frac{(X'_{qi} - X''_{qi})}{(X'_{qi} - X'_{\ell si})} \psi_{2qi} \right. \\ \left. + j \frac{(X''_{di} - X'_{\ell si})}{(X'_{di} - X'_{\ell si})} E'_{qi} + j \frac{(X'_{di} - X''_{di})}{(X'_{di} - X'_{\ell si})} \psi_{1di} \right] e^{j(\delta_i - \frac{\pi}{2})} + \sum_{k=1}^n (G''_{ik} + jB''_{ik}) V_k e^{j\theta_k} \\ i = 1, \dots, m \quad (6.104)$$

$$0 = \sum_{k=1}^n (G''_{ik} + jB''_{ik}) V_k e^{j\theta_k} \quad i = m+1, \dots, n \quad (6.105)$$

where $G''_{ik} + jB''_{ik}$ is the ik^{th} entry of the bus admittance matrix, including all “constant impedance” loads and $1/(R_{si} + jX''_{di})$ on the i^{th} diagonal.

Clearly, all of the $V_k e^{j\theta_k}$ ($k = 1, \dots, n$) can be eliminated by solving (6.104) and (6.105) and substituting into (6.103) to obtain m complex equations that are linear in I_{di} , I_{qi} ($i = 1, \dots, m$). These can, in principle, be solved through the inverse of a matrix that would be a function of δ_i , E'_{di} , ψ_{2qi} , E'_{qi} , ψ_{1di} ($i = 1, \dots, m$). This inverse can be avoided if the following simplification is made:

$$X''_{qi} = X''_{di} \quad i = 1, \dots, m. \quad (6.106)$$

With this assumption, (6.104) and (6.105) can be solved for $V_k e^{j\theta_k}$ and substituted into (6.103) to obtain

$$\begin{aligned} I_{di} + jI_{qi} = \sum_{k=1}^m (G''_{ik}^{\text{red}} + jB''_{ik}^{\text{red}}) & \left[\frac{(X''_{qk} - X_{\ell sk})}{(X'_{qk} - X_{\ell sk})} E'_{dk} - \frac{(X'_{qk} - X''_{qk})}{(X'_{qk} - X_{\ell sk})} \psi_{2qk} \right. \\ & \left. + j \frac{(X''_{dk} - X_{\ell sk})}{(X'_{dk} - X_{\ell sk})} E'_{qk} + j \frac{(X'_{dk} - X''_{dk})}{(X'_{dk} - X_{\ell sk})} \psi_{1dk} \right] e^{j(\delta_k - \delta_i)} \quad i = 1, \dots, m \end{aligned} \quad (6.107)$$

where $G''_{ik}^{\text{red}} + jB''_{ik}^{\text{red}}$ is the ik^{th} entry of an $m \times m$ admittance matrix (often called the matrix reduced to “internal nodes”). This can easily be solved for I_{di} , I_{qi} ($i = 1, \dots, m$) and substituted into the differential equations (6.85)–(6.95). Substitution of I_{di} , I_{qi} into (6.98) also gives V_i as a function of the states (needed for (6.93)), so the resulting dynamic model is in explicit form without algebraic equations.

6.4 Multimachine Two-Axis Model

The reduced-order model of the last section still contains the damper-winding dynamics ψ_{1di} and ψ_{2qi} . If T''_{doi} and T''_{qoi} are sufficiently small, there is an integral manifold for these dynamic states. A first approximation of the fast damper-winding integral manifold is found by setting T''_{doi} and T''_{qoi} equal to zero in (6.86)–(6.88) to obtain

$$0 = -\psi_{1di} + E'_{qi} - (X'_{di} - X_{\ell si})I_{di} \quad i = 1, \dots, m \quad (6.108)$$

$$0 = -\psi_{2qi} - E'_{di} - (X'_{qi} - X_{\ell si})I_{qi} \quad i = 1, \dots, m. \quad (6.109)$$

When used to eliminate ψ_{1di} and ψ_{2qi} , the synchronous machine dynamic circuit is changed from Figure 6.2 to Figure 6.5, giving the following multimachine two-axis model:

$$T'_{doi} \frac{dE'_{qi}}{dt} = -E'_{qi} - (X_{di} - X'_{di})I_{di} + E_{fdi} \quad i = 1, \dots, m \quad (6.110)$$

$$T'_{qoi} \frac{dE'_{di}}{dt} = -E'_{di} + (X_{qi} - X'_{qi})I_{qi} \quad i = 1, \dots, m \quad (6.111)$$

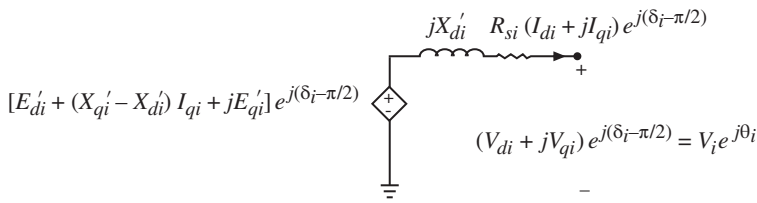


Figure 6.5 Synchronous machine two-axis model dynamic circuit ($i = 1, \dots, m$).

$$\frac{d\delta_i}{dt} = \omega_i - \omega_s \quad i = 1, \dots, m \quad (6.112)$$

$$\frac{2H_i}{\omega_s} \frac{d\omega_i}{dt} = T_{Mi} - E'_{di} I_{di} - E'_{qi} I_{qi} - (X'_{qi} - X'_{di}) I_{di} I_{qi} - T_{FWi} \quad i = 1, \dots, m \quad (6.113)$$

$$T_{Ei} \frac{dE_{fdi}}{dt} = -(K_{Ei} + S_{Ei}(E_{fdi})) E_{fdi} + V_{Ri} \quad i = 1, \dots, m \quad (6.114)$$

$$T_{Fi} \frac{dR_{fi}}{dt} = -R_{fi} + \frac{K_{Fi}}{T_{Fi}} E_{fdi} \quad i = 1, \dots, m \quad (6.115)$$

$$T_{Ai} \frac{dV_{Ri}}{dt} = -V_{Ri} + K_{Ai} R_{fi} - \frac{K_{Ai} K_{Fi}}{T_{Fi}} E_{fdi} + K_{Ai} (V_{refi} - V_i) \quad i = 1, \dots, m \quad (6.116)$$

$$T_{CHi} \frac{dT_{Mi}}{dt} = -T_{Mi} + P_{SVi} \quad i = 1, \dots, m \quad (6.117)$$

$$T_{SVi} \frac{dP_{SVi}}{dt} = -P_{SVi} + P_{Ci} - \frac{1}{R_{Di}} \left(\frac{\omega_i}{\omega_s} - 1 \right) \quad i = 1, \dots, m \quad (6.118)$$

with the limit constraints

$$V_{Ri}^{\min} \leq V_{Ri} \leq V_{Ri}^{\max} \quad i = 1, \dots, m \quad (6.119)$$

$$0 \leq P_{SVi} \leq P_{SVi}^{\max} \quad i = 1, \dots, m \quad (6.120)$$

and the algebraic constraints

$$0 = V_i e^{j\theta_i} + (R_{si} + jX'_{di})(I_{di} + jI_{qi}) e^{j(\delta_i - \frac{\pi}{2})} - \left[E'_{di} + (X'_{qi} - X'_{di}) I_{qi} + jE'_{qi} \right] e^{j(\delta_i - \frac{\pi}{2})} \quad i = 1, \dots, m \quad (6.121)$$

$$V_i e^{j\theta_i} (I_{di} - jI_{qi}) e^{-j(\delta_i - \frac{\pi}{2})} + P_{Li}(V_i) + jQ_{Li}(V_i) = \sum_{k=1}^n V_i V_k Y_{ik} e^{j(\theta_i - \theta_k - \alpha_{ik})} \quad i = 1, \dots, m \quad (6.122)$$

$$P_{Li}(V_i) + jQ_{Li}(V_i) = \sum_{k=1}^n V_i V_k Y_{ik} e^{j(\theta_i - \theta_k - \alpha_{ik})} \quad i = m+1, \dots, n. \quad (6.123)$$

As before, for given functions $P_{Li}(V_i)$ and $Q_{Li}(V_i)$, the $n+m$ complex algebraic equations must be solved for V_i , θ_i ($i = 1, \dots, m$) and I_{di} , I_{qi} ($i = 1, \dots, m$) in terms of the states δ_i , E'_{di} , E'_{qi} ($i = 1, \dots, m$). The currents can clearly be explicitly eliminated by solving either (6.121) or (6.122) and substituting into the differential equations and remaining algebraic equations. This would leave only n complex algebraic equations to be solved for the n complex voltages $V_i e^{j\theta_i}$.

6.4.1 The Special Case of “Impedance Loads”

In some cases, this two-axis dynamic model can be put in explicit closed form without algebraic equations. We make the special assumptions about the load representations

$$P_{Li}(V_i) = k_{P2i} V_i^2 \quad i = 1, \dots, n \quad (6.124)$$

$$Q_{Li}(V_i) = k_{Q2i} V_i^2 \quad i = 1, \dots, n. \quad (6.125)$$

In this case, the loads and $R_{si} + jX'_{di}$ can be added into the bus admittance matrix diagonal entries to obtain the following simplified algebraic equations for the two-axis model with “constant impedance” loads

$$(I_{di} + jI_{qi})e^{j(\delta_i - \frac{\pi}{2})} = \left(\frac{1}{R_{si} + jX'_{di}} \right) [E'_{di} + (X'_{qi} - X'_{di})I_{qi} + jE'_{qi}] e^{j(\delta_i - \frac{\pi}{2})} - \left(\frac{1}{R_{si} + jX'_{di}} \right) V_i e^{j\theta_i} \quad i = 1, \dots, m \quad (6.126)$$

$$0 = - \left(\frac{1}{R_{si} + jX'_{di}} \right) [E'_{di} + (X'_{qi} - X'_{di})I_{qi} + jE'_{qi}] e^{j(\delta_i - \frac{\pi}{2})} + \sum_{k=1}^n (G'_{ik} + jB'_{ik}) V_k e^{j\theta_k} \quad i = 1, \dots, m \quad (6.127)$$

$$0 = \sum_{k=1}^n (G'_{ik} + jB'_{ik}) V_k e^{j\theta_k} \quad i = m+1, \dots, n \quad (6.128)$$

where $G'_{ik} + jB'_{ik}$ is the ik^{th} entry of the admittance matrix, including all “constant impedance” loads and $1/(R_{si} + jX'_{di})$ on the i^{th} diagonal.

Clearly, all of the $V_k e^{j\theta_k}$ ($k = 1, \dots, n$) can be eliminated by solving (6.127) and (6.128) and substituting into (6.126) to obtain m complex equations that are linear in I_{di} , I_{qi} ($i = 1, \dots, m$). These can, in principle, be solved through the inverse of a matrix that would be a function of the states δ_i , E'_{qi} , E'_{di} ($i = 1, \dots, m$). This inverse can be avoided if the following simplification is made:

$$X'_{qi} = X'_{di} \quad i = 1, \dots, m. \quad (6.129)$$

With this assumption, (6.127) and (6.128) can be solved for $V_k e^{j\theta_k}$ and substituted into (6.126) to obtain

$$I_{di} + jI_{qi} = \sum_{k=1}^m \left(G'_{\text{red}} + jB'_{\text{red}} \right)_{ik} [E'_{dk} + jE'_{qk}] e^{j(\delta_k - \delta_i)} \quad i = 1, \dots, m \quad (6.130)$$

where $G'_{\text{red}} + jB'_{\text{red}}$ is the ik^{th} entry of an $m \times m$ admittance matrix (often called the matrix reduced to “internal nodes”). This can easily be solved for I_{di} , I_{qi} ($i = 1, \dots, m$) and substituted into the differential equations (6.110)–(6.18). Substitution of I_{di} , I_{qi} into (6.121) also gives V_i as a function of the states (needed for (6.116)), so the resulting dynamic model is in explicit form without algebraic equations.

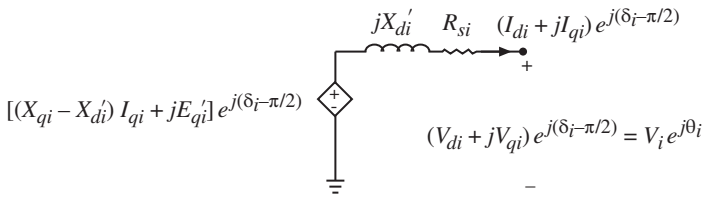


Figure 6.6 Synchronous machine flux-decay model dynamic circuit ($i = 1, \dots, m$).

6.5 Multimachine Flux-Decay Model

The reduced-order model of the last section still contains the damper-winding dynamics E'_{di} . If T'_{qoi} for all $i = 1, \dots, m$ are sufficiently small, there is an integral manifold for these dynamic states. A first approximation of the remaining fast damper-winding integral manifold is found by setting T'_{qoi} equal to zero in (6.111) to obtain

$$0 = -E'_{di} + (X_{qi} - X'_{qi})I_{qi} \quad i = 1, \dots, m. \quad (6.131)$$

When used to eliminate E'_{di} , the synchronous machine dynamic circuit is changed from Figure 6.5 to Figure 6.6, giving the following multimachine one-axis or flux-decay model:

$$T'_{doi} \frac{dE'_{qi}}{dt} = -E'_{qi} - (X_{di} - X'_{di})I_{di} + E_{fdi} \quad i = 1, \dots, m \quad (6.132)$$

$$\frac{d\delta_i}{dt} = \omega_i - \omega_s \quad i = 1, \dots, m \quad (6.133)$$

$$\frac{2H_i}{\omega_s} \frac{d\omega_i}{dt} = T_{Mi} - E'_{qi}I_{qi} - (X_{qi} - X'_{di})I_{di}I_{qi} - T_{FWi} \quad i = 1, \dots, m \quad (6.134)$$

$$T_{Ei} \frac{dE_{fdi}}{dt} = -(K_{Ei} + S_{Ei}(E_{fdi}))E_{fdi} + V_{Ri} \quad i = 1, \dots, m \quad (6.135)$$

$$T_{Fi} \frac{dR_{fi}}{dt} = -R_{fi} + \frac{K_{Fi}}{T_{Fi}}E_{fdi} \quad i = 1, \dots, m \quad (6.136)$$

$$T_{Ai} \frac{dV_{Ri}}{dt} = -V_{Ri} + K_{Ai}R_{fi} - \frac{K_{Ai}K_{fi}}{T_{Fi}}E_{fdi} + K_{Ai}(V_{refi} - V_i) \quad i = 1, \dots, m \quad (6.137)$$

$$T_{CHi} \frac{dT_{Mi}}{dt} = -T_{Mi} + P_{SVi} \quad i = 1, \dots, m \quad (6.138)$$

$$T_{SVi} \frac{dP_{SVi}}{dt} = -P_{SVi} + P_{Ci} - \frac{1}{R_{Di}} \left(\frac{\omega_i}{\omega_s} - 1 \right) \quad i = 1, \dots, m \quad (6.139)$$

with the limit constraints

$$V_{Ri}^{\min} \leq V_{Ri} \leq V_{Ri}^{\max} \quad i = 1, \dots, m \quad (6.140)$$

$$0 \leq P_{SVi} \leq P_{SVi}^{\max} \quad i = 1, \dots, m \quad (6.141)$$

and the algebraic constraints

$$0 = V_i e^{j\theta_i} + (R_{si} + jX'_{di})(I_{di} + jI_{qi}) e^{j(\delta_i - \frac{\pi}{2})} - [(X_{qi} - X'_{di})I_{qi} + jE'_{qi}] e^{j(\delta_i - \frac{\pi}{2})} \\ i = 1, \dots, m \quad (6.142)$$

$$V_i e^{j\theta_i} (I_{di} - jI_{qi}) e^{-j(\delta_i - \frac{\pi}{2})} + P_{Li}(V_i) + jQ_{Li}(V_i) = \sum_{k=1}^n V_i V_k Y_{ik} e^{j(\theta_i - \theta_k - \alpha_{ik})} \\ i = 1, \dots, m \quad (6.143)$$

$$P_{Li}(V_i) + jQ_{Li}(V_i) = \sum_{k=1}^n V_i V_k Y_{ik} e^{j(\theta_i - \theta_k - \alpha_{ik})} \quad i = m + 1, \dots, n. \quad (6.144)$$

As before, for given functions $P_{Li}(V_i)$ and $Q_{Li}(V_i)$, the $n+m$ complex algebraic equations must be solved for V_i , θ_i ($i = 1, \dots, n$), I_{di} , I_{qi} ($i = 1, \dots, m$) in terms of the states δ_i , E'_{qi} ($i = 1, \dots, m$). The currents can clearly be explicitly eliminated by solving either (6.142) or (6.143) and substituting into the differential equations and remaining algebraic equations. This would leave only n complex algebraic equations to be solved for the n complex voltages $V_i e^{j\theta_i}$.

6.5.1 The Special Case of “Impedance Loads”

In some cases, this flux-decay dynamic model can be put in explicit closed form without algebraic equations. We make the special assumptions about the load representations

$$P_{Li}(V_i) = k_{P2i} V_i^2 \quad i = 1, \dots, n \quad (6.145)$$

$$Q_{Li}(V_i) = k_{Q2i} V_i^2 \quad i = 1, \dots, n. \quad (6.146)$$

In this case, the loads and $R_{si} + jX'_{di}$ can be added into the bus admittance matrix diagonal entries to obtain the following simplified algebraic equations for the flux-decay model with “constant impedance” loads

$$(I_{di} + jI_{qi}) e^{j(\delta_i - \frac{\pi}{2})} = \frac{1}{(R_{si} + jX'_{di})} [(X_{qi} - X'_{di})I_{qi} + jE'_{qi}] e^{j(\delta_i - \frac{\pi}{2})} \\ - \frac{1}{(R_{si} + jX'_{di})} V_i e^{j\theta_i} \quad i = 1, \dots, m \quad (6.147)$$

$$0 = -\frac{1}{(R_{si} + jX'_{di})} [(X_{qi} - X'_{di})I_{qi} + jE'_{qi}] e^{j(\delta_i - \frac{\pi}{2})} \\ + \sum_{k=1}^n (G'_{ik} + jB'_{ik}) V_k e^{j\theta_k} \quad i = 1, \dots, m \quad (6.148)$$

$$0 = \sum_{k=1}^n (G'_{ik} + jB'_{ik}) V_k e^{j\theta_k} \quad i = m + 1, \dots, n \quad (6.149)$$

where $G'_{ik} + jB'_{ik}$ is the ik^{th} entry of the admittance matrix, including all “constant impedance” loads and $1/(R_{si} + jX'_{di})$ on the i^{th} diagonal.

Clearly, all of the $V_k e^{j\theta_k}$ ($k = 1, \dots, n$) can be eliminated by solving (6.148) and (6.149) and substituting into (6.147) to obtain m complex equations that are linear in I_{di} ,

I_{qi} ($i = 1, \dots, m$). These can, in principle, be solved through the inverse of a matrix that would be a function of the states δ_i, E'_{qi} ($i = 1, \dots, m$). This inverse can be avoided if the following simplification (usually not considered valid) is made:

$$X_{qi} = X'_{di} \quad i = 1, \dots, m. \quad (6.150)$$

With this simplification, (6.148) and (6.149) can be solved for $V_k e^{j\theta_k}$ and substituted into (6.147) to obtain

$$I_{di} + jI_{qi} = \sum_{k=1}^m (G'_{\text{red}} + jB'_{\text{red}}) E'_{qk} e^{j(\delta_k - \delta_i)} \quad i = 1, \dots, m \quad (6.151)$$

where $G'_{\text{red}} + jB'_{\text{red}}$ is an $m \times m$ admittance matrix (often called the matrix reduced to “internal nodes”). This can easily be solved for I_{di}, I_{qi} ($i = 1, \dots, m$) and substituted into the differential equations (6.132)–(6.139). Substitution of I_{di}, I_{qi} into (6.142) also gives V_i as a function of the states (needed for (6.137)) so that the resulting dynamic model is in explicit form without algebraic equations. We emphasize that the simplification of (6.150) is usually not considered valid for most machines.

6.6 Multimachine Classical Model

As in the single machine/infinite bus case of Chapter 5, the derivation of the classical model requires assumptions that cannot be rigorously supported. Returning to the multimachine two-axis model, rather than assuming $T'_{qoi} = 0$ ($i = 1, \dots, m$), we assume that an integral manifold exists for $E'_{di}, E'_{qi}, E_{fdi}, R_f, V_{Ri}$ ($i = 1, \dots, m$) that as a first approximation, gives each E'_{qi} equal to a constant and each $(E'_{di} + (X'_{qi} - X'_{di})I_{qi})$ equal to a constant. For this constant based on initial values $E'^o_{di}, I'^o_{qi}, E'^o_{qi}$, we define the constant voltage

$$E'_i \stackrel{\Delta}{=} \sqrt{\left(E'^o_{di} + (X'_{qi} - X'_{di})I'^o_{qi}\right)^2 + (E'^o_{qi})^2} \quad (6.152)$$

and the constant angle

$$\delta'_i \stackrel{\Delta}{=} \tan^{-1} \left(\frac{E'^o_{qi}}{E'^o_{di} + (X'_{qi} - X'_{di})I'^o_{qi}} \right) - \frac{\pi}{2}. \quad (6.153)$$

The classical model dynamic circuit is then shown in Figure 6.7. Because the classical model is usually used with the assumption of constant shaft torque, we assume

$$T_{CHi} = \infty. \quad (6.154)$$

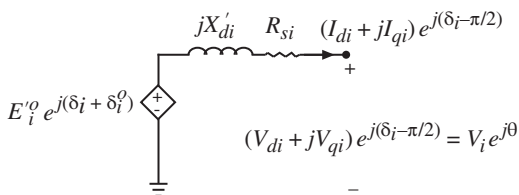


Figure 6.7 Synchronous machine classical model dynamic circuit ($i = 1, \dots, m$).

The classical model is then a $2m$ -order system (obtained from (6.110)–(6.123))

$$\frac{d\delta_i}{dt} = \omega_i - \omega_s \quad i = 1, \dots, m \quad (6.155)$$

$$\frac{2H_i}{\omega_s} \frac{d\omega_i}{dt} = T_{Mi}^o - \text{Real} \left[(E_i'^o e^{j(\delta_i + \delta_i'^o)} (I_{di} - jI_{qi}) e^{-j(\delta_i - \frac{\pi}{2})}) \right] - T_{FWi} \quad i = 1, \dots, m \quad (6.156)$$

and the algebraic constraints

$$0 = V_i e^{j\theta_i} + (R_{si} + jX'_{di})(I_{di} + jI_{qi}) e^{j(\delta_i - \frac{\pi}{2})} - E_i'^o e^{j(\delta_i + \delta_i'^o)} \quad i = 1, \dots, m \quad (6.157)$$

$$V_i e^{j\theta_i} (I_{di} - jI_{qi}) e^{-j(\delta_i - \frac{\pi}{2})} + P_{Li}(V_i) + jQ_{Li}(V_i) = \sum_{k=1}^n V_i V_k Y_{ik} e^{j(\theta_i - \theta_k - \alpha_{ik})} \quad (6.158)$$

$$P_{Li}(V_i) + jQ_{Li}(V_i) = \sum_{k=1}^n V_i V_k Y_{ik} e^{j(\theta_i - \theta_k - \alpha_{ik})} \quad i = m+1, \dots, n. \quad (6.159)$$

As before, for given functions $P_{Li}(V_i)$ and $Q_{Li}(V_i)$, the $n+m$ complex algebraic equations must be solved for V_i , θ_i ($i = 1, \dots, n$) and I_{di} , I_{qi} ($i = 1, \dots, m$) in terms of the states δ_i . The currents can easily be explicitly eliminated by solving either (6.157) or (6.158) and substituting into the differential equations and remaining algebraic equations. This would leave only n complex equations to be solved for the n complex voltages $V_i e^{j\theta_i}$.

6.6.1 The Special Case of “Impedance Loads”

In some cases, this classical model can be put in explicit closed form without algebraic equations. We make the special assumptions about the load representations

$$P_{Li}(V_i) = k_{P2i} V_i^2 \quad i = 1, \dots, n \quad (6.160)$$

$$Q_{Li}(V_i) = k_{Q2i} V_i^2 \quad i = 1, \dots, n. \quad (6.161)$$

In this case, the loads and $R_{si} + jX'_{di}$ can be added into the bus admittance matrix diagonal entries to obtain the following simplified algebraic equations for the classical model with “constant impedance” loads

$$(I_{di} + jI_{qi}) e^{j(\delta_i - \frac{\pi}{2})} = \frac{1}{(R_{si} + jX'_{di})} E_i'^o e^{j(\delta_i + \delta_i'^o)} - \frac{1}{(R_{si} + jX'_{di})} V_i e^{j\theta_i} \quad i = 1, \dots, m \quad (6.162)$$

$$0 = -\frac{1}{(R_{si} + jX'_{di})} E_i'^o e^{j(\delta_i + \delta_i'^o)} + \sum_{k=1}^n (G'_{ik} + jB'_{ik}) V_k e^{j\theta_k} \quad i = 1, \dots, m \quad (6.163)$$

$$0 = \sum_{k=1}^n (G'_{ik} + jB'_{ik}) V_k e^{j\theta_k} \quad i = m+1, \dots, n \quad (6.164)$$

where $G'_{ik} + jB'_{ik}$ is the ik^{th} entry of the admittance matrix, including all “constant impedance” loads and $1/(R_{si} + jX'_{di})$ on the i^{th} diagonal.

Clearly, all of the $V_k e^{j\theta_k}$ ($k = 1, \dots, n$) can be eliminated by solving (6.163) and (6.164) and substituting into (6.162) to obtain m complex equations of the form

$$(I_{di} + jI_{qi})e^{j(\delta_i - \frac{\pi}{2})} = \sum_{k=1}^m (G'_{\text{red}} + jB'_{\text{red}}) E_k'^o e^{j(\delta_k + \delta_k'^o)} \quad (6.165)$$

where $G'_{\text{red}} + jB'_{\text{red}}$ is the ik^{th} entry of an $m \times m$ admittance matrix (often called the matrix reduced to “internal nodes”). Defining

$$\delta_{\text{classical}} \stackrel{\Delta}{=} \delta_i + \delta_i'^o \quad i = 1, \dots, m \quad (6.166)$$

the multimachine classical model with constant impedance loads is found by substituting (6.165) into (6.156):

$$\frac{d\delta_{\text{classical}}}{dt} = \omega_i - \omega_s \quad i = 1, \dots, m \quad (6.167)$$

$$\begin{aligned} \frac{2H_i d\omega_i}{\omega_s dt} &= T_{Mi} - \sum_{k=1}^m E_k'^o E_k'^o G'_{\text{red}} \cos(\delta_{\text{classical}_i} - \delta_{\text{classical}_k}) \\ &\quad - \sum_{k=1}^m E_k'^o E_k'^o B'_{\text{red}} \sin(\delta_{\text{classical}_i} - \delta_{\text{classical}_k}) - T_{FWi} \quad i = 1, \dots, m. \end{aligned} \quad (6.168)$$

The classical model can also be obtained formally from the two-axis model by setting $X'_{qi} = X'_{di}$, and $T_{CHi} = T'_{qoi} = T'_{doi} = \infty$ ($i = 1, \dots, m$), or from the one-axis model by setting $X_{qi} = X_{di}$, and $T'_{qoi} = 0$, $T_{CHi} = T'_{doi} = \infty$ ($i = 1, \dots, m$). In this latter case, $\delta_i'^o$ is equal to zero, so that $\delta_{\text{classical}}$ is equal to δ_i and $E_i'^o$ is equal to E_{qi}' ($i = 1, \dots, m$).

6.7 Multimachine Damping Torques

As in the single machine/infinite bus case of Chapter 5, the multimachine flux-decay and classical models do not have explicit speed-damping torques. The friction and windage torque term could be specified as

$$T_{FW} = D_{FW}\omega \text{ or } D'_{FW}\omega^2. \quad (6.169)$$

While this would provide some damping, the effect of all damper windings has been lost in the reduction process. As in the single machine/infinite bus case, it is possible to justify the addition of speed-damping torques. The mathematical derivation of these damping torque terms proceeds in a direct extension to the multimachine case. For example, the integral manifold for each machine E'_{di} must be approximated more accurately, as done in Section 5.7. The resulting improved integral manifolds have the following general form:

$$E'_{di} = \sum_{k=1}^m f_{oik}(\delta_i - \delta_k, E'_{qi}, E'_{qk}) - T'_{qoi} \sum_{k=1}^m f_{1ik}(\delta_i - \delta_k, E'_{qi}, E'_{qk}, E_{fdi}, E_{fdk}, \omega_i, \omega_k) \quad (6.170)$$

where f_{oik} is the same as (6.131) written after elimination of I_{qi} . The functions f_{1ik} contain all the speeds of all machines. Rather than use the complicated form of (6.170), it is customary to simply recognize that this additional term involving speeds will contribute speed-damping torques, which can be approximated by

$$T_{Di} = \sum_{k=1}^m D_{ik}(\omega_k - \omega_s) \quad (6.171)$$

with D_{ik} treated as a constant. The swing equation for each machine would then be

$$\frac{2H_i}{\omega_s} \frac{d\omega_i}{dt} = T_{Mi} - T_{ELEC_i} - T_{Di} - T_{FWi} \quad (6.172)$$

with T_{ELEC_i} and all other dynamics evaluated using the simple integral manifold approximation for E'_{di} in (6.131). In order of accuracy, it is emphasized that the most accurate model would keep all damper-winding dynamics. The second most accurate model would use a good integral manifold approximation for the damper windings (6.170). The least accurate model would use the crude integral manifold for the damper windings (6.131), together with a constant D_{ik} cross-damping torque term (6.171).

6.8 Multimachine Models with Saturation

The dynamic models of (6.10)–(6.24), (6.85)–(6.100), (6.110)–(6.123), (6.132) –(6.144), and (6.155)–(6.159) began with the assumption of a linear magnetic circuit. In order to account for saturation, it is necessary to repeat this analysis with the saturation functions included. For this case, we assume the saturation functions of [37], given in (3.204)–(3.209). With these functions and the assumption that saturation does not significantly affect time scales, the stator/network transients can still be formally eliminated to obtain the same dynamic circuits of Figures 6.2 to 6.4 and the following multimachine dynamic model:

$$T'_{doi} \frac{dE'_{qi}}{dt} = -E'_{qi} - (X_{di} - X'_{di}) \left[I_{di} - \frac{(X'_{di} - X''_{di})}{(X'_{di} - X'_{\ell si})^2} (\psi_{1di} + (X'_{di} - X'_{\ell si})I_{di} - E'_{qi}) \right] - S_{fdi}^{(2)} + E_{fdi} \quad i = 1, \dots, m \quad (6.173)$$

$$T''_{doi} \frac{d\psi_{1di}}{dt} = -\psi_{1di} + E'_{qi} - (X'_{di} - X'_{\ell si})I_{di} \quad i = 1, \dots, m \quad (6.174)$$

$$T'_{qoi} \frac{dE'_{di}}{dt} = -E'_{di} + (X_{qi} - X'_{qi}) \left[I_{qi} - \frac{(X'_{qi} - X''_{qi})}{(X'_{qi} - X'_{\ell si})^2} (\psi_{2qi} + (X'_{qi} - X'_{\ell si})I_{qi} + E'_{di}) \right] + S_{1qi}^{(2)} \quad i = 1, \dots, m \quad (6.175)$$

$$T''_{qoi} \frac{d\psi_{2qi}}{dt} = -\psi_{2qi} - E'_{di} - (X'_{qi} - X'_{\ell si})I_{qi} \quad i = 1, \dots, m \quad (6.176)$$

$$\frac{d\delta_i}{dt} = \omega_i - \omega_s \quad i = 1, \dots, m \quad (6.177)$$

$$\begin{aligned} \frac{2H_i}{\omega_s} \frac{d\omega_i}{dt} = T_{Mi} - \frac{(X''_{di} - X'_{\ell si})}{(X'_{di} - X'_{\ell si})} E'_{qi} I_{qi} - \frac{(X'_{di} - X''_{di})}{(X'_{di} - X'_{\ell si})} \psi_{1di} I_{qi} - \frac{(X''_{qi} - X'_{\ell si})}{(X'_{qi} - X'_{\ell si})} E'_{di} I_{di} \\ + \frac{(X'_{qi} - X''_{qi})}{(X'_{qi} - X'_{\ell si})} \psi_{2qi} I_{di} - (X''_{qi} - X''_{di}) I_{di} I_{qi} - T_{FWi} \quad i = 1, \dots, m \end{aligned} \quad (6.178)$$

$$T_{Ei} \frac{dE_{fdi}}{dt} = -(K_{Ei} + S_{Ei}(E_{fdi})) E_{fdi} + V_{Ri} \quad i = 1, \dots, m \quad (6.179)$$

$$T_{Fi} \frac{dR_{fi}}{dt} = -R_{Fi} + \frac{K_{Fi}}{T_{Fi}} E_{fdi} \quad i = 1, \dots, m \quad (6.180)$$

$$T_{Ai} \frac{dV_{Ri}}{dt} = -V_{Ri} + K_{Ai} R_{fi} - \frac{K_{Ai} K_{Fi}}{T_{Fi}} E_{fdi} + K_{Ai} (V_{refi} - V_i) \quad i = 1, \dots, m \quad (6.181)$$

$$T_{CHi} \frac{dT_{Mi}}{dt} = -T_{Mi} + P_{SVi} \quad i = 1, \dots, m \quad (6.182)$$

$$T_{SVi} \frac{dP_{SVi}}{dt} = -P_{SVi} + P_{Ci} - \frac{1}{R_{Di}} \left(\frac{\omega_i}{\omega_s} - 1 \right) \quad i = 1, \dots, m \quad (6.183)$$

with the limit constraints

$$V_{Ri}^{\min} \leq V_{Ri} \leq V_{Ri}^{\max} \quad i = 1, \dots, m \quad (6.184)$$

$$0 \leq P_{SVi} \leq P_{SVi}^{\max} \quad i = 1, \dots, m \quad (6.185)$$

and the algebraic constraints

$$\begin{aligned} 0 = V_i e^{j\theta_i} + (R_{si} + jX''_{di})(I_{di} + jI_{qi}) e^{j(\delta_i - \frac{\pi}{2})} - \left[(X''_{qi} - X''_{di}) I_{qi} + \frac{(X''_{qi} - X'_{\ell si})}{(X'_{qi} - X'_{\ell si})} E'_{di} \right. \\ \left. - \frac{(X'_{qi} - X''_{qi})}{(X'_{qi} - X'_{\ell si})} \psi_{2qi} + j \frac{(X''_{di} - X'_{\ell si})}{(X'_{di} - X'_{\ell si})} E'_{qi} + j \frac{(X'_{di} - X''_{di})}{(X'_{di} - X'_{\ell si})} \psi_{1di} \right] e^{j(\delta_i - \frac{\pi}{2})} \\ i = 1, \dots, m \end{aligned} \quad (6.186)$$

$$\begin{aligned} V_i e^{j\theta_i} (I_{di} - jI_{qi}) e^{-j(\delta_i - \frac{\pi}{2})} + P_{Li}(V_i) + jQ_{Li}(V_i) = \sum_{k=1}^n V_i V_k Y_{ik} e^{j(\theta_i - \theta_k - \alpha_{ik})} \\ i = 1, \dots, m \end{aligned} \quad (6.187)$$

$$P_{Li}(V_i) + jQ_{Li}(V_i) = \sum_{k=1}^n V_i V_k Y_{ik} e^{j(\theta_i - \theta_k - \alpha_{ik})} \quad i = m+1, \dots, n \quad (6.188)$$

and finally the saturation function relations

$$S_{fdi}^{(2)} \stackrel{\Delta}{=} \frac{\psi''_{di}}{|\psi''_i|} S_{smi}(|\psi''_i|) \quad i = 1, \dots, m \quad (6.189)$$

$$S_{1qi}^{(2)} \stackrel{\Delta}{=} \frac{\psi''_{qi}(X_{qi} - X'_{\ell si})}{|\psi''_i|(X_{di} - X'_{\ell si})} S_{smi}(|\psi''_i|) \quad i = 1, \dots, m \quad (6.190)$$

where

$$|\psi_i''| \stackrel{\Delta}{=} (\psi_{di}''^2 + \psi_{qi}''^2)^{\frac{1}{2}} \quad i = 1, \dots, m \quad (6.191)$$

$$\psi_{di}'' \stackrel{\Delta}{=} \frac{(X_{di}'' - X_{\ell si})}{(X_{di}' - X_{\ell si})} E_{qi}' + \frac{(X_{di}' - X_{di}'')}{(X_{di}' - X_{\ell si})} \psi_{1di} \quad i = 1, \dots, m \quad (6.192)$$

$$\psi_{qi}'' \stackrel{\Delta}{=} -\frac{(X_{qi}'' - X_{\ell si})}{(X_{qi}' - X_{\ell si})} E_{di}' + \frac{(X_{qi}' - X_{qi}'')}{(X_{qi}' - X_{\ell si})} \psi_{2qi} \quad i = 1, \dots, m \quad (6.193)$$

and S_{smi} are given nonlinear functions that are zero at $|\psi_i''| = 0$ and increase exponentially with $|\psi_i''|$.

With our choice of saturation functions, the special case of impedance loads still leads to an explicit set of differential equations without algebraic equations. This should be clear, since the only added terms are $S_{fdi}^{(2)}$ and $S_{1qi}^{(2)}$, which are assumed functions of dynamic states. This will not impair the elimination of currents and voltages needed to obtain the reduced admittance matrix formulation. If saturation of network transformers were considered, this elimination would involve nonlinearities in algebraic states that would make an explicit formulation difficult, if not impossible.

6.8.1 The Multimachine Two-Axis Model with Synchronous Machine Saturation

To obtain a two-axis model with saturation included as above, we again assume that T_{doi}'' and T_{goi}'' are sufficiently small so that an integral manifold exists for each ψ_{1di} and ψ_{2qi} . A first approximation of the fast damper-winding integral manifold is found by setting T_{doi}'' and T_{goi}'' equal to zero in (6.174) and (6.176) to obtain

$$0 = -\psi_{1di} + E_{qi}' - (X_{di}' - X_{\ell si}) I_{di} \quad i = 1, \dots, m \quad (6.194)$$

$$0 = -\psi_{2qi} - E_{di}' - (X_{qi}' - X_{\ell si}) I_{qi} \quad i = 1, \dots, m. \quad (6.195)$$

When used to eliminate ψ_{1di} and ψ_{2qi} , the synchronous machine dynamic circuit is changed from Figure 6.2 to Figure 6.5, giving the following multimachine two-axis dynamic model with synchronous machine saturation:

$$T'_{doi} \frac{dE_{qi}'}{dt} = -E_{qi}' - (X_{di} - X_{di}') I_{di} - S_{fdi}^{(3)} + E_{fdi} \quad i = 1, \dots, m \quad (6.196)$$

$$T'_{goi} \frac{dE_{di}'}{dt} = -E_{di}' + (X_q - X_{qi}') I_{qi} + S_{1qi}^{(3)} \quad i = 1, \dots, m \quad (6.197)$$

$$\frac{d\delta_i}{dt} = \omega_i - \omega_s \quad i = 1, \dots, m \quad (6.198)$$

$$\frac{2H_i d\omega_i}{\omega_s dt} = T_{Mi} - E_{di}' I_{di} - E_{qi}' I_{qi} - (X_{qi}' - X_{di}') I_{di} I_{qi} - T_{FWi} \quad i = 1, \dots, m \quad (6.199)$$

$$T_{Ei} \frac{dE_{fdi}}{dt} = -(K_{Ei} + S_{Ei}(E_{fdi})) E_{fdi} + V_{Ri} \quad i = 1, \dots, m \quad (6.200)$$

$$T_{Fi} \frac{dR_{fi}}{dt} = -R_{fi} + \frac{K_{Fi}}{T_{Fi}} E_{fdi} \quad i = 1, \dots, m \quad (6.201)$$

$$T_{Ai} \frac{dV_{Ri}}{dt} = -V_{Ri} + K_{Ai}R_{fi} - \frac{K_{Ai}K_{Fi}}{T_{Fi}}E_{fdi} + K_{Ai}(V_{refi} - V_i) \quad i = 1, \dots, m \quad (6.202)$$

$$T_{CHi} \frac{dT_{Mi}}{dt} = -T_M + P_{SVi} \quad i = 1, \dots, m \quad (6.203)$$

$$T_{SVi} \frac{dP_{SVi}}{dt} = -P_{SVi} + P_{Ci} - \frac{1}{R_{Di}} \left(\frac{\omega_i}{\omega_s} - 1 \right) \quad i = 1, \dots, m \quad (6.204)$$

with the limit constraints

$$V_{Ri}^{\min} \leq V_{Ri} \leq V_{Ri}^{\max} \quad i = 1, \dots, m \quad (6.205)$$

$$0 \leq P_{SVi} \leq P_{SVi}^{\max} \quad i = 1, \dots, m \quad (6.206)$$

and the algebraic constraints

$$0 = V_i e^{j\theta_i} + (R_{si} + jX'_{di})(I_{di} + jI_{qi})e^{j(\delta_i - \frac{\pi}{2})} - [E'_{di} + (X'_{qi} - X'_{di})I_{qi} + jE'_{qi}]e^{j(\delta_i - \frac{\pi}{2})} \quad i = 1, \dots, m \quad (6.207)$$

$$V_i e^{j\theta_i} (I_{di} - jI_{qi})e^{-j(\delta_i - \frac{\pi}{2})} + P_{Li}(V_i) + jQ_{Li}(V_i) = \sum_{k=1}^n V_i V_k Y_{ik} e^{j(\theta_i - \theta_k - \alpha_{ik})} \quad i = 1, \dots, m \quad (6.208)$$

$$P_{Li}(V_i) + jQ_{Li}(V_i) = \sum_{k=1}^n V_i V_k Y_{ik} e^{j(\theta_i - \theta_k - \alpha_{ik})} \quad i = m+1, \dots, n \quad (6.209)$$

and finally the saturation function relations

$$S_{fdi}^{(3)} \triangleq \frac{E'_{qi}}{|\psi'_i|} S_{smi}(|\psi'_i|) \quad i = 1, \dots, m \quad (6.210)$$

$$S_{1qi}^{(3)} \triangleq \frac{-E'_{di}(X_{qi} - X_{\ell si})}{|\psi'_i|(X_{di} - X_{\ell si})} S_{smi}(|\psi'_i|) \quad i = 1, \dots, m \quad (6.211)$$

where

$$|\psi'_i| \triangleq (E'^2_{qi} + E'^2_{di})^{\frac{1}{2}} \quad i = 1, \dots, m. \quad (6.212)$$

We have made the assumption that when ψ_{1di} and ψ_{2qi} are eliminated by the approximate integral manifold of (6.194) and (6.195), the saturation function can be approximated by using $\psi''_{di} \approx E'_{qi}$, $\psi''_{qi} \approx -E'_{di}$. This prevents I_{di} or I_{qi} from entering the saturation function explicitly.

As before, the special case of impedance loads still leads to a dynamic model in explicit form without algebraic equations, because the saturation functions are assumed to be functions of only the dynamic states E'_{di} and E'_{qi} .

6.8.2 The Multimachine Flux-Decay Model with Synchronous Machine Saturation

To obtain a flux-decay model with saturation included, we again assume that T'_{gqi} is sufficiently small so that an integral manifold exists for each E'_{di} . A first approximation

of this integral manifold is found by setting T'_{qoi} equal to zero in (6.197) to obtain:

$$0 = -E'_{di} + (X_{qi} - X'_{qi})I_{qi} + S_{1qi}^{(3)} \quad i = 1, \dots, m. \quad (6.213)$$

As in the single machine/infinite bus case, there is now a problem, since (6.213) must be solved for each E'_{di} (recall that each $S_{1qi}^{(3)}$ is a function of E'_{di} and E'_{qi}). While we could simply carry (6.213) along as another algebraic equation, we can again recognize that since we have already approximated the integral manifold (and, of course, neglected all off-manifold dynamics) we may as well simplify further and set $S_{1qi}^{(3)} \approx 0$. This gives the following flux-decay model with saturation only in the field axis.

$$T'_{doi} \frac{dE'_{qi}}{dt} = -E'_{qi} - (X_{di} - X'_{di})I_{di} - S_{fdi}^{(4)} + E_{fdi} \quad i = 1, \dots, m \quad (6.214)$$

$$\frac{d\delta_i}{dt} = \omega_i - \omega_s \quad i = 1, \dots, m \quad (6.215)$$

$$\frac{2H_i}{\omega_s} \frac{d\omega_i}{dt} = T_{Mi} - E'_{qi}I_{qi} - (X_{qi} - X'_{di})I_{di}I_{qi} - T_{FWi} \quad i = 1, \dots, m \quad (6.216)$$

$$T_{Ei} \frac{dE_{fdi}}{dt} = -(K_{Ei} + S_{Ei}(E_{fdi}))E_{fdi} + V_{Ri} \quad i = 1, \dots, m \quad (6.217)$$

$$T_{Fi} \frac{dR_{fi}}{dt} = -R_{fi} + \frac{K_{Fi}}{T_{Fi}}E_{fdi} \quad i = 1, \dots, m \quad (6.218)$$

$$T_{Ai} \frac{dV_{Ri}}{dt} = -V_{Ri} + K_{Ai}R_{fi} - \frac{K_{Ai}K_{Fi}}{T_{Fi}}E_{fdi} + K_{Ai}(V_{refi} - V_i) \quad i = 1, \dots, m \quad (6.219)$$

$$T_{CHi} \frac{dT_{Mi}}{dt} = -T_{Mi} + P_{SVi} \quad i = 1, \dots, m \quad (6.220)$$

$$T_{SVi} \frac{dP_{SVi}}{dt} = -P_{SVi} + P_{Ci} - \frac{1}{R_{Di}} \left(\frac{\omega_i}{\omega_s} - 1 \right) \quad i = 1, \dots, m \quad (6.221)$$

with the limit constraints

$$V_{Ri}^{\min} \leq V_{Ri} \leq V_{Ri}^{\max} \quad i = 1, \dots, m \quad (6.222)$$

$$0 \leq P_{SVi} \leq P_{SVi}^{\max} \quad i = 1, \dots, m \quad (6.223)$$

and the algebraic constraints

$$0 = V_i e^{j\theta_i} + (R_{si} + jX'_{di})(I_{di} + jI_{qi})e^{j(\delta_i - \frac{\pi}{2})} - [(X_{qi} - X'_{di})I_{qi} + jE'_{qi}]e^{j(\delta_i - \frac{\pi}{2})} \\ i = 1, \dots, m \quad (6.224)$$

$$V_i e^{j\theta_i} (I_{di} - jI_{qi})e^{-j(\delta_i - \frac{\pi}{2})} + P_{Li}(V_i) + jQ_{Li}(V_i) = \sum_{k=1}^n V_i V_k Y_{ik} e^{j(\theta_i - \theta_k - \alpha_{ik})} \\ i = 1, \dots, m \quad (6.225)$$

$$P_{Li}(V_i) + jQ_{Li}(V_i) = \sum_{k=1}^n V_i V_k Y_{ik} e^{j(\theta_i - \theta_k - \alpha_{ik})} \quad i = 1, \dots, m \quad (6.226)$$

and finally the saturation function relation

$$S_{fdi}^{(4)} = S_{smi}(E'_{qi}) \quad i = 1, \dots, m. \quad (6.227)$$

As before, the special case of impedance loads still leads to a dynamic model without algebraic equations, since the additional saturation terms are functions only of the dynamic states E'_{qi} .

There is little point in trying to incorporate saturation into the multimachine classical model, since it essentially assumes constant flux linkage.

6.9 Frequency During Transients

The steady-state relationship between voltages and currents in loads clearly depends on frequency. For inductive loads, the reactance increases with frequency. For induction motors, the nominal speed increases with frequency. During transients, frequency does not have any meaning, since voltage and current waveforms are not pure sinusoids. It is, however, possible to define a quantity during transients that reflects the concept of frequency and is equal to frequency in the sinusoidal steady state. This can be done by considering the algebraic variables V_{Di} , V_{Qi} introduced earlier in the synchronously rotating reference frame together with their polar forms:

$$V_{Di} + jV_{Qi} = V_i e^{j\theta_i} \quad i = 1, \dots, n. \quad (6.228)$$

From the inverse transformation, the scaled *abc* voltages are (with $V_{Oi} = 0$):

$$V_{ai} = \sqrt{2}V_i \cos(\omega_s t + \theta_i) \quad i = 1, \dots, n \quad (6.229)$$

$$V_{bi} = \sqrt{2}V_i \cos\left(\omega_s t + \theta_i - \frac{2\pi}{3}\right) \quad i = 1, \dots, n \quad (6.230)$$

$$V_{ci} = \sqrt{2}V_i \cos\left(\omega_s t + \theta_i + \frac{2\pi}{3}\right) \quad i = 1, \dots, n. \quad (6.231)$$

We emphasize that these forms are valid for both transient and steady-state analyses. In general, V_i and θ_i will both change during a transient. A logical definition of a “dynamic frequency” is

$$\omega_{di} \stackrel{\Delta}{=} \omega_s + \frac{d\theta_i}{dt} \quad i = 1, \dots, n. \quad (6.232)$$

If the multimachine system is in synchronism with all machines turning at a constant speed, the system frequency is equal to this dynamic frequency (possibly above or below ω_s). During transients, each bus will have a dynamic frequency determined by $d\theta_i/dt$. We emphasize that this definition is only one of many possible such quantities that have the property of being equal to true frequency in steady state.

Adding frequency dependence into the load model by using $P_{Li}(V_i, \omega_{di})$, $Q_{Li}(V_i, \omega_{di})$ instead of $P_{Li}(V_i)$, and $Q_{Li}(V_i)$ requires that $\theta_i (i = 1, \dots, n)$ become dynamic state variables. This is done by simply adding the following n additional differential equations:

$$\frac{d\theta_i}{dt} = \omega_{di} - \omega_s \quad i = 1, \dots, n. \quad (6.233)$$

The n dynamic frequencies ω_{di} are algebraic variables that must be eliminated together with all other algebraic variables (I_{di} , I_{qi} , V_i). Since this normally cannot be done easily, it is customary to avoid making the θ_i dynamic states by approximating the frequency dependence. This is done by keeping each ω_{di} constant over one time step of numerical integration (Δt) as

$$\omega_{di}(t) \approx \frac{\theta_i(t) - \theta_i(t - \Delta t)}{\Delta t} + \omega_s \quad (6.234)$$

where t is the current time. In this method, the θ_i remain as algebraic variables and are simply monitored at each time step to update the frequency-dependent terms of $P_{Li}(V_i, \omega_{di})$ and $Q_{Li}(V_i, \omega_{di})$ for the next time step.

6.10 Angle References and an Infinite Bus

The multimachine dynamic models of the last sections have at least one more differential equation than is needed to solve an m machine, n bus problem, because every rotational system must have a reference for angles. To illustrate this, we define the angles relative to machine 1 as

$$\delta'_i \stackrel{\Delta}{=} \delta_i - \delta_1 \quad i = 1, \dots, m \quad (6.235)$$

$$\theta'_i \stackrel{\Delta}{=} \theta_i - \delta_1 \quad i = 1, \dots, n \quad (6.236)$$

with derivatives for the new dynamic states

$$\frac{d\delta'_1}{dt} = 0 \quad (6.237)$$

$$\frac{d\delta'_i}{dt} = \omega_i - \omega_1 \quad i = 2, \dots, m. \quad (6.238)$$

Inspection of the algebraic equations that accompany all of the previous models will reveal that all angles can be written in terms of δ'_i and θ'_i . This means that the full system models have the same form as before, with the following modifications:

- Replace δ_i with δ'_i (and $\delta'_1 = 0$).
- Replace θ_i with θ'_i .
- Replace ω_s in the time derivative of δ'_i with ω_1 .

With this formulation, the order of the system is formally reduced by 1, since

$$\delta'_1 = 0. \quad (6.239)$$

While δ'_1 remains at zero for all time, ω_1 changes during a transient. The original δ_1 can be obtained by integrating $\omega_1 - \omega_s$ over time. The original $\delta_i (i = 2, \dots, m)$ and $\theta_i (i = 1, \dots, n)$ can be recovered easily from δ'_i , θ_i and δ'_1 through (6.235)–(6.236), if desired.

The dynamic system order can be further reduced either if H_1 is set to infinity (machine 1 has constant speed) or if speeds do not explicitly appear on the right-hand

side of any dynamic equations (no speed-damping torques and no governor action). This could be formally done by defining

$$\omega'_i \stackrel{\Delta}{=} \omega_i - \omega_1 \quad i = 1, \dots, m \quad (6.240)$$

so that

$$\frac{d\delta'_i}{dt} = \omega'_i \quad i = 1, \dots, m \quad (6.241)$$

and ω'_i replaces ω_i as a dynamic state. In this case, there is no need to include either the angle or the speed equation for machine 1, since all other dynamics would depend only on $\delta'_i (i = 2, \dots, m)$ and $\omega'_i (i = 2, \dots, m)$. This situation also arises when the only speed terms on the right-hand side appear in the swing equations with uniform damping ($H_i/D_i = H_k/D_k, i, k = 1, \dots, m$).

A common transformation used in transient stability analysis is the center-of-inertia (COI) reference. Rather than reference each angle to a specific machine (i.e., δ_1), the COI reference transformation defines the COI angle and speeds as

$$\delta_{COI} \stackrel{\Delta}{=} \frac{1}{M_T} \sum_{i=1}^m M_i \delta_i \quad (6.242)$$

$$\omega_{COI} \stackrel{\Delta}{=} \frac{1}{M_T} \sum_{i=1}^m M_i \omega_i \quad (6.243)$$

where

$$M_T \stackrel{\Delta}{=} \sum_{i=1}^m M_i \quad (6.244)$$

and

$$M_i \stackrel{\Delta}{=} \frac{2H_i}{\omega_s}. \quad (6.245)$$

The COI-referenced angles and speeds are

$$\hat{\delta}_i \stackrel{\Delta}{=} \delta_i - \delta_{COI} \quad i = 1, \dots, m \quad (6.246)$$

$$\hat{\omega}_i \stackrel{\Delta}{=} \omega_i - \omega_{COI} \quad i = 1, \dots, m. \quad (6.247)$$

With the introduction of δ_{COI} and ω_{COI} , it is possible to use these as dynamic states together with any other $m - 1$ pairs of COI-referenced mechanical pairs. Choosing $2, \dots, m$, the new mechanical state-space would consist of $\delta_{COI}, \omega_{COI}, \hat{\delta}_i, \hat{\omega}_i (i = 2, \dots, m)$. This would require the elimination of δ_1 and ω_1 in terms of $\delta_{COI}, \omega_{COI}$ and $\hat{\delta}_i, \hat{\omega}_i (i = 2, \dots, m)$. The resulting system would have M_T multiplying the time derivative of ω_{COI} . Since M_T represents the total system inertia, it is usually quite large relative to any single M_i . For this reason, it is often taken to be infinity, in which case the COI mechanical pair is eliminated, reducing the dynamic order by 2. It is important to emphasize that simply using COI-referenced variables does not, in itself, reduce the dynamic order. The reduction requires the use of COI-referenced variables together with the approximation that M_T is infinity. The resulting swing equations are complicated by the COI

reference, since an inertia-weighted form of “system” acceleration is subtracted from each machine’s true acceleration.

6.11 Automatic Generation Control (AGC)

One of the most interesting issues in power systems is the answer to the question “What happens when you turn on a light?” While the answer is rather complicated, it can be divided into five stages:

1. Speed of light – currents redistribute almost instantly while voltages remain almost constant.
2. New currents create a mismatch in power/torque at every generator causing a change in speed from Newton’s Second Law because the mechanical power cannot change fast enough.
3. The speed governors sense the change in speed and react with a preset “droop.”
4. Load Frequency Control (LFC) detects the change in area frequency and initiates the Automatic Generation Control algorithm to change the scheduled power out of each unit.
5. Economic Dispatch (ED) or Optimal Power Flow (OPF) detects the change in total load and reacts with a change in scheduling of unit outputs to result in the most economical operation.

The following section discusses and illustrates these five stages with a one-area example. Load Frequency Control (LFC) maintains area frequency and area interchange flows. Economic Dispatch maintains the economic operation of all the units in one area. Automatic Generation Control is the combination of these two efforts.

In each of the previous multi-machine dynamic models, there are essentially two ways in which the power output (or speed/frequency) of a generating unit can be changed. Either the power control set point (P_{C_i}) could be changed up or down, or the speed control setpoint (ω_s) could be changed up or down. This governor action can be automated to ensure certain criteria are satisfied. One of these criteria involves a quantity called Area Control Error (ACE) and an algorithm called Load Frequency Control (LFC). This control is typically done within an “area” or a designated “balancing authority.”

The frequency of the voltage output of the synchronous machine is determined by its speed, which is determined by the prime mover (i.e., turbine). The torque produced by the prime mover is typically controlled by the opening or closing of a valve (i.e., steam valve). As discussed earlier, there is a time delay associated with that valve action. The amount of action needed is determined by the governor and its scheduled speed and “droop” settings. In addition, there is a scheduled “export” of real power for each area based on agreements or contracts.

There are two conventions with the definition of ACE – either the “What you have done” version, or the “What you should do” version. NERC uses the “What you have done” version of ACE – When the ACE is positive, the area is generating too much and should lower the generation. The notation used in [79] gives the “What you should do” version of ACE which has the opposite sign – so that if the ACE is positive you should increase generation. It clearly does not matter which definition is used, but it does affect the equations that are used in the model.

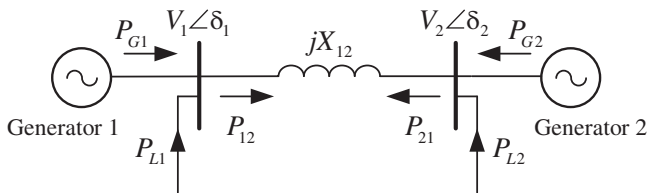


Figure 6.8 Single-area system for illustrating frequency governing and AGC.

The outputs of each generating unit “on AGC” in an area are sent to each location every few seconds for deciding how much each generator should be producing in order to meet the total amount needed at that time. The sum of these generator outputs is considered to be the total area load at that time. Approximately every 5 minutes, an Economic Dispatch (ED) solution gives updated “base points” for each generator. This computation must consider many constraints including the unit production costs, maximum/minimum ramping rates of each unit, the desired tie-line export, plus network voltage and line flow constraints. The desired rate of change of each unit with respect to the total over time is called the “participation factor” (i.e., a decimal percentage) for that unit. Every few seconds, the scheduled (set point) value of each unit is then computed as the latest base economic dispatch amount plus the participation factor times the change in total load (and change in scheduled export) since the last economic dispatch calculation. The actual value of each generating unit output (P_{Gi}) minus its scheduled (set point) value (P_{Ci}) is called the unit error.

The NERC Area Control Error (ACE) is defined as the summation of actual real power export minus the scheduled real power export minus the “Bias Factor” times the actual frequency minus the scheduled or desired frequency (see (6.252)). This “Bias Factor” is a negative number so that if the frequency is too high, the ACE will be positive which implies too much generation. Similarly, if the actual real power export minus the scheduled real power export is positive, this also implies too much generation, both resulting in positive ACE. The sum of all unit errors could be added to the basic ACE to form a composite error signal. To see how this all works, consider a single-area system with two generators (rated at 500 MW each) with a single tie-line between them (Figure 6.8). The over-simplified models (neglecting the internal reactance) for generators which are assumed to be round rotor with constant internal voltage are

$$\begin{aligned} \frac{d\delta_1}{dt} &= \omega_1 - \omega_s \\ \frac{2H_1}{\omega_s} \frac{d\omega_1}{dt} &= T_{M1} - \frac{V_2 V_1}{X_{12}} \sin(\delta_1 - \delta_2) - D_1(\omega_1 - \omega_s) + P_{L1} \\ \frac{d\delta_2}{dt} &= \omega_2 - \omega_s \\ \frac{2H_2}{\omega_s} \frac{d\omega_2}{dt} &= T_{M2} - \frac{V_2 V_1}{X_{12}} \sin(\delta_2 - \delta_1) - D_2(\omega_2 - \omega_s) + P_{L2} \end{aligned} \quad (6.248)$$

where $\omega_s = 2\pi 60$ rad/sec, P_{L1} and P_{L2} are negative as the “injected” notation is used, and

$$P_{G1} = \frac{V_1 V_2}{X_{12}} \sin(\delta_1 - \delta_2) - P_{L1}, \quad P_{G2} = \frac{V_2 V_1}{X_{12}} \sin(\delta_2 - \delta_1) - P_{L2} \quad (6.249)$$

The loads are assumed to be directly connected to the generators at buses 1 and 2. Assume the beginning condition of unity power factor loads:

$$\begin{aligned} P_{G1} &= 300 \text{ MW}, & P_{L1} &= -400 \text{ MW} \\ P_{G2} &= 500 \text{ MW}, & P_{L2} &= -400 \text{ MW} \end{aligned} \quad (6.250)$$

Assume the voltages at both buses in the area are 1.0 pu magnitude with $\delta_1 = -0.1 \text{ rad}$ and $\delta_2 = 0 \text{ rad}$, and these magnitudes do not change because of fast voltage regulators. The impedance of the line between the two generators 1 and 2 has $R_{12} = 0$ and $X_{12} = 0.1 \text{ pu}$. The inertia constant H_i is 3.0 sec and the machine damping coefficient D_i is 0.1 sec for each machine. Following (4.100) and (4.116), the turbine/governor for each generator has the following model:

$$\begin{aligned} T_{CHi} \frac{dT_{Mi}}{dt} &= -T_{Mi} + P_{SVi} \\ T_{SVi} \frac{dP_{SVi}}{dt} &= -P_{SVi} + P_{Ci} - \frac{1}{R_{Di}} \left(\frac{\omega}{\omega_s} - 1 \right) \end{aligned} \quad (6.251)$$

Without AGC, the governor scheduled powers P_{Ci} would be constant.

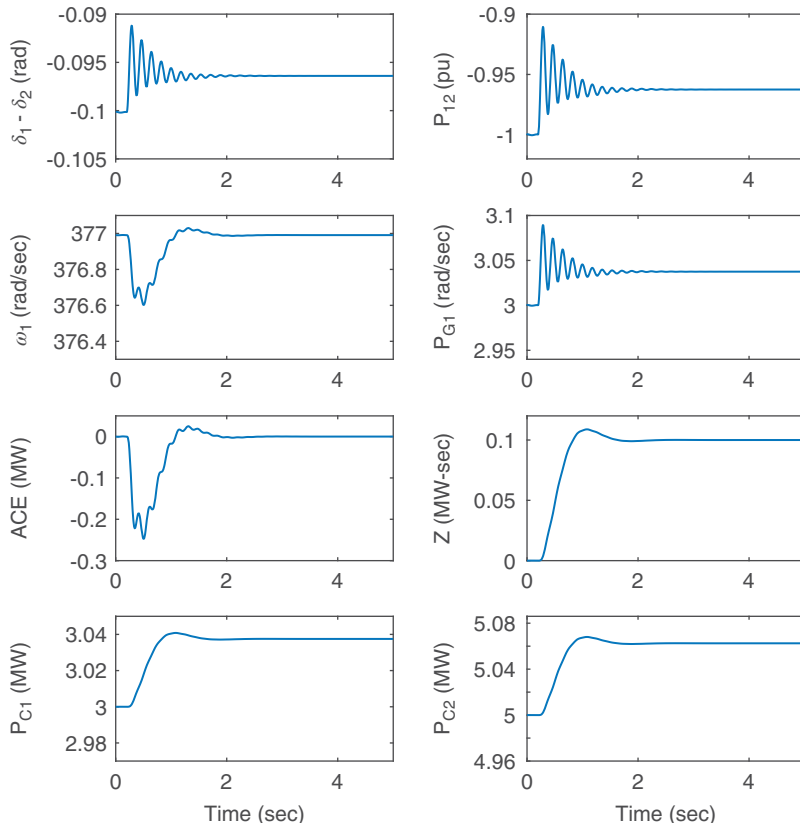


Figure 6.9 Frequency response with governor action and AGC.

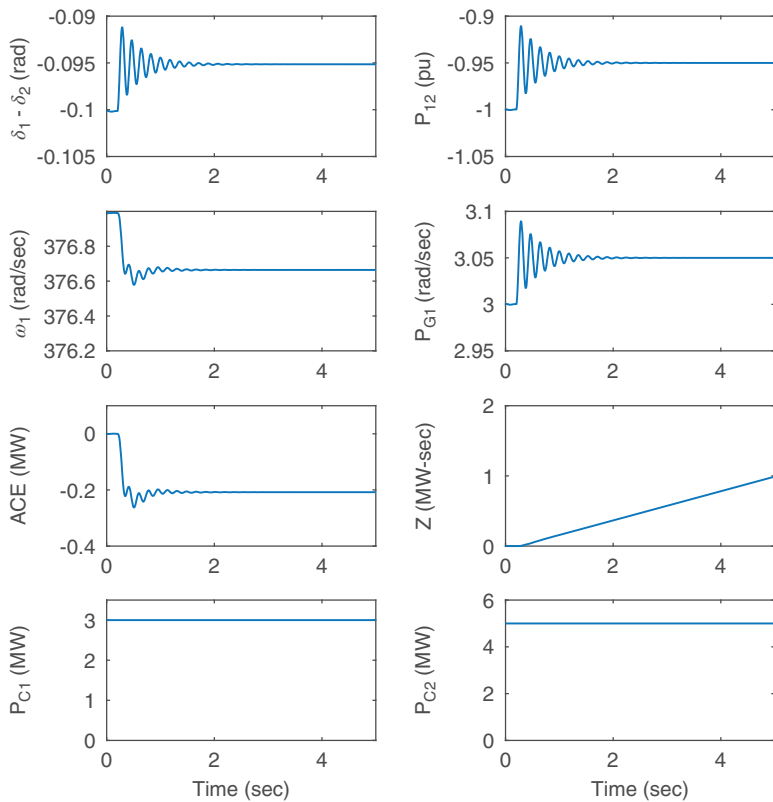


Figure 6.10 Frequency response with governor action only.

The system is initially in steady state with $\omega_i = \omega_s$ rad/sec for each machine. Assume that the system operator for the single area with a nominal frequency of 60 Hz has an AGC system that monitors the ACE which is computed as

$$\text{ACE} = \text{Pexport}_{\text{act}} - \text{Pexport}_{\text{sch}} - 10B(f - 60) \quad (6.252)$$

Since there is only one area, $\text{Pexport}_{\text{act}} = \text{Pexport}_{\text{sch}} = 0$. In this definition, the bias factor B is negative and has the units of MW/0.1 Hz and f is the frequency in Hz obtained as $\omega/(2\pi)$. We need a control that will drive the ACE to zero. The LFC equation for the single area during the period (while waiting for the economic dispatch update of P_{Ci}^{ED}) is

$$\frac{dZ}{dt} = -\text{ACE} \quad (6.253)$$

with $Z(0) = 0$ (time 0 for this computation is when a new economic dispatch solution is given). The generator output scheduled set points are continuously computed to be equal to the given initial economic dispatch set point plus a constant participation factor pf_i of generator i times the AGC variable Z

$$P_{Ci} = P_{Ci}^{\text{ED}} + \text{pf}_i Z \quad (6.254)$$

Note that the generator participation factors add to unity within an area, that is, $\text{pf}_1 + \text{pf}_2 = 1.0$. The individual pf_i reflects the estimated economic split between the

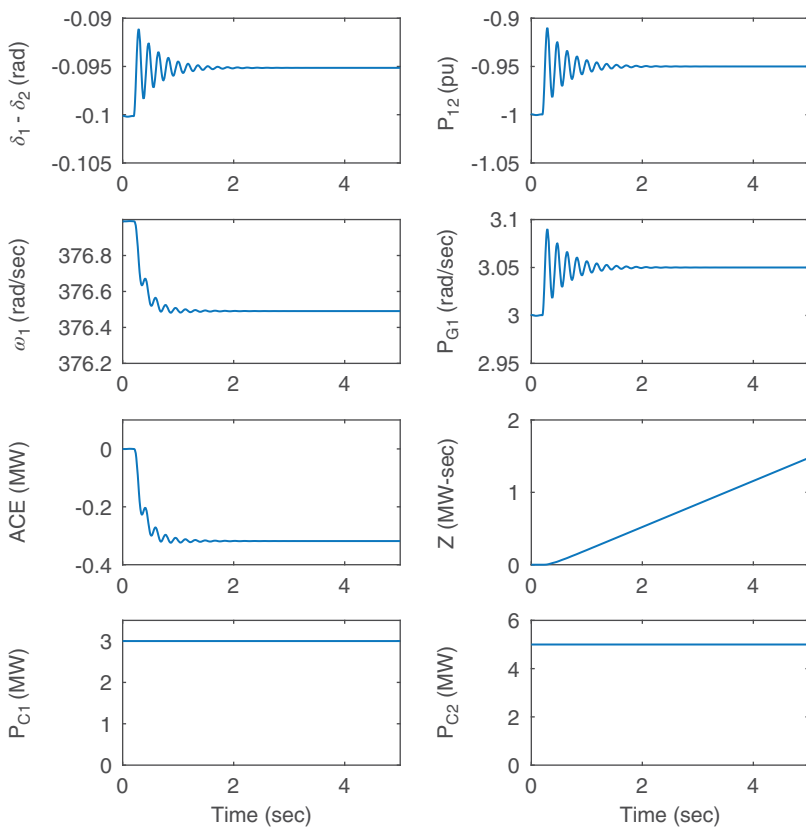


Figure 6.11 Frequency response with no governor action and no AGC.

two units. A simple calculation of these factors is to use the ratio of each economic dispatch set point divided by the total load (assumed equal to the total generation).

For this example, assume that the real power load at bus 2 increases by 0.1 pu and each generator has a 5% droop ($R_{Di} = 0.05$) and a Bias Factor B_i equal to $-40 \text{ MW}/0.1 \text{ Hz}$ ($10B_i = -400 \text{ MW}/\text{Hz}$). The time constants T_{Chi} and T_{SVi} are each 0.1 sec. The economic dispatch solution at time zero is $P_{C1}^{\text{ED}} = 3.0 \text{ pu}$ and $P_{C2}^{\text{ED}} = 5.0 \text{ pu}$. The participation factors are taken to be in that same ratio: $pf_1 = 0.375$ and $pf_2 = 0.625$ (unit 1 is expensive and unit 2 is cheap). What is the response before an update of P_{Ci}^{ED} if the base three-phase power is 100 MW? Use a time step of 0.001 sec for 5 seconds and change the load at bus 2 from 4 to 4.1 after the first 200 time steps.

The solution with full AGC control should be:

$$\text{ACE} = 0$$

$$f = 60.0 \text{ Hz} \text{ (for each machine)}$$

$$Z = 0.1 \text{ pu} \text{ (the change in load)}$$

$$T_{M1} = P_{SV1} = P_{C1} = P_{G1} = 3.0375 \text{ pu}$$

$$T_{M2} = P_{SV2} = P_{C2} = P_{G2} = 5.0625 \text{ pu}$$

$$\delta_{21} = \delta_2 - \delta_1 = 0.0964 \text{ radians}$$

The following figures give the results for three possible cases:

1. Governor plus Load Frequency Control plus participation factor dispatch (Figure 6.9)
2. Governor control only (simulated by setting $p_f_1 = p_f_2 = 0$) (Figure 6.10)
3. No governor control (set T_{CHi} and T_{SVi} both to be 1×10^{12} ensuring constant T_{M1} and T_{M2}) (Figure 6.11)

These results are generated using EXCEL files which is available for download.

Notice that in this simulation we could reduce the order of this dynamic model by one through the introduction of the variable $\delta_{12} = \delta_1 - \delta_2$ which replaces two states with one and the related state equation

$$\frac{d\delta_{12}}{dt} = \omega_1 - \omega_2 \quad (6.255)$$

The model would still compute the two speeds and therefore could recover the two individual angles if needed.

It is also important to enforce ramp rate limits when studying AGC. Reference [80] indicates that for thermal power plants 2% is a typical maximum continuous rating/minute ramp rate. In contrast, for hydro plants this would be as high as 100%/min. For the 500 MW plants in this example, the 2% ramp rate limit would be 10 MW per minute. This example used a 0.1 pu sudden load increase which corresponds to 10 MW (recall that the per unit power base was selected as 100 MW).

7

Multimachine Simulation

In this chapter, we consider simulation techniques for a multimachine power system using a two-axis machine model with no saturation and neglecting both the stator and the network transients. The resulting differential-algebraic model is systematically derived. Both the partitioned-explicit (PE) and the simultaneous-implicit (SI) methods for integration are discussed. The SI method is preferred in both research grade programs and industry programs, since it can handle “stiff” equations very well. After explaining the SI method consistent with our analytical development so far, we then explain the equivalent but notationally different method, the well-known EPRI-ETMSP (Extended Transient Midterm Stability Program) [72, 73]. A numerical example to illustrate the systematic computation of initial conditions is presented.

7.1 Differential-Algebraic Model

We first rewrite the two-axis model of Section 6.4 in a form suitable for simulation after neglecting the subtransient reactances and saturation. We also neglect the turbine governor dynamics resulting in T_{Mi} being a constant. The limit constraints on V_{Ri} are also deleted, since we wish to concentrate on modeling and simulation. We assume a linear damping term $T_{FWi} = D_i(\omega_i - \omega_s)$. The resulting differential-algebraic equations follow from (6.196)–(6.209) for the m machine, n bus system with the IEEE-Type I exciter as

1. Differential Equations

$$T'_{doi} \frac{dE'_{qi}}{dt} = -E'_{qi} - (X_{di} - X'_{di})I_{di} + E_{fdi} \quad i = 1, \dots, m \quad (7.1)$$

$$T'_{qoi} \frac{dE'_{di}}{dt} = -E'_{di} + (X_{qi} - X'_{qi})I_{qi} \quad i = 1, \dots, m \quad (7.2)$$

$$\frac{d\delta_i}{dt} = \omega_i - \omega_s \quad i = 1, \dots, m \quad (7.3)$$

$$\begin{aligned} \frac{2H_i}{\omega_s} \frac{d\omega_i}{dt} = & T_{Mi} - E'_{di}I_{di} - E'_{qi}I_{qi} - (X'_{qi} - X'_{di})I_{di}I_{qi} \\ & - D_i(\omega_i - \omega_s) \quad i = 1, \dots, m \end{aligned} \quad (7.4)$$

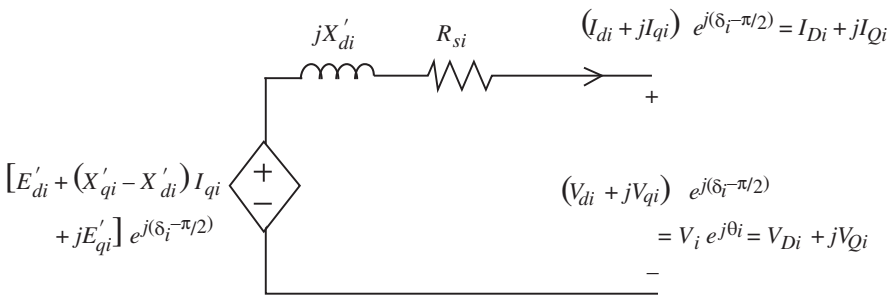


Figure 7.1 Synchronous machine two-axis model dynamic circuit ($i = 1, \dots, m$).

$$T_{Ei} \frac{dE_{fdi}}{dt} = -(K_{Ei} + S_{Ei}(E_{fdi}))E_{fdi} + V_{Ri} \quad i = 1, \dots, m \quad (7.5)$$

$$T_{Fi} \frac{dR_{fi}}{dt} = -R_{fi} + \frac{K_{Fi}}{T_{Fi}} E_{fdi} \quad i = 1, \dots, m \quad (7.6)$$

$$T_{Ai} \frac{dV_{Ri}}{dt} = -V_{Ri} + K_{Ai} R_{fi} - \frac{K_{Ai} K_{Fi}}{T_{Fi}} E_{fdi} + K_{Ai} (V_{refi} - V_i) \quad i = 1, \dots, m. \quad (7.7)$$

Equation (7.4) has dimensions of torque in per-unit. When the stator transients were neglected, the electrical torque became equal to the per-unit power associated with the internal voltage source.

2. Algebraic Equations The algebraic equations consist of the stator algebraic equations and the network equations. The stator algebraic equations directly follow from the dynamic equivalent circuit of Figure 6.5, which is reproduced in Figure 7.1. Application of Kirchhoff's Voltage Law (KVL) to Figure 7.1 yields the stator algebraic equations:

- (a) Stator algebraic equations

$$0 = V_i e^{j\theta_i} + (R_{si} + jX'_{di})(I_{di} + jI_{qi})e^{j(\delta_i - \frac{\pi}{2})} \\ - [E'_i + (X'_{qi} - X'_{di}) I_{qi} + jE'_{qi}] e^{j(\delta_i - \frac{\pi}{2})} \quad i = 1, \dots, m. \quad (7.8)$$

- (b) Network equations

The dynamic circuit, together with the static network and the loads, is shown in Figure 7.2. The network equations written at the n buses are in complex form. From (6.208) and (6.209), these network equations are

7.1.1 Generator Buses

$$V_i e^{j\theta_i} (I_{di} - jI_{qi}) e^{-j(\delta_i - \frac{\pi}{2})} + P_{Li}(V_i) + jQ_{Li}(V_i) \\ = \sum_{k=1}^n V_i V_k Y_{ik} e^{j(\theta_i - \theta_k - \alpha_{ik})} \quad i = 1, \dots, m \quad (7.9)$$

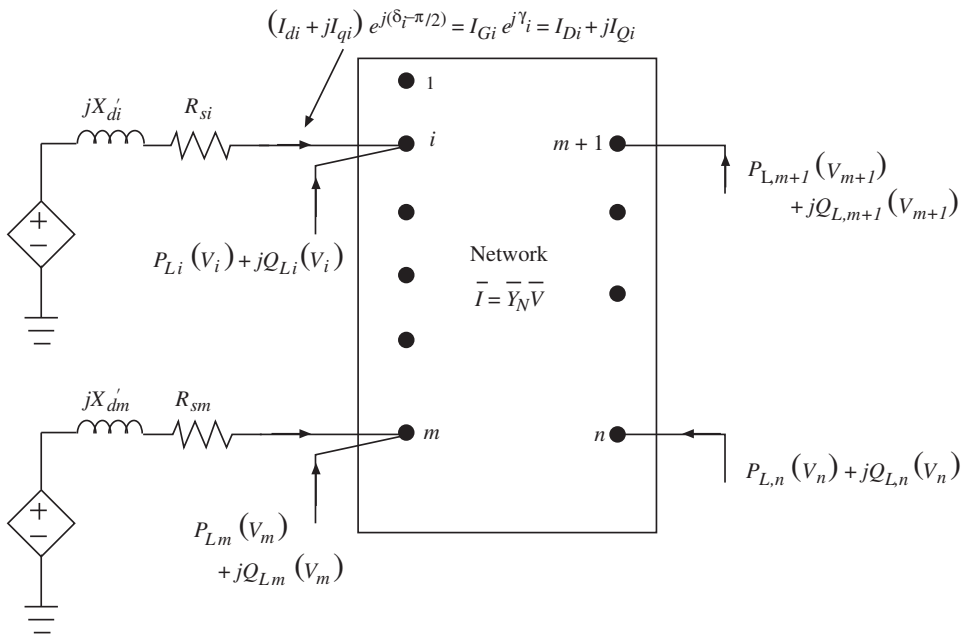


Figure 7.2 Interconnection of synchronous machine dynamic circuit and the rest of the network.

7.1.2 Load Buses

$$P_{Li}(V_i) + jQ_{Li}(V_i) = \sum_{k=1}^n V_i V_k Y_{ik} e^{j(\theta_i - \theta_k - \alpha_{ik})} \quad i = m+1, \dots, n. \quad (7.10)$$

In (7.9), $V_i e^{j\theta_i} (I_{di} - jI_{qi}) e^{-j(\delta_i - \pi/2)} \stackrel{\Delta}{=} P_{Gi} + jQ_{Gi}$ is the complex power “injected” into bus i due to the generator. Thus, (7.9) and (7.10) are only the real and reactive power balance equation at all the n buses. Equation (7.9), which constitutes the power balance equations at the generator buses, shows the interaction of the algebraic variables and the state variables δ_i , E'_{qi} , and E'_{di} . We thus have

1. Seven differential equations (d.e.’s) for each machine, that is, $7m$ d.e.’s ((7.1)–(7.7)).
2. One complex stator algebraic equation (7.8) (two real equations) for each machine, that is, $2m$ real equations.
3. One complex network equation (7.9) and (7.10) (two real equations) at each network bus, that is, $2n$ real equations.

We have $7m + 2m + 2n$ equations with $x = [x_1^t \dots x_m^t]^t$ as the *state* vector where $x_i = [E'_{qi} \quad E'_{di} \quad \delta_i \quad \omega_i \quad E_{fdi} \quad R_{fi} \quad V_{Ri}]^t$ as the state vector for each machine. $y = [I_{d-q}^t \quad V^t \quad \theta^t]^t$ is the set of algebraic variables where

$$\begin{aligned} I_{d-q} &= [I_{d1} \quad I_{q1} \dots I_{dm} I_{qm}]^t \\ V &= [V_1 \dots V_n]^t, \quad \theta = [\theta_1 \dots \theta_n]^t, \quad \bar{V} = [\bar{V}_1 \dots \bar{V}_n]^t. \end{aligned}$$

Functionally, therefore, the differential equations (7.1)–(7.7), together with the stator algebraic equations (7.8) and the network equations (7.9)–(7.10), form a set of differential-algebraic equations of the form

$$\dot{x} = f(x, y, u) \quad (7.11)$$

$$0 = g(x, y) \quad (7.12)$$

$u = [u_1^t \dots u_m^t]^t$ with $u_i = [\omega_s \ T_{mi} \ V_{\text{ref}_i}]^t$ as the input vector for each machine. We now formally put (7.1)–(7.10) in the form (7.11) and (7.12).

7.2 Stator Algebraic Equations

There are several different ways of writing the stator algebraic equations (7.8) as two real equations for computational purposes. The idea is to express I_{di} , I_{qi} in terms of the state and network variables. Both the polar form and the rectangular form will be explained.

7.2.1 Polar Form

In this form, the network voltages appear in polar form. If we multiply (7.8) by $e^{-j(\delta_i - \frac{\pi}{2})}$ and equate the real and imaginary parts, we obtain

$$E'_{di} - V_i \sin(\delta_i - \theta_i) - R_{si} I_{di} + X'_{qi} I_{qi} = 0 \quad i = 1, \dots, m \quad (7.13)$$

$$E'_{qi} - V_i \cos(\delta_i - \theta_i) - R_{si} I_{qi} - X'_{di} I_{di} = 0 \quad i = 1, \dots, m. \quad (7.14)$$

We define

$$\begin{bmatrix} R_{si} & -X'_{qi} \\ X'_{di} & R_{si} \end{bmatrix} \triangleq Z_{d-q,i}.$$

Then, from (7.13) and (7.14):

$$\begin{bmatrix} I_{di} \\ I_{qi} \end{bmatrix} = [Z_{d-q,i}]^{-1} \begin{bmatrix} E'_{di} - V_i \sin(\delta_i - \theta_i) \\ E'_{qi} - V_i \cos(\delta_i - \theta_i) \end{bmatrix} \quad i = 1, \dots, m. \quad (7.15)$$

Equations (7.13) and (7.14) are implicit in I_{di} , I_{qi} , whereas in (7.15) they are expressed explicitly in terms of the state variables x_i and the algebraic variables V_i , θ_i . Thus

$$\begin{bmatrix} I_{di} \\ I_{qi} \end{bmatrix} = h_{pi}(x_i, V_i, \theta_i) \quad i = 1, \dots, m. \quad (7.16)$$

7.2.2 Rectangular Form

This can be easily derived by recognizing the fact that

$$\bar{V}_i = V_{Di} + jV_{Qi} = V_i e^{j\theta_i} = V_i \cos \theta_i + jV_i \sin \theta_i. \quad (7.17)$$

By expanding (7.13) and (7.14) and noting from (7.17) that $V_{Di} = V_i \cos \theta_i$ and $V_{Qi} = V_i \sin \theta_i$, we obtain the implicit form in rectangular coordinates as

$$E'_{di} - V_{Di} \sin \delta_i + V_{Qi} \cos \delta_i - R_{si} I_{di} + X'_{qi} I_{qi} = 0 \quad (7.18)$$

$$E'_{qi} - V_{Di} \cos \delta_i - V_{Qi} \sin \delta_i - R_{si} I_{qi} - X'_{di} I_{di} = 0. \quad (7.19)$$

To obtain the explicit form, I_{di} , I_{qi} in (7.18) and (7.19) can be expressed in terms of E'_{di} , E'_{qi} , δ_i , V_{Di} , and V_{Qi} . Alternatively, the right-hand side of (7.15) is expanded as

$$\begin{bmatrix} I_{di} \\ I_{qi} \end{bmatrix} = [Z_{d-q,i}]^{-1} \begin{bmatrix} E'_{di} \\ E'_{qi} \end{bmatrix} - [Z_{d-q,i}]^{-1} \begin{bmatrix} V_i(\sin \delta_i \cos \theta_i - \cos \delta_i \sin \theta_i) \\ V_i(\cos \delta_i \cos \theta_i + \sin \delta_i \sin \theta_i) \end{bmatrix}. \quad (7.20)$$

Using the fact from (7.17) that $V_{Di} = V_i \cos \theta_i$ and $V_{Qi} = V_i \sin \theta_i$, (7.20) becomes

$$\begin{bmatrix} I_{di} \\ I_{qi} \end{bmatrix} = [Z_{d-q,i}]^{-1} \begin{bmatrix} E'_{di} \\ E'_{qi} \end{bmatrix} - [Z_{d-q,i}]^{-1} \begin{bmatrix} \sin \delta_i & -\cos \delta_i \\ \cos \delta_i & \sin \delta_i \end{bmatrix} \begin{bmatrix} V_{Di} \\ V_{Qi} \end{bmatrix} \quad (7.21)$$

$$= h_{ri}(x_i, V_{Di}, V_{Qi}) \quad i = 1, \dots, m. \quad (7.22)$$

Note that (7.21) can be obtained directly from (7.18) and (7.19). Symbolically, (7.16) or (7.22) can be expressed for all machines as

$$\begin{aligned} I_{d-q} &= h_p(x, V, \theta) \text{ or } h_r(x, V_D, V_Q) \\ &\stackrel{\Delta}{=} h(x, \bar{V}). \end{aligned} \quad (7.23)$$

7.2.3 Alternate Form of Stator Algebraic Equations

In much of the literature, a block diagram representation of stator equations is done through an “interface” block that reflects the machine–network transformation. The machine–network transformation is given by

$$\begin{bmatrix} F_{di} \\ F_{qi} \end{bmatrix} = \begin{bmatrix} \sin \delta_i & -\cos \delta_i \\ \cos \delta_i & \sin \delta_i \end{bmatrix} \begin{bmatrix} F_{Di} \\ F_{Qi} \end{bmatrix} \quad i = 1, \dots, m \quad (7.24)$$

and

$$\begin{bmatrix} F_{Di} \\ F_{Qi} \end{bmatrix} = \begin{bmatrix} \sin \delta_i & \cos \delta_i \\ -\cos \delta_i & \sin \delta_i \end{bmatrix} \begin{bmatrix} F_{di} \\ F_{qi} \end{bmatrix} \quad i = 1, \dots, m \quad (7.25)$$

where F may be either I or V . Figure 7.3 is a graphical representation of (7.24) and (7.25) illustrated for the voltage $\bar{V}_i = V_i e^{j\theta_i}$. Using (7.24) in (7.21), we obtain

$$\begin{bmatrix} I_{di} \\ I_{qi} \end{bmatrix} = [Z_{d-q,i}]^{-1} \begin{bmatrix} E'_{di} - V_{di} \\ E'_{qi} - V_{qi} \end{bmatrix} \quad i = 1, \dots, m \quad (7.26)$$

Thus

$$\begin{bmatrix} E'_{di} - V_{di} \\ E'_{qi} - V_{qi} \end{bmatrix} = [Z_{d-q,i}] \begin{bmatrix} I_{di} \\ I_{qi} \end{bmatrix} \quad i = 1, \dots, m \quad (7.27)$$

The interface block in the block diagram in Figure 7.5 is now consistent with (7.24), (7.25), and (7.26). Note that, in this formulation, algebraic equation (7.26) or (7.27) is

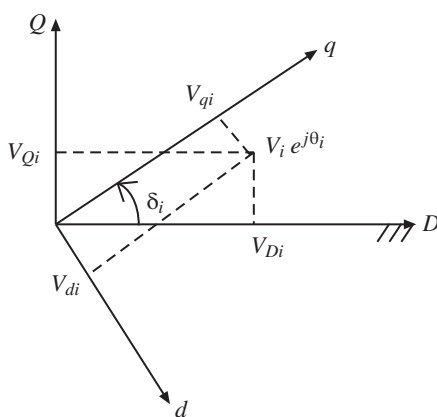


Figure 7.3 Graphical representation.

in machine reference only, whereas (7.24) and (7.25) act as an “interface” between the machine and the network.

7.3 Network Equations

The network equations can be expressed either in power-balance or current-balance form. The latter form is more popular with the industry software packages. We discuss both of them now.

7.3.1 Power-Balance Form

The network equations for the generator buses (7.9) are separated into real and imaginary parts for $i = 1, \dots, m$

$$I_{di}V_i \sin(\delta_i - \theta_i) + I_{qi}V_i \cos(\delta_i - \theta_i) + P_{Li}(V_i) - \sum_{k=1}^n V_i V_k Y_{ik} \cos(\theta_i - \theta_k - \alpha_{ik}) = 0 \quad (7.28)$$

$$I_{di}V_i \cos(\delta_i - \theta_i) - I_{qi}V_i \sin(\delta_i - \theta_i) + Q_{Li}(V_i) - \sum_{k=1}^n V_i V_k Y_{ik} \sin(\theta_i - \theta_k - \alpha_{ik}) = 0. \quad (7.29)$$

For the load buses, a similar procedure using (7.10) gives for $i = m+1, \dots, n$

$$P_{Li}(V_i) - \sum_{k=1}^n V_i V_k Y_{ik} \cos(\theta_i - \theta_k - \alpha_{ik}) = 0 \quad (7.30)$$

$$Q_{Li}(V_i) - \sum_{k=1}^n V_i V_k Y_{ik} \sin(\theta_i - \theta_k - \alpha_{ik}) = 0. \quad (7.31)$$

Note that load can be present at the generator as well as at the load buses. The network equations (7.28)–(7.31) can be rearranged so that the real power equations appear first and the reactive power equations appear next, as follows.

7.3.2 Real Power Equations

$$\begin{aligned} I_{di}V_i \sin(\delta_i - \theta_i) + I_{qi}V_i \cos(\delta_i - \theta_i) + P_{Li}(V_i) \\ - \sum_{k=1}^n V_i V_k Y_{ik} \cos(\theta_i - \theta_k - \alpha_{ik}) = 0 \quad i = 1, \dots, m \end{aligned} \quad (7.32)$$

$$P_{Li}(V_i) - \sum_{k=1}^n V_i V_k Y_{ik} \cos(\theta_i - \theta_k - \alpha_{ik}) = 0 \quad i = m+1, \dots, n. \quad (7.33)$$

7.3.3 Reactive Power Equations

$$\begin{aligned} I_{di}V_i \cos(\delta_i - \theta_i) - I_{qi}V_i \sin(\delta_i - \theta_i) + Q_{Li}(V_i) \\ - \sum_{k=1}^n V_i V_k Y_{ik} \sin(\theta_i - \theta_k - \alpha_{ik}) = 0 \quad i = 1, \dots, m \end{aligned} \quad (7.34)$$

$$Q_{Li}(V_i) - \sum_{k=1}^n V_i V_k Y_{ik} \sin(\theta_i - \theta_k - \alpha_{ik}) = 0 \quad i = m+1, \dots, n. \quad (7.35)$$

Thus, the differential-algebraic equation (DAE) model is:

1. The differential equations (7.1)–(7.7)
2. The stator algebraic equations of the form (7.23) in the polar form
3. The network equations (7.32)–(7.35) in the power-balance form

The differential-algebraic equations are now written symbolically as

$$\dot{x} = f_o(x, I_{d-q}, \bar{V}, u) \quad (7.36)$$

$$I_{d-q} = h(x, \bar{V}) \quad (7.37)$$

$$0 = g_o(x, I_{d-q}, \bar{V}). \quad (7.38)$$

Substitution of (7.37) into (7.36) and (7.38) gives

$$\dot{x} = f_1(x, \bar{V}, u) \quad (7.39)$$

$$0 = g_1(x, \bar{V}). \quad (7.40)$$

Note that (7.40) is in the power-balance form. This is the differential-algebraic equation (DAE) analytical model with the network algebraic variables in the polar form. We prefer this form, since in load-flow equations the voltages are generally in polar form. Simplified forms of this model result from the reduced-order model of the synchronous machine as well as the exciter, which will be discussed later.

7.3.4 Current-Balance Form

Instead of the power-balance form of (7.32)–(7.35), one can have the current-balance form, which is essentially the nodal set of equations

$$\bar{I} = \bar{Y}_N \bar{V} \quad (7.41)$$

where \bar{Y}_N is the $n \times n$ bus admittance matrix of the network with elements $\bar{Y}_{ik} = Y_{ik}e^{j\alpha_{ik}} = G_{ik} + jB_{ik}$, \bar{I} is the net injected current vector and \bar{V} is the bus voltage vector. Depending on how \bar{I} is expressed, it can take different forms, as discussed below. Equation (7.41) can also be derived from (7.9)–(7.10) by dividing both sides of the equation by $V_i e^{j\theta_i}$ and then taking the complex conjugate as follows.

$$(I_{di} + jI_{qi})e^{j(\delta_i - \pi/2)} + \frac{P_{Li}(V_i) - jQ_{Li}(V_i)}{V_i e^{-j\theta_i}} = \sum_{k=1}^n Y_{ik} e^{j\alpha_{ik}} V_k e^{j\theta_k} \quad i = 1, \dots, m \quad (7.42)$$

$$\frac{P_{Li}(V_i) - jQ_{Li}(V_i)}{V_i e^{-j\theta_i}} = \sum_{k=1}^n Y_{ik} e^{j\alpha_{ik}} V_k e^{j\theta_k} \quad i = m+1, \dots, n. \quad (7.43)$$

These equations are the same as (6.83) and (6.84). Equations (7.42) and (7.43) can be symbolically denoted in matrix form as

$$\bar{I}_o(I_{d-q}, x, \bar{V}) = \bar{Y}_N \bar{V}. \quad (7.44)$$

The other algebraic equation is

$$I_{d-q} = h(x, \bar{V}). \quad (7.45)$$

Substitution of (7.45) in (7.36) and (7.44) leads to the DAE model

$$\begin{aligned} \dot{x} &= f_1(x, \bar{V}, u) \\ \bar{I}_1(x, \bar{V}) &= \bar{Y}_N \bar{V}. \end{aligned} \quad (7.46)$$

Example 7.1 We illustrate the DAE models discussed in the previous section with a numerical example. We consider the popular Western System Coordinating Council (WECC) 3-machine, 9-bus system [74–76] shown in Figure 7.4. This is also the system appearing in [77] and widely used in the literature. The base MVA is 100, and system frequency is 60 Hz. The converged load-flow data obtained using the EPRI-IPFLOW program [78] is given in Table 7.1.

The \bar{Y}_{bus} for the network (also denoted as \bar{Y}_N) can be written by inspection from Figure 7.4 and is shown in Table 7.2. The machine data and the exciter data are given in Table 7.3.¹ The exciter is assumed to be identical for all the machines and is of the IEEE-Type I. Define $\frac{2H_i}{\omega_s} \triangleq M_i$. Assume that $\frac{D_1}{M_1} = 0.1$, $\frac{D_2}{M_2} = 0.2$, and $\frac{D_3}{M_3} = 0.3$ (all in pu).

¹ Note that Machine 1 is a hydraulic generator. Table 7.3 shows that $X'_{q1} = X_{q1}$, which is quite common for hydraulic generators. As a result, the q -axis dynamics are not needed (see (7.2)), which requires removing the E'_{d1} state from the model. Here E'_{d1} will be kept, by setting a non-zero value 0.31 for the q -axis time constant. This will result in a pole at $-1/0.31 = -3.2258$ which is fixed as it is not impacted by any other states, as can be seen from the eigenvalue tables that follow.

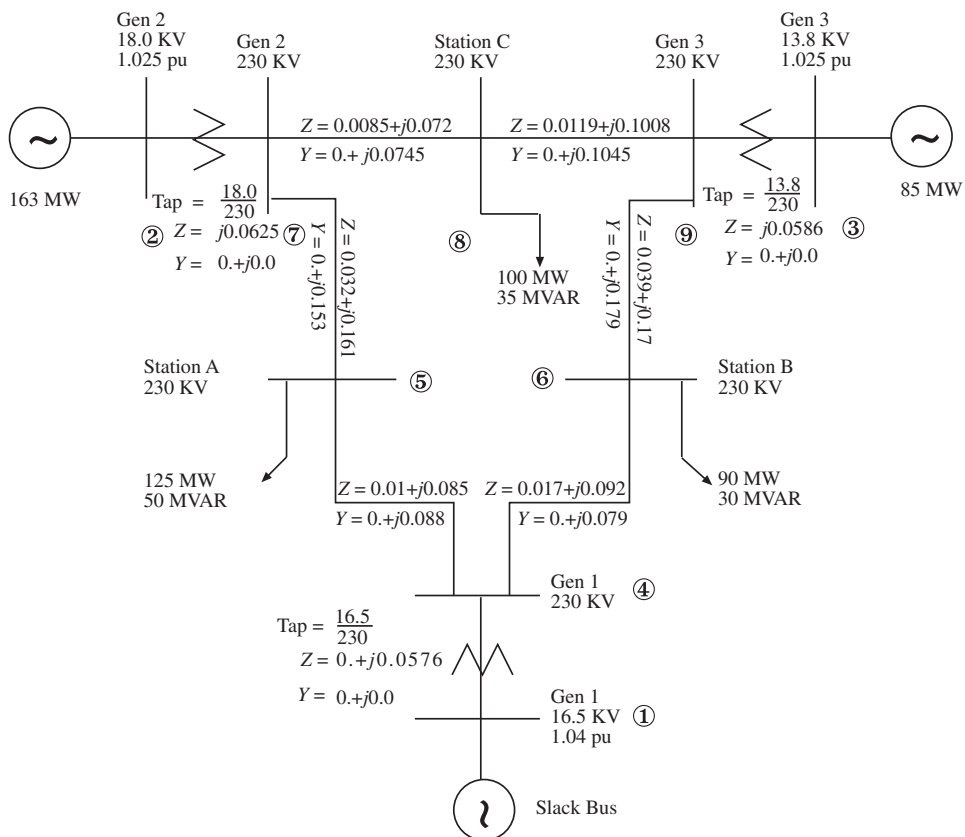


Figure 7.4 WECC 3-machine, 9-bus system; the value of Y is half the line charging. Source: Courtesy of EPRI 1977 [76]. Reproduced with permission of EPRI.

Table 7.1 Load-Flow Results of the WECC 3-Machine, 9-Bus System.

Bus #	Voltage (pu)	P_G (pu)	Q_G (pu)	$-P_L$ (pu)	$-Q_L$ (pu)
1 (swing)	1.04	0.716	0.27	–	–
2 (P-V)	$1.025\angle9.3^\circ$	1.63	0.067	–	–
3 (P-V)	$1.025\angle4.7^\circ$	0.85	-0.109	–	–
4 (P-Q)	$1.026\angle-2.2^\circ$	–	–	–	–
5 (P-Q)	$0.996\angle-4.0^\circ$	–	–	1.25	0.5
6 (P-Q)	$1.013\angle-3.7^\circ$	–	–	0.9	0.3
7 (P-Q)	$1.026\angle3.7^\circ$	–	–	–	–
8 (P-Q)	$1.016\angle0.7^\circ$	–	–	1.00	0.35
9 (P-Q)	$1.032\angle2.0^\circ$	–	–	–	–

Table 7.2 \bar{Y}_N for the Network in Figure 7.4.

	1	2	3	4	5	6	7	8	9
1	$-j17.361$	0	0	$j17.361$	0	0	0	0	0
2	0	$-j16$	0	0	0	0	$j16$	0	0
3	0	0	$-j17.065$	0	0	0	0	0	$j17.065$
4	$j17.361$	0	0	3.307	-1.365	-1.942	0	0	0
				$-j39.309$	$+j11.604$	$+j10.511$			
5	0	0	0	-1.365	2.553	0	-1.188	0	0
				$+j11.604$	$-j17.338$		$+j5.975$		
6	0	0	0	-1.942	0	3.224	0	0	-1.282
				$+j10.511$		$-j15.841$			$+j5.588$
7	0	$j16$	0	0	-1.188	0	2.805	-1.617	0
					$+j5.975$		$-j35.4460$	$+j13.698$	
8	0	0	0	0	0	0	-1.617	2.772	-1.155
							$+j13.698$	$-j23.303$	$+j9.784$
9	0	0	$j17.065$	0	0	-1.282	0	-1.155	2.437
						$+j5.588$		$+j9.784$	$-j32.1540$

Table 7.3 Machine and Exciter Data.

Machine Data			
Parameters	M/C 1	M/C 2	M/C 3
H(secs)	23.64	6.4	3.01
X_d (pu)	0.146	0.8958	1.3125
X'_d (pu)	0.0608	0.1198	0.1813
X_q (pu)	0.0969	0.8645	1.2578
X'_q (pu)	0.0969	0.1969	0.25
T'_{do} (sec)	8.96	6.0	5.89
T'_{qo} (sec)	0.31	0.535	0.6

Exciter Data			
Parameters	Exciter 1	Exciter 2	Exciter 3
K_A	20	20	20
T_A (sec)	0.2	0.2	0.2
K_E	1.0	1.0	1.0
T_E (sec)	0.314	0.314	0.314
K_F	0.063	0.063	0.063
T_F (sec)	0.35	0.35	0.35

$$S_{Ei}(E_{fdi}) = 0.0039e^{1.555E_{fdi}} \quad i = 1, 2, 3$$

The differential equations corresponding to (7.1)–(7.7) are

$$\begin{bmatrix} \dot{E}'_{qi} \\ \dot{E}'_{di} \\ \dot{\delta}_i \\ \dot{\omega}_i \\ \dot{E}'_{fdi} \\ \dot{R}_{fi} \\ \dot{V}_{Ri} \end{bmatrix} = [A_i] \begin{bmatrix} E'_{qi} \\ E'_{di} \\ \delta_i \\ \omega_i \\ E'_{fdi} \\ R_{fi} \\ V_{Ri} \end{bmatrix} + R_i(E'_{qi}, E'_{di}, E_{fdi}, I_{di}, I_{qi}, V_i) + C_i u_i \quad i = 1, 2, 3 \quad (7.47)$$

where

$$A_i = \begin{bmatrix} -\frac{1}{T'_{doi}} & 0 & 0 & 0 & \frac{1}{T'_{doi}} & 0 & 0 \\ 0 & \frac{-1}{T'_{qoi}} & 0 & 0 & 0 & 0 & 0 \\ 0 & 0 & 0 & 1 & 0 & 0 & 0 \\ 0 & 0 & 0 & \frac{-D_i}{M_i} & 0 & 0 & 0 \\ 0 & 0 & 0 & 0 & -\frac{K_{Ei}}{T_{Ei}} & 0 & \frac{1}{T_{Ei}} \\ 0 & 0 & 0 & 0 & \frac{K_{Fi}}{T_{Fi}^2} & \frac{-1}{T_{Fi}} & 0 \\ 0 & 0 & 0 & 0 & \frac{-K_{Ai}K_{Fi}}{T_{Ai}T_{Fi}} & \frac{K_{Ai}}{T_{Ai}} & \frac{-1}{T_{Ai}} \end{bmatrix} \quad i = 1, 2, 3 \quad (7.48)$$

$$R_i = \begin{bmatrix} \frac{-(X_{di} - X'_{di})I_{di}}{T'_{doi}} \\ \frac{(X_{qi} - X'_{qi})I_{qi}}{T'_{qoi}} \\ 0 \\ \frac{-\omega_s[(E'_{di}I_{di} + E'_{qi}I_{qi}) + (X'_{qi} - X'_{di})I_{di}I_{qi}]}{2H_i} \\ -\frac{S_{Ei}(E_{fdi})}{T_{Ei}} \\ 0 \\ \frac{-K_{Ai}}{T_{Ai}}V_i \end{bmatrix}$$

$$C_i = \begin{bmatrix} 0 & 0 & 0 \\ 0 & 0 & 0 \\ -1 & 0 & 0 \\ \frac{D_i}{M_i} & \frac{1}{M_i} & 0 \\ 0 & 0 & 0 \\ 0 & 0 & 0 \\ 0 & 0 & \frac{K_{Ai}}{T_{Ai}} \end{bmatrix}, \quad u_i = \begin{bmatrix} \omega_s \\ T_{Mi} \\ V_{\text{ref}i} \end{bmatrix}, i = 1, 2, 3. \quad (7.49)$$

Substituting the numerical values, we obtain

$$A_1 = \begin{bmatrix} -0.112 & 0 & 0 & 0 & 0.112 & 0 & 0 \\ 0 & -3.226 & 0 & 0 & 0 & 0 & 0 \\ 0 & 0 & 0 & 1 & 0 & 0 & 0 \\ 0 & 0 & 0 & -0.1 & 0 & 0 & 0 \\ 0 & 0 & 0 & 0 & -3.185 & 0 & 3.185 \\ 0 & 0 & 0 & 0 & 0.514 & -2.86 & 0 \\ 0 & 0 & 0 & 0 & -18 & 100 & -5 \end{bmatrix}$$

$$A_2 = \begin{bmatrix} -0.167 & 0 & 0 & 0 & 0.167 & 0 & 0 \\ 0 & -1.87 & 0 & 0 & 0 & 0 & 0 \\ 0 & 0 & 0 & 1 & 0 & 0 & 0 \\ 0 & 0 & 0 & -0.2 & 0 & 0 & 0 \\ 0 & 0 & 0 & 0 & -3.185 & 0 & 3.185 \\ 0 & 0 & 0 & 0 & 0.514 & -2.86 & 0 \\ 0 & 0 & 0 & 0 & -18 & 100 & -5 \end{bmatrix}$$

$$A_3 = \begin{bmatrix} -0.17 & 0 & 0 & 0 & 0.17 & 0 & 0 \\ 0 & -1.67 & 0 & 0 & 0 & 0 & 0 \\ 0 & 0 & 0 & 1 & 0 & 0 & 0 \\ 0 & 0 & 0 & -0.3 & 0 & 0 & 0 \\ 0 & 0 & 0 & 0 & -3.185 & 0 & 3.185 \\ 0 & 0 & 0 & 0 & 0.514 & -2.86 & 0 \\ 0 & 0 & 0 & 0 & -18 & 100 & -5 \end{bmatrix} \quad (7.50)$$

$$R_1 = \begin{bmatrix} -0.0095I_{d1} \\ 0 \\ 0 \\ -8(E'_{d1}I_{d1} + E'_{q1}I_{q1}) \\ -0.29I_{d1}I_{q1} \\ -0.0124e^{1.555E_{fd1}} \\ 0 \\ -100V_1 \end{bmatrix}, R_2 = \begin{bmatrix} -0.13I_{d2} \\ 1.25I_{q2} \\ 0 \\ -29.5(E'_{d2}I_{d2} + E'_{q2}I_{q2}) \\ -2.27I_{d2}I_{q2} \\ -0.0124e^{1.555E_{fd2}} \\ 0 \\ -100V_2 \end{bmatrix},$$

$$R_3 = \begin{bmatrix} -0.19I_{d3} \\ 1.7I_{q3} \\ 0 \\ -62.6(E'_{d3}I_{d3} + E'_{q3}I_{q3}) \\ -4.3I_{d3}I_{q3} \\ -0.0124e^{1.555E_{fd3}} \\ 0 \\ -100V_3 \end{bmatrix} \quad (7.51)$$

$$C_1 = \begin{bmatrix} 0 & 0 & 0 \\ 0 & 0 & 0 \\ -1 & 0 & 0 \\ 0.1 & 8 & 0 \\ 0 & 0 & 0 \\ 0 & 0 & 0 \\ 0 & 0 & 100 \end{bmatrix}, C_2 = \begin{bmatrix} 0 & 0 & 0 \\ 0 & 0 & 0 \\ -1 & 0 & 0 \\ 0.2 & 29.5 & 0 \\ 0 & 0 & 0 \\ 0 & 0 & 0 \\ 0 & 0 & 100 \end{bmatrix},$$

$$C_3 = \begin{bmatrix} 0 & 0 & 0 \\ 0 & 0 & 0 \\ -1 & 0 & 0 \\ 0.3 & 62.6 & 0 \\ 0 & 0 & 0 \\ 0 & 0 & 0 \\ 0 & 0 & 100 \end{bmatrix}. \quad (7.52)$$

The stator algebraic equations corresponding to (7.13) and (7.14) (assuming $R_{si} \equiv 0$) are

$$\begin{aligned} E'_{d1} - V_1 \sin(\delta_1 - \theta_1) + 0.0969I_{q1} &= 0 \\ E'_{q1} - V_1 \cos(\delta_1 - \theta_1) - 0.0608I_{d1} &= 0 \\ E'_{d2} - V_2 \sin(\delta_2 - \theta_2) + 0.1969I_{q2} &= 0 \\ E'_{q2} - V_2 \cos(\delta_2 - \theta_2) - 0.1198I_{d2} &= 0 \\ E'_{d3} - V_3 \sin(\delta_3 - \theta_3) + 0.2500I_{q3} &= 0 \\ E'_{q3} - V_3 \cos(\delta_3 - \theta_3) - 0.1813I_{d3} &= 0. \end{aligned} \quad (7.53)$$

The network equations are (with the notation $\theta_{ij} = \theta_i - \theta_j$) as follows. The constant power loads are treated as injected into the buses.

Real Power Equations

$$\begin{aligned} I_{d1}V_1 \sin(\delta_1 - \theta_1) + I_{q1}V_1 \cos(\delta_1 - \theta_1) \\ - 17.36V_1V_4 \sin\theta_{14} &= 0 \\ I_{d2}V_2 \sin(\delta_2 - \theta_2) + I_{q2}V_2 \cos(\delta_2 - \theta_2) \\ - 16.00V_2V_7 \sin\theta_{27} &= 0 \\ I_{d3}V_3 \sin(\delta_3 - \theta_3) + I_{q3}V_3 \cos(\delta_3 - \theta_3) \\ - 17.06V_3V_9 \sin\theta_{39} &= 0 \end{aligned}$$

$$\begin{aligned}
& -17.36V_4V_1 \sin \theta_{41} - 3.31V_4^2 + 1.36V_4V_5 \cos \theta_{45} - 11.6V_4V_5 \sin \theta_{45} \\
& \quad + 1.942V_4V_6 \cos \theta_{46} - 10.51V_4V_6 \sin \theta_{46} = 0 \\
& -1.25 + 1.36V_5V_4 \cos \theta_{54} - 11.6V_5V_4 \sin \theta_{54} + 1.19V_5V_7 \cos \theta_{57} \\
& \quad - 5.97V_5V_7 \sin \theta_{57} - 2.55V_5^2 = 0 \\
& -0.9 + 1.94V_6V_4 \cos \theta_{64} - 10.51V_6V_4 \sin \theta_{64} - 3.22V_6^2 \\
& \quad + 1.28V_6V_9 \cos \theta_{69} - 5.59V_6V_9 \sin \theta_{69} = 0 \\
& -16V_7V_2 \sin \theta_{72} + 1.19V_7V_5 \cos \theta_{75} - 5.98V_7V_5 \sin \theta_{75} \\
& \quad - 2.8V_7^2 + 1.62V_7V_8 \cos \theta_{78} \\
& \quad - 13.7V_7V_8 \sin \theta_{78} = 0 \\
& -1 + 1.62V_8V_7 \cos \theta_{87} - 13.7V_8V_7 \sin \theta_{87} - 2.77V_8^2 \\
& \quad + 1.16V_8V_9 \cos \theta_{89} - 9.8V_8V_9 \sin \theta_{89} = 0 \\
& -17.065V_9V_3 \sin \theta_{93} + 1.28V_9V_6 \cos \theta_{96} - 5.59V_9V_6 \sin \theta_{96} \\
& \quad + 1.15V_9V_8 \cos \theta_{98} - 9.78V_9V_8 \sin \theta_{98} \\
& \quad - 2.4V_9^2 = 0. \tag{7.54}
\end{aligned}$$

Reactive Power Equations

$$\begin{aligned}
& I_{d1}V_1 \cos(\delta_1 - \theta_1) - I_{q1}V_1 \sin(\delta_1 - \theta_1) \\
& \quad + 17.36V_1V_4 \cos \theta_{14} - 17.36V_1^2 = 0 \\
& I_{d2}V_2 \cos(\delta_2 - \theta_2) - I_{q2}V_2 \sin(\delta_2 - \theta_2) \\
& \quad + 16V_2V_7 \cos \theta_{27} - 16V_2^2 = 0 \\
& I_{d3}V_3 \cos(\delta_3 - \theta_3) - I_{q3}V_3 \sin(\delta_3 - \theta_3) \\
& \quad + 17.07V_3V_9 \cos \theta_{39} - 17.07V_3^2 = 0 \\
& 17.36V_4V_1 \cos \theta_{41} - 39.3V_4^2 + 1.36V_4V_5 \sin \theta_{45} \\
& \quad + 11.6V_4V_5 \cos \theta_{45} + 1.94V_4V_6 \sin \theta_{46} \\
& \quad + 10.52V_4V_6 \cos \theta_{46} = 0 \\
& -0.5 + 1.37V_5V_4 \sin \theta_{54} + 11.6V_5V_4 \cos \theta_{54} - 17.34V_5^2 \\
& \quad + 1.19V_5V_7 \sin \theta_{57} + 5.98V_5V_7 \cos \theta_{57} = 0 \\
& -0.3 + 1.94V_6V_4 \sin \theta_{64} + 10.51V_6V_4 \cos \theta_{64} - 15.84V_6^2 \\
& \quad + 1.28V_6V_9 \sin \theta_{69} + 5.59V_6V_9 \cos \theta_{69} = 0 \\
& 16V_7V_2 \cos \theta_{72} + 1.19V_7V_5 \sin \theta_{75} + 5.98V_7V_5 \cos \theta_{75} \\
& \quad - 35.45V_7^2 + 1.62V_7V_8 \sin \theta_{78} + 13.67V_7V_8 \cos \theta_{78} = 0 \\
& -0.35 + 1.62V_8V_7 \sin \theta_{87} + 13.67V_8V_7 \cos \theta_{87} - 23.3V_8^2 + 1.15V_8V_9 \sin \theta_{89} \\
& \quad + 9.78V_8V_9 \cos \theta_{89} = 0 \\
& 17.065V_9V_3 \cos \theta_{93} + 1.28V_9V_6 \sin \theta_{96} + 5.59V_9V_6 \cos \theta_{96} \\
& \quad + 1.16V_9V_8 \sin \theta_{98} + 9.78V_9V_8 \cos \theta_{98} - 32.15V_9^2 = 0. \tag{7.55}
\end{aligned}$$

It is easy to solve (7.53) for I_{di}, I_{qi} ($i = 1, 2, 3$), substitute them in (7.47) and (7.54)–(7.55), and obtain the equations $\dot{x} = f_1(x, \bar{V}, u)$ and $0 = g_1(x, \bar{V})$. This is left as an exercise for the reader. \square

Example 7.2 In this example, we put the DAE model with the network equations in the current-balance form.

The differential equations (7.47) and the stator algebraic equations (7.53) are unchanged. The network equations are

$$\bar{I}_o(I_{d-q}, x, \bar{V}) = \bar{Y}_N \bar{V} \quad (7.56)$$

where

$$\bar{I}_o(I_{d-q}, x, \bar{V}) = \begin{bmatrix} (I_{d1} + jI_{q1})e^{j(\delta_1 - \pi/2)} \\ (I_{d2} + jI_{q2})e^{j(\delta_2 - \pi/2)} \\ (I_{d3} + jI_{q3})e^{j(\delta_3 - \pi/2)} \\ 0 + j0 \\ (-1.25 + j0.5)/\bar{V}_5^* \\ (-0.9 + j0.3)/\bar{V}_6^* \\ 0 + j0 \\ (-1 + j0.35)/\bar{V}_8^* \\ 0 + j0 \end{bmatrix}. \quad (7.57)$$

It is an easy exercise to substitute I_{d-q} from (7.53) in (7.57) to obtain the network equations for the form $\bar{I}_1(x, \bar{V}) = \bar{Y}_N \bar{V}$. \square

7.4 Industry Model

We now present an equivalent but alternative formulation that is used widely in commercial power system simulation packages [75]. The principal difference is in terms of suitably rearranging the equations from a programming point of view. This will be referred to as the *industry* model. From (7.15) we have

$$\begin{bmatrix} I_{di} \\ I_{qi} \end{bmatrix} = [Z_{d-q,i}]^{-1} \begin{bmatrix} E'_{di} - V_i \sin(\delta_i - \theta_i) \\ E'_{qi} - V_i \cos(\delta_i - \theta_i) \end{bmatrix} i = 1, \dots, m. \quad (7.58)$$

Also from (7.21):

$$\begin{bmatrix} I_{di} \\ I_{qi} \end{bmatrix} = [Z_{d-q,i}]^{-1} \begin{bmatrix} E'_{di} \\ E'_{qi} \end{bmatrix} - [Z_{d-q,i}]^{-1} \begin{bmatrix} \sin \delta_i & -\cos \delta_i \\ \cos \delta_i & \sin \delta_i \end{bmatrix} \begin{bmatrix} V_{Di} \\ V_{Qi} \end{bmatrix} i = 1, \dots, m. \quad (7.59)$$

Hence, I_{di} , I_{qi} are functions of either $(E'_{di}, E'_{qi}, \delta_i, V_i, \theta_i)$ or $(E'_{di}, E'_{qi}, \delta_i, V_{Di}, V_{Qi})$. For ease in programming, the electric power output of machine i in (7.4) is defined as

$$\begin{aligned} P_{ei} &\stackrel{\Delta}{=} E'_{di} I_{di} + E'_{qi} I_{qi} + (X'_{qi} - X'_{di}) I_{di} I_{qi} \\ &= P_{epi}(E'_{di}, E'_{qi}, \delta_i, V_i, \theta_i) \quad \text{or} \quad P_{eri}(E'_{di}, E'_{qi}, \delta_i, V_{Di}, V_{Qi}) \end{aligned} \quad (7.60)$$

if we substitute for I_{di} and I_{qi} from (7.58) or (7.59). The terminal voltage V_i is

$$V_i = \sqrt{V_{Di}^2 + V_{Qi}^2} = \sqrt{V_{di}^2 + V_{qi}^2}. \quad (7.61)$$

We define two vectors

$$E \stackrel{\Delta}{=} [E'_{d1} E'_{q1} \dots E'_{dm} E'_{qm} \delta_1 \dots \delta_m]^t \quad (7.62)$$

and

$$W \stackrel{\Delta}{=} [I_{d1} I_{q1} \dots I_{dm} I_{qm} P_{e1} \dots P_{em} V_1 \dots V_m]^t. \quad (7.63)$$

E is a subset of the state vector x and W is a vector of algebraic variables. With these definitions, we can express the differential equations (7.1)–(7.7) as

$$\dot{x} = F(x, W, u). \quad (7.64)$$

The stator algebraic equations (7.58) or (7.59), together with (7.60) and (7.61), are expressed as

$$W = G(E, \bar{V}) \quad (7.65)$$

The network equations from (7.46) are

$$\bar{I}_2(E, \bar{V}) = \bar{Y}_N \bar{V} \quad (7.66)$$

since E is a subset of the vector x . Thus, assembling (7.64), (7.65), and (7.66) results in

$$\dot{x} = F(x, W, u) \quad (7.67)$$

$$W = G(E, \bar{V}) \quad (7.68)$$

$$\bar{I}_2(E, \bar{V}) = \bar{Y}_N \bar{V}. \quad (7.69)$$

Equation (7.67) has the structure

$$\dot{x} = A(x)x + BW + Cu \quad (7.70)$$

The only dependency of $A(x)$ on x comes through the saturation function in the exciter. $A(x), B$, and C are matrices having a block structure with each block belonging to a machine. G contains the stator algebraic equations and intermediate equations for P_{ei} and V_i in terms of (E, \bar{V}) . This formulation is easy to program. Alternatively, we can substitute (7.68) in (7.67) to obtain

$$\begin{aligned}\dot{x} &= f_1(x, \bar{V}, u) \\ \bar{I}_1(x, \bar{V}) &= \bar{Y}_N \bar{V}\end{aligned}\quad (7.71)$$

which is precisely equal to (7.46).

The DAE model with the network equations in the current-balance form is the preferred industry model, since the network-admittance matrix has to be refactored only if there is a network change. Otherwise, the initial factorization will remain. The DAE model with network equations in power-balance form (discussed in Section 7.3.1) has the advantage that the Jacobian of the network equations contains the power flow Jacobian, a fact useful in small-signal analysis and voltage collapse studies, as discussed in Chapter 8.

Equations (7.67)–(7.69) can be interpreted as a block diagram, as shown in Figure 7.5.

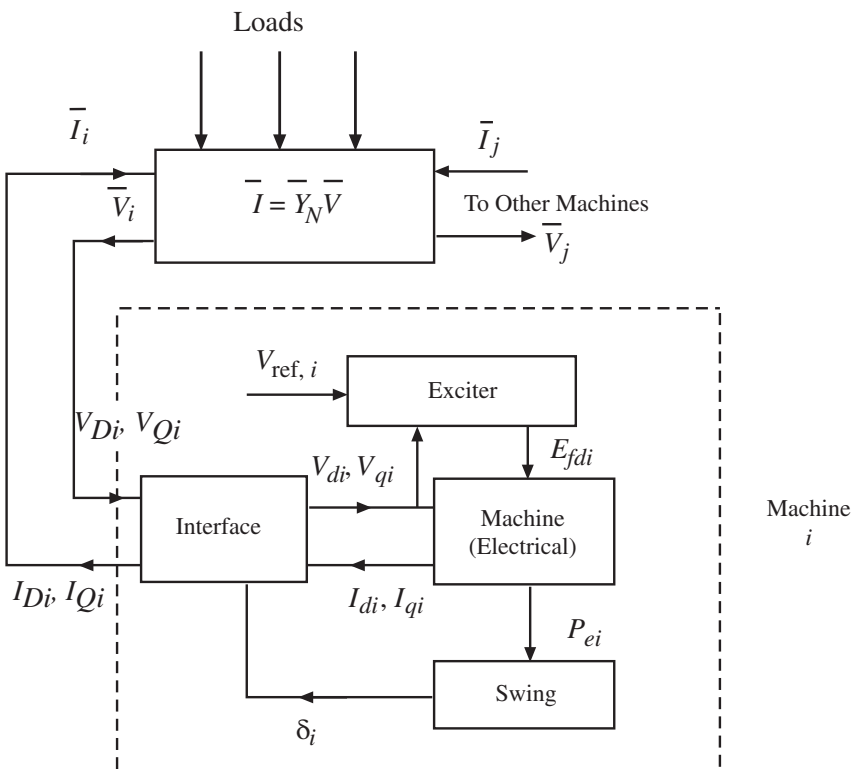


Figure 7.5 Block diagram conceptualization of (7.67)–(7.69).

Example 7.3 We will express the 3-machine system in Example 7.1 in the form of (7.67)–(7.69). Thus (7.67)–(7.68) become

$$\begin{bmatrix} \dot{x}_1 \\ \dot{x}_2 \\ \dot{x}_3 \end{bmatrix} = \begin{bmatrix} A_1 & 0 & 0 \\ 0 & A_2 & 0 \\ 0 & 0 & A_3 \end{bmatrix} \begin{bmatrix} x_1 \\ x_2 \\ x_3 \end{bmatrix} + \begin{bmatrix} B_1 & 0 & 0 \\ 0 & B_2 & 0 \\ 0 & 0 & B_3 \end{bmatrix} \begin{bmatrix} W_1 \\ W_2 \\ W_3 \end{bmatrix} + Cu \quad (7.72)$$

where

$$A_i = \begin{bmatrix} \frac{-1}{T'_{doi}} & 0 & 0 & 0 & \frac{1}{T'_{doi}} & 0 & 0 \\ 0 & \frac{-1}{T'_{qoi}} & 0 & 0 & 0 & 0 & 0 \\ 0 & 0 & 0 & 1 & 0 & 0 & 0 \\ 0 & 0 & 0 & \frac{-D_i}{M_i} & 0 & 0 & 0 \\ 0 & 0 & 0 & 0 & \frac{-(K_{Ei} + S_{Ei}(E_{fdi}))}{T_{Ei}} & 0 & \frac{1}{T_{Ei}} \\ 0 & 0 & 0 & 0 & \frac{K_{Fi}}{T_{Fi}^2} & \frac{-1}{T_{Fi}} & 0 \\ 0 & 0 & 0 & 0 & \frac{-K_{Ai}K_{Fi}}{T_{Fi}T_{Ai}} & \frac{K_{Ai}}{T_{Ai}} & \frac{-1}{T_{Ai}} \end{bmatrix} \quad i = 1, 2, 3 \quad (7.73)$$

$$B_i = \begin{bmatrix} \frac{-(X_{di} - X'_{di})}{T'_{doi}} & 0 & 0 & 0 \\ 0 & \frac{(X_{qi} - X'_{qi})}{T'_{qoi}} & 0 & 0 \\ 0 & 0 & 0 & 0 \\ 0 & 0 & \frac{-1}{M_i} & 0 \\ 0 & 0 & 0 & 0 \\ 0 & 0 & 0 & -\frac{K_{Ai}}{T_{Ai}} \end{bmatrix} \quad i = 1, 2, 3$$

$$W_i = \begin{bmatrix} I_{di} \\ I_{qi} \\ P_{ei} \\ V_i \end{bmatrix} \quad i = 1, 2, 3. \quad (7.74)$$

C is $\text{Diag}(C_i)$ and $u = \text{Diag}(u_i)$, where C_i and u_i are given by (7.49). The stator algebraic equations and the intermediate equations corresponding to (7.68) are

$$W_i = \begin{bmatrix} [Z_{d-q,i}]^{-1} \begin{bmatrix} E'_{di} \\ E'_{qi} \end{bmatrix} - [Z_{d-q,i}]^{-1} \begin{bmatrix} \sin \delta_i & -\cos \delta_i \\ \cos \delta_i & \sin \delta_i \end{bmatrix} \begin{bmatrix} V_{Di} \\ V_{Qi} \end{bmatrix} \\ E'_{di} I_{di} + E'_{qi} I_{qi} + (X'_{qi} - X'_{di}) I_{di} I_{qi} \\ \sqrt{V_{Di}^2 + V_{Qi}^2} \end{bmatrix} \quad i = 1, 2, 3. \quad (7.75)$$

If I_{di} and I_{qi} in P_{ei} are expressed from the first two equations, then $W_i = G_i(E_i, \bar{V}_i)$. A similar substitution for I_{di}, I_{qi} in (7.56) and (7.57) leads to

$$\bar{I}_1(x, \bar{V}) = \bar{Y}_N \bar{V}. \quad (7.76)$$

Substitution of numerical values in the above equations is trivial, and is left as an exercise for the reader. \square

Before we discuss the important issue of initial condition computation, we consider two simplifications that yield models far simpler than the two-axis model. They are also amenable to a network theoretic approach. Using these simplifications, we develop later (1) the structure-preserving flux-decay model, (2) the structure-preserving classical model, and (3) the internal node model using the classical machine model and constant impedance loads. Both (1) and (2) can have nonlinear load representations.

7.5 Simplification of the Two-Axis Model

Two simplifications can be made in the two-axis model—one regarding X'_d and X'_q , and the other regarding the nature of loads. These can be done independently or together, resulting in simplified models.

7.5.1 Simplification #1 (Neglecting Transient Saliency in the Synchronous Machine)

Transient saliency corresponds to different values of X'_{di} and X'_{qi} . If $X'_{qi} = X'_{di}$, then the stator algebraic equation (7.8) is simplified as

$$0 = V_i e^{j\theta_i} + (R_{si} + jX'_{di})(I_{di} + jI_{qi})e^{j(\delta_i - \pi/2)} - (E'_{di} + jE'_{qi})e^{j(\delta_i - \pi/2)}. \quad (7.77)$$

The equivalent circuit for machine i is shown in Figure 7.6.

The machine–network transformation gives

$$(E'_{di} + jE'_{qi})e^{j(\delta_i - \pi/2)} = E'_{Di} + jE'_{Qi} \quad (7.78)$$

$$(I_{di} + jI_{qi})e^{j(\delta_i - \pi/2)} = I_{Di} + jI_{Qi}. \quad (7.79)$$

Thus, with all the quantities in the synchronous reference frame, we have the equivalent circuit shown in Figure 7.7. Writing the KVL equation for Figure 7.7, we get $(E'_{Di} + jE'_{Qi}) = (R_{si} + jX'_{di})(I_{Di} + jI_{Qi}) + V_i e^{j\theta_i}$, which is equivalent to (7.77).

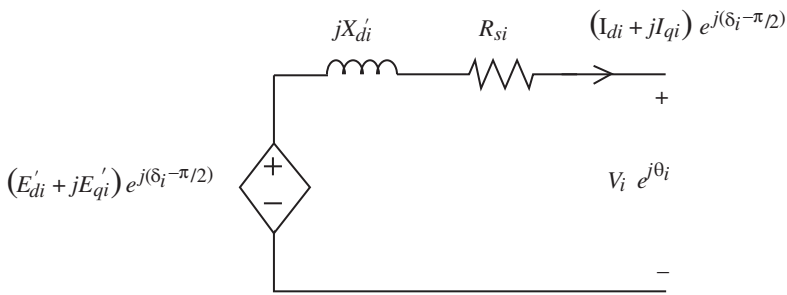


Figure 7.6 Equivalent circuit with $X'_{di} = X'_{qi}$.

In the differential equations, the expression for electric power P_{ei} given by (7.60) is simplified as

$$P_{ei} = E'_{di} I_{di} + E'_{qi} I_{qi}. \quad (7.80)$$

It can be verified that the right-hand side of (7.80) is also equal to $E'_{D_i} I_{D_i} + E'_{Q_i} I_{Q_i}$ by taking the complex conjugate of (7.79), multiplying it by (7.78), and equating the real part.

This assumption of $X'_{di} = X'_{qi}$ is often called “neglecting transient saliency.” The advantage is that, in the equivalent circuit, all variables are in the network reference frame, and it is particularly useful in the current-balance form of Section 7.3.2. In (7.46), the algebraic equations that are equivalent to (7.42) and (7.43) can be directly expressed in terms of I_{D_i} , I_{Q_i} , and \bar{V}_i using $(I_{di} + jI_{qi}) e^{j(\delta_i - \pi/2)} = I_{D_i} + jI_{Q_i}$.

7.5.2 Simplification #2 (Constant Impedance Load in the Transmission System)

Here, the loads are assumed to be of the constant impedance type, that is,

$$P_{Li}(V_i) = k_{P2i} V_i^2 \quad (7.81)$$

$$Q_{Li}(V_i) = k_{Q2i} V_i^2. \quad (7.82)$$

Then

$$P_{Li}(V_i) + jQ_{Li}(V_i) = (k_{P2i} + jk_{Q2i}) V_i^2. \quad (7.83)$$

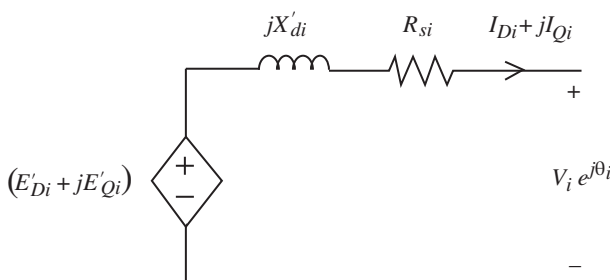
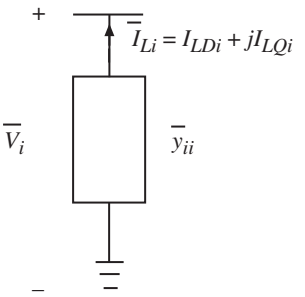


Figure 7.7 Equivalent circuit (all quantities in network reference frame).

Figure 7.8 Load admittance representation.

Since $(P_{Li} + jQ_{Li}) = \bar{V}_i \bar{I}_{Li}^*$, where \bar{I}_{Li} is the injected current,

$$\bar{V}_i \bar{I}_{Li}^* = V_i^2 (k_{P2i} + jk_{Q2i}). \quad (7.84)$$

But $V_i^2 = \bar{V}_i \bar{V}_i^*$ and conjugating (7.84), we obtain

$$(k_{P2i} - jk_{Q2i}) = \frac{\bar{I}_{Li}}{\bar{V}_i} = -\bar{y}_{ii}. \quad (7.85)$$

Because of the orientation of \bar{V}_i and \bar{I}_{Li} , there is a negative sign in front of the load admittance \bar{y}_{ii} in (7.85). From Figure 7.8, we can verify that

$$\frac{P_{Li}(V_i) - jQ_{Li}(V_i)}{\bar{V}_i^*} = \bar{I}_{Li} = -\bar{y}_{ii} \bar{V}_i. \quad (7.86)$$

Hence

$$\bar{y}_{ii} = -\frac{(P_{Li}(V_i) - jQ_{Li}(V_i))}{V_i^2}.$$

This is consistent with the fact that P_{Li} and Q_{Li} are injected loads. \bar{y}_{ii} is the complex admittance due to the loads. Since $(I_{di} + jI_{qi})e^{j(\delta_i - \pi/2)} = I_{Di} + jI_{Qi}$, for $i = 1, \dots, m$ and using (7.86), the network equations (7.42) and (7.43) become

$$(I_{Di} + jI_{Qi}) = \sum_{k=1}^n V_k e^{j\theta_k} Y_{ik} e^{j\alpha_{ik}} + \bar{y}_{ii} V_i e^{j\theta_i} \quad i = 1, \dots, m \quad (7.87)$$

$$0 = \sum_{k=1}^n V_k e^{j\theta_k} Y'_{ik} e^{j\alpha'_{ik}} + \bar{y}_{ii} V_i e^{j\theta_i} \quad i = m+1, \dots, n$$

that is,

$$I_{Di} + jI_{Qi} = \sum_{k=1}^n V_k e^{j\theta_k} Y'_{ik} e^{j\alpha'_{ik}} \quad i = 1, \dots, m \quad (7.88)$$

$$0 = \sum_{k=1}^n V_k e^{j\theta_k} Y'_{ik} e^{j\alpha'_{ik}} \quad i = m+1, \dots, n$$

where

$$\begin{aligned} Y'_{ik} e^{j\alpha'_{ik}} &= Y_{ik} e^{j\alpha_{ik}} \quad i \neq k \\ Y'_{ii} e^{j\alpha'_{ii}} &= Y_{ii} e^{j\alpha_{ii}} + \bar{y}_{ii}. \end{aligned}$$

Equation (7.88) can be written as

$$\begin{bmatrix} \bar{I}_1 \\ \vdots \\ \bar{I}_m \\ 0 \\ \vdots \\ 0 \end{bmatrix} = [\bar{Y}'] \begin{bmatrix} \bar{V}_1 \\ \vdots \\ \bar{V}_n \end{bmatrix} \quad (7.89)$$

where $\bar{I}_1, \dots, \bar{I}_m$ are the complex injected generator currents at the generator buses. Let the modified \bar{Y}_{bus} denoted as \bar{Y}' be partitioned as

$$[\bar{Y}'] = \begin{array}{c|c} m & n-m \\ \hline \bar{Y}_1 & \bar{Y}_2 \\ \hline - & - \\ \bar{Y}_3 & \bar{Y}_4 \end{array}. \quad (7.90)$$

Since there are no injections at buses $m+1, \dots, n$, we can eliminate them to get

$$\begin{bmatrix} \bar{I}_1 \\ \vdots \\ \bar{I}_m \end{bmatrix} = [\bar{Y}_{\text{red}}] \begin{bmatrix} \bar{V}_1 \\ \vdots \\ \bar{V}_m \end{bmatrix} \quad (7.91)$$

where $\bar{Y}_{\text{red}} = (\bar{Y}_1 - \bar{Y}_2 \bar{Y}_4^{-1} \bar{Y}_3)$.

Note that we can make either or both of the above two simplifications. If we make only the constant impedance approximation, then we can obtain a passive reduced network, as in Figure 7.9, but the source will be a dependent one, as in Figure 7.1. On the other hand, if we make the assumption $X'_{di} = X'_{qi}$ only, then we obtain the source representation, as in Figure 7.9, but the network equations will remain in (7.42) and (7.43). If we make both assumptions, then we obtain a passive reduced network, as in Figure 7.9, and the voltage $\bar{E}'_i = E'_{Di} + jE'_{Qi}$.

Example 7.4 Based on the load-flow results in Table 7.1, convert the loads as constant admittances, and then obtain a \bar{Y}_{red} representation (all in pu).

Solution

Note that the load specified in Table 7.1 is the negative of the injected load. Hence, at buses 5, 6, and 8, \bar{y}_{ii} is given by

$$\begin{aligned} \bar{y}_{55} &= \frac{1.25-j0.5}{(0.9956)^2} = 1.26 - j0.504, \\ \bar{y}_{66} &= \frac{0.9-j0.3}{(1.013)^2} = 0.877 - j0.292 \\ \bar{y}_{88} &= \frac{1-j0.35}{(1.016)^2} = 0.969 - j0.339. \end{aligned}$$

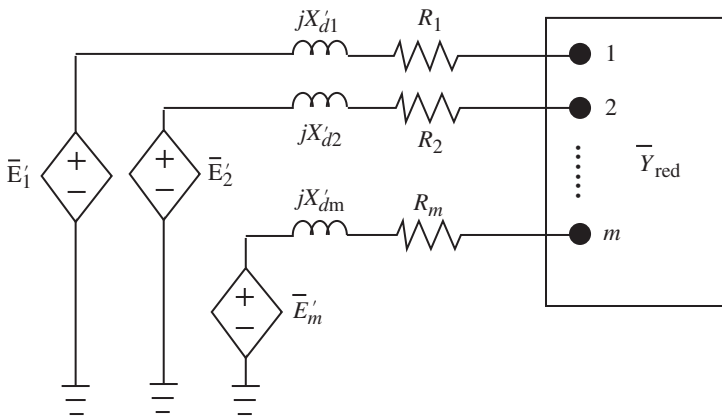


Figure 7.9 Network reduced at generator nodes and $X'_{di} = X'_{qi}$.

These elements are now added to the \bar{Y}_{55} , \bar{Y}_{66} , and \bar{Y}_{88} elements of the \bar{Y}_{bus} matrix in Table 7.2, resulting in \bar{Y}' as

$$\bar{Y}' = \begin{pmatrix} 1 & 2 & 3 & 4 & 5 & 6 & 7 & 8 & 9 \\ 1 & -j17.361 & 0 & 0 & j17.361 & 0 & 0 & 0 & 0 \\ 2 & 0 & -j16 & 0 & 0 & 0 & 0 & j16 & 0 \\ 3 & 0 & 0 & -j17.065 & 0 & 0 & 0 & 0 & j17.065 \\ 4 & j17.361 & 0 & 0 & (3.3074 & (-1.3652 & (-1.9422 & 0 & 0 \\ & & & -j39.3089 & +j11.604) & +j10.5107) & 0 & 0 & 0 \\ 5 & 0 & 0 & 0 & (-1.365 & (3.814 & 0 & (-1.188 & 0 \\ & & & +j11.604) & -j17.842) & & & +j5.975) & 0 \\ 6 & 0 & 0 & 0 & (-1.942 & 0 & (4.102 & 0 & (-1.282 \\ & & & +j10.511) & & -j16.133) & & & +j5.588) \\ 7 & 0 & j16 & 0 & 0 & (-1.188 & 0 & (2.805 & (-1.617 \\ & & & & +j5.975) & & -j35.464) & +j13.698) & 0 \\ 8 & 0 & 0 & 0 & 0 & 0 & 0 & (-1.617 & (3.741 \\ & & & & & & & +j13.698) & -j23.642) & (-1.155 \\ 9 & 0 & 0 & j17.065 & 0 & 0 & (-1.282 & 0 & (-1.155 \\ & & & & & & +j5.588) & +j9.784) & (2.437 \\ & & & & & & & & -j32.154) \end{pmatrix}.$$

\bar{Y}_{red} is obtained by eliminating the buses 4 to 9 from \bar{Y}' . The resulting \bar{Y}_{red} is given by

$$\bar{Y}_{\text{red}} = \begin{bmatrix} 1.105 - j4.695 & 0.096 + j2.253 & 0.004 + j2.275 \\ 0.096 + j2.257 & 0.735 - j5.114 & 0.123 + j2.826 \\ 0.004 + j2.275 & 0.123 + j2.826 & 0.721 - j5.023 \end{bmatrix}.$$

With this simplification, we have $\bar{I} = \bar{Y}_{\text{red}} \bar{V}$. □

7.6 Initial Conditions (Full Model)

The initial conditions of the state variables for the model in Section 7.1 are computed by systematically solving the load-flow equations of the network first, and then computing the other algebraic and state variables. The load-flow equations are part of the network equations, as shown below.

7.6.1 Load-Flow Formulation

We now revert to the formulation of the network equations that were written as real and reactive power-balance equations at the nodes, that is, (7.32)–(7.35). We reproduce them below by writing real power equations first, followed by the reactive power equations

$$\begin{aligned} I_{di} V_i \sin(\delta_i - \theta_i) + I_{qi} V_i \cos(\delta_i - \theta_i) + P_{Li}(V_i) \\ - \sum_{k=1}^n V_i V_k Y_{ik} \cos(\theta_i - \theta_k - \alpha_{ik}) = 0 \quad i = 1, \dots, m \end{aligned} \quad (7.92)$$

$$P_{Li}(V_i) - \sum_{k=1}^n V_i V_k Y_{ik} \cos(\theta_i - \theta_k - \alpha_{ik}) = 0 \quad i = m+1, \dots, n \quad (7.93)$$

$$\begin{aligned} I_{di} V_i \cos(\delta_i - \theta_i) - I_{qi} V_i \sin(\delta_i - \theta_i) + Q_{Li}(V_i) \\ - \sum_{k=1}^n V_i V_k Y_{ik} \sin(\theta_i - \theta_k - \alpha_{ik}) = 0 \quad i = 1, \dots, m \end{aligned} \quad (7.94)$$

$$Q_{Li}(V_i) - \sum_{k=1}^n V_i V_k Y_{ik} \sin(\theta_i - \theta_k - \alpha_{ik}) = 0 \quad i = m+1, \dots, n. \quad (7.95)$$

It follows from the dynamic circuit in Figure 7.10 that

$$\begin{aligned} P_{Gi} + j Q_{Gi} &= \bar{V}_i \bar{I}_{Gi}^* = V_i e^{j\theta_i} (I_{di} - j I_{qi}) e^{-j(\delta_i - \pi/2)} \\ &= V_i (\cos \theta_i + j \sin \theta_i) (I_{di} - j I_{qi}) (\sin \delta_i + j \cos \delta_i). \end{aligned} \quad (7.96)$$

$$\bar{I}_{Gi} = (I_{di} + j I_{qi}) e^{j(\delta_i - \pi/2)}$$

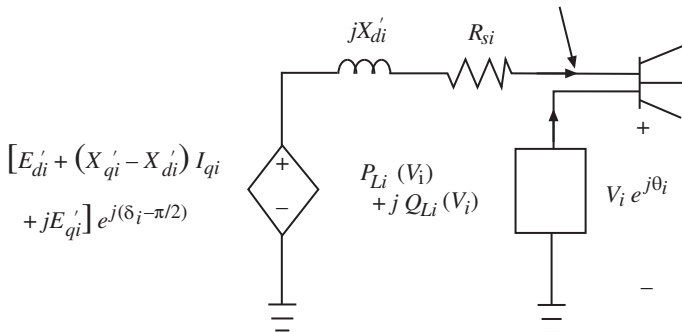


Figure 7.10 Synchronous machine dynamic circuit.

Now we equate the real and imaginary parts along with the use of trigonometric identities. It can be shown from (7.96) that

$$P_{Gi} = I_{di} V_i \sin(\delta_i - \theta_i) + I_{qi} V_i \cos(\delta_i - \theta_i) \quad (7.97)$$

and

$$Q_{Gi} = I_{di} V_i \cos(\delta_i - \theta_i) - I_{qi} V_i \sin(\delta_i - \theta_i) \quad (7.98)$$

$$\bar{I}_{Gi} \stackrel{\Delta}{=} I_{Gi} e^{j\gamma_i} = (I_{di} + jI_{qi}) e^{j(\delta_i - \pi/2)} \quad (7.99)$$

is the injected generator current at the generator bus in the synchronous reference frame. Figure 7.10 explains the equations at the generator bus.

We further define net injected power at a bus as

$$\begin{aligned} P_i(\delta_i, I_{di}, I_{qi}, V_i, \theta_i) + jQ_i(\delta_i, I_{di}, I_{qi}, V_i, \theta_i) = \\ (P_{Gi} + P_{Li}(V_i)) + j(Q_{Gi} + Q_{Li}(V_i)) \quad i = 1, \dots, m. \end{aligned} \quad (7.100)$$

Thus, the power-balance equations at the buses $1, \dots, n$ are

$$P_i(\delta_i, I_{di}, I_{qi}, V_i, \theta_i) = \sum_{k=1}^n V_i V_k Y_{ik} \cos(\theta_i - \theta_k - \alpha_{ik}) \quad i = 1, \dots, m \quad (7.101)$$

$$P_{Li}(V_i) = \sum_{k=1}^n V_i V_k Y_{ik} \cos(\theta_i - \theta_k - \alpha_{ik}) \quad i = m+1, \dots, n \quad (7.102)$$

$$Q_i(\delta_i, I_{di}, I_{qi}, V_i, \theta_i) = \sum_{k=1}^n V_i V_k Y_{ik} \sin(\theta_i - \theta_k - \alpha_{ik}) \quad i = 1, \dots, m \quad (7.103)$$

$$Q_{Li}(V_i) = \sum_{k=1}^n V_i V_k Y_{ik} \sin(\theta_i - \theta_k - \alpha_{ik}) \quad i = m+1, \dots, n. \quad (7.104)$$

7.6.2 Standard Load Flow

Load flow has been the traditional mechanism for computing a proposed steady-state operating point. We now define standard load flow as follows, using (7.101)–(7.104). Loads are of the constant power type.

1. Specify bus voltage magnitudes numbered 1 to m .
2. Specify bus voltage angle at bus number 1 (slack bus).
3. Specify net injected real power P_i at buses numbered 2 to m .
4. Specify load powers P_{Li} and Q_{Li} at buses numbered $m+1$ to n .

The following equations result from (7.101), (7.102), and (7.104) chosen according to criteria (3) and (4). These are known as the *load-flow equations*. Thus, we have

$$0 = -P_i + \sum_{k=1}^n V_i V_k Y_{ik} \cos(\theta_i - \theta_k - \alpha_{ik}) \quad \begin{matrix} i=2, \dots, m \\ (\text{PV buses}) \end{matrix} \quad (7.105)$$

$$0 = -P_{Li} + \sum_{k=1}^n V_i V_k Y_{ik} \cos(\theta_i - \theta_k - \alpha_{ik}) \quad \begin{matrix} i=m+1, \dots, n \\ (\text{PQ buses}) \end{matrix} \quad (7.106)$$

$$0 = -Q_{Li} + \sum_{k=1}^n V_i V_k Y_{ik} \sin(\theta_i - \theta_k - \alpha_{ik}) \quad (PQ \text{ buses}) \quad (7.107)$$

where P_i ($i = 2, \dots, m$), V_i ($i = 1, \dots, m$), P_{Li} ($i = m+1, \dots, n$), Q_{Li} ($i = m+1, \dots, n$), and θ_1 are specified numbers. The standard load flow solves (7.105)–(7.107) for $\theta_2, \dots, \theta_n, V_{m+1}, \dots, V_n$. After the load-flow solution, we compute the net injected powers at the slack bus and the net injected reactive power at the generator buses as

$$P_1 + jQ_1 = \sum_{k=1}^n V_i V_k Y_{ik} e^{j(\theta_1 - \theta_k - \alpha_{ik})} \quad (7.108)$$

$$Q_i = \sum_{k=1}^n V_i V_k Y_{ik} \sin(\theta_i - \theta_k - \alpha_{ik}) \quad i = 2, \dots, m. \quad (7.109)$$

The generator powers are given by $P_{G1} = P_1 - P_{L1}$ and $Q_{Gi} = Q_i - Q_{Li}$ ($i = 1, \dots, m$). This standard load flow has many variations, including the addition of other devices such as tap-changing-under-load (TCUL) transformers, switching VAR sources, HVDC converters, and nonlinear load representation. It can also include inequality constraints on quantities such as Q_{Gi} at the generators, and can also have more than one slack bus. For details, refer to [15, 16, 18].

One important point about load flow should be emphasized. Load flow is normally used to evaluate operation at a specific load level (specified by a given set of powers). For a specified load and generation schedule, the solution is independent of the actual load model. That is, it is certainly possible to evaluate the voltage at a constant impedance load for a specific case where that impedance load consumes a specific amount of power. Thus, the use of “constant power” in load-flow analysis does not require or even imply that the load is truly a constant power device. It merely gives the voltage at the buses when the loads (any type) consume a specific amount of power. The load characteristic is important when the analyst wants to study the system in response to a change, such as contingency analysis or dynamic analysis. For these purposes, standard load flow is computed on the basis of constant PQ loads and usually provides the “initial conditions” for the dynamic system.

7.6.3 Initial Conditions for Dynamic Analysis

We use the model in the power-balance form from (7.36)–(7.38)

$$\dot{x} = f_o(x, I_{d-q}, \bar{V}, u) \quad (7.110)$$

$$I_{d-q} = h(x, \bar{V}) \quad (7.111)$$

$$0 = g_o(x, I_{d-q}, \bar{V}). \quad (7.112)$$

It is necessary to compute the initial values of all the dynamic states and the fixed inputs T_{Mi} and V_{ref_i} ($i = 1, \dots, m$). In power system dynamic analysis, the fixed inputs and initial conditions are normally found from a base case load-flow solution. That is, the values of V_{ref_i} are computed such that the m generator voltages are as specified in the load flow. The values of T_{Mi} are computed such that the m generator real power outputs P_{Gi} are as specified and computed in the load flow for rated speed ω_s . To see how this is done, we assume that a load-flow solution (as defined in previous section) has been found, that is,

solution of (7.105)–(7.107). The first step in computing the initial conditions is normally the calculation of generator currents from (7.96), as $\bar{I}_{Gi} = I_{Gi} e^{j\gamma_i} = (P_{Gi} - jQ_{Gi})/\bar{V}_i^*$.

Step 1: Since $P_{Gi} = P_i - P_{Li}$ and $Q_{Gi} = Q_i - Q_{Li}$:

$$I_{Gi} e^{j\gamma_i} = ((P_i - P_{Li}) - j(Q_i - Q_{Li}))/(\bar{V}_i e^{-j\theta_i}), \quad i = 1, \dots, m. \quad (7.113)$$

This current is in the network reference frame and is equal to $(I_{di} + jI_{qi}) e^{j(\delta_i - \pi/2)}$.

In steady state, all the derivatives are zero in the differential equations (7.1)–(7.7). The first step is to calculate the rotor angles δ_i at all the machines. We use the complex stator algebraic equation (7.8) and the algebraic equation obtained from (7.2) by setting $\dot{E}_{di} = 0$. From the latter, we obtain

$$E'_{di} = (X_{qi} - X'_{qi})I_{qi} \quad i = 1, \dots, m. \quad (7.114)$$

Substitution of (7.114) in (7.8) results in

$$\begin{aligned} V_i e^{j\theta_i} + (R_{si} + jX'_{di})(I_{di} + jI_{qi})e^{j(\delta_i - \pi/2)} \\ - [(X_{qi} - X'_{qi})I_{qi} + (X'_{qi} - X'_{di})I_{qi} + jE'_{qi}]e^{j(\delta_i - \pi/2)} = 0 \quad i = 1, \dots, m \end{aligned} \quad (7.115)$$

that is,

$$\begin{aligned} V_i e^{j\theta_i} + R_{si}(I_{di} + jI_{qi})e^{j(\delta_i - \pi/2)} + jX'_{di}(I_{di} + jI_{qi})e^{j(\delta_i - \pi/2)} \\ - [(X_{qi} - X'_{di})I_{qi} + jE'_{qi}]e^{j(\delta_i - \pi/2)} = 0 \quad i = 1, \dots, m \end{aligned} \quad (7.116)$$

that is,

$$\begin{aligned} V_i e^{j\theta_i} + R_{si}(I_{di} + jI_{qi})e^{j(\delta_i - \pi/2)} + jX'_{di}I_{di}e^{j(\delta_i - \pi/2)} - X_{qi}I_{qi}e^{j(\delta_i - \pi/2)} \\ - jE'_{qi}e^{j(\delta_i - \pi/2)} = 0, \quad i = 1, \dots, m. \end{aligned} \quad (7.117)$$

Adding and subtracting $jX_{qi}I_{di}e^{j(\delta_i - \pi/2)}$ from the left-hand side of (7.117) results in

$$\begin{aligned} V_i e^{j\theta_i} + (R_{si} + jX_{qi})(I_{di} + jI_{qi})e^{j(\delta_i - \pi/2)} \\ - j[(X_{qi} - X'_{di})I_{di} + E'_{qi}]e^{j(\delta_i - \pi/2)} = 0 \quad i = 1, \dots, m. \end{aligned} \quad (7.118)$$

Replace $(I_{di} + jI_{qi})e^{j(\delta_i - \pi/2)}$ by $I_{Gi} e^{j\gamma_i}$, which is already calculated in (7.113):

$$V_i e^{j\theta_i} + (R_{si} + jX_{qi})I_{Gi} e^{j\gamma_i} = ((X_{qi} - X'_{di})I_{di} + E'_{qi})e^{j\delta_i} \quad i = 1, \dots, m. \quad (7.119)$$

The right-hand side of (7.119) is a voltage behind the impedance $(R_{si} + jX_{qi})$ and has an angle δ_i . The voltage has a magnitude $(E'_{qi} + (X_{qi} - X'_{di})I_{di})$ and an angle $\delta_i = \text{angle of } (V_i e^{j\theta_i} + (R_{si} + jX_{qi})I_{Gi} e^{j\gamma_i})$. The complex number representation for computing δ_i from (7.119) is shown in Figure 7.11. This representation is generally known as “phasor diagram” in the literature and “locating the q axis” of the machine.

Step 2: δ_i is computed as $\delta_i = \text{angle on } (V_i e^{j\theta_i} + (R_{si} + jX_{qi})I_{Gi} e^{j\gamma_i})$.

Step 3: Compute I_{di} , I_{qi} , V_{di} , V_{qi} for the machines as

$$I_{di} + jI_{qi} = I_{Gi} e^{j(\gamma_i - \delta_i + \pi/2)} \quad i = 1, \dots, m \quad (7.120)$$

$$V_{di} + jV_{qi} = V_i e^{j(\theta_i - \delta_i + \pi/2)} \quad i = 1, \dots, m. \quad (7.121)$$

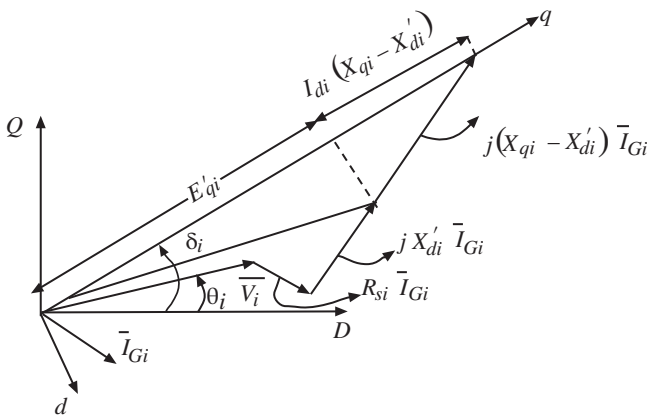


Figure 7.11 Representation of stator algebraic equations in steady state.

Step 4: Compute E'_{di} from (7.27):

$$E'_{di} = V_{di} + R_{si} I_{di} - X'_{qi} I_{qi} \quad i = 1, \dots, m \quad (7.122)$$

which from (7.114) is also equal to $(X_{qi} - X'_{qi}) I_{qi}$. This serves as a check on the calculations.

Step 5: Compute E'_{qi} from (7.27)

$$E'_{qi} = V_{qi} + R_{si} I_{qi} + X'_{di} I_{di} \quad i = 1, \dots, m. \quad (7.123)$$

Step 6: Compute E_{fdi} from (7.1) (after setting the derivative equal to zero):

$$E_{fdi} = E'_{qi} + (X_{di} - X'_{di}) I_{di} \quad i = 1, \dots, m. \quad (7.124)$$

Step 7: With the field voltage E_{fdi} known, the other variables R_{fi} , V_{Ri} and V_{refi} can be found from (7.5)–(7.7) (after setting the derivatives equal to zero):

$$V_{Ri} = (K_{Ei} + S_{Ei}(E_{fdi})) E_{fdi} \quad i = 1, \dots, m \quad (7.125)$$

$$R_{fi} = \frac{K_{Fi}}{T_{Fi}} E_{fdi} \quad i = 1, \dots, m \quad (7.126)$$

$$V_{refi} = V_i + (V_{Ri}/K_{Ai}) \quad i = 1, \dots, m. \quad (7.127)$$

Note that if the machine saturation is included, the calculation for E'_{qi} and E'_{di} may be iterative. The mechanical states ω_i and T_{Mi} are found from (7.3) and (7.4) (after setting the derivatives equal to zero):

$$\omega_i = \omega_s \quad i = 1, \dots, m \quad (7.128)$$

$$T_{Mi} = E'_{di} I_{di} + E'_{qi} I_{qi} + (X'_{qi} - X'_{di}) I_{di} I_{qi} \quad i = 1, \dots, m. \quad (7.129)$$

This completes the computation of all dynamic-state initial conditions and fixed inputs. Thus, we have computed $x(o)$, $y(o)$, and u from the load-flow data.

For a given disturbance, the inputs remain fixed throughout the simulation. If the disturbance occurs due to a fault or a network change, the algebraic states must change

instantaneously. The dynamic states cannot change instantaneously. Thus, it will be necessary to solve all the algebraic equations inclusive of the stator equations with the dynamic states specified at their values just prior to the disturbance as initial conditions to determine the new initial values of the algebraic states.

From the above description, it is clear that once a standard load-flow solution is found, the remaining dynamic states and inputs can be found in a systematic manner. The machine rotor angles δ_i can always be found, provided that:

$$V_i e^{j\theta_i} + (R_{si} + jX_{qi}) I_{Gi} e^{j\gamma_i} \neq 0 \quad i = 1, \dots, m \quad (7.130)$$

If control limits are enforced, a solution satisfying these limits may not exist. In this case, the state that is limited would have to be fixed at its limiting value and a corresponding new steady-state solution would have to be found. This would require a new load flow by specifying either different values of generator voltages, different generator real powers, or possibly specifying generator-reactive power injections, thus allowing generator voltage to be a part of the load-flow solution. In fact, the use of reactive power limits in load flow can usually be traced to an attempt to consider excitation system limits or generator capability limits.

Example 7.5 For Example 7.1, compute the initial conditions. The solved load-flow data are given in Table 7.1 (all in pu).

Machine 1

Step 1:

$$\begin{aligned} I_{G1} e^{j\gamma_1} &= \frac{P_{G1} - jQ_{G1}}{\bar{V}_1^*} = \frac{0.716 - j0.27}{1.04\angle 0^\circ} \\ &= 0.736\angle -20.66^\circ. \end{aligned}$$

Step 2:

$$\begin{aligned} \delta_1(0) &= \text{Angle of}(V_1 e^{j\theta_1} + (R_{s1} + jX_{q1}) I_{G1} e^{j\gamma_1}) \\ &= \text{Angle of}((1.04\angle 0^\circ + j0.0969)(0.736\angle -20.66^\circ)) \\ &= 3.58^\circ. \end{aligned}$$

Step 3:

$$\begin{aligned} I_{d1} + jI_{q1} &= I_{G1} e^{j\gamma_1} e^{-j(\delta_1 - \pi/2)} \\ &= (0.736\angle -20.66^\circ)(1\angle 86.42^\circ) \\ &= 0.302 + j0.671 \end{aligned}$$

$$I_{d1} = 0.302 \quad I_{q1} = 0.671$$

$$\begin{aligned} V_{d1} + jV_{q1} &= V_1 e^{j\theta_1} e^{-j(\delta_1 - \pi/2)} \\ &= (1.04\angle 0^\circ)(1\angle 86.42^\circ) \\ &= 0.065 + j1.038 \end{aligned}$$

$$V_{d1} = 0.065, V_{q1} = 1.038.$$

Step 4:

$$\begin{aligned} E'_{d1} &= (X_{q1} - X'_{q1})I_{q1} \\ &= (0.0969 - 0.0969)(0.671) \\ &= 0. \end{aligned}$$

It can be verified that this is also equal to $V_{d1} + R_{s1}I_{d1} - X'_{q1}I_{q1}$.

Step 5:

$$\begin{aligned} E'_{q1} &= V_{q1} + R_{s1}I_{q1} + X'_{d1}I_{d1} \\ &= 1.038 + 0 + (0.0608)(0.302) \\ &= 1.056. \end{aligned}$$

Step 6:

$$\begin{aligned} E_{fd1} &= E'_{q1} + (X_{d1} - X'_{d1})I_{d1} \\ &= 1.056 + (0.146 - 0.0608)(0.302) \\ &= 1.082. \end{aligned}$$

Step 7:

$$V_{R1} = (K_{E1} + 0.0039e^{1.555E_{fd1}})E_{fd1} = (1.021)(1.082) = 1.105$$

$$R_{f1} = \frac{K_{F1}}{T_{F1}}E_{fd1} = \left(\frac{0.063}{0.35}\right)1.082 = 0.195$$

$$\begin{aligned} V_{\text{ref1}} &= V_1 + \frac{V_{R1}}{K_{A1}} = 1.04 + \frac{1.105}{20} \\ &= 1.095. \end{aligned}$$

The mechanical input T_{M1} is computed as follows:

$$\begin{aligned} T_{M1} &= E'_{d1}I_{d1} + E'_{q1}I_{q1} + (X'_{q1} - X'_{d1})I_{d1}I_{q1} \\ &= (0)(0.302) + (1.056)(0.671) + (0.0969 - 0.0608)(0.302)(0.671) \\ &= 0.716. \end{aligned}$$

Similarly, for other machines, we can compute the state and the algebraic variables as

$$\begin{aligned} \delta_2(o) &= 61.1^\circ & \delta_3(o) &= 54.2^\circ \\ I_{d2} &= 1.29 & I_{d3} &= 0.562 \\ I_{q2} &= 0.931 & I_{q3} &= 0.619 \\ V_{d2} &= 0.805 & V_{d3} &= 0.779 \\ V_{q2} &= 0.634 & V_{q3} &= 0.666 \\ E'_{d2} &= 0.622 & E'_{d3} &= 0.624 \\ E'_{q2} &= 0.788 & E'_{q3} &= 0.768 \\ E_{fd2} &= 1.789 & E_{fd3} &= 1.403 \\ R_{f2} &= 0.322 & R_{f3} &= 0.252 \\ V_{R2} &= 1.902 & V_{R3} &= 1.453 \\ V_{\text{ref2}} &= 1.12 & V_{\text{ref3}} &= 1.09 \\ T_{M2} &= 1.63 & T_{M3} &= 0.85. \end{aligned}$$

□

7.6.4 Angle Reference, Infinite Bus, and COI Reference

As explained in Section 6.10, by taking one of the angles as a reference, the order of the dynamic system can be reduced from $7m$ to $7m - 1$. Furthermore, if the inertia constant on this reference angle machine is infinity, the order of the system can be reduced to $7m - 2$. This is also possible if the machines have zero or uniform damping. Finally, we can also use center-of-angle formulation instead of relative rotor angle formulation. The center-of-angle formulation is discussed in Chapter 9.

7.7 Numerical Solution: Power-Balance Form

The number of algorithms that have been proposed for the numerical solution of the DAE system of equations is very large. There are basically two approaches used in power system simulation packages.

1. Simultaneous-implicit (SI) method.
2. Partitioned-explicit (PE) method.

The SI is numerically more stable than the PE method. It is also the method used in the EPRI 1208 stability program known as the ETMSP (Extended Transient Midterm Stability Program) program [73]. We illustrate the SI method on the WECC system with a two-axis model for the machine and with the exciter on all the three machines.

7.7.1 SI Method

We illustrate with the differential-algebraic model in power-balance form.

$$\dot{x} = f_o(x, I_{d-q}, \bar{V}, u) \quad (7.131)$$

$$I_{d-q} = h(x, \bar{V}) \quad (7.132)$$

$$0 = g_o(x, I_{d-q}, \bar{V}). \quad (7.133)$$

All the initial conditions at $t = 0$ have been computed. In the SI method, the differential equations in (7.131) are algebraized using either implicit Euler's method or a trapezoidal integration method. These resulting algebraic equations are then solved simultaneously with the remaining algebraic equations (7.132)–(7.133) using Newton's method at each time step.

7.7.2 Review of Newton's Method

Let $f(x) = 0$ be the set of nonlinear algebraic equations, that is,

$$\begin{aligned} f_1(x_1, \dots, x_n) &= 0 \\ f_2(x_1, \dots, x_n) &= 0 \\ &\vdots \\ f_n(x_1, \dots, x_n) &= 0. \end{aligned} \quad (7.134)$$

Assume an initial guess $x_1^{(o)}, \dots, x_n^{(o)}$. Expand the equations in a Taylor series and retain only the linear term.

$$f(x^{(o)}) + \left. \frac{\partial f}{\partial x} \right|_{x=x^{(o)}} (x - x^{(o)}) \approx 0. \quad (7.135)$$

Solving for x results in an improved estimate for x :

$$x^{(1)} = x^{(o)} - \left[\left. \frac{\partial f}{\partial x} \right|_{x=x^{(o)}} \right]^{-1} f(x^{(o)}). \quad (7.136)$$

In general,

$$x^{(k+1)} = x^{(k)} - [J^{(k)}]^{-1} f(x^{(k)}) \quad (7.137)$$

where k is the iteration count and $[J] \stackrel{\Delta}{=} \frac{\partial f}{\partial x}$ is called the Jacobian. In an expanded version:

$$[J] = \begin{bmatrix} \frac{\partial f_1}{\partial x_1} & \dots & \frac{\partial f_1}{\partial x_n} \\ \vdots & & \vdots \\ \frac{\partial f_n}{\partial x_1} & \dots & \frac{\partial f_n}{\partial x_n} \end{bmatrix}. \quad (7.138)$$

Define

$$\Delta x^{(k)} = x^{(k+1)} - x^{(k)}. \quad (7.139)$$

Equation (7.137) can be recast as follows:

$$[J^{(k)}] \Delta x^{(k)} = -f(x^{(k)}), k = 0, 1, 2, \dots \quad (7.140)$$

Equation (7.140) is a linear one and has to be solved for $\Delta x^{(k)}$. Then from (7.139)

$$x^{(k+1)} = x^{(k)} + \Delta x^{(k)}, k = 0, 1, 2, \dots \quad (7.141)$$

With an initial value of $x^{(o)}$, steps corresponding to (7.140) and (7.141) are repeated and at the end of each iteration compute $\max_i |f_i(x^{(k+1)})|$. If this is $< \epsilon$ where ϵ is the specified tolerance, the Newton iterates have converged.

7.7.3 Numerical Solution Using SI Method

Let the subscripts n and $n + 1$ denote the time instants t_n and t_{n+1} , respectively. Then, integrating the differential equations in (7.131) from t_n to t_{n+1} using the trapezoidal rule and solving the resulting algebraic equations with the remaining algebraic equations at t_{n+1} , obtain

$$x_{n+1} = x_n + \int_{t_n}^{t_{n+1}} f_o(x, I_{d-q}, \bar{V}, u) dt \quad (7.142)$$

that is,

$$x_{n+1} = x_n + \frac{\Delta t}{2} [f_o(x_{n+1}, I_{d-q,n+1}, \bar{V}_{n+1}, u_{n+1}) + f_o(x_n, I_{d-q,n}, \bar{V}_n, u_n)] \quad (7.143)$$

$$0 = I_{d-q,n+1} - h(x_{n+1}, \bar{V}_{n+1}) \quad (7.144)$$

$$0 = g_o(x_{n+1}, I_{d-q,n+1}, \bar{V}_{n+1}) \quad (7.145)$$

where $\Delta t = t_{n+1} - t_n$ is the integration time step. Rearranging (7.143)–(7.145),

$$\begin{aligned} & [x_{n+1} - \frac{\Delta t}{2} f_o(x_{n+1}, I_{d-q,n+1}, \bar{V}_{n+1}, u_{n+1})] - [x_n + \frac{\Delta t}{2} f_o(x_n, I_{d-q,n}, \bar{V}_n, u_n)] \\ & \stackrel{\Delta}{=} F_1(x_{n+1}, I_{d-q,n+1}, \bar{V}_{n+1}, u_{n+1}, x_n, I_{d-q,n}, \bar{V}_n, u_n) = 0 \end{aligned} \quad (7.146)$$

$$I_{d-q,n+1} - h(x_{n+1}, \bar{V}_{n+1}) \stackrel{\Delta}{=} F_2(x_{n+1}, I_{d-q,n+1}, \bar{V}_{n+1}) = 0 \quad (7.147)$$

$$g_o(x_{n+1}, I_{d-q,n+1}, \bar{V}_{n+1}) \stackrel{\Delta}{=} F_3(x_{n+1}, I_{d-q,n+1}, \bar{V}_{n+1}) = 0. \quad (7.148)$$

At each time step, (7.146)–(7.148) are solved by Newton's method. The Newton iterates are

$$\begin{matrix} 7m & 2m & 2n & (k) \\ 7m & \left(\begin{array}{ccc} J_1 & J_2 & J_3 \\ J_4 & J_5 & J_6 \\ J_7 & J_8 & J_9 \end{array} \right) & \left[\begin{array}{c} \Delta x_{n+1} \\ \Delta I_{d-q,n+1} \\ \Delta \bar{V}_{n+1} \end{array} \right]^{(k)} & = - \left[\begin{array}{c} F_1 \\ F_2 \\ F_3 \end{array} \right] \end{matrix} \quad (7.149)$$

$$x_{n+1}^{(k+1)} = x_{n+1}^{(k)} + \Delta x_{n+1}^{(k)} \quad (7.150)$$

$$I_{d-q,n+1}^{(k+1)} = I_{d-q,n+1}^{(k)} + \Delta I_{d-q,n+1}^{(k)} \quad (7.151)$$

$$\bar{V}_{n+1}^{(k+1)} = \bar{V}_{n+1}^{(k)} + \Delta \bar{V}_{n+1}^{(k)} \quad (7.152)$$

where k is the iteration number at time step t_{n+1} . $x_{n+1}^{(o)}$ is the converged value x_n at the previous time step. The iterations are continued until the norm of the mismatch vector $[F_1, F_2, F_3]^t$ is close to zero. This completes the computation at time step t_{n+1} .

If there is a change in reference input V_{ref} , or T_{Mi} , the DAE (differential algebraic equation) model can be integrated with known values of all variables. But if there is a disturbance in the network, a different procedure has to be adopted, as explained below.

7.7.4 Disturbance Simulation

The typical disturbance corresponds to a network disturbance, such as a fault where the parameters in the algebraic equations change at $t = 0$. The algebraic variables can change instantaneously, whereas the state variables do not. Hence, at $t = 0+$, with the network disturbance reflected in the network equations, we solve the set of algebraic equations for $I_{d-q}(0+)$, $\bar{V}(0+)$ as

$$I_{d-q}(0+) = h^f(x(0), \bar{V}(0+)) \quad (7.153)$$

$$0 = g_o^f(x(0), I_{d-q}(0+), \bar{V}(0+)) \quad (7.154)$$

where the superscript f indicates that the algebraic equations correspond to the faulted state. With the value of $I_{d-q}(0+)$, $\bar{V}(0+)$ so obtained, the trapezoidal method is then applied. Note that the initial guess for the vector $[x^t I_{d-q}^t \bar{V}^t]^t$ at time instant t_{n+1} is the converged value at the previous time instant, that is,

$$\begin{bmatrix} x_{n+1} \\ I_{d-q,n+1} \\ \bar{V}_{n+1} \end{bmatrix}^{(o)} = \begin{bmatrix} x_n \\ I_{d-q,n} \\ \bar{V}_n \end{bmatrix}, n = 0, 1, 2, \dots \quad (7.155)$$

If there is a change in generation or load, this is simply taken care of by changing P_{Gi} and Q_{Gi} or P_{Li} and Q_{Li} in (7.153) and (7.154), and computing I_{d-q} and \bar{V} at $t = 0+$. If there is a short circuit at bus i , then set $\bar{V}_i \equiv 0$ and delete the P and Q equations at bus i from $g_o(x, I_{d-q}, \bar{V})$ to obtain $g_o^f(x, I_{d-q}, \bar{V})$.

7.7.5 PE Method

1. Incorporate the system disturbance and solve for $\bar{V}(0+)$, $I_{d-q}(0+)$ as in (7.153) and (7.154).
2. Using the values of $I_{d-q}(0+)$, $\bar{V}(0+)$ integrate the differential equations

$$\dot{x} = f_o(x, I_{d-q}, \bar{V}), x(0) = x^o \quad (7.156)$$

to obtain $x(1)$.

3. Go to Step 1 and solve for $I_{d-q}(1)$, $\bar{V}(1)$ again from the algebraic equations.

$$I_{d-q}(1) = h^f(x(1), \bar{V}(1)) \quad (7.157)$$

$$0 = g_o^f(x(1), I_{d-q}(1), \bar{V}(1)) \quad (7.158)$$

4. Integrate the differential equations to obtain $x(2)$, and again solve the algebraic equation to obtain $I_{d-q}(2)$, $\bar{V}(2)$.
5. This procedure is repeated until $t = T_{\text{desired}}$ or there is a change in the configuration. In the second case, a similar procedure is followed.

The PE scheme, although conceptually simple, has numerical convergence problems such as interface errors, and so on [76].

7.8 Numerical Solution: Current-Balance Form

In this section, we explain the industrial approach to implement the SI method forming the structured approach to the problem. It is the basis of the well-known ETMSP program of EPRI [73]. The current-balance approach is favored, since the bus admittance matrix is easily formed and factorized. The DAE model from (7.36), (7.44), and (7.45) is

$$\dot{x} = f_o(x, I_{d-q}, \bar{V}, u) \quad (7.159)$$

$$I_{d-q} = h(x, \bar{V}) \quad (7.160)$$

$$\bar{I}_o(I_{d-q}, x, \bar{V}) = \bar{Y}_N \bar{V}. \quad (7.161)$$

The use of the SI method to solve these equations yields the set of algebraic equations:

$$F_1(x_{n+1}, I_{d-q,n+1}, \bar{V}_{n+1}, u_{n+1}, x_n, I_{d-q,n}, \bar{V}_n, u_n) = 0 \quad (7.162)$$

$$F_2(x_{n+1}, I_{d-q,n+1}, \bar{V}_{n+1}) = 0 \quad (7.163)$$

$$\bar{I}_o(I_{d-q,n+1}, x_{n+1}, \bar{V}_{n+1}) = \bar{Y}_N \bar{V}_{n+1}. \quad (7.164)$$

Instead of treating x and I_{d-q} as separate vectors, we form a new vector $X = [X_1^t \dots X_m^t]^t$. Associate $I_{d-q,i}$ with the respective x_i so that $X_i = [x_i^t I_{d-q,i}^t]^t$. Equations (7.162) and (7.163) are replaced by

$$F_M(X_{n+1}, V_{n+1}^e, u_{n+1}, X_n, V_n^e, u_n) = 0.$$

Also, we replace (7.164) by its rectangular equivalent $I^e(X_{n+1}, V_{n+1}^e) = Y_N^e V_{n+1}^e$, where e stands for expanded form, that is,

$$\begin{aligned} I^e &= [I_{D1} I_{Q1} \dots I_{Dn} I_{Qn}]^t \\ V^e &= [V_{D1} V_{Q1} \dots V_{Dn} V_{Qn}]^t \end{aligned}$$

and Y_N^e consists of 2×2 square matrices with real numbers. With this, the application of Newton's method yields the following equations.

$$\left[\begin{array}{cc|c} A_{GG1} & & B_{GV1} \\ \ddots & & \vdots \\ \hline C_{VG1} & \dots & C_{VGm} \end{array} \right] \left[\begin{array}{c} \Delta X_1 \\ \vdots \\ \frac{\Delta X_m}{\Delta V_1^e} \\ \vdots \\ \Delta V_n^e \end{array} \right] = \left[\begin{array}{c} R_{G1} \\ \vdots \\ \frac{R_{Gm}}{R_{V1}^e} \\ \vdots \\ R_{Vn}^e \end{array} \right]. \quad (7.165)$$

The various elements of the Jacobian are defined as

$$\begin{aligned} A_{GGi} &\stackrel{\Delta}{=} \frac{\partial F_M}{\partial X_{n+1,i}}, B_{GVi} &\stackrel{\Delta}{=} \frac{\partial F_M}{\partial V_{n+1,i}^e} \\ C_{VGi} &\stackrel{\Delta}{=} -\frac{\partial I^e}{\partial X_{n+1,i}} \quad i = 1, 2, \dots, m \end{aligned}$$

and

$$Y_L^e = -\frac{\partial I^e}{\partial V_{n+1}^e}.$$

For ease of understanding, V_i^e can be considered as a vector $(V_{Di}, V_{Qi})^t$, and $I_i^e = (I_{Di}, I_{Qi})^t$. Y_N^e becomes a $2n \times 2n$ matrix of real elements. The right-hand sides of (7.165) are the residuals. In Newton's method for solving $f(x) = 0$, the residuals at any iteration k are $-f(x^{(k)})$. Y_L^e is computed as follows (the suffix $n + 1$ is dropped for ease of notation):

$$Y_L^e \stackrel{\Delta}{=} -\left[\frac{\partial I^e}{\partial V^e} \right] \quad (7.166)$$

Y_L^e consists of 2×2 blocks of the type

$$-\begin{bmatrix} \frac{\partial I_{Di}}{\partial V_{Di}} & \frac{\partial I_{Di}}{\partial V_{Qi}} \\ \frac{\partial I_{Qi}}{\partial V_{Di}} & \frac{\partial I_{Qi}}{\partial V_{Qi}} \end{bmatrix}. \quad (7.167)$$

The solution method to solve the linear equation (7.165) is as follows. We recognize that the nonzero columns in B_{GVi} correspond to ΔV_i^e , and that those in C_{GVi} correspond to ΔX_i . Thus, from (7.165)

$$\Delta X_i = A_{GGi}^{-1}(R_{Gi} - B_{GVi}\Delta V^e) \quad i = 1, \dots, m. \quad (7.168)$$

From (7.165),

$$[Y_N^e + Y_L^e] \Delta V^e + \sum_{i=1}^m (C_{VGi} \Delta X_i) = [R_V^e]. \quad (7.169)$$

Substituting ΔX_i from (7.168),

$$\left[Y^e + Y_L^e - \sum_{i=1}^m (C_{VGi} A_{GGi}^{-1} B_{GVi}) \right] [\Delta V^e] = [R_V^{e'}] \quad (7.170)$$

where $R_V^{e'} = R_V^e - \sum_{i=1}^m C_{VGi} A_{GGi}^{-1} R_{Gi}$.

Thus, the algorithm first solves for ΔV^e in (7.170) and then solves (7.169) iteratively to convergence for $\Delta X_i (i = 1, \dots, m)$. The same computations are then repeated at the next time instant and so on.

7.8.1 Some Practical Details [73]

The Jacobian in (7.165) is expensive to compute at each iteration. Let $J_{n+1}^{(k)}$ be the Jacobian evaluated at $t = t_{n+1}$ and k represent the iteration count at that time instant. Solving (7.169) and (7.170) results in

$$\begin{bmatrix} X^{(k+1)} \\ V^{e(k+1)} \end{bmatrix} = \begin{bmatrix} X^{(k)} \\ V^{e(k)} \end{bmatrix} + \begin{bmatrix} \Delta X^{(k)} \\ \Delta V^{e(k)} \end{bmatrix} \quad k = 0, 1, 2, \dots \quad (7.171)$$

The very dishonest Newton method (VDHN) holds the Jacobian in (7.165) fixed for a period of time. Thus

$$\left[J_{n+1}^{(o)} \right] \begin{bmatrix} \Delta X^{(k)} \\ \Delta V^{e(k)} \end{bmatrix} = \begin{bmatrix} R_\ell^{(k)} \end{bmatrix} \quad (7.172)$$

where the time instant $\ell \geq n + 1$.

This means that the initial Jacobian at $t = t_{n+1}$ is held constant for some time steps after t_{n+1} . This reduces the overall cost of computation. The choice of when to reevaluate the Jacobian is based on experience. The Jacobian must be reevaluated at any major system change. Between time steps, it is reevaluated if the previous time-step iteration was considered too slow (took three or more iterations). Within a time step, a maximum of five iterations are taken using the same Jacobian.

7.8.2 Prediction [73]

Whenever a Jacobian is evaluated at the beginning of a time step, instead of taking the converged values of the previous time step, we can use a linear prediction for generator variables and geometric prediction for network voltages. Thus, at time instant t_{n+1} , the initial estimate in the evaluation of the Jacobian would be

$$X_{n+1}^{(o)} = X_n + (X_n - X_{n-1}) \quad (7.173)$$

where X_n, X_{n-1} are the previous converged values at the previous time steps.

For the network variables, each voltage initial guess is

$$V_{n+1}^{(o)} = \frac{(V_n)^2}{V_{n-1}}. \quad (7.174)$$

7.9 Reduced-Order Multimachine Models

While many types of reduced-order multimachine models are possible, we discuss three specific ones.

1. Flux-decay model with a fast exciter. The network structure is preserved.
2. Structure-preserving model with a classical machine model.
3. Classical model with network nodes eliminated.

7.9.1 Flux-Decay Model

This model is widely used in eigenvalue analysis and power-system stabilizer design. If the damper-winding constants are very small, then we can set them to zero (i.e., there is an integral manifold for these states, as discussed in Section 6.5), and we obtain from (7.2):

$$0 = -E'_{di} + (X_{qi} - X'_{qi})I_{qi} \quad i = 1, \dots, m. \quad (7.175)$$

We eliminate E'_{di} from (7.4) and (7.8) using (7.175). The synchronous machine dynamic circuit is modified as shown in Figure 7.12. It is also common, while using the flux-decay model, to have a simplified exciter with one gain and one time constant, as shown in Figure 7.13. The complete set of differential-algebraic equations (7.1)–(7.10) becomes (assuming no governor and no damping).

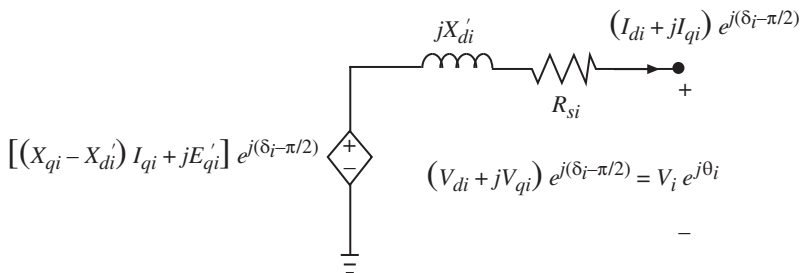


Figure 7.12 Synchronous machine flux-decay model dynamic circuit.

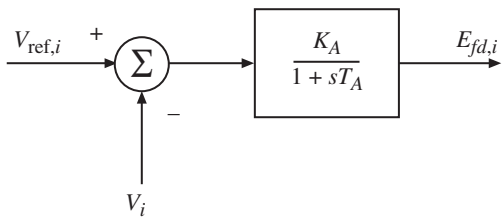


Figure 7.13 Static exciter (one gain–one time constant).

7.9.2 Generator Equations

$$T'_{dot} \frac{dE'_{qi}}{dt} = -E'_{qi} - (X_{di} - X'_{di})I_{di} + E_{fdi} \quad i = 1, \dots, m \quad (7.176)$$

$$\frac{d\delta_i}{dt} = \omega_i - \omega_s \quad i = 1, \dots, m \quad (7.177)$$

$$\frac{2H_i}{\omega_s} \frac{d\omega_i}{dt} = T_{Mi} - E'_{qi}I_{qi} - (X_{qi} - X'_{di})I_{di}I_{qi} \quad i = 1, \dots, m \quad (7.178)$$

$$T_{Ai} \frac{dE_{fdi}}{dt} = -E_{fdi} + K_{Ai}(V_{refi} - V_i) \quad i = 1, \dots, m. \quad (7.179)$$

7.9.3 Stator Equations

Assuming $R_{si} = 0$, and substituting for E'_{di} from (7.175), we obtain the stator equations (7.13) and (7.14) in polar form as

$$V_i \sin(\delta_i - \theta_i) - X_{qi}I_{qi} = 0 \quad i = 1, \dots, m \quad (7.180)$$

$$V_i \cos(\delta_i - \theta_i) + X'_{di}I_{di} - E'_{qi} = 0 \quad i = 1, \dots, m. \quad (7.181)$$

7.9.4 Network Equations

The network equations can be written in the power-balance form as in Section 7.3.1, or in the current-balance form as in Section 7.3.2.

7.9.5 Initial Conditions

The steps to compute the initial conditions of the multimachine flux-decay model DAE system are given below.

Step 1 From the load flow, compute $I_{Gi}e^{j\gamma_i}$ as in (7.113) as $(P_{Gi} - jQ_{Gi})/V_i e^{-j\theta_i}$.

Step 2 Compute δ_i as angle of $[V_i e^{j\theta_i} + jX_{qi} I_{Gi} e^{j\gamma_i}]$.

Step 3 Compute $\omega_i = \omega_s$ from (7.177).

Step 4 Compute I_{di}, I_{qi} from $(I_{di} + jI_{qi}) = I_{Gi} e^{j(\gamma_i - \delta_i + \pi/2)}$.

Step 5 Compute E'_{qi} from (7.181) as $E'_{qi} = V_i \cos(\delta_i - \theta_i) + X'_{di}I_{di}$.

Step 6 Compute E_{fdi} from (7.176) as $E_{fdi} = E'_{qi} + (X_{di} - X'_{di})I_{di}$.

Step 7 Compute V_{refi} from (7.179) as $V_{refi} = \frac{E_{fdi}}{K_{Ai}} + V_i$.

Step 8 Compute T_{Mi} from (7.178) as $T_{Mi} = E'_{qi}I_{qi} + (X_{qi} - X'_{di})I_{di}I_{qi}$.

7.9.6 Structure-Preserving Classical Model

To obtain the classical model, we set $T'_{doi} = \infty$ and $X_{qi} = X'_{di}$ in (7.176) and (7.178), respectively. This results in E'_{qi} being a constant equal to the initial value E'_{qi}^0 . Ignoring (7.176) and (7.179), the resulting differential equations are

$$\frac{d\delta_i}{dt} = \omega_i - \omega_s \quad i = 1, \dots, m \quad (7.182)$$

$$\frac{2H_i}{\omega_s} \frac{d\omega_i}{dt} = T_{Mi} - E'_{qi}^0 I_{qi} \quad i = 1, \dots, m. \quad (7.183)$$

These are known as the swing equations in the literature. The stator algebraic equations (7.180) and (7.181) are added after multiplying the former by $-j$. We replace X_{qi} by X'_{di} and E'_{qi} by E'_{qi}^0 . Thus

$$\begin{aligned} E'_{qi}^0 &= X'_{di}(I_{di} + jI_{qi}) + V_i(\cos(\delta_i - \theta_i) - j \sin(\delta_i - \theta_i)) \\ &= X'_{di}(I_{di} + jI_{qi}) + V_i e^{-j(\delta_i - \theta_i)}. \end{aligned} \quad (7.184)$$

Equation (7.184) can be rearranged as

$$\begin{aligned} E'_{qi}^0 e^{j\delta_i} &= jX'_{di}(I_{di} + jI_{qi}) e^{j(\delta_i - \pi/2)} + V_i e^{j\theta_i} \\ &= jX'_{di}(I_{Di} + jI_{Qi}) + V_i e^{j\theta_i}. \end{aligned} \quad (7.185)$$

This represents a voltage $\bar{E}_i = E'_{qi}^0 e^{j\delta_i}$ of constant magnitude behind a transient reactance X'_{di} as shown in Figure 7.14. Henceforth, we will denote $E'_{qi}^0 i = E_i$. This forms the basis of the structure-preserving model, which, is discussed next.

7.9.6.1 Structure-Preserving Model with Constant Voltage Behind Reactance

This model is widely used in structure-preserving transient energy function and voltage collapse literature that uses energy functions. It consists of the swing equations (7.182) and (7.183) and the network algebraic equations at the nodes $1, \dots, n$. In Figure 7.15, the n bus transmission network is shown augmented by the constant voltage behind reactances at the generator buses $1, \dots, m$. The generator internal nodes are denoted as

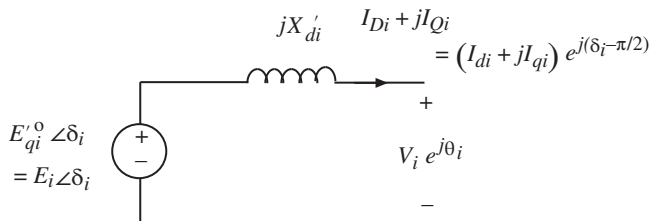


Figure 7.14 Constant voltage behind transient reactance.

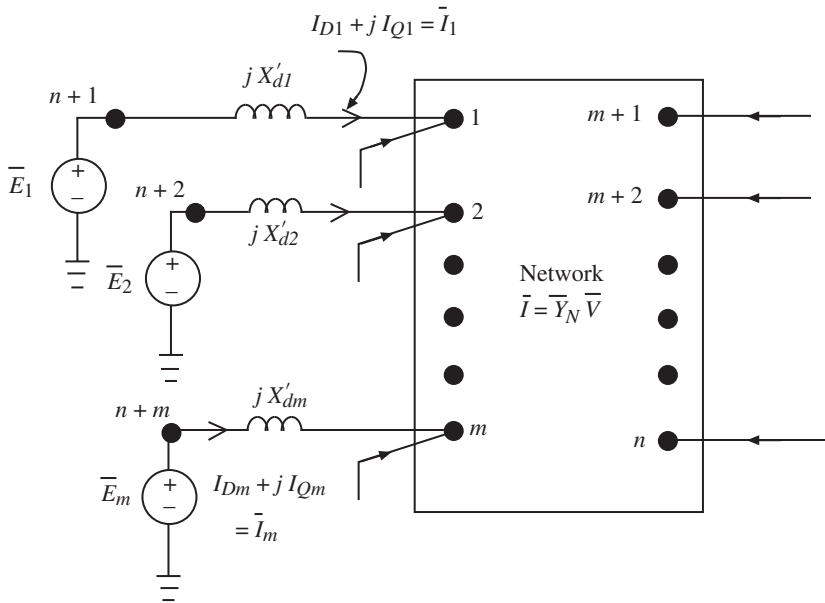


Figure 7.15 Structure-preserving model with constant voltage behind reactance.

$n+1, \dots, n+m$. The complex power output at the i^{th} internal node in Figure 7.15 can be expressed as

$$\begin{aligned}
 \bar{E}_i \bar{I}_i^* &= E_i e^{j\delta_i} ((\bar{E}_i - \bar{V}_i) / jX'_{di})^* \\
 &= E_i e^{j\delta_i} (E_i e^{-j\delta_i} - V_i e^{-j\theta_i}) / (-jX'_{di}) \\
 &= j \frac{E_i^2}{X'_{di}} - j \frac{E_i V_i}{X'_{di}} ((\cos(\delta_i - \theta_i) + j \sin(\delta_i - \theta_i)) \\
 &= \frac{E_i V_i \sin(\delta_i - \theta_i)}{X'_{di}} + j \left(\frac{E_i^2}{X'_{di}} - \frac{E_i V_i \cos(\delta_i - \theta_i)}{X'_{di}} \right).
 \end{aligned} \tag{7.186}$$

Alternatively,

$$\begin{aligned}
 \bar{E}_i \bar{I}_i^* &= E_i e^{j\delta_i} (I_{di} - jI_{qi}) e^{-j(\delta_i - \pi/2)} \\
 &= E_i I_{qi} + j E_i I_{di}.
 \end{aligned} \tag{7.187}$$

Comparing (7.186) and (7.187), the real and reactive power output at the generator internal nodes are given, respectively, by

$$\text{Real power } E_i I_{qi} = \frac{E_i V_i \sin(\delta_i - \theta_i)}{X'_{di}} \tag{7.188}$$

$$\text{Reactive power } E_i I_{di} = \frac{E_i^2}{X'_{di}} - \frac{E_i V_i}{X'_{di}} \cos(\delta_i - \theta_i). \tag{7.189}$$

This shows that real power P is associated with I_q and reactive power is associated with I_d . At the generator buses $1, \dots, m$, we can express the complex power due to the generators as

$$\begin{aligned}
P_{Gi} + jQ_{Gi} &= \bar{V}_i \bar{I}_i^* \\
\bar{V}_i \bar{I}_i^* &= V_i e^{j\theta_i} \left[(\bar{E}_i - \bar{V}_i) / jX'_{di} \right]^* \\
&= V_i e^{j\theta_i} (E_i e^{-j\delta_i} - V_i e^{-j\theta_i}) / (-jX'_{di}) \\
&= E_i V_i (\cos(\theta_i - \delta_i) + j \sin(\theta_i - \delta_i)) \frac{j}{X'_{di}} - \frac{jV_i^2}{X'_{di}} \\
&= -\frac{E_i V_i \sin(\theta_i - \delta_i)}{X'_{di}} + j \left(\frac{-V_i^2}{X'_{di}} + \frac{E_i V_i \cos(\theta_i - \delta_i)}{X'_{di}} \right). \tag{7.190}
\end{aligned}$$

Therefore

$$P_{Gi} = \frac{-E_i V_i \sin(\theta_i - \delta_i)}{X'_{di}} = \frac{E_i V_i \sin(\delta_i - \theta_i)}{X'_{di}} \tag{7.191}$$

$$Q_{Gi} = \frac{-V_i^2}{X'_{di}} + \frac{E_i V_i \cos(\theta_i - \delta_i)}{X'_{di}}. \tag{7.192}$$

The structure-preserving model consists of the swing and the network equations (neglecting resistance) as

$$\dot{\delta}_i = \omega_i - \omega_s \quad i = 1, \dots, m \tag{7.193}$$

$$\frac{2H_i}{\omega_s} \dot{\omega}_i = T_{Mi} - \frac{E_i V_i \sin(\delta_i - \theta_i)}{X'_{di}} \quad i = 1, \dots, m \tag{7.194}$$

$$P_{Li}(V_i) + P_{Gi} = \sum_{j=1}^n V_i V_j B_{ij} \sin(\theta_i - \theta_j) \quad i = 1, \dots, n \tag{7.195}$$

$$Q_{Li}(V_i) + Q_{Gi} = - \sum_{j=1}^n V_i V_j B_{ij} \cos(\theta_i - \theta_j) \quad i = 1, \dots, n \tag{7.196}$$

where P_{Gi} and Q_{Gi} for $i = 1, \dots, m$ are given by (7.191) and (7.192), and $P_{Gi} = Q_{Gi} = 0$ for $i = m+1, \dots, n$. The right-hand sides of (7.195) and (7.196) are the sums of real and reactive power on the lines emanating from bus i under the assumption of negligible transmission line resistance. This is shown as follows. If we neglect transmission line resistances, then the network admittance matrix is $\bar{Y}_N = [jB_{ij}]$, and the total complex power in the network transmission lines from bus i is given by

$$\bar{V}_i \left(\sum_{j=1}^n jB_{ij} \bar{V}_j \right)^*. \tag{7.197}$$

Expanding the expression (7.197) results in

$$\begin{aligned} V_i e^{j\theta_i} \sum_{j=1}^n -jB_{ij} V_j e^{-j\theta_j} &= \sum_{j=1}^n -jV_i V_j B_{ij} (\cos(\theta_i - \theta_j) + j \sin(\theta_i - \theta_j)) \\ &= \sum_{j=1}^n V_i V_j B_{ij} \sin(\theta_i - \theta_j) - j \sum_{j=1}^n V_i V_j B_{ij} \cos(\theta_i - \theta_j). \end{aligned} \quad (7.198)$$

The real and imaginary parts of (7.198) are the right-hand sides of (7.195) and (7.196), respectively. The model given by (7.191)–(7.196) is called the *structure-preserving classical model*.

An interesting observation from (7.189) and (7.192) regarding reactive power is the following. The reactive power absorbed by X'_{di} is obtained by subtracting Q_{Gi} from $E_i I_{di}$, resulting in

$$E_i I_{di} - Q_{Gi} = (E_i^2 - 2E_i V_i \cos(\delta_i - \theta_i) + V_i^2) / X'_{di}. \quad (7.199)$$

An alternative form of the structure-preserving model is to consider the augmented Y matrix obtained by including the admittance corresponding to the transient reactances of the machines. Thus, with proper ordering,

$$\bar{Y}_{\text{aug}} = \begin{array}{c} \begin{matrix} & n+1 \dots n+m & & 1 \dots m & & m+1 \dots n \\ \begin{matrix} n+1 \\ \vdots \\ n+m \end{matrix} & \left| \begin{matrix} \bar{y} & & & -\bar{y} & & 0 \\ \hline \cdots & \cdots & \cdots & \cdots & \cdots & \cdots \end{matrix} \right| \end{matrix} \\ \begin{matrix} 1 \\ \vdots \\ m \end{matrix} & \left| \begin{matrix} -\bar{y} & & \\ \hline \cdots & \cdots & \end{matrix} \right| \\ \begin{matrix} m+1 \\ \vdots \\ n \end{matrix} & \left| \begin{matrix} 0 & & \\ \hline \end{matrix} \right| \end{array} \quad (7.200)$$

where

$$\bar{y} = \text{Diag} \left(\frac{1}{jX'_{di}} \right) \quad i = 1, \dots, m$$

and

$$\bar{Y}_{N1} = \bar{Y}_N + \begin{bmatrix} \bar{y} & 0 \\ 0 & 0 \end{bmatrix}.$$

Considering $\bar{Y}_{\text{aug}} = [jB_{ij}]$, (7.193)–(7.196) can be written more compactly as (denoting, temporarily, δ_i 's as θ_i 's and E_i 's as V_i 's)

$$\dot{\theta}_i = \omega_i - \omega_s \quad i = n+1, \dots, n+m \quad (7.201)$$

$$\frac{2H_i}{\omega_s} \dot{\omega}_i = T_{Mi} - \sum_{j=1}^{n+m} V_i V_j B_{ij} \sin(\theta_i - \theta_j) \quad i = n+1, \dots, n+m \quad (7.202)$$

$$P_{Li}(V_i) = \sum_{j=1}^{n+m} V_i V_j B_{ij} \sin(\theta_i - \theta_j) i = 1, \dots, n \quad (7.203)$$

$$Q_{Li}(V_i) = - \sum_{j=1}^{n+m} V_i V_j B_{ij} \cos(\theta_i - \theta_j) i = 1, \dots, n. \quad (7.204)$$

It can be verified that, in (7.202), the second term on the right-hand side is only $E_i V_i \sin(\delta_i - \theta_i) / X'_{di}$. It is easy to verify the equivalence of (7.203) and (7.204) with (7.195) and (7.196), respectively. Note that, in this model, we are allowed to have nonlinear load representation. This model is used in voltage stability studies by means of the energy function method [124].

7.9.7 Internal-Node Model

This is a widely used model in first-swing transient stability analysis. In this model, the loads are assumed to be constant impedances and converted to admittances as

$$\bar{y}_{Li} = \frac{-(P_{Li} - jQ_{Li})}{V_i^2} \quad i = 1, \dots, n. \quad (7.205)$$

There is a negative sign for \bar{y}_{Li} , since loads are assumed as injected quantities. Adding these to the diagonal elements of the \bar{Y}_{N1} matrix in (7.200) makes it $\bar{Y}_{N2} = \bar{Y}_{N1} + \text{Diag}(\bar{y}_{Li})$. The modified augmented Y matrix becomes

$$Y_{\text{aug}}^{\text{new}} = \begin{matrix} & \begin{matrix} n+1 \dots n+m & | & 1 \dots m & | & m+1 \dots n \end{matrix} \\ \begin{matrix} n+1 \\ \vdots \\ n+m \end{matrix} & \left(\begin{array}{ccccc} \bar{y} & | & -\bar{y} & | & 0 \\ \hline --- & --- & --- & --- & --- \\ -\bar{y} & | & & & \\ \hline --- & & & & \bar{Y}_{N2} \\ 0 & | & & & \end{array} \right) \\ \begin{matrix} 1 \\ \vdots \\ m \end{matrix} & \\ \begin{matrix} m+1 \\ \vdots \\ n \end{matrix} & \end{matrix}. \quad (7.206)$$

The passive portion of the network is shown in Figure 7.16.

The network equations for the new augmented network can be rewritten as

$$\frac{m}{n} \begin{bmatrix} \bar{I}_A \\ 0 \end{bmatrix} = \frac{m}{n} \begin{pmatrix} \bar{Y}_A & \bar{Y}_B \\ \bar{Y}_C & \bar{Y}_D \end{pmatrix} \begin{bmatrix} \bar{E}_A \\ \bar{V}_B \end{bmatrix} \quad (7.207)$$

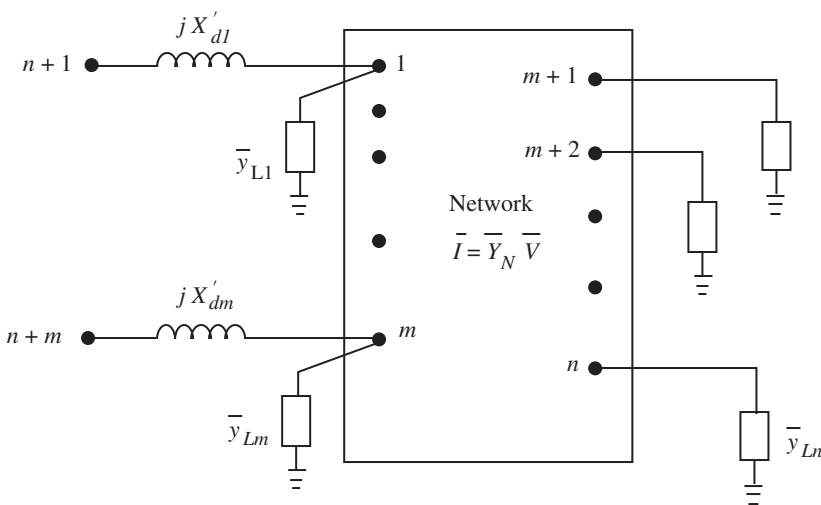


Figure 7.16 Augmented Y matrix with constant impedance.

where $\bar{Y}_A = \bar{y}$, $\bar{Y}_B = [-\bar{y} \mid 0]$, $\bar{Y}_C = [\frac{-\bar{y}}{0}]$, and $\bar{Y}_D = \bar{Y}_{N2}$. The n network buses can be eliminated, since there is no current injection at these buses. Thus

$$\begin{aligned}\bar{I}_A &= \left(\bar{Y}_A - \bar{Y}_B \bar{Y}_D^{-1} \bar{Y}_C \right) \bar{E}_A \\ &= \bar{Y}_{\text{int}} \bar{E}_A\end{aligned}\quad (7.208)$$

where the elements of \bar{I}_A and \bar{E}_A are, respectively, $\bar{I}_i = (I_{di} + jI_{qi})e^{j(\delta_i - \pi/2)} = I_{Di} + jI_{Qi}$ and $\bar{E}_i = E_i \angle \delta_i$. The elements of \bar{Y}_{int} are $\bar{Y}_{ij} = G_{ij} + jB_{ij}$. Since the network buses have been eliminated, we may renumber the internal nodes as $1, \dots, m$ for ease of notation

$$\bar{I}_i = \sum_{j=1}^m \bar{Y}_{ij} \bar{E}_j \quad i = 1, \dots, m. \quad (7.209)$$

Real electrical power out of the internal node i in Figure 7.16 is given by

$$\begin{aligned}P_{ei} &= \text{Re}[\bar{E}_i \bar{I}_i^*] \\ &= \text{Re} \left[E_i e^{j\delta_i} \sum_{j=1}^m \bar{Y}_{ij}^* \bar{E}_j^* \right] \\ &= \text{Re} \left[E_i e^{j\delta_i} \sum_{j=1}^m (G_{ij} - jB_{ij}) E_j e^{-j\delta_j} \right] \\ &= \text{Re} \left[\sum_{j=1}^m (G_{ij} - jB_{ij}) E_i E_j [\cos(\delta_i - \delta_j) + j \sin(\delta_i - \delta_j)] \right].\end{aligned}\quad (7.210)$$

Define

$$\delta_i - \delta_j \stackrel{\Delta}{=} \delta_{ij}. \quad (7.211)$$

Then

$$\begin{aligned} P_{ei} &= \sum_{j=1}^m E_i E_j (G_{ij} \cos \delta_{ij} + B_{ij} \sin \delta_{ij}) \\ &= E_i^2 G_{ii} + \sum_{\substack{j=1 \\ \neq i}}^m (C_{ij} \sin \delta_{ij} + D_{ij} \cos \delta_{ij}) \end{aligned} \quad (7.212)$$

where

$$C_{ij} = E_i E_j B_{ij} \quad (7.213)$$

$$D_{ij} = E_i E_j G_{ij}. \quad (7.214)$$

Thus, the classical model is

$$\frac{d\delta_i}{dt} = \omega_i - \omega_s \quad (7.215)$$

$$\frac{2H_i}{\omega_s} \frac{d\omega_i}{dt} = T_{Mi} - P_{ei} \quad i = 1, \dots, m \quad (7.216)$$

where P_{ei} is given by (7.212). Since P_{ei} is a function of the δ_i 's, (7.215)–(7.216) can be integrated by any numerical algorithm.

7.10 Initial Conditions

Step 1 From the load flow, compute $\bar{I}_i = I_{Di} + jI_{Qi}$ as $(P_{Gi} - jQ_{Gi})/V_i e^{-j\theta_i}$.

Step 2 Using (7.185), compute $E_i \angle \delta_i$ as $E_i \angle \delta_i = V_i e^{j\theta_i} + jX'_{di}(I_{Di} + jI_{Qi})$.

Step 3 From (7.193) or (7.215), $\omega_i = \omega_s$.

Thus, computation of initial conditions is simple when a classical model is used.

Example 7.6 Compute $E_i \angle \delta_i$ ($i = 1, 2, 3$) and \bar{Y}_{int} for Example 7.1 using the classical model (all in pu).

We first compute \bar{I}_i ($i = 1, 2, 3$)

$$\bar{I}_1 = \frac{0.716 - j0.27}{1.04 \angle 0^\circ} = 0.7358 \angle -20.66^\circ$$

$$\bar{I}_2 = \frac{1.63 - j0.067}{1.025 \angle -9.3^\circ} = 1.5916 \angle 6.947^\circ$$

$$\bar{I}_3 = \frac{0.85 + j0.109}{1.02 \angle -4.7^\circ} = 0.8361 \angle 12.0^\circ$$

$$E_1 \angle \delta_1 = 1.04 \angle 0^\circ + j0.068 \bar{I}_1 = 1.054 \angle 2.267^\circ$$

$$E_2 \angle \delta_2 = 1.025 \angle 9.3^\circ + j0.1198 \bar{I}_2 = 1.050 \angle 19.75^\circ$$

$$E_3 \angle \delta_3 = 1.02 \angle 4.7^\circ + j0.1813 \bar{I}_3 = 1.017 \angle 13.2^\circ$$

$$Y_{\text{aug}}^{\text{new}} = \begin{bmatrix} & 10, 11, 12 & & 1, 2, 3 & & 4 \dots 9 \\ 10 & \bar{y} & | & -\bar{y} & | & 0 \\ 11 & & | & & | & \\ 12 & & | & & | & \\ \hline 1 & -\bar{y} & | & & & \\ 2 & & | & & & \\ 3 & & | & & \bar{Y}_{N2} & \\ \hline 4 & 0 & | & & & \\ \vdots & & | & & & \\ 9 & & | & & & \end{bmatrix}$$

where

$$\bar{y} = \begin{bmatrix} -j16.45 & 0 & 0 \\ 0 & -j8.35 & 0 \\ 0 & 0 & -j5.52 \end{bmatrix}$$

$$\text{and } \bar{Y}_{N2} = \bar{Y}_N + \begin{bmatrix} \bar{y} & 0 \\ 0 & 0 \end{bmatrix} + \text{Diag}(\bar{y}_{Li}).$$

\bar{Y}_{int} is obtained by eliminating nodes 1 ... 9 as in (7.208), and is given by

$$\bar{Y}_{\text{int}} = \begin{bmatrix} 0.845 - j2.988 & 0.287 + j1.513 & 0.210 + j1.226 \\ 0.287 + j1.513 & 0.420 - j2.724 & 0.213 + j1.088 \\ 0.210 + j1.226 & 0.213 + j1.088 & 0.277 - j2.368 \end{bmatrix}.$$

□

7.11 Conclusion

This chapter has discussed the formulation of a multimachine system model with the two-axis model, as well as the reduced-order flux-decay model and the classical model. The computation of initial conditions and solution methodology for the two-axis model using the simultaneous-implicit method has been discussed. The methodology of the ETMSP program of EPRI has also been discussed. The reduced-order flux-decay model and the classical model, as well as the computation of initial conditions, are discussed. We also discussed the structure-preserving classical model.

7.12 Problems

- 7.1** Perform a load flow for the 3-machine system of Example 7.1 by varying the load at bus 5 in increments of 0.5 until $P_L = 4.5$ pu. Plot the voltage magnitude at bus 5 as a function of the load. This is called a *PV* curve.

- 7.2** In Problem 7.1, the increased load at each increment is allocated to slack bus 1. In practice, the AGC system allocates it through the area control error, etc. As an alternative, consider allocating the increased load in proportion to the inertias of the machine, that is, ΔP_{L5} is allocated to buses 2 and 3 as $P_{G2}^{k+1} = P_{G2}^k + \frac{H_2}{H_T} \Delta P_{L5}$ and $P_{G3}^{k+1} = P_{G3}^k + \frac{H_3}{H_T} \Delta P_{L5}$, where P_{G2}^k and P_{G3}^k are the generator powers before the load is increased and $H_T = H_1 + H_2 + H_3$. Again draw the PV curve.
- 7.3** Repeat Problems 7.1 and 7.2 for a contingency of lines 5 to 7 being outaged. Draw the PV curves for the pre-contingency state and the contingent case on the same graph.
- 7.4** This problem and Problem 7.5 can be done using symbolic software. As explained at the end of Example 7.1, I_{di}, I_{qi} can be eliminated from (7.47) as well as (7.54) and (7.55) using (7.53). Express the resulting equations in the form

$$\begin{aligned}\dot{x} &= f_1(x, \bar{V}, u) \\ 0 &= g_1(x, \bar{V}).\end{aligned}$$

This is the DAE model with the algebraic equations in the power-balance form ((7.39) and (7.40)).

- 7.5** Using (7.53), substitute for $I_{di}, I_{qi}(i = 1, 2, 3)$ in (7.57) to express the DAE in the form

$$\begin{aligned}\dot{x} &= f(x, \bar{V}, u) \\ \bar{I}_1(x, \bar{V}) &= \bar{Y}_N \bar{V}.\end{aligned}$$

- 7.6** Derive $\bar{I}_1(x, \bar{V}) = \bar{Y}_N \bar{V}$ directly in Problem 7.5 from $0 = g_1(x, \bar{V})$ computed in Problem 7.4. (Hint: See Section 7.3.2.)

- 7.7** Express Example 7.1 in the form

$$\begin{aligned}\dot{x} &= A(x) + BW + Cu \\ W &= G(E, \bar{V}) \\ 0 &= g_1(x, \bar{V})\end{aligned}$$

and Example 7.2 in the form

$$\begin{aligned}\dot{x} &= A(x) + BW + Cu \\ W &= G(E, \bar{V}) \\ \bar{I}_1(x, \bar{V}) &= \bar{Y}_N \bar{V}.\end{aligned}$$

- 7.8** In Example 7.1, loads (both real and reactive) at buses 5 and 6 are increased by 50 percent. With the new load flow compute the initial conditions for the variables, $I_{di}, I_{qi}, V_{di}, V_{qi}, V_{\text{refi}}$ and $T_{Mi}(i = 1, 2, 3)$.

- 7.9** Under nominal loading conditions of Example 7.1, there is a three-phase ground fault at bus 5 that is self-clearing in six cycles. Do the dynamic simulation using the SI method or any available commercial software for 0–2 sec. Use the two-axis model and the IEEE-Type 1 exciter data in Example 7.1. You may use the model obtained in Problems 7.4, 7.5, or 7.7.
- 7.10** Repeat Problem 7.8 for the flux-decay model and a fast exciter with $K_A = 25$ and $T_A = 0.2$ sec. Do the simulation as in Problem 7.9.
- 7.11** In Problems 7.9 and 7.10, find the gain K_A at which the system will become unstable. (Instability occurs when relative rotor angles diverge.)
- 7.12** In Problems 7.9 and 7.10, find by repetitive simulation the value t_{cr} , the critical-clearing time at which the system becomes unstable.
- 7.13** Repeat Problems 7.9 and 7.10 for the fault at bus 5 followed by clearing of lines 5 to 7. Assume $t_{cl} =$ six cycles. Also find the critical-clearing time t_{cr} .
- 7.14** For Example 7.1, write the structure-preserving model in the form of (7.201)–(7.204).
- 7.15** Obtain \bar{Y}_{int} for the system in Example 7.1 for both the faulted state and post-fault states for (a) self-clearing fault at bus 5 and (b) fault at bus 5 followed by switching of the lines 5 to 7. Write the equations in the form (7.215)–(7.216).
- 7.16** Find t_{cr} in Problem 7.15 for both cases by repetitive simulation, and compare the results with Problems 7.12 and 7.13, respectively.

8

Small-Signal Stability

8.1 Background

In this chapter, we consider linearized analysis of multimachine power systems that is necessary for the study of both steady-state and voltage stability. In many cases, instability and eventual loss of synchronism are initiated by some spurious disturbance in the system resulting in oscillatory behavior that, if not damped, may eventually build up. This is very much a function of the operating condition of the power system. Oscillations, even if undamped at low frequencies, are undesirable because they limit power transfers on transmission lines and, in some cases, induce stress in the mechanical shaft. The source of inter-area oscillations is difficult to diagnose. Extensive research has been done in both of these areas. In recent years, there has been considerable interest in dynamic voltage collapse. As regional transfers vary over a wide range due to restructuring and open transmission access, certain parts of the system may face increased loading conditions. Earlier, this phenomenon was analyzed purely on the basis of static considerations, i.e., load-flow equations. In this chapter, we develop a comprehensive dynamic model to study both low-frequency oscillations and voltage stability using a two-axis model with IEEE-Type I exciter, as well as the flux-decay model with a high-gain fast exciter. Both the electromechanical oscillations and their damping, as well as dynamic voltage stability, are discussed. The electromechanical oscillation is of two types:

1. Local mode, typically in the 1 to 3-Hz range between a remotely located power station and the rest of the system.
2. Inter-area oscillations in the range of less than 1 Hz.

Two kinds of analysis are possible: (1) A multimachine linearized analysis that computes the eigenvalues and also finds those machines that contribute to a particular eigenvalue (both local and inter-area oscillations can be studied in such a framework); (2) a single-machine infinite-bus system case that investigates only local oscillations.

Dynamic voltage stability is analyzed by monitoring the eigenvalues of the linearized system as a power system is progressively loaded. Instability occurs when a pair of complex eigenvalues cross to the right-half plane. This is referred to as dynamic voltage instability. Mathematically, it is called Hopf bifurcation. *More details on voltage stability can be found in [81–83].*

Also discussed in this chapter is the role of a power system stabilizer that stabilizes a machine with respect to the local mode of oscillation. A brief review of the approaches to the design of the stabilizers is given. For detailed design procedures, it is necessary to refer to the literature. References [84] and [85] are the basic works in this area.

8.2 Basic Linearization Technique

A unified framework is presented in this section for the linear analysis of multimachine systems. The nonlinear model derived in Chapter 7, using a two-axis model with IEEE-Type I exciter or flux-decay model with a static exciter, is of the form

$$\dot{x} = f(x, y, u) \quad (8.1)$$

$$0 = g(x, y) \quad (8.2)$$

where the vector y includes both the I_{d-q} and \bar{V} vectors. Thus, (8.1) is of dimension $7m$, and (8.2) is of dimension $2(n + m)$.

Equation (8.2) consists of the stator algebraic equations and the network equations in the power-balance form. To show explicitly the traditional load-flow equations and the other algebraic equations, we partition y as

$$\begin{aligned} y &= \begin{bmatrix} I_{d-q}^t & \theta_1 V_1 \dots V_m \mid \theta_2 \dots \theta_n V_{m+1} \dots V_n \end{bmatrix}^t \\ &= [y_a^t \mid y_b^t]^t. \end{aligned} \quad (8.3)$$

Here, the vector y_b corresponds to the load-flow variables, and the vector y_a corresponds to the other algebraic variables. Bus 1 is taken as the slack bus and buses $2, \dots, m$ are the PV buses with the buses $m + 1, \dots, n$ being the PQ buses. The dimension of x is $7m$. Linearizing (8.1) and (8.2) around an operating point gives

$$\begin{bmatrix} \frac{d}{dt} \Delta x \\ 0 \\ 0 \end{bmatrix} = \left[\begin{array}{c|cc} A & B \\ \hline D_{11} & D_{12} \\ D_{21} & J_{LF} \end{array} \right] \begin{bmatrix} \Delta x \\ \Delta y_a \\ \Delta y_b \end{bmatrix} + E[\Delta u]. \quad (8.4)$$

Define

$$J_{AE} = \begin{bmatrix} D_{11} & D_{12} \\ D_{21} & J_{LF} \end{bmatrix}. \quad (8.5)$$

Eliminating $\Delta y_a, \Delta y_b$ we get $\Delta \dot{x} = A_{\text{sys}} \Delta x$ where $A_{\text{sys}} = (A - BJ_{AE}^{-1}C)$. J_{LF} is the load-flow Jacobian. The model represented by (8.4) is useful in both small-signal stability, analysis and voltage stability, since J_{LF} is explicitly shown as part of the system differential-algebraic Jacobian.

We use the above formulation for a multimachine system with a two-axis machine model and the IEEE-Type I exciter (model A) and indicate a similar extension for the flux-decay model with a fast exciter (model B). The methodology is based on [86] and [87].

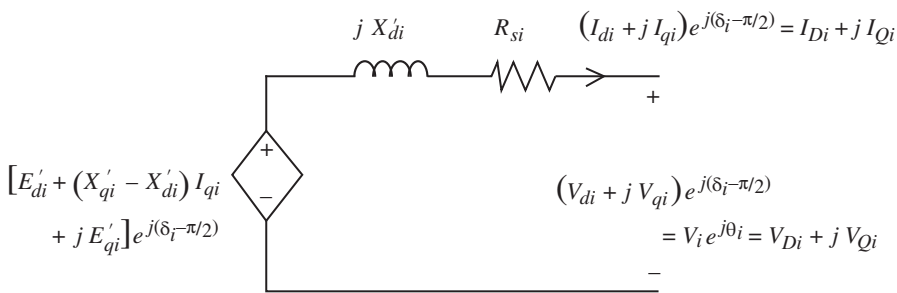


Figure 8.1 Synchronous machine two-axis model dynamic circuit ($i = 1, \dots, m$).

8.2.1 Linearization of Model A

The differential equations of the machine and the exciter are the same as in Chapter 7, except that the state variables are reordered. The synchronous machine dynamic circuit and the IEEE-Type I exciter are shown in Figures 8.1 and 8.2, respectively. The differential and algebraic equations follow.

8.2.2 Differential Equations

$$\frac{d\delta_i}{dt} = \omega_i - \omega_s \quad (8.6)$$

$$\frac{d\omega_i}{dt} = \frac{T_{Mi}}{M_i} - \frac{[E'_{qi} - X'_{di} I_{di}] I_{qi}}{M_i} - \frac{[E'_{di} + X'_{qi} I_{qi}] I_{di}}{M_i} - \frac{D_i(\omega_i - \omega_s)}{M_i} \quad (8.7)$$

$$\frac{dE'_{qi}}{dt} = -\frac{E'_{qi}}{T'_{doi}} - \frac{(X_{di} - X'_{di}) I_{di}}{T'_{doi}} + \frac{E_{fdi}}{T'_{doi}} \quad (8.8)$$

$$\frac{dE'_{di}}{dt} = -\frac{E'_{di}}{T'_{qoi}} + \frac{I_{qi}}{T'_{qoi}} (X_{qi} - X'_{qi}) \quad (8.9)$$

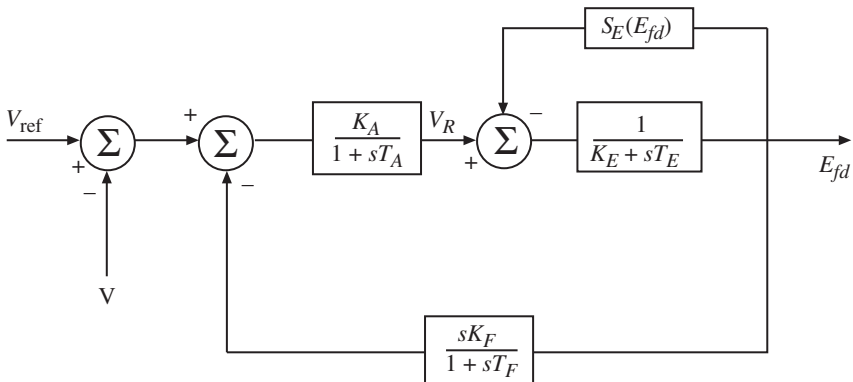


Figure 8.2 IEEE-Type I exciter model.

$$\frac{dE_{fdi}}{dt} = -\frac{K_{Ei} + S_E(E_{fdi})}{T_{Ei}}E_{fdi} + \frac{V_{Ri}}{T_{Ei}} \quad (8.10)$$

$$\frac{dV_{Ri}}{dt} = -\frac{V_{Ri}}{T_{Ai}} + \frac{K_{Ai}}{T_{Ai}}R_{fi} - \frac{K_{Ai}K_{Fi}}{T_{Ai}T_{Fi}}E_{fdi} + \frac{K_{Ai}}{T_{Ai}}(V_{refi} - V_i) \quad (8.11)$$

$$\frac{dR_{Fi}}{dt} = -\frac{R_{Fi}}{T_{Fi}} + \frac{K_{Fi}}{(T_{Fi})^2}E_{fdi} \quad \text{for } i = 1, \dots, m. \quad (8.12)$$

8.2.3 Stator Algebraic Equations

The stator algebraic equations in polar form are

$$E'_{di} - V_i \sin(\delta_i - \theta_i) - R_{si}I_{di} + X'_{qi}I_{qi} = 0 \quad (8.13)$$

$$E'_{qi} - V_i \cos(\delta_i - \theta_i) - R_{si}I_{qi} - X'_{di}I_{di} = 0 \quad \text{for } i = 1, \dots, m. \quad (8.14)$$

8.2.4 Network Equations

The network equations are

$$\begin{aligned} I_{di}V_i \sin(\delta_i - \theta_i) + I_{qi}V_i \cos(\delta_i - \theta_i) + P_{Li}(V_i) \\ - \sum_{k=1}^n V_i V_k Y_{ik} \cos(\theta_i - \theta_k - \alpha_{ik}) = 0 \end{aligned} \quad (8.15)$$

$$\begin{aligned} I_{di}V_i \cos(\delta_i - \theta_i) - I_{qi}V_i \sin(\delta_i - \theta_i) + Q_{Li}(V_i) \\ - \sum_{k=1}^n V_i V_k Y_{ik} \sin(\theta_i - \theta_k - \alpha_{ik}) = 0 \quad i = 1, 2, \dots, m \end{aligned} \quad (8.16)$$

$$P_{Li}(V_i) - \sum_{k=1}^n V_i V_k Y_{ik} \cos(\theta_i - \theta_k - \alpha_{ik}) = 0 \quad (8.17)$$

$$Q_{Li}(V_i) - \sum_{k=1}^n V_i V_k Y_{ik} \sin(\theta_i - \theta_k - \alpha_{ik}) = 0 \quad \text{for } i = m+1, \dots, n. \quad (8.18)$$

Equations (8.6)–(8.18) are linearized analytically, as explained below. The linearization of the differential equations (8.6)–(8.12) yields

$$\frac{d\Delta\delta_i}{dt} = \Delta\omega_i \quad (8.19)$$

$$\begin{aligned} \frac{d\Delta\omega_i}{dt} &= \frac{1}{M_i}\Delta T_{Mi} - \frac{E'_{qio}}{M_i}\Delta I_{qi} + \frac{X'_{di}I_{dio}}{M_i}\Delta I_{qi} + \frac{X'_{di}I_{qio}}{M_i}\Delta I_{di} - \frac{I_{qio}}{M_i}\Delta E'_{qi} \\ &\quad - \frac{E'_{dio}}{M_i}\Delta I_{di} - \frac{I_{dio}}{M_i}\Delta E_{di} - \frac{X'_{qi}I_{dio}}{M_i}\Delta I_{qi} - \frac{X'_{qi}I_{qio}}{M_i}\Delta I_{di} - \frac{D_i}{M_i}\Delta\omega_i \end{aligned} \quad (8.20)$$

$$\frac{d\Delta E'_{qi}}{dt} = -\frac{\Delta E'_{qi}}{T'_{doi}} - \frac{(X_{di} - X'_{di})\Delta I_{di}}{T'_{doi}} + \frac{\Delta E_{fdi}}{T'_{doi}} \quad (8.20)$$

$$\frac{d\Delta E'_{di}}{dt} = -\frac{\Delta E'_{di}}{T'_{qoi}} + \frac{(X_{qi} - X'_{qi})}{T'_{qoi}}\Delta I_{qi} \quad (8.21)$$

$$\frac{d\Delta E_{fdi}}{dt} = f_{si}(E_{fdio})\Delta E_{fdi} + \frac{\Delta V_{Ri}}{T_{Ei}} \quad (8.22)$$

$$\frac{d\Delta V_{Ri}}{dt} = -\frac{\Delta V_{Ri}}{T_{Ai}} + \frac{K_{Ai}}{T_{Ai}}\Delta R_{Fi} - \frac{K_{Ai}K_{Fi}}{T_{Ai}T_{Fi}}\Delta E_{fdi} - \frac{K_{Ai}}{T_{Ai}}\Delta V_i + \frac{K_{Ai}}{T_{Ai}}\Delta V_{refi} \quad (8.23)$$

$$\frac{d\Delta R_{Fi}}{dt} = -\frac{\Delta R_{Fi}}{T_{Fi}} + \frac{K_{Fi}}{(T_{Fi})^2}\Delta E_{fdi} \quad \text{for } i = 1, \dots, m \quad (8.24)$$

where $f_{si}(E_{fdio}) = -\frac{K_{Ei} + E_{fdio}\partial S_E(E_{fdio}) + S_E(E_{fdio})}{T_{Ei}}$ where the symbol ∂ stands for partial derivative. Writing (8.19) through (8.24) in matrix notation, we obtain

$$\begin{aligned} \begin{bmatrix} \Delta\dot{\delta}_i \\ \Delta\dot{\omega}_i \\ \Delta\dot{E}'_{qi} \\ \Delta\dot{E}'_{di} \\ \Delta\dot{E}'_{fdi} \\ \Delta\dot{V}_{Ri} \\ \Delta\dot{R}_{Fi} \end{bmatrix} &= \begin{bmatrix} 0 & 1 & 0 & 0 & 0 & 0 & 0 \\ 0 & -\frac{D_i}{M_i} & -\frac{I_{qio}}{M_i} & -\frac{I_{dio}}{M_i} & 0 & 0 & 0 \\ 0 & 0 & -\frac{1}{T'_{doi}} & 0 & \frac{1}{T'_{doi}} & 0 & 0 \\ 0 & 0 & 0 & -\frac{1}{T'_{qoi}} & 0 & 0 & 0 \\ 0 & 0 & 0 & 0 & f_{si}(E_{fdio}) & \frac{1}{T_{Ei}} & 0 \\ 0 & 0 & 0 & 0 & -\frac{K_{Ai}K_{Fi}}{T_{Ai}T_{Fi}} & -\frac{1}{T_{Ai}} & \frac{K_{Ai}}{T_{Ai}} \\ 0 & 0 & 0 & 0 & \frac{K_{Fi}}{(T_{Fi})^2} & 0 & -\frac{1}{T_{Fi}} \end{bmatrix} \begin{bmatrix} \Delta\delta_i \\ \Delta\omega_i \\ \Delta E'_{qi} \\ \Delta E'_{di} \\ \Delta E'_{fdi} \\ \Delta V_{Ri} \\ \Delta R_{Fi} \end{bmatrix} \\ &+ \begin{bmatrix} 0 & 0 \\ \frac{I_{qio}(X'_{di} - X'_{qi}) - E'_{dio}}{M_i} & \frac{I_{dio}(X'_{di} - X'_{qi}) - E'_{qio}}{M_i} \\ -\frac{(X_{di} - X'_{di})}{T'_{doi}} & 0 \\ 0 & \frac{X_{qi} - X'_{qi}}{T'_{qoi}} \\ 0 & 0 \\ 0 & 0 \\ 0 & 0 \end{bmatrix} \begin{bmatrix} \Delta I_{di} \\ \Delta I_{qi} \end{bmatrix} \\ &+ \begin{bmatrix} 0 & 0 \\ 0 & 0 \\ 0 & 0 \\ 0 & 0 \\ 0 & 0 \\ 0 & -\frac{K_{Ai}}{T_{Ai}} \\ 0 & 0 \end{bmatrix} \begin{bmatrix} 0 & 0 \\ \frac{1}{M_i} & 0 \\ 0 & 0 \\ 0 & 0 \\ 0 & 0 \\ 0 & \frac{K_{Ai}}{T_{Ai}} \\ 0 & 0 \end{bmatrix} \begin{bmatrix} \Delta T_{Mi} \\ \Delta V_{refi} \end{bmatrix} \quad i = 1, \dots, m. \quad (8.25) \end{aligned}$$

Denoting $\begin{bmatrix} \Delta I_{di} \\ \Delta I_{qi} \end{bmatrix} = \Delta I_g$, $\begin{bmatrix} \Delta \theta_i \\ \Delta V_i \end{bmatrix} = \Delta V_g$, and $\begin{bmatrix} \Delta T_{Mi} \\ \Delta V_{\text{refi}} \end{bmatrix} = \Delta u_i$, (8.25) can be written as

$$\Delta \dot{x}_i = A_{1i} \Delta x_i + B_{1i} \Delta I_{gi} + B_{2i} \Delta V_{gi} + E_i \Delta u_i \text{ for } i = 1, \dots, m. \quad (8.26)$$

For the m -machine system, (8.26) can be expressed in matrix form as

$$\Delta \dot{x} = A_1 \Delta x + B_1 \Delta I_g + B_2 \Delta V_g + E_1 \Delta U \quad (8.27)$$

where A_1 , B_1 , B_2 , and E_1 are block diagonal matrices.

We now linearize the stator algebraic equations (8.13) and (8.14):

$$\begin{aligned} \Delta E'_{di} - \sin(\delta_{io} - \theta_{io}) \Delta V_i - V_{io} \cos(\delta_{io} - \theta_{io}) \Delta \delta_i + V_{io} \cos(\delta_{io} - \theta_{io}) \Delta \theta_i \\ - R_{si} \Delta I_{di} + X'_{qi} \Delta I_{qi} = 0 \end{aligned} \quad (8.28)$$

$$\begin{aligned} \Delta E'_{qi} - \cos(\delta_{io} - \theta_{io}) \Delta V_i + V_{io} \sin(\delta_{io} - \theta_{io}) \Delta \delta_i - V_{io} \sin(\delta_{io} - \theta_{io}) \Delta \theta_i \\ - R_{si} \Delta I_{qi} - X'_{di} \Delta I_{di} = 0 \quad i = 1, \dots, m. \end{aligned} \quad (8.29)$$

Writing (8.28) and (8.29) in matrix form, we have

$$\begin{bmatrix} -V_{io} \cos(\delta_{io} - \theta_{io}) & 0 & 0 & 1 & 0 & 0 & 0 \\ V_{io} \sin(\delta_{io} - \theta_{io}) & 0 & 1 & 0 & 0 & 0 & 0 \end{bmatrix} \begin{bmatrix} \Delta \delta_i \\ \Delta \omega_i \\ \Delta E'_{qi} \\ \Delta E'_{di} \\ \Delta E_{fdi} \\ \Delta V_{Ri} \\ \Delta R_{Fi} \end{bmatrix} + \begin{bmatrix} -R_{si} & X'_{qi} \\ -X'_{di} & -R_{si} \end{bmatrix} \begin{bmatrix} \Delta I_{di} \\ \Delta I_{qi} \end{bmatrix} \\ + \begin{bmatrix} V_{io} \cos(\delta_{io} - \theta_{io}) & -\sin(\delta_{io} - \theta_{io}) \\ -V_{io} \sin(\delta_{io} - \theta_{io}) & -\cos(\delta_{io} - \theta_{io}) \end{bmatrix} \begin{bmatrix} \Delta \theta_i \\ \Delta V_i \end{bmatrix} = 0 \quad i = 1, \dots, m. \quad (8.30)$$

Rewriting (8.30), we obtain

$$0 = C_{1i} \Delta x_i + D_{1i} \Delta I_{gi} + D_{2i} \Delta V_{gi} \quad i = 1, \dots, m. \quad (8.31)$$

In matrix notation, (8.31) can be written as

$$0 = C_1 \Delta x + D_1 \Delta I_g + D_2 \Delta V_g \quad (8.32)$$

where C_1 , D_1 , and D_2 are block diagonal. Linearizing the network equations (8.15) and (8.16), which pertain to generators, we obtain

$$\begin{aligned} V_{io} \sin(\delta_{io} - \theta_{io}) \Delta I_{di} + I_{dio} \sin(\delta_{io} - \theta_{io}) \Delta V_i + I_{dio} V_{io} \cos(\delta_{io} - \theta_{io}) \Delta \delta_i \\ - I_{dio} V_{io} \cos(\delta_{io} - \theta_{io}) \Delta \theta_i + V_{io} \cos(\delta_{io} - \theta_{io}) \Delta I_{qi} \\ + I_{qio} \cos(\delta_{io} - \theta_{io}) \Delta V_i - I_{qio} V_{io} \sin(\delta_{io} - \theta_{io}) \Delta \delta_i \\ + I_{qio} V_{io} \sin(\delta_{io} - \theta_{io}) \Delta \theta_i - \left[\sum_{k=1}^n V_{ko} Y_{ik} \cos(\theta_{io} - \theta_{ko} - \alpha_{ik}) \right] \Delta V_i \\ - V_{io} \sum_{k=1}^n [Y_{ik} \cos(\theta_{io} - \theta_{ko} - \alpha_{ik})] \Delta V_k \end{aligned}$$

$$\begin{aligned}
& + \left[V_{io} \sum_{\substack{k=1 \\ \neq i}}^n V_{ko} Y_{ik} \sin(\theta_{io} - \theta_{ko} - \alpha_{ik}) \right] \Delta \theta_i \\
& - V_{io} \sum_{\substack{k=1 \\ \neq i}}^n [V_{ko} Y_{ik} \sin(\theta_{io} - \theta_{ko} - \alpha_{ik})] \Delta \theta_k + \frac{\partial P_{Li}(V_i)}{\partial V_i} \Delta V_i = 0
\end{aligned} \tag{8.33}$$

$$\begin{aligned}
& V_{io} \cos(\delta_{io} - \theta_{io}) \Delta I_{di} + I_{dio} \cos(\delta_{io} - \theta_{io}) \Delta V_i - I_{dio} V_{io} \sin(\delta_{io} - \theta_{io}) \Delta \delta_i \\
& + I_{dio} V_{io} \sin(\delta_{io} - \theta_{io}) \Delta \theta_i - V_{io} \sin(\delta_{io} - \theta_{io}) \Delta I_{qi} \\
& - I_{qio} \sin(\delta_{io} - \theta_{io}) \Delta V_i - I_{qio} V_{io} \cos(\delta_{io} - \theta_{io}) \Delta \delta_i \\
& + I_{qio} V_{io} \cos(\delta_{io} - \theta_{io}) \Delta \theta_i - \left[\sum_{k=1}^n V_{ko} Y_{ik} \sin(\theta_{io} - \theta_{ko} - \alpha_{ik}) \right] \Delta V_i \\
& - V_{io} \sum_{k=1}^n [Y_{ik} \sin(\theta_{io} - \theta_{ko} - \alpha_{ik})] \Delta V_k \\
& - \left[V_{io} \sum_{\substack{k=1 \\ \neq i}}^n V_{ko} Y_{ik} \cos(\theta_{io} - \theta_{ko} - \alpha_{ik}) \right] \Delta \theta_i \\
& + V_{io} \sum_{\substack{k=1 \\ \neq i}}^n [V_{ko} Y_{ik} \cos(\theta_{io} - \theta_{ko} - \alpha_{ik})] \Delta \theta_k + \frac{\partial Q_{Li}(V_i)}{\partial V_i} \Delta V_i = 0 \\
& i = 1, 2, \dots, m.
\end{aligned} \tag{8.34}$$

Rewriting (8.33) and (8.34) in matrix form, we obtain

$$\begin{aligned}
0 &= \begin{bmatrix} C_{21} & & \\ & \ddots & \\ & & C_{2m} \end{bmatrix} \begin{bmatrix} \Delta x_1 \\ \vdots \\ \Delta x_m \end{bmatrix} + \begin{bmatrix} D_{31} & & \\ & \ddots & \\ & & D_{3m} \end{bmatrix} \begin{bmatrix} \Delta I_{g1} \\ \vdots \\ \Delta I_{gm} \end{bmatrix} \\
& + \begin{bmatrix} D_{41,1} & \cdots & D_{41,m} \\ \vdots & \ddots & \vdots \\ D_{4m,1} & \cdots & D_{4m,m} \end{bmatrix} \begin{bmatrix} \Delta V_{g1} \\ \vdots \\ \Delta V_{gm} \end{bmatrix} + \begin{bmatrix} D_{51,m+1} & \cdots & D_{51,n} \\ \vdots & \ddots & \vdots \\ D_{5m,m+1} & \cdots & D_{5m,n} \end{bmatrix} \begin{bmatrix} \Delta V_{\ell m+1} \\ \vdots \\ \Delta V_{\ell n} \end{bmatrix}
\end{aligned} \tag{8.35}$$

where the various submatrices of (8.35) can be easily identified. In matrix notation, (8.35) is

$$0 = C_2 \Delta x + D_3 \Delta I_g + D_4 \Delta V_g + D_5 \Delta V_\ell \tag{8.36}$$

where

$$\Delta V_{\ell i} = \begin{bmatrix} \Delta \theta_i \\ \Delta V_i \end{bmatrix}$$

for the non-generator buses $i = m + 1, \dots, n$.

Note that C_2, D_3 are block diagonal, whereas D_4, D_5 are full matrices. Linearizing network equations (8.17) and (8.18) for the load buses (PQ buses), we obtain

$$\begin{aligned} 0 &= \frac{\partial P_{Li}(V_i)}{\partial V_i} \Delta V_i - \left[\sum_{k=1}^n V_{ko} Y_{ik} \cos(\theta_{io} - \theta_{ko} - \alpha_{ik}) \right] \Delta V_i \\ &\quad + \left[\sum_{\substack{k=1 \\ \neq i}}^n V_{io} V_{ko} Y_{ik} \sin(\theta_{io} - \theta_{ko} - \alpha_{ik}) \right] \Delta \theta_i \\ &\quad - V_{io} \sum_{k=1}^n [Y_{ik} \cos(\theta_{io} - \theta_{ko} - \alpha_{ik})] \Delta V_k \\ &\quad - V_{io} \sum_{\substack{k=1 \\ \neq i}}^n [V_{ko} Y_{ik} \sin(\theta_{io} - \theta_{ko} - \alpha_{ik})] \Delta \theta_k \end{aligned} \quad (8.37)$$

$$\begin{aligned} 0 &= \frac{\partial Q_{Li}(V_i)}{\partial V_i} \Delta V_i - \left[\sum_{k=1}^n V_{ko} Y_{ik} \sin(\theta_{io} - \theta_{ko} - \alpha_{ik}) \right] \Delta V_i \\ &\quad - \left[\sum_{\substack{k=1 \\ \neq i}}^n V_{io} V_{ko} Y_{ik} \cos(\theta_{io} - \theta_{ko} - \alpha_{ik}) \right] \Delta \theta_i \\ &\quad - V_{io} \sum_{k=1}^n [Y_{ik} \sin(\theta_{io} - \theta_{ko} - \alpha_{ik})] \Delta V_k \\ &\quad + V_{io} \sum_{\substack{k=1 \\ \neq i}}^n [V_{ko} Y_{ik} \cos(\theta_{io} - \theta_{ko} - \alpha_{ik})] \Delta \theta_k \quad i = m+1, \dots, n. \end{aligned} \quad (8.38)$$

Rewriting (8.37) and (8.38) in matrix form gives

$$0 = \begin{bmatrix} D_{6m+1,1} & \cdots & D_{6m+1,m} \\ \vdots & \ddots & \vdots \\ D_{6n,1} & \cdots & D_{6n,m} \end{bmatrix} \begin{bmatrix} \Delta V_{g1} \\ \vdots \\ \Delta V_{gm} \end{bmatrix} + \begin{bmatrix} D_{7m+1,m+1} & \cdots & D_{7m+1,n} \\ \vdots & \ddots & \vdots \\ D_{7n,m+1} & \cdots & D_{7n,n} \end{bmatrix} \begin{bmatrix} \Delta V_{\ell m+1} \\ \vdots \\ \Delta V_{\ell n} \end{bmatrix} \quad (8.39)$$

where, again, the various submatrices in (8.39) can be identified from (8.37) and (8.38). Rewriting (8.39) in a compact notation,

$$0 = D_6 \Delta V_g + D_7 \Delta V_\ell \quad (8.40)$$

where D_6, D_7 are full matrices. Rewriting (8.27), (8.32), (8.36), and (8.40) together,

$$\Delta \dot{x} = A_1 \Delta x + B_1 \Delta I_g + B_2 \Delta V_g + E_1 \Delta u \quad (8.41)$$

$$0 = C_1 \Delta x + D_1 \Delta I_g + D_2 \Delta V_g \quad (8.42)$$

$$0 = C_2 \Delta x + D_3 \Delta I_g + D_4 \Delta V_g + D_5 \Delta V_\ell \quad (8.43)$$

$$0 = D_6 \Delta V_g + D_7 \Delta V_\ell \quad (8.44)$$

where

$$\begin{aligned} x &= [x_1^t \dots x_m^t]^t \\ x_i &= [\delta_i \omega_i E'_{qi} E'_{di} E_{fdi} V_{Ri} R_{fi}]^t \\ I_g &= [I_{d1} I_{q1} \dots I_{dm} I_{qm}]^t \\ V_g &= [\theta_1 V_1 \dots \theta_m V_m]^t \\ V_\ell &= [\theta_{m+1} V_{m+1} \dots \theta_n V_n]^t \\ u &= [u_1^t \dots u_m^t]^t \\ u_i &= [T_{Mi} V_{\text{refi}}]^t. \end{aligned}$$

This is the linearized DAE model for the multimachine system. Equations (8.41)–(8.44) are equivalent to the linear model of (8.4), except that in these equations the dependence of loads on the voltages has not been specified, whereas in (8.4) the loads were assumed to be of the constant power type. This model is quite general and can easily be expanded to include frequency or V dependence at the load buses. The power system stabilizer (PSS) dynamics can also be included easily. In the above model, ΔI_g is not of interest and, hence, is eliminated from (8.41) and (8.43) using (8.42). Thus, from (8.42),

$$\Delta I_g = -D_1^{-1} C_1 \Delta x - D_1^{-1} D_2 \Delta V_g. \quad (8.45)$$

Substituting (8.45) into (8.43), we get

$$C_2 \Delta x + D_3 (-D_1^{-1} C_1 \Delta x - D_1^{-1} D_2 \Delta V_g) + D_4 \Delta V_g + D_5 \Delta V_\ell = 0 \quad (8.46)$$

Let

$$[D_4 - D_3 D_1^{-1} D_2] \stackrel{\Delta}{=} K_1$$

and

$$[C_2 - D_3 D_1^{-1} C_1] \stackrel{\Delta}{=} K_2. \quad (8.47)$$

Note that D_1^{-1} involves taking a series of 2×2 inverses of $Z_{d-q,i}$ ($i = 1, \dots, m$). Equation (8.46) is now expressed as

$$K_2 \Delta x + K_1 \Delta V_g + D_5 \Delta V_\ell = 0. \quad (8.48)$$

If (8.45) is substituted in (8.41) to eliminate ΔI_g , the new overall differential-algebraic model is given by

$$\Delta \dot{x} = (A_1 - B_1 D_1^{-1} C_1) \Delta x + (B_2 - B_1 D_1^{-1} D_2) \Delta V_g + E_1 \Delta u \quad (8.49)$$

$$0 = K_2 \Delta x + K_1 \Delta V_g + D_5 \Delta V_\ell \quad (8.50)$$

$$0 = D_6 \Delta V_g + D_7 \Delta V_\ell. \quad (8.51)$$

Equations (8.49)–(8.51) can be put in the more compact form

$$\begin{bmatrix} \Delta \dot{x} \\ 0 \end{bmatrix} = \begin{bmatrix} A' & B' \\ C' & D' \end{bmatrix} \begin{bmatrix} \Delta x \\ \Delta V_N \end{bmatrix} + \begin{bmatrix} E_1 \\ 0 \end{bmatrix} \Delta u \quad (8.52)$$

where $\Delta V_N = \begin{bmatrix} \Delta V_g \\ \Delta V_\ell \end{bmatrix}$. Reorder the variables in the voltage vector and define $\Delta V_p = [\Delta y_c^t \Delta y_b^t]^t = [\Delta\theta_1 \Delta V_1 \dots \Delta V_m \mid \Delta\theta_2 \dots \Delta\theta_n \Delta V_{m+1} \dots \Delta V_n]^t$. Δy_b is the set of load-flow variables, and Δy_c is the set of other algebraic variables in the network equations. Note that we have eliminated the stator algebraic variables.

In any rotational system, the reference for angles is arbitrary. The order of the dynamical system in (8.52) is $7m$, and can be reduced to $(7m - 1)$ by introducing relative rotor angles. Selecting δ_1 as the reference, we have

$$\begin{aligned}\delta'_i &= \delta_i - \delta_1 & i = 2, \dots, m \\ \delta'_1 &= 0 \\ \dot{\delta}'_i &= \omega_i - \omega_1 & i = 2, \dots, m \\ \dot{\delta}'_1 &= 0 \\ \theta'_i &= \theta_i - \delta_1 & i = 1, \dots, n.\end{aligned}$$

Since the angles $\delta_i (i = 1, \dots, m)$ and $\theta_i (i = 1, \dots, n)$ always appear as differences, we can retain the notation with the understanding that these angles are referred to δ_1 . This implies that the differential equation corresponding to δ_1 can be deleted from (8.52) and also from the column corresponding to $\Delta\delta_1$ in A' and C' . The differential equations $\Delta\dot{\delta}_i = \omega_i (i = 2, \dots, m)$ are replaced by $\Delta\dot{\delta}'_i = \Delta\omega_i - \Delta\omega_1$. This means that in the A' matrix we place minus 1 in the intersections of the rows corresponding to $\Delta\dot{\delta}_i (i = 2, \dots, m)$ and the column corresponding to $\Delta\omega_1$. This process is analytically neat, but is not carried out in linear analysis packages. Since angles appear as differences, they are computed to within a constant. Hence, a zero eigenvalue is always present. Recognizing this fact, we retain the formulation corresponding to (8.52). We rewrite the differential-algebraic (DAE) system (8.52) after the reordering of algebraic variables as

$$\begin{bmatrix} \Delta\dot{x} \\ 0 \\ 0 \end{bmatrix} = \begin{bmatrix} A' & B'_1 & B'_2 \\ C'_1 & D'_{11} & D'_{12} \\ C'_2 & D'_{21} & D'_{22} \end{bmatrix} \begin{bmatrix} \Delta x \\ \Delta y_c \\ \Delta y_b \end{bmatrix} + \begin{bmatrix} E_1 \\ 0 \\ 0 \end{bmatrix} \Delta u. \quad (8.53)$$

For voltage-dependent loads, only the appropriate diagonal elements of D'_{11} and D'_{22} will be affected. Now, D'_{22} is the load-flow Jacobian J_{LF} modified by the load representation and

$$\begin{bmatrix} D'_{11} & D'_{12} \\ D'_{21} & D'_{22} \end{bmatrix} = J'_{AE} \quad (8.54)$$

the network algebraic Jacobian with voltage dependencies of the load included. Note that, compared to the algebraic Jacobian J_{AE} of (8.4), the stator algebraic variables have been eliminated to obtain J'_{AE} . The system A_{sys} matrix is obtained as

$$\Delta\dot{x} = A_{sys} \Delta x + E \Delta u \quad (8.55)$$

where

$$A_{sys} = A' - [B'_1 B'_2] [J'_{AE}]^{-1} \begin{bmatrix} C'_1 \\ C'_2 \end{bmatrix}. \quad (8.56)$$

This model is used later to examine the effects of increased loading on the eigenvalues of A_{sys} and the determinants of J'_{AE} and J_{LF} for (1) constant power case, (2) constant current case, and (3) constant impedance case for the models A and B.

We now show that the model in (8.53) is consistent with the development from the nonlinear model in power balance form from Chapter 7. These are (7.36)–(7.38):

$$\dot{x} = f_o(x, I_{d-q}, \bar{V}, u) \quad (8.57)$$

$$I_{d-q} = h(x, \bar{V}) \quad (8.58)$$

$$0 = g_o(x, I_{d-q}, \bar{V}). \quad (8.59)$$

By substituting I_{d-q} from (8.58) in (8.57) and (8.59), we obtain

$$\dot{x} = f_1(x, \bar{V}, u) \quad (8.60)$$

$$0 = g_1(x, \bar{V}). \quad (8.61)$$

Linearizing (8.60) and (8.61) results in

$$\Delta \dot{x} = \frac{\partial f_1}{\partial x} \Delta x + \frac{\partial f_1}{\partial V_p} \Delta V_p + \frac{\partial f_1}{\partial u} \Delta u$$

$$0 = \frac{\partial g_1}{\partial x} \Delta x + \frac{\partial g_1}{\partial V_p} \Delta V_p$$

where $V_p = [\theta_1 \ V_1 \dots V_m \ | \ \theta_2 \dots \theta_n \ V_{m+1} \dots V_n]^t$, then we can identify

$$\begin{aligned} \frac{\partial f_1}{\partial x} &= A', \quad \frac{\partial f_1}{\partial V_p} = [B'_1 \ B'_2] \\ \frac{\partial g_1}{\partial x} &= \begin{bmatrix} C'_1 \\ C'_2 \end{bmatrix}, \quad \frac{\partial g_1}{\partial V_p} = \begin{bmatrix} D'_{11} & D'_{12} \\ D'_{21} & D'_{22} \end{bmatrix}, \quad \frac{\partial f_1}{\partial u} = \begin{bmatrix} E_1 \\ 0 \\ 0 \end{bmatrix}. \end{aligned}$$

8.2.5 Linearization of Model B

As discussed in Chapter 7, the multimachine model with the flux-decay model and fast exciter (Figures 8.3 and 8.4) is given by the following set of differential-algebraic equations:

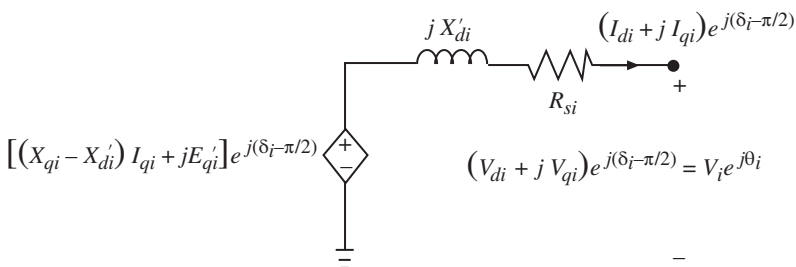


Figure 8.3 Dynamic circuit for the flux-decay model.

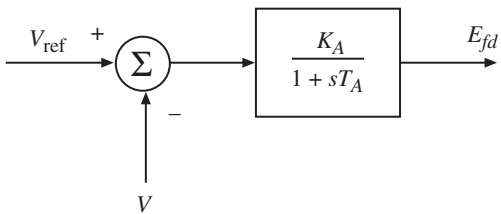


Figure 8.4 Static exciter model.

8.2.6 Differential Equations

$$\frac{d\delta_i}{dt} = \omega_i - \omega_s \quad (8.62)$$

$$\frac{d\omega_i}{dt} = \frac{T_{Mi}}{M_i} - \frac{E'_{qi} I_{qi}}{M_i} - \frac{(X_{qi} - X'_{di})}{M_i} I_{di} I_{qi} - \frac{D_i(\omega_i - \omega_s)}{M_i} \quad (8.63)$$

$$\frac{dE'_{qi}}{dt} = -\frac{E'_{qi}}{T'_{doi}} - \frac{(X_{di} - X'_{di})}{T'_{doi}} I_{di} + \frac{E_{fdi}}{T'_{doi}} \quad (8.64)$$

$$\frac{dE_{fdi}}{dt} = -\frac{E_{fdi}}{T_{Ai}} + \frac{K_{Ai}}{T_{Ai}} (V_{ref,i} - V_i) \quad \text{for } i = 1, \dots, m. \quad (8.65)$$

8.2.7 Stator Algebraic Equations

The stator algebraic equations are

$$V_i \sin(\delta_i - \theta_i) + R_{si} I_{di} - X_{qi} I_{qi} = 0 \quad (8.66)$$

$$E'_{qi} - V_i \cos(\delta_i - \theta_i) - R_{si} I_{qi} - X'_{di} I_{di} = 0 \quad \text{for } i = 1, \dots, m. \quad (8.67)$$

8.2.8 Network Equations

The network equations are the same as (8.15)–(8.18). The linearization of this model is done in the same manner as in model A and, hence, is not discussed.

8.3 Participation Factors

Due to the large size of the power system, it is often necessary to construct reduced-order models for dynamic stability studies by retaining only a few modes. The appropriate definition and determination as to which state variables significantly participate in the selected modes become very important. This requires a tool for identifying the state variables that have significant participation in a selected mode. It is natural to suggest that the significant state variables for an eigenvalue λ_i are those that correspond to large entries in the corresponding eigenvector v_i . But the entries in the eigenvector are dependent on the dimensions of the state variables which are, in general, incommensurable (for example, angle, velocities, and flux). Verghese et al. [88] have suggested a related but dimensionless measure of state variable participation called participation factors.

Participation factor analysis aids in the identification of how each dynamic variable affects a given mode or eigenvalue. Specifically, given a linear system

$$\dot{x} = Ax \quad (8.68)$$

a participation factor is a sensitivity measure of an eigenvalue to a diagonal entry of the system A matrix. This is defined as

$$p_{ki} = \frac{\partial \lambda_i}{\partial a_{kk}} \quad (8.69)$$

where λ_i is the i^{th} system eigenvalue, a_{kk} is a diagonal entry in the system A matrix, and p_{ki} is the participation factor relating the k^{th} state variable to the i^{th} eigenvalue. The participation factor may also be defined by

$$p_{ki} = \frac{w_{ki} v_{ki}}{w_i^t v_i} \quad (8.70)$$

where w_{ki} and v_{ki} are the k^{th} entries in the left and right eigenvector associated with the i^{th} eigenvalue. The right eigenvector v_i and the left eigenvector w_i associated with the i^{th} eigenvalue λ_i satisfy

$$Av_i = \lambda_i v_i \quad (8.71)$$

$$w_i^t A = w_i^t \lambda_i. \quad (8.72)$$

It is not obvious that the definitions given in (8.69) and (8.70) are equivalent. We establish the equivalence as follows. Consider the system

$$[A - \lambda_i I]v_i = 0 \quad (8.73)$$

$$w_i^t [A - \lambda_i I] = 0 \quad (8.74)$$

where v_i and w_i need not be normalized eigenvectors. It is our goal to examine the sensitivity of the eigenvalue to a diagonal element of the A matrix. From (8.68), assuming that the eigenvalues and eigenvectors vary continuously with respect to the elements of the A matrix, we write the perturbation equation as

$$(A + \Delta A)(v_i + \Delta v_i) = (\lambda_i + \Delta \lambda_i)(v_i + \Delta v_i). \quad (8.75)$$

Expansion yields

$$[Av_i] + [\Delta A v_i + A \Delta v_i] + [\Delta A \Delta v_i] = [\lambda_i v_i] + [\Delta \lambda_i v_i + \lambda_i \Delta v_i] + [\Delta \lambda_i \Delta v_i]. \quad (8.76)$$

Neglecting the second-order terms $\Delta A \Delta v_i$ and $\Delta \lambda_i \Delta v_i$ and using (8.71), we obtain

$$[A - \lambda_i I]\Delta v_i + \Delta A v_i = \Delta \lambda_i v_i. \quad (8.77)$$

Multiply (8.77) by the left eigenvector w_i^t to give

$$w_i^t [A - \lambda_i I]\Delta v_i + w_i^t \Delta A v_i = w_i^t \Delta \lambda_i v_i. \quad (8.78)$$

The first term in the left-hand side of (8.78) is identically zero in view of (8.74), leaving

$$w_i^t \Delta A v_i = w_i^t \Delta \lambda_i v_i. \quad (8.79)$$

Now, the sensitivities of λ_i with respect to diagonal entries of A are related to the participation factors, as follows. Assume only that the k^{th} diagonal entry of A is perturbed so that

$$\Delta A = \begin{bmatrix} 0 & \dots & 0 & 0 \\ 0 & \Delta a_{kk} & 0 \\ 0 & \dots & 0 & 0 \end{bmatrix}. \quad (8.80)$$

Then, in (8.79), the left-hand side can be simplified, resulting in

$$w_i^t \Delta A v_i = w_{ki} \Delta a_{kk} v_{ki} = w_i^t \Delta \lambda_i v_i \quad (8.81)$$

Solving for the sensitivity gives the participation factor as

$$\frac{\Delta \lambda_i}{\Delta a_{kk}} = \frac{w_{ki} v_{ki}}{w_i^t v_i} = p_{ki}. \quad (8.82)$$

Equation (8.82) thus shows that (8.69) and (8.70) are equivalent.

An eigenvector may be scaled by any value resulting in a new vector, which is also an eigenvector. We can use this property to choose a scaling that simplifies the use of participation factors, for instance, choosing the eigenvectors such that $w_i^t v_i = 1$ simplifies the definition of the participation factor. In any case, since $\sum_{k=1}^n w_{ki} v_{ki} = w_i^t v_i$, it follows from (8.82) that the sum of all the participation factors associated with a given eigenvalue is equal to 1, that is,

$$\sum_{k=1}^n p_{ki} = 1. \quad (8.83)$$

This property is useful, since all participation factors lie on a scale from zero to one. To handle participation factors corresponding to complex eigenvalues, we introduce some modifications as follows. The eigenvectors corresponding to a complex eigenvalue will have complex elements. Hence, p_{ki} is defined as

$$p_{ki} = \frac{|v_{ki}| \|w_{ki}\|}{\sum_{k=1}^n |v_{ki}| \|w_{ki}\|} \quad (8.84)$$

A further normalization can be done by making the largest of the participation factors equal to unity.

Example 8.1 Compute the participation factors of the 2×2 matrix $\dot{x} = Ax$, where

$$A = \begin{bmatrix} 1 & 4 \\ 3 & 2 \end{bmatrix}.$$

The eigenvalues are $\lambda_1 = 5$, $\lambda_2 = -2$. The right eigenvectors are

$$v_1 = \begin{bmatrix} 1 \\ 1 \end{bmatrix}$$

and

$$v_2 = \begin{bmatrix} 4 \\ -3 \end{bmatrix}.$$

The left eigenvectors are computed as $w_1^t = [3 \quad 4]$ and $w_2^t = [1 \quad -1]$. Verify that $w_2^t v_1 = w_1^t v_2 = 0$. Also, $w_1^t v_1 = 7 = w_2^t v_2$. Letting $i = 1$ and $k = 1, 2$, successively, we obtain the participation of the state variables x_1, x_2 in the mode $\lambda_1 = 5$ as

$$p_{11} = \frac{w_{11}v_{11}}{w_1^t v_1} = \left(\frac{(3)(1)}{7} \right) = \frac{3}{7}$$

$$p_{21} = \frac{w_{21}v_{21}}{w_2^t v_2} = \left(\frac{(4)(1)}{7} \right) = \frac{4}{7}.$$

Letting $i = 2$ and $k = 1, 2$, we obtain the participation of the state variables x_1, x_2 in the mode $\lambda_2 = -2$ as

$$p_{12} = \frac{w_{12}v_{12}}{w_2^t v_2} = \frac{4}{7}$$

$$p_{22} = \frac{w_{22}v_{22}}{w_2^t v_2} = \frac{3}{7}.$$

The participation matrix is therefore

$$P = \begin{bmatrix} p_{11} & p_{12} \\ p_{21} & p_{22} \end{bmatrix} = \begin{bmatrix} \frac{3}{7} & \frac{4}{7} \\ \frac{4}{7} & \frac{3}{7} \end{bmatrix}.$$

Normalizing the largest participation factor as equal to 1 in each column results in

$$P_{\text{norm}} = \begin{bmatrix} 0.75 & 1 \\ 1 & 0.75 \end{bmatrix}.$$

□

The i^{th} column entries in the P or P_{norm} matrix are the sensitivities of the i^{th} eigenvalue with respect to the states.

Example 8.2 Compute the participation factors corresponding to the complex eigenvalue of

$$A = \begin{bmatrix} -0.4 & 0 & -0.01 \\ 1 & 0 & 0 \\ -1.4 & 9.8 & -0.02 \end{bmatrix}.$$

The eigenvalues are $\lambda_1 = -0.6565$ and $\lambda_{2,3} = 0.1183 \pm j0.3678$. The right and left eigenvectors corresponding to the complex eigenvalue $\lambda_2 = 0.1183 + j0.3678$ are

$$v_2 = \begin{bmatrix} 0.0138 - j0.0075 \\ -0.0075 - j0.04 \\ -0.9918 - j0.1203 \end{bmatrix}, \quad w_2 = \begin{bmatrix} 0.838 - j0.0577 \\ 0.4469 + j0.307 \\ -0.0061 + j0.0205 \end{bmatrix}.$$

Using the formula in the previous section, we obtain

$$p_{21} = 0.2332, \quad p_{22} = 0.3896, \quad p_{23} = 0.3772.$$

Note $p_{21} + p_{22} + p_{23} = 1$. We can normalize with respect to p_{22} by making it unity, in which case $p_{21(\text{norm})} = 0.598$, $p_{22(\text{norm})} = 1$ and $p_{23(\text{norm})} = 0.968$.

□

Table 8.1 Eigenvalues of the 3-Machine System.

-0.7209 $\pm j12.7486$
-0.1908 $\pm j8.3672$
-5.4875 $\pm j7.9487$
-5.3236 $\pm j7.9220$
-5.2218 $\pm j7.8161$
-5.1761
-3.3995
-0.4445 $\pm j1.2104$
-0.4394 $\pm j0.7392$
-0.4260 $\pm j0.4960$
-0.0000
-0.0000
-3.2258

Example 8.3 The numerical Example 7.1 is used to illustrate the eigenvalue computation. Compute the eigenvalues, as well as the participation factors, for the eigenvalues for the nominal loading of Example 7.1. The damping $D_i \equiv 0 (i = 1, 2, 3)$. The machine and exciter data are given in Table 7.3. Loads are assumed as constant power type.

Solution

Following the linearization procedure results in a 21×21 sized A_{sys} matrix. Because of zero-damping, two zero eigenvalues are obtained. The eigenvalues are shown in Table 8.1. The participation factors associated with the eigenvalues are given in Table 8.2. Only the participation factors greater than 0.2 are listed. Also shown are the state variables and the machines associated with these state variables. From a practical point of view, this information is very useful. \square

8.4 Studies on Parametric Effects

In this section, the effect of various parameters on the small-signal stability of the system is studied.

8.4.1 Effect of Loading

The WSCC 3-machine, 9-bus system of Chapter 7 is considered. The real or reactive loads at a particular bus/buses are increased continuously. At each step, the initial conditions of the state variables are computed, after running the load flow, and linearization of the equations is done. Ideally, the increase in load is picked up by the generators through the economic load dispatch scheme. To simplify matters, the load increase is allocated among the generators (real power) in proportion to their inertias. In the case

Table 8.2 Eigenvalues and Their Participation Factors.

Eigenvalue	Machine Number	Machine Variable	PF
$-0.7209 \pm j12.7486$	3	δ, ω	1.0, 1.0
	2	δ, ω	0.22, 0.22
$-0.1908 \pm j8.3672$	2	δ, ω	1.0, 1.0
	1	δ, ω	0.42, 0.42
$-5.4875 \pm j7.79487$	2	V_R, E_{fd}	1.0, 0.98
	2	R_f	0.29
$-5.3236 \pm j7.9220$	3	V_R, E_{fd}	1.0, 0.98
	3	R_f	0.29
$-5.2218 \pm j7.8161$	1	V_R, E_{fd}	1.0, 0.97
	1	R_f	0.31
-5.1761	2	E'_d	1.0
	3	E'_d	0.92
-3.3995	3	E'_d	1.0
-3.2258	2	E'_d	0.89
$-0.4445 \pm j1.2104$	1	E'_q, R_f	1.0, 0.74
	2	E'_q, R_f	0.67, 0.48
	3	E'_q, R_f	0.38, 0.28
$-0.4394 \pm j0.7392$	1	E'_q, R_f	1.0, 0.78
	2	E'_q, R_f	0.78, 0.60
	3	E'_q	0.22
$-0.4260 \pm j0.4960$	3	E'_q, R_f	1.0, 0.83
	2	E'_q, R_f	0.43, 0.33
0.0000	1	δ, ω	1.0, 1.0
	2	δ, ω	0.26, 0.26
0.0000	1	δ, ω	1.0, 1.0
	2	δ, ω	0.26, 0.26

of increase of reactive power, it is picked up by the *PV* buses. The A_{sys} matrix is formed, and its eigenvalues are checked for stability. Also $\det J_{LF}$ and $\det J'_{AE}$ are computed. The step-by-step algorithm is as follows:

1. Increase the load at bus/buses for a particular generating unit model.
2. If the real load is increased, then distribute the load among the various generators in proportion to their inertias.
3. Run the load flow.
4. Stop, if the load flow fails to converge.
5. Compute the initial conditions of the state variables, as discussed in Chapter 7.

Table 8.3 Eigenvalues with Model A, $K_A = 20$.

Load at Bus 5	$sgn(\det J_{LF})$	$sgn(\det J'_{AE})$	Critical Eigenvalue(s)	Associated States
4.3	+	+	$-0.1618 \pm j1.9769$	E'_{q1}, R_{f1}
4.4	+	+	$-0.0522 \pm j2.1102$	E'_{q1}, R_{f1}
4.5 (A)	+	+	$0.1268 \pm j2.2798$	E'_{q1}, R_{f1}
4.6	+	+	$0.4446 \pm j2.4911$	E'_{q1}, E'_{q2}
4.7	+	+	$1.0825 \pm j2.7064$	$E'_{q1}, E'_{q2}, E'_{d2}$
4.8	+	+	$2.6051 \pm j2.4392$	$E'_{d2}, E'_{q1}, E'_{q2}, E'_{d3}$
4.9	+	+	17.568, 1.7849	E'_{d2}, E'_{q1}
5.0 (B)	+	-	1.0526	E'_{q1}
5.1	+	-	0.6553	E'_{q1}
5.2	+	-	0.3505	E'_{q1}
5.3	+	-	0.0496	$E'_{q1}, \delta_1, \delta_2$
5.35	-	-	-0.1454	ω_1
5.45	LF does not converge			

6. From the linearized DAE model, compute the various matrices.
7. Compute $\det J_{LF}$, $\det J'_{AE}$, and the eigenvalues of A_{sys} .
8. If A_{sys} is stable, then go to step (1).
9. If unstable, identify the states associated with the unstable eigenvalue(s) of A_{sys} using the participation factor method, and go to step (1).

The above algorithm is implemented for models A and B. Nonuniform damping is assumed by choosing $D_1 = 0.0254$, $D_2 = 0.0066$, and $D_3 = 0.0026$. The results are summarized in Tables 8.3 and 8.4. It is observed that for constant power load, with model A and the IEEE-Type I slow exciter, it is the voltage control mode that goes unstable at $P_{L5} = 4.5$ pu. Examination of the participation factor indicates that the pair of state variables E'_q, R_f of machine 1 in the excitation system is responsible for this model. In the case of model B, the mode that goes unstable is due to the electromechanical variables δ, ω of machine 2 at a load of 4.6 pu. A value of $K_A = 45$ is assumed. The point at which the eigenvalues cross over to the right-half plane is called the Hopf bifurcation point, and the point at which the $\det J'_{AE}$ changes sign is the singularity-induced bifurcation. These are discussed in the literature in detail [89, 92].

8.4.2 Effect of K_A

It was found that, for model A, the increase in K_A alone did not lead to any instability. The stabilizing feedback in the IEEE-Type I exciter was removed, and then an increase in K_A led to instability for this model, as well. For model B, a sufficient increase in K_A led to instability even for a nominal load.

Table 8.4 Eigenvalues with Model B, $K_A = 45$.

Load at Bus 5	$sgn(\det J_{LF})$	$sgn(\det J'_{AE})$	Critical Eigenvalue(s)	Associated States
4.3	+	+	$-0.1119 \pm j8.8738$	δ_2, ω_2
4.4	+	+	$-0.0729 \pm j8.8401$	δ_2, ω_2
4.5	+	+	$-0.0035 \pm j8.8183$	δ_2, ω_2
4.6 (A)	+	+	$0.0901 \pm j8.8421$	δ_2, ω_2
4.7	+	+	$0.1587 \pm j8.9371$	δ_2, ω_2
4.8	+	+	$0.1292 \pm j9.0538$	δ_2, ω_2
4.9	+	+	$0.7565 \pm j20.1162$ $0.0471 \pm j9.0902$	E'_{q1}, E'_{d1} δ_2, ω_2
5.0 (B)	+	-	14.7308	E'_{q1}, E'_{d1}
5.1	+	-	7.1144	E'_{q1}
5.2	+	-	4.2567	E'_{q1}
5.3	+	-	2.3120	E'_{q1}
5.4	-	-	$-0.0597 \pm j8.7819$	δ_2, ω_2
5.5	<i>LF does not converge</i>			

8.4.3 Effect of Type of Load

Appropriate voltage-dependent load modeling can be incorporated into the dynamic model by specifying the load functions. The load at any bus i is given by

$$P_{Li} = P_{Lio} \left(\frac{V_i}{V_{io}} \right)^{n_{pi}} \quad i = 1, \dots, n \quad (8.85)$$

$$Q_{Li} = Q_{Lio} \left(\frac{V_i}{V_{io}} \right)^{n_{qi}} \quad i = 1, \dots, n \quad (8.86)$$

where P_{Lio} and Q_{Lio} are the nominal real and reactive powers, respectively, at bus i , with the corresponding voltage magnitude V_{io} , and n_{pi} , n_{qi} are the load indices. Three types of load are considered.

1. Constant power type ($n_p = n_q = 0$).
2. Constant current type ($n_p = n_q = 1$).
3. Constant impedance type ($n_p = n_q = 2$).

The step-by-step procedure of analysis for a given generating-unit model is as follows:

1. Select the type of the load at various buses (i.e., choose values of n_p and n_q at each bus).
2. Compute the system matrix.
3. Compute the eigenvalues of A_{sys} for stability analysis.

For the three types of loads mentioned earlier, the eigenvalues of model A for increased values of load P_{Lo} at bus 5 are listed in Tables 8.5 and 8.6.

Table 8.5 Eigenvalues for Different Types of Load at Bus 5 for model A ($P_{Lo} = 1.5 \text{ pu}$; $Q_{Lo} = 0.5 \text{ pu}$):
 (a) constant power; (b) constant current; (c) constant impedance.

Constant Power (a)	Constant Current (b)	Constant Impedance (c)
$-0.7927 \pm j12.7660$	$-0.7904 \pm j12.7686$	$-0.7887 \pm j12.7706$
$-0.2849 \pm j8.3675$	$-0.2768 \pm j8.3447$	$-0.2703 \pm j8.3271$
$-5.5187 \pm j7.9508$	$-5.5214 \pm j7.9516$	$-5.5236 \pm j7.9523$
$-5.3325 \pm j7.9240$	$-5.3335 \pm j7.9247$	$-5.3344 \pm j7.9253$
$-5.2238 \pm j7.8156$	$-5.2273 \pm j7.8259$	$-5.2301 \pm j7.8337$
-5.2019	-5.2030	-5.2039
-3.4040	-3.4462	-3.4801
$-0.4427 \pm j1.2241$	$-0.4537 \pm j1.1822$	$-0.4617 \pm j1.1489$
$-0.4404 \pm j0.7413$	$-0.4412 \pm j0.7416$	$-0.4419 \pm j0.7418$
-0.0000	-0.0000	-0.0000
-0.1975	-0.1974	-0.1973
$-0.4276 \pm j0.4980$	$-0.4276 \pm j0.4980$	$-0.4277 \pm j0.4980$
-3.2258	-3.2258	-3.2258

Table 8.6 Eigenvalues for Different Types of Load at Bus 5 for Model A ($P_{Lo} = 4.5 \text{ pu}$; $Q_{Lo} = 0.5 \text{ pu}$):
 (a) constant power; (b) constant current; (c) constant impedance. All other loads are modeled as constant power.

Constant Power (a)	Constant Current (b)	Constant Impedance (c)
$-0.7751 \pm j12.7373$	$-0.7335 \pm j12.7842$	$-0.7285 \pm j12.7936$
$-0.2845 \pm j8.0723$	$-0.2497 \pm j8.0650$	$-0.2444 \pm j8.0659$
$-6.7291 \pm j7.8883$	$-6.7669 \pm j7.9730$	$-6.7760 \pm j7.9895$
$-5.6034 \pm j7.9238$	$-5.6287 \pm j7.9557$	$-5.6338 \pm j7.9639$
$-5.2935 \pm j7.6433$	$-5.2812 \pm j7.8419$	$-5.2938 \pm j7.8712$
-5.2541	-5.2715	-5.2790
$0.1268 \pm j2.2798$	-3.5296	-3.8105
-2.5529	$-0.5020 \pm j1.2531$	$-0.5303 \pm j1.0434$
$-0.4858 \pm j0.7475$	-0.0000	$-0.4950 \pm j0.7653$
-0.0000	$-0.4910 \pm j0.7561$	$-0.5371 \pm j0.5336$
$-0.5341 \pm j0.5306$	$-0.5360 \pm j0.5324$	-0.0000
-0.1976	-0.1972	-0.1970
-3.2258	-3.2258	-3.2258

Table 8.7 Eigenvalues for Different Types of Load at Bus 5 for Model B with $K_A = 175$ ($P_{Lo} = 4.6$ pu, $Q_{Lo} = 0.5$ pu): (a) constant power; (b) constant current; (c) constant impedance. All other loads are modeled as constant power. The machine data used are slightly different from those given in Table 7.3.

Constant Power (a)	Constant Current (b)	Constant Impedance (c)
$-1.9610 \pm j19.3137$	$-0.2039 \pm j15.5128$	$-0.2054 \pm j15.5285$
$-0.1237 \pm j15.5812$	$-2.2586 \pm j12.4273$	$-2.1834 \pm j11.1128$
$0.4495 \pm j9.1844$	$0.1441 \pm j9.0636$	$-0.0607 \pm j9.1218$
$-3.1711 \pm j8.2119$	$-3.1359 \pm j8.1099$	$-3.0930 \pm j8.0364$
$-2.7621 \pm j7.1753$	$-2.7599 \pm j7.1594$	$-2.7575 \pm j7.1462$
-0.0000	-0.0000	-0.0000
-0.1987	-0.1989	-0.1990

First of all, the relative stability of constant power, constant current, and constant impedance-type load has been shown for a nominal operating point $P_{Lo} = 1.5$ pu and $Q_{Lo} = 0.5$ pu (Table 8.5). We observe that the system is dynamically stable for all types of loads. For an increased value of load at bus 5 ($P_{Lo} = 4.5$ pu, $Q_{Lo} = 0.5$ pu), a new power flow is solved and the eigenvalues are listed in Table 8.6. From Table 8.6 we observe that, for this increased load at bus 5, the system becomes dynamically unstable if the load is treated as a constant power type, whereas for the other two types of loads the system remains stable. Finally, we take another case ($P_{Lo} = 4.6$ pu, $Q_{Lo} = 0.5$ pu), in which we show that the constant impedance type load is more stable than the constant current type. To demonstrate this condition, we take model B with a high gain of the exciter ($K_A = 175$). The eigenvalues for various kind of loads are listed in Table 8.7. Both the constant power and constant current cases are unstable, whereas the constant impedance type is stable. These results corroborate the observation in the literature that constant power gives poor results as far as network loadability is concerned [91].

8.4.4 Hopf Bifurcation

For model A, when the load is increased at bus 5, it is observed that the critical modes for the unstable eigenvalues are the electrical ones associated with the exciter, and are complex (Table 8.3). At a load of 4.5 pu, the eigenvalues cross the $j\omega$ axis. This is known as Hopf bifurcation (point A). When the load is increased from 4.8 pu to 4.9 pu, the complex pair of unstable eigenvalues splits into real ones that move in opposite directions along the real axis. The one moving along the positive real axis eventually comes back to the left-half plane via $+\infty$ when the load at bus 5 is increased from 4.9 pu to 5.0 pu (point B). This is the point at which $\det J'_{AE}$ changes sign. This is also known as singularity-induced bifurcation in the literature [92]. The other unstable real eigenvalue moves to the left, and is sensitive to the variable E'_{q1} of the exciter. This eigenvalue returns to the left-half plane at a loading of approximately 5.4 pu, and the system is again dynamically stable (point C). For the load at bus 5 = 5.5 pu, the load flow does not converge. It is possible through other algebraic techniques to reach the nose of the PV curve

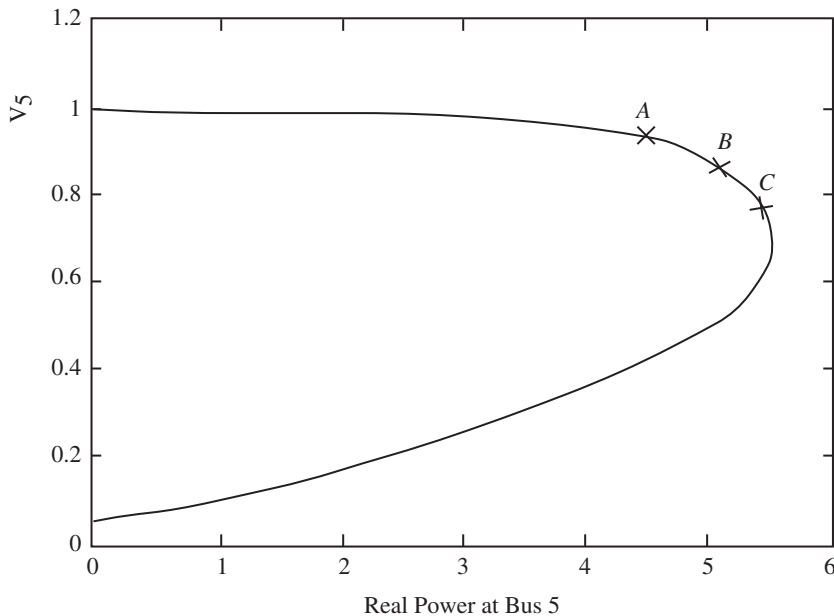


Figure 8.5 PV curve for bus 5 with model A.

or the saddle node bifurcation. This phenomenon is pictorially indicated in the *PV* curve for model A and also is the locus of critical eigenvalue(s) in the *s*-plane (Figures 8.5 and 8.6). At point A, Hopf bifurcation occurs, and it has been shown to be subcritical, i.e., the limit cycle corresponding to the $E'_q - R_f$ pair is unstable [93]. However, load-flow solution still exists. In this region, E'_q and R_f state variables are clearly dominant initially. As the eigenvalues become real and positive, other state variables start participating substantially in the unstable eigenvalues, as indicated in Table 8.3. For model B, which has the fast static exciter with a single time constant, the modes that go unstable are the electromechanical ones (Table 8.4).

When the Hopf bifurcation phenomenon in power systems was first discussed in the literature for a single-machine case, the electromechanical mode was considered

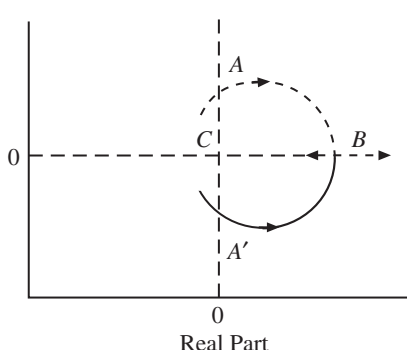


Figure 8.6 The qualitative behavior of the critical modes of A_{sys} as a function of the load at bus 5 (model A).

as the critical one [85, 94]. It was called low-frequency oscillatory instability. In studies relating to voltage collapse, it was shown that the exciter mode may go unstable first [89]. From Tables 8.3 and 8.4, it is seen that both the exciter modes and the electromechanical modes are critical in steady-state stability and voltage collapse, and that they both participate in the dynamic instability depending on the machine and exciter models. Hence, decoupling the QV dynamics from the $P\delta$ dynamics as suggested in the literature may not always hold. It may be true for special system configuration/operating conditions. Load dynamics, if included, can be considered as fast dynamics, and the phenomenon of $\det J'_{AE}$ changing sign will still exist. In conventional bifurcation-theory terms, one can think of solving $g(x, y) = 0$ for $y = h(x)$ in (8.2) and substituting this in the differential equation (8.1) to get $\dot{x} = f(x, h(x))$. The change in sign of $\det J'_{AE}$ (which generally agrees with the sign of J_{AE} in (8.5)) is the instant at which the solution of y is no longer possible. This is also tied in with the concept of the implicit function theorem in singular perturbation theory.

8.5 Electromechanical Oscillatory Modes

These are the modes associated with the rotor angles of the machines. These can be identified through a participation factor analysis in the detailed model. In the classical model with internal node description, we have only the rotor angle modes. We now discuss the computation of these modes as a special case. The equations have been derived in Chapter 7 and are reproduced below.

$$\frac{d\delta_i}{dt} = \omega_i - \omega_s \quad i = 1, \dots, m \quad (8.87)$$

$$\begin{aligned} \frac{2H_i}{\omega_s} \frac{d\omega_i}{dt} &= T_{Mi} - \left[E_i^2 G_{ii} + \sum_{\substack{j=1 \\ \neq i}}^m (C_{ij} \sin \delta_{ij} + D_{ij} \cos \delta_{ij}) \right] \\ &= T_{Mi} - P_{ei} \quad i = 1, \dots, m. \end{aligned} \quad (8.88)$$

Linearization around an operating point o gives

$$\frac{d}{dt} \Delta\delta_i = \Delta\omega_i \quad (8.89)$$

$$\frac{d}{dt} \Delta\omega_i = \frac{\omega_s}{2H_i} [\Delta T_{Mi} - \Delta P_{ei}]. \quad (8.90)$$

Because $T_{Mi} = \text{constant}$, and $\Delta P_{ei} = \sum_{j=1}^m \frac{\partial P_{ei}}{\partial \delta_j} \Delta\delta_j$, we get

$$\frac{d}{dt} \Delta\delta_i = \Delta\omega_i \quad (8.91)$$

$$\frac{d}{dt} \Delta\omega_i = -\frac{\omega_s}{2H_i} \sum_{j=1}^m \left(\frac{\partial P_{ei}}{\partial \delta_j} \Delta\delta_j \right) \quad (8.92)$$

where

$$-\frac{\partial P_{ei}}{\partial \delta_j} = \begin{cases} -\sum_{j=1, j \neq i}^m (C_{ij} \cos \delta_{ij}^o - D_{ij} \sin \delta_{ij}^o) & j = i \\ C_{ij} \cos \delta_{ij}^o - D_{ij} \sin \delta_{ij}^o & j \neq i \end{cases} \quad (8.93)$$

In matrix form we have

$$\begin{bmatrix} \Delta \dot{\delta}_1 \\ \vdots \\ \Delta \dot{\delta}_m \\ \hline \Delta \dot{\omega}_1 \\ \vdots \\ \Delta \dot{\omega}_m \end{bmatrix} = \begin{bmatrix} 0 & I \\ A_\omega & 0 \end{bmatrix} \begin{bmatrix} \Delta \delta_1 \\ \vdots \\ \Delta \delta_m \\ \hline \Delta \omega_1 \\ \vdots \\ \Delta \omega_m \end{bmatrix}. \quad (8.94)$$

The elements of A_ω are given by $\frac{-\omega_s}{2H_i} \frac{\partial P_{ei}}{\partial \delta_j}$. The matrix A_ω can be written as

$$A_\omega = \begin{bmatrix} \frac{-\omega_s}{2H_1} \frac{\partial P_{e1}}{\partial \delta_1} & \dots & \frac{-\omega_s}{2H_1} \frac{\partial P_{e1}}{\partial \delta_m} \\ \vdots & \ddots & \vdots \\ \frac{-\omega_s}{2H_m} \frac{\partial P_{em}}{\partial \delta_1} & \dots & \frac{-\omega_s}{2H_m} \frac{\partial P_{em}}{\partial \delta_m} \end{bmatrix}_o. \quad (8.95)$$

The elements of A_ω can also be expressed in a polar notation by noting that

$$C_{ij} = E_i E_j B_{ij} = E_i E_j Y_{ij} \sin \alpha_{ij}$$

and

$$D_{ij} = E_i E_j G_{ij} = E_i E_j Y_{ij} \cos \alpha_{ij}.$$

Hence, in (8.93)

$$C_{ij} \cos \delta_{ij}^o - D_{ij} \sin \delta_{ij}^o = E_i E_j Y_{ij} \sin (\alpha_{ij} - \delta_{ij}^o). \quad (8.96)$$

Therefore

$$-\frac{\partial P_{ei}}{\partial \delta_j} = \begin{cases} -\sum_{j=1, j \neq i}^m E_i E_j Y_{ij} \sin (\alpha_{ij} - \delta_{ij}^o) & j = i \\ E_i E_j Y_{ij} \sin (\alpha_{ij} - \delta_{ij}^o) & j \neq i \end{cases} \quad (8.97)$$

For the 3-machine case

$$A_\omega = \omega_s \begin{bmatrix} \frac{-1}{2H_1} [E_1 E_2 Y_{12} \sin (\alpha_{12} - \delta_{12}^o)] + E_1 E_3 Y_{13} \sin (\alpha_{13} - \delta_{13}^o) \\ \frac{1}{2H_2} [E_1 E_2 Y_{21} \sin (\alpha_{21} - \delta_{21}^o)] + E_2 E_3 Y_{23} \sin (\alpha_{23} - \delta_{23}^o) \\ \frac{1}{2H_3} [E_3 E_1 Y_{13} \sin (\alpha_{31} - \delta_{31}^o)] + E_2 E_1 Y_{23} \sin (\alpha_{32} - \delta_{32}^o) \end{bmatrix} \begin{bmatrix} \frac{1}{2H_1} [E_1 E_2 Y_{12} \sin (\alpha_{12} - \delta_{12}^o)] \\ \frac{1}{2H_2} [E_2 E_1 Y_{21} \sin (\alpha_{21} - \delta_{21}^o)] \\ \frac{1}{2H_3} [E_3 E_2 Y_{23} \sin (\alpha_{23} - \delta_{23}^o)] \end{bmatrix} \begin{bmatrix} \frac{1}{2H_1} [E_1 E_3 Y_{13} \sin (\alpha_{13} - \delta_{13}^o)] \\ \frac{1}{2H_2} [E_2 E_3 Y_{23} \sin (\alpha_{23} - \delta_{23}^o)] \\ \frac{1}{2H_3} [E_3 E_1 Y_{13} \sin (\alpha_{31} - \delta_{31}^o)] + E_2 E_1 Y_{23} \sin (\alpha_{32} - \delta_{32}^o) \end{bmatrix} \quad (8.98)$$

A_ω is not symmetric, since $\delta_{ij} = -\delta_{ji}$, although $\alpha_{ij} = \alpha_{ji}$. However, the sum of the three columns = 0, hence, the rank of A_ω = 2. This means that one eigenvalue of A_ω = 0. A_ω can be expressed as $A_\omega = M^{-1}K$, where $M^{-1} = [\text{diag}(\frac{\omega_s}{2H_i})]$ and $K = [K_{ij}]$:

$$K_{ij} = - \sum_{j=1, j \neq i}^m E_i E_j Y_{ij} \sin(\alpha_{ij} - \delta_{ij}^o) \quad j = i \quad (8.99)$$

$$= E_i E_j Y_{ij} \sin(\alpha_{ij} - \delta_{ij}^o) \quad j \neq i. \quad (8.100)$$

K_{ij} 's are called the synchronizing coefficients, and are equivalent to those in (8.93).

8.5.1 Eigenvalues of A and A_ω

Case (a): Transfer conductances are neglected, i.e., $G_{ij} = 0$.

This implies $\alpha_{ij} = \frac{\pi}{2}$ and $K_{ij} = K_{ji}$ by inspection from (8.99) and (8.100). Hence, the matrix K is symmetric. It can be shown mathematically that (1) the eigenvalues of

$$A = \begin{bmatrix} 0 & | & U \\ M^{-1}K & | & 0 \end{bmatrix} \quad (8.101)$$

are the square roots of the eigenvalues of $A_\omega = M^{-1}K$. (2) The eigenvalues of A_ω are real, including one zero eigenvalue. The zero eigenvalue is due to the fact that a reference angle is necessary, and the angles appear only as differences. Hence, A has a pair of zero eigenvalues. If the real eigenvalues of A_ω are negative, then A has complex pairs of eigenvalues on the imaginary axis. The nonzero eigenvalues $\pm j\omega_k$ of A ($k = 1, 2, \dots, m-1$) define the *electromechanical modes*. If A_ω has a positive real eigenvalue, then A has at least one positive real eigenvalue, and, hence, the system is unstable.

Case (b): $G_{ij} \neq 0$ ($i \neq j$).

K is not symmetric. However, A_ω will still have a zero eigenvalue. Hence, A will also have two zero eigenvalues. It appears that the eigenvalues of A are also the square roots of the eigenvalues of A_ω .

Example 8.4 Compute the electromechanical modes with and without transfer conductances for the 3-machine system. In Example 7.6, the voltages behind transient reactances and the reduced-order model at the internal buses around the operating point have been computed. They are reproduced below

$$\bar{E}_1 = 1.054 \angle 2.27^\circ \quad \bar{E}_2 = 1.05 \angle 19.75^\circ \quad \bar{E}_3 = 1.02 \angle 13.2^\circ.$$

The \bar{Y}_{int} matrix is given by

$$\bar{Y}_{\text{int}} = \begin{bmatrix} 0.845 - j2.988 & 0.287 + j1.513 & 0.210 + j1.226 \\ 0.287 + j1.513 & 0.420 - j2.724 & 0.213 + j1.088 \\ 0.210 + j1.226 & 0.213 + j1.088 & 0.277 - j2.368 \end{bmatrix}.$$

The elements of A_ω are calculated as follows

$$\frac{\omega_s}{2H_1} = 7.974, \frac{\omega_s}{2H_2} = 29.453, \frac{\omega_s}{2H_3} = 62.625$$

$$C_{12} = 1.678, C_{13} = 1.321, G_{11} = 0.845, |\bar{E}_1| = 1.054$$

$$D_{12} = 0.318, D_{13} = 0.226$$

$$C_{21} = 1.678, C_{23} = 1.165, G_{22} = 0.420, |\bar{E}_2| = 1.05$$

$$D_{21} = 0.318, D_{23} = 0.228$$

$$C_{31} = 1.313, C_{32} = 1.165, C_{33} = 0.277, |\bar{E}_3| = 1.02$$

$$D_{31} = 0.226, D_{32} = 0.228$$

$$\delta_{12}^o = -17.46^\circ, \delta_{13}^o = -10.91^\circ, \delta_{23}^o = 6.55^\circ.$$

We next obtain the following quantities for use in computing elements of A_ω

$$C_{12} \cos \delta_{12}^o - D_{12} \sin \delta_{12}^o = 1.696$$

$$C_{13} \cos \delta_{13}^o - D_{13} \sin \delta_{13}^o = 1.332$$

$$C_{21} \cos \delta_{21}^o - D_{21} \sin \delta_{21}^o = 1.506$$

$$C_{23} \cos \delta_{23}^o - D_{23} \sin \delta_{23}^o = 1.139$$

$$C_{31} \cos \delta_{31}^o - D_{31} \sin \delta_{31}^o = 1.246$$

$$C_{32} \cos \delta_{32}^o - D_{32} \sin \delta_{32}^o = 1.191.$$

From (8.93), we can now calculate the elements of A_ω .

Case (a): A_ω for $G_{ij} \neq 0$ is

$$A_\omega = \begin{bmatrix} -24.209 & 13.521 & 10.688 \\ 44.356 & -77.902 & 33.546 \\ 78.031 & 74.586 & -152.617 \end{bmatrix}.$$

Case (b): With $G_{ij} = 0$

$$A_\omega = \begin{bmatrix} -23.83 & 13.15 & 10.68 \\ 45.64 & -79.04 & 33.40 \\ 78.48 & 74.28 & -152.76 \end{bmatrix}.$$

The eigenvalues of A are obtained as

Case (a):

$$0, 0, \pm j8.7326, \pm j13.393$$

Case (b):

$$0, 0, \pm j9.807, \pm j13.435$$

Notice the difference by neglecting G_{ij} . □

8.6 Power System Stabilizers

So far we have discussed the linearized model, eigenvalues, and its application to voltage stability in the context of a multimachine power system. We now discuss a stabilizing device, called the power system stabilizer (PSS), used to damp out the low-frequency oscillations. Although considerable research is being done in designing PSS for a multimachine system, no definitive results have been applied in the field. The design is still done on the basis of a single machine infinite bus (SMIB) system. The parameters are then tuned on-line to suppress the modes, both the local and inter-area modes. We explain the basic approach based on control theory, and illustrate it with an example.

8.6.1 Basic Approach

The differential-algebraic nonlinear model of a single machine connected to an infinite bus is given by

$$\dot{x} = f(x, y, u) \quad (8.102)$$

$$0 = g(x, y) \quad (8.103)$$

where x is the state vector, y is the vector of algebraic variables, and g consists of the stator algebraic and the network equations. Let the operating point be x^o, y^o, u^o . The perturbed variables are $x = x^o + \Delta x$, $y = y^o + \Delta y$, and $u = u^o + \Delta u$. Linearization of (8.102) and (8.103) leads to

$$\Delta\dot{x} = A\Delta x + B\Delta y + E\Delta u \quad (8.104)$$

$$0 = C\Delta x + D\Delta y. \quad (8.105)$$

If D is invertible,

$$\Delta y = -D^{-1}C\Delta x \quad (8.106)$$

Therefore

$$\Delta\dot{x} = (A - BD^{-1}C)\Delta x + E\Delta u = A_{\text{sys}}\Delta x + E\Delta u. \quad (8.107)$$

A, B, C, D , and E are appropriate Jacobians of (8.102) and (8.103) evaluated at the operating point. We illustrate the procedure for a single-machine system. Equation (8.103) consists of the two stator algebraic equations and the network equations in either the power-balance or the current-balance form.

8.6.2 Derivation of $K1 - K6$ Constants [78,88]

Historically, when low-frequency oscillations were first investigated analytically, they took a two-step approach. A single machine connected to an infinite bus is chosen to analyze the local (plant) mode of oscillation in the 1- to 3-Hz range. A flux-decay model is linearized with E_{fd} as an input, and the model so obtained is put in a block diagram form. Then a fast-acting exciter between ΔV_t and ΔE_{fd} is introduced in the block diagram. In the resulting state-space model, certain constants called the $K1 - K6$ are identified. These constants are functions of the operating point. The state-space model is then used to examine the eigenvalues, as well as to design supplementary controllers to

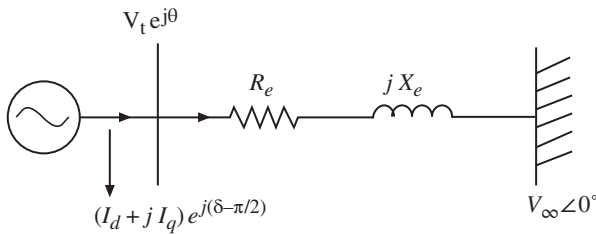


Figure 8.7 Single-machine infinite-bus system.

ensure adequate damping of the dominant modes. The real and imaginary parts of the electromechanical mode are associated with the damping and synchronizing torques, respectively. We now outline this approach, which is a special case of the general development discussed in the earlier sections of this chapter.

The single machine connected to an infinite bus through an external reactance X_e and resistance R_e is the widely used configuration with a flux-decay model and stator resistance equal to zero. No local load is assumed at the generator bus. Figure 8.7 shows the system. The flux-decay model of the machine only is given by (8.62)–(8.64), with E_{fd} being treated as an input; the equations are given below.

$$\dot{E}'_q = -\frac{1}{T'_{do}}(E'_q + (X_d - X'_d)I_d - E_{fd}) \quad (8.108)$$

$$\dot{\delta} = \omega - \omega_s \quad (8.109)$$

$$\dot{\omega} = \frac{\omega_s}{2H}[T_M - (E'_q I_q + (X_q - X'_d)I_d I_q + D(\omega - \omega_s))]. \quad (8.110)$$

The stator algebraic equations are given by (8.66) and (8.67), and we assume $R_s = 0$. We use V_t to denote the magnitude of the generator terminal voltage. The equations are

$$X_q I_q - V_t \sin(\delta - \theta) = 0 \quad (8.111)$$

$$E'_q - V_t \cos(\delta - \theta) - X'_d I_d = 0. \quad (8.112)$$

Now

$$(V_d + j V_q) e^{j(\delta - \pi/2)} = V_t e^{j\theta}.$$

Hence

$$V_d + j V_q = V_t e^{j\theta} e^{-j(\delta - \pi/2)}. \quad (8.113)$$

Expansion of the right-hand side results in

$$V_d + j V_q = V_t \sin(\delta - \theta) + j V_t \cos(\delta - \theta). \quad (8.114)$$

Hence, $V_d = V_t \sin(\delta - \theta)$ and $V_q = V_t \cos(\delta - \theta)$. Substituting for V_d and V_q in (8.111) and (8.112), we get the stator algebraic equations

$$X_q I_q - V_d = 0 \quad (8.115)$$

$$E'_q - V_q - X'_d I_d = 0. \quad (8.116)$$

The network equation is (assuming zero phase angle at the infinite bus)

$$(I_d + jI_q)e^{j(\delta-\pi/2)} = \frac{(V_d + jV_q)e^{j(\delta-\pi/2)} - V_\infty \angle 0^\circ}{R_e + jX_e} \quad (8.117)$$

$$(I_d + jI_q) = \frac{(V_d + jV_q) - V_\infty e^{-j(\delta-\pi/2)}}{R_e + jX_e}. \quad (8.118)$$

Cross-multiplying and separating into real and imaginary parts,

$$R_e I_d - X_e I_q = V_d - V_\infty \sin \delta \quad (8.119)$$

$$X_e I_d + R_e I_q = V_q - V_\infty \cos \delta. \quad (8.120)$$

We thus have, for the single-machine case, the differential equations (8.108)–(8.110) and the algebraic equations (8.115), (8.116), (8.119), and (8.120). We linearize them around an operating point, and eliminate the algebraic variables $I_d, I_q, \theta, V_d, V_q$ as follows.

8.6.3 Linearization

Step 1: Linearize the algebraic equations (8.115) and (8.116):

$$\begin{bmatrix} \Delta V_d \\ \Delta V_q \end{bmatrix} = \begin{bmatrix} 0 & X_q \\ -X'_d & 0 \end{bmatrix} \begin{bmatrix} \Delta I_d \\ \Delta I_q \end{bmatrix} + \begin{bmatrix} 0 \\ \Delta E'_q \end{bmatrix}. \quad (8.121)$$

Step 2: Linearize the load-flow equations (8.119) and (8.120):

$$\begin{bmatrix} \Delta V_d \\ \Delta V_q \end{bmatrix} = \begin{bmatrix} R_e & -X_e \\ X_e & R_e \end{bmatrix} \begin{bmatrix} \Delta I_d \\ \Delta I_q \end{bmatrix} + \begin{bmatrix} V_\infty \cos \delta^o \\ -V_\infty \sin \delta^o \end{bmatrix} \Delta \delta. \quad (8.122)$$

Step 3: Equate the right-hand sides of (8.121) and (8.122), and simplify

$$\begin{bmatrix} R_e & -(X_e + X_q) \\ (X_e + X'_d) & R_e \end{bmatrix} \begin{bmatrix} \Delta I_d \\ \Delta I_q \end{bmatrix} = \begin{bmatrix} 0 \\ \Delta E'_q \end{bmatrix} + \begin{bmatrix} -V_\infty \cos \delta^o \\ V_\infty \sin \delta^o \end{bmatrix} \Delta \delta. \quad (8.123)$$

Now

$$\begin{bmatrix} R_e & -(X_e + X_q) \\ (X_e + X'_d) & R_e \end{bmatrix}^{-1} = \frac{1}{\Delta} \begin{bmatrix} R_e & (X_e + X_q) \\ -(X_e + X'_d) & R_e \end{bmatrix} \quad (8.124)$$

where the determinant Δ is given by

$$\Delta = R_e^2 + (X_e + X_q)(X_e + X'_d).$$

Solve for $\Delta I_d, \Delta I_q$ in (8.123), to get (after simplification)

$$\begin{bmatrix} \Delta I_d \\ \Delta I_q \end{bmatrix} = \frac{1}{\Delta} \begin{bmatrix} (X_e + X_q) & | & -R_e V_\infty \cos \delta^o + V_\infty \sin \delta^o (X_q + X_e) \\ R_e & | & R_e V_\infty \sin \delta^o + V_\infty \cos \delta^o (X'_d + X_e) \end{bmatrix} \begin{bmatrix} \Delta E'_q \\ \Delta \delta \end{bmatrix}. \quad (8.125)$$

Step 4: Linearize the differential equations (8.108)–(8.110). We introduce the normalized frequency $\nu = \frac{\omega}{\omega_s}$ so that the linearized differential equations become

$$\begin{bmatrix} \Delta \dot{E}'_q \\ \Delta \dot{\delta} \\ \Delta \dot{v} \end{bmatrix} = \begin{bmatrix} -\frac{1}{T'_{do}} & 0 & 0 \\ \frac{T'_{do}}{2H} & 0 & \omega_s \\ -I_q^o & 0 & -\frac{D\omega_s}{2H} \end{bmatrix} \begin{bmatrix} \Delta E'_q \\ \Delta \delta \\ \Delta v \end{bmatrix} + \begin{bmatrix} -\frac{1}{T'_{do}}(X_d - X'_d) & 0 & 0 \\ \frac{1}{2H} I_q^o (X'_d - X_q) & 0 & 0 \\ \frac{1}{2H} (X'_d - X_q) I_d^o - \frac{1}{2H} E_q'^o & \frac{1}{2H} (X'_d - X_q) I_d^o & \frac{1}{2H} E_q'^o \end{bmatrix} \begin{bmatrix} \Delta I_d \\ \Delta I_q \\ \Delta T_M \end{bmatrix} + \begin{bmatrix} \frac{1}{T'_{do}} & 0 \\ 0 & 0 \\ 0 & \frac{1}{2H} \end{bmatrix} \begin{bmatrix} \Delta E_{fd} \\ \Delta T_M \end{bmatrix}. \quad (8.126)$$

Step 5: Substitute for ΔI_d , ΔI_q from (8.125) into (8.126) to obtain

$$\Delta \dot{E}'_q = -\frac{1}{K_3 T'_{do}} \Delta E'_q - \frac{K_4}{T'_{do}} \Delta \delta + \frac{1}{T'_{do}} \Delta E_{fd} \quad (8.127)$$

$$\Delta \dot{\delta} = \omega_s \Delta \nu \quad (8.128)$$

$$\Delta \dot{v} = -\frac{K_2}{2H} \Delta E'_q - \frac{K_1}{2H} \Delta \delta - \frac{D\omega_s}{2H} \Delta \nu + \frac{1}{2H} \Delta T_M \quad (8.129)$$

where

$$\frac{1}{K_3} = 1 + \frac{(X_d - X'_d)(X_q + X_e)}{\Delta} \quad (8.130)$$

$$K_4 = \frac{V_\infty (X_d - X'_d)}{\Delta} [(X_q + X_e) \sin \delta^o - R_e \cos \delta^o] \quad (8.131)$$

$$K_2 = \frac{1}{\Delta} [I_q^o \Delta - I_q^o (X'_d - X_q) (X_q + X_e) - R_e (X'_d - X_q) I_d^o + R_e E_q'^o] \quad (8.132)$$

$$\begin{aligned} K_1 = & -\frac{1}{\Delta} [I_q^o V_\infty (X'_d - X_q) \{(X_q + X_e) \sin \delta^o - R_e \cos \delta^o\} \\ & + V_\infty \{(X'_d - X_q) I_d^o - E_q'^o\} \{(X'_d + X_e) \cos \delta^o + R_e \sin \delta^o\}]. \end{aligned} \quad (8.133)$$

Since

$$\begin{aligned} V_t &= \sqrt{V_d^2 + V_q^2} \\ V_t^2 &= V_d^2 + V_q^2 \\ 2V_t \Delta V_t &= 2V_d^o \Delta V_d + 2V_q^o \Delta V_q \\ \Delta V_t &= \frac{V_d^o}{V_t} \Delta V_d + \frac{V_q^o}{V_t} \Delta V_q. \end{aligned} \quad (8.134)$$

Substituting (8.125) in (8.121) results in

$$\begin{aligned} \begin{bmatrix} \Delta V_d \\ \Delta V_q \end{bmatrix} &= \frac{1}{\Delta} \begin{bmatrix} 0 & X_q \\ -X'_d & 0 \end{bmatrix} \begin{bmatrix} X_q + X_e \\ R_e \end{bmatrix} \begin{bmatrix} -R_e V_\infty \cos \delta^o + V_\infty (X_q + X_e) \sin \delta^o \\ R_e V_\infty \sin \delta^o + V_\infty \cos \delta^o (X'_d + X_e) \end{bmatrix} \\ &\quad \times \begin{bmatrix} \Delta E'_q \\ \Delta \delta \end{bmatrix} + \begin{bmatrix} 0 \\ \Delta E'_q \end{bmatrix} \\ &= \frac{1}{\Delta} \begin{bmatrix} X_q R_e & X_q (R_e V_\infty \sin \delta^o + V_\infty \cos \delta^o (X'_d + X_e)) \\ -X'_d (X_q + X_e) & -X'_d (-R_e V_\infty \cos \delta^o + V_\infty (X_q + X_e) \sin \delta^o) \end{bmatrix} \\ &\quad \times \begin{bmatrix} \Delta E'_q \\ \Delta \delta \end{bmatrix} + \begin{bmatrix} 0 \\ \Delta E'_q \end{bmatrix}. \end{aligned} \quad (8.135)$$

Substituting (8.135) in (8.134) gives

$$\Delta V_t = K_5 \Delta \delta + K_6 \Delta E'_q \quad (8.136)$$

where

$$\begin{aligned} K_5 &= \frac{1}{\Delta} \left\{ \frac{V_d^o}{V_t} X_q [R_e V_\infty \sin \delta^o + V_\infty \cos \delta^o (X'_d + X_e)] \right. \\ &\quad \left. + \frac{V_q^o}{V_t} [X'_d (R_e V_\infty \cos \delta^o - V_\infty (X_q + X_e) \sin \delta^o)] \right\} \end{aligned} \quad (8.137)$$

$$K_6 = \frac{1}{\Delta} \left\{ \frac{V_d^o}{V_t} X_q R_e - \frac{V_q^o}{V_t} X'_d (X_q + X_e) \right\} + \frac{V_q^o}{V_t}. \quad (8.138)$$

The constants that we have derived are called the *K1–K6*, developed by Heffron-Phillips [95], and later by DeMello-Concordia [85], for the study of local low-frequency oscillations.

Example 8.5 In Figure 8.7, assume that $R_e = 0$, $X_e = 0.5$ pu, $V_t \angle \theta = 1 \angle 15^\circ$ pu, and $V_\infty \angle 0^\circ = 1.05 \angle 0^\circ$ pu. The machine data are $H = 3.2$ sec, $T'_{do} = 9.6$ sec, $K_A = 400$, $T_A = 0.2$ sec, $R_s = 0.0$ pu, $X_q = 2.1$ pu, $X_d = 2.5$ pu, $X'_d = 0.39$ pu, $D = 0$, and $\omega_s = 377$. Using the flux-decay model, find (1) the initial values of state and algebraic variables, as well as V_{ref} , T_M , and (2) *K1–K6* constants.

1. Computation of Initial Conditions

The technique discussed in Section 7.6 is followed. The superscript *o* on the algebraic and state variables is omitted.

$$I_G e^{j\gamma} = (I_d + jI_q) e^{j(\delta - \pi/2)} = \frac{1 \angle 15^\circ - 1.05 \angle 0^\circ}{j0.5} = 0.5443 \angle 18^\circ$$

$$\delta(0) = \text{angle of } \bar{E} \text{ where } \bar{E} = V_t e^{j\theta} + (R_s + jX_q) I_G e^{j\gamma}.$$

$$\bar{E} = 1 \angle 15^\circ + (j2.1)(0.5443 \angle 18^\circ)$$

$$= 1.4788 \angle 65.52^\circ.$$

Therefore $\delta(0) = 65.52^\circ$. $I_d + jI_q = I_G e^{j\gamma} e^{-j(\delta-\pi/2)} = 0.5443 \angle 42.48^\circ$, $I_d = 0.4014$, and $I_q = 0.3676$

$$\begin{aligned} V_d + jV_q &= V e^{j\theta} e^{-j(\delta-\pi/2)} \\ &= 1 \angle 39.48^\circ. \end{aligned}$$

Hence

$$V_d = 0.77185, V_q = 0.63581.$$

From (8.116):

$$\begin{aligned} E'_q &= V_q + X'_d I_d \\ &= 0.63581 + (0.39)(0.4014) = 0.7924. \end{aligned}$$

From (8.62)–(8.65), setting derivatives = 0,

$$\begin{aligned} E_{fd} &= E'_q + (X_d - X'_d) I_d \\ &= 0.7924 + (2.5 - 0.39)0.4014 = 1.6394 \\ V_{\text{ref}} &= V_t + \frac{E_{fd}}{K_A} = 1 + \frac{1.6394}{400} = 1.0041 \\ \omega_s &= 377, T_M = E'_q I_q + (X_q - X'_d) I_d I_q \\ &= (0.7924)(0.3676) + (2.1 - 0.39)(0.4014)(0.3676) \\ &= 0.5436. \end{aligned}$$

This completes the calculation of the initial values.

2. Computation of K1–K6 Constants

The formulas given in (8.130)–(8.134) and (8.137)–(8.138) are used.

$$\begin{aligned} \Delta &= R_e^2 + (X_e + X_q)(X_e + X'_d) \\ &= 2.314 \end{aligned}$$

$$\begin{aligned} \frac{1}{K_3} &= 1 + \frac{(X_d - X'_d)(X_q + X_e)}{\Delta} \\ &= 3.3707 \end{aligned}$$

$$K_3 = 0.296667$$

$$\begin{aligned} K_4 &= \frac{V_\infty (X_d - X'_d)}{\Delta} [(X_q + X_e) \sin \delta^\circ - R_e \cos \delta^\circ] \\ &= 2.26555 \end{aligned}$$

$$\begin{aligned} K_2 &= \frac{1}{\Delta} [I_q^o \Delta - I_q^o (X'_d - X_q)(X_q + X_e) - R_e (X'_d - X_q) I_d^o + R_e E_q'^o] \\ &= 1.0739. \end{aligned}$$

Similarly, K_1 , K_5 , and K_6 are calculated as

$$K_1 = 0.9224$$

$$K_5 = 0.005$$

$$K_6 = 0.3572.$$

□

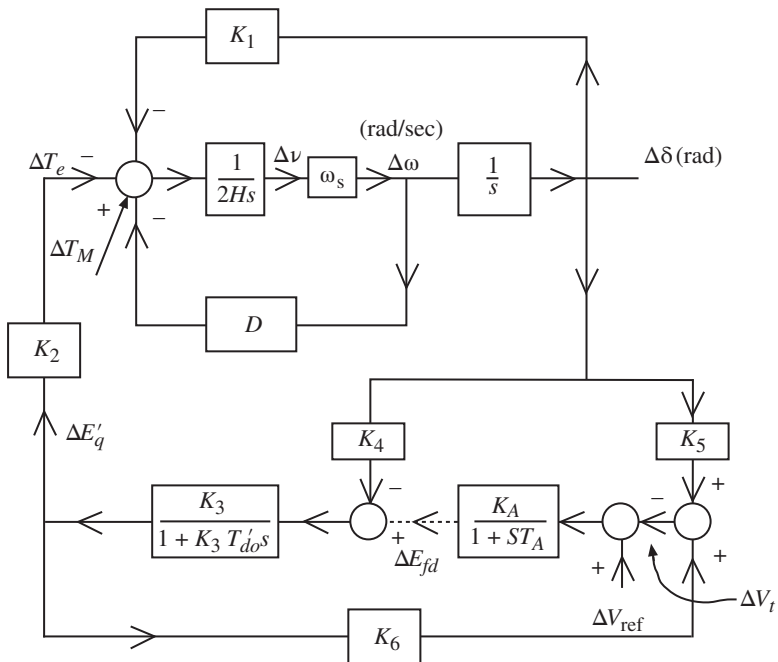


Figure 8.8 Block diagram of the incremental flux-decay model with fast exciter (dotted portion represents the exciter).

8.6.4 Synchronizing and Damping Torques

To the single-machine infinite-bus system of Figure 8.7, we add a fast exciter whose state-space equation is

$$T_A \dot{E}_{fd} = -E_{fd} + K_A(V_{\text{ref}} - V_t). \quad (8.139)$$

The linearized form of (8.139) is

$$T_A \Delta \dot{E}_{fd} = -\Delta E_{fd} + K_A(\Delta V_{\text{ref}} - \Delta V_t). \quad (8.140)$$

Then the machine differential equations (8.127)–(8.129), the exciter equation (8.140), and the algebraic equation (8.136) can be put in the block diagram form shown in Figure 8.8. Both the normalized frequency ν and ω in rad/sec are shown. System loading, as well as the external network parameter X_e , affect the parameters K_1 – K_6 . Generally these are > 0 , but under heavy loading, K_5 might become negative, contributing to negative damping and instability, as we explain below.

8.6.5 Damping of Electromechanical Modes

There are two ways to explain the damping phenomena:

1. State-space analysis [96]
2. Frequency-domain analysis [85]

1. State-space analysis (assume that $\Delta T_M \equiv 0$)

Equations (8.127)–(8.129) are rewritten in matrix form as

$$\begin{bmatrix} \Delta \dot{E}'_q \\ \Delta \dot{\delta} \\ \Delta \dot{v} \end{bmatrix} = \begin{bmatrix} -\frac{1}{K_3 T'_{do}} & \frac{-K_4}{T'_{do}} & 0 \\ 0 & 0 & \omega_s \\ \frac{-K_2}{2H} & \frac{-K_1}{2H} & -\frac{D\omega_s}{2H} \end{bmatrix} \begin{bmatrix} \Delta E'_q \\ \Delta \delta \\ \Delta v \end{bmatrix} + \begin{bmatrix} \frac{1}{T'_{do}} \\ 0 \\ 0 \end{bmatrix} \Delta E_{fd}. \quad (8.141)$$

Note that, instead of $\Delta\omega$, we have used the normalized frequency deviation $\Delta v = \Delta\omega/\omega_s$. Hence, the last row in (8.141) is

$$\Delta \dot{v} = -\frac{K_2}{2H} \Delta E'_q - \frac{K_1}{2H} \Delta \delta - \frac{D\omega_s}{2H} \Delta v. \quad (8.142)$$

ΔE_{fd} is the perturbation in the field voltage. Without the exciter, the machine is said to be on “manual control.” The matrix generally has a pair of complex eigenvalues and a negative real eigenvalue. The former corresponds to the electromechanical mode (1 to 3-Hz range), and the latter the flux-decay mode. Without the exciter (i.e., $K_A = 0$), there are three loops in the block diagram (Figure 8.8), the top two loops corresponding to the complex pair of eigenvalues, and the bottom loop due to $\Delta E'_q$ through K_4 , resulting in the real eigenvalue. Note that the bottom loop contributes to positive feedback. Hence, the torque-angle eigenvalues tend to move to the left-half plane, and the negative real eigenvalue to the right. Thus, with constant E_{fd} , there is “natural” damping. With enough gain, the real pole may go to the right-half plane. This is referred to as monotonic instability. In the power literature, this twofold effect is described in more graphic physical terms. The effect of the lag associated with the time constant T'_{do} is to increase the damping torque but to decrease the synchronizing torque. Now, if we add the exciter through the simplified representation, the state-space equation will now be modified by making ΔE_{fd} a state variable. The equation for ΔE_{fd} is given by (8.140) as

$$\begin{aligned} \Delta \dot{E}_{fd} &= -\frac{1}{T_A} \Delta E_{fd} + \frac{K_A}{T_A} (\Delta V_{ref} - \Delta V_t) \\ &= -\frac{1}{T_A} \Delta E_{fd} - \frac{K_A K_5}{T_A} \Delta \delta - \frac{K_A K_6}{T_A} \Delta E'_q + \frac{K_A}{T_A} \Delta V_{ref}. \end{aligned} \quad (8.143)$$

Ignoring the dynamics of the exciter for the moment, if $K_5 < 0$ and K_A is large enough, then the gain through T'_{do} is approximately $-(K_4 + K_A K_5)K_3$. This gain may become positive, resulting in negative feedback for the torque-angle loop and pushing the complex pair to the right-half plane. Hence, this complicated action should be studied carefully. The overall state-space model for Figure 8.8 becomes

$$\begin{bmatrix} \Delta \dot{E}'_q \\ \Delta \dot{\delta} \\ \Delta \dot{v} \\ \Delta \dot{E}_{fd} \end{bmatrix} = \begin{bmatrix} -1 & \frac{-K_4}{T'_{do}} & 0 & \frac{1}{T'_{do}} \\ \frac{K_3 T'_{do}}{T_A} & 0 & \omega_s & 0 \\ 0 & 0 & 0 & 0 \\ \frac{-K_2}{2H} & \frac{-K_1}{2H} & -\frac{D\omega_s}{2H} & 0 \\ \frac{-K_A K_6}{T_A} & \frac{-K_A K_5}{T_A} & 0 & \frac{-1}{T_A} \end{bmatrix} \begin{bmatrix} \Delta E'_q \\ \Delta \delta \\ \Delta v \\ \Delta E_{fd} \end{bmatrix} + \begin{bmatrix} 0 \\ 0 \\ 0 \\ \frac{K_A}{T_A} \end{bmatrix} \Delta V_{ref}. \quad (8.144)$$

The exciter introduces an additional negative real eigenvalue.

Example 8.6 For the following two test systems whose $K_1 - K_6$ constants and other parameters are given, find the eigenvalues for $K_A = 50$. Plot the root locus for varying K_A . Note that in system 1 $K_5 > 0$, and in system 2 $K_5 < 0$.

Test System 1

$$\begin{aligned} K_1 &= 3.7585 & K_2 &= 3.6816 \\ K_3 &= 0.2162 & K_4 &= 2.6582 \\ K_5 &= 0.0544 & K_6 &= 0.3616 \\ T'_{do} &= 5 \text{ sec} & H &= 6 \text{ sec} \\ T_A &= 0.2 \text{ sec.} \end{aligned}$$

Test System 2

$$\begin{aligned} K_1 &= 0.9831 & K_2 &= 1.0923 \\ K_3 &= 0.3864 & K_4 &= 1.4746 \\ K_5 &= -0.1103 & K_6 &= 0.4477 \\ T'_{do} &= 5 \text{ sec} & H &= 6 \text{ sec} \\ T_A &= 0.2 \text{ sec.} \end{aligned}$$

The eigenvalues for $K_A = 50$ are shown below using (8.144).

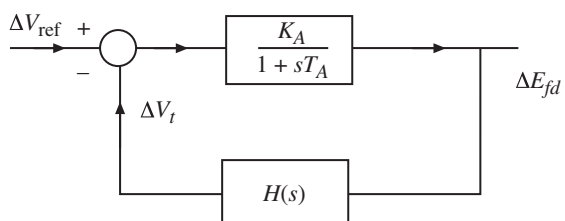
Test System 1	Test System 2
$-0.353 \pm j10.946$	$0.015 \pm j5.38$
$-2.61 \pm j3.22$	$-2.77 \pm j2.88$

Notice that test system 2 is unstable for this value of gain. The root loci for the two systems can be drawn using MATLAB. An alternative way to draw the root locus is to remove the exciter and compute the transfer function $\frac{\Delta V_t(s)}{\Delta E_{fd}(s)} = H(s)$ in Figure 8.8. Note that $H(s)$ includes all the dynamics except that of the exciter. With the $G(s) = \frac{K_A}{1+0.2s}$, we can view $H(s)$ as a feedback transfer function, as in Figure 8.9. $H(s)$ can be computed for each of the two systems as

System 1

$$H(s) = \frac{0.0723s^2 + 7.2811}{s^3 + 0.9251s^2 + 118.0795s + 47.74}.$$

Figure 8.9 Small-signal model viewed as a feedback system.



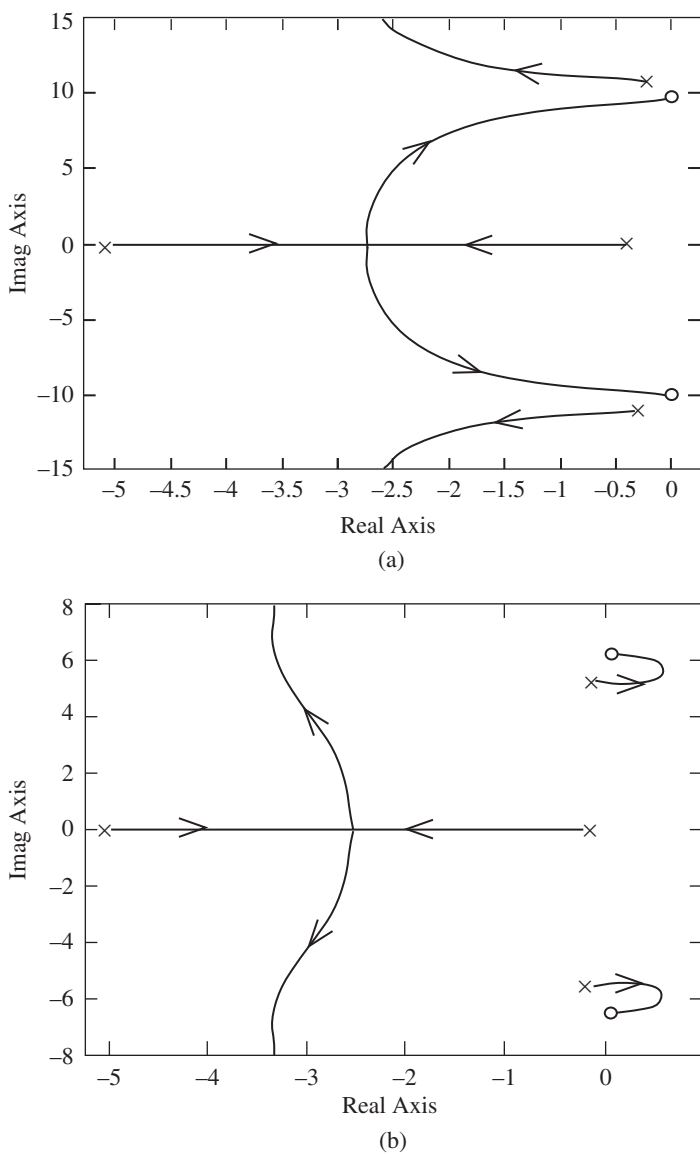


Figure 8.10 Root loci for (a) test system and (b) test system 2.

System 2

$$H(s) = \frac{0.0895s^2 + 3.5225}{s^3 + 0.5176s^2 + 30.886s^2 + 5.866}.$$

The closed-loop characteristic equation is given by $1 + G(s)H(s) = 0$, where $G(s) = \frac{K_A}{1+0.2s}$. The root locus for each of the two test systems is shown in Figure 8.10. System 1 is stable for all values of gain, whereas system 2 becomes unstable for $K_A = 22.108$. \square

2. Frequency-domain analysis through block diagram

For simplicity, assume that the exciter is simply a high constant gain K_A , i.e., assume $T_A = 0$ in Figure 8.10. Now, we can compute the transfer function $\Delta E'_q(s)/\Delta\delta(s)$ as

$$\frac{\Delta E'_q(s)}{\Delta\delta(s)} = \frac{-K_3(K_4 + K_A K_5)}{1 + K_A K_3 K_6 + s K_3 T'_{do}}. \quad (8.145)$$

This assumes that $\Delta V_{ref} = 0$. The effect of the feedback around T'_{do} is to reduce the time constant. If $K_5 > 0$, the overall situation does not differ qualitatively from the case without the exciter, i.e., the system has three open loop poles, with one of them being complex and positive feedback. Thus, the real pole tends to move into the right-half plane. If $K_5 < 0$ and, consequently, $K_4 + K_A K_5 < 0$, the feedback from $\Delta\delta$ to ΔT_e changes from positive to negative, and, with a large enough gain K_A , the electromechanical modes may move to the right-half plane and the real eigenvalue to the left on the real axis. The situation is changed in detail, but not in its general features, if a more detailed exciter model is considered.

Thus, a fast-acting exciter is bad for damping, but it has beneficial effects also. It minimizes voltage fluctuations, increases the synchronizing torque, and improves transient stability. With the time constant T_A present,

$$\frac{\Delta E'_q(s)}{\Delta\delta(s)} = \frac{-[(K_4(1 + sT_A) + K_A K_5)K_3]}{K_A K_6 K_3 + (1 + K_3 T'_{do})s(1 + sT_A)}. \quad (8.146)$$

The contribution of this expression to the torque-angle loop is given by

$$\frac{\Delta T_e(s)}{\Delta\delta(s)} = K_2 \frac{\Delta E'_q(s)}{\Delta\delta(s)} \stackrel{\Delta}{=} H(s). \quad (8.147)$$

8.6.6 Torque-Angle Loop

Letting $\Delta T_M = 0$, the torque-angle loop is given by Figure 8.11. The undamped frequency of the torque-angle loop ($D \equiv 0$) is given by the roots of the characteristic equation

$$\frac{2H}{\omega_s} s^2 + K_1 = 0 \quad (8.148)$$

$$s_{1,2} = \pm j \sqrt{\frac{K_1 \omega_s}{2H}} \text{ rad/sec.} \quad (8.149)$$

With a higher synchronizing torque coefficient K_1 and lower H , $s_{1,2}$ is higher. K_1 is a complicated expression involving loading conditions and external reactances. The value of D is generally small and, hence, neglected.

We wish to compute the damping due to E'_q . The overall block diagram neglecting damping is shown in Figure 8.12. From this diagram and the closed-loop transfer function, it can be verified that the characteristic equation is given by

$$\frac{2H}{\omega_s} s^2 \Delta\delta + K_1 \Delta\delta + H(s) \Delta\delta = 0. \quad (8.150)$$

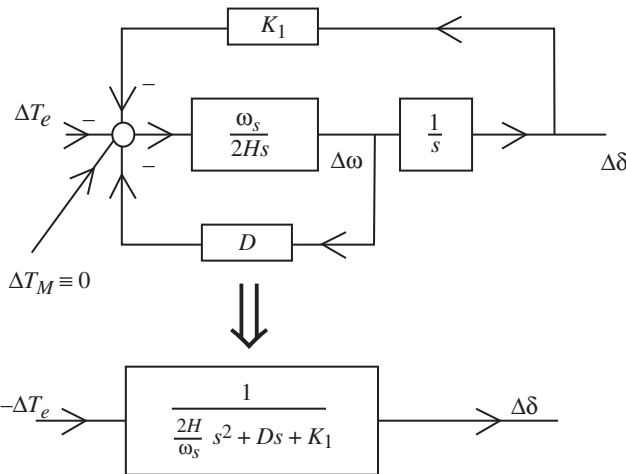


Figure 8.11 Torque-angle loop.

$H(s)\Delta\delta$ therefore contributes to both the synchronizing torque and the damping torque. The contributions are now computed approximately. At oscillation frequencies of 1 to 3 Hz, it can be shown that K_4 has negligible effect.

Neglecting the effect of K_4 in Figure 8.8, we get from (8.147)

$$H(s) = \frac{-K_2 K_A K_5}{\frac{1}{K_3} + K_A K_6 + s \left(\frac{T_A}{K_3} + T'_{do} \right) + s^2 T'_{do} T_A}. \quad (8.151)$$

Let $s = j\omega$. Then

$$\begin{aligned} H(j\omega) &= \frac{-K_2 K_A K_5}{\left(\frac{1}{K_3} + K_A K_6 - \omega^2 T'_{do} K_A \right) + j\omega \left(\frac{T_A}{K_3} + T'_{do} \right)} \\ &= \frac{-K_2 K_A K_5 (x - jy)}{x^2 + y^2} \end{aligned} \quad (8.152)$$

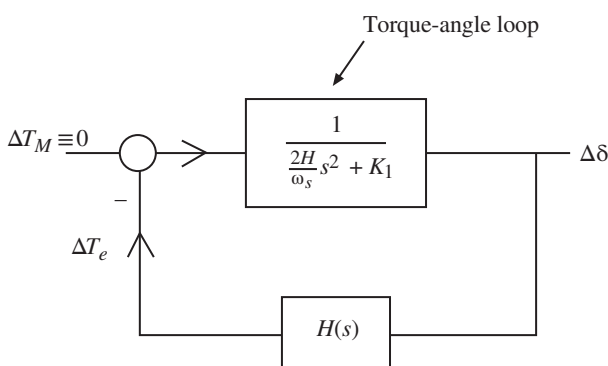


Figure 8.12 Torque-angle loop with other dynamics added.

where

$$x = \frac{1}{K_3} + K_A K_6 - \omega^2 T'_{do} T_A \quad (8.153)$$

$$y = \omega \left(\frac{T_A}{K_3} + T'_{do} \right). \quad (8.154)$$

From (8.150), it is clear that, at the oscillation frequency, if $\text{Im}[H(j\omega)] > 0$, positive damping is implied, that is, the roots move to the left-half plane. If $\text{Im}[H(j\omega)] < 0$, it tends to make the system unstable, i.e., negative damping results. Thus

$$\begin{aligned} \text{Re}[H(j\omega)] &= \frac{-K_2 K_A K_5 x}{x^2 + y^2} \stackrel{\Delta}{=} \text{contribution to the synchronizing} \\ &\quad \text{torque component due to } H(s) \end{aligned} \quad (8.155)$$

$$\begin{aligned} \text{Im}[H(j\omega)] &= \frac{+K_2 K_A K_5 y}{x^2 + y^2} \stackrel{\Delta}{=} \text{contribution to damping} \\ &\quad \text{torque component due to } H(s) \end{aligned} \quad (8.156)$$

8.6.7 Synchronizing Torque

For low frequencies, we set $\omega \approx 0$. Thus, from (8.155):

$$\text{Re}[H(j\omega)] = \frac{-K_2 K_A K_5}{\frac{1}{K_3} + K_A K_6} \approx \frac{-K_2 K_5}{K_6} \text{ for high } K_A. \quad (8.157)$$

Thus, the total synchronizing component is $K_1 - \frac{K_2 K_5}{K_6} > 0$. K_1 is usually high, so that even with $K_5 > 0$ (low to medium external impedance and low-to-medium loadings), $\frac{K_1 - K_2 K_5}{K_6} > 0$. With $K_5 < 0$ (moderate to high external impedance and heavy loadings), the synchronizing torque is enhanced positively.

8.6.8 Damping Torque

$$\text{Im}[H(j\omega)] = \frac{K_2 K_A K_5 \left(\frac{T_A}{K_3} + T'_{do} \right) \omega}{x^2 + y^2}. \quad (8.158)$$

This expression contributes to positive damping for $K_5 > 0$ but negative damping for $K_5 < 0$, which is a cause for concern. Further, with $K_5 < 0$, a higher K_A spells trouble (see Figure 8.10). This may offset the inherent machine damping torque D . To introduce damping, a power system stabilizer (PSS) is therefore introduced. The stabilizing signal may be Δv , ΔP_{acc} , or a combination of both. We discuss this briefly next. For an extensive discussion of PSS design, the reader is referred to the literature [84, 85].

8.6.9 Power System Stabilizer Design

Speed Input PSS

Stabilizing signals derived from machine speed, terminal frequency, or power are processed through a device called the power system stabilizer (PSS) with a transfer function $G(s)$ and its output connected to the input of the exciter. Figure 8.13 shows the PSS with speed input and the signal path from Δv to the torque-angle loop.

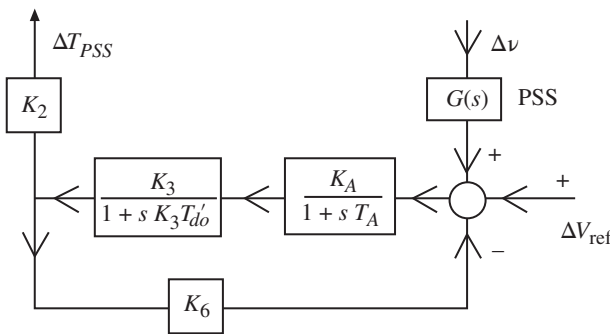


Figure 8.13 Speed input PSS.

8.6.10 Frequency-Domain Approach [85]

From Figure 8.13, the contribution of the PSS to the torque-angle loop is (assuming $\Delta V_{\text{ref}} \equiv 0$ and $\Delta\delta \equiv 0$)

$$\begin{aligned}
 \frac{\Delta T_{\text{PSS}}}{\Delta v} &= \frac{G(s)K_2K_AK_3}{K_AK_3K_6 + (1 + sK_3T'_{do})(1 + sT_A)} \\
 &= \frac{G(s)K_2K_A}{\left(\frac{1}{K_3} + K_AK_6\right) + s\left(\frac{T_A}{K_3} + T'_{do}\right) + s^2T'_{do}T_A} \\
 &= G(s)\text{GEP}(s).
 \end{aligned} \tag{8.159}$$

For the usual range of constants [85], the above expression can be approximated as

$$\approx \frac{G(s)K_2K_A}{\left(\frac{1}{K_3} + K_AK_6\right)[1 + s(T'_{do}/K_AK_6)](1 + sT_A)}. \tag{8.160}$$

For large values of K_A (high gain exciter), this is further approximated by

$$\frac{\Delta T_{\text{PSS}}}{\Delta v} = \frac{K_2}{K_6} \frac{G(s)}{[1 + s(T'_{do}/K_AK_6)][1 + sT_A]}. \tag{8.161}$$

If this were to provide pure damping throughout the frequency range, then $G(s)$ should be a pure lead function with zeros, that is, $G(s) = K_{\text{PSS}}[1 + s(T'_{do}/K_AK_6)](1 + sT_A)$ where K_{PSS} = gain of the PSS. Such a function is not physically realizable. Hence, we have a compromise resulting in what is called a lead-lag type transfer function such that it provides enough phase lead over the expected range of frequencies. For design purposes, $G(s)$ is of the form

$$G(s) = K_{\text{PSS}} \frac{(1 + sT_1)(1 + sT_3)}{(1 + sT_2)(1 + sT_4)} \frac{sT_W}{(1 + sT_W)} = K_{\text{PSS}}G_1(s). \tag{8.162}$$

The time constants T_1 , T_2 , T_3 , T_4 should be set to provide damping over the range of frequencies at which oscillations are likely to occur. Over this range they should compensate for the phase lag introduced by the machine and the regulator. A typical

technique [84] is to compensate for the phase lag in the absence of PSS such that the net phase lag is:

1. Between 0 to 45° from 0.3 to 1 Hz.
2. Less than 90° up to 3 Hz.

Typical values of the parameters are:

K_{PSS} is in the range of 0.1 to 50

T_1 is the lead time constant, 0.2 to 1.5 sec

T_2 is the lag time constant, 0.02 to 0.15 sec

T_3 is the lead time constant, 0.2 to 1.5 sec

T_4 is the lag time constant, 0.02 to 0.15 sec.

The desired stabilizer gain is obtained by first finding the gain at which the system becomes unstable. This may be obtained by actual test or by root locus study. T_W , called the washout time constant, is set at 10 sec. The purpose of this constant is to ensure that there is no steady-state error of voltage reference due to speed deviation. K_{PSS} is set at $\frac{1}{3}K_{PSS}^*$, where K_{PSS}^* is the gain at which the system becomes unstable [84].

It is important to avoid interaction between the PSS and the torsional modes of vibration. Analysis has revealed that such interaction can occur on nearly all modern excitation systems, as they have relatively high gain at high frequencies. A stabilizer-torsional instability with a high-response excitation system may result in shaft damage, particularly at light generator loads where the inherent mechanical damping is small. Even if shaft damage does not occur, such an instability can cause saturation of the stabilizer output, causing it to be ineffective, and possibly causing saturation of the voltage regulator, resulting in loss of synchronism and tripping the unit. It is imperative that stabilizers do not induce torsional instabilities. Hence, the PSS is put in series with another transfer function $FILT(s)$ [84]. A typical value of $FILT(s) \approx \frac{570}{570+35s+s^2}$. The overall transfer function of PSS is $G(s)FILT(s)$.

8.6.11 Design Procedure Using the Frequency-Domain Method

The following procedure is adapted from [96, 97]. In Figure 8.13, let

$$\frac{\Delta T_{PSS}}{\Delta v} = GEP(s)G(s) \quad (8.163)$$

where $GEP(s)$ from (8.159) is given by

$$GEP(s) = \frac{K_2 K_A K_3}{K_A K_3 K_6 + (1 + sT'_{do} K_3)(1 + sT_A)}. \quad (8.164)$$

Step 1: Neglecting the damping due to all other sources, find the undamped natural frequency ω_n in rad/sec of the torque-angle loop from

$$\frac{2H}{\omega_s} s^2 + K_1 = 0, \text{ i.e., } s_{1,2} = \pm j\omega_n, \text{ where } \omega_n = \sqrt{\frac{K_1 \omega_s}{2H}}. \quad (8.165)$$

Step 2: Find the phase lag of $GEP(s)$ at $s = j\omega_n$ in (8.164).

Step 3: Adjust the phase lead of $G(s)$ in (8.163) such that

$$\angle G(s) \mid_{s=j\omega_n} + \angle GEP(s) \mid_{s=j\omega_n} = 0. \quad (8.166)$$

Let

$$G(s) = K_{PSS} \left(\frac{1+sT_1}{1+sT_2} \right)^k \quad (8.167)$$

ignoring the washout filter whose net phase contribution is approximately zero. $k = 1$ or 2 with $T_1 > T_2$. Thus, if $k = 1$:

$$\angle 1 + j\omega_n T_1 = \angle 1 + j\omega_n T_2 - \angle GEP(j\omega_n). \quad (8.168)$$

Knowing ω_n and $\angle GEP(j\omega_n)$, we can select T_1, T_2 can be chosen as some value between 0.02 to 0.15 sec.

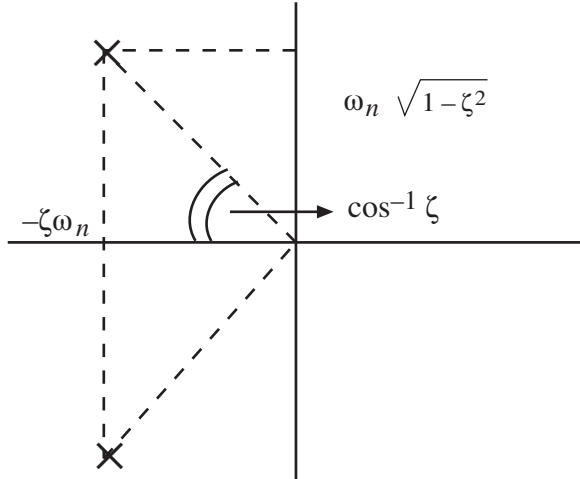
Step 4: To compute K_{PSS} , we can compute K_{PSS}^* , i.e., the gain at which the system becomes unstable using the root locus, and then have $K_{PSS} = \frac{1}{3}K_{PSS}^*$. An alternative procedure that avoids having to do the root locus is to design for a damping ratio ξ due to PSS alone. In a second-order system whose characteristic equation is

$$\frac{2H}{\omega_s} s^2 + Ds + K_1 = 0. \quad (8.169)$$

The damping ratio is $\xi = \frac{1}{2}D/\sqrt{MK_1}$ where $M = 2H/\omega_s$. This is shown in Figure 8.14. The characteristic roots of (8.169) are

$$\begin{aligned} s_{1,2} &= -\frac{-\frac{D}{M} \pm \sqrt{\left(\frac{D}{M}\right)^2 - \frac{4K_1}{M}}}{2} \\ &= -\frac{D}{2M} \pm j\sqrt{\frac{K_1}{M} - \left(\frac{D}{2M}\right)^2} \text{ if } \left(\frac{D}{M}\right)^2 < \frac{4K_1}{M} \\ &= -\xi\omega_n \pm j\omega_n\sqrt{1-\xi^2}. \end{aligned}$$

Figure 8.14 Damping ratio.



We note that $\omega_n = \sqrt{\frac{K_1}{M}}$. Therefore

$$\xi = \frac{D}{2M\omega_n} = \frac{D}{2M} \sqrt{\frac{M}{K_1}} = \frac{D}{2\sqrt{K_1 M}}. \quad (8.170)$$

Verify that

$$\omega_n^2 \xi^2 = \frac{K_1}{M} \cdot \frac{D^2}{4K_1 M} = \left(\frac{D}{2M} \right)^2.$$

To revert to step 4, since the phase lead of $G(s)$ cancels phase lag due to $GEP(s)$ at the oscillation frequency, the contribution of the PSS through $GEP(s)$ is a pure damping torque with a damping coefficient D_{PSS} . Thus, again ignoring the phase contribution of the washout filter,

$$D_{PSS} = K_{PSS} | GEP(s) |_{s=j\omega_n} || G_1(s) |_{s=j\omega_n} |. \quad (8.171)$$

Therefore, the characteristic equation is

$$s^2 + \frac{D_{PSS}}{M}s + \frac{K_1}{M} = 0 \quad (8.172)$$

that is, $s^2 + 2\xi\omega_n s + \omega_n^2 = 0$. As a result,

$$D_{PSS} = 2\xi\omega_n M = K_{PSS} | GEP(j\omega_n) || G_1(j\omega_n) |. \quad (8.173)$$

We can thus find K_{PSS} , knowing ω_n and the desired ξ . A reasonable choice for ξ is between 0.1 and 0.3.

Step 5: Design of the washout time constant is now discussed. The PSS should be activated only when low-frequency oscillations develop and should be automatically terminated when the system oscillation ceases. It should not interfere with the regular function of the excitation system during steady-state operation of the system frequency. The washout stage has the transfer function

$$G_W(s) = \frac{sT_W}{1+sT_W}. \quad (8.174)$$

Since the washout filter should not have any effect on phase shift or gain at the oscillating frequency, it can be achieved by choosing a large value of T_W so that sT_W is much larger than unity

$$G_W(j\omega_n) \approx 1. \quad (8.175)$$

Hence, its phase contribution is close to zero. The PSS will not have any effect on the steady state of the system since, in steady state,

$$\Delta v = 0 \quad (8.176)$$

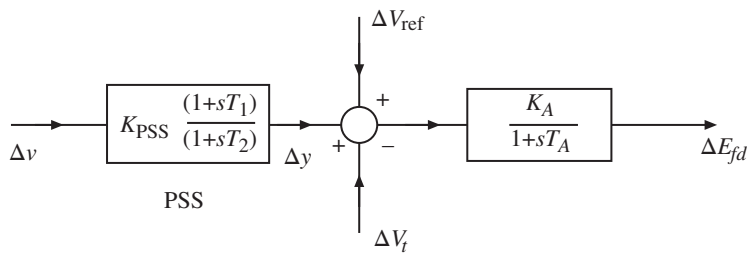


Figure 8.15 Exciter with PSS.

Example 8.7 The purpose of this example is to show that the introduction of the PSS will improve the damping of the electromechanical mode. Without the PSS, the A matrix, for example, 8.5, is calculated as

$$\begin{bmatrix} -0.3511 & -0.236 & 0 & 0.104 \\ 0 & 0 & 377 & 0 \\ -0.1678 & -0.144 & 0 & 0 \\ -714.4 & -10 & 0 & -5 \end{bmatrix}.$$

The eigenvalues are $\lambda_{1,2} = -0.0875 \pm j7.11$, $\lambda_{3,4} = -2.588 \pm j8.495$. The electromechanical mode $\lambda_{1,2}$ is poorly damped. Instead of a two-stage lag lead compensator, we will have a single-stage lag-lead PSS. Assume that the damping D in the torque-angle loop is zero. The input to the stabilizer is Δv . An extra state equation will be added. The washout stage is omitted, since its objective is to offset only the dc steady-state error. Hence, it does not play any role in the design. The block diagram in Figure 8.15 shows a single lag-lead stage of the PSS. The added state equation due to the PSS is

$$\begin{aligned} \Delta \dot{y} &= -\frac{1}{T_2} \Delta y + \frac{K_{PSS}}{T_2} \Delta v + K_{PSS} \frac{T_1}{T_2} \Delta \dot{v} \\ &= -\frac{1}{T_2} \Delta y + \frac{K_{PSS}}{T_2} \Delta v + K_{PSS} \frac{T_1}{T_2} \left(\frac{-K_2}{2H} \Delta E'_q - \frac{K_1}{2H} \Delta \delta \right). \end{aligned} \quad (8.177)$$

The new A matrix is given as

$$\begin{bmatrix} -1 & -K_4 & 0 & \frac{1}{T'_do} & 0 \\ K_3 T'_{do} & T'_{do} & 377 & 0 & 0 \\ 0 & 0 & 0 & 0 & 0 \\ \frac{-K_2}{2H} & \frac{-K_1}{2H} & 0 & 0 & 0 \\ \frac{K_A K_6}{T_A} & \frac{-K_A K_5}{T_A} & 0 & \frac{-1}{T_A} & \frac{K_A}{T_A} \\ \frac{-K_2 T_1}{T_2} \left(\frac{K_{PSS}}{2H} \right) & \frac{-K_1 T_1}{T_2} \left(\frac{K_{PSS}}{2H} \right) & \frac{K_{PSS}}{T_2} & 0 & \frac{-1}{T_2} \end{bmatrix}.$$

With a choice of $K_{PSS} = 0.5$, $T_1 = 0.5$, $T_2 = 0.1$, the new A matrix is

$$\begin{bmatrix} -0.3511 & -0.236 & 0 & 0.104 & 0 \\ 0 & 0 & 377 & 0 & 0 \\ -0.1678 & -0.144 & 0 & 0 & 0 \\ -714.4 & -10 & 0 & -5 & 2000 \\ -0.42 & -0.36 & 5 & 0 & -10 \end{bmatrix}$$

and the eigenvalues are $\lambda_{1,2} = -0.8612 \pm j7.0742$, $\lambda_{3,4} = -1.6314 \pm j8.5504$, $\lambda_5 = -10.3661$. Note the improvement in damping of the electromechanical mode $\lambda_{1,2}$. \square

8.7 Conclusion

In this chapter, we have discussed linear models of single and multimachine systems with different degrees of machine and load modeling. The effect of different types of loading on the steady-state stability was discussed for the multimachine case; Hopf bifurcation in the context of voltage collapse was discussed. The design of a power-system stabilizer for damping the local mode of oscillation was discussed for the single-machine infinite-bus case.

8.8 Problems

- 8.1** The single line diagram for the two-area system is given in Figure 8.16.

The transmission line data, machine data, excitation system data, and load-flow results are given in Tables 8.8, 8.9, 8.10, and 8.11.

1. Using the two-axis model for the generator and constant power load representation, obtain eigenvalues of the linearized system.
2. Repeat (a) with one tie line out of service. Any comments?

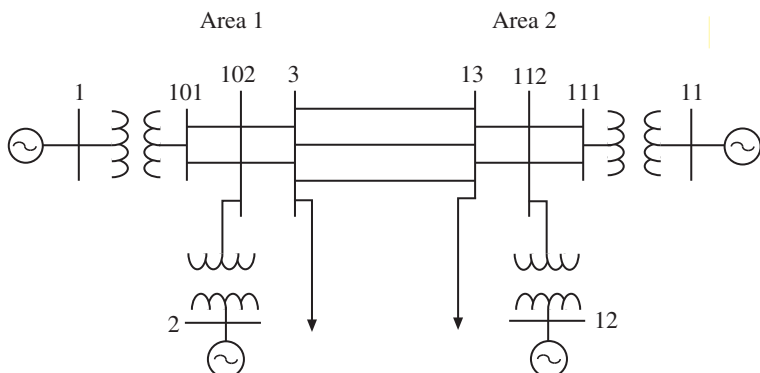


Figure 8.16 Two-area system.

Table 8.8 Transmission Line Data on 100 MVA Base.

From Bus Number	To Bus Number	Series Resistance (R_s) pu	Series Reactance (X_s) pu	Shunt Susceptance (B) pu
1	101	0.001	0.012	0.00
2	102	0.001	0.012	0.00
3	13	0.022	0.22	0.33
3	13	0.022	0.22	0.33
3	13	0.022	0.22	0.33
3	102	0.002	0.02	0.03
3	102	0.002	0.02	0.03
11	111	0.001	0.012	0.00
12	112	0.001	0.012	0.00
13	112	0.002	0.02	0.03
13	112	0.002	0.02	0.03
101	102	0.005	0.05	0.075
101	102	0.005	0.05	0.075
111	112	0.005	0.05	0.075
111	112	0.005	0.05	0.075

Table 8.9 Machine Data.

Variable	Machine at Bus 1	Machine at Bus 2	Machine at Bus 11	Machine at Bus 12
X_1 (pu)	0.022	0.022	0.022	0.022
R_s (pu)	0.00028	0.00028	0.00028	0.00028
X_d (pu)	0.2	0.2	0.2	0.2
X'_d (pu)	0.033	0.033	0.033	0.033
T'_{do} (sec)	8.0	8.0	8.0	8.0
X_q (pu)	0.19	0.19	0.19	0.19
X'_q (pu)	0.061	0.061	0.061	0.061
T'_{qo} (sec)	0.4	0.4	0.4	0.4
H (sec)	54.0	54.0	63.0	63.0
D (pu)	0.0	0.0	0.0	0.0

Table 8.10 Excitation System Data.

Variable	Machine at Bus 1	Machine at Bus 2	Machine at Bus 11	Machine at Bus 12
K_A (pu)	200	200	200	200
T_A (sec)	.1	.1	.1	.1

Table 8.11 Load-Flow Results for the System.

Bus Number	Bus Type	Voltage Magnitude (pu)	Angle (degrees)	Real Power Gen. (pu)	Reactive Power Gen. (pu)	Real Power Load (pu)	Reactive Power Load (pu)
1	PV	1.03	8.2154	7.0	1.3386	0.0	0.0
2	PV	1.01	-1.5040	7.0	1.5920	0.0	0.0
11	Swing	1.03	0.0	7.2172	1.4466	0.0	0.0
12	PV	1.01	-10.2051	7.0	1.8083	0.0	0.0
101	PQ	1.0108	3.6615	0.0	0.0	0.0	0.0
102	PQ	0.9875	-6.2433	0.0	0.0	0.0	0.0
111	PQ	1.0095	-4.6977	0.0	0.0	0.0	0.0
112	PQ	0.9850	-14.9443	0.0	0.0	0.0	0.0
3	PQ	0.9761	-14.4194	0.0	0.0	11.59	-0.7350
13	PQ	0.9716	-23.2922	0.0	0.0	15.75	-0.8990

- 8.2** With three tie lines in service, add a PSS at bus 12 with the following parameters. $K_{PSS} = 25$, $T_W = 10$ sec, $T_1 = 0.047$ sec, $T_2 = 0.021$ sec, $T_3 = 3.0$ sec, and $T_4 = 5.4$ sec. What are the new eigenvalues?

- 8.3** Repeat Problem 8.2 with two tie lines in service.

- 8.4** Consider the single machine connected to an infinite bus in Figure 8.7. Assume that $V_\infty = 1.0$. The parameters are as follows:

Line: $R_e = 0.0$, $X_e = 0.4$ pu

Generator: $X_d = 1.6$ pu, $X_q = 1.55$ pu, $X'_d = 0.32$ pu, $T'_{do} = 6.0$ sec, $H = 3.0$ sec
Injected power into the bus: $P = 0.8$ pu, $Q = 0.4$ pu

Exciter: $K_A = 50$, $T_A = 0.05$ sec.

1. Compute the $K1 - K6$ constants.

2. Compute the eigenvalues. (ans: $-14.5662, -5.7351, -0.0808 \pm j8.55$)

- 8.5** In a single-machine-infinite-bus system (Figure 8.17), there is a local load at the generator bus. The parameters are

Line: $R_E = -0.034$ pu, $X_E = 0.977$ pu

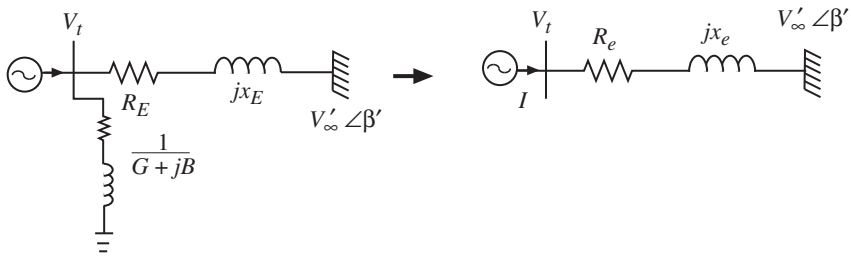


Figure 8.17 Single-machine infinite-bus case (local load).

Generator: $X_D = 0.973$ pu, $X_q = 0.550$ pu, $X'_d = 0.230$ pu, $T'_{do} = 7.76$ sec, $H = 4.63$ sec

Injected power: $P = 1.0$ pu, $Q = 0.015$ pu

Generator terminal voltage: $V_t = 1.05$ pu

Local load (constant impedance): $G = 0.249$ pu, $B = 0.262$ pu

Exciter: $K_A = 50$, $T_A = 0.05$ sec

1. Assuming $\bar{V}_t = V_t \angle 0^\circ$, compute $\bar{V}_\infty = V_\infty \angle \beta$.
2. Compute the Thevenin equivalent looking into the external network from the generator bus as $\bar{V}_{th} = V'_\infty \angle \beta'$ in series with an impedance Z_{th} . Show that

$$R_e + jX_e = \frac{R_E + jX_E}{1 + (R_E + jX_E)(G + jB)}$$

and

$$\bar{V}_{th} = V_\infty \angle \beta \frac{1}{1 + (R_E + jX_E)(G + jB)} = V'_\infty \angle \beta'.$$

3. Compute $\delta(0)$.
4. To apply the results of Section 8.6.2, we set $\beta' = 0$ and replace $\delta(0)$ by $\delta(0) - \beta'$. This makes the infinite bus a reference bus with phase-angle zero.
5. Compute the $K1-K6$ constants and the eigenvalues. (ans: $-10.316 \pm j3.2644$, $-0.2838 \pm j4.9496$)

- 8.6** For each of the two test systems below (Example 8.6), whose $K1-K6$ constants and other parameters are given:

1. Write the state space model in the form (8.144). Assume $D \equiv 0$.
2. Plot the root locus as K_A is varied from a small to a high value. At what value of K_A does instability occur and what are the unstable eigenvalues.
3. Find the eigenvalues at $K_A = 50$.

Test System 1: $K_1 = 3.7585$, $K_2 = 3.6816$, $K_3 = 0.2162$, $K_4 = 2.6582$, $K_5 = 0.0544$, $K_6 = 0.3616$, $T'_{do} = 5$ sec, $H = 6$ sec, $T_A = 0.2$ sec.

Test System 2: $K_1 = 0.9831$, $K_2 = 1.0923$, $K_3 = 0.3864$, $K_4 = 1.4746$, $K_5 = -0.1103$, $K_6 = 0.4477$, $T'_{do} = 5$ sec, $H = 6$ sec, $T_A = 0.24$ sec.

- 8.7** A single machine with a flux-decay model and a fast exciter is connected to an infinite bus through a reactance of $j0.5$ pu. The generator terminal voltage is $1 \angle 15^\circ$

and the infinite bus voltage is $1.05\angle 0^\circ$. The parameters and initial conditions of the state variables are given below.

Parameters

$$\begin{aligned} H &= 3.2 \text{ sec}, T'_{do} = 9.6 \text{ sec}, K_A = 400, T_A = 0.2 \text{ sec} \\ R_s &= 0.0017 \text{ pu}, X_q = 2.1 \text{ pu}, X_d = 2.5 \text{ pu}, X'_d = 0.39 \text{ pu} \\ D &\equiv 0, \omega_s = 377 \text{ rad/sec} \end{aligned}$$

Initial conditions using the flux-decay model and the fast exciter

$$\delta(0) = 65.52^\circ, V_d(0) = 0.7719, V_q(0) = 0.6358$$

$$I_d(0) = 0.3999, I_q(0) = 0.3662$$

$$E'_q(0) = 0.7949, E_{fd}(0) = 1.6387, \omega(0) = 377 \text{ rad/sec}$$

$$V_{\text{ref}} = 1.0041, T_M = 0.542$$

1. Compute the $K1-K6$ constants and the undamped natural frequency of the torque-angle loop.
2. Compute the eigenvalues.

- 8.8** Find the participation factors of the eigenvalues for the following systems, where $\dot{x} = Ax$.

$$1. \quad A = \begin{bmatrix} 3 & 8 \\ 2 & 3 \end{bmatrix}$$

$$2. \quad A = \begin{bmatrix} 1 & 2 & 1 \\ 0 & 3 & 1 \\ 0 & 5 & -1 \end{bmatrix}.$$

9

Energy Function Methods

9.1 Background

In this chapter, we discuss energy function methods for transient stability analysis. In transient stability, we are interested in computing the critical clearing time of circuit breakers to clear a fault when the system is subjected to large disturbances. In real-world applications, the critical clearing time can be interpreted in terms of meaningful quantities such as maximum power transfer in the prefault state. The energy function methods have proved to be reliable after many decades of research [100, 103]. It is now considered a promising tool in dynamic security assessment.

9.2 Physical and Mathematical Aspects of the Problem

The ultimate objective of nonlinear dynamic simulation of power systems is to see whether synchronism is preserved in the event of a disturbance. This is judged by the variation of rotor angles as a function of time. If the rotor angle δ_i of a machine or a group of machines continues to increase with respect to the rest of the system, the system is unstable. The rotor angle δ_i of each machine is measured with respect to a fixed rotating reference frame that is the synchronous network reference frame. Hence, instability of a machine means that the rotor angle of machine i pulls away from the rest of the system. Thus, relative rotor angles rather than absolute rotor angles must be monitored to test stability/instability. Figure 9.1 shows the rotor angles for the cases of stability and instability. Figure 9.1(a) shows that all relative rotor angles are finite, as $t \rightarrow \infty$. In Figure 9.1(b), the rotor angle of one machine is increasing with respect to the rest of the system; hence, it is a single-machine instability. Figure 9.1(c) is a group of two machines going unstable with respect to the rest of the system.

In its simplest form, a power system undergoing a disturbance can be described by a set of three differential equations:

$$\dot{x}(t) = f^I(x(t)) \quad -\infty < t \leq 0 \quad (9.1)$$

$$\dot{x}(t) = f^F(x(t)) \quad 0 < t \leq t_{cl} \quad (9.2)$$

$$\dot{x}(t) = f(x(t)) \quad t_{cl} < t < \infty \quad (9.3)$$

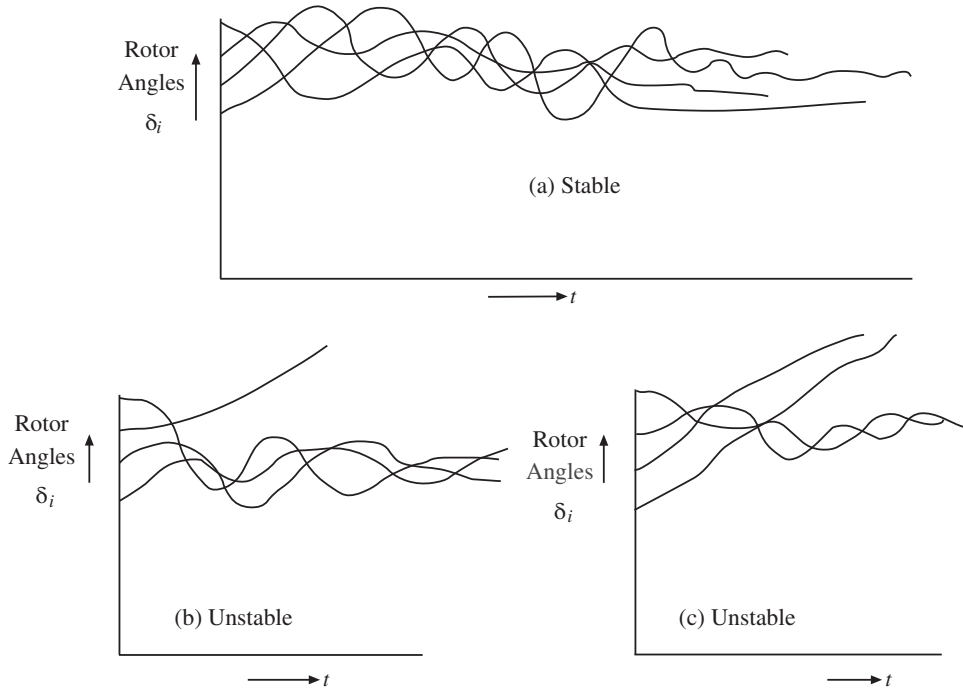


Figure 9.1 Behavior of rotor angles for the (a) stable, and (b), (c) the unstable cases.

$x(t)$ is the vector of state variables of the system at time t . At $t = 0$, a fault occurs in the system and the dynamics change from f^I to f^F . During $0 < t \leq t_{cl}$, called the faulted period, the system is governed by the fault-on dynamics f^F . Actually, before the fault is cleared at $t = t_{cl}$, we may have several switchings in the network, each giving rise to a different f^F . For simplicity, we have taken a single f^F , indicating that there are no structural changes between $t = 0$ and $t = t_{cl}$. When the fault is cleared at $t = t_{cl}$, we have the postfault system with its dynamics $f(x(t))$. In the prefault period $-\infty < t \leq 0$, the system would have settled down to a steady state, so that $x(0) = x_o$ is known. Therefore, we need not discuss (9.1). We then have only

$$\begin{aligned}\dot{x}(t) &= f^F(x(t)) \quad 0 < t \leq t_{cl} \\ x(0) &= x_o\end{aligned}\tag{9.4}$$

and

$$\dot{x}(t) = f(x(t)) \quad t > t_{cl}\tag{9.5}$$

with the initial condition $x(t_{cl})$ for (9.5) provided by the solution of the faulted system (9.4) evaluated at $t = t_{cl}$. Viewed in another manner, the solution of (9.4) provides at each instant of time the possible initial conditions for (9.5). Let us assume that (9.5) has a stable equilibrium point x_s . The question is whether the trajectory $x(t)$ for (9.5) with the initial condition $x(t_{cl})$ will converge to x_s as $t \rightarrow \infty$. The largest value of t_{cl} for which this holds true is called the critical clearing time t_{cr} .

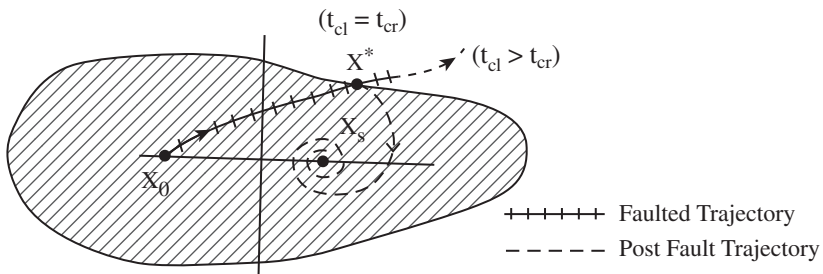


Figure 9.2 Region of attraction and computation of t_{cr} .

From this discussion, it is clear that if we have an accurate estimate of the region of attraction of the postfault stable equilibrium point (s.e.p) x_s , then t_{cr} is obtained when the trajectory of (9.4) exits the region of attraction of (9.5) at $x = x^*$. Figure 9.2 illustrates this concept for a two-dimensional system. The computation of the region of attraction for a general nonlinear dynamical system is far from easy. It is not, in general, a closed region. In the case of power systems with simple-machine models, the characterization of this region has been discussed theoretically in the literature. The stability region consists of surfaces passing through the unstable equilibrium points (u.e.p's) of (9.5). For each fault, the mode of instability (i.e., one or more machines going unstable) may be different if the fault is not cleared in time. We may describe the interior of the region of attraction of the postfault system (9.5) through an inequality of the type $V(x) < V_{cr}$, where $V(x)$ is the Lyapunov or energy function for (9.5). $V(x)$ is generally the sum of the kinetic and potential energies of the postfault system. The computation of V_{cr} , called the critical energy, is different for each fault and is a difficult step. There are currently three basic methods, with a number of variations on each method.

These methods are:

1. Lowest energy u.e.p method [106]

$V_{cr} = V(x^{uc})$, where x^{uc} is the unstable equilibrium point (u.e.p) resulting in the lowest value of V_{cr} among the u.e.p's lying on the stability boundary of (9.5). This requires the computation of many u.e.p's of the postfault system and, hence, is not computationally attractive. Moreover, it gives conservative results. Reference [106] was the first systematic application of Lyapunov's method for transient stability.

2. Potential Energy Boundary Surface (PEBS) method

V_{cr} = maximum value of the potential energy component of $V(x)$ along the trajectory of (9.4). This is known as the potential energy boundary surface (PEBS) method [107].

3. Controlling u.e.p method

$V_{cr} = V(x^u)$, at which x^u is the relevant or controlling u.e.p, that is, the u.e.p closest to the point where the fault-on trajectory of (9.4) exits the region of attraction of (9.5). This is called the controlling u.e.p method first proposed in [104]. The boundary-controlling u.e.p (BCU) method [105] (also called the exit-point method) is an efficient technique to compute this controlling u.e.p.

We will discuss the PEBS method (2) and the controlling u.e.p method (3) in detail. The computation of t_{cr} involves the following steps.

1. Computing x_s , the stable equilibrium point of the postfault system given by (9.5).
2. Formulating $V(x)$ for (9.5). This is not a difficult step. Generally, $V(x)$ is the sum of kinetic and potential energies of the postfault system, i.e., $V(x) = V_{KE} + V_{PE}$.
3. Computation of V_{cr} .
In the PEBS method (2), V_{cr} is obtained by integrating the faulted trajectory in (9.4) until the potential energy part V_{PE} of $V(x)$ reaches a maximum V_{PE}^{\max} . This value is taken as V_{cr} in the PEBS method. In the controlling u.e.p method (3) we integrate (9.4) for a short interval followed by either a minimization problem to get the controlling u.e.p, or integration of a reduced-order postfault system after the PEBS is reached (BCU method) [105] to get the controlling u.e.p x^u . V_{cr} is given by $V(x^u) = V_{PE}(x^u)$, since V_{KE} is zero at an u.e.p.
4. Calculating the time instant t_{cr} when $V(x) = V_{cr}$ on the faulted trajectory of (9.4). The faulted trajectory has to be integrated for all the three methods to obtain t_{cr} . In the PEBS method (2), the faulted trajectory is already available while computing V_{cr} . It is also available in the BCU method. The computation time is least for the PEBS method (2). The relative merits of these various methods and their variations are discussed extensively in the literature [108].

9.3 Lyapunov's Method

In 1892, A. M. Lyapunov, in his famous Ph.D. dissertation [125], proposed that the stability of the equilibrium point of a nonlinear dynamic system of dimension n

$$\dot{x} = f(x) \quad f(0) = 0 \quad (9.6)$$

can be ascertained without numerical integration. He said that if there exists a scalar function $V(x)$ for (9.6) that is positive-definite, i.e., $V(x) > 0$ around the equilibrium point "0" and the derivative $\dot{V}(x) < 0$, then the equilibrium is asymptotically stable. $\dot{V}(x)$ is obtained as $\sum_{i=1}^n \frac{\partial V}{\partial x_i} \dot{x}_i = \sum_{i=1}^n \frac{\partial V}{\partial x_i} f_i(x) = \nabla V^T \cdot f(x)$ where n is the order of the system in (9.6). Thus, $f(x)$ enters directly in the computation of $\dot{V}(x)$. The condition $\dot{V}(x) < 0$ can be relaxed to $\dot{V}(x) \leq 0$, provided that $\dot{V}(x)$ does not vanish along any other solution with the exception of $x = 0$.

$V(x)$ is actually a generalization of the concept of the energy of a system. Since 1948, when the results of Lyapunov appeared in the English language together with potential applications, there has been extensive literature surrounding this topic. Application of the energy function method to power system stability began with the early work of Magnusson [109] and Aylett [110], followed by a formal application of the more general Lyapunov's method by El-Abiad and Nagappan [106]. Reference [106] provided an algorithmic procedure to compute the critical clearing time. It used the lowest energy u.e.p method to compute V_{cr} . Although many different Lyapunov functions have been tried since then, the first integral of motion, which is the sum of kinetic and potential energies, seemed to have provided the best result. In the power literature, Lyapunov's method has become synonymous with the transient energy function (TEF) method and has been applied successfully [100, 105]. Today, this technique has proved to be a

practical tool in dynamic security assessment. To make it a practical tool, it is necessary to compute the region of stability of the equilibrium point of (9.5). In physical systems, it is finite and not the whole state-space. An estimate of the region of stability or attraction is characterized by an inequality of the type $V(x) < V_{cr}$. The computation of V_{cr} remained a formidable barrier for a long time. In the case of a multimachine classical model with loads being treated as constant impedances, there are well-proved algorithms. Extensions to multimachine systems with detailed models have been made [111, 113].

9.4 Modeling Issues

In applying the TEF technique, we must consider the model in two time frames, as follows:

1. Faulted system

$$\dot{x} = f^F(x(t)), \quad 0 < t \leq t_{cl}. \quad (9.7)$$

2. Postfault system

$$\dot{x} = f(x(t)), \quad t > t_{cl}. \quad (9.8)$$

In reality, the model is a set of differential-algebraic equations (DAE), that is,

$$\dot{x} = f^F(x(t), y(t)) \quad (9.9)$$

$$0 = g^F(x(t), y(t)), \quad 0 < t \leq t_{cl} \quad (9.10)$$

and

$$\dot{x} = f(x(t), y(t)) \quad (9.11)$$

$$0 = g(x(t), y(t)), \quad t > t_{cl}. \quad (9.12)$$

The function g represents the nonlinear algebraic equations of the stator and the network, while the differential equations represent the dynamics of the generating unit and its controls. In Chapter 7, the modeling of equations in the form of (9.9) and (9.10) or (9.11) and (9.12) has been covered extensively. Reduced-order models, such as a flux-decay model and a classical model, have also been discussed. In the classical model representation, we can either preserve the network structure (structure-preserving model) or eliminate the load buses (assuming constant impedance load) to obtain the internal-node model. These have also been discussed in Chapter 7. Structure-preserving models involve nonlinear algebraic equations in addition to dynamic equations, and can incorporate nonlinear load models leading to the concept of structure-preserving energy function (SPEF) $V(x, y)$, while models consisting of differential equations lead only to closed-form types of energy functions $V(x)$. The work on SPEF by Bergen and Hill [111] has been extended to more detailed models in [112–115].

It is not clear at this stage whether a more detailed generator or load model will lead to more accurate estimates of t_{cr} . What appears to be true, however, from extensive simulation studies by researchers is that, for the so-called first-swing stability (i.e., instability occurring in 1 to 2 sec interval), the classical model with the loads represented as constant impedance will suffice. This results in only differential equations, as opposed

to DAE equations. Both the PEBS and BCU methods give satisfactory results for this model. We first discuss this in the multimachine context. The swing equations have been derived in Section 7.9.3 (using $P_{mi} = T_{Mi}$) as

$$\frac{2H_i}{\omega_s} \frac{d^2\delta_i}{dt^2} + D_i \frac{d\delta_i}{dt} = P_{mi} - P_{ei}, \quad i = 1, \dots, m \quad (9.13)$$

where

$$P_{ei} = E_i^2 G_{ii} + \sum_{\substack{j=1 \\ \neq i}}^m (C_{ij} \sin \delta_{ij} + D_{ij} \cos \delta_{ij}). \quad (9.14)$$

Denoting $\frac{2H_i}{\omega_s} \stackrel{\Delta}{=} M_i$ and $P_i \stackrel{\Delta}{=} P_{mi} - E_i^2 G_{ii}$, we get

$$M_i \frac{d^2\delta_i}{dt^2} + D_i \frac{d\delta_i}{dt} = P_i - \sum_{j=1 \neq i}^m (C_{ij} \sin \delta_{ij} + D_{ij} \cos \delta_{ij}) \quad (9.15)$$

which can be written as

$$M_i \frac{d^2\delta_i}{dt^2} + D_i \frac{d\delta_i}{dt} = P_i - P_{ei}(\delta_1, \dots, \delta_m), \quad i = 1, \dots, m. \quad (9.16)$$

Let α_i be the rotor angle with respect to a fixed reference. Then $\dot{\delta}_i = \alpha_i - \omega_s t$. $\ddot{\delta}_i = \frac{d\alpha_i}{dt} - \omega_s = \omega_i - \omega_s$, where ω_i is the angular velocity of the rotor and ω_s is the synchronous speed in radians per sec. Thus, both δ_i and $\dot{\delta}_i$ are expressed with respect to a synchronously rotating reference frame. Equation (9.16) is converted to a set of first-order differential equations by introducing the state variables δ_i and ω_i :

$$\dot{\delta}_i = \omega_i - \omega_s \quad (9.17)$$

$$\dot{\omega}_i = \frac{1}{M_i} (P_i - P_{ei}(\delta_1, \dots, \delta_m) - D_i(\omega_i - \omega_s)) \quad i = 1, \dots, m. \quad (9.18)$$

Equations (9.17) and (9.18) are applicable both to the faulted state and the postfault state, with the difference that P_{ei} is different in each case, because the internal node admittance matrix is different for the faulted and postfault system. The model corresponding to (9.17)–(9.18) is known as the internal-node model since the physical buses have been eliminated by network reduction.

9.5 Energy Function Formulation

Prior to 1979, there was considerable research in constructing a Lyapunov function for the system (9.15) using the state-space model given by (9.17) and (9.18) [116–119]. However, analytical Lyapunov functions can be constructed only if the transfer conductances are zero, that is, $D_{ij} \equiv 0$. Since these terms have to be accounted for properly, the first integrals of motion of the system are constructed, and these are called energy functions. We have two options, to use either the relative rotor angle formulation or the center of inertia formulation. We use the latter, since there are some advantages. Since the angles are referred to a center of inertia, the resulting energy function is called the transient energy function (TEF).

In this formulation, the angle of the center of inertia (COI) is used as the reference angle, since it represents the “mean motion” of the system. Although the resulting energy function is identical to $V(\delta, \omega)$ (using relative rotor angles), it has the advantage of being more symmetric and easier to handle in terms of the path-dependent terms. Synchronous stability of all machines is judged by examining the angles referenced only to COI instead of relative rotor angles. Modern literature invariably uses the COI formulation. The energy function in the COI notation, including D_{ij} terms (transfer conductances), was first proposed by Athay et al. [104].

We derive the transient energy function for the conservative system (assuming $D_i \equiv 0$). The center of inertia (COI) for the whole system is defined as

$$\delta_o = \frac{1}{M_T} \sum_{i=1}^m M_i \delta_i \text{ and the center of speed as } \omega_o = \frac{1}{M_T} \sum_{i=1}^m M_i \omega_i \quad (9.19)$$

where $M_T = \sum_{i=1}^m M_i$. We then transform the variables δ_i, ω_i to the COI variables as $\theta_i = \delta_i - \delta_o$, $\tilde{\omega}_i = \omega_i - \omega_o$. It is easy to verify

$$\begin{aligned} \dot{\theta}_i &= \dot{\delta}_i - \dot{\delta}_o \\ &= \omega_i - \omega_o \\ &\stackrel{\Delta}{=} \tilde{\omega}_i. \end{aligned}$$

The swing equations (9.15) with $D_i = 0$ become (omitting the algebra):

$$M_i \frac{d^2\theta_i}{dt^2} = P_i - \sum_{j=1, j \neq i}^m (C_{ij} \sin \theta_{ij} + D_{ij} \cos \theta_{ij}) - \frac{M_i}{M_T} P_{COI} \stackrel{\Delta}{=} f_i(\theta) \quad i = 1, \dots, m \quad (9.20)$$

where

$$P_i = P_{mi} - E_i^2 G_{ii}, \quad P_{COI} = \sum_{i=1}^m P_i - 2 \sum_{i=1}^m \sum_{j=i+1}^m D_{ij} \cos \theta_{ij}.$$

If one of the machines is an infinite bus, say, m whose inertia constant M_m is very large, then $\frac{M_i}{M_T} P_{COI} \approx 0$ ($i \neq m$) and also $\delta_o \approx \delta_m$ and $\omega_o \approx \omega_m$. The COI variables become $\theta_i = \delta_i - \delta_m$ and $\tilde{\omega}_i = \omega_i - \omega_m$. In the literature where the BCU method is discussed [105], δ_m is simply taken as zero. Equation (9.20) is modified accordingly, and there will be only $(m - 1)$ equations after omitting the equation for machine m .

We consider the general case in which all M_i 's are finite. Corresponding to the faulted and the postfault states, we have two sets of differential equations,

$$M_i \frac{d\tilde{\omega}_i}{dt} = f_i^F(\theta) \quad 0 < t \leq t_{cl} \frac{d\theta_i}{dt} = \tilde{\omega}_i, \quad i = 1, 2, \dots, m \quad (9.21)$$

and

$$M_i \frac{d\tilde{\omega}_i}{dt} = f_i(\theta) \quad t > t_{cl} \frac{d\theta_i}{dt} = \tilde{\omega}_i, \quad i = 1, 2, \dots, m. \quad (9.22)$$

Let the postfault system given by (9.22) have the stable equilibrium point at $\theta = \theta^s$, $\tilde{\omega} = 0$. θ^s is obtained by solving the nonlinear algebraic equations

$$f_i(\theta) = 0, \quad i = 1, \dots, m. \quad (9.23)$$

Since $\sum_{i=1}^m M_i \theta_i = 0$, θ_m can be expressed in terms of the other θ_i 's and substituted in (9.23), which is then equivalent to

$$f_i(\theta_1, \dots, \theta_{m-1}) = 0, \quad i = 1, \dots, m-1. \quad (9.24)$$

The basic procedure for computing the critical clearing time consists of the following steps:

1. Construct an energy or Lyapunov function $V(\theta, \tilde{\omega})$ for the system (9.22), that is, the postfault system.
2. Find the critical value of $V(\theta, \tilde{\omega})$ for a given fault denoted by V_{cr} .
3. Integrate (9.21), that is, the faulted equations, until $V(\theta, \tilde{\omega}) = V_{cr}$. This instant of time is called the critical clearing time t_{cr} .

While this procedure is common to all the methods, they differ from one another in steps 2 and 3, that is, finding V_{cr} and integrating the swing equations. There is general agreement that the first integral of motion of (9.22) constitutes a proper energy function and is derived as follows [101–102].

From (9.22) we have, for $i = 1, \dots, m$

$$dt = \frac{M_1 d\tilde{\omega}_1}{f_1(\theta)} = \frac{d\theta_1}{\tilde{\omega}_1} = \frac{M_2 d\tilde{\omega}_2}{f_2(\theta)} = \frac{d\theta_2}{\tilde{\omega}_2} = \dots = \frac{M_m d\tilde{\omega}_m}{f_m(\theta)} = \frac{d\theta_m}{\tilde{\omega}_m}. \quad (9.25)$$

Integrating the pairs of equations for each machine between $(\theta_i^s, 0)$, the postfault s.e.p to $(\theta_i, \tilde{\omega}_i)$ results in

$$V_i(\theta, \tilde{\omega}) = \frac{1}{2} M_i \tilde{\omega}_i^2 - \int_{\theta_i^s}^{\theta_i} f_i(\theta) d\theta_i, \quad i = 1, \dots, m. \quad (9.26)$$

This is known in the literature as the individual machine energy function [110]. Adding these functions for all the machines, we obtain the first integral of motion for the system as (omitting the algebra):

$$V(\theta, \tilde{\omega}) = \frac{1}{2} \sum_{i=1}^m M_i \tilde{\omega}_i^2 - \sum_{i=1}^m \int_{\theta_i^s}^{\theta_i} f_i(\theta) d\theta_i \quad (9.27)$$

$$\begin{aligned} &= \frac{1}{2} \sum_{i=1}^m M_i \tilde{\omega}_i^2 - \sum_{i=1}^m P_i(\theta_i - \theta_i^s) - \sum_{i=1}^{m-1} \sum_{j=i+1}^m \left[C_{ij} (\cos \theta_{ij} - \cos \theta_{ij}^s) \right. \\ &\quad \left. - \int_{\theta_i^s + \theta_j^s}^{\theta_i + \theta_j} D_{ij} \cos \theta_{ij} d(\theta_i + \theta_j) \right] \end{aligned} \quad (9.28)$$

$$= V_{KE}(\tilde{\omega}) + V_{PE}(\theta) \quad (9.29)$$

since

$$\sum_{i=1}^m \frac{M_i}{M_T} \int_{\theta_i^s}^{\theta_i} P_{COI} d\theta_i = 0.$$

Note that (9.28) contains path-dependent integral terms. In view of this, we cannot assert that V_i and V are positive-definite. If $D_{ij} \equiv 0$, it can be shown that $V(\theta, \bar{\omega})$ constitutes a proper Lyapunov function [100, 106, 107].

9.6 Potential Energy Boundary Surface (PEBS)

We first discuss the PEBS method because of its simplicity and its natural relationship to the equal-area criterion.

Ever since it was first proposed by Kakimoto et al. [107] and Athay et al. [104], the method has received wide attention by researchers because it avoids computing the controlling (relevant) u.e.p and requires only a quick fault-on system integration to compute V_{cr} . We can even avoid computing the postfault s.e.p., as discussed in Section 9.6.5. In this section, we will first motivate the method through application to a single-machine infinite-bus system, establish the equivalence between the energy function and the equal-area criterion, and, finally, explain the multimachine PEBS method.

9.6.1 Single-Machine Infinite-Bus System

Consider a single-machine infinite-bus system (Figure 9.3). Two parallel lines each having a reactance of X_1 connect a generator having transient reactance of X'_d through a transformer with a reactance of X_t to an infinite bus whose voltage is $E_2 \angle 0^\circ$. A three-phase fault occurs at the middle of one of the lines at $t = 0$, and is subsequently cleared at $t = t_{cl}$ by opening the circuit breakers at both ends of the faulted line. The prefault, faulted, and postfault configurations and their reduction to a two-machine equivalent are shown in Figures 9.4, 9.5, and 9.6. The electric power P_e during prefault, faulted, and postfault states are $\frac{E_1 E_2}{X'} \sin \delta$, $\frac{E_1 E_2 \sin \delta}{X^F}$, and $\frac{E_1 E_2 \sin \delta}{X}$, respectively. The computation of X' for the prefault system and X for the postfault system is straightforward, as shown in Figures 9.4 and 9.6.

Example 9.1 Compute X^F for the faulted system in Figure 9.3. X^F is the reactance between the internal node of the machine and the infinite bus. It can be computed for this network by performing a $Y - \Delta$ transformation in Figure 9.5(b). It is more instructive to illustrate a general method that is applicable to the multimachine case as well. Figure 9.5(a) is redrawn after labeling the various nodes (Figure 9.7). The point at which the fault occurs is labeled node 4. $X_g = X'_d + X_t$. There are current injections at nodes

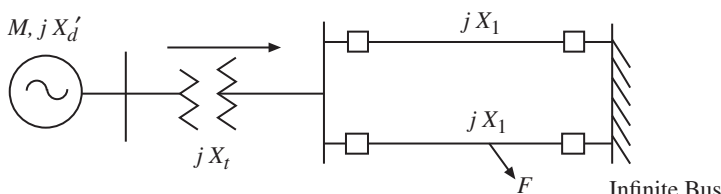


Figure 9.3 Single-machine infinite-bus system.

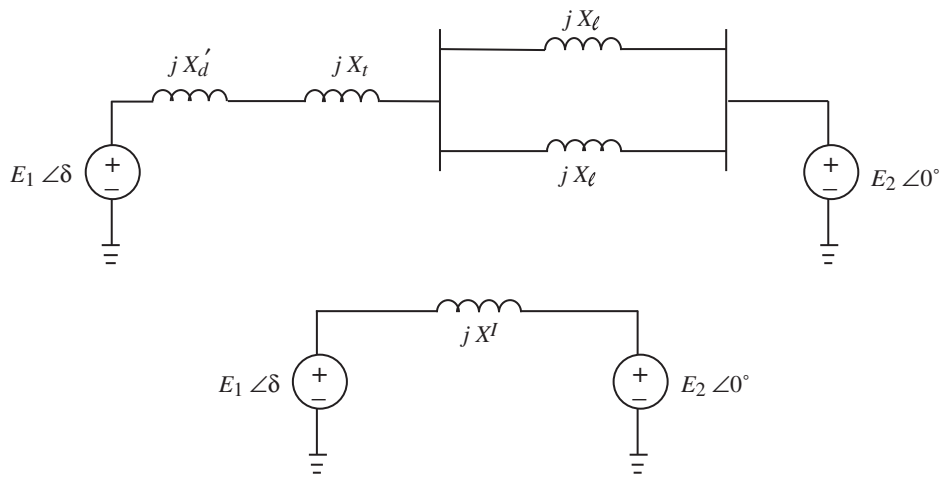


Figure 9.4 Prefault system and its two-machine equivalent.

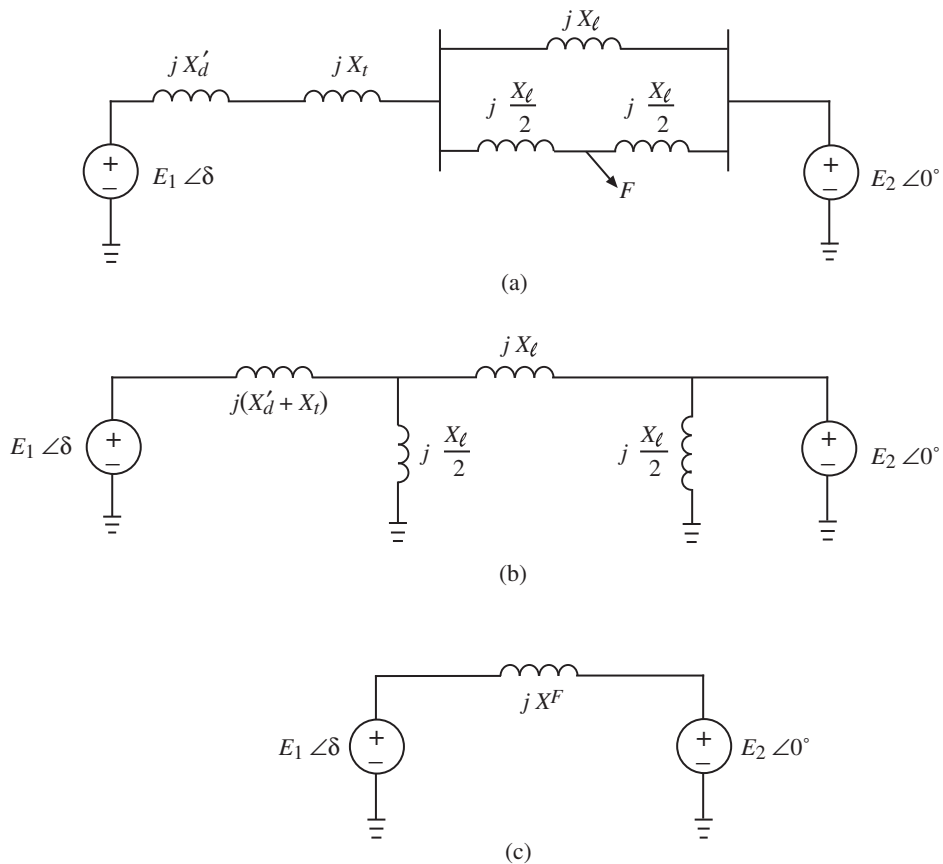
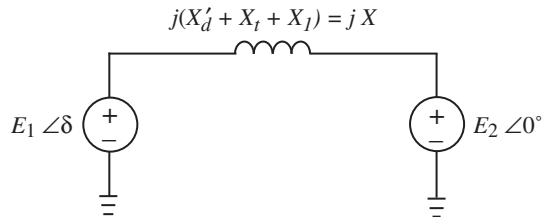


Figure 9.5 Faulted system and its two-machine equivalent.

Figure 9.6 Postfault system and its two-machine equivalent.



1, 2, and 4, and none at node 3. The nodal equation is

$$\begin{bmatrix} I_1 \\ I_2 \\ 0 \\ I_4 \end{bmatrix} = \begin{bmatrix} Y_{11} & 0 & Y_{13} & 0 \\ 0 & Y_{22} & Y_{23} & Y_{24} \\ Y_{31} & Y_{32} & Y_{33} & Y_{34} \\ 0 & Y_{42} & Y_{43} & Y_{44} \end{bmatrix} \begin{bmatrix} E_1 \\ E_2 \\ V_3 \\ V_4 \end{bmatrix}.$$

Since the fault is at node 4 with the fault impedance equal to zero, $V_4 \equiv 0$. Hence, we can delete row 4 and column 4, resulting in

$$\begin{bmatrix} I_1 \\ I_2 \\ 0 \end{bmatrix} = \begin{bmatrix} Y_{11} & 0 & Y_{13} \\ 0 & Y_{22} & Y_{23} \\ Y_{31} & Y_{32} & Y_{33} \end{bmatrix} \begin{bmatrix} E_1 \\ E_2 \\ V_3 \end{bmatrix}.$$

Node 3 is eliminated by expressing V_3 from the third equation in terms of E_1 and E_2 and substituting in the first two equations. This results in (omitting the algebra):

$$\begin{bmatrix} I_1 \\ I_2 \end{bmatrix} = \begin{bmatrix} Y_{11} - Y_{13}Y_{33}^{-1}Y_{31} & -Y_{13}Y_{33}^{-1}Y_{32} \\ -Y_{23}Y_{33}^{-1}Y_{31} & Y_{22} - Y_{23}Y_{33}^{-1}Y_{32} \end{bmatrix} \begin{bmatrix} E_1 \\ E_2 \end{bmatrix}.$$

X^F can be computed from the off-diagonal entry as

$$\frac{1}{jX^F} = Y_{13}Y_{33}^{-1}Y_{32}.$$

Now

$$Y_{13}Y_{33}^{-1}Y_{32} = \left(\frac{-1}{jX_g} \right) \left(\frac{1}{jX_g} + \frac{1}{jX_1} + \frac{1}{j\frac{X_1}{2}} \right)^{-1} \left(\frac{-1}{jX_1} \right) = \frac{1}{j(X_1 + 3X_g)}.$$

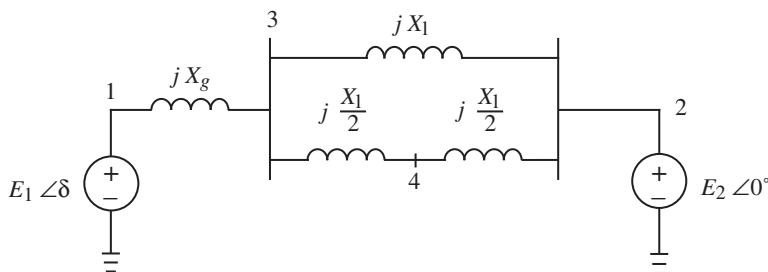


Figure 9.7 Faulted system.

Hence

$$X^F = X_1 + 3X_g.$$

We do not require the other elements of the reduced Y matrix. \square

9.6.2 Energy Function for a Single-Machine Infinite-Bus System

The energy function is *always* constructed for the postfault system. In the SMIB case, the postfault equations are

$$M \frac{d^2\delta}{dt^2} = P_m - P_e^{\max} \sin \delta \quad (9.30)$$

where $P_e^{\max} = \frac{E_1 E_2}{X}$, δ is the angle relative to the infinite bus, and $\frac{d\delta}{dt} = \omega$ is the relative rotor-angle velocity. The right-hand side of (9.30) can be written as $\frac{-\partial V_{PE}}{\partial \delta}$, where

$$V_{PE}(\delta) = -P_m \delta - P_e^{\max} \cos \delta. \quad (9.31)$$

Multiplying (9.30) by $\frac{d\delta}{dt}$, it can be rewritten as

$$\frac{d}{dt} \left[\frac{M}{2} \left(\frac{d\delta}{dt} \right)^2 + V_{PE}(\delta) \right] = 0$$

that is,

$$\frac{d}{dt} \left[\frac{1}{2} M \omega^2 + V_{PE}(\delta) \right] = 0$$

that is,

$$\frac{d}{dt} [V(\delta, \omega)] = 0. \quad (9.32)$$

Hence, the energy function is

$$V(\delta, \omega) = \frac{1}{2} M \omega^2 + V_{PE}(\delta). \quad (9.33)$$

It follows from (9.32) that the quantity inside the brackets $V(\delta, \omega)$ is a constant. The equilibrium point is given by the solution of $0 = P_m - P_e^{\max} \sin \delta$, that is, $\delta^s = \sin^{-1}(\frac{P_m}{P_e^{\max}})$. This is a stable equilibrium point surrounded by two unstable equilibrium points $\delta^u = \pi - \delta^s$ and $\hat{\delta}_u = -\pi - \delta^s$. If we make a change of coordinates so that $V_{PE} = 0$ at $\delta = \delta^s$, then (9.31) becomes

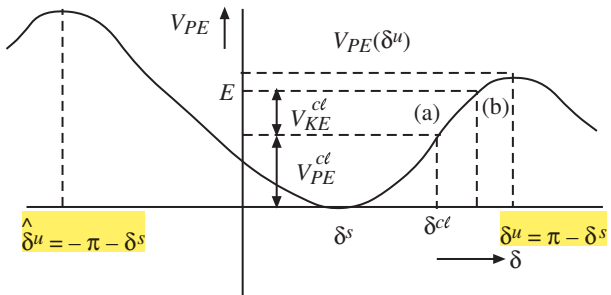
$$V_{PE}(\delta, \delta^s) = -P_m(\delta - \delta^s) - P_e^{\max}(\cos \delta - \cos \delta^s). \quad (9.34)$$

With this, the energy function $V(\delta, \omega)$ can be written as

$$V(\delta, \omega) = \frac{1}{2} M \omega^2 - P_m(\delta - \delta^s) - P_e^{\max}(\cos \delta - \cos \delta^s) = V_{KE} + V_{PE}(\delta, \delta^s) \quad (9.35)$$

where $V_{KE} = \frac{1}{2} M \omega^2$ is the transient kinetic energy and $V_{PE}(\delta, \delta^s) = -P_m(\delta - \delta^s) - P_e^{\max}(\cos \delta - \cos \delta^s)$ is the potential energy. From (9.32) it follows that $V(\delta, \omega)$ is equal to a constant E , which is the sum of the kinetic and potential energies, and remains

Figure 9.8 Potential energy “well”.



constant once the fault is cleared since the system is conservative. $V(\delta, \omega)$ evaluated at $t = t_{cl}$ from the faulted trajectory represents the total energy E present in the system at $t = t_{cl}$. This energy must be absorbed by the system once the fault is cleared if the system is to be stable. The kinetic energy is always positive, and is the difference between E and $V_{PE}(\delta, \delta^s)$. This is shown graphically in Figure 9.8, which is the potential energy curve.

At $\delta = \delta^s$, the postfault s.e.p., both the V_{KE} and the V_{PE} are zero, since $\omega = 0$ and $\delta = \delta^s$ at this point. Suppose that, at the end of the faulted period $t = t_{cl}$, the rotor angle is $\delta = \delta^{cl}$, and the velocity is ω^{cl} . Then

$$V^{cl}(\delta^{cl}, \omega^{cl}) = \frac{1}{2}M\omega^{cl}_2 - P_m(\delta^{cl} - \delta^s) - P_e^{\max}(\cos \delta^{cl} - \cos \delta^s) = V_{KE}^{cl} + V_{PE}^{cl}. \quad (9.36)$$

This is the value of E . There are two other equilibrium points of the system (9.30), namely, $\delta^u = \pi - \delta^s$ and $\hat{\delta}^u = -\pi - \delta^s$. Both of these are unstable and, in fact, are Type 1 (saddle-type) e.p.’s. Type 1 e.p.’s are characterized by the fact that the linearized system at that e.p. has one real eigenvalue in the right-half plane. The potential energy is zero at $\delta = \delta^s$ and has a relative maximum at $\delta = \delta^u$ and $\delta = \hat{\delta}^u$. At the point (a), δ^{cl} and ω^{cl} are known from the faulted trajectory; hence, $V(\delta^{cl}, \omega^{cl}) = E$ is known. This is shown as point (b). If $E < V_{PE}(\delta^u)$, then since the system is conservative, the cleared system at point (a) will accelerate until point (b), and then start decelerating. If $E > V_{PE}(\delta^u)$, then the cleared system will accelerate beyond δ^u and, hence, the system is unstable. $V_{PE}(\delta^u)$ is obtained from (9.34) as $-P_m(\pi - 2\delta^s) + 2P_e^{\max} \cos \delta^s$. If δ decreases due to deceleration for $t > 0$, then the system is unstable if $E > V(\hat{\delta}^u)$. The points δ^u and $\hat{\delta}^u$ constitute the zero-dimensional PEBS for the single-machine system. Some researchers restate the above idea by saying that if the V_{PE} is initialized to zero at δ^{cl} , V_{KE}^{cl} represents the excess kinetic energy injected into the system. Then stability of the system is determined by the ability of the postfault system to absorb this excess kinetic energy (i.e., the system is stable if $V_{PE}(\delta^u) - V_{PE}(\delta^{cl}) > V_{KE}^{cl}$).

Most of the stability concepts can be interpreted as if the moment of inertia M is assumed as a particle that slides without friction within a “hill” with the shape $V_{PE}(\delta)$. Motions within a potential “well” are bounded and, hence, stable. It is interesting to relate the potential “well” concept to the stability of equilibrium points for small disturbances. Using (9.31), (9.30) can be written as

$$M \frac{d^2\delta}{dt^2} = -\frac{\partial V_{PE}(\delta)}{\partial \delta}. \quad (9.37)$$

We can expand the right-hand side of (9.37) in a Taylor series about an equilibrium point δ^* , i.e., $\delta = \delta^* + \Delta\delta$, and retain only the linear term. Then

$$M \frac{d^2 \Delta\delta}{dt^2} = -\left. \frac{\partial^2 V_{PE}(\delta)}{\partial \delta^2} \right|_{\delta^*} \Delta\delta \quad (9.38)$$

that is,

$$M \frac{d^2 \Delta\delta}{dt^2} + \left. \frac{\partial^2 V_{PE}(\delta)}{\partial \delta^2} \right|_{\delta^*} \Delta\delta = 0. \quad (9.39)$$

If $\left. \frac{\partial^2 V_{PE}}{\partial \delta^2} \right|_{\delta^*} < 0$, the equilibrium is unstable. If $\left. \frac{\partial^2 V_{PE}}{\partial \delta^2} \right|_{\delta^*} > 0$, then it is an oscillatory system, and the oscillations around δ^* are bounded. Since there is always some positive damping, we may call it stable. In the case of (9.30), it can be verified that δ^s is a stable equilibrium point and that both δ^u and $\hat{\delta}^u$ are unstable equilibrium points using this criterion.

The energy function, Lyapunov function, and the PEBS are thus all equivalent in the case of a single-machine infinite-bus system. It is in the case of multimachine systems and nonconservative systems that each method gives only approximations to the true stability boundary! In the case of multimachine systems, the second derivative of V_{PE} is the Hessian matrix.

Example 9.2 Consider an SMIB system whose postfault equation is given by

$$0.2 \frac{d^2 \delta}{dt^2} = 1 - 2 \sin \delta - 0.02 \frac{d\delta}{dt}.$$

The equilibrium points are given by $\delta^s = \sin^{-1}(\frac{1}{2})$. Hence, $\delta^s = \frac{\pi}{6}$, $\delta^u = \pi - \frac{\pi}{6} = \frac{5\pi}{6}$, $\hat{\delta}^u = -\pi - \frac{\pi}{6} = \frac{-7\pi}{6}$. Linearizing around an equilibrium point "0" results in

$$0.2 \frac{d^2 \Delta\delta}{dt^2} = -2 \cos \delta^o \Delta\delta - 0.02 \frac{d\Delta\delta}{dt}.$$

This can be put in the state-space form by defining $\Delta\delta$, $\Delta\omega = \dot{\Delta\delta}$ as the state variables.

$$\begin{bmatrix} \Delta\dot{\delta} \\ \Delta\dot{\omega} \end{bmatrix} = \begin{bmatrix} 0 & 1 \\ -10 \cos \delta^o & -0.1 \end{bmatrix} \begin{bmatrix} \Delta\delta \\ \Delta\omega \end{bmatrix}$$

For $\delta^o = \delta^s = \frac{\pi}{6}$, eigenvalues of this matrix are $\lambda_{1,2} = -0.05 \pm j2.942$. It is a stable equilibrium point called the focus. For $\delta^o = \delta^u$ or $\hat{\delta}^u$, the eigenvalues are $\lambda_1 = 2.993$ and $\lambda_2 = -2.893$. Both are saddle points. Since there is only one eigenvalue in the right-half plane, it is called a Type 1 u.e.p. \square

Example 9.3 Construct the energy function for Example 9.2. Verify the stability of the equilibrium points by using (9.39).

The energy function is constructed for the undamped system, that is, the coefficient of $\frac{d\delta}{dt}$ is set equal to zero. $M = 0.2$, $P_m = 1$, $P_e^{\max} = 2$, $\delta^s = \frac{\pi}{6}$. The energy function is

$$\begin{aligned} V(\delta, \omega) &= \frac{1}{2}(0.2)\omega^2 - 1(\delta - \pi/6) - 2 \left(\cos \delta - \cos \frac{\pi}{6} \right) \\ &= 0.1\omega^2 - \left(\delta - \frac{\pi}{6} \right) - 2(\cos \delta - 0.866) \\ V_{PE}(\delta, \delta^s) &= - \left(\delta - \frac{\pi}{6} \right) - 2(\cos \delta - 0.866) \\ \frac{\partial^2 V_{PE}(\delta, \delta^s)}{\partial \delta} &= 2 \cos \delta. \end{aligned}$$

At $\delta = \delta^s = \pi/6$, $2 \cos \delta > 0$; hence δ^s is a stable equilibrium point. At $\delta = \delta^u = \frac{5\pi}{6}$ or $\hat{\delta}^u = \frac{-7\pi}{6}$, $2 \cos \delta < 0$. Hence, both δ^u and $\hat{\delta}^u$ are unstable equilibrium points. \square

9.6.3 Equal-Area Criterion and the Energy Function

The prefault, faulted, and postfault power angle curves P_e for the single-machine infinite-bus system are shown in Figure 9.9.

The system is initially at $\delta = \delta^o$. We shall now show that the area A_1 represents the kinetic energy injected into the system during the fault, which is the same as V_{KE}^{cl} in Figure 9.8. A_2 represents the ability of the postfault system to absorb this energy. In terms of Figure 9.8, A_2 represents $V_{PE}(\delta^u) - V_{PE}(\delta^{cl})$. By the equal-area criterion, the system is stable if $A_1 < A_2$.

Let the faulted and postfault equations, respectively, be

$$M \frac{d^2\delta}{dt^2} = P_m - P_e^F \sin \delta \quad (9.40)$$

and

$$M \frac{d^2\delta}{dt^2} = P_m - P_e^{\max} \sin \delta \quad (9.41)$$

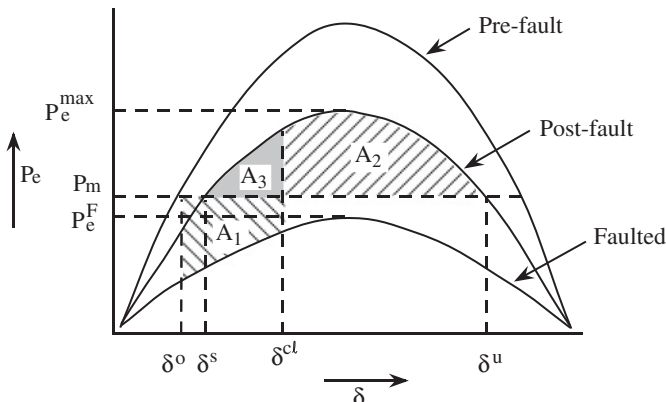


Figure 9.9 Equal-area criterion for the SMIB case.

where

$$P_e^F = \frac{E_1 E_2}{X^F}$$

and

$$P_e^{\max} = \frac{E_1 E_2}{X}.$$

The area A_1 is given by

$$\begin{aligned} A_1 &= \int_{\delta^o}^{\delta^{cl}} (P_m - P_e^F \sin \delta) d\delta \\ &= \int_{\delta^o}^{\delta^{cl}} M \frac{d\omega}{dt} d\delta \\ &= \int_{\delta^o}^{\delta^{cl}} M \frac{d\omega}{dt} \omega dt \\ &= \int_o^{\omega^{cl}} M \omega d\omega = \frac{1}{2} M (\omega^{cl})^2. \end{aligned} \quad (9.42)$$

Hence, A_1 is the kinetic energy injected into the system due to the fault. Area A_2 is given by

$$\begin{aligned} A_2 &= \int_{\delta^{cl}}^{\delta^u} (P_e^{\max} \sin \delta - P_m) d\delta = -P_e^{\max} (\cos \delta^u - \cos \delta^{cl}) - P_m (\delta^u - \delta^{cl}) \\ &= V_{PE}(\delta^u) - V_{PE}(\delta^{cl}) \end{aligned}$$

from (9.31). If we add area A_3 to both sides of the criterion $A_1 < A_2$, the result is

$$A_1 + A_3 < A_2 + A_3. \quad (9.43)$$

Now

$$A_3 = \int_{\delta^s}^{\delta^{cl}} (P_e^{\max} \sin \delta - P_m) d\delta = -P_m (\delta^{cl} - \delta^s) - P_e^{\max} (\cos \delta^{cl} - \cos \delta^s). \quad (9.44)$$

Changing δ^{cl}, ω^{cl} to any δ, ω and adding A_1 to A_3 , gives

$$A_1 + A_3 = \frac{1}{2} M \omega^2 - P_m (\delta - \delta^s) - P_e^{\max} (\cos \delta - \cos \delta^s). \quad (9.45)$$

This is the same as $V(\delta, \omega)$ as in (9.35). Now, from Figure 9.9:

$$A_2 + A_3 = \int_{\delta^s}^{\pi - \delta^s} (P_e^{\max} \sin \delta - P_m) d\delta = 2P_e^{\max} \cos \delta^s - P_m (\pi - 2\delta^s). \quad (9.46)$$

The right-hand side of (9.46) is also verified to be the sum of the areas A_2 and A_3 , for which analytical expressions have been derived. It may be verified from (9.35) that

$$\begin{aligned} V(\delta, \omega) \Big|_{\delta=\delta^u, \omega=0} &= -P_m (\pi - 2\delta^s) + 2P_e^{\max} \cos \delta^s = A_2 + A_3 \\ &= V_{PE}(\delta^u) \\ &\stackrel{\Delta}{=} V_{cr}. \end{aligned} \quad (9.47)$$

Thus, the equal-area criterion $A_1 < A_2$ is equivalent to $A_1 + A_3 < A_2 + A_3$, which in turn is equivalent to

$$V(\delta, \omega) < V_{cr} \quad (9.48)$$

where $V_{cr} = V_{PE}(\delta^u)$. Note that δ, ω are obtained from the faulted equation.

Example 9.4 For Example 9.2, (1) state analytically the equal-area criterion. (2) If the faulted system is given by

$$\frac{0.2d^2\delta}{dt^2} = 1 - \sin \delta - 0.02 \frac{d\delta}{dt}$$

compute t_{cr} using the results of part (1). Note that the energy function is for a conservative system, while the faulted system is not conservative.

The energy function is given by

$$\begin{aligned} V(\delta, \omega) &= \frac{1}{2}(0.2)\omega^2 - 1\left(\delta - \frac{\pi}{6}\right) - 2\left(\cos \delta - \cos \frac{\pi}{6}\right) \\ &= 0.1\omega^2 - \left(\delta - \frac{\pi}{6}\right) - 2\cos \delta + 1.732 \\ &= 0.1\omega^2 - \delta - 2\cos \delta + 2.256 \\ V(\delta^u, 0) &= -P_m(\pi - 2\delta^s) + 2P_e^{\max} \cos \delta^s \\ &= -\left(\pi - \frac{2\pi}{6}\right) + 4 \cos \frac{\pi}{6} \\ &= -2.09 + 3.464 = 1.374. \end{aligned}$$

Hence, the equal-area criterion is

$$V(\delta, \omega) < 1.374$$

where δ, ω are calculated from the fault-on trajectory. To obtain t_{cr} , the faulted equations are integrated and $V(\delta, \omega)$ are computed at each time point. When $V(\delta, \omega) = 1.374$, the time instant is t_{cr} . \square

9.6.4 Multimachine PEBS

In the previous section, we mentioned that the points δ^u and $\hat{\delta}^u$ were the zero-dimensional PEBS for the SMIB system. In the case of multimachine systems, the PEBS is quite complex in the rotor-angle space. A number of unstable equilibrium points surround the stable equilibrium point of the postfault system. The potential energy boundary surface therefore constitutes a multidimensional surface passing through the u.e.p.s. The theory behind the characterization of the PEBS is quite detailed, and is dealt with in the literature [100, 101]. We can extend the concept of computing V_{cr} using the PEBS method for a multimachine system as follows.

In the previous section, we showed that in the SMIB case $V_{cr} = V_{PE}(\delta^u)$, that is, $V(\delta, \omega)$ is evaluated at the nearest equilibrium point $(\delta^u, 0)$ if the machine loses synchronism by acceleration. δ^u is therefore not only the nearest, but also the relevant (or controlling), u.e.p in this case. In the case of the multimachine system, depending on the location and nature of the fault, the system may lose synchronism by one or more

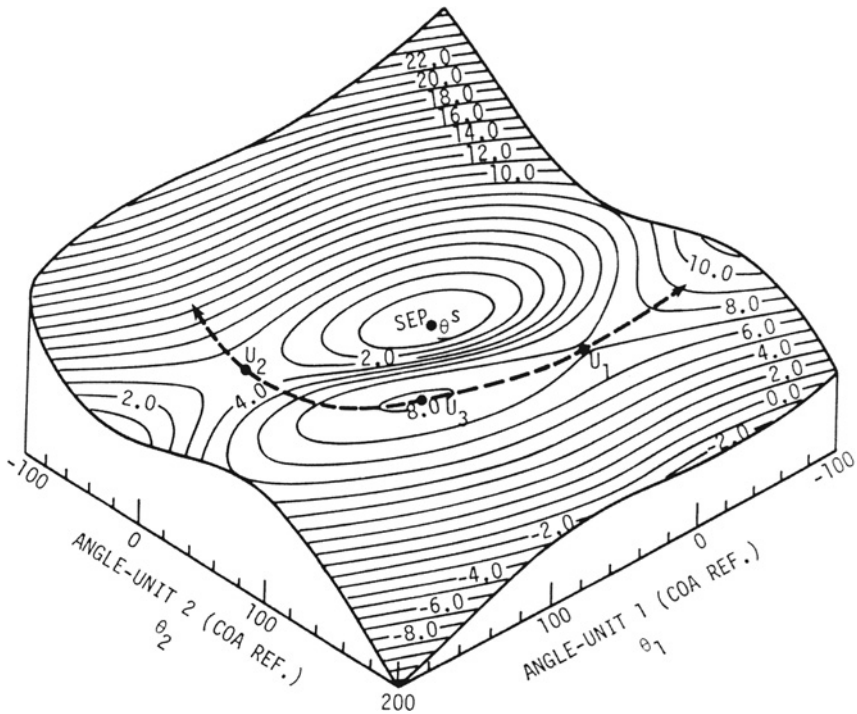


Figure 9.10 The potential energy boundary surface Source: Yu 1983 [97]. Reproduced with permission of Elsevier.

machines going unstable. Hence, each disturbance gives rise to what is called a mode of instability (MOI) [121]. Associated with each MOI is an u.e.p that we call the controlling u.e.p for that particular disturbance. A number of u.e.p's surround the s.e.p of the postfault system. Mathematically, these are the solutions of (9.23). From the pre-fault s.e.p, if the faulted system is integrated and cleared critically, then the postfault trajectory approaches a particular u.e.p depending on the mode of instability. This u.e.p is called the controlling u.e.p for that disturbance. In the multimachine PEBS, we can visualize a multidimensional potential “well” analogous to Figure 9.8 for the SMIB case. For a three-machine system, one such “well” is shown in Figure 9.10 where the axes are the COI-referenced rotor angles θ_1, θ_2 of two machines. The vertical axis represents $V_{PE}(\theta)$. Equipotential contours are shown, as well as the three nearby u.e.p's U_1, U_2, U_3 . The dotted line connecting these u.e.p's is orthogonal to the equipotential curves and is called the PEBS. If at the instant of fault-clearing the system state in the angle space has crossed the PEBS, the system will be unstable. If the fault is cleared early enough, then the postfault trajectory in the angle space will tend to return to equilibrium eventually because of the damping in the system. The critical clearing time t_{cr} is defined to be the time instant such that the postfault trajectory just stays within the “well.” It is a conjecture that the critically cleared trajectory passes “very close” to the controlling u.e.p. This is called the “first swing” stable phenomenon. To find the critical value of $V(\delta, \omega)$, the fault-on trajectory is monitored until it crosses the PEBS at a point θ^* . In many cases, θ^* ,

the controlling u.e.p, is close to θ^* , so that $V_{PE}(\theta^u) \approx V_{PE}(\theta^*) \stackrel{\Delta}{=} V_{cr}$. This is the essence of the PEBS method. A key question here is the detection of the PEBS crossing. This crossing is also approximately the point at which $V_{PE}(\theta)$ is maximum along the faulted trajectory. Hence, V_{cr} can be taken as equal to $V_{PE}^{\max}(\theta)$ along the faulted trajectory. It can be shown [104] that the PEBS crossing is also the point at which $f^T(\theta) \cdot (\theta - \theta^s) = 0$. $f(\theta)$ is the accelerating power in the postfault system. That this is the same point at which $V_{PE}(\theta)$ is maximum has been shown to be true for a conservative system [100]. In recent years, this PEBS crossing method has been the basis of improved algorithms such as the “second kick” method [122]. We now explain the basic PEBS algorithm in detail. It will help in understanding the newer algorithms. The energy function given by (9.28) is repeated here:

$$V(\theta, \tilde{\omega}) = \frac{1}{2} \sum_{i=1}^m M_i \tilde{\omega}_i^2 - \sum_{i=1}^m P_i(\theta_i - \theta_i^s) - \sum_{i=1}^m \sum_{j=i+1}^m \left[C_{ij} (\cos \theta_{ij} - \cos \theta_{ij}^s) - \int_{\theta_i^s + \theta_j^s}^{\theta_i + \theta_j} D_{ij} \cos \theta_{ij} d(\theta_i + \theta_j) \right]. \quad (9.49)$$

The last term on the right-hand side of (9.49) denoted by $V_d(\theta)$ is a path-dependent term. This can be evaluated using trapezoidal integration as

$$V_d(\theta) = \sum_{i=1}^{m-1} \sum_{j=i+1}^m I_{ij} \quad (9.50)$$

where at the k^{th} step

$$I_{ij}(k) = I_{ij}(k-1) + \frac{1}{2} D_{ij} [\cos(\theta_i(k) - \theta_j(k)) + \cos(\theta_i(k-1) - \theta_j(k-1))] [\theta_i(k) + \theta_j(k) - \theta_i(k-1) - \theta_j(k-1)] \quad (9.51)$$

with

$$I_{ij}(0) = 0.$$

This evaluation of $I_{ij}(0)$ is correct when the postfault system is the same as the prefault system, but is somewhat inaccurate if there is line-switching. This is explained in the next section. Equation (9.49) is rewritten as

$$V(\theta, \tilde{\omega}) = V_{KE}(\tilde{\omega}) + V_p(\theta) + V_d(\theta) \quad (9.52)$$

where

$$V_{PE}(\theta) = V_p(\theta) + V_d(\theta) \quad (9.53)$$

$$V_p(\theta) = - \sum_{i=1}^m P_i(\theta_i - \theta_i^s) - \sum_{i=1}^m \sum_{j=i+1}^m C_{ij} (\cos \theta_{ij} - \cos \theta_{ij}^s)$$

and $V_d(\theta)$ is given by (9.50). It can be shown [104] that the points θ on the PEBS are defined by $\sum_{i=1}^m f_i(\theta)(\theta_i - \theta_i^s) = 0$. This is the characterization of the PEBS. In vector form, this can be written as $f^T(\theta) \cdot (\theta - \theta^s) = 0$. Denoting $\theta - \theta^s = \hat{\theta}$, we can show by analogy to the zero transfer conductance case that inside the PEBS $f^T(\theta) \cdot \hat{\theta} < 0$, and

outside the PEBS it is > 0 [100]. In the absence of transfer conductances, $f(\theta) = -\frac{\partial V_{PE}(\theta)}{\partial \theta}$. When θ is away from θ^s , within the potential multidimensional “well,” $\frac{\partial V_{PE}(\theta)}{\partial \theta}$ (which is the gradient of the potential energy function) and $\hat{\theta}$ (i.e., $(\theta - \theta^s)$) are both > 0 . Hence, $f^T(\theta) \cdot \hat{\theta} < 0$ inside the “well.” Outside the “well,” $\theta - \theta^s$ is > 0 and $\frac{\partial V_{PE}(\theta)}{\partial \theta} < 0$, resulting in $f^T(\theta) \cdot \hat{\theta} > 0$. On the PEBS, the product $f^T(\theta) \cdot \hat{\theta}$ is equal to zero.

The steps to compute t_{cr} using the PEBS method are as follows:

1. Compute the postfault s.e.p θ^s by solving (9.23).
2. Compute the fault-on trajectory given by (9.21).
3. Monitor $f^T(\theta) \cdot \hat{\theta}$ and $V_{PE}(\theta)$ at each time step. The parameters in $f(\theta)$ and $V_{PE}(\theta)$ pertain to the postfault configuration.
4. Inside the potential “well” $f^T(\theta) \cdot \hat{\theta} < 0$. Continue steps 2 and 3 until $f^T(\theta) \cdot \hat{\theta} = 0$. This is the PEBS crossing $(t^*, \theta^*, \tilde{\omega}^*)$. At this point, find $V_{PE}(\theta^*)$. This is a good estimate of V_{cr} for that fault.
5. Find when $V(\tilde{\theta}, \tilde{\omega}) = V_{cr}$ from the fault-on trajectory. This gives a good estimate of t_{cr} .

One can replace steps 3 and 4 by monitoring when $V_{PE}^{\max}(\theta)$ is reached, and taking it as V_{cr} . There will be some error in either of the algorithms.

9.6.5 Initialization of $V_{PE}(\theta)$ and its Use in PEBS Method

In this section, we outline a further simplification of the PEBS method that works well in many cases, particularly when θ^s is “close” to θ^o . While integrating the faulted trajectory given by (9.21), the initial conditions on the states are $\theta_i(0) = \theta_i^o$ and $\tilde{\omega}_i(0) = 0$. In the energy function (9.29), the reference angle and velocity variables are θ_i^s and $\tilde{\omega}_i(0) = 0$. Thus, at $t = 0$, we evaluate $V_{PE}(\theta)$ in (9.29) as

$$\begin{aligned} V_{PE}(\theta^o) &= - \sum_{i=1}^m \int_{\theta_i^s}^{\theta_i^o} f_i(\theta) d\theta_i \\ &= - \sum_{i=1}^m P_i (\theta_i^o - \theta_i^s) - \sum_{i=1}^{m-1} \sum_{j=i+1}^m \\ &\quad \left[C_{ij} (\cos \theta_{ij}^o - \cos \theta_{ij}^s) - \int_{\theta_i^s + \theta_j^s}^{\theta_i^o + \theta_j^o} D_{ij} \cos \theta_{ij} d(\theta_i + \theta_j) \right] \\ &= K \text{ (a constant)}. \end{aligned} \tag{9.54}$$

The path-dependent integral term in (9.54) is evaluated using the trapezoidal rule:

$$I_{ij}(0) = \frac{1}{2} D_{ij} \left[\cos (\theta_i^o - \theta_j^o) + \cos (\theta_i^s - \theta_j^s) \right] \left[(\theta_i^o + \theta_j^o) - (\theta_i^s + \theta_j^s) \right]. \tag{9.55}$$

If the postfault network is the same as the prefault network, then $K = 0$. Otherwise, this value of K should be included in the energy function.

If one uses the potential energy boundary surface (PEBS) method, then when the post-fault network is not equal to the prefault network, this term can be subtracted from the energy function, that is,

$$V(\theta, \tilde{\omega}) = V_{KE}(\tilde{\omega}) + V_{PE}(\theta) - V_{PE}(\theta^o). \quad (9.56)$$

Hence, the potential energy can be defined, with θ^o as the datum, as

$$\begin{aligned} \hat{V}_{PE}(\theta) &\stackrel{\Delta}{=} V_{PE}(\theta) - V_{PE}(\theta^o) = - \left[\sum_{i=1}^m \int_{\theta_i^s}^{\theta_i} f_i(\theta) d\theta_i - \sum_{i=1}^m \int_{\theta_i^s}^{\theta_i^o} f_i(\theta) d\theta_i \right] \\ &= - \sum_{i=1}^m \int_{\theta_i^o}^{\theta_i} f_i(\theta) d\theta_i. \end{aligned} \quad (9.57)$$

If the path-dependent integral term in (9.57) is evaluated, using trapezoidal integration as in (9.51), $I_{ij}(0) = 0$. At the PEBS crossing θ^* , $\hat{V}_{PE}(\theta^*)$ gives a good approximation to V_{cr} . The PEBS crossing has been shown as approximately the point at which the potential energy V_{PE} reaches a maximum value. Hence, one can directly monitor \hat{V}_{PE} and thus avoid having to monitor the dot product $f^T(\theta) \cdot (\theta - \theta^s)$ as in step 4 of the previous section. This leads to the important advantage of not having to compute θ^s . In fast screening of contingencies, this could result in a significant saving of computation. On large-scale systems, this has not been investigated in the literature so far.

Example 9.5 Compute the \bar{Y}_{int} for Example 7.1, using the classical model for the fault at bus 7 followed clearing lines of 7–5. Using the PEBS method, compute t_{cr} . Use $f^T(\theta) \cdot \hat{\theta}$ as the criterion for PEBS crossing.

\bar{Y}_{int} with fault at bus 7 (faulted system)

In the Y_{aug}^{new} matrix of Example 7.6, since $V_7 = 0$, we delete the row and column corresponding to bus 7. Then eliminate all buses except the internal nodes 10, 11, and 12. The result is

$$\bar{Y}_{int}^F = \begin{bmatrix} 0.6567 - j3.8159 & 0.0000 - j0.0000 & 0.0701 + j0.6306 \\ 0.0000 - j0.0000 & 0.0000 - j5.4855 & 0.0000 - j0.0000 \\ 0.0701 + j0.6306 & 0.0000 - j0.0000 & 0.1740 - j2.7959 \end{bmatrix}.$$

\bar{Y}_{int} with lines 7–5 cleared (postfault system)

$\bar{Y}_{bus} = \bar{Y}_N$ is first computed with lines 7–5 removed, and the rest of the steps are as in Example 7.6. Buses 1 to 9 are eliminated, resulting in

$$\bar{Y}_{int} = \begin{bmatrix} 1.1386 - 2.2966i & 0.1290 + 0.7064i & 0.1824 + 1.0637i \\ 0.1290 + 0.7064i & 0.3744 - 2.0151i & 0.1921 + 1.2067i \\ 0.1824 + 1.0637i & 0.1921 + 1.2067i & 0.2691 - 2.3516i \end{bmatrix}.$$

The initial rotor angles are $\delta_1(0) = 0.0396$ rad, $\delta_2(0) = 0.344$ rad, and $\delta_3(0) = 0.23$ rad. The COA is calculated as $\delta_o = \frac{1}{M_T} \sum_{i=1}^3 M_i \delta_i(0) = 0.116$ rad, where $M_T = M_1 + M_2 + M_3$. Hence, we have $\theta_1(0) = \delta_1(0) - \delta_o = -0.0764$ rad, $\theta_2(0) = \delta_2(0) - \delta_o = 0.229$ rad,

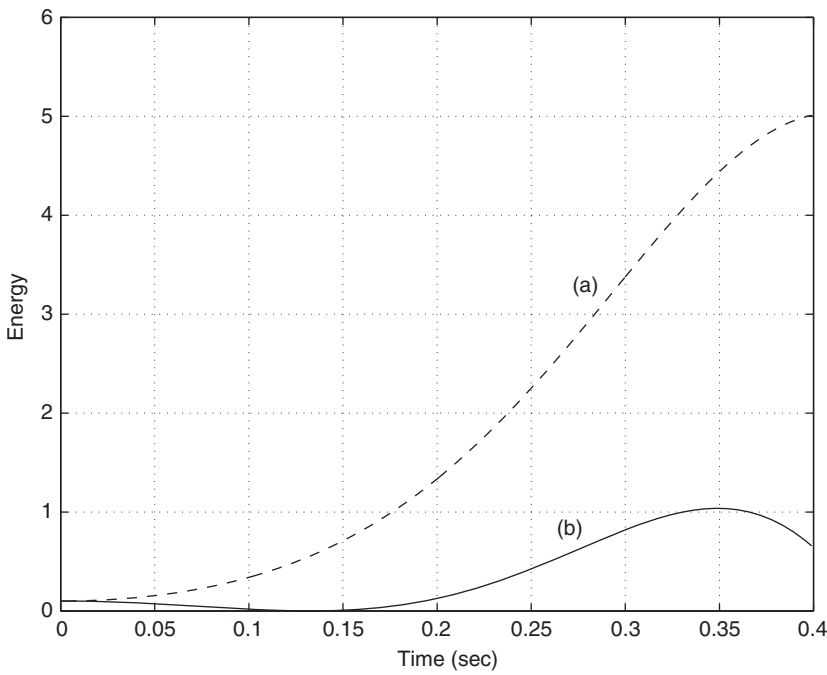


Figure 9.11 Total and potential energies: (a) $V(\theta, \tilde{\omega})$ (dashed line); (b) $V_{PE}(\theta)$ (solid line).

and $\theta_3(0) = \delta_3(0) - \delta_o = 0.114$ rad, $\tilde{\omega}_1(0) = \tilde{\omega}_2(0) = \tilde{\omega}_3(0) = 0$. The postfault s.e.p is calculated as $\theta_1^s = -0.1782$, $\theta_2^s = 0.5309$, $\theta_3^s = 0.2711$. The steps in computing t_{cr} are given below.

1. From the entries in Y_{int} for faulted and postfault systems, the appropriate C_{ij} and D_{ij} 's are calculated to put the equations in the form of (9.21) and (9.22).
2. $V(\theta, \omega)$ is given by $V_{KE} + V_{PE}(\theta)$, where $V_{KE} = \frac{1}{2}M_i\tilde{\omega}_i^2$ and $V_{PE}(\theta)$ is given by (9.53). The path-integral term is evaluated as in (9.51), with $I_{ij}(0) = 0$, and the term (9.55) is added to $V_{PE}(\theta)$.
3. The faulted system corresponding to (9.21) is integrated and at each time step $V(\theta, \tilde{\omega})$ as well as $V_{PE}(\theta)$ are computed. Also the dot product $f^T(\theta) \cdot \hat{\theta}$ is monitored. The plots of $V(\theta, \tilde{\omega})$ and $V_{PE}(\theta)$ are shown in Figure 9.11. Figure 9.12 shows the plot of $f^T(\theta) \cdot \hat{\theta}$.
4. $V_{PE}^{\max} = 1.0377$ is reached at approximately 0.36 sec. Note from Figure 9.12 that the zero crossing of $f^T(\theta) \cdot \hat{\theta}$ occurs at approximately the same time.
5. From the graph for $V(\theta, \tilde{\omega})$, $t_{cr} = 0.179$ sec when $V(\theta, \tilde{\omega}) = 1.0377$. □

9.7 The Boundary Controlling u.e.p (BCU) Method

This method [105] provided another breakthrough in applying energy function methods to stability analysis after the work of Athay et al. [104], which originally proposed the

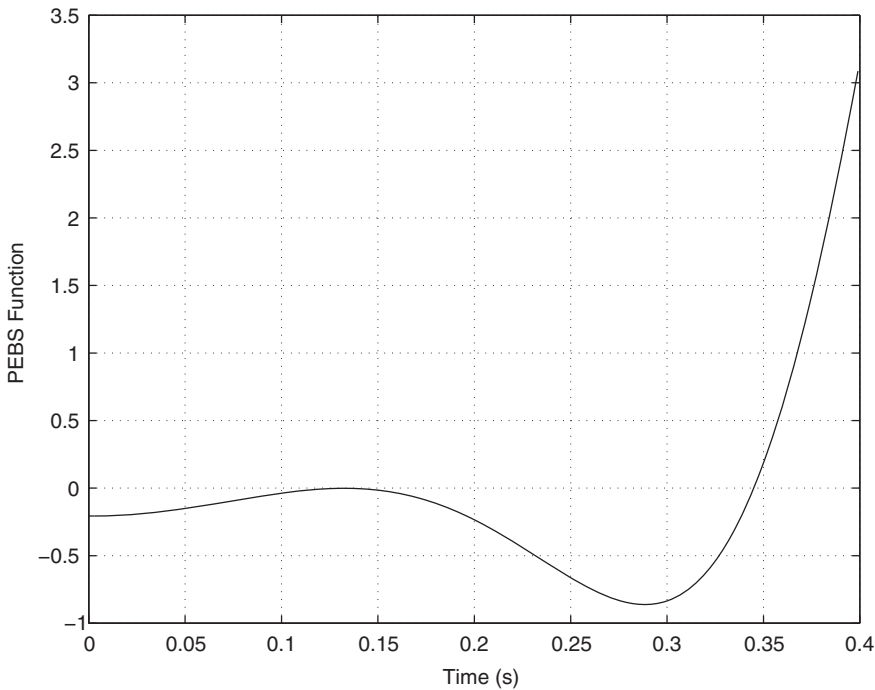


Figure 9.12 The monitoring of the PEBS crossing by $f^T(\theta) \cdot \dot{\theta}$.

controlling u.e.p method. The equations of the postfault system (9.22) can be put in the state-space form as

$$\begin{aligned}\dot{\theta} &= \tilde{\omega}_i \\ M_i \ddot{\omega}_i &= f'_i(\theta) \\ &= -\frac{\partial V_{PE}(\theta)}{\partial \theta_i} \quad i = 1, \dots, m.\end{aligned}\tag{9.58}$$

Now

$$\begin{aligned}\dot{V}(\theta, \tilde{\omega}) &= \frac{\partial V}{\partial \theta} \dot{\theta} + \frac{\partial V}{\partial \tilde{\omega}} \dot{\tilde{\omega}} \\ &= \frac{\partial V_{PE}(\theta)}{\partial \theta} \dot{\theta} + \frac{\partial V_{KE}(\tilde{\omega})}{\partial \tilde{\omega}} \dot{\tilde{\omega}} \\ &= -\sum_{i=1}^m f_i(\theta) \dot{\theta}_i + \sum_{i=1}^m M_i \tilde{\omega}_i \dot{\tilde{\omega}}_i \\ &= \sum_{i=1}^m \tilde{\omega}_i (-f_i(\theta) + M_i \dot{\tilde{\omega}}_i) \\ &= 0,\end{aligned}\tag{9.59}$$

Hence, $V(\theta, \tilde{\omega})$, is a valid energy function.

The equilibrium points of (9.58) lie on the subspace $\theta, \tilde{\omega}$ such that $\theta \in \mathbb{R}^m, \tilde{\omega} = 0$. In the previous section, we have qualitatively characterized the PEBS as the hypersurfaces

connecting the u.e.p's. We make it somewhat more precise now. Consider the gradient system

$$\dot{\theta} = \frac{-\partial V_{PE}(\theta)}{\partial \theta}. \quad (9.60)$$

Note that the gradient system has dimension m , which is half the order of the system (9.58). It has been shown by Chiang et al. [105] that the region of attraction of (9.58) is the union of the stable manifolds of u.e.p's lying on the stability boundary. If this region of attraction is projected onto the angle space, it can be characterized by

$$\partial A(\theta^s) = \cup_i W^s(\theta_i^{ub}) \quad (9.61)$$

where θ_i^{ub} is an u.e.p on the stability boundary in the angle space. The stable manifold $W^s(\theta_i^{ub})$ of θ_i^{ub} is defined as the set of trajectories that converge to θ_i^{ub} as $t \rightarrow +\infty$. Since the gradient of $V_{PE}(\theta)$ is a vector orthogonal to the level surfaces $V_{PE}(\theta) = \text{constant}$ in the direction of increased values of $V_{PE}(\theta)$, the PEBS in the direction of decreasing values of $V_{PE}(\theta)$ can be described by the differential equations $\dot{\theta} = -\frac{\partial V_{PE}(\theta)}{\partial \theta} = f(\theta)$. Hence, when the fault-on trajectory reaches the PEBS at $\theta = \theta^*$ corresponding to $t = t^*$, we can integrate the set of equations for $t > t^*$ as

$$\dot{\theta} = f(\theta), \quad \theta(t^*) = \theta^* \quad (9.62)$$

where $f(\theta)$ pertains to the postfault system. This will take $\theta(t)$ along the PEBS to the saddle points (u.e.p's U_1 or U_2 in Figure 9.10 depending on θ^*). The integration of (9.62) requires very small time steps since it is "stiff." Hence, we stop the integration until $\|f(\theta)\|$ is minimum. At this point, let $\theta = \theta_{app}^u$. If we need the exact θ^u , we can solve for $f(\theta) = 0$ in (9.23) using θ_{app}^u as an initial guess. The BCU method is now explained in an algorithmic manner.

9.7.1 Algorithm

- For a given contingency that involves either line switching or load/generation change, compute the postdisturbance s.e.p. θ^s as follows.

The s.e.p and u.e.p's are solutions of the real power equations

$$f_i(\theta) = P_i - P_{ei}(\theta) - \frac{M_i}{M_T} P_{COI}(\theta) = 0 \quad i = 1, \dots, m. \quad (9.63)$$

$\theta_m = \frac{-1}{M_m} \sum_{i=1}^{m-1} M_i \theta_i$, it is sufficient to solve for

$$f_i(\theta) = 0 \quad i = 1, \dots, m-1 \quad (9.64)$$

with θ_m being substituted in (9.64) in terms of $\theta_1, \dots, \theta_{m-1}$. Generally, the s.e.p. θ^s is close to θ^o the prefault e.p. Hence, using θ^o as the starting point, (9.64) can be solved using the Newton-Raphson method.

- Next, compute the controlling u.e.p. θ^u as follows:
 - Integrate the faulted system (9.21) and compute $V(\theta, \tilde{\omega}) = V_{KE}(\tilde{\omega}) + V_{PE}(\theta)$ given in (9.52) at each time step. As in the PEBS algorithm of the previous section, determine when the PEBS is crossed at $\theta = \theta^*$ corresponding to $t = t^*$. This is best done by finding when $f^T(\theta) \cdot (\theta - \theta^s) = 0$.
 - After the PEBS is crossed, the faulted swing equations are no longer integrated. Instead, the gradient system (9.62) of the postfault system is used. This is a

reduced-order system in that only the θ dynamics are considered as explained earlier, i.e., for $t > t^*$

$$\dot{\theta} = f(\theta), \theta(t^*) = \theta^*. \quad (9.65)$$

Equation (9.65) is integrated while looking for a minimum of

$$\sum_{i=1}^m |f_i(\theta)|. \quad (9.66)$$

At the first minimum of the norm given by (9.66), $\theta = \theta_{\text{app}}^u$ and $V_{PE}(\theta_{\text{app}}^u) = V_{cr}$ is a good approximation to the critical energy of the system. The value of θ_{app}^u is almost the relevant or the controlling u.e.p.

- (c) The exact u.e.p can be obtained by solving $f(\theta) = 0$ and using θ_{app}^u as a starting point to arrive at θ^u . Note that since $f(\theta)$ is nonlinear, some type of minimization routine must be used to arrive at θ^u . Generally, θ_{app}^u is so close to θ^u that it makes very little difference in the value of V_{cr} whether θ^u or θ_{app}^u is used.
- 3. V_{cr} is approximated as $V_{cr} = V(\theta^u, 0) = V_{PE}(\theta^u)$.

Because of the path-dependent integral term in V_{PE} , this computation also involves approximation. Unlike computing $V_{PE}(\theta)$ from the faulted trajectory where θ was known, here we do not know the trajectory from the full system. Hence, an approximation has to be used. The most convenient one is the straight-line path of integration. $V_{PE}(\theta^u)$ is evaluated as [104]:

$$V_{PE}(\theta^u) = - \sum_{i=1}^m P_i (\theta_i^u - \theta_i^s) - \sum_{i=1}^{m-1} \sum_{j=i+1}^m \left[C_{ij} \left(\cos \theta_{ij}^u - \cos \theta_{ij}^s \right) - \frac{(\theta_i^u - \theta_i^s) + (\theta_j^u - \theta_j^s)}{(\theta_i^u - \theta_i^s) - (\theta_j^u - \theta_j^s)} D_{ij} \left(\sin \theta_{ij}^u - \sin \theta_{ij}^s \right) \right]. \quad (9.67)$$

We derive the third term of (9.67) as follows. Assume a ray from θ_i^s to θ_i^u and then any point on the ray is $\theta_i = \theta_i^s + p(\theta_i^u - \theta_i^s)$ ($0 \leq p \leq 1$). Thus, $d(\theta_i + \theta_j) = dp(\theta_i^u - \theta_i^s + \theta_j^u - \theta_j^s)$. The path-dependent term $V_d(\theta)$ in (9.49) is now evaluated at θ^u as $V_d(\theta) = \sum_{i=1}^{m-1} \sum_{j=i+1}^m I_{ij}$.

$$\begin{aligned} I_{ij} &= \left[(\theta_i^u - \theta_i^s) + (\theta_j^u - \theta_j^s) \right] \int_0^1 D_{ij} \cos \left[(\theta_i^s - \theta_j^s) + p \left((\theta_i^u - \theta_i^s) - (\theta_j^u - \theta_j^s) \right) \right] dp \\ &= \frac{(\theta_i^u - \theta_i^s) + (\theta_j^u - \theta_j^s)}{(\theta_i^u - \theta_i^s) - (\theta_j^u - \theta_j^s)} D_{ij} \left[\sin \left(\theta_i^s - \theta_j^s \right) + p \left((\theta_i^u - \theta_i^s) - (\theta_j^u - \theta_j^s) \right) \right] \Big|_{p=0}^{p=1} \\ &= \frac{(\theta_i^u - \theta_i^s) + (\theta_j^u - \theta_j^s)}{(\theta_i^u - \theta_i^s) - (\theta_j^u - \theta_j^s)} D_{ij} \left[\sin \theta_{ij}^u - \sin \theta_{ij}^s \right]. \end{aligned} \quad (9.68)$$

4. To compute t_{cr} , we go back to the already-computed value of $V(\theta, \tilde{\omega})$ from the fault-on trajectory in the case of a fault, or the postdisturbance trajectory in the case of load/generation change, and find the time when $V(\theta, \tilde{\omega}) = V_{cr}$. In the case of a fault this time instant gives t_{cr} and the system is stable if the fault is set to clear at a time $t < t_{cr}$. In the case of load/generation change, the system is stable if $V(\theta, \tilde{\omega}) < V_{cr}$ for all t .

Example 9.6 Compute t_{cr} using the BCU method for Example 9.5. Use θ_{app}^u instead of the exact controlling u.e.p θ^u to compute V_{cr} .

The PEBS crossing is computed as in Example 9.5. t^* is obtained as 0.3445 sec and $\theta_1^* = -0.7290$ rad, $\theta_2^* = 2.3988$ rad and $\theta_3^* = 0.6248$ rad.

The gradient system for $t \geq t^*$ is given by

$$\dot{\theta} = f(\theta), \quad \theta(t^*) = \theta^*$$

where $f(\theta)$ is given by (9.63) with the parameters C_{ij} and D_{ij} pertaining to the postfault system. The equations are now integrated until $\|f(\theta)\| = \sum_{i=1}^3 |f_i(\theta)|$ is minimum (Figure 9.13). The minimum obtained is $\|f\| = 0.985$. At this point, $\theta_{app1}^u = -0.7451$ rad, $\theta_{app2}^u = 2.3909$ rad, and $\theta_{app3}^u = 0.6487$ rad. With this, $V_{cr} = V_{PE}(\theta_{app}^u)$ is calculated using (9.67) as 1.0815. Hence, from the fault-on trajectory in Figure 9.11, t_{cr} is between

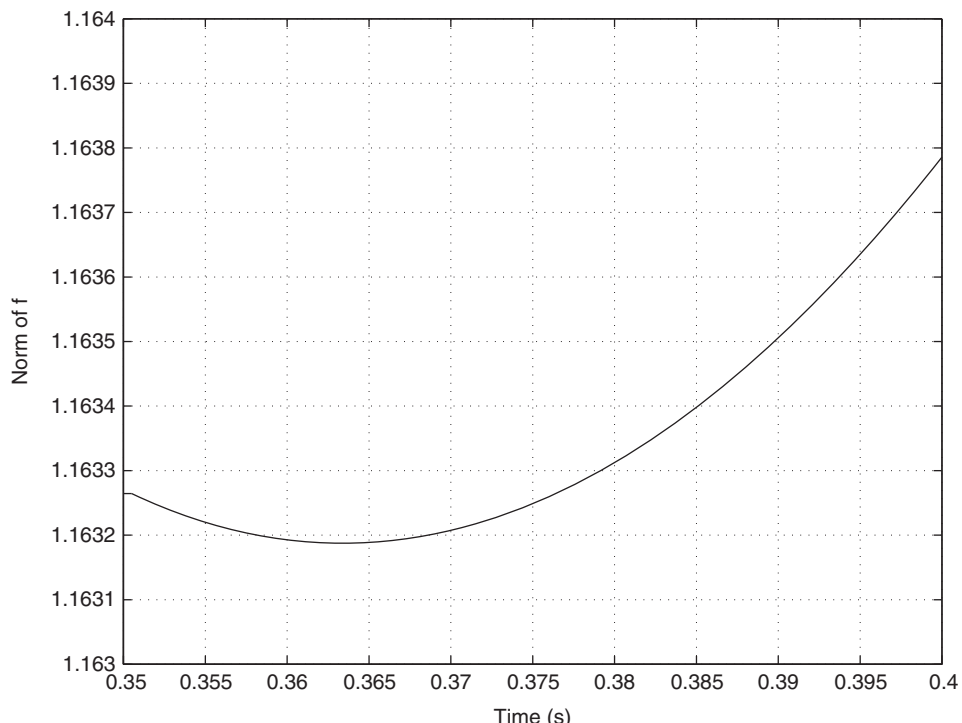


Figure 9.13 Plot $\|f(\theta)\|$ as a function of time in the gradient system.

0.180 and 0.184 sec. In this case, t_{cr} by both the PEBS and BCU method is about the same. The effect of loading, as well as the closed-form approximation to the path-dependent integral on t_{cr} , is discussed in [127]. \square

9.8 Structure-Preserving Energy Functions

The structure-preserving model (7.201)–(7.204) is reproduced below.

$$\dot{\theta}_i = \omega_i - \omega_s \quad (9.69)$$

$$M_i \dot{\omega}_i = T_{Mi} - \sum_{j=1}^{n+m} V_i V_j B_{ij} \sin(\theta_i - \theta_j) \quad i = n+1, \dots, n+m \quad (9.70)$$

$$P_{Li}(V_i) = \sum_{j=1}^{n+m} V_i V_j B_{ij} \sin(\theta_i - \theta_j) \quad i = 1, \dots, n \quad (9.71)$$

$$Q_L(V_i) = - \sum_{j=1}^{n+m} V_i V_j B_{ij} \cos(\theta_i - \theta_j) \quad i = 1, \dots, n. \quad (9.72)$$

Note that the rotor angles δ_i 's are also denoted as θ_i 's. Here, we are assuming constant real power loads so that $P_{Li}(V_i) = P_{Li}$, and reactive power as nonlinear voltage-dependent loads. If the angles are referred to the COI $\delta_o = \frac{1}{M_T} \sum_{i=1}^m M_i \theta_i$, then the angles referenced to COI become $\tilde{\theta}_i = \theta_i - \delta_o$ ($i = 1, \dots, n+m$). It can be shown [101] that the energy function is given by

$$V(\tilde{\omega}, \tilde{\theta}, V) = V_{KE}(\tilde{\omega}) + V_{P1}(\tilde{\theta}, V) + V_{P2}(\tilde{\theta}) \quad (9.73)$$

where

$$V_{KE}(\tilde{\omega}) = \frac{1}{2} \sum_{i=1}^m M_i \tilde{\omega}_i^2$$

$$V_{P1}(\tilde{\theta}, V) = - \sum_{i=n+1}^{n+m} T_{Mi} (\tilde{\theta}_i - \tilde{\theta}_i^s) + \sum_{i=1}^n \int_{V_i^s}^{V_i} \frac{Q_{Li}(V_i)}{V_i} dV_i \quad (9.74)$$

$$\frac{1}{2} \sum_{i=1}^n B_{ii} \left(V_i^2 - (V_i^s)^2 \right) \quad (9.75)$$

$$- \sum_{i=1}^{n+m-1} \sum_{j=i+1}^{n+m} B_{ij} \left(V_i V_j \cos \tilde{\theta}_{ij} - V_i^s V_j^s \cos \tilde{\theta}_{ij}^s \right) \quad (9.76)$$

$$V_{P2}(\tilde{\theta}) = - \sum_{i=1}^n P_{Li} (\tilde{\theta}_i - \tilde{\theta}_i^s). \quad (9.77)$$

This energy function has been used for both transient-stability and voltage-stability analyses. In the second case, only the *PE* term is used, along with the concepts of high- and low-power flow solutions [123, 124].

9.9 Conclusion

In this chapter, we have discussed in detail the transient energy function method for angle stability. The basis of the method has been shown to be the famous Lyapunov's direct method [125]. The equivalence of the energy function to the equal-area criterion has been shown for the single-machine case. For the multimachine case, the PEBS and the BCU have been explained in detail. The TEF method can be used to act as a filter to screen out contingencies in a dynamic security assessment framework [126]. The BCU method is known to be sensitive with respect to the PEBS crossing θ^* . The method can be made more robust by tracking the stable manifold to the controlling u.e.p using what is called "shadowing" method [128]. Finally, the structure-preserving energy function (SPEF) has been derived. The SPEF is an active area of research [129].

9.10 Problems

- 9.1** A single machine connected to an infinite bus has the following faulted and post-fault equations.

Faulted

$$0.0133 \frac{d^2\delta}{dt^2} = 0.91 \quad 0 < t \leq t_{cl}.$$

Postfault

$$0.0133 \frac{d^2\delta}{dt^2} = 0.91 - 3.24 \sin \delta \quad t > t_{cl}.$$

The prefault system is the same as the postfault system.

- (a) Find $V(\delta, \omega)$ and V_{cr} using the u.e.p formulation.
- (b) Explain stability test of (a) using the equal-area criterion. Sketch the areas A_1, A_2, A_3 .
- (c) Find t_{cr} using V_{cr} .
- (d) Find t_{cr} using PEBS method.

- 9.2** For the 3-machine system of Example 7.1, a fault occurs at bus 7 and is cleared at t_{cl} with no line switching.

- (a) Based on prefault load flow and using the classical model, compute the voltages behind transient reactances and the rotor angles at $t = 0^-$.
- (b) Find \bar{Y}_{int} for the faulted and the postfault cases.
- (c) Write the energy function $V(\theta, \tilde{\omega})$, assuming $G_{ij} = 0(i \neq j)$.
- (d) Write the faulted equations in COI notation, together with the initial conditions.
- (e) Compute t_{cr} using the PEBS method.
- (f) Repeat (c), (d), and (e), assuming $G_{ij} \neq 0$.

- 9.3** For Problem 8.1 using the classical model, compute \bar{Y}_{int} for prefault and \bar{Y}_{int} for a fault at bus 112.
- 9.4** Compute for Problem 8.1 the voltages behind transient reactances and the rotor angles at $t = 0^-$.
- (a) Using results of Problem 9.3, write the energy function $V(\theta, \tilde{\omega})$. Assume that the fault at bus 112 is self-clearing.
- (b) Using the PEBS method, compute t_{cr} .
- 9.5** Use the BCU method to compute t_{cr} for Problems 9.2 and 9.4. Do this first for $G_{ij} = 0(i \neq j)$ and then for $G_{ij} \neq 0$. Compare the results with the PEBS method.

10

Synchronized Phasor Measurement

10.1 Background

An AC power network operates with sinusoidal voltages and currents at the nominal system frequency. Each of these voltage and current quantities can be represented by a phasor with a frequency, magnitude, and phase. If the sinusoidal voltage and current waveforms are measured and their magnitude and phase quantities are calculated, then the power flow on the transmission lines can be obtained. Phasor computation is a digital technology of estimating the phasor components from the measured analog waveforms. Devices to perform such digital signal processing are called phasor measurement units (PMUs) [130].

Phasors can be used in many applications beside power flow computation. With advanced monitoring and protection needs, it is necessary to measure the magnitude and phase of power system three-phase waveforms so that dynamic phenomena can be captured. Phasors can also be used for the monitoring of ambient and disturbance conditions in power systems. Coupled with GPS time pulses, the estimates from PMUs in geographically dispersed areas can be analyzed as a complete system to observe the propagation and impact of large disturbances, such as generator trips and system separation. These time-synchronized phasor measurements are also referred to as synchrophasors.

A sinusoidal waveform in the time domain is defined as (Figure 10.1)

$$x(t) = \sqrt{2}A \cos(\omega t + \phi) = \sqrt{2}A \cos(2\pi ft + \phi) = \operatorname{Re}\{\sqrt{2}Ae^{j(2\pi ft+\phi)}\} \quad (10.1)$$

where A is the rms value of the amplitude, ω is the frequency in rad/sec, and f is the frequency in Hz. The phase ϕ is defined relative to a time reference denoted by $t = 0$. The signal can be represented as a phasor (denoted by the $\tilde{\cdot}$ symbol)

$$\tilde{X} = Ae^{j\phi} = A\angle\phi = X_r + jX_i \quad (10.2)$$

where $X_r = A \cos \phi$ and $X_i = A \sin \phi$ are the real and imaginary parts of \tilde{X} , and the frequency f is not explicitly shown. In a PMU, the frequency f , nominally at the system frequency of 50 or 60 Hz, is also estimated to account for off-nominal frequency operation.

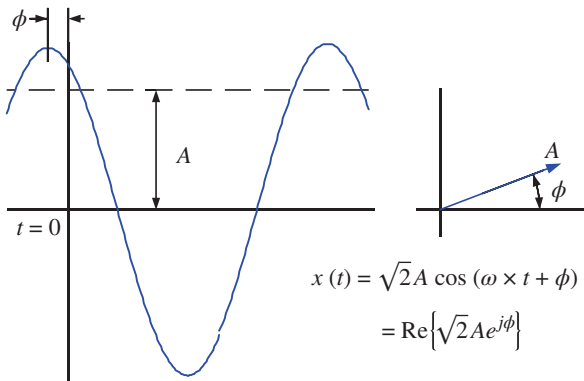


Figure 10.1 Sinusoidal waveform in time domain and vector form.

The first part of this chapter provides a description of methods in computing the phasor quantities, in particular, at off-nominal frequencies. The second part discusses a few applications of PMU data to monitor the impact of disturbances on a power system and extract power system disturbance information. PMU data is also useful for reinforcing some of the power system dynamics concepts developed in the earlier chapters.

Even though the phasor measurement technology was invented in the late 1980s, it has only been recently (early 2010s) that large numbers of phasor measurement units have been installed in many countries, particularly in US and China. Such a denser coverage of PMUs will promote the use of new algorithms to enhance power system reliability, with the ultimate goal of eliminating cascading failures. In this fast moving technology area, the applications discussed in this book hopefully will only be the tip of the iceberg.

10.2 Phasor Computation

The basic method used to compute the phasor representation of a sinusoidal signal $x(t)$ is the discrete Fourier transform (DFT) [131]. Denote the system fundamental frequency as f_o , and let the uniform sampling rate be $f_s = Nf_o$, where N is an integer, such that $x(t)$ is sampled at a sampling period $\tau = 1/f_s$ with N points per cycle of the fundamental frequency. The sampled signal is denoted by $x_k = x(k\tau)$, $k = 0, 1, \dots$.

10.2.1 Nominal Frequency Phasors

If the voltage or current signal $x(t)$ is precisely at f_o , then the phasor \tilde{X} representation in rectangular form with the RMS value for the amplitude can be readily computed from the sampled data x_k using DFT as

$$\tilde{X} = \frac{1}{\sqrt{2}} \frac{2}{N} (X_c - jX_s) = \frac{\sqrt{2}}{N} (X_c - jX_s) \quad (10.3)$$

where

$$X_c = \sum_{k=0}^{N-1} x_k \cos k\theta, \quad X_s = \sum_{k=0}^{N-1} x_k \sin k\theta \quad (10.4)$$

and

$$\theta = \frac{2\pi}{N} = 2\pi f_o \tau \quad (10.5)$$

The phasor can also be computed in polar coordinates as

$$\tilde{X} = \frac{\sqrt{2}}{N} \sum_{k=0}^{N-1} x_k e^{-j \frac{2\pi k}{N}} \quad (10.6)$$

Note that the DFT (10.3)–(10.4) can be computed recursively by replacing the first point in the DFT with a newly measured point [130]. However, care must be taken to prevent the cumulation of truncation error in such recursive methods.

10.2.2 Off-Nominal Frequency Phasors

When a power system is operated at precisely the nominal frequency f_o , the computation of a phasor (10.6) is quite straightforward. The instantaneous frequency of a practical power system, however, typically fluctuates in a narrow band (normally within ± 20 mHz) about the nominal frequency f_o every few seconds or minutes, as the system operators take frequency corrective actions. Thus a reliable phasor computation scheme needs to adapt the DFT computation (10.3) to frequencies that are slightly different from f_o . Figure 10.2 shows two possible architectures used in real-time phasor computation. Both schemes use analog anti-aliasing filtering

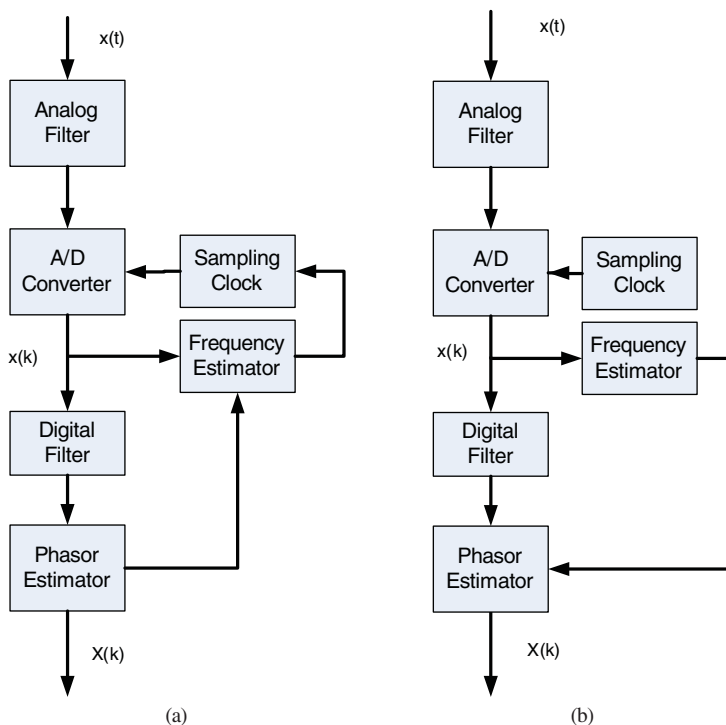


Figure 10.2 Phasor estimation architectures: (a) Frequency Tracking, and (b) Frequency Compensation [130]. Source: Phadke 2008 [130]. Reproduced with permission of Springer.

to limit the bandwidth of the input signal. Furthermore, digital filtering may also be used to provide band-pass filtering and remove frequency components that may create difficulties for specific applications.

The main difference between the two architectures in Figure 10.2 is the sampling rate. The frequency tracking architecture uses the instantaneous frequency to compute the phasor. To accomplish this, it requires over-sampling at a sufficiently high frequency and then resampling to the estimated instantaneous frequency. The drawback of this approach is the additional computational burden for over-sampling and resampling. The technicalities of these schemes are quite advanced [132, 133] and the implementations of such schemes can be computationally intensive.

A non-DFT variant of the frequency tracking method is to use an estimation method to directly compute the phasor representation of an off-nominal frequency sinusoidal signal. Most of these estimation methods employ an iterative nonlinear least-squares or Newton-like method to simultaneously estimate the amplitude, phase, and frequency of the signal [134]. In addition, some methods will also estimate the significant harmonic frequencies in the signal, in addition to the fundamental frequency.

The second group of algorithms samples the signals at a fixed frequency with a fixed data window length. The actual frequency is estimated and the calculated phasor is compensated as a function of the frequency deviation [132]. This approach is simpler and largely used in commercial PMUs. It will be discussed here, following the treatment in [130].

Let an off-nominal frequency signal be given by a continuous-time signal

$$x(t) = X_m \cos(\omega t + \phi), \quad \omega = \omega_o + \Delta\omega \quad (10.7)$$

where $\Delta\omega$ is the frequency deviation from the nominal frequency ω_o . The phasor representation of this signal in RMS values is

$$\tilde{X} = (X_m / \sqrt{2}) e^{j\phi} \quad (10.8)$$

such that the signal $x(t)$ can be recovered as

$$x(t) = \sqrt{2} \operatorname{Re}\{\tilde{X} e^{j\omega t}\} \quad (10.9)$$

Let \tilde{X}^* be the complex conjugate of \tilde{X} . Then $x(t)$ can be expressed as

$$x(t) = (1/\sqrt{2})(\tilde{X} e^{j\omega t} + \tilde{X}^* e^{-j\omega t}) \quad (10.10)$$

At the sampling time $t = k\tau$, the discrete-time signal is

$$x_k = (1/\sqrt{2})(\tilde{X} e^{jk\omega\tau} + \tilde{X}^* e^{-jk\omega\tau}) \quad (10.11)$$

The DFT of the signal x_k for one period of the nominal frequency using x_r as the first sample will yield a quantity

$$\tilde{X}'_r = \frac{\sqrt{2}}{N} \sum_{k=r}^{r+N-1} x_k e^{-jk\omega_o\tau} = \frac{1}{N} \sum_{k=r}^{r+N-1} (\tilde{X} e^{jk\omega\tau} + \tilde{X}^* e^{-jk\omega\tau}) e^{-jk\omega_o\tau} \quad (10.12)$$

Note that \tilde{X}'_r at $r = 0$ is not the same as the phasor \tilde{X} unless $\omega = \omega_o$.

Using the identities

$$e^{j\theta} - 1 = e^{j\theta/2}(e^{j\theta/2} - e^{-j\theta/2}) = 2je^{j\theta/2} \sin(\theta/2) \quad (10.13)$$

and

$$\sum_{k=0}^{N-1} e^{jk\theta} = \frac{e^{jN\theta} - 1}{e^{j\theta} - 1} \quad (10.14)$$

(10.12) can be rewritten as

$$\tilde{X}'_r = P\tilde{X}e^{jr(\omega-\omega_o)\tau} + Q\tilde{X}^*e^{-jr(\omega+\omega_o)\tau} \quad (10.15)$$

where

$$P = \left\{ \frac{\sin \frac{N(\omega-\omega_0)\tau}{2}}{N \sin \frac{(\omega-\omega_0)\tau}{2}} \right\} e^{j(N-1)\frac{(\omega-\omega_0)\tau}{2}} \quad (10.16)$$

$$Q = \left\{ \frac{\sin \frac{N(\omega+\omega_0)\tau}{2}}{N \sin \frac{(\omega+\omega_0)\tau}{2}} \right\} e^{-j(N-1)\frac{(\omega+\omega_0)\tau}{2}} \quad (10.17)$$

With $\omega = \omega_o + \Delta\omega$, these expressions can be represented by

$$\tilde{X}'_r = P\tilde{X}e^{jr\Delta\omega\tau} + Q\tilde{X}^*e^{-jr(2\omega_o+\Delta\omega)\tau} \quad (10.18)$$

$$P = \left\{ \frac{\sin \frac{N\Delta\omega\tau}{2}}{N \sin \frac{\Delta\omega\tau}{2}} \right\} e^{j(N-1)\frac{\Delta\omega\tau}{2}} \quad (10.19)$$

$$Q = \left\{ \frac{\sin \frac{N(2\omega_0+\Delta\omega)\tau}{2}}{N \sin \frac{(2\omega_0+\Delta\omega)\tau}{2}} \right\} e^{-j(N-1)\frac{(2\omega_0+\Delta\omega)\tau}{2}} \quad (10.20)$$

Note that P and Q are complex quantities dependent on $\Delta\omega$. The values of P and Q for $\Delta f = 0, \pm 0.5, \pm 1.0$ Hz are shown in Table 10.1 for $f_o = 60$ Hz and $\tau = 1/1440$ sec, that is, 24 samples per cycle.

For a small $\Delta\omega$, the time-varying phasor X'_r can be considered as mainly due to the first component $P\tilde{X}e^{jr\Delta\omega\tau} \approx \tilde{X}$, superimposed with a time-varying quantity $Q\tilde{X}^*e^{-jr(2\omega_o+\Delta\omega)\tau}$ that oscillates about \tilde{X} at about twice the nominal frequency. This second harmonic component is visible as a modulation of $|X'_r|$ and is illustrated in the following example.

Table 10.1 Values of P and Q for several values of Δf .

Δf (Hz)	$ P $	$\angle P$ (deg)	$ Q $	$\angle(\text{sgn}(\Delta f)Q)$ (deg)
-1.0	0.9995	-2.87	0.0085	17.87
-0.5	0.9999	-1.44	0.0042	16.44
0	1.0000	0	0	15.00
0.5	0.9999	1.44	0.0042	13.56
1.0	0.9995	2.87	0.0084	12.12

Example 10.1 Consider a sinusoidal signal $x(t)$ of unity amplitude with a frequency of 59.9 Hz

$$x(t) = \cos(2\pi \times 59.9t + \pi/3) = \cos(2\pi \times 59.9t + 1.0472 \text{ rad}) \quad (10.21)$$

Sampling this signal at 1,440 Hz results in the discrete-time signal

$$x_k = \cos(2\pi \times 59.9 \times (k/1440) + \pi/3), \quad k = 0, 1, 2, \dots \quad (10.22)$$

Compute X'_r , assuming that the signal is at 60 Hz.

Solution:

The number of points per cycle at the nominal frequency is

$$N = f_s/f_o = 1440/60 = 24 \quad (10.23)$$

The first 24 samples of the signal is shown in the Table 10.2.

The phasor starting at the first point, assuming a frequency of 60 Hz, can be computed as

$$\tilde{X}'_0 = \frac{\sqrt{2}}{N} \sum_{n=0}^{N-1} x_n e^{-j\frac{2\pi n}{N}} = 0.3562 + j0.6110 = 0.7073 \angle 1.0430 \text{ rad} \quad (10.24)$$

which is not identical to the phasor $\tilde{X} = 0.7071 \angle 1.0472 \text{ rad}$ at 59.9 Hz, as explained earlier. Table 10.3 shows the values of \tilde{X}'_r , for $r = 0, 1, \dots, 23$. \square

Note that the signal $x(t)$ in Example 10.1 is only 0.1 Hz below the nominal frequency of 60 Hz. Thus $P \approx 1$ and Q is quite small. If the frequency of the signal $x(t)$ deviates by a higher value, say 5 Hz, the impact of P and Q will become more significant. Figure 10.3

Table 10.2 First 24 samples of the 59.9 Hz signal (10.22).

Sample no.	x_k	Sample no.	x_k
0	0.5000	12	-0.5045
1	0.2592	13	-0.2643
2	0.0009	14	-0.0061
3	-0.2576	15	0.2525
4	-0.4985	16	0.4939
5	-0.7056	17	0.7018
6	-0.8647	18	0.8621
7	-0.9651	19	0.9637
8	-1.0000	20	1.0000
9	-0.9669	21	0.9683
10	-0.8682	22	0.8708
11	-0.7105	23	0.7142

Table 10.3 Values of \tilde{X}'_r , for $r = 0, 1, \dots, 23$.

r	$ \tilde{X}'_r $	$\angle\tilde{X}'_r$ (deg)	r	$ \tilde{X}'_r $	$\angle\tilde{X}'_r$ (deg)
0	0.7073	59.7593	12	0.7072	-120.5406
1	0.7075	74.7220	13	0.7075	-105.5776
2	0.7077	89.6755	14	0.7077	-90.6240
3	0.7077	104.6256	15	0.7077	-75.6739
4	0.7075	119.5788	16	0.7075	-60.7208
5	0.7073	134.5410	17	0.7073	-45.7589
6	0.7070	149.5156	18	0.7070	-30.7845
7	0.7067	164.5028	19	0.7067	-15.7976
8	0.7065	179.4992	20	0.7065	-0.8013
9	0.7065	-165.5008	21	0.7065	14.1987
10	0.7067	-150.5039	22	0.7067	29.1957
11	0.7069	-135.5161	23	0.7069	44.1838

shows the phasor computation for the 55 Hz continuous-time signal

$$x(t) = 100\sqrt{2} \cos(2\pi \times 55t + \pi/3) \quad (10.25)$$

sampled at 1,440 point/sec. Note that in Figure 10.3(b), the second harmonic component modulates the signal magnitude of 100.

10.2.3 Post Processing

Under off-nominal frequency operation, the phasor expression (10.12) requires a post-processing step to correct for the effects caused by the leakage phenomenon, resulting from the truncation of sampled data outside the data window. If the off-nominal frequency is known, the correction factors P (10.16) and Q (10.17) can be readily computed and applied to correct for \tilde{X}_r . The second harmonic component cannot be compensated with just a fixed value. However, it can be removed with filtering such as the technique described in [135, 136].

A simple way to minimize the impact of the second harmonic component is to use a three-point-average filter [130]. For a sinusoidal signal at the fundamental frequency, the sum of three points, each 120° apart, will equal zero. As the undesired signal is the second harmonic component, the three points on the fundamental frequency signal would be only 60° apart. A three-point-average filter can be implemented in various ways. Here the three-point-average filter for \tilde{X}'_r is implemented as

$$(\tilde{X}'_r)^{3pf} = |(\tilde{X}'_r)^{3pf}| \angle\tilde{X}'_r \quad (10.26)$$

where the magnitude is averaged as

$$|(X'_r)^{3pf}| = (|\tilde{X}'_r| + |\tilde{X}'_{r+N/6}| + |\tilde{X}'_{r+2N/6}|)/3 \quad (10.27)$$

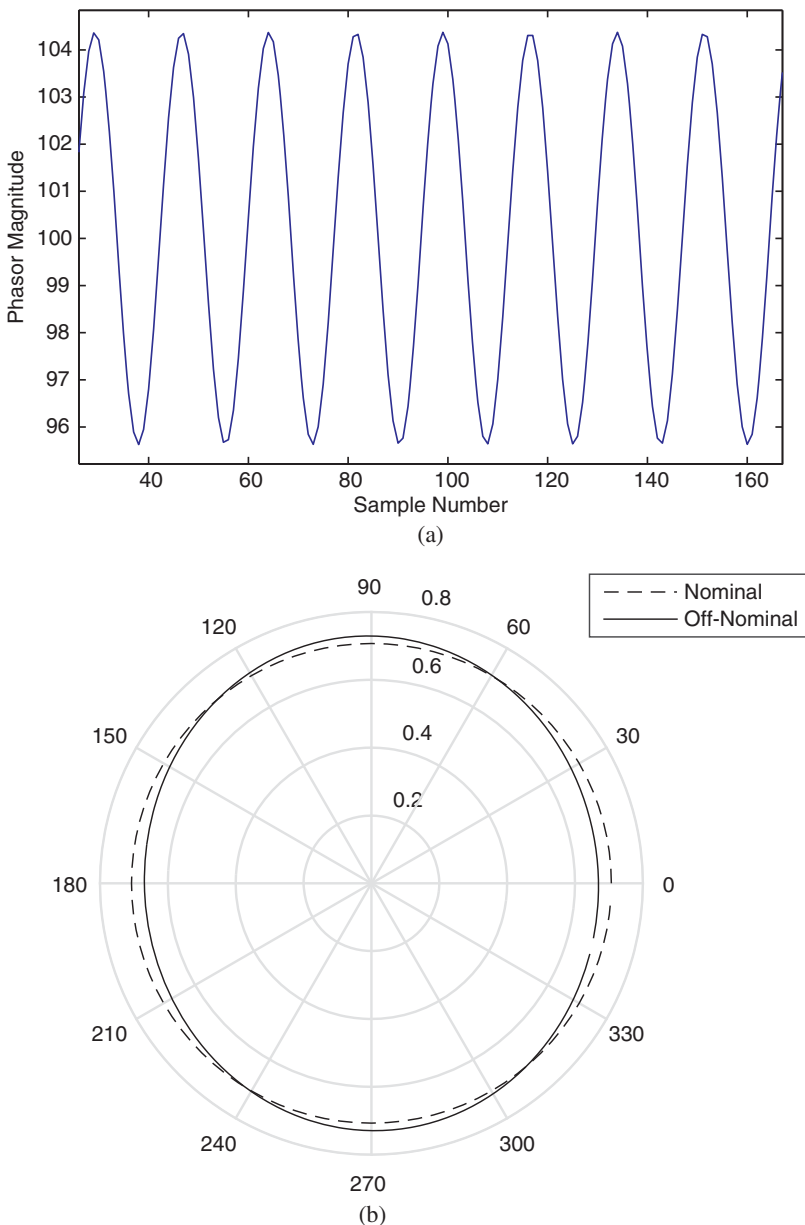


Figure 10.3 \tilde{X}'_r of the 55 Hz signal $x(t)$ (10.25): (a) $|\tilde{X}'_r|$ and (b) polar plot of \tilde{X}'_r .

where N is the number of data points per cycle, and presumed to be a multiple of 6. This filtering will remove the \tilde{X}^* component of \tilde{X}'_r (10.15), so that an estimate of \tilde{X}_r is

$$\tilde{X}_r^{\text{est}} = (\tilde{X}'_r)^{3\text{pf}} / P \quad (10.28)$$

Example 10.2 For the signal in Example 10.1, use (10.26) and (10.28) to compute \tilde{X}_0^{est} from \tilde{X}'_0 , where $N = 24$.

Solution

Using the data points in Table 10.3

$$|(\tilde{X}'_0)|^{3\text{pf}} = (|\tilde{X}'_0| + |\tilde{X}'_4| + |\tilde{X}'_8|)/3 = 0.7071 \quad (10.29)$$

The scale factor P is computed as

$$P = \left\{ \frac{\sin \frac{24(-0.1)\frac{1}{1440}}{2}}{24 \sin \frac{(-0.1)\frac{1}{1440}}{2}} \right\} e^{j(24-1)\frac{(-0.1)\frac{1}{1440}}{2}} = 1.0000 \angle -0.2875^\circ \quad (10.30)$$

such that

$$\tilde{X}_0^{\text{est}} = (\tilde{X}'_0)^{3\text{pf}}/P = 0.7071 \angle 60.0468^\circ \quad (10.31)$$

which differs from $\tilde{X}_0 = 0.7071 \angle 60^\circ$ by a phase angle of only 0.0468° . \square

10.2.4 Positive-Sequence Signals

The signal processing technique discussed earlier can be applied individually to each of the three voltage and current phases of an AC power network. These single-phase phasors can be streamed from a phasor measurement unit (PMU) to a phasor data concentrator for visualization and monitoring. For most monitoring functions, only the positive-sequence quantities need to be streamed from the PMU. This section shows that second harmonics filtering is not needed for positive-sequence quantities if the system is operating in balanced three-phase condition.

The transformation from the abc phases to the zero (0), positive (1), and negative (2) sequence quantities is given by

$$\begin{bmatrix} \tilde{X}_0 \\ \tilde{X}_1 \\ \tilde{X}_2 \end{bmatrix} = \frac{1}{3} \begin{bmatrix} 1 & 1 & 1 \\ 1 & \alpha & \alpha^2 \\ 1 & \alpha^2 & \alpha \end{bmatrix} \begin{bmatrix} \tilde{X}_a \\ \tilde{X}_b \\ \tilde{X}_c \end{bmatrix} \quad (10.32)$$

where $\alpha = 1 \angle 120^\circ$, and phase α is taken to align with the positive sequence.

Let \tilde{X}'_{rk} , $k = a, b, c$, be the measured phase- a , b , and c phasors at the data point r , respectively. Then the measured sequence phasors are given by

$$\begin{bmatrix} \tilde{X}'_{r0} \\ \tilde{X}'_{r1} \\ \tilde{X}'_{r2} \end{bmatrix} = \frac{1}{3} \begin{bmatrix} 1 & 1 & 1 \\ 1 & \alpha & \alpha^2 \\ 1 & \alpha^2 & \alpha \end{bmatrix} \begin{bmatrix} \tilde{X}'_{ra} \\ \tilde{X}'_{rb} \\ \tilde{X}'_{rc} \end{bmatrix} \quad (10.33)$$

$$\begin{aligned} &= \frac{1}{3} \begin{bmatrix} P(\tilde{X}_a + \tilde{X}_b + \tilde{X}_c)e^{jr\Delta\omega\tau} + Q(\tilde{X}_a^* + \tilde{X}_b^* + \tilde{X}_c^*)e^{-jr(2\omega_o + \Delta\omega)\tau} \\ P(\tilde{X}_a + \alpha\tilde{X}_b + \alpha^2\tilde{X}_c)e^{jr\Delta\omega\tau} + Q(\tilde{X}_a^* + \alpha\tilde{X}_b^* + \alpha^2\tilde{X}_c^*)e^{-jr(2\omega_o + \Delta\omega)\tau} \\ P(\tilde{X}_a + \alpha^2\tilde{X}_b + \alpha\tilde{X}_c)e^{jr\Delta\omega\tau} + Q(\tilde{X}_a^* + \alpha^2\tilde{X}_b^* + \alpha\tilde{X}_c^*)e^{-jr(2\omega_o + \Delta\omega)\tau} \end{bmatrix} \end{aligned} \quad (10.34)$$

For balanced 3-phase operation, (10.34) reduces to

$$\begin{bmatrix} \tilde{X}'_{r0} \\ \tilde{X}'_{r1} \\ \tilde{X}'_{r2} \end{bmatrix} = \begin{bmatrix} 0 \\ P\tilde{X}_a e^{jr\Delta\omega\tau} \\ Q\tilde{X}_a^* e^{-jr(2\omega_o + \Delta\omega)\tau} \end{bmatrix} \quad (10.35)$$

that is, the positive-sequence quantities will not have second harmonic components, although the second harmonic components will dominate the negative-sequence quantities. Thus second harmonics filtering is not needed for positive-sequence quantities.

10.2.5 Frequency Estimation

Power system frequency is important in phasor computation for two reasons. First, a phasor has to be associated with a frequency, in addition to its magnitude and phase. Second, the frequency deviation is needed in computing the correction factor P (10.16). The frequency of a power system is not an instantaneously measured value, like the current flowing in a transmission line. Instead, frequency is calculated from a voltage waveform data window. Several frequency measurement methodologies can be found in [137–141]. The method used in [138, 140, 141] to compute the frequency deviation will be discussed here.

Suppose during a period $t = 0$ to $t = T$, the initial frequency deviation is $\Delta\omega$ and the frequency in the period is changing at a constant rate of $d\omega/dt$. Then the frequency within the period would be represented by

$$\omega(t) = \omega_o + \Delta\omega + \frac{d\omega}{dt}t, \quad 0 \leq t \leq T \quad (10.36)$$

and the phase angle would be

$$\varphi(t) = \int_{\tau=0}^t \omega(\tau)d\tau = \varphi_o + t\omega_o + t\Delta\omega + \frac{1}{2}t^2 \frac{d\omega}{dt} \quad (10.37)$$

where φ_o is the value of φ at $t = 0$.

Define two time points t_1 and $t_2 > t_1$ that are a few cycles apart. For small $t = (t_2 - t_1)$, the rate of change in frequency $d\omega/dt$ can be neglected, such that

$$\varphi(t_2) - \varphi(t_1) = (t_2 - t_1)\Delta\omega \quad (10.38)$$

yielding the off-nominal frequency estimate as

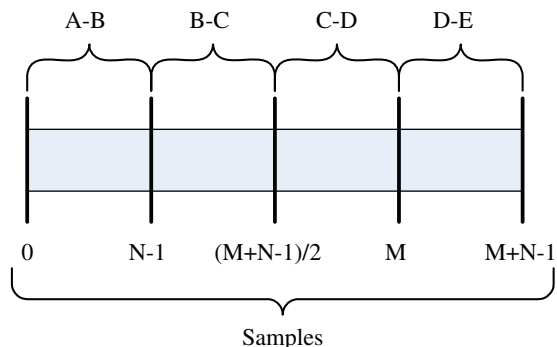
$$\Delta\omega = (\varphi(t_2) - \varphi(t_1))/(t_2 - t_1) \quad (10.39)$$

Figure 10.4 illustrates this method in which the phase angles of a signal are computed for the data windows AB and DE , each with N data points. The integer M can be taken as the size of the data window for frequency calculation. Here the frequency deviation is computed as

$$\Delta\omega = \frac{\varphi^{DE} - \varphi^{AB}}{M\tau} \quad (10.40)$$

The following example illustrates frequency estimation using the signal in Example 10.1.

Figure 10.4 Phasor-based frequency estimation. Source: Fan 2007 [140]. Reproduced with permission of IEEE.



Example 10.3 For the 59.9 Hz signal in Example 10.1, use (10.40) to estimate the frequency of the signal.

Solution

In this example, $M = 4N = 96$ is chosen, which represents 4 cycles. The phase angle of the first cycle has already been computed in Example 10.2. The time domain samples from the fifth cycle are shown in the Table 10.4. The phasor can be computed as

$$\tilde{X}_{5\text{th}} = \frac{\sqrt{2}}{N} \sum_{n=M}^{M+N-1} x_n e^{-j\frac{2\pi n}{N}} = 0.3814 + j0.5955 = 0.7072 \angle 1.0011 \text{ rad} \quad (10.41)$$

Thus the frequency deviation can be estimated as

$$\Delta f = \frac{1}{2\pi} \frac{1.0430 - 1.0011}{(96/1440)} = -0.10 \text{ Hz} \quad (10.42)$$

such that the frequency of the signal is 59.9 Hz. □

Table 10.4 Fifth cycle samples of the 59.9 Hz signal (10.21).

Sample no.	x_k	Sample no.	x_k
0	0.5358	12	-0.5402
1	0.2995	13	-0.3044
2	0.0427	14	-0.0480
3	-0.2169	15	0.2118
4	-0.4617	16	0.4571
5	-0.6753	17	0.6714
6	-0.8429	18	0.8401
7	-0.9533	19	0.9517
8	-0.9990	20	0.9987
9	-0.9768	21	0.9779
10	-0.8882	22	0.8906
11	-0.7393	23	0.7429

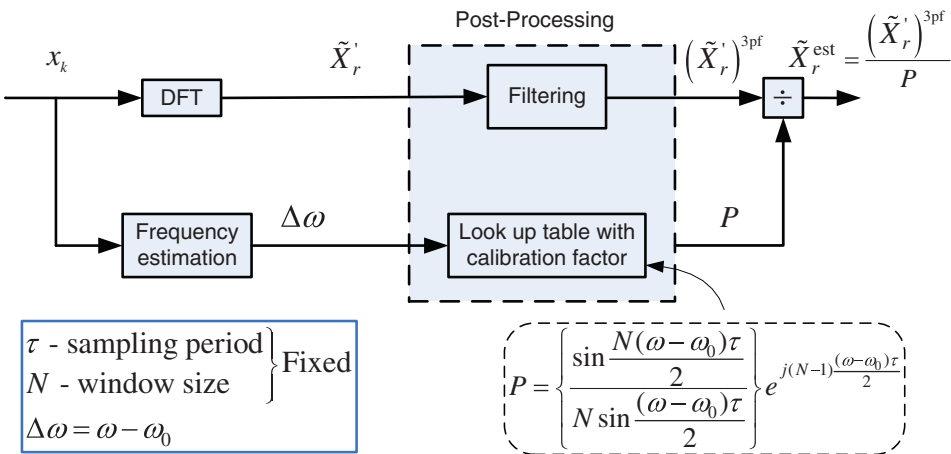


Figure 10.5 Phasor processing algorithm for uniform sampling [143].

This multi-step process of phasor computation with frequency estimation is shown in Figure 10.5.

10.2.6 Phasor Data Accuracy

Many PMU applications require using PMU data from multiple substations, with PMUs which may be supplied by different vendors. Thus it is important that all PMUs adhere to a common standard on the estimated synchrophasor values. In the IEEE Synchrophasor Standard C37.118.1 [142], the accuracy of the phasor computation of a PMU is specified using a real quantity called the total vector error given by

$$\text{TVE}(k) = \sqrt{\frac{(X_{\text{re}}^{\text{est}}(k) - X_{\text{re}}(k))^2 + (X_{\text{im}}^{\text{est}}(k) - X_{\text{im}}(k))^2}{X_{\text{re}}(k)^2 + X_{\text{im}}(k)^2}} \quad (10.43)$$

where $X_{\text{re}}^{\text{est}}(k)$ and $X_{\text{im}}^{\text{est}}(k)$ are the real and imaginary parts, respectively, of the estimated phasor, and $X_{\text{re}}(k)$ and $X_{\text{im}}(k)$ are the real and imaginary parts, respectively, of the input signal at the sampling time k . The circular region in Figure 10.6 is within 1% of the TVE, which is the accuracy required by the C37.118 standard.

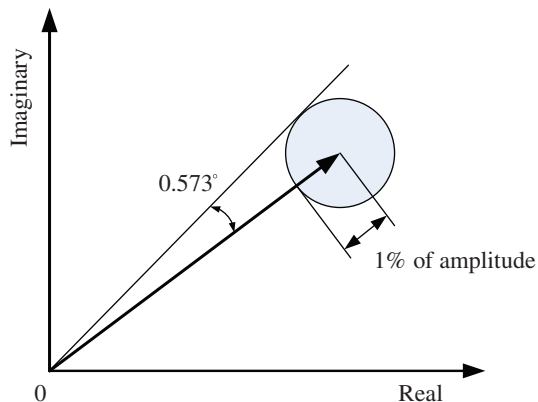
An alternative means of specifying the accuracy of a phasor is to define the magnitude error (ME) and the phase error (PE) separately as

$$\text{ME} = \left| \frac{X_m^{\text{est}} - X_r}{X_r} \right|, \quad \text{PE} = |\phi_m^{\text{est}} - \phi_r| \quad (10.44)$$

where X_m^{est} and X_r are the estimated and reference amplitude, and ϕ_m^{est} and ϕ_r are the estimated and reference phase of the signal. This method of accuracy specification is used in China [144].

The performance of a PMU for various signal conditions can be tested under the following signal conditions:

Figure 10.6 A 1% TVE shown on the end of a phasor.



1. Magnitude modulation test - change in the amplitude of the signal
2. Frequency modulation test - change in the frequency of the signal
3. Step test - a step change in the signal frequency from the nominal to an off-nominal value
4. Frequency ramp test - a ramp change in the signal frequency from the nominal to an off-nominal value over a set time period

Some test methodologies and results can be found in [145, 146]. Such tests would evaluate steady-state and dynamic performance of a PMU to amplitude and frequency variations of an input sinusoidal signal close to the nominal frequency.

10.2.7 PMU Simulator

To foster advances in PMUs, researchers from many countries have contributed to the development of an open model for PMU technology [147–149]. However, most of them need hardware components and may require a laboratory environment. The PMU simulator, presented in [136], is based on the MATLAB SIMULINK™ platform and does not rely on hardware components. The main goal is to replicate the device architecture and phasor computation algorithms available in the literature [130] for education and research, and for exploring the algorithms involved in the phasor measurement process. In the SIMULINK™ environment, the PMU Simulator shows the various functional blocks within a practical PMU, and can be readily used for simulation and symmetrical component estimation. The relevant parameters such as the input sinusoidal wave amplitude, frequency, and phase, can be changed on-the-fly. This software tool will provide hands-on experience for understanding the algorithms and tradeoffs involved in the phasor measurement process, such as:

1. Off-nominal frequency operation
2. Unbalanced phase operation
3. Impact of correction factors for off-nominal frequency signal
4. Process real measured raw PMU data

The PMU Simulator can be downloaded from a link on the third author's website.

10.3 Phasor Data Communication

PMU data is often used by control centers to monitor the dynamics in a power system. This is accomplished by having PMUs in substations streaming the time-tagged phasor data, at a rate of 30/50/60 Hz, to a phasor data concentrator (PDC) located in the independent system operator (ISO). In a typical configuration, the PMUs in substations owned by the same transmission operator (TO) will be first streamed to a TO PDC. If a substation has more than one PMU, their data streams can be collected by a local PDC, which will send the PMU data out as a single data stream. The TO PDC will then assemble all the incoming phasor streams for a particular time tag and forward the collected data as a larger, single phasor stream to the ISO PDC. In addition, the ISO PDC may share some of its PMU data with neighboring ISOs. This communication structure is shown in Figure 10.7.

For a PDC to accept phasor data from PMUs made by different vendors, PMU data is streamed in prespecified message frames. The information contained in each data frame includes the following fields:

1. IDCODE - PMU/PDC identification number
2. SOC - second-of-century time-stamp
3. FRACSEC - fraction of second and time quality
4. PHASORS - estimates of single-phase or positive-sequence voltage and current phasors in either rectangular or polar coordinates
5. FREQ - frequency

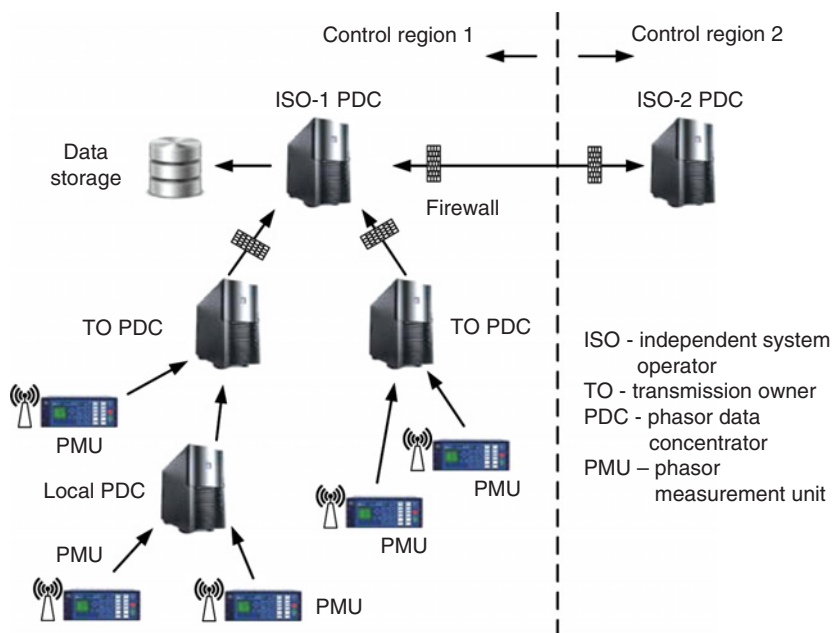


Figure 10.7 Communication infrastructure for phasor data.

6. DFREQ - rate of change of frequency
7. ANALOG - analog (non-sinusoidal) data such as a control signal or transducer value
8. DIGITAL - digital data such as a bitmapped status or flag

A complete list of fields with detailed explanations can be found in the IEEE Synchrophasor Standard C37.118.2 [147].

To transport the data frames over the internet, the sending and receiving hosts' addresses and network protocol are added to the data packets, defining the transportation mode [150]. Typically, the User Datagram Protocol (UDP) is more suitable for data communication when time-sensitive information is required, such as applications for control actions. UDP uses a simple connectionless transmission model with a minimum of protocol mechanism and does not require an acknowledgement from the receiving host. The Transmission Control Protocol (TCP) is more suitable when reliable transmission is desired, like data storage for archival purposes. TCP provides reliable and error-checked delivery of data stream running on hosts communicating over the Internet. Thus TCP requires a slightly longer time for message transmittal.

10.4 Power System Frequency Response

Power systems operate within a narrow range of the nominal frequency to maintain reliability and minimize stability problems. System frequency is supported by dispatching an appropriate amount of generation to supply load, often via an economic dispatch function in a control center. In case of a trip of a large generator, governors on steam and hydraulic turbines are used to restore the frequency, as discussed in Chapter 4 (Sections 4.4 and 4.5). This section shows the use of PMU data to compute the so-called "frequency response" of a large interconnected power system.

The frequency variation in a large interconnected power system can be modeled as a first-order differential equation

$$2H\dot{f} = P_{\text{acc}} = P_m - P_e \quad (10.45)$$

where H is the aggregate inertia in sec of the generators in the system, f is the average system frequency in Hz, P_m is the aggregate mechanical power in MW driving all the generators, P_e is the electrical power in MW representing all the load consumption and transmission losses, and P_{acc} is the accelerating power. In this formulation, assuming that there are no voltage stability and transient stability problems, the reactive power and the generator rotor angles are not considered.

In an off-nominal frequency event, the turbine power under governing control would be, following the notation in (4.118),

$$P_m = P_{mo} + \Delta P_m = P_{mo} + \frac{1}{R_D} \frac{1}{1 + sT_G} (f_o - f) \quad (10.46)$$

where P_{mo} is the pre-disturbance mechanical input power equilibrium value, f_o the nominal frequency, f the actual frequency, R_D the aggregate governor droop, and T_G a composite time constant representing the aggregate turbine-governor time response.

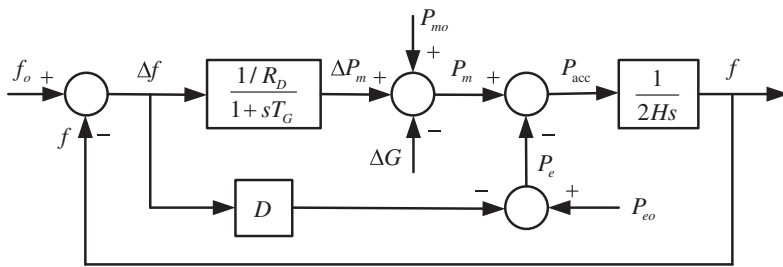


Figure 10.8 Model for studying system frequency response.

In frequency regulation studies, the load power consumption is assumed to vary linearly in frequency¹ such that

$$\frac{\partial P_e}{\partial f} = D \quad (10.47)$$

Thus the electrical power is represented by

$$P_e = P_{eo} + D(f_o - f) \quad (10.48)$$

where $P_{eo} = P_{mo}$ is the pre-disturbance electrical power equilibrium value. The combination of (10.46) and (10.48) results in the block diagram shown in Figure 10.8.

Figure 10.8 includes the generation loss ΔG in a generator-trip event as an input variable. The transfer function from ΔG to the frequency deviation Δf is

$$\Delta f = \frac{1}{2Hs} P_{acc} = \frac{1}{2Hs} [(P_{mo} + \Delta P_m - \Delta G) - (P_{eo} - D\Delta f)] \quad (10.49)$$

or

$$s\Delta f = \frac{1}{2H} \left(-\Delta G + \left(\frac{1}{R_D} \frac{1}{1+sT_G} + D \right) \Delta f \right) \quad (10.50)$$

Initially at the instant of the generator trip, the rate of change of frequency (RoCoF) is given by

$$\frac{d\Delta f}{dt} = -\frac{\Delta G}{2H} \quad (10.51)$$

by setting $\Delta f = 0$ on the RHS of (10.50). Thus the RoCoF is mainly determined by the system total inertia.

In steady state, $P_{acc} = 0$ such that

$$\Delta f = \frac{1}{D + 1/R_D} \Delta G = \frac{1}{\beta} \Delta G \quad (10.52)$$

where $\beta = D + 1/R_D$ is known as the “frequency response” [151].² Figure 10.9 shows the typical frequency response of a large generator trip in the US western interconnection

1 Note that the load model (6.81) and (6.82) does not contain a frequency sensitive component, which is not needed in transient stability investigations. Frequency sensitive loads are mostly attributed to motor loads.

2 Note that the frequency response β is for an entire interconnection, whereas the bias factor B (6.252) is used for each control region.

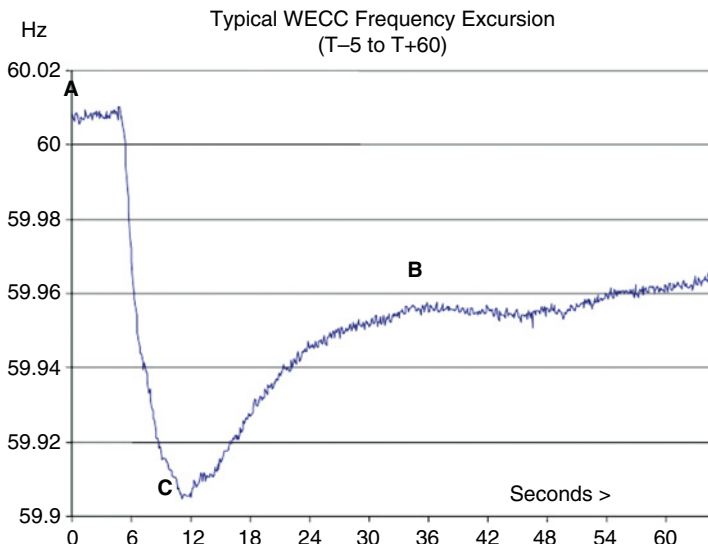


Figure 10.9 Frequency response of a loss of generation event in WECC. Source: Courtesy of NERC 2011 [151]. Reproduced with permission of NERC.

(WECC). At the time instant of the unit trip (point A), the system frequency dropped rapidly, at a rate given by RoCoF (10.51). The frequency eventually settled to a quasi-steady state (point B). The value of β can be estimated by dividing the amount of generation loss (available from the operator's log in control centers) by the frequency drop from Point A to Point B. During the transient period, the frequency would dip to Point C (known as the nadir) which is mainly determined by the frequency sensitivity of load and the total generator inertia. Then the governor action would restore the frequency to Point B.

The value of β has been tracked regularly based on historical generator trip analysis [152]. In general, the larger the interconnection, the higher the value of β . For example, the US Eastern Interconnection (EI) has a $\beta \approx 2,760$ MW/0.1 Hz, the Western Interconnection (WECC) has a $\beta \approx 1,482$ MW/0.1 Hz, and the Texas Interconnection (ERCOT) has a $\beta \approx 650$ MW/0.1 Hz. The value of β is roughly proportional to the size of the interconnection.

The value of β also depends on the participation of the generator governors. Note that governors are equipped with a deadband to prevent the control valves from responding to small frequency changes. In case of a large frequency deviation, such as the situation in Figure 10.9, it would be reasonable to assume that all governors with deadbands would have responded. For generators that are already dispatched to their maximum active power loading, their governors will no longer be able to respond to provide additional power. The lack of governors participating in generator trip events in the US Eastern Interconnection is evident from Figure 10.10 for several remote generator-tripping events recorded at the Northfield substation in Massachusetts [153]. The frequency drop was about 30 mHz in those events, and the lack of governor response was quite evident.

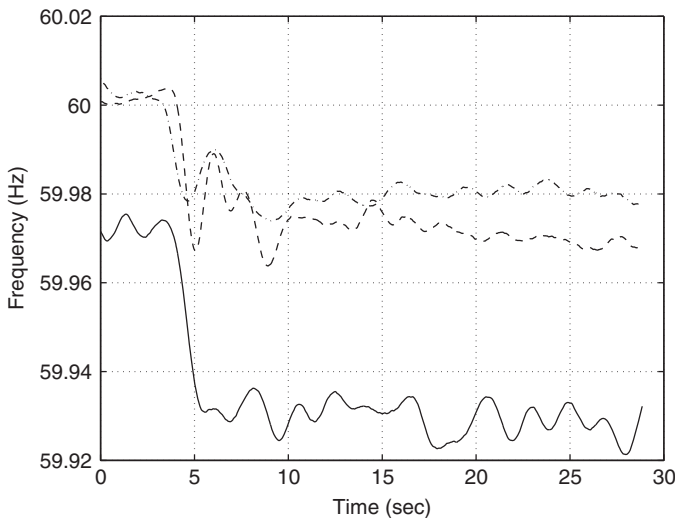


Figure 10.10 Frequency response recording at Northfield for remote generator trips. Source: Adapted from Bykhovsky 2003 [153].

10.5 Power System Disturbance Propagation

The frequency response is, in general, a composite frequency profile derived from the individual bus frequencies. However, the frequency drop in a power system due to a generator trip does not occur instantaneously at all locations in the system. Instead, this disturbance effect will spread from the trip location to the rest of the network according to the network impedances and the generator inertias. The phenomenon can be explained using a wave equation, similar to the study of electromagnetic transients on transmission lines in Chapter 2 [154–156].

Consider a chained generator system in Figure 10.11, consisting of N identical generators connected radially with a uniform reactance X . The generator is represented by a classical model with an inertia $M = 2H$ and a fixed voltage E' behind the direct-axis transient reactance X'_d . To simplify the analysis, it is assumed that $X'_d = 0$ and $E' = 1$, such that the bus voltage angle and the rotor angle are the same, that is, $\theta_i = \delta_i$. In addition, electrical power is supplied from the first generator to the last generator, which acts as a load.

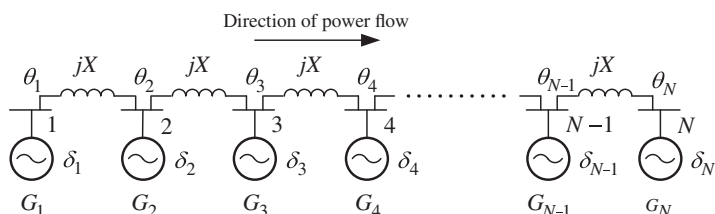


Figure 10.11 Chain of uniformly connected identical generators, where δ denotes the generator rotor angle, θ the bus voltage angle, and X the line reactance.

The dynamic equations of Generator i , $i = 2, \dots, N - 1$, in the system are given by

$$\dot{\delta}_i = \Omega\omega_i, \quad M\dot{\omega}_i = -P_{ei} = -(P_{i,i+1} - P_{i-1,i}) \quad (10.53)$$

where P_{ei} is the electrical power acting on Generator i , $P_{i-1,i}$ the electrical power flow from Bus $i - 1$ to Bus i , and $P_{i,i+1}$ the electrical power flow from Bus i to Bus $i + 1$, such that

$$P_{i-1,i} = (\delta_{i-1} - \delta_i)/X, \quad P_{i,i+1} = (\delta_i - \delta_{i+1})/X \quad (10.54)$$

in which the DC power flow expression is used.

Consider the chained generator system as a distributed parameter system with $N \rightarrow \infty$ and ℓ the transmission line length between adjacent buses, such that the system parameters can be parameterized by

$$m = M/\ell, \quad k = (X/\ell)^{-1} = \ell/X \quad (10.55)$$

where m is the inertia per unit length and k is the inverse of the reactance per unit length X/ℓ .

Denoting x as the distance of Generator i from the first generator, the accelerating power on Generator i is represented by

$$P_{i,i+1} - P_{i-1,i} = (\partial P/\partial x)\ell \quad (10.56)$$

where $\partial P/\partial x$ is the incremental variation of the power P along the reactance between adjacent buses. Thus (10.53) becomes

$$M \frac{\partial \omega}{\partial t} = -\frac{\partial P}{\partial x}\ell \quad \rightarrow \quad m \frac{\partial \omega}{\partial t} = -\frac{\partial P}{\partial x} \quad (10.57)$$

The power angle variation along the transmission line can be represented as

$$\delta_{i-1} - \delta_i = -\frac{\partial \delta}{\partial x}\ell \quad (10.58)$$

such that (10.54) becomes

$$\frac{P\ell}{k} = -\frac{\partial \delta}{\partial x}\ell \quad \rightarrow \quad \frac{\partial P}{\partial t} = -k \frac{\partial}{\partial t} \frac{\partial \delta}{\partial x} = -k\Omega \frac{\partial \omega}{\partial x} \quad (10.59)$$

Taking the partial derivative of (10.57) with respect to t and the partial derivative of (10.54) with respect to x , the results can be combined to form

$$\frac{\partial^2 \omega}{\partial t^2} = \frac{k\Omega}{m} \frac{\partial^2 \omega}{\partial x^2} = c^2 \frac{\partial^2 \omega}{\partial x^2} \quad (10.60)$$

which is a one-dimensional electromechanical wave equation similar to that used to model electromagnetic wave propagation on a transmission line (2.12)–(2.13). Note that similar wave equations can be developed for δ and P as well.

From (10.60), the speed of electromechanical wave propagation can be computed as³

$$c = \sqrt{\frac{k\Omega}{m}} \text{ pu-length/s} \quad (10.61)$$

³ Here the transmission line length is defined in pu reactance. One can also express the speed using line length in km.

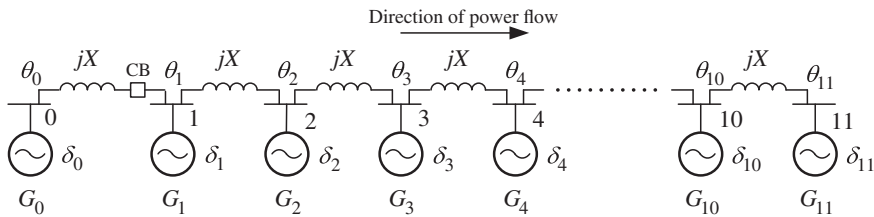


Figure 10.12 Chain of uniformly connected identical generators for Example 10.5.

The general solution to (10.61) is

$$\omega(x, t) = \omega_f(x - ct) + \omega_r(x + ct) \quad (10.62)$$

where ω_f is the forward wave and ω_r the reflected wave. The actual solution is a function of the boundary condition.

The following example simulates a “lumped” generator system, which still shows dynamic behaviors predicted by the wave equation solution (10.62).

Example 10.4 A lossless chained generator system with 12 generators (0–11) is given in Figure 10.12 in which the reactances connecting the generators are uniform with a value of $X = 0.1$ pu on a 100 MVA base and all the bus voltages are at 1 pu. All the generators are identical and represented by a classical model with a rating of 200 MVA. The generator inertia is $H = 3.0$ pu, damping constant $D = 1$ pu, and $X'_d = 0.245$ pu, all on the machine base. The load of 150 MW is represented by Generator 11 with a negative generation. Generators 2–10 are supplying local loads so the generation and load net to zero on Buses 2–10. The load on Bus 11 is supplied in two parts: Generator 1 supplying 145 MW and Generator 0 supplying 5 MW. At time $t = 0.1$ s, the circuit breaker (CB) is opened (without any fault) so that Generator 0 is disconnected, resulting in a generation deficiency situation. Simulate this disturbance and plot the machine speeds vs time. Find the speed of the electromechanical wave.

Solution

First the power flow is solved yielding the following bus angles:

θ_1	θ_2	θ_3	θ_4	θ_5	θ_6	θ_7	θ_8	θ_9	θ_{10}	θ_{11}
0°	-4.30°	-12.93°	-21.56°	-30.18°	-38.81°	-47.44°	-56.06°	-64.69°	-73.31°	-81.94°

Note that the bus angle separation is 82° from Bus 1 to Bus 11, which is not uncommon for large interconnected power systems. The generation drop is 0.05 pu or $5 \text{ MW}/150 \text{ MW} = 3.3\%$ of the total load and the total connected generation of $11 \times 2 = 22$ pu. In addition, because there are no governors modeled in the generators, the damping parameter D is used to model the impact of both governing and load sensitivity to frequency, which has been discussed in the last section. If $D = 0$, the frequency would not settle to a steady state.

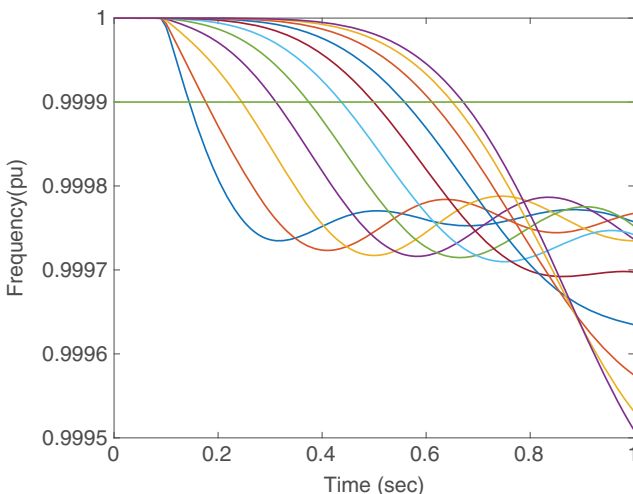


Figure 10.13 Generator rotor speeds in response to generator trip for Example 10.4: Generator 1 is the first curve from the left, and Generator 11 is the last curve to the right.

Figure 10.13 shows the generator rotor speed response for the first second. Normally disturbances are detected based on df/dt exceeding a threshold. For this discussion the frequency drop can be used. Suppose a drop of 0.0001 pu or 6 mHz signifies the detection of the disturbance, which in this case, is the advancing frequency wave. Generator 1 sees the frequency drop in 0.05 sec, and Generator 11 sees the frequency drop in 0.58 sec, that is, almost 0.53 sec later.

Taking the length of the transmission line between two adjacent buses as $\ell = 0.1$ unit such that $k = \ell/X = 0.1/0.1 = 1$ pu-length/pu-reactance and

$$m = 2 \times 3 \times (200/100)/0.1 = 120 \text{ pu-inertia/pu-length} \quad (10.63)$$

The expression (10.61) predicts the electromechanical wave propagation speed as

$$c = \sqrt{377/120} = 1.773 \text{ pu-length/s} \quad (10.64)$$

Thus the time for the frequency deviation to reach from Generator 1 to Generator 11 (1 pu total reactance) is $1/c = 0.564$ s, which is close to the 0.53 sec travel time shown in Figure 10.13.

To see a more complete evolution of the disturbance, a 5-sec simulation is shown in Figure 10.14. A three-dimensional plot showing the spatial-temporal aspects of the disturbance is shown in Figure 10.15. For the first 0.6 second, the frequency wave is advancing from Generator 1 to Generator 11. Once the wave reaches the last generator, the reflected wave becomes important, which reaches Generator 1 at about 1.4 s. The back-and-forth dynamics help the generators to synchronize, that is, to collectively organize into the electromechanical modes. Commencing from $t = 1.5$ sec, the oscillations become repetitive or periodic, which can be regarded as the linear response of the system. Such oscillations can be identified using modal analysis techniques, which will be discussed in Section 10.8. \square

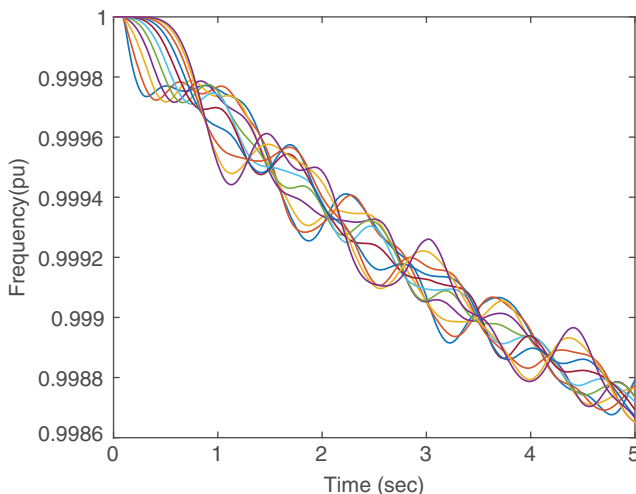


Figure 10.14 Generator rotor speeds in response to generator trip for Example 10.4.

The system discussed here is a radial system. A real power system is most likely a two-dimensional meshed system. The wave equation model can also be applied to a uniformly gridded power system, as discussed in [154] and [157].

Note that PMUs are normally installed at substations and measure bus voltage angles and frequencies. Figure 10.16 shows a generation-and-load trip event in Florida in which more load than generation was tripped, resulting in frequency rise starting from the disturbance location. The frequency wave then moved from Florida to Tennessee, before finally reaching Manitoba and Maine two seconds later. The synchronization of the oscillations in Florida, Manitoba, and Maine started a few more seconds later.

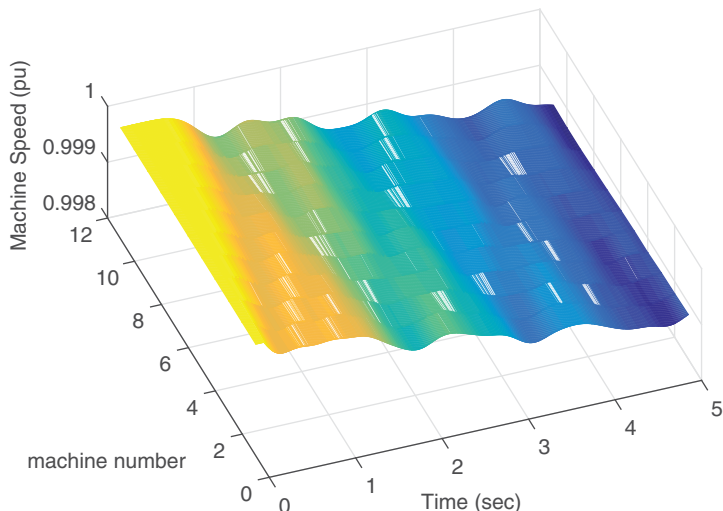


Figure 10.15 3D plot of generator rotor speeds in response to generator trip for Example 10.4.

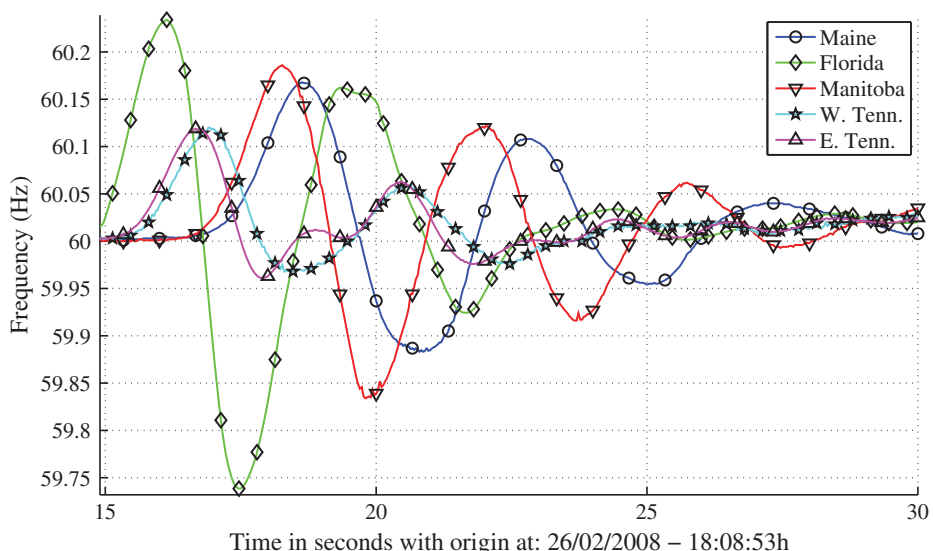


Figure 10.16 Frequency wave propagation in a generation-load trip event in Florida, 2008.

The frequency wave travel time can be used to locate generator trip using some kind of triangulation methods based on the frequency wave arrival times at several locations close to the disturbance. The FNET system at the University of Tennessee collects frequency measurements at many locations in the US, and uses several methods of triangulation to arrive at a consensus of the generation trip location [158], normally within a small radius (about 50 miles) of the actual trip location.

10.5.1 Disturbance Triggering

One of the benefits of PMU data is to detect the onset of a disturbance. For switching events, such as generator trip and line switching, the rate-of-change-of-frequency (RoCoF) is usually a good indicator, by implementing a function that will trigger if the magnitude of RoCoF exceeds a certain threshold. Typically the PMUs that are closest to the disturbance will give the highest RoCoF values and detect the disturbances immediately, as evidenced by the disturbance propagation waves shown in Figure 10.13. However, triggering on other types of disturbances, such as oscillations, may require combining RoCoF with other signal variations.

10.6 Power System Disturbance Signatures

In power system stability analysis using a dynamic simulation package, the typical disturbance is a three-phase short-circuit fault close to a large turbine-generator. However, there are a variety of disturbances and network switching events that produce distinct dynamic signatures that can be observed from PMU data. The following discussion on disturbance characteristics will rely on a reader being familiar with the materials developed in the earlier chapters.

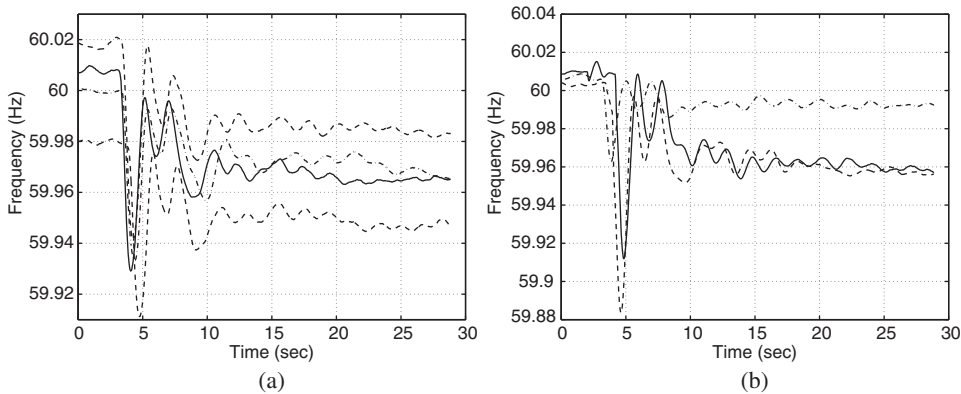


Figure 10.17 Dynamics recorded for: (a) several Millstone unit trip events, and (b) several HVDC 1-pole trip events.

Most power system disturbance and switching events can be divided into the following 5 categories. Real PMU recordings of such events will be used as illustrations.

10.6.1 Generator or Load Trip

The signature of a sudden generation trip, already discussed in Section 10.4, is a frequency drop in the whole interconnection as a function of the system frequency response β . As a result, this kind of disturbances is visible throughout the interconnection, as typified by the responses shown in Figure 10.10. For substations close to a generator-trip event, local swing modes may also be visible in the bus frequency measurements. Figure 10.17 shows two sets of generation-trip events recorded at the Northfield substation [153], which is connected to a hydraulic generator. Figure 10.17(a) shows the response of the generator to four trip-of-the-Millstone-unit events on different days. Due to the generator dynamic swing, the initial frequency drop was about twice as much as the steady-state frequency drop. Note the similarity of the frequency dynamics, after adjusting for the different pre-disturbance frequency levels. Figure 10.17(b) shows the response of the generator to three New England HVDC single-pole trip events. Similar conclusions can be drawn that the initial frequency drop was about twice the steady-state frequency drop.

In the case of a load-trip event, the interconnection frequency will go up. However, the sudden loss of a large amount of load, like the blackout of a load center, is relatively rare. A more common situation is the shut down of a large pumped-hydraulic unit at the end of its pumping cycle. Figure 10.18 shows the PMU frequency data at six substations (each substation is one to two hundred miles apart to the nearest substation) due to the shut down of a remote pumped-hydraulic unit. Note that the frequency does not change as abruptly as in generator-trip events. In addition, Figure 10.18 shows that the bus frequencies at the substations track each other very closely. This is generally the case in steady-state operation of a connected AC grid, until a large disturbance such as a generator trip causes a frequency wave to propagate through the system.

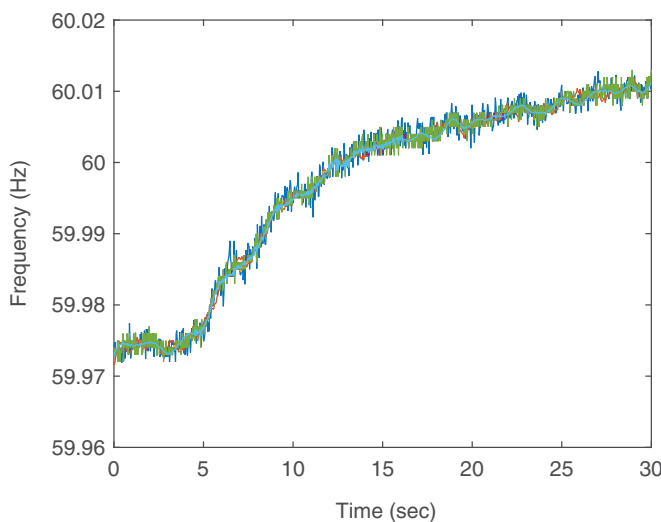


Figure 10.18 Bus frequencies at various substations for a remote pumped-hydraulic unit disconnection.

10.6.2 Oscillations

One of the first applications of PMU data is to detect and analyze lightly damped or unstable interarea oscillations in the US Western Interconnections. With a sampling rate of 30 Hz and higher, PMU data is well suited to capture electromechanical oscillations from interarea modes of 0.25–1 Hz to local and intra-plant modes of 1 to 3 Hz. An important concern is lightly damped (damping ratio less than 2–3%) or even unstable swing modes. Figure 10.19 shows a growing oscillation on the Pacific AC Intertie due to

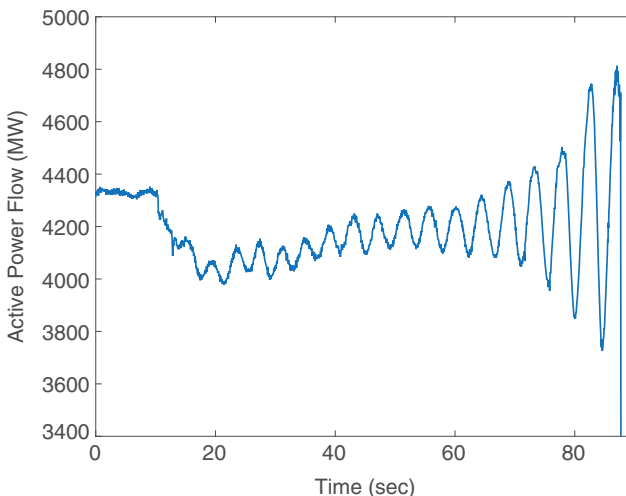


Figure 10.19 Active power oscillation on the California-Oregon Intertie on August 10, 1996. Source: Data from Dmitry Kosterev.

the disconnection of the Alberta power system from the rest of WECC on August 10, 1996, which subsequently resulted in the blackout of WECC [159].

Once an electromechanical mode oscillation starts, it can be observed in many signals, including bus frequency, bus voltage magnitude and angle, and active power flows on transmission lines. The oscillatory frequency and damping ratio can be computed using modal analysis methods [160], which will be discussed in Section 10.8. Online oscillation detection and damping assessment software packages have also been developed [161, 162].

10.6.3 Fault and Line Switching

Line switching events, including those due to line-to-ground faults cleared quickly by protective relays without generator trips, are events that can be detected only locally. The PMU current reading on the tripped line will drop to zero. The power flow on the tripped line will be dispersed to parallel lines, causing the measured PMU bus frequency, voltage angle, and current magnitude values to change abruptly at the onset of the fault. These effects would diminish for PMUs that are located farther away from the disturbance, so that the disturbance would not be detectable from remote PMUs.

Figure 10.20 shows the recording of a line-trip event. At the onset (about 46 sec) of a fault on a transmission line, the voltage, frequency and current flow PMU data all exhibited significant variations. Once the fault was cleared, the frequency and voltage data showed much less variations. The faulted line was tripped and as a result, its current measurement dropped to zero.

Line trips due to faults may sometimes be reclosed after a period of 15–30 seconds. Figure 10.20 shows a successful reclosing at 62 sec, about 15 sec after the fault was cleared.

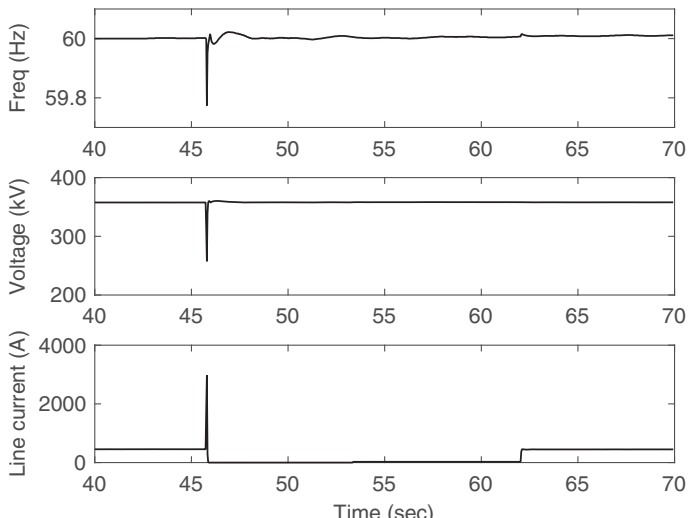


Figure 10.20 Frequency measurement of a line trip and its successful reclosing at a substation in New England. Source: Data from David Bertagnoli.

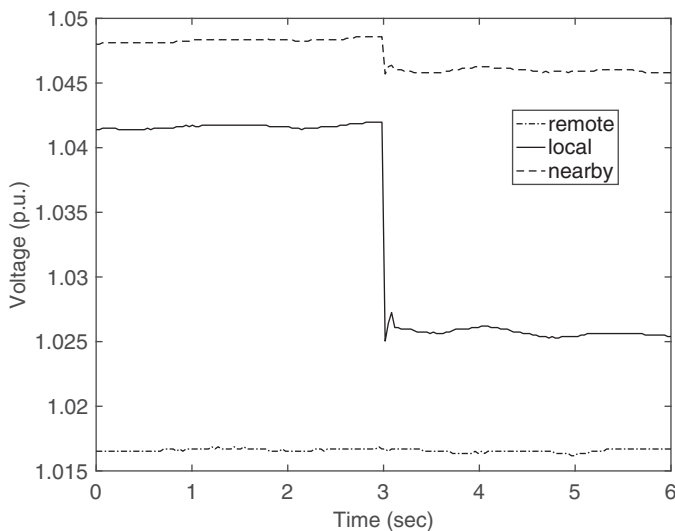


Figure 10.21 Voltage magnitude measurement of a shunt switching event at three substations.

10.6.4 Shunt Capacitor or Reactor Switching

Shunt capacitor or reactor switching events are also local in nature. In these events, the PMU voltage measurements at a few nearby buses will exhibit a jump or drop in the voltage magnitude. However, the voltage angles would not be affected much as these shunt components only affect reactive power flow. These switching events are typically planned and are not considered as disturbances. Figure 10.21 shows the PMU voltage magnitude measurements at a local substation, a nearby substation, and a remote substation, of switching on a shunt reactor. The local substation shows the largest drop of the bus voltage, whereas the remote substation shows no voltage impact.

10.6.5 Voltage Collapse

Dynamic voltage instability, briefly mentioned in Chapter 8, had contributed to some major blackouts, even though it might not be the only cause. Dynamic voltage collapse typically manifests in a matter of 5–10 seconds. Figure 10.22 shows the voltage collapse in WECC leading to the July 2, 1996 blackout. The Malin voltage decay is due to insufficient voltage support along the Pacific AC interties in central Oregon, possibly exacerbated by various irrigation and air conditioning loads [163]. Generator over-excitation limiter operation might also have contributed to the collapse, although there was no definitive confirmation. Since the 1996 event, additional reactive power support had been installed around the Malin area to reduce the probability of future voltage collapse.

10.7 Phasor State Estimation

SCADA-based static state estimation (SE) using 5-sec measured analog data is an important function performed in a power system control center [163, 164] to support

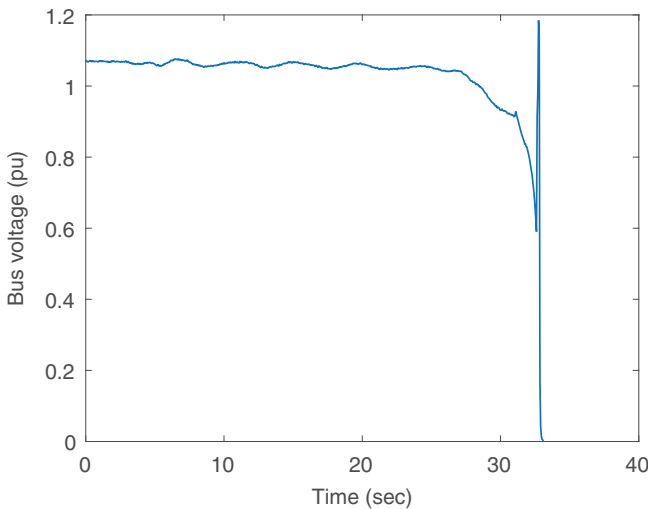


Figure 10.22 Dynamic voltage response at Malin on July 2, 1996. Source: Data from Dmitry Kosterev.

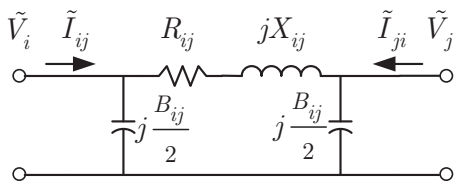


Figure 10.23 Transmission line admittances, voltages, and currents.

contingency analysis and electricity market dispatch. PMU data can be readily used to augment a static SE by incorporating the phase angle measurements in an iterative least-squares solution method [165]. PMU data can also be used to improve the robustness of a SE when PMU data is used to supplement the critical measurements [166].⁴ Further improvement to this scheme is possible if the analog SCADA data is also time tagged, so that the SCADA data can be synchronized to the PMU data.

The discussion in this section will focus on a SE approach using only PMU data [167]. Assuming that all the buses in a transmission network are equipped with PMUs to measure the voltage phasors, the line current flowing from Bus i to Bus j shown in Figure 10.23 can be estimated as

$$\tilde{I}_{ij} = (\tilde{V}_i - \tilde{V}_j)/(R_{ij} + jX_{ij}) + j(B_{ij}/2)\tilde{V}_i \quad (10.65)$$

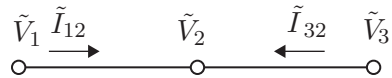
If the line current phasor \tilde{I}_{ij} is also measured, then a least-squares estimation problem can be formulated to reduce measurement noise. By formulating the voltages in rectangular coordinates, the state estimation becomes linear as the entries in the coefficient matrix to solve for the unknown voltage variables are line impedances $R_{ij} + jX_{ij}$ and susceptances B_{ij} and are not dependent on the bus angles (see Example 10.5) as in a SCADA state estimator [164]. This least-squares solution can then be obtained directly without any iterations.

⁴ If a critical measurement is lost, a part of the system will become unobservable.

Figure 10.24 Four-bus radial system (admittances not shown) with PMU measurements of \tilde{V}_1 , \tilde{I}_{12} , \tilde{V}_4 , and \tilde{I}_{43} .



Figure 10.25 Three-bus radial system with PMU measurements of \tilde{V}_1 , \tilde{I}_{12} , \tilde{V}_3 , and \tilde{I}_{32} .



Not all buses in a real power system are equipped with PMUs. In this situation, the PMU data can be used to extend the visibility of the network. Consider the situation in Figure 10.23 in which the PMU at Bus i measures both the voltage phasor \tilde{V}_i and current phasor \tilde{I}_{ij} . Then the voltage phasor on Bus j can be estimated as

$$\hat{\tilde{V}}_j = \tilde{V}_i - (\tilde{I}_{ij} - j(B_{ij}/2)\tilde{V}_i)(R_{ij} + jX_{ij}) \quad (10.66)$$

which is called a virtual or pseudo PMU measurement. This extended observability property is important, as illustrated by Figure 10.24, which has 4 buses connected radially with voltage and current phasor measurements on Buses 1 and 4 as indicated. In this configuration, the virtual PMU measurements \tilde{V}_2 and \tilde{V}_3 can be estimated, and thus the current phasor on Line 2–3 can also be computed, without knowing any bus injections. This is possible because the phase angles of Buses 2 and 3 are known, which cannot be replicated in the SCADA-based SE. In the following example, the linear state estimator [167] is illustrated using the 3-bus system in Figure 10.25.

Example 10.5 The parameters of the 3-bus system in Figure 10.25 are given in pu by

$$\begin{aligned} R_{12} &= 0.00003, & X_{12} &= 0.00042, & B_{12} &= 0 \\ R_{32} &= 0.00251, & X_{32} &= 0.0346, & B_{32} &= 0.592 \end{aligned} \quad (10.67)$$

The PMU data with the same time tag for Buses 1 and 3 are shown in the second column of Table 10.5. Use the linear state estimator (LSE) method to estimate \tilde{V}_i , $i = 1, 2, 3$.

Solution

In this example, the 4 measured phasor quantities will be used to estimate 5 phasor quantities \tilde{V}_1 , \tilde{V}_2 , \tilde{V}_3 , \tilde{I}_{12} , and \tilde{I}_{32} . Thus in addition to the unknown voltage \tilde{V}_2 , the

Table 10.5 PMU data for Example 10.5.

PMU data	LSE solution
\tilde{V}_1	$1.0361\angle-15.9120^\circ$
\tilde{V}_3	$1.0275\angle-24.1200^\circ$
\tilde{I}_{12}	$2.2731\angle149.8560^\circ$
\tilde{I}_{32}	$5.8465\angle159.4880^\circ$
\tilde{V}_2	not measured
	$1.0373\angle-14.3246^\circ$

measured phasors are also included in the estimation to reduce measurement noise. Thus the unknowns in rectangular coordinates are the estimated values

$$\mathbf{x} = [\hat{V}_{1r} \quad \hat{V}_{1i} \quad \hat{V}_{2r} \quad \hat{V}_{2i} \quad \hat{V}_{3r} \quad \hat{V}_{3i} \quad \hat{I}_{12r} \quad \hat{I}_{12i} \quad \hat{I}_{32r} \quad \hat{I}_{32i}]^T \quad (10.68)$$

where the subscripts r and i denote the real and imaginary part of the phasors, respectively.

Writing (10.66) for Buses 1 and 2 in rectangular coordinates results in

$$V_{2r} = V_{1r} - \left(R_{12}I_{12r} - X_{12}I_{12i} + \frac{X_{12}B_{12}}{2}V_{1r} + \frac{R_{12}B_{12}}{2}V_{1i} \right) \quad (10.69)$$

$$V_{2i} = V_{1r} - \left(X_{12}I_{12r} + R_{12}I_{12i} - \frac{R_{12}B_{12}}{2}V_{1r} + \frac{X_{12}B_{12}}{2}V_{1i} \right) \quad (10.70)$$

A similar set of circuit equations can be developed for the line connecting Buses 2 and 3.

In the linear state estimator, a linear equation $Ax = b$ relating the unknowns to the measurements is developed. The A matrix is derived from the circuit equations, and is defined by the line parameters as

$$\begin{bmatrix} 1 & 0 & 0 & 0 & 0 & 0 & 0 & 0 & 0 \\ 0 & 1 & 0 & 0 & 0 & 0 & 0 & 0 & 0 \\ 0 & 0 & 0 & 0 & 1 & 0 & 0 & 0 & 0 \\ 0 & 0 & 0 & 0 & 0 & 1 & 0 & 0 & 0 \\ 0 & 0 & 0 & 0 & 0 & 0 & 1 & 0 & 0 \\ 0 & 0 & 0 & 0 & 0 & 0 & 0 & 1 & 0 \\ 0 & 0 & 0 & 0 & 0 & 0 & 0 & 0 & 1 \\ 0 & 0 & 0 & 0 & 0 & 0 & 0 & 1 & 0 \\ 1 - X_{12}\bar{B}_{12} & -R_{12}\bar{B}_{12} & -1 & 0 & 0 & 0 & -R_{12} & X_{12} & 0 \\ R_{12}\bar{B}_{12} & 1 - X_{12}\bar{B}_{12} & 0 & -1 & 0 & 0 & -X_{12} & -R_{12} & 0 \\ 0 & 0 & -1 & 0 & 1 - X_{32}\bar{B}_{32} & -R_{32}\bar{B}_{32} & 0 & 0 & -R_{32} & X_{32} \\ 0 & 0 & 0 & -1 & R_{32}\bar{B}_{32} & 1 - X_{32}\bar{B}_{32} & 0 & 0 & -X_{32} & -R_{32} \end{bmatrix} \quad (10.71)$$

where $\bar{B}_{ij} = B_{ij}/2$. The b vector contains the measurements and is given by

$$[\bar{V}_{1r} \quad \bar{V}_{1i} \quad \bar{V}_{3r} \quad \bar{V}_{3i} \quad \bar{I}_{12r} \quad \bar{I}_{12i} \quad \bar{I}_{32r} \quad \bar{I}_{32i} \quad 0 \quad 0 \quad 0 \quad 0]^T \quad (10.72)$$

The circuit equations (10.69)–(10.70) are important in the state estimation and therefore are weighted more heavily. Thus the last four rows of A and b are weighted by a factor of 100. Unity weights are used for the measurement equations, which form rows 1 to 8 of the A matrix. The weights form the diagonal entries of the weighting matrix W .

For the given PMU data, the linear state estimator is solved in one step using the least-squares estimation formula

$$\hat{\mathbf{x}} = ((WA)^T(WA))^{-1}(WA)Wb \quad (10.73)$$

yielding the result shown in the third column of Table 10.5. Because the Line 1–2 impedance is much smaller than the Line 3–2 impedance, the phase difference between

Buses 1 and 2 is much smaller in magnitude than that between Buses 3 and 2. Here Bus 2 is a generator bus, and is exporting active power to both Buses 1 and 3. Thus even though there is no PMU on the generator bus, virtual PMU data can be computed such that the active and reactive power generation can be monitored. \square

If there is some a-priori information on the accuracy of the PMU measurements, higher weights can be applied to the more accurate measurements in the LSE solution. PMU data can also be used to perform three-phase state estimation [168]. Such individual phase information can be useful for monitoring power systems operating with significant imbalances in voltages and currents.

The LSE generates a power network solution at the same sampling rate as a PMU. The dynamics of the power system will be visible from the LSE solution, although no dynamic equations such as generator models and electromagnetic equations are used. This LSE approach is justified because (1) the machine states are “frozen” during the LSE solution, and (2) the electromagnetic transients have already decayed such that the power network is in quasi-steady state. The LSE solution can also be useful for dynamic state estimation. For example, virtual measurements can be computed at the terminal buses for generators without PMUs. Then the computed terminal bus voltage phasors and current injections can be used to validate and/or identify generator and excitation system model parameters. More details on dynamic state estimation can be found in [169–171].

A more advanced method of a phasor-only state estimator is to use the redundancy in the measured data to correct for PMU phase angle and current scaling errors, and to estimate transformer tap ratio [169, 170]. In this approach, the least-squares estimation problem is nonlinear and has to be solved iteratively. Note that in Example 10.5, the measured and calculated voltage angles of Buses 1 and 2 differ by about 1.5° , which is about 3 times as much as the maximum error specification of a PMU. The method in [170] was able to identify that the current scaling factor for Line 3-2 was off by 19%. Problem 10.13 asks a reader to apply this current scaling factor and compute a new least-squares solution.

10.8 Modal Analyses of Oscillations

A major concern in power systems with long distance power transfer is small-signal instability characterized by growing oscillations. Such oscillations are not captured in 4-sec SCADA data, but can be clearly visible in PMU data [163]. Many signal processing techniques have been applied to PMU data for oscillation monitoring, some of which have been implemented in software packages used by power grid operators. These software packages are developed for two types of oscillation analysis: ring down and ambient conditions. This section will deal with only ring-down analyses. A reader interested in ambient condition analyses is referred to [178].

When a power system is subjected to a large disturbance, the time response immediately after the onset of the disturbance can be quite nonlinear. It is then followed by decaying oscillations which can be modeled as an unforced linear system. The latter response is called a ring down, with clearly visible swing-mode oscillations of several cycles. A ring-down analysis is to identify the frequencies and damping of the swing

modes visible in the time response. In this setting, the measured signal y is modeled as a discrete-time signal

$$y(k) = y(kT) = \sum_{i=1}^m R_i z_i^k, \quad k = 0, \dots, N - 1 \quad (10.74)$$

where T is the sampling time, z_i is the i th mode of the linear discrete-time system, R_i is the residue of mode z_i , m is the number of modes, and N is the number of samples. If the characteristic polynomial governing y is

$$d(z) = 1 - (a_1 z^{-1} + \dots + a_m z^{-m}) \quad (10.75)$$

then the measured samples are related by the auto-regressive equation

$$y(k) = a_1 y(k-1) + \dots + a_m y(k-m) \quad (10.76)$$

In the Prony method, the coefficients a_i are solved by sequencing the sampled signal through (10.76) repeatedly to form the linear matrix equation

$$\begin{bmatrix} y(m-1) & y(m-2) & \dots & y(0) \\ y(m-0) & y(m-1) & \dots & y(1) \\ \vdots & \vdots & \vdots & \vdots \\ y(N-2) & y(N-3) & \dots & y(N-m-1) \end{bmatrix} \begin{bmatrix} a_1 \\ a_2 \\ \vdots \\ a_m \end{bmatrix} = \begin{bmatrix} y(m) \\ y(m+1) \\ \vdots \\ y(N-1) \end{bmatrix} \quad (10.77)$$

The data matrix on the left side of (10.77) is also known as a Hankel matrix.

From the characteristic polynomial solution of (10.77), the roots z_i can be computed and transformed to equivalent continuous-time poles λ_i using the expressions $z_i = e^{s_i T}$ or $s_i = \ln(z_i)/T$. The Prony method was first proposed for power system oscillation analysis in [160] for a scalar signal. When multiple signals containing similar modes are available, a multi-channel Prony method [172] can be used, as (10.77) also holds for y being a vector signal. Using multiple signals improves the accuracy of the modal estimation results.

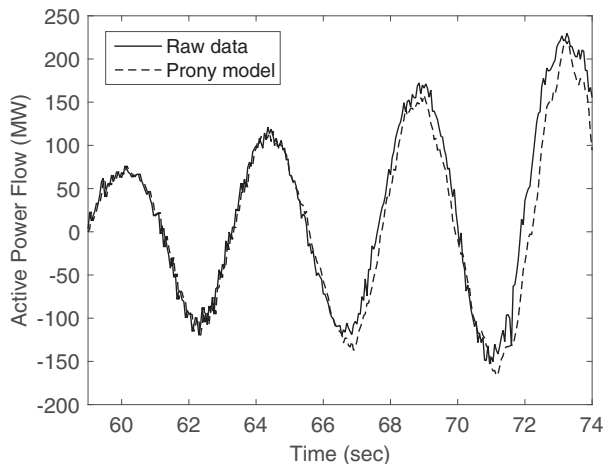
The following example applies the `prony` function available in MATLAB™ to the oscillation event shown in Figure 10.19, using a 15-second segment of the signal. It would be more difficult to analyze the complete waveform in one shot because nonlinearity can be a problem for a long duration signal. In addition, detrending would be necessary to remove slowly varying components due to changes in operating conditions.

Example 10.6 Use the Prony method to find the frequency and damping ratio of the dominant mode in the oscillation signal from 59 to 74 seconds shown in Figure 10.26. Note that a steady-state value of 4200 MW has been subtracted out of the line flow.

Solution

Although it is quite obvious from Figure 10.26 that there is only one dominant unstable mode (a pair of complex poles) in the signal, in the presence of noise and with the possibility of some nonlinearities, specifying a second-order model directly in Prony analysis would normally give erroneous results. Instead, a two-stage approach is used. First, a high-order Prony model fit is obtained, and then a lower order model is

Figure 10.26 Line active power for identifying oscillatory mode.



extracted. For this identification problem, the number of data points used is 301, which is 15 second long with a sampling rating of 20 samples per second.⁵ First a 100th order model is used in the Prony model identification. The impulse response of the resulting discrete-time model is shown as the dashed curve in Figure 10.26 and matches the raw PMU data quite well.⁶ In the discrete-time model, the dominant pair of poles is determined to be $z_{1,2} = 1.00039 \pm 0.07137$, which correspond to the continuous-time system poles $s_{1,2} = 0.0588 \pm 1.4250$, having a frequency of 0.2268 Hz and a negative damping ratio of -0.0412 .

Then a modal decomposition is used to extract a second-order discrete-time model

$$G_2(z) = \frac{12.5367z - 6.7863}{z^2 - 2.0008z + 1.0059} \quad (10.78)$$

The impulse response of this reduced system is shown in Figure 10.27, which provides just as good an approximation to the raw PMU data as that provided by the 100th order model. \square

In addition to the Prony method, there is also a class of techniques for computing the poles z_i directly from the sampled signals without having to first obtain the characteristic polynomial. The Eigensystem Realization Algorithm (ERA) [173] performs a singular value decomposition of the Hankel matrix, whereas the matrix pencil method [174, 175] formulates a generalized eigenvalue problem using two Hankel matrices. Both the ERA and matrix pencil methods readily handle signals from multiple channels. Comparison of these and other ring down methods can be found in [176, 177].

⁵ The data was recorded by an older PMU with a sampling rate less than 30 samples per second.

⁶ Note that in MATLAB™, the magnitude of an impulse response needs to be scaled by the sampling period to match a continuous-time signal.

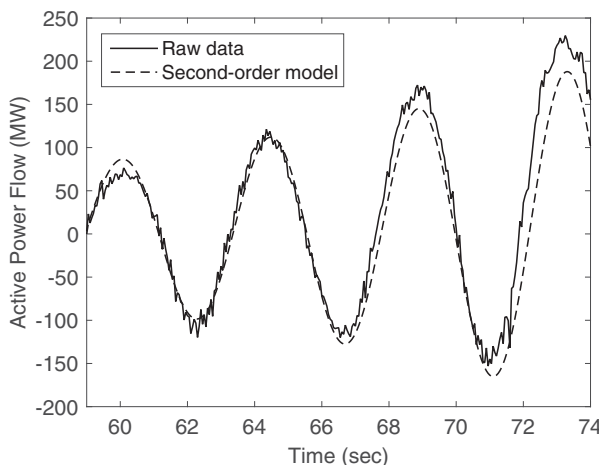


Figure 10.27 Line active power approximated by a second-order system.

10.9 Energy Function Analysis

The use of energy functions to determine transient stability has been discussed in Chapter 9. This section provides some additional insights into energy functions using PMU data from a disturbance event. The system involved several generating units at a remote substation sending power to a load center via two parallel lines. For some undetermined reasons, oscillations of 0.578 Hz were observed at the generating units and recorded by PMUs near the generating units and at the load center. For practical purposes, the generating units can be lumped into a single aggregate generator, which is connected to the load center modeled as an infinite bus. To construct the energy function and demonstrate it using the PMU data, it is also necessary to estimate the single-machine infinite-bus model by computing the aggregate generator inertia and the reactance of the transmission system. This section will assume that this model estimation part is done. A reader can refer to [179, 180] for additional details.

The angular difference θ and the frequency difference ω between the generating units and the load center are shown in Figures 10.28(a) and (b), respectively. Note that the oscillations started at about 60 seconds and lasted for over 200 seconds.

Using the methods in [179, 180], it was estimated that the pre-disturbance and post-disturbance equivalent reactances between the equivalent generator and the infinite bus were $x_e = 0.070$ pu and $x_e = 0.077$ pu, respectively, and the inertia H of the aggregate machine was 129 pu, all on 100 MVA base. These parameters can be used to compute the power-angle curve, which is shown in Figure 10.29(a). Combining the line flow PMU data in Figure 10.29(b) and the angle separation data in Figure 10.28(a), the system dynamic response can be plotted on the power-angle curves.

The bus frequency difference is mostly mono-modal, but the angle difference shows a distinct quasi-steady-state variation. Bandpass filtering is used to separate the oscillation and the quasi-steady-state components of θ as shown in Figures 10.30(a) and (b), respectively.

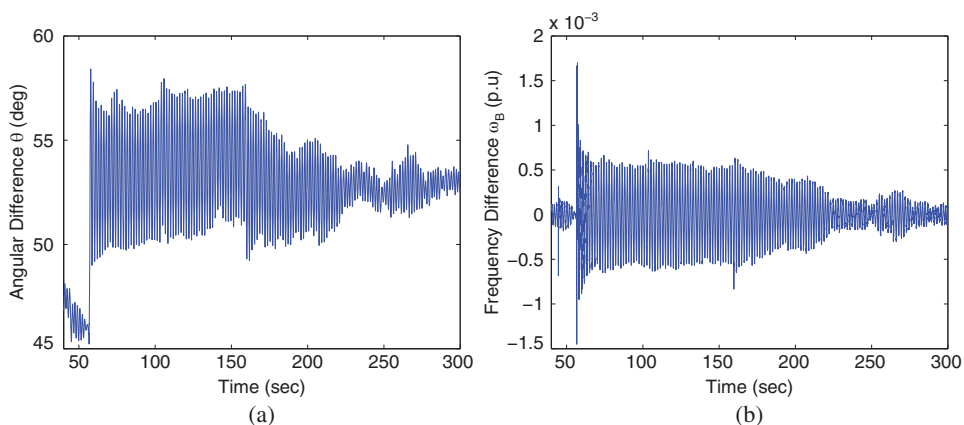


Figure 10.28 Recorded dynamics of (a) angular difference θ , and (b) frequency difference ω .

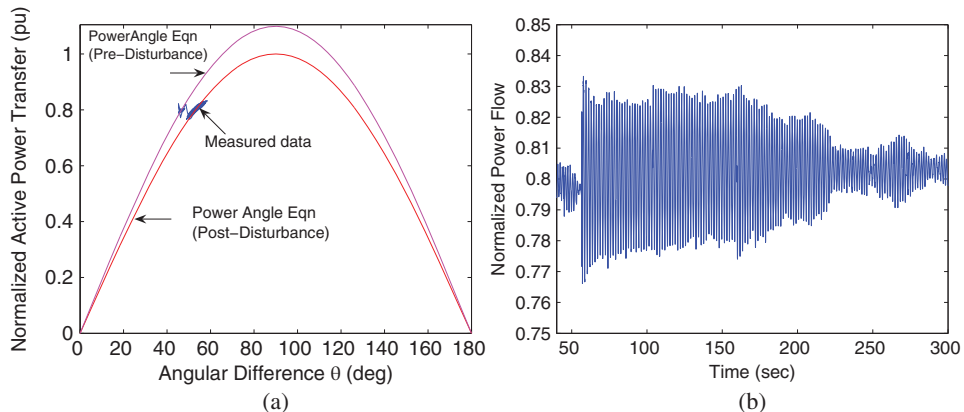


Figure 10.29 (a) Power-angle curves, and (b) transmission line power flow PMU data.

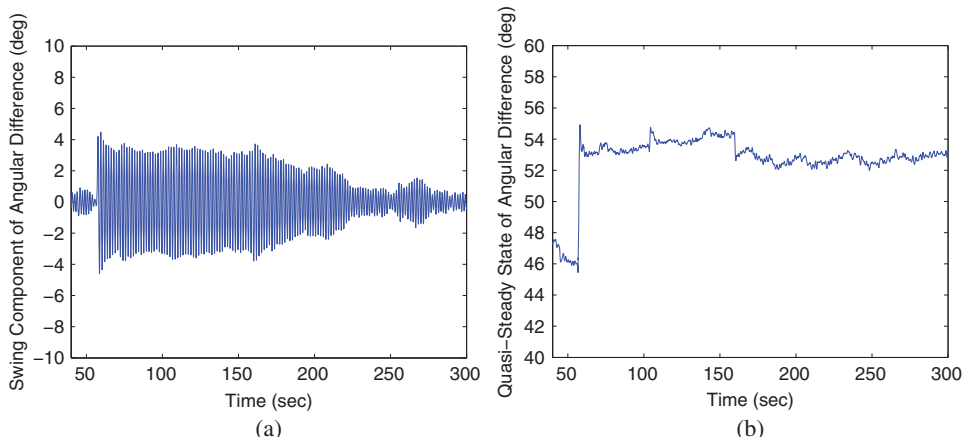


Figure 10.30 Angular separation showing (a) swing component, and (b) quasi-steady-state component.

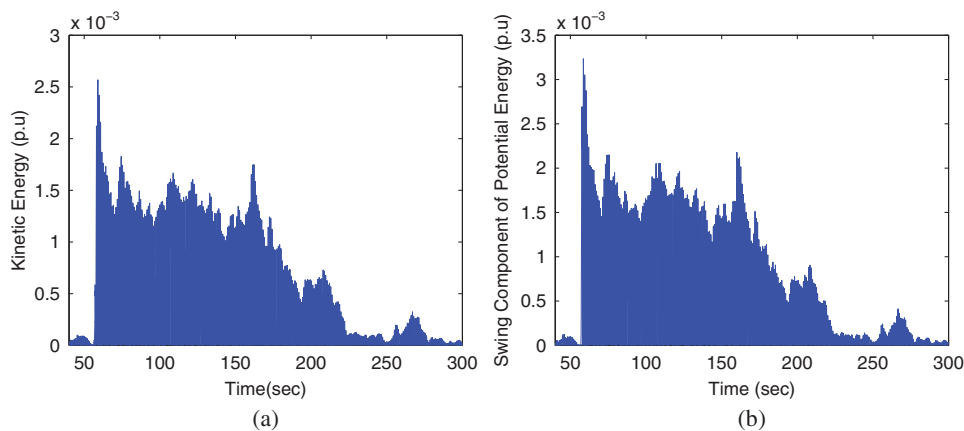


Figure 10.31 (a) Kinetic energy, and (b) potential energy.

Based on the above discussion, the energy function (9.29) to model the power swing in the system is

$$\hat{V}_E(t) = \hat{V}_{KE}(t) + \hat{V}_{PE}(t) \quad (10.79)$$

where the potential energy is

$$\hat{V}_{PE} = \frac{\bar{V}_1 \bar{V}_2}{x'_e} (\cos(\theta_{qss}) - \cos(\theta) + \sin(\theta_{qss})(\theta_{qss} - \theta)) \quad (10.80)$$

and the kinetic energy is

$$\hat{V}_{KE}(t) = H\Omega\omega(t)^2 \quad (10.81)$$

where ω is the frequency deviation from the nominal value and θ_{qss} is quasi-steady-state value obtained by bandpass filtering the θ measurement.

Figures 10.31 and 10.32 show the various energy functions \hat{V}_{KE} , \hat{V}_{PE} , \hat{V}_E . Note that oscillations are clearly visible in \hat{V}_{KE} and \hat{V}_{PE} and yet they literally disappear when \hat{V}_E

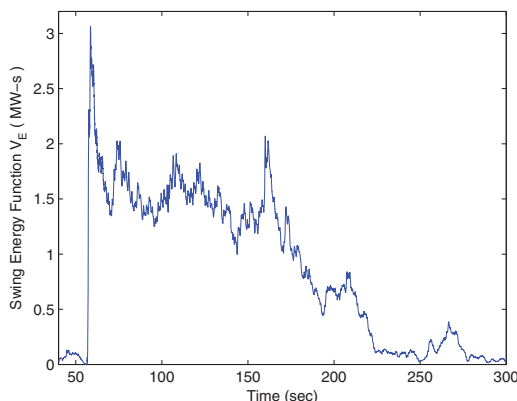


Figure 10.32 Total energy of the disturbance.

and \hat{V}_{PE} are added together to form \hat{V}_E . The maximum energy resulting from the disturbance is 3 MW-sec.

The oscillation is small-signal stable, although the damping is quite low, and \hat{V}_E eventually decays to a level commensurate with random perturbations on the system. If the system were negatively damped, \hat{V}_E would grow. The quasi-steady angle θ_{qss} indicates that the sending end and receiving end of the transfer path remains synchronized, that is, transiently stable. A jump in θ_{qss} indicates most likely the loss of a portion of the transmission system. If the disturbance had caused a separation of the transfer path, θ_{qss} would grow as synchronism would be lost.

10.10 Control Design Using PMU Data

The availability of high-sampling-rate time-tagged data and a system to communicate the data throughout the power network would enable more intelligent protection systems (which can be viewed as open-loop control systems) and feedback control functions. In a practical control problem, a designer has to find the best feasible input signals to use such that the controller is effective and its complexity is manageable. If a local signal with many modal contents is used, a controller often has to be implemented with multiple filters so that the control system has minimal impact on modes that are not central to the control design problem. If the PMU data is available remotely, a controller can selectively generate new input signals containing only the modes of interest. For example, in the damping of an interarea mode between two areas, one can select the average frequency measurement in each of the areas. Then the difference of these two frequency measurements will predominantly be the interarea mode, with a much smaller amount of local modes within the areas. Thus using PMU data as input signals to damp interarea mode has a strong appeal, as the controllers, such as power system stabilizers, can be made more effective.

Control designs using PMU data, including linear optimal control, have been proposed [130]. The authors of this book have not prepared its readers for such advanced control designs. However, it is useful in this section to provide a reader with a sense of the impact of latency due to computation and communication delays [181] on controller design. With dedicated optical communication channels, PMU data can be relayed to controllers within 100–150 ms, including PMU phasor processing time [182].

In control system design, a time delay when viewed in the frequency domain becomes a phase lag. For example, a time delay of $T_d = 100$ ms at an interarea mode of $\omega = 3$ rad/s is equivalent to a phase lag of

$$\theta_{lag} = \omega \times T_d = 3 \times 0.1 = 0.3 \text{ rad} = 17.19^\circ \quad (10.82)$$

Time delays reduce the stability of feedback systems and prevent the use of high-gain feedback, as root-locus branches will move into the right-half plane (RHP) [183]. Thus a control design, such as the lead-lag compensation method for power system stabilizers, has to take the additional phase lag into account.

For control design and performance simulation purposes, a time delay T_d can be represented by a first-order Padé approximant [183] as

$$e^{-T_d s} \simeq \frac{1 - (T_d s/2)}{1 + (T_d s/2)} \quad (10.83)$$

The right-half-plane zero at $s = 2/T_d$ in (10.83) would render the control design more complex.

To illustrate a control design taking into account T_d , the PSS design for the power system model presented in Example 8.7 will be extended to account for the delay in the speed feedback signal. Note that in this model, the lightly damped local mode is at about 7 rad/s, implying a larger phase lag than (10.82).

Example 10.7 Suppose for the PSS design in Example 8.7 that the speed input signal has a delay of 100 ms. Investigate the impact of this delay modeled as (10.83) on the root-locus plot in the PSS design. Then redesign the PSS so as to recover a performance similar to that shown in Example 8.7.

Solution

The root-locus plot associated with the PSS in Example 8.7

$$G(s) = K_{\text{PSS}} \left(\frac{1 + sT_1}{1 + sT_2} \right) = K_{\text{PSS}} \left(\frac{1 + 0.5s}{1 + 0.1s} \right) \quad (10.84)$$

is shown in Figure 10.33(a). Note that the phase compensation is effective as the root-locus branch leaving the local mode moves in the direction of increased damping (that is, parallel to the negative real axis).

With the Padé transfer function

$$\frac{1 - (T_d s/2)}{1 + (T_d s/2)} = \frac{1 - (0.1s/2)}{1 + (0.1s/2)} \quad (10.85)$$

in the loop, the root-locus plot is shown in Figure 10.33(b). Note that the root-locus branch leaving the local mode at a frequency of 7 rad/s moves upward and turns around towards the RHP, indicating that the phase compensation is no longer appropriate.

To compensate for the delay, a second lead-lag stage is added to $G(s)$ to compensate for $0.1 \times 7 = 0.7$ rad = 40.11° at a frequency of 7 rad. Referring to the phase compensation method in control textbooks, such as p. 350 in [183], the lead-lag stage needs a pole-zero ratio of about 5. Thus using

$$T_3 = 1/(7/\sqrt{5}) = 0.3194, \quad T_4 = T_3/5 = 1/(7 \times \sqrt{5}) = 0.0639 \quad (10.86)$$

the redesigned PSS transfer function is

$$G'(s) = K_{\text{PSS}} \left(\frac{1 + sT_1}{1 + sT_2} \right) \left(\frac{1 + sT_3}{1 + sT_4} \right) = K_{\text{PSS}} \left(\frac{1 + 0.5s}{1 + 0.1s} \right) \left(\frac{1 + 0.3194s}{1 + 0.0639s} \right) \quad (10.87)$$

The root-locus plot for this controller is shown in Figure 10.33(c), which resembles that of Figure 10.33(a).

Picking a value of $K_{\text{PSS}} = 0.2$, in the closed-loop power system with a time delay of 100 ms, the swing mode poles are located at $-0.7702 \pm j6.9848$ and the exciter modes

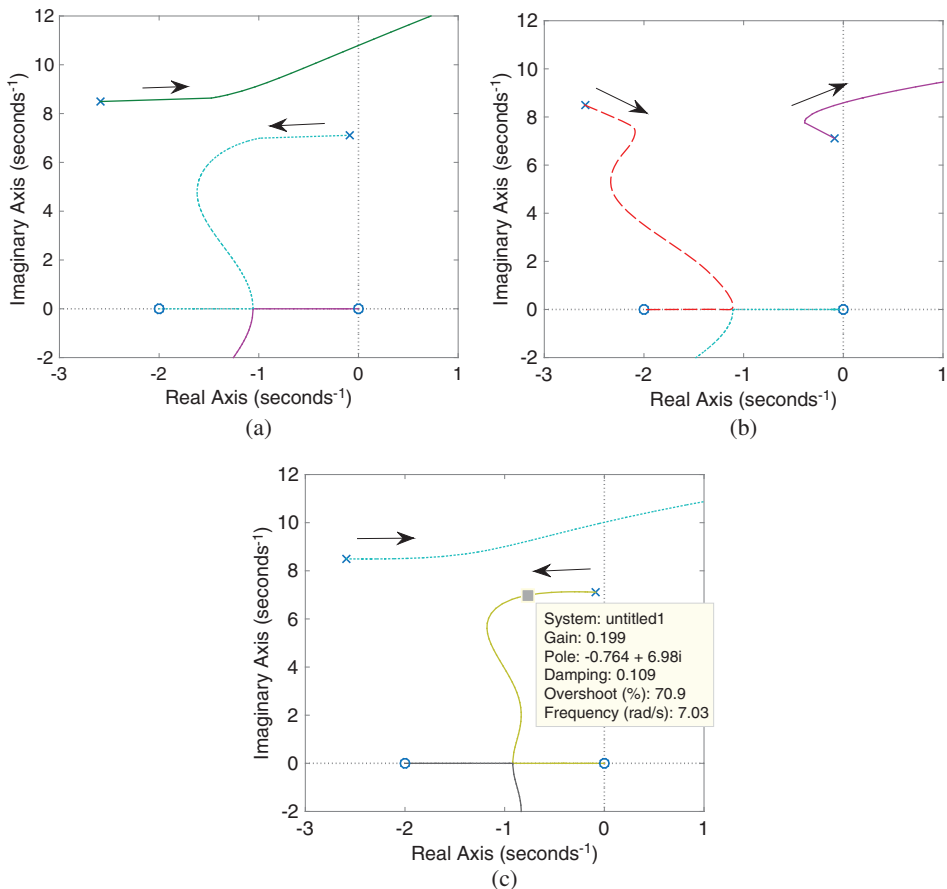


Figure 10.33 PSS design root-locus plots for (a) $G(s)$ (10.84), (b) $G(s)$ (10.84) with delay, and (c) $G'(s)$ (10.87) with delay.

are at $-1.4388 \pm j8.6758$, as compared to the design in Example 8.7 with the closed-loop poles at $-0.8612 \pm j7.0742$ and $-1.6314 \pm j8.5504$, respectively. \square

In a realistic power system, the arrival time of PMU data at a controller may have variable delays. Thus an adaptive phase compensation scheme based on the actual time delay may be used. One of such schemes is described in [184].

10.11 Conclusions and Remarks

Synchrophasor is a relatively new technology which has high potentials for enhancing the reliability of power system operation. This chapter describes the process of phasor computation, especially for off-nominal frequency conditions, and some applications of synchrophasor data. It is envisioned that new applications using synchrophasor data for

real-time visualization, situation awareness, and stability margin calculation will continue to be developed. These methods will be needed in light of the extensive deployment of renewable resources such as wind energy and photovoltaic systems in the not-too-distant future.

10.12 Problems

Some of the problems require using real PMU data and MATLABTM files. They can be found in the zipped folder downloadable from the third author's website. Note that some of the MATLABTM files used in the examples are also available in the zipped folder.

- 10.1** For the 60 Hz signal

$$x(t) = 100\sqrt{2} \cos(2\pi 60t + \pi/4) \quad (10.88)$$

sampled at a frequency of 1,440 Hz, apply DFT (MATLABTM `fft` function) to one cycle of the sampled signal x_k to compute \tilde{X} . Divide the magnitude by $N/2$ where N is the number of points used. Then divide again by $\sqrt{2}$ to get the RMS value.

- 10.2** Derive the P and Q expressions (10.16) and (10.17).

- 10.3** Compute the P and Q values in Table 10.1.

- 10.4** Compute the phasor representation \tilde{X}'_r of the 59 Hz sinusoidal signal

$$x(t) = 100\sqrt{2} \cos(2\pi 59t + \pi/4) \quad (10.89)$$

using a sampling frequency of 1,440 Hz and generate a table similar to Table 10.3. This is computed as if the signal were at 60 Hz. Develop two cycles of this signal to generate the table. Make a polar plot of the resulting computation (MATLABTM `polar` function).

- 10.5** Use the results of the previous problem and the three-point-average filter equation (10.27) to estimate the magnitude of the phasor representation of the 59 Hz signal.

- 10.6** For the 59 Hz signal, generate 5 cycles of data to compute \tilde{X}'_r for the first and the 4th cycle. Then apply (10.40) to estimate the frequency deviation of the 59 Hz signal referenced to a 60 Hz signal.

- 10.7** Let a true voltage phasor be $\tilde{X} = 100\angle\pi/4$ rad and its estimated phasor be $\tilde{X}_r = 100.5\angle0.79$ rad. Compute the TVE of the estimated signal.

- 10.8** The three-phase voltage and current data for a generator load rejection event is shown in Figure 10.34. Use the PMU Simulator [136] to compute the phasors of the individual phases, and the positive-, negative-, and zero-sequence phasors

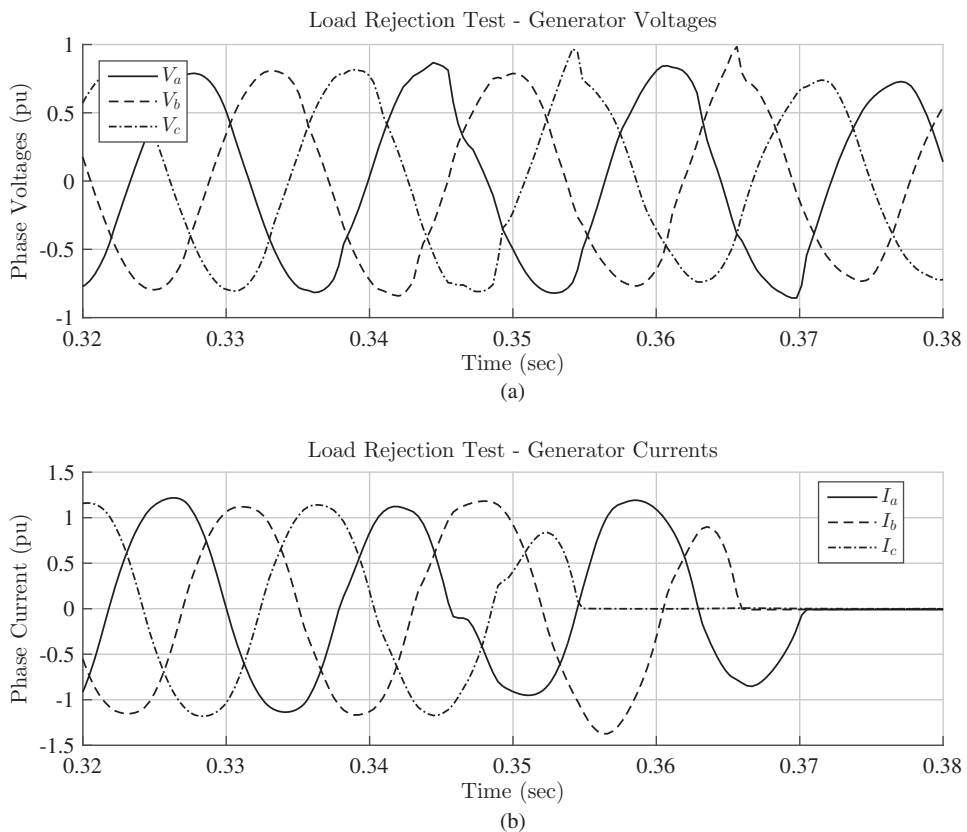


Figure 10.34 Dynamic data recorded for a load rejection test: (a) three-phase voltages, and (b) three-phase currents.

of the measured data. (The PMU simulator can be downloaded from a link on the third author's website.)

10.9 Calculate β for the various generator trip events shown in the Table 10.6.

10.10 For the system in Example 10.4, change the line reactance to 0.2 pu and simulate the disturbance waveform. What is the waveform travel speed?

Table 10.6 Generator trip events [152].

Year	Generator Name	MW lost	Hz change
1998	Gavin 1	1150	0.044
1998	Gavin 1	1150	0.038
1998	Millstone 3	1160	0.029
1998	Millstone 3	1150	0.033

- 10.11** For the system in Example 10.4, double the machine inertias and simulate the disturbance waveform. What is the waveform travel speed?
- 10.12** Repeat Example 10.4 by extending the radial chain of generators in Figure 10.12 by attaching 10 more radially connected generators (Generators 12 to 21) to Generator 11. Use the same machine inertia and line reactance for the additional generators. The load of 150 MW is moved from Generator 11 to Generator 21. Simulate the system dynamic response due to the tripping of Generator 0. Show the generator rotor speeds in 2D and 3D plots. Estimate the electromechanical wave propagation speed.
- 10.13** Repeat Example 10.5 with the Line 3-2 current magnitude adjusted down by 19% (the adjusted current magnitude is 4.9130 pu). Apply the LSE and evaluate the accuracy of the PMU data.
- 10.14** Use the Prony method to identify the dominant oscillatory mode for the unstable oscillation event in Figure 10.19 using the PMU data from 70–85 sec (data is in `Prob10-14.xls`). First obtain a 100th-order Prony model. Then put the identified model into a state-space model and perform a modal decomposition. From the modal decomposition, keep only the pair associated with the unstable oscillatory mode and form a 2nd-order reduced model. (Note that there are other unstable modes in the identified model.) Then perform an impulse response to check the accuracy of the identified model.
- 10.15** Redesign the PSS in Example 10.7 with a time delay of 150 ms in the machine speed signal. The linearized model data of the system in Example 10.7 can be found in the file `Example_10_7.m`.

11

Power System Toolbox

11.1 Background

Planning and operation of a large power system require dynamic simulations to ensure the stability of the system subject to all credible contingencies. Commercial power flow and dynamic simulation programs are capable of analyzing transient stability of very large systems with tens of thousands of buses and machines. In addition, there are also specialized programs available for voltage stability and small-signal stability analysis. Many models and algorithms used in dynamic simulation have been discussed in this book. The purpose of this chapter is to provide some insights into these simulation programs and typical model parameters so that a reader can become a more proficient user.

The discussion and examples in this chapter will make use of the Power System Toolbox (PST), a MATLABTM-based power system simulation software, which is fairly straightforward to learn and use [185].¹ Because the source code is provided, it is possible for an ambitious reader to incorporate new models into PST.

More specifically the objectives of this chapter are to:

1. Discuss data requirement for power system simulation
2. Explain the structures of simulation programs
3. Provide simulation examples
4. Reinforce the materials discussed in the other chapters

Although the discussion is based on PST, it is generally applicable to commercial power system simulation programs. Although PST does not have an interactive user interface (beside the MATLAB command window) or an extensive model library as commercial software packages, it is quite adequate for dealing with small-size systems used for illustrating power system concepts. A user can also readily use the graphics capability of MATLAB to display the simulation results.

¹ There is a link on the website of the third author to download a free copy of the software and a user manual [186].

This chapter will discuss three main aspects of PST for power system computer simulation and analysis, with references to materials already covered in the other chapters:

1. Power flow solution, which can also be used to analyze voltage stability (Section 8.4) and to initialize a dynamic simulation (Section 7.6)
2. Dynamic simulation, for performing transient stability investigations (Chapters 3 and 7) and evaluating the performance of damping controllers in the time domain (Section 8.6)
3. Linear analysis, which is useful for determining small-signal stability (Section 8.5) and designing power swing damping controllers such as power system stabilizers (Section 8.6)

The descriptions of the algorithmic aspects of these simulations and analyses have been covered in the previous chapters. Thus only a summary with some additional insights for using the simulation software will be provided. A reader is also referred to [187] for a more detailed treatment of power system simulation.

11.2 Power Flow Computation

Power flow computation is the determination of the steady-state flow of power from the generators to the loads. The assumptions made in computing the power flow solution include:

- The generator bus voltages are fixed, as they are supported by adequate reactive power supplied from the excitation systems and the field voltages of the generators.
- All generator active power outputs are fixed, except for one generator, which is used as the swing or slack bus because its generation is also needed to make up for the transmission losses. In practice, the generator output is determined most likely by an optimal power flow dispatch.
- The active and reactive power components of the loads are given.

This section covers the power flow data requirements, provides brief descriptions of the algorithms, and illustrates with an example.

11.2.1 Data Requirement

A power flow formulation requires generation and load as the bus data, and the power network connections as the branch data.

The bus data contains generator output and load consumption, given in MW/MVar or in pu. A commonly used system base is 100 MVA. The bus voltages in kV are also listed in the bus data and used for determining the transformer ratios. The active power P_L and reactive power Q_L loads are fixed at each bus, and the generator active power output P_G is also fixed, except for the swing generator.

The bus voltages on the generator buses are fixed, with the assumption that the excitation systems will provide adequate reactive power support to maintain the voltage. As a result, the reactive power output Q_G of a generator bus is not fixed, but is allowed to vary between a minimum value and a maximum value, which are determined from the generator's reactive power capability curve.

The branch data connects a from-bus to a to-bus and consists of two types: transmission lines and transformers. Transmission line data uses a π model (Section 2.2) consisting of a resistance R , a reactance X , and a line charging C , given in pu on the system base. A transmission line at a higher voltage level will have a smaller X and a larger C than a transmission line of the same length at a lower voltage level. In addition, the values of X and C both increase linearly as the line length is increased. The line charging can be neglected in short lines. The resistance R is typically 5–10% of the X value. Some production grade software allows a transmission line to have multiple sections. Series-capacitor-compensated lines can be modeled in this way allowing one of the sections to contain the series capacitor, with a negative X value.

Underground or submarine cables, found in cities and harbors, have a significantly larger line charging C than overhead lines as the phases in a cable are packed close together. Shunt reactors are typically switched in during low-load period to prevent excessively high voltage due to the Ferranti effect [188]. Some long 765 kV overhead lines would also need shunt reactors during low-load periods.

The transformer data is used to model fixed and variable-tap transformers. Power grids standardize on a small set of voltage levels to minimize the number of transformers needed. For example, the main transmission system voltage level in New York and New England system is 345 kV, and no transformer is needed in this interconnection of about 150 substations. Step down transformers are needed to deliver power to the 230/138/115 kV subtransmission lines and even lower-voltage distribution lines. A fixed transformer is represented by a resistance R , a reactance X , and a fixed tap ratio. The reactance X is the leakage reactance of the transformer [189]. The resistance R is normally small and thus set to zero. Variable-tap transformers are used to achieve some voltage control in the network. The taps are not moved very often due to mechanical wear-and-tear considerations. The number of taps and the step-size are required transformer data, so that a power flow program can adjust the taps if some bus voltages are outside of the desired voltage ranges.

Step-up transformers are used to connect generators to the high-voltage grid. If the transformer parameters are not given, it can be assumed to have a (leakage) reactance value of 15% on the transformer rating. For example, the step-up transformer for a 600 MVA generator would have a reactance value of $0.15 \times 100/600 = 0.025$ pu when put on a system base of 100 MVA. Such step-up transformers are normally fixed tap as the generator excitation systems can be used for voltage control.

Phase-shifting transformers are practically all variable taps. One of the main functions of a phase-shifting transformer is to control active power loop flow or balance the active power flows on parallel paths. They are quite commonly found at the interfaces between control regions, for example, between New York and New Jersey. A phase-shifting transformer is represented by the number of taps and the step-size. The transformer reactance value is also required.

The bus data also requires a bus name and a bus number. The bus numbers do not have to be consecutive, as the computer software will assign a consecutive internal bus number (a technique loosely called “second indexing”) to a bus as its data is being read. The from-bus and to-bus of a branch will also be automatically indexed to the internal bus numbers. This is a significant convenience to a user with a large power system data set provided by many different companies.

Table 11.1 Power flow bus types and variables.

Bus type	V	θ	P	Q
PQ (load bus)	computed	computed	specified	specified
PV (generator)	specified	computed	specified	computed
Swing (slack) bus	specified	$\theta = 0^\circ$	computed	computed

11.2.2 Power Flow Formulation and Solution

A nonlinear power flow program solves for the bus voltages and angles given the loads and the generator active power outputs and voltages, with a swing generator to balance the active power generation against the active power loads and losses on transmission lines. Table 11.1 shows three different types of buses used in a power flow solution, and their fixed and computed values.

A load bus is a PQ bus with known consumption of P_L and Q_L . A generator bus is a PV bus with fixed P_G and V . One of the generators is designated as a swing bus with fixed V and phase θ , which is normally set to 0° , but unspecified P_G and Q_G . Because power transfer across a branch is a function of the angle difference between the from-bus and the to-bus, one of the bus angles needs to be fixed. Otherwise, there will be an infinite number of solutions (which are all equivalent). Furthermore, the P generation at the swing bus is not specified, as the active power losses are not known ahead of time.

A power flow program solves the nonlinear network flow equations listed in Section 7.3. An early approach is to use the Gauss-Seidel iterative method, which has been abandoned because its convergence is only linear. Instead all power flow computation in commercial software uses the Newton-Raphson method which has a quadratic convergence rate when the iterations get close to the solution. The power flow is formulated using the admittance matrix Y (see Table 7.2 for an example). The Y matrix is sparse and an entry in Y is non-zero only if there is a branch connecting the respective buses. It is built one connection at a time for each branch data as it is read into the program. The Y matrix normally averages 4–5 non-zero entries per row, reflecting the configuration of a real power system. The partial derivatives of the power flow equations with respect to the bus voltage magnitudes and angles, also known as the Jacobian matrix J , is also sparse. Thus very efficient LU decomposition using sparse factorization algorithms, first proposed in [190], can be used to solve power flow for systems with more than 30,000 buses. At various times, methods have been proposed for using the impedance matrix Z , which unfortunately is not suitable for large systems due to Z being a full matrix.

As discussed earlier, generators have reactive power output limits. If the power flow solution determines that the reactive power output of a generator exceeds its limits, this generator will be reset to a PQ bus with its active power load as $-P_G$ and reactive power load as the negative value of the appropriate limit. If the solution converges, then the reactive power limits for that generator would not be violated. However, the desired voltage at this generator bus would no longer be maintained.

The NR power flow method will converge very fast if the initial guess is close to the solution. Starting from a default voltage magnitude of 1 and phase of 0° on all the

unspecified buses, which is known as a *cold start*, this initial condition may be quite far away from the solution and require quite a few iterations. However, if a similar power flow solution has already been obtained previously, it can be used to initiate the current power flow solution. This *warm start* will improve the efficiency of the NR solution.

As expected, the majority of the computing time is spent with building the Jacobian matrix J (7.165) and performing the LU decomposition. Several alternative methods have been proposed. One approach is the dishonest Newton method in which J is not updated at every iteration.² Another approach is the decoupled power flow method which decomposes J into two parts: one for active power flow to solve for the voltage angles and the other for the reactive power flow to solve for the voltage magnitudes. Most power system simulation programs provide options for a user to choose these alternative methods. An in-depth power flow algorithm survey is provided in [191].

The following example is intended to demonstrate the use of the power flow function `loadflow` in PST and interpret the power flow solution.

Example 11.1 A two-area, four-machine system is shown in Figure 8.16, with the system parameters shown in Tables 8.8–8.11. Use the `loadflow` function to

1. Solve the base case power flow shown in Table 8.11.
2. Increase the active power load on Bus 13 to 16.75 pu and reduce the active power load on Bus 3 to 10.59 pu. The reactive power loads on these buses remain the same. Solve the power flow.

Solution

1. The power flow solution obtained based on a cold-start data file³ is shown in Figure 11.1. Note that the power flow values on identical parallel lines are not shown. The reactive power generations of all the generators are within the reactive power capability of ± 2 pu. The total active power losses are computed by subtracting the sum of all the active power loads from the sum of the generator active power output. The total reactive power losses are computed in the same way for reactive power loads and generation, which include the contributions from line charging. The NR algorithm converges in 4 iterations to a user-specified tolerance of 10^{-6} .
2. The bus solution of the new power flow from a cold start data file⁴ is shown in Figure 11.2. First, the increased power flow on the lines connecting Buses 3 and 13 causes the angular separation of these two buses to increase to 13.46° from 8.87° , indicating a higher stress on the system. Second, the increased power flow to Bus 13 requires additional reactive power compensation. The generator on Bus 12 provides increased reactive power supply such that it reaches its maximum reactive power capability. As a result, the bus voltage drops below 1.01 pu. The voltages at Buses 112, 3, and 13 also decrease. In particular, the voltage on Bus 13 drops to 0.9641 pu from the value 0.9717 pu in Part (1). Further load increases on Bus 13 will cause voltage collapse in the system. □

² An imprecise J can still give reasonably good descent directions for convergence.

³ The data file is `Example_11_1_1.m`

⁴ The data file is `Example_11_1_2.m`

LOAD-FLOW STUDY
REPORT OF POWER FLOW CALCULATIONS

10-Dec-2015

SWING BUS : BUS 3
 NUMBER OF ITERATIONS : 4
 SOLUTION TIME : 0.003 sec.
 TOTAL TIME : 0.005 sec.
 TOTAL REAL POWER LOSSES : 0.877231.
 TOTAL REACTIVE POWER LOSSES: 7.82055.

BUS	VOLTS	ANGLE	GENERATION		LOAD	
			REAL	REACTIVE	REAL	REACTIVE
1.0000	1.0300	8.2170	7.0000	1.3393	0	0
2.0000	1.0100	-1.5026	7.0000	1.5940	0	0
11.0000	1.0300	0	7.2172	1.4462	0	0
12.0000	1.0100	-10.2050	7.0000	1.8070	0	0
101.0000	1.0108	3.6631	0	0	0.0000	-0.0000
102.0000	0.9875	-6.2419	0	0	0.0000	-0.0000
111.0000	1.0095	-4.6977	0	0	0.0000	-0.0000
112.0000	0.9850	-14.9442	0	0	0.0000	-0.0000
3.0000	0.9761	-14.4184	0	0	11.5900	-0.7350
13.0000	0.9717	-23.2918	0	0	15.7500	-0.8990

LINE FLOWS					
LINE	FROM BUS	TO BUS	REAL	REACTIVE	
1.0000	1.0000	101.0000	7.0000	1.3393	
2.0000	2.0000	102.0000	7.0000	1.5940	
3.0000	3.0000	13.0000	0.6654	-0.1527	
6.0000	3.0000	102.0000	-6.7931	0.5965	
8.0000	11.0000	111.0000	7.2172	1.4462	
9.0000	12.0000	112.0000	7.0000	1.8070	
10.0000	13.0000	112.0000	-6.8922	0.5366	
12.0000	101.0000	102.0000	3.4761	0.3824	
14.0000	111.0000	112.0000	3.5831	0.4167	
1.0000	101.0000	1.0000	-6.9521	-0.7647	
2.0000	102.0000	2.0000	-6.9495	-0.9877	
3.0000	13.0000	3.0000	-0.6552	-0.0580	
6.0000	102.0000	3.0000	6.8908	0.3511	
8.0000	111.0000	11.0000	-7.1662	-0.8334	
9.0000	112.0000	12.0000	-6.9488	-1.1922	
10.0000	112.0000	13.0000	6.9935	0.4474	
12.0000	102.0000	101.0000	-3.4161	0.1427	
14.0000	112.0000	111.0000	-3.5191	0.1487	

Figure 11.1 Base case power flow solution for Example 11.1.

BUS	VOLTS	ANGLE	GENERATION		LOAD	
			REAL	REACTIVE	REAL	REACTIVE
1.0000	1.0300	12.5821	7.0000	1.3836	0	0
2.0000	1.0100	2.8478	7.0000	1.7264	0	0
11.0000	1.0300	0	7.2667	1.5894	0	0
12.0000	1.0076	-10.3343	7.0000	2.0000	0.0000	-0.0000
101.0000	1.0103	8.0283	0	0	0.0000	-0.0000
102.0000	0.9859	-1.8915	0	0	0.0000	-0.0000
111.0000	1.0079	-4.7305	0	0	0.0000	-0.0000
112.0000	0.9802	-15.0972	0	0	0.0000	-0.0000
3.0000	0.9728	-10.0982	0	0	10.5900	-0.7350
13.0000	0.9641	-23.5627	0	0	16.7500	-0.8990

Figure 11.2 Power flow solution for Example 11.1 with increased load at Bus 13.

11.2.3 Nonconvergent Power Flow

If the power system data is not consistent, the power flow may converge to a bad solution or not converge at all. Some common problems are:

1. Incorrect MVA bases used for the line, generator, and load parameters.
2. Some wrong line parameters are used, resulting in higher reactance lines that would not permit the desired power flow values.
3. There is not enough reactive power support, forcing some generators to reach their maximum reactive power limits and load buses to reach their minimum voltage levels. Most power flow programs would indicate the buses that have reached their minimum voltage levels. Thus a user can temporarily put synchronous condensers on these buses and make them *PV* buses with sufficient amounts of reactive power supply. A synchronous condenser is a generator that supplies only reactive power to regulate the bus voltage. The low bus voltage may also be avoided by raising the generator terminal voltages.

Once a converged power flow solution has been obtained, a user can look at the results and strategically adjust the loads and reactive power supply to achieve a bus voltage profile within the range 0.98–1.05 pu. The generator buses typically will have higher voltages than the load buses, because the generators normally supply reactive power as well as active power.

11.3 Dynamic Simulation

A power system consists of many dynamic components coupled by the electrical network. Referring to Figure 1.2, for dynamic studies in the slower time-scales, such as transient stability, network transient phenomenon can be neglected and the power circuits represented by the positive-sequence network. Thus disturbance simulation of power systems is based on the electrical network modeled as algebraic equations. The algebraic equations are linear if the loads are modeled as constant impedance. For other load models, these equations are nonlinear. Figure 11.3 shows the interactions between the dynamic and algebraic components of a power system model.

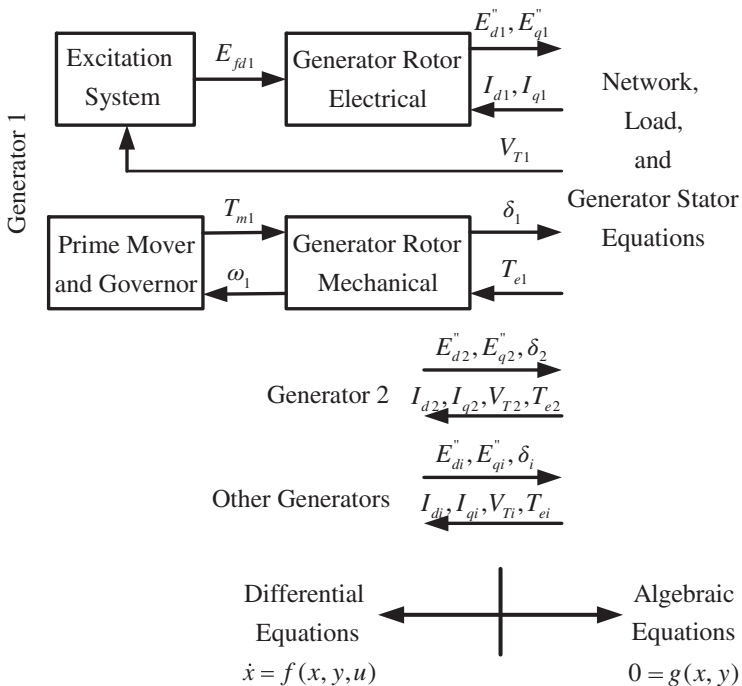


Figure 11.3 Power system computation variable flow diagram. *Source:* Adapted from Price 1980 [192].

This section discusses the structure of a power system simulation program suitable for very large power systems. The modeling approach is referred to as the Industry Model in Section 7.4. The complexity arises from initializing the equilibrium values of the states (such as generator fluxes) before the start of a disturbance and then solving the network solution required for each time step of integration after the disturbance has been applied. In addition, the program also needs to handle various models of generators (such as steam and hydraulic units) and excitation systems (AC and DC sources). A flowchart of the steps involved in power system dynamic simulation is shown in Figure 11.4 and will be discussed in the sequel.

11.3.1 Dynamic Models and Per-Unit Parameter Values

A general purpose simulation program provides a large variety of dynamic models to choose from. These models are standardized so that equipment manufacturers can provide dynamic data for performance verification in simulation programs. For example, various generator models and their usage are described in [193]. Excitation systems are grouped into DC (direct current), AC (alternating current), and ST (static excitation) according to the types of exciter voltage sources [57]. Turbines are grouped into steam, hydraulic, and combustion models [61, 62, 194].

The dynamic models are programmed using the differential equation representations of their dynamic behavior, many of which have already been discussed in previous chapters. For example, in generator models, the swing equation is used to model the acceleration of the rotor states (angle and speed) according to the difference of the mechanical

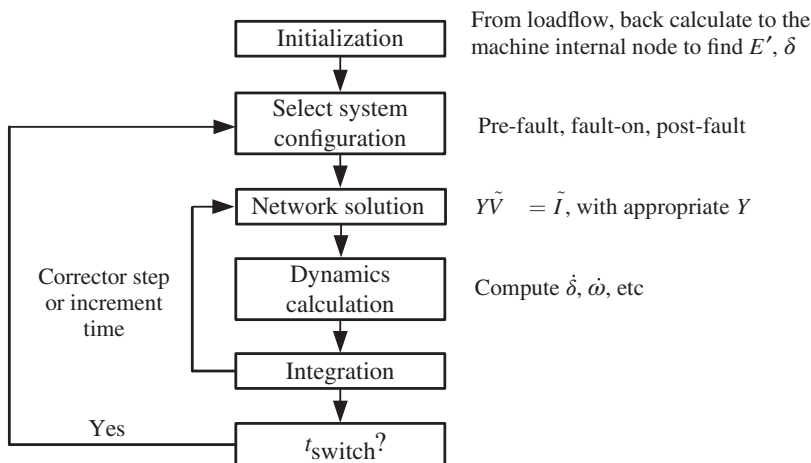


Figure 11.4 Power system dynamic simulation flowchart.

power determined by the output of the turbine, and the electrical power determined by the network power flow. Each piece of data for a dynamic model would contain a model type so that an appropriate model can be applied.

The generator model parameters as provided by the manufacturers are typically in per unit on the generator rating, which is a MVA value required for the generator data. The per-unit values have the advantage of normalizing across generator units of different sizes. For example, on the machine MVA base, the direct-axis transient reactance X'_d is normally in the range of 0.2–0.3 pu regardless of the generator type (steam, hydraulic, etc.). The combined turbine-generator inertia H ranges from a low value of 2.5 pu for a hydraulic turbine to 6 pu for a steam unit with multiple turbine sections at various pressure levels. In this way, an experienced power engineer can readily spot any anomalies in the machine parameters, because the parameters for practical generators are known to be in certain ranges [80], as determined by the machine windings and physical laws. In fact, some simulation programs would warn a user if certain parameter values are outside the normal ranges. Within a simulation program, the pu values of the generator parameters will be converted to pu values on the system base before the start of the simulation.

11.3.2 Initialization

In disturbance simulation, a power system is expected to be in steady state before the disturbance is applied. The initialization process starts from a converged power flow solution with specified loads and computed generator output. As discussed in Section 7.6, a “back-tracking” process is used to first compute for each synchronous machine, the generator currents and internal voltages, and then the generator rotor angle, as shown in Figure 7.11. Note that in this calculation, the only variables needed are the terminal bus voltage \tilde{V}_T and the generator current \tilde{I}_G for that generator. Because the generator is providing active power to the network, the rotor angle δ would be higher than the terminal bus voltage angle θ .

Next, the computed generator field voltage is used to initialize the states in the excitation system, including the reference voltage value V_{ref} . Note that V_{ref} is not the same as the terminal bus voltage V_T , because most voltage regulators are of the proportional gain type and not the integral type, resulting in a small steady-state error acted upon by the voltage regulator gain K_A . If the generator is providing reactive power to the network, than V_{ref} would be higher than V_T .

The mechanical input power P_m required by the generator will be used to initialize the turbine-governor state variables. Here the speed reference will be the nominal system frequency, and the turbine power will be set to exactly the value of the generator mechanical input power. Thus the turbine will be rotating at synchronous speed and the generator rotor angle will be at a constant value.

Note that the initialization process for each generator and its control equipment is independent of the other generators.⁵ Thus if computers with multiple processors or cores are used, the initialization process can be performed in parallel, reducing the computing time.

11.3.3 Network Solution

After the generation voltages (fluxes) have been determined, they and the loads will “drive” the electrical network. In essence, given the generator voltages, the network currents will be computed. These currents will in turn determine the bus voltages including the generator terminal voltage V_T , and the electrical power (torque) P_e (T_e) drawn from the generators. Then the swing equation will use P_e to determine the rate of change of the rotor speed and angle, and the excitation system will determine the field voltage E_{fd} based on the value of V_T . The resulting values of δ , E''_q and E''_d (or E'_q and E'_d for transient model) will be used to determine the network current flow, thus repeating the process.

Much of this process has already been discussed in Chapter 7. Here a two-step current and voltage calculation is illustrated. The voltage-current relationship in a power network is determined by

$$Y_N \tilde{V} = \tilde{I} \quad (11.1)$$

where Y_N is the network admittance matrix, \tilde{V} is a vector of bus voltages, and \tilde{I} is a vector of current injections at the buses. The admittance matrix Y_N includes the line resistances, reactances, and charging, shunt capacitors and reactors, and transformer taps (which are generally fixed during dynamic simulation). The positive direction of \tilde{I} means the current is flowing from a bus into the network.

Separating the generation and load buses, (11.1) can be rewritten as

$$\begin{bmatrix} Y_{11} & Y_{12} \\ Y_{21} & Y_{22} \end{bmatrix} \begin{bmatrix} \tilde{V}_G \\ \tilde{V}_L \end{bmatrix} = \begin{bmatrix} \tilde{I}_G \\ \tilde{I}_L \end{bmatrix} \quad (11.2)$$

where \tilde{V}_G and \tilde{V}_L are the voltages and \tilde{I}_G and \tilde{I}_L are the current injections of the generator and load buses, respectively.

⁵ Cross-compound units may be exceptions.

For the treatment here, the loads are assumed to be of the constant-impedance type so that

$$\tilde{I}_L = -Y_L \tilde{V}_L \quad (11.3)$$

where Y_L is the diagonal load admittance matrix. For Generator i , the output current is determined by

$$\tilde{I}_{Gi} = \frac{1}{jX''_{di}} (\tilde{E}''_i - \tilde{V}_{Gi}) \quad (11.4)$$

where $\tilde{E}''_i = E''_{di} + jE''_{qi}$ and $X''_{qi} = X''_{di}$ (subtransient saliency neglected). Let Y_G be the diagonal matrix of $1/(jX''_{di})$. Then

$$Y_G (\tilde{E}'' - \tilde{V}_G) = \tilde{I}_G \quad (11.5)$$

Note that for a transient model, E'_{di} , E'_{qi} , and X'_{di} will replace E''_{di} , E''_{qi} , and X''_{di} , respectively, in these equations.

Combine (11.2)–(11.5) into a single equation to form the network equation extended to the generator internal node as

$$\begin{bmatrix} Y_G & -Y_G & 0 \\ -Y_G & Y'_{11} & Y_{12} \\ 0 & Y_{21} & Y'_{22} \end{bmatrix} \begin{bmatrix} \tilde{E}'' \\ \tilde{V}_G \\ \tilde{V}_L \end{bmatrix} = \begin{bmatrix} \tilde{I}_G \\ 0 \\ 0 \end{bmatrix} \quad (11.6)$$

where $Y'_{11} = Y_{11} + Y_G$ and $Y'_{22} = Y_{22} + Y_L$.

The network equation (11.6) is solved in two stages.

- Stage 1:

Extract \tilde{V}_G and \tilde{V}_L from (11.6) to form

$$\begin{bmatrix} Y'_{11} & Y_{12} \\ Y_{21} & Y'_{22} \end{bmatrix} \begin{bmatrix} \tilde{V}_G \\ \tilde{V}_L \end{bmatrix} = Y_{GL} \begin{bmatrix} \tilde{V}_G \\ \tilde{V}_L \end{bmatrix} = \begin{bmatrix} Y_G \\ 0 \end{bmatrix} \tilde{E}'' \quad (11.7)$$

and use LU decomposition to solve for \tilde{V}_G and \tilde{V}_L , as the generator voltage phasor \tilde{E}'' is known. Note that the admittance matrix is fixed for a given network configuration, so only one factorization is needed.

- Stage 2:

Compute

$$\tilde{I}_G = Y_G (\tilde{E}'' - \tilde{V}_G) \quad (11.8)$$

From the solution of (11.8), the electrical power $P_e = \text{Re}(\tilde{E}'' \tilde{I}_G^*)$ can be computed. Note that Q_e is not needed, unless its limit needs to be checked.

Alternatively, from (11.7), \tilde{V}_G and \tilde{V}_L can be expressed in terms of \tilde{E}'' as

$$\begin{bmatrix} \tilde{V}_G \\ \tilde{V}_L \end{bmatrix} = Y_{GL}^{-1} \begin{bmatrix} Y_G \\ 0 \end{bmatrix} \tilde{E}'' = H_{VR} \tilde{E}'' \quad (11.9)$$

The matrix H_{VR} is known as the (complex) voltage reconstruction matrix and is dimensionless. Note that although Y_N is not invertible, the admittance matrix Y_{GL} is, because of the generator reactance terms in the diagonal entries of Y'_{11} .

It follows that the generator currents can be computed from

$$\tilde{I}_G = (Y_d + [-Y_d \quad 0] H_{\text{VR}}) \tilde{E}'' = Y_{\text{red}} \tilde{E}'' \quad (11.10)$$

The matrix Y_{red} is known as the admittance matrix reduced to the machine internal node or the reduced admittance matrix. It is a full matrix because the voltage reconstruction bus is a full matrix. Thus even though Y_{red} is smaller in size than Y_N , sparse factorization cannot be applied to Y_{red} , and hence, Y_{red} is not used in simulation programs for large power systems. Instead, \tilde{I}_G is solved from (11.8).

11.3.4 Integration Methods

To simulate the impact of a disturbance on a power system, an integration method is applied to the dynamic models to compute the states as they deviate from the initial equilibrium point. The power system states are governed by a system of first-order nonlinear differential equations of mechanical and electrical dynamics, represented by

$$\dot{x} = f(x, u, t), \quad x(t_0) = x_0, \quad x, f \in R^n, \quad u \in R^m \quad (11.11)$$

where x is the state vector of dimension n , u is the input vector of dimension m , and f is the vector of the nonlinear dynamics governing the system.

Let the solution of (11.11) be

$$x(t_0) = x_0, x(t_1) = x_1, \dots, x(t_k) = x_k, x(t_{k+1}) = x_{k+1}, \dots \quad (11.12)$$

where t_i is the time at the i th time step and the time increment h is uniform, that is, $t_{k+1} = t_k + h$. The parameter h is also known as the integration stepsize.

The Taylor Series expansion of the solution up to the $(r+1)$ st order is given by

$$x_{k+1} = x_k + h\dot{x}_k + \frac{h^2}{2}\ddot{x}_k + \dots + \frac{h^r}{r!}x_k^{(r)} + \frac{h^{r+1}}{(r+1)!}x_k^{(r+1)}(\xi) \quad (11.13)$$

where $t_k \leq \xi \leq t_{k+1}$ and the superscript r in $x_k^{(r)}$ denotes the r th derivative of x_k . The expansion (11.13) is used to determine the order and the local truncation error of an integration routine.

In the Euler method, a nonlinear differential equation is solved for a fixed stepsize h from $t = t_0$ to $t = t_f = t_0 + N_h h$, using the formula

$$x(t_{k+1}) = x(t_k) + h\dot{x}(t_k) = x_k + h\dot{x}_k, \quad k = 0, 1, \dots, N_h - 1 \quad (11.14)$$

The Euler's method is a first-order Runge-Kutta (RK) method. The local truncation error is [194, 195]

$$\varepsilon = \frac{h^2}{2}\ddot{x}(\xi) \simeq \frac{h^2}{2}\ddot{x}_k \simeq \frac{h^2}{2} \frac{(\dot{x}_{k+1} - \dot{x}_k)}{h} = \frac{h}{2}(\dot{x}_{k+1} - \dot{x}_k) \quad (11.15)$$

Due to its low accuracy, the Euler's method is seldom used in power system dynamic simulations, because a very small stepsize is needed to capture the lightly damped oscillations accurately.

A second-order integration method is the Euler full-step modification method, which performs the integration in two stages. First the value of x_{k+1} is predicted as

$$\hat{x}_{k+1} = x_k + h\dot{x}_k = x_k + hf(x_k, u_k, t_k) \quad (11.16)$$

Then the time-derivative of \hat{x}_{k+1} is computed as

$$\dot{\hat{x}}_{k+1} = f(\hat{x}_{k+1}, u_{k+1}, t_{k+1}) \quad (11.17)$$

and used to correct the predicted values \hat{x}_{k+1} using the average value of \dot{x}_k and $\dot{\hat{x}}_{k+1}$

$$x_{k+1} = x_k + \frac{h}{2}(\dot{x}_k + \dot{\hat{x}}_{k+1}) \quad (11.18)$$

This predictor-corrector method is a 2nd-order RK method, as the local truncation error is $\varepsilon \simeq (h^3/6)x_k^{(3)}$.⁶ The improved accuracy comes with the expense of requiring two evaluations of f at each integration step.

A few commercial simulation software packages⁷ use the Adams-Basforth Second-Order (AB2) method [195] for numerical integration. Using AB2, the integration of (11.11) is performed as

$$x_{k+1} = x_k + h[1.5f(x_k) - 0.5f(x_{k-1})] \quad (11.19)$$

This method is a multi-step method because the new value depends not only on the current value, but also on a previous value. See [195] for a proof of the selection of the coefficients used in (11.19). For the initialization of AB2, the Euler method is used to integrate from x_0 to x_1 .

11.3.5 Disturbance Specifications

Dynamic simulation is used to determine the stability of a power system subject to a large number of contingencies. Most system operators are concerned with the so-called $N-1$ contingencies [196], interpreted as all equipment (of which there are N of them) working properly except for one.

The most common disturbance would be a short circuit on a transmission line due to a fault such as a lightning strike. The fault is cleared by relay operation, resulting in tripping the faulted transmission line. The short-circuit fault may differ in severity. In contingency analysis, the most severe fault is usually considered, which is the three-phase-to-ground short-circuit fault, cleared by removing all three phases. The rationale here is that if the generator or system under consideration remains stable under the most severe fault conditions, it should also be stable under less severe fault conditions.

The disturbance simulation is specified by a “script” containing the following elements:

1. An initial short period of time (0.1 to 1.0 sec) with no disturbance: the purpose is to ensure that the power system initializes in steady state.
2. The time when the fault is applied, and the fault type, including single-phase-to-ground, two-phase-to-ground, line-to-line, three-phase-to-ground, and impedance-to-ground.
3. The location at which the fault is applied: to maximize the impact of a fault, the fault is applied on a line close to a generator bus.

⁶ The Euler full-step modification method is used in the Power System Toolbox for the simulation of power system disturbances.

⁷ The Siemens-PTI PSS/ETM program and the GE PSLFTM program.

4. The time when the fault is cleared and the faulted line is tripped: typical relaying operation time is 4-6 cycles.
5. The time when the simulation ends.

The stepsize of integration also needs to be specified and can be changed during the simulation. For the fault-on period and immediately after a fault is cleared, a small step size like 2.5 ms should be used. After the initial transient period, a larger step size like 5 or 10 ms can be used.

In the following, dynamic simulation will be illustrated with 2 examples. The first example is on the initialization of the 3-machine system in Section 7.3, and the second example is on the time simulation of a single-machine infinite-bus system to illustrate system dynamic response and transient energy functions.

Example 11.2 Section 7.6 describes the analytical steps of obtaining the initial conditions of the generators and their control equipment in a simulation program. Example 7.5 uses the procedure to obtain the equilibrium values of the 3-machine system in Figure 7.4. Now repeat Example 7.4 using PST to obtain the initial conditions.

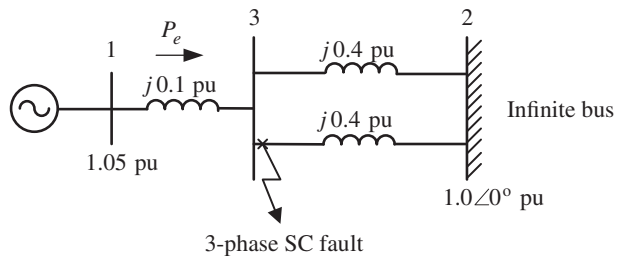
Solution

The PST `s_simu` function is used to perform a simulation with a short period of steady-state condition at the start. The initial conditions for the machine and exciter states can be extracted from the simulation at $t = 0$, and are listed in Table 11.2. The top row of the labels contains the variables used in this book, and the bottom row contains the corresponding variable names in PST. Note that these values agree well with those obtained in Example 7.5, except for one discrepancy, arising from a different definition of the state R_f in PST. If the R_f values from PST are scaled by $K_F/T_F = 0.063/0.35$, the resulting values of R_f would be equal to those given in Example 7.5. \square

Table 11.2 Initial conditions for Example 11.2 (all values in pu except for angles in degrees).

Machine	\bar{V} V	δ mac_ang	I_d curd	I_q curq	V_d ed	V_q eq
1	1.040∠0°	3.586°	0.3026	0.6712	0.0650	1.0380
2	1.025∠9.280°	61.098°	1.2901	0.9320	0.8057	0.6336
3	1.025∠4.665°	54.137°	0.5615	0.6194	0.7797	0.6661
E'_d edprime	E'_q eqprime	E_{fd} Efd	V_R v_R	R_f R_f	V_{ref} exc_con(:, 3)	T_M pmech
0.0242	1.0564	1.0821	1.1049	1.0821	1.0952	0.7164
0.6941	0.7882	1.7893	1.9021	1.7893	1.1201	1.6300
0.6668	0.7679	1.4030	1.4515	1.4040	1.0976	0.8500

Figure 11.5 SMIB system for Example 11.3.



Example 11.3 A single-machine infinite-bus system is shown in Figure 11.5. The electromechanical model parameters of Generator 1 on Bus 1 are: base MVA = 991, $H = 2.8756$ pu, $D = 1.0$ pu, and $X'_d = 0.245$ pu. The voltage at the infinite bus is 1.0 pu. The line parameters are given on the generator MVA base.

1. Solve the loadflow for the system with $P_e = 0.90$ pu, using the infinite bus as the swing bus. Plot the power-angle (P - δ) curve.
2. Simulate the system response up to 5 sec using the following script: no-fault simulation for 0.1 sec, a three-phase short-circuit fault on one of lines connecting Buses 2 and 3 on the Bus 3 side at 0.1 sec, and the fault cleared by opening the faulted line at 0.2 sec (6-cycle fault) at Bus 3 and 0.22 sec later at Bus 2. Repeat the simulation by delaying the opening of the faulted line to 0.247 sec at Bus 3 and 0.249 sec (about 9 cycles) later at Bus 2.
 - a) Determine the system stability with respect to these two contingencies and plot $\delta(t)$ (in degrees) and $\omega(t)$ (in pu) versus time t .
 - b) Make a phase plot of $(\delta(t), \omega(t))$.
 - c) Superimpose $P_e(t)$ versus $\delta(t)$ on the pre-fault P - δ curve for the 6-cycle fault clearing case.
 - d) Plot together the various energy functions: V_{KE} , V_{PE} , and V_E for the 6-cycle fault clearing case.

Solution

The power flow solution shows that $V_1 = 1.05\angle 14.90^\circ$, $V_2 = 1.0\angle 0^\circ$, and $V_3 = 1.0257\angle 10.10^\circ$. The disturbance simulations of Generator 1 machine angle and speed with respect to the two contingencies are shown in Figures 11.6(a) and (b). For the 6-cycle fault clearing time, the system response is stable and the time response is damped because of the nonzero D value. However, the 9-cycle fault clearing time resulted in an unstable transient response. Only the beginning part of the unstable time response is shown in those figures.

The phase plot of $\delta(t)$ versus $\omega(t)$ is shown in Figure 11.6(c). In the stable response, the fault-on trajectory leaves the pre-fault equilibrium point with monotonically increasing machine speed and angle. At the fault-clearing point, the trajectory starts to spiral inward clockwise towards the post-fault equilibrium point. Thus the trajectory remains inside the region of stability. However, for the 9-cycle fault clearing time, the fault-on trajectory has moved outside the region of stability. When the fault is cleared, the rotor angle continues to increase, as the rotor speed deviation remains positive.

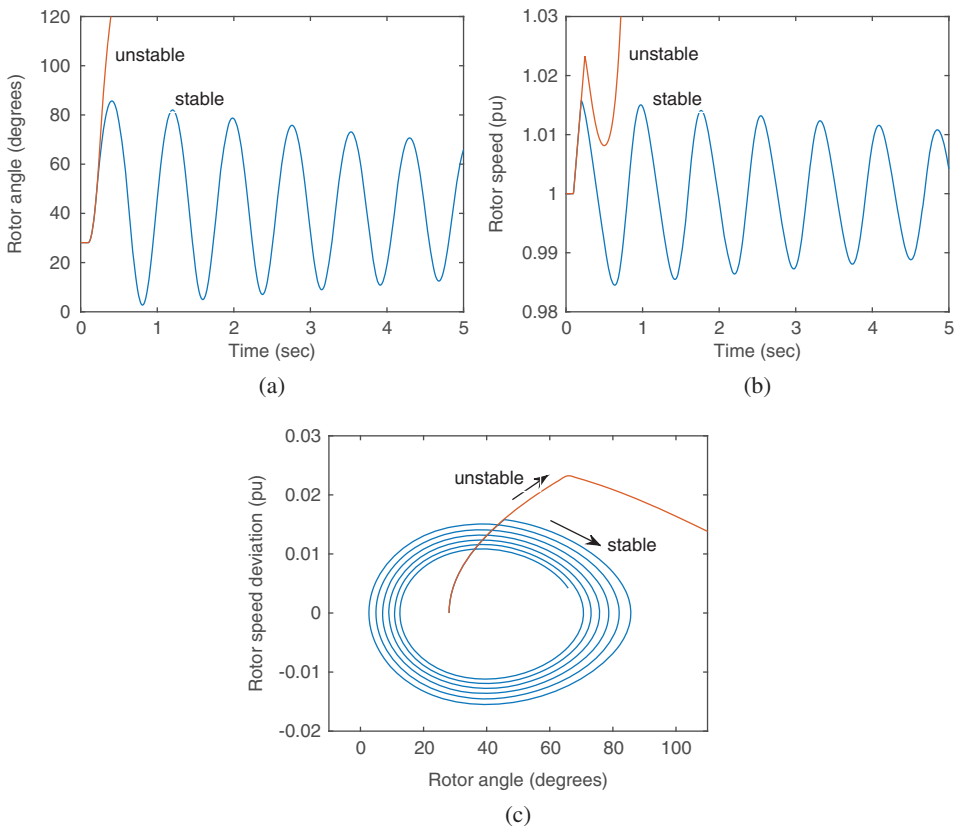


Figure 11.6 Stable and unstable disturbance response for (a) rotor angle, (b) rotor speed, and (c) phase plot of rotor angle vs rotor speed.

The pre-fault power-angle (P - δ) curve is shown in Figure 11.7. The intersection of the curve with the constant mechanical power line at 0.9 pu is the pre-fault equilibrium angle. During the fault-on period, the rotor angle increases as the electrical power drops to zero. In the stable case, when the fault is cleared, the rotor angle will continue to increase until the speed deviation becomes negative. This trajectory forms part of the post-fault power-angle curve. Figure 11.7 can be used to determine the critical clearing time (see Figure 9.9).

Using the expression of the energy function V_E (9.35), the potential (V_{PE}), kinetic (V_{KE}), and total energy (V_E) functions are plotted in Figure 11.8. Note that the swing oscillations are observable in the potential and kinetic energy functions. However, the total energy function is a monotonic decaying function. Note that the energy decay is non-uniform, because the energy loss is due to the generator damping term D such that the energy dissipation is small when the machine speed deviation is small.

In this example with the damping coefficient $D > 0$, the time responses are damped, although the damping is small. If $D = 0$, the oscillations would be undamped. As a result, the total energy function will remain constant at the fault-clearing time energy level. \square

Figure 11.7 P - δ curve for Example 11.3.

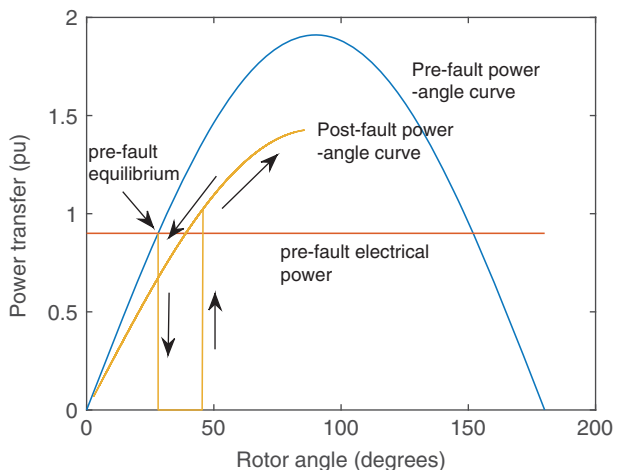
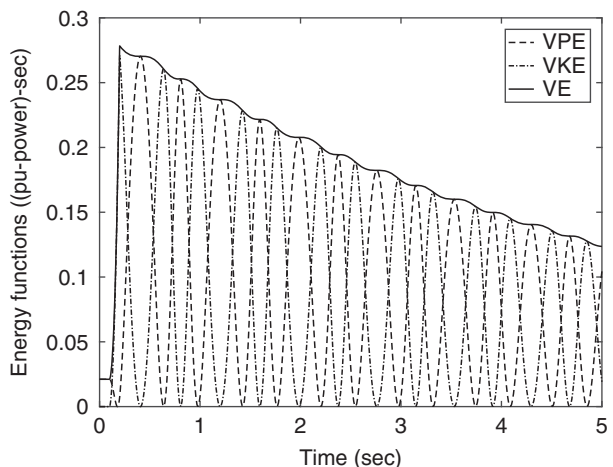


Figure 11.8 Potential, kinetic, and total energy functions for Example 11.3.



11.4 Linear Analysis

Chapter 8 discusses linear models of power systems in the form of

$$\Delta \dot{x} = A \Delta x + B \Delta u, \quad \Delta y = C \Delta x + D \Delta u \quad (11.20)$$

where x , u , and y are the vectors of the state, input, and output variables, respectively, A , B , C , and D are the state, input, output, and feedforward matrices, respectively, and Δ denotes small perturbations of the variables. The model (11.20) is useful in determining the stability of the swing modes and the machines participating in each of the swing modes, and for designing power system stabilizers. Linearization involves solving for the equilibrium of a nonlinear dynamic system and then performing partial derivatives of the state and output equations, as shown in Section 8.2.1. Analytical linearization using partial derivatives can be found in [197].

An alternative approach is to use numerical perturbations to perform the partial derivative computation. Consider the nonlinear model (8.60)–(8.61), repeated here as

$$\dot{x} = f_1(x, V, \theta, u), \quad 0 = g_1(x, V, \theta) \quad (11.21)$$

where the equilibrium values are $(x_o, V_o, \theta_o, u_o)$, and V and θ are the vectors of the bus voltage magnitudes and angles.

Suppose the state x is a scalar variable and is perturbed from the equilibrium value x_o to $x_o + \Delta x$, where Δx is small. The impact of Δx on the changes ΔV and $\Delta \theta$ of V and θ , respectively, is solved from

$$0 = g_1(x_o + \Delta x, V_o + \Delta V, \theta + \Delta \theta) \quad (11.22)$$

Then the partial derivative $\partial f_1 / \partial x$ is approximated by

$$\frac{\partial f_1}{\partial x} \approx \frac{f_1(x_o + \Delta x, V_o + \Delta V, \theta + \Delta \theta, u_o)}{\Delta x} \quad (11.23)$$

For improved accuracy, the perturbation is performed for a positive Δx and repeated for a negative Δx . The average of the two (11.23) is then taken as a more accurate partial derivative.

The advantage of the numerical perturbation approach is that it can be readily accomplished in a simulation program without much additional code, because the computation of $f_1(x_o + \Delta x, V_o + \Delta V, \theta + \Delta \theta, u_o)$ is already available in the dynamics calculation part of a simulation program (the fourth block in Figure 11.4). In addition, the solution of the voltage variable perturbations ΔV and $\Delta \theta$ (11.22) is computed in the network solution part of the program (the third block in Figure 11.4).

The Power System Toolbox uses this numerical perturbation technique to generate linearized models with the `svm_mgen` function. The system matrix A is fixed. However, a user can pick a variety of inputs to build the input B matrix and output variables to build the output C matrix.

The next two examples illustrate the use of linearized models to compute the swing modes in a power system and find the K_i parameters discussed in Section 8.6.2.

Example 11.4 Use PST to generate the linearized A matrix of the 3-machine, 9-bus model of Example 7.1 at the nominal loading condition, and compute the eigenvalues.

Solution

The $21 \times 21 A$ matrix is not shown here but can be readily computed from the `svm_mgen` function using the data file `data3m9b_example_11_4.m`. The eigenvalues of the A matrix are given in Table 11.3. Note that these eigenvalues are slightly different from those obtained in Example 8.3, because in PST transient saliency is neglected for the transient model. Also the pair of eigenvalues $\pm j0.0101$, which are the system modes, should be at the origin. However, as the linearized model is generated using the perturbation approach, small numerical errors would arise. \square

Example 11.5 Consider the single-machine infinite-bus system shown in Figure 11.5. The 991 MVA generator is now modeled with a subtransient model with the parameters $x_f = 0.15$ pu, $r_a = 0$, $X_d = 2.0$ pu, $X'_d = 0.245$ pu, $X''_d = 0.2$ pu, $T'_{do} = 5.0$ s, $T''_{do} = 0.031$ s, $X_q = 1.91$ pu, $X'_q = 0.42$ pu, $X''_q = 0.2$ pu, $T'_{qo} = 0.66$ s, $T''_{qo} = 0.061$ s, and

Table 11.3 Eigenvalues/modes of the 3-machine, 9-bus system with constant power loads, computed using PST.

Electromechanical	Exciter	E'_d	E'_q and exciter
$-0.9567 \pm j13.0396$	$-5.4840 \pm j7.9599$	-6.3315	$-0.4427 \pm j1.2122$
$-0.3514 \pm j8.6741$	$-5.3187 \pm j7.9318$	-3.7068	$-0.4400 \pm j0.7382$
$\pm j0.0101$	$-5.2293 \pm j7.8210$	-3.2915	$-0.4264 \pm j0.4940$

$H = 2.8756$ pu, all on the generator base. The parameters of the static excitation system (IEEE Type ST3 model [57]) are $K_A = 7.04$, $T_A = 0.4$ s, $T_B = 6.67$ s, $T_C = 1.0$ s, $V_{R\max} = 7.57$ pu, $V_{R\min} = 0$ pu, $V_{I\max} = 0.2$ pu, $V_{I\min} = -0.2$ pu, $K_J = 200$, $K_p = 4.365$, $\theta_p = 20^\circ$, $K_I = 4.83$, $X_L = 0.091$ pu, $K_C = 1.096$, $E_{fd\max} = 6.53$ pu, $K_G = 1$, and $V_{G\max} = 6.53$ pu. Use PST to obtain the linearized state matrix A of the system and compute its eigenvalues. Also use appropriate entries in the A matrix and the C matrix rows corresponding to the generator rotor angle and the terminal voltage to find the coefficients K_1 and K_5 discussed in Section 8.6.2.

Solution

Applying the `svm_mgen` function to the data file `datasmib_example_11_5.m` results in the linear model

$$\dot{x} = Ax \quad (11.24)$$

where

$$x = [\Delta\delta \quad \Delta\omega \quad \Delta E'_q \quad \Delta\psi_{kd} \quad \Delta E'_d \quad \Delta\psi_{kq} \quad V_A \quad E_{fd}]^t \quad (11.25)$$

$$A = \begin{bmatrix} 0 & 377.0 & 0 & 0 & 0 & 0 & 0 & 0 \\ -0.368 & 0 & -0.187 & -0.168 & -0.023 & -0.099 & 0 & 0 \\ 0.137 & 0 & -2.147 & 2.307 & -0.020 & -0.089 & 0 & 1.214 \\ -6.268 & 0 & 29.033 & -35.161 & 0 & 0 & 0 & 0 \\ -0.293 & 0 & 0 & 0 & -8.483 & 6.132 & 0 & 0 \\ -3.101 & 0 & 0 & 0 & 14.754 & -23.606 & 0 & 0 \\ 3.084 & 0 & -5.112 & -4.601 & 2.805 & 12.341 & -0.150 & 0 \\ 8.975 & 0 & -89.751 & -145.380 & 51.139 & 225.008 & 14.961 & -109.326 \end{bmatrix} \quad (11.26)$$

The eigenvalues of this system are the exciter mode -108.96 , the subtransient flux modes -34.775 and -28.21 , the exciter and transient flux modes -4.417 and $-0.892 \pm j0.767$, and the lightly damped local modes $-0.366 \pm j11.29$.

A user of PST can also select signals to build the output C matrix. The output matrix corresponding to the generator electrical torque and terminal bus voltage is found to be (from the PST matrix variables `c_t` and `c_v`)

$$\begin{bmatrix} \Delta T_e \\ \Delta V_t \end{bmatrix} = Cx \quad (11.27)$$

where

$$C = \begin{bmatrix} 2.117 & 0 & 1.076 & 0.968 & 0.130 & 0.571 & 0 & 0 \\ -0.103 & 0 & 0.170 & 0.153 & -0.0935 & -0.412 & 0 & 0 \end{bmatrix} \quad (11.28)$$

A reader may notice that the first row of C when multiplied by $-2H$ is the same as the second row of A and the second row of C multiplied by $-K_J/T_B = -30$ equals the first 6 entries of the 7th row of A .

Based on the definitions in Figure 8.8, K_1 and K_5 can be readily found from (11.28) as

$$K_1 = 2.117, \quad K_5 = -0.103 \quad (11.29)$$

The other K_i parameters are not defined for this model as there are now 4 flux variables for the generator. Note that K_5 is negative, due to the loading of the generator and the relatively high value of the system equivalent reactance. Thus it contributes to a destabilizing effect of the local mode. \square

The use of the linearized model to perform control design has been discussed in Example 10.7, and thus will not be repeated here.

11.5 Conclusions and Remarks

A primer for using the Power System Toolbox has been provided in this chapter. The focus here is on using the software for various tasks in power system analysis and research.

The problems at the end of this chapter are intended to give a reader more practice on using PST or similar power system simulation software. Several problems ask for power flow solutions or disturbance simulations in which models or components are changed. They then ask a reader to compare the results and make appropriate observations. This approach is a common industry practice in which various components and simulation models are used so as to establish the validity of the evaluation. If the simulation results are contrary to the prediction from analysis or experience, additional investigations should be performed to understand the sources of discrepancies.

This chapter does not include a section on how to build new component models to be used in PST, although a discussion on how PST works has been provided. To this effect, a reader who wants to develop new models is advised to start from the MATLAB function of an existing model and follow its code structure. This approach has served well the PST development team which includes many former and current students at Rensselaer Polytechnic Institute.

11.6 Problems

The following problems can be solved using PST.

- 11.1** For the power system in Example 11.1, increase the active power load on Bus 13 to 17.75 pu and reduce the active power load on Bus 3 to 9.59 pu. The reactive power load will remain the same. Solve the power flow with $Q_{\max} = 2$ pu on Generator Buses 2 and 12. Then add a shunt capacitor of 100 MVar to Bus 13 and re-solve the power flow. Compare these two power flow solutions.

- 11.2** For the power system in part 2 of Example 11.1, set the minimum voltage at Bus 13 to 0.98 pu and solve the power flow. If the power flow does not converge, increase the voltages at the Generator Buses 11 and 12 to 1.04 pu. It may also be necessary to increase the maximum reactive power supply at these two buses.
- 11.3** Find the initial conditions for the three-machine nine-bus system of Example 7.5. If PST is used, the initial values of the variables can be found in the first column of the arrays `mac_ang` (δ), `mac_spd` (ω), `curd` (I_d), `curq` (I_q), `ed` (V_d), `eq` (V_q), `edprime` (E'_d), `eqprime` (E'_q), `Efd` (E_{fd}), `R_f` (R_f), `V_R` (V_R), `exc_pot` (third column) (V_{ref}), and `pmech` (T_M). The PST values will be identical to those in Example 7.5, except for (1) E'_d (because PST ignores saliency) and (2) V_R (because a slightly different way of computing the coefficients of the saturation model). Furthermore, in PST, $V_R = E_{fd}$, as it is not scaled by K_F/T_F . Also note that `exc_pot` is deleted after a successful completion of a simulation run. To see its values, a user needs to abort the program using `ctrl-C` in the MATLAB command window when `s_simu` is still executing. The data is in the file `data3m9b_problem_11_3.m`.
- 11.4** Repeat Example 11.3 with $D = 0$ for Generator 1, using the 6-cycle fault clearing case. Without damping the oscillation will not decay and the total energy function will be constant. Note that the base MVA of the system is 991.
- 11.5** Find the critical clearing time, to 0.01 sec accuracy, of the three-machine system in Figure 7.4 for a three-phase short-circuit fault near Bus 7, cleared by tripping the line connecting Buses 7 and 5. The synchronous machine and exciter data can be found in Table 7.2. Add a damping term of $D = 2$ pu on the machine base to all the machines. Use the constant impedance model for all the loads.
- 11.6** Repeat Problem 11.5, but use the constant current model for real power loads and the constant impedance model for reactive power loads. Take the system to be unstable if the nonconforming load iteration fails to converge because of very low bus voltages.
- 11.7** Linearize the New England 16-machine system using the classical model for all the generators and the constant impedance model for all the loads, and compute the electromechanical modes. A diagram of the 16-machine system can be found in [69]. The bus, line, and machine data can be found in the file `data16em.m` in the PST data folder.
- 11.8** Find the critical clearing time, to 0.01 sec accuracy, of Generator 9 in the New England 16-machine system given a fault close to Bus 29, cleared by opening the line connecting Buses 29 and 28. Use the constant impedance model for all the loads.

Bibliography

- 1 IEEE Working Group on Dynamic System Performance of the System Planning Subcommittee, IEEE Power Engineering Society Power System Engineering Committee, "Symposium on Adequacy and Philosophy of Modeling: Dynamic System Performance," *IEEE Publication 75 CHO 970-4-PWR IEEE*, New York, 1975.
- 2 P. Kokotovic, H. K. Khalil and J. O'Reilly, *Singular Perturbation Methods In Control: Analysis and Design*, Academic Press, Orlando, FL, 1986.
- 3 North American Electric Reliability Council, "Reliability Assessment 1995–2004," *NERC*, Sept. 1995.
- 4 U. S. Energy Research and Development Administration, "Systems Engineering for Power: Status and Prospects," *Proceedings Engineering Foundation Conference, CONF-750867*, Henniker, NH, Aug. 17–22, 1975.
- 5 Electric Power Research Institute, "Power System Planning and Operations: Future Problems and Research Needs," *EPRI Special Report EL-377-SR*, Feb. 1977.
- 6 E. G. Gate, K. Hemmaplardh, J. W. Manke, and D. P. Gelopoulos, "Time Frame Notion and Time Response of the Models in Transient, Mid-Term and Long-Term Stability Programs," *IEEE Trans. Power Appar. Syst., PAS-103*, 1, Jan. 1984, 143–150.
- 7 E. Kuffel and M. Abdullah, *High-Voltage Engineering*, Pergamon Press, Oxford, England, 1970.
- 8 Electric Power Research Institute, "User Survey and Implementation Plan for EMTP Enhancements," *EPRI Report EL-3668*, Palo Alto, CA, Sept. 1984.
- 9 Electric Power Research Institute, "Electromagnetic Transients Program (EMTP) Primer," *EPRI Report EL-4202*, Palo Alto, CA, Sept. 1985.
- 10 J. J. Grainger and W. D. Stevenson, *Power System Analysis*, McGraw-Hill, New York, 1994.
- 11 C. A. Gross, *Power System Analysis*, John Wiley & Sons, Inc., New York, 1986.
- 12 A. R. Bergen and V. Vittal, *Power System Analysis*, 2nd edition, Prentice-Hall, Inc., Englewood Cliffs, NJ, 2000.
- 13 S. Ramo, J. R. Whinnery, and T. Van Duzer, *Fields and Waves in Communication Electronics*, John Wiley & Sons, Inc., New York, 1965.
- 14 H. W. Dommel, "Digital Computer Solution of Electromagnetic Transients in Single and Multiphase Networks," *IEEE Trans. PAS*, 88, 4, April 1969, 388–399.
- 15 G. W. Stagg and A. H. El-Abiad, *Computer Methods in Power System Analysis*, McGraw-Hill Book Co., New York, 1968.

- 16 M. A. Pai and D. Chatterjee, *Computer Techniques in Power System Analysis*, 3rd edition, Tata McGraw-Hill, New Delhi, India, 2014.
- 17 L. O. Chua and P. M. Lin, *Computer-Aided Analysis of Electronic Circuits*, Prentice-Hall, Inc., Englewood Cliffs, NJ, 1975.
- 18 G. T. Heydt, *Computer Analysis Methods for Power Systems*, Macmillan Publishing Co., New York, 1986.
- 19 IEEE PES Engineering Education Committee, "IEEE Tutorial Course: Digital Simulation of Electrical Transient Phenomena," *IEEE Tutorial 81 EHO 173-5-PWR*, IEEE, New York, 1980.
- 20 P. C. Krause, O. Wasynszuk, S. D. Sudhoff, and S. Pekarek, *Analysis of Electric Machinery and Drive Systems*, 3rd edition, McGraw-Hill, New York, 2013.
- 21 A. E. Fitzgerald, C. Kingsley, and S. D. Umans, *Electric Machinery*, 7th edition, McGraw-Hill Book Co., New York, 2014.
- 22 E. W. Kimbark, *Power System Stability: Synchronous Machines*, Dover Publications, Inc., New York, 1956.
- 23 B. Adkins, *The General Theory of Electrical Machines*, Chapman and Hall Ltd., London, 1962.
- 24 F. P. DeMello and L. N. Hannett, "Determination of Synchronous Machine Stability Study Constants," *EPRI Report EL-1424*, 3, Electric Power Research Institute, Palo Alto, CA, June 1980.
- 25 D. P. Gelopoulos, "Midterm Simulation of Electric Power Systems," *EPRI Report EL-596*, Electric Power Research Institute, Palo Alto, CA, June 1979.
- 26 D. W. Olive, "New Techniques for the Calculation of Dynamic Stability," *IEEE Trans. Power Appar. Sys., PAS-85*, 7, July 1966.
- 27 C. Concordia, *Synchronous Machine*, John Wiley & Sons, New York, 1951.
- 28 A. W. Rankin, "Per-unit Impedance of Synchronous Machines," *AIEE Trans.*, 64, Aug. 1945.
- 29 M. R. Harris, P. J. Lawrenson, and J. M. Stephenson, *Per-unit Systems with Special Reference to Electrical Machines*, Cambridge University Press, Cambridge, England, 1970.
- 30 I. M. Canay, "Causes of Discrepancies on Calculation of Rotor Quantities and Exact Equivalent Diagrams of the Synchronous Machine," *IEEE Trans. Power Appar. Syst., PAS-88*, 7, July 1969.
- 31 H. H. Woodson and J. R. Melcher, *Electromechanical Dynamics Part I: Discrete Systems*, John Wiley & Sons, Inc., New York, 1968.
- 32 T. S. Peterson, *Calculus with Analytic Geometry*, Harper & Row Publishers, Inc., New York, 1960.
- 33 R. G. Bartle, *The Elements of Real Analysis*, John Wiley & Sons, Inc., New York, 1976.
- 34 E. Kreyszig, *Advanced Engineering Mathematics*, John Wiley & Sons, Inc., New York, 1972.
- 35 C. C. Young, "The Synchronous Machine," *IEEE Tutorial Course on Modern Concepts of Power System Dynamics*, 70 M 62-PWR, Institute of Electrical and Electronics Engineers, New York, 1970.
- 36 P. M. Anderson and A. A. Fouad, *Power System Control and Stability*, Iowa State University Press, Ames, IA, 1977.
- 37 F. P. DeMello and L. N. Hannett, "Representation of Saturation in Synchronous Machines," *IEEE Trans. Power Syst., PWRS-1*, 4, Nov. 1986, 8–18.

- 38 P. L. Dandeno et al., "Current Usage and Suggested Practices in Power System Stability Simulations for Synchronous Machines," *IEEE Trans. Energy Conversion*, EC-1, 1, Mar. 1986, 77–93.
- 39 G. Shackshaft, "Model of Generator Saturation for Use in Power System Studies," *Proc. IEE*, 126, 8, 759–763.
- 40 G. Xie and R. S. Ramshaw, "Nonlinear Model of Synchronous Machines with Saliency," *Paper 85 SM 347-0*, IEEE/PES 1985 Summer Meeting, Vancouver, BC, July 14–19, 1985.
- 41 K. Prabhashankar and W. Janischewskyj, "Digital Simulation of Multimachine Power Systems for Stability Studies," *IEEE Trans. on Power Appar. Syst.*, PAS-87, 1, Jan. 1968, 73–79.
- 42 J. E. Brown, K. P. Kovacs, and P. Vas, "A Method of Including the Effects of Main Flux Path Saturation in the Generalized Equations of A.C. Machines," *IEEE Trans. Power Appar. Syst.*, PAS-102, 1, Jan. 1983, 96–102.
- 43 I. M. Canay, "Determination of Model Parameters of Synchronous Machines," *IEE Proc.*, 130, Part B, 2, Mar. 1983, 86–94.
- 44 W. B. Jackson and R. L. Winchester, "Direct and Quadrature Axis Equivalent Circuits for Solid-Rotor Turbine Generators," *IEEE Trans. Power Appar. Syst.*, PAS-88, 7, July 1969, 1121–1136.
- 45 P. L. Dandeno, P. Kundur, and R. P. Schulz, "Recent Trends and Progress in Synchronous Machine Modeling in the Electric Utility Industry," *IEEE Proc.*, 62, 7, July 1974, 941–950.
- 46 S. H. Minnich et al., "Saturation Functions for Synchronous Generators from Finite Elements," *Paper 87 WM 207-4*, IEEE/PES 1987 Winter Meeting, New Orleans, Feb. 1–6, 1987.
- 47 S. H. Minnich, "Small Signal, Large Signals and Saturation in Generator Modeling," *IEEE Trans. Energy Conversion*, EC-1, 1, Mar. 1986, 94–102.
- 48 T. J. Hammons and D. J. Winning, "Comparisons of Synchronous Machine Models in the Study of the Transient Behaviour of Electrical Power Systems," *Proc. IEEE*, 118, 10, Oct. 1971, 1442–1458.
- 49 IEEE, "Symposium on Synchronous Machine Modeling for Power System Studies," 83TH0101-6-PWR, Tutorial at IEEE/PES 1983 Winter Meeting, New York, 1983.
- 50 J. D. Ojo and T. A. Lipo, "An Improved Model for Saturated Salient Pole Synchronous Motors," *Paper 88 SM 614-0*, IEEE/PES 1988 Summer Meeting, Portland, OR, July 24–29, 1988.
- 51 P. W. Sauer, "Constraints on Saturation Modeling in AC Machines," *IEEE Trans. Energy Conversion*, 7, 1, Mar. 1992, 161–167.
- 52 M. E. Coultes and W. Watson, "Synchronous Machine Models by Standstill Frequency Response Tests," *IEEE Trans. Power Appar. Syst.*, PAS-100, 4, Apr. 1981, 1480–1489.
- 53 IEEE Std 115A-1987, "IEEE Standard Procedures for Obtaining Synchronous Machine Parameters by Standstill Frequency Response Testing," *Supplement to ANSI/IEEE Std. 115-1983*, IEEE, New York, 1987.
- 54 A. E. Fitzgerald and C. Kingsley, *Electric Machinery*, McGraw-Hill Book Co., New York, 1961.
- 55 IEEE Committee report, "Computer Representation of Excitation Systems," *IEEE Trans. Power Appar. Syst.*, PAS-87, 6, June 1968, 1460–1464.

- 56** IEEE Committee report, "Excitation System Models for Power System Stability Studies," *IEEE Trans. Power Appar. Syst., PAS-100*, 2, Feb. 1981, 494–509.
- 57** IEEE Std 421.5-1992, "IEEE Recommended Practice for Excitation System Models for Power System Stability Studies," IEEE, New York, 1992.
- 58** D. G. Ramey and J. W. Skooglund, "Detailed Hydrogovernor Representation for System Stability Studies," *IEEE Trans. Power Appar. and Syst., PAS-89*, 1, Jan. 1970, 106–112.
- 59** C. C. Young, "Equipment and System Modeling for Large Scale Stability Studies," *IEEE Trans. Power Appar. and Syst., PAS-91*, 1, Jan./Feb. 1972, 99–109.
- 60** IEEE Committee report, "Dynamic Models for Steam and Hydro Turbines in Power System Studies," *IEEE Trans. Power Appar. and Syst., PAS-92*, 6, Nov/Dec 1973, 1904–1915.
- 61** IEEE Committee Report, "Hydraulic Turbine and Turbine Control Models for System Dynamic Studies," *IEEE Transactions on Power Systems*, vol. 7, 1, pp. 167–179, 1992.
- 62** IEEE Committee Report, "Dynamic Models for Fossil Fueled Steam Units in Power System Studies," *IEEE Transactions on Power Systems*, vol. 6, 2, pp. 753–761, May 1991.
- 63** Systems Control Inc., "Development of Dynamic Equivalents for Transient Stability Studies," *Final Report EPRI EL-456*, Electric Power Research Institute, Palo Alto, CA, Apr. 1977.
- 64** O. I. Elgerd, *Electric Energy System Theory, An Introduction*, McGraw-Hill Book Co., New York, 1982.
- 65** C. C. Young and R. M. Webler, "A New Stability Program for Predicting the Dynamic Performance of Electric Power Systems," *Proceedings of the American Power Conference*, 29, Chicago, 1967, 1126–1138.
- 66** P. W. Sauer, D. J. LaGesse, S. Ahmed-Zaid and M. A. Pai, "Reduced Order Modeling of Interconnected Multimachine Power Systems Using Time-Scale Decomposition," *IEEE Trans. Power Syst., PWRS-2*, 2, May 1987, 310–320.
- 67** P. W. Sauer, S. Ahmed-Zaid, and P. V. Kokotovic, "An Integral Manifold Approach to Reduced Order Dynamic Modeling of Synchronous Machines," *IEEE Trans. Power Syst.*, 3, 1, Feb. 1988, 17–23.
- 68** P. V. Kokotovic and P. W. Sauer, "Integral Manifold as a Tool for Reduced Order Modeling of Nonlinear Systems: A Synchronous Machine Case Study," *IEEE Trans. Circuits Syst., 36*, 3, Mar. 1989, 403–410.
- 69** J. H. Chow, Ed., "Time-Scale Modeling of Dynamic Networks with Applications to Power Systems," vol. 46 of lecture notes in *Control and Information Sciences*, Springer-Verlag, New York, 1982.
- 70** P. V. Kokotovic, H. K. Khalil, and J. O'Reilly, *Singular Perturbation Methods in Control: Analysis and Design*, Academic Press Inc., London, 1986.
- 71** P. W. Sauer, "Reduced Order Dynamic Modeling of Machines and Power Systems," *Proceedings of the American Power Conference*, 49, Chicago, 1987, 789–794.
- 72** P. W. Sauer, S. Ahmed-Zaid, and M. A. Pai, "Systematic Inclusion of Stator Transients in Reduced Order Synchronous Machine Models," *IEEE Trans. Power Appar. Syst., PAS-103*, 6, June 1984, 1348–1354.
- 73** "Extended Transient-Midterm Stability Package (ETMSP)," *Final Report EPRI EL-4610*, Electric Power Research Institute, Palo Alto, Jan. 1987.
- 74** P. W. Sauer and M. A. Pai, "Simulation of Multimachine Power System Dynamics," *Control and Dynamic System* (C. T. Leondes, Ed.), 43, Part 3, Academic Press, San Diego, 1991.

- 75 B. Stott, "Power System Dynamic Response Calculations," *Proc. IEEE*, 67, Feb. 1979, 219–241.
- 76 "Power System Dynamic Analysis-Phase I," *EPRI Report EL-484*, Electric Power Research Institute, July 1977.
- 77 P. M. Anderson and A. A. Fouad, "Power System Control and Stability," Iowa State University Press, Ames, IA, 1977.
- 78 "Interactive Power Flow (IPFLOW)," *Final Report TR-103643*, 1, May 1994.
- 79 A. J. Wood, B. F. Wollenberg, and G. B. Sheble, *Power Generation, Operation, and Control*, 3rd Edition, John Wiley and Sons, 2014.
- 80 P. Kundur, *Power System Stability and Control*, McGraw-Hill, New York, 1994.
- 81 C. Taylor, *Power System Voltage Stability*, McGraw Hill, 1994.
- 82 T. Van Cutsem and C. Vournas, *Voltage Stability of Electric Power Systems*, Springer, 1998.
- 83 V. Ajjarapu, *Computational Techniques for Voltage Stability Assessment and Control*, Springer, 2006.
- 84 E. V. Larsen and D. A. Swann, "Applying Power System Stabilizers, Part I: General Concepts, Part II: Performance Objectives and Tuning Concepts, Part III: Practical Considerations," *IEEE Power Appar. Syst., PAS-100*, 12, Dec. 1981, 3017–3046.
- 85 F. P. DeMello and C. Concordia, "Concepts of Synchronous Machine Stability as Affected by Excitation Control," *IEEE Trans., PAS-88*, Apr. 1969, 316–329.
- 86 P. W. Sauer and M. A. Pai, "Power System Steady State Stability and the Load Flow Jacobian," *IEEE Trans. Power Appar. Syst., PAS-5*, Nov. 1990, 1374–1383.
- 87 R. K. Ranjan, M. A. Pai, and P. W. Sauer, "Analytical Formulation of Small Signal Stability Analysis of Power Systems with Nonlinear Load Models," in *Sadhana, Proc. in Eng. Sci.*, Indian Acad. Sci., Bangalore, India, 18, 5, Sept. 1993, 869–889, Errata, 20, 6, Dec. 1995, 971.
- 88 G. C. Verghese, I. J. Perez-Arriaga and F. C. Scheweppe, "Selective Modal Analysis with Applications to Electric Power Systems, Part I and II," *IEEE Trans. Power Appar. Syst., PAS-101*, Sept. 1982, 3117–3134.
- 89 C. Rajagopalan, B. Lesieutre, P. W. Sauer, and M. A. Pai, "Dynamic Aspects of Voltage/Power Characteristics," *IEEE Trans. Power Syst.*, 7, Aug. 1992, 990–1000.
- 90 B. C. Lesieutre, P. W. Sauer, and M. A. Pai, "Sufficient Conditions on Static Load Models for Network Solvability," in *Proc. 24th Annu. North Amer. Power Symp.*, Reno, Oct. 1992, 262–271.
- 91 P. W. Sauer and B. C. Lesieutre, "Power System Load Modeling," *System and Control Theory for Power Systems* (J. H. Chow et al., Eds.), Springer-Verlag, 64, 1995.
- 92 V. Venkatasubramanian, H. Schattler, and J. Zaborszky, "Voltage Dynamics: Study of a Generator with Voltage Control, Transmission and Matched MW Load," *IEEE Trans. Autom. Contr.*, 37, Nov. 1992, 1717–1733.
- 93 C. Rajagopalan, "Dynamic of Power Systems at Critical Load Levels," Ph.D. thesis, University of Illinois, Urbana-Champaign, 1989.
- 94 E. H. Abed and P. Varaiya, "Nonlinear Oscillations in Power Systems," *Int. J. Elect. Power Energy Syst.*, 6, 1984, 37–43.
- 95 W. G. Heffron and R. A. Phillips, "Effects of Modern Amplidyne Voltage Regulator in Underexcited Operation of Large Turbine Generators," *AIEE Trans., PAS-71*, Aug. 1952, 692–697.

- 96** A. R. Bergen, "Analytical Methods for the Problem of Dynamic Stability," *Proc. International Symposium on Circuits and Systems*, 1977.
- 97** Y. N. Yu, *Electric Power System Dynamics*, Academic Press, New York, 1983.
- 98** P. Kundur, M. Klein, G. J. Rogers, and M. S. Zywno, "Application of Power System Stabilizer for Enhancement of Overall System Stability," *IEEE Trans., PWRS-4*, May 1989, 614–626.
- 99** F.-P. DeMello, P. J. Nolan, T. F. Laskowski and J. M. Undrill, "Coordinated Application of Stabilizers in Multimachine Power Systems," *IEEE Trans. Power Appar. Syst., PAS-99*, May-June 1980, 892–901.
- 100** M. A. Pai, *Power System Stability*, North Holland Publishing Co., New York, 1981.
- 101** M. A. Pai, *Energy Function Analysis for Power System Stability*, Kluwer Academic Publishers, Boston, 1989.
- 102** A. A. Fouad and V. Vittal, *Power System Transient Stability Analysis Using the Transient Energy Function Method*, Prentice Hall, Englewood Cliffs, 1991.
- 103** M. Pavella and P. G. Murthy, *Transient Stability of Power Systems: Theory and Practice*, John Wiley & Sons, Inc., New York, 1994.
- 104** T. Athay, R. Podmore, and S. Virmani, "A Practical Method for Direct Analysis of Transient Stability," *IEEE Trans. Power Appar. Syst., PAS-98*, 2, Mar./Apr. 1979, 573–584.
- 105** H. D. Chiang, F. F. Wu, and P. P. Varaiya, "Foundations of Direct Methods for Power System Transient Stability Analysis," *IEEE Trans. Circuits Syst., CAS-34*, Feb. 1987, 160–173.
- 106** A. H. El-Abiad and K. Nagappan, "Transient Stability Region of Multi-Machine Power Systems," *IEEE Trans. Power Appar. Syst., PAS-85*, 2, Feb. 1966, 169–178.
- 107** N. Kakimoto, Y. Ohsawa, and M. Hayashi, "Transient Stability Analysis of Electric Power Systems Via Lure Type Lyapunov Functions, Parts I and II," *Trans. IEE of Japan*, 98, 5/6, May/June 1978.
- 108** F. A. Rahimi, M. G. Lauby, J. N. Wrubel, and K. W. Lee, "Evaluation of the Transient Energy Function Method for On-line Dynamic Security Analysis," *IEEE Transactions on Power Systems*, 8, 2, May 1993, 497–506.
- 109** P. C. Magnusson, "Transient Energy Method of Calculating Stability," *AIEE Trans.*, 66, 1947, 747–755.
- 110** P. D. Aylett, "The Energy-Integral Criterion of Transient Stability Limits of Power Systems," *Proc. of the Institution of Electrical Engineers (London)*, 105C, 8, Sept. 1958, 257–536.
- 111** A. R. Bergen and D. J. Hill, "Structure Preserving Model for Power System Stability Analysis," *IEEE Trans. Power Appar. Syst., PAS-100*, 1, Jan. 1981.
- 112** K. R. Padiyar and H. S. Y. Sastry, "Topological Energy Function Analysis of Stability of Power Systems," *Int. Electr. Power and Energy Syst.*, 9, 1, Jan. 1987, 9–16.
- 113** K. R. Padiyar and K. K. Ghosh, "Direct Stability Evaluation of Power Systems with Detailed Generator Models Using Structure Preserving Energy Functions," *Int. J. Electr. Power and Energy Syst.*, 11, 1, Jan. 1989, 47–56.
- 114** P. W. Sauer, A. K. Behera, M. A. Pai, J. R. Winkelman, and J. H. Chow, "Trajectory Approximations for Direct Energy Methods That Use Sustained Faults with Detailed Power System Models," *IEEE Transactions on Power Systems*, 4, 2, May 1988, 499–506.
- 115** A. R. Bergen, D. J. Hill, and C. L. DeMarco, "A Lyapunov Function for Multi-Machine Power Systems with Generator Flux Decay and Voltage Dependent Loads," *Int. J. of Electric Power and Energy Syst.*, 8, 1, Jan. 1986, 2–10.

- 116 M. A. Pai, "Power System Stability Studies by Lyapunov-Popov Approach," *Proc. 5th IFAC World Congress*, Paris, 1972.
- 117 J. Willems, "Direct Methods for Transient Stability Studies in Power System Analysis," *IEEE Trans. Autom. Control, AC-16*, 4, July-Aug. 1971, 1469–81.
- 118 M. Ribbens-Pavella and F. J. Evans, "Direct Methods for Studying of the Dynamics of Large Scale Electric Power Systems - A Survey," *Automatica*, 21, 1, 1985, 1–21.
- 119 A. A. Fouad and S. E. Stanton, "Transient Stability of Multi-Machine Power Systems, Part I and II," *IEEE Trans. Power Appar. Syst., PAS-100*, 1951, 3408–3424.
- 120 A. N. Michel, A. A. Fouad, and V. Vittal, "Power System Transient Stability Using Individual Machine Energy Functions," *IEEE Trans. Circuits Syst., CAS-30*, 5, May 1983, 266–276.
- 121 M. A. El-Kady, C. K. Tang, V. F. Carvalho, A. A. Fouad, and V. Vittal, "Dynamic Security Assessment Utilizing the Transient Energy Function Method," *IEEE Trans. Power Syst., PWRS1*, 3, Aug. 1986, 284–291.
- 122 Y. Mansour, E. Vaahedi, A. Y. Chang, B. R. Corns, B. W. Garrett, K. Demaree, T. Athay, and K. Cheung, "B. C. Hydro's On-Line Transient Stability Assessment (TSA): Model Development, Analysis and Post-Processing," *IEEE Trans. Power Syst., 10*, 1, Feb. 1995, 241–253.
- 123 H. D. Chiang, "Analytical results on direct methods for power system transient stability assessment," *Control and Dynamic Systems* (C. T. Leondes, Ed.), 43, Academic Press, San Diego, 1991, 275–334.
- 124 C. L. DeMarco and T. J. Overbye, "An Energy Based Measure for Assessing Vulnerability to Voltage Collapse," *IEEE Trans. Power Syst., 5*, 2, May 1990, 582–591.
- 125 A. M. Lyapunov, *The General Problem of the Stability of Motion* (in Russian), The Mathematical Society of Kharkov, Russia, 1892. English translation, Taylor and Francis Ltd., London, 1992.
- 126 A. A. Fouad and V. Vittal, "Power System Transient Stability Assessment Using the Transient Energy Function Method," *Control and Dynamic Systems* (C. T. Leondes, Ed.), 43, Academic Press, San Diego, 1991, 115–184.
- 127 M. A. Pai, M. Laufenberg, and P. W. Sauer, "Some Clarification in the Transient Energy Function Method," *Int. Journal of Elec. Power and Energy Systems*, 18, 1, 1996, 65–72.
- 128 R. T. Treinen, V. Vittal, and W. Kliemann, "An Improved Technique to Determine the Controlling Unstable Equilibrium Point in a Power System," *IEEE Transactions on Circuits and Systems-I: Fundamental Theory and Application*, 43, 4, Apr. 1996, 313–323.
- 129 K. R. Padiyar, *Structure Preserving Energy Functions in Power Systems: Theory and Applications*, CRC Press, 2013.
- 130 A. G. Phadke and J. S. Thorp, *Synchronized Phasor Measurements and Their Applications*, New York, NY, USA: Springer, 2008.
- 131 A. V. Oppenheim and R. W. Schafer, *Discrete-Time Signal Processing*, 3rd Edition, Pearson, 2009.
- 132 W. Premerlani, B. Kasztenny, and M. Adamiak, "Development and Implementation of a Synchrophasor Estimator Capable of Measurements under Dynamic Conditions," *IEEE Trans. on Power Delivery*, vol. 23, no. 1, pp. 109–123, Jan. 2008.
- 133 G. C. Zweigle, L. S. Anderson, and A. Guzman-Casillas, "Apparatus and Method for Estimating Synchronized Phasors at Pre-determined Times Referenced to an Absolute Time Standard in an Electrical System," US Patent 20070086134, 2009.

- 134 V. Terzija, D. Cai, V. Stanojevic, and G. Strbac, "Frequency and Power Components Estimation from Instantaneous Power Signal," *IEEE Trans. on Instrumentation and Measurement*, vol. 60, no. 11, pp. 3640–3649, 2010.
- 135 D. Dotta and J.H. Chow, "Second Harmonic Filtering in Phasor Measurement Estimation," *IEEE Trans. on Power Delivery*, vol. 28, no. 2, pp. 1240–1241, 2013.
- 136 D. Dotta, J. H. Chow, and D. B. Bertagnolli, "A Teaching Tool for Phasor Measurement Estimation," *IEEE Trans. on Power Systems*, vol. 29, no. 4, pp. 1981–1988, July 2014.
- 137 D. W. P. Thomas and M. S. Woolfson, "Evaluation of Frequency Tracking Methods," *IEEE Trans. on Power Delivery*, vol. 16, no. 3, pp. 367–371, 2001.
- 138 M. M. Begovic, P. M. Djuric, S. Dunlap, and A. G. Phadke, "Frequency Tracking in Power Networks in the Presence of Harmonics," vol. 8, no. 2, pp. 480–486, 1993.
- 139 M. Akke, "Frequency Estimation by Demodulation of Two Complex Signals," *IEEE Trans. on Power Delivery*, vol. 12, no. 1, pp. 157–163, 1997.
- 140 D. Fan and V. Centeno, "Phasor-based Synchronized Frequency Measurement in Power Systems," *IEEE Trans. on Power Delivery*, vol. 22, no. 4, pp. 2010–2016, 2007.
- 141 D. Fan and V. Centeno, "Least-Squares Estimation in Phasor-based Synchronized Frequency Measurements," *Proc. IEEE Power and Energy Society General Meeting*, pp. 1–6, 2008.
- 142 IEEE C37.118.1, *Standard for Synchrophasor Measurements for Power Systems*, IEEE Standards, 2011.
- 143 M. Akke and J. S. Thorp, "Sample Value Adjustment Improves Phasor Estimation at Off-Nominal Frequencies," *IEEE Trans. on Power Delivery*, vol. 25, no. 4, pp. 2255–2263, 2010.
- 144 *Test Specification for Synchrophasor Measurement Unit for Power System*, GB/T 26862-2011, July 2011 (Chinese). Available: <http://www.csres.com/detail/219479.html>.
- 145 P. Komarnicki, C. Dzienis, Z. A. Styczynski, J. Blumschein, and V. Centeno, "Practical Experience with PMU System Testing and Calibration Requirements," *Proc. IEEE PES General Meeting*, Pittsburgh, 2008.
- 146 H. Liu, T. Bi, and Q. Yang, "The PMU Performance Evaluation," *Proc. of Conference on Precision Electromagnetic Measurements*, pp. 416–417, 2012.
- 147 IEEE C37.118.2, *Standard for Synchrophasor Data Transfer for Power Systems*, IEEE Standards, 2011.
- 148 D. Laverty, R. Best, P. Brogan, I. Al Khatib, L. Vanfretti, and D. Morrow, "The OpenPMU Platform for Open-Source Phasor Measurements," *IEEE Trans. Instrum. Meas.*, vol. 62, no. 4, pp. 701–709, 2013.
- 149 R. Garcia-Valle, G.-Y. Yang, K. Martin, A. Nielsen, and J. Ostergaard, "DTU PMU laboratory Development, Testing and Validation," *Proc. 2010 IEEE PES InnovativeSmart Grid Technologies Conf. Europe (ISGT Europe)*, pp. 1–6.
- 150 J. F. Kurose and K. W. Ross, "Computer Networking: A Top-Down Approach," 6th edition, Pearson, 2012.
- 151 NERC Technical Report, *Balancing and Frequency Response*, 2011; available: www.nerc.com.
- 152 J. Ingleson and M. Nagle, "Decline of Eastern Interconnection Frequency Response," Georgia Tech Fault and Disturbance Conference, 1999.
- 153 A. Bykhovsky and J. H. Chow, "Dynamic Data Recording in the New England Power System and an Event Analyzer for the Northfield Monitor," *Electric Power and Energy Journal*, vol. 25, pp. 787–795, 2003.

- 154 A. Semlyen, "Analysis of Disturbance Propagation in Power Systems based on a Homogeneous Dynamic Model," *IEEE Trans. on Power Apparatus and Systems*, vol. PAS-93, vol. 2, pp. 676–684, 1974.
- 155 R. Cresap and J. Hauer, "Analysis of Disturbance Propagation in Power Systems based on a Homogeneous Dynamic Model," *IEEE Trans. on Power Apparatus and Systems*, vol. PAS-93, vol. 2, pp. 676–684, 1974.
- 156 M. Parashar, J. S. Thorp, and C. E. Seyler, "Continuum Modeling of Electromechanical Dynamics in Large-Scale Power Systems," *IEEE Trans. on Circuits and Systems-I*, vol. 51, no. 9, pp. 1848–1858, 2004.
- 157 M. Mahmoudi, J. Dong, K. Tomsovic, and S. Djouadi, "Application of Distributed Control to Mitigate Disturbance Propagations in Large Power Networks," *Proc. North American Power Symposium (NAPS)*, pp. 1–6, 2015.
- 158 T. Xia, et al., "Wide-area Frequency Based Event Location Estimation," *Proc. IEEE PES General Meeting*, pp. 1–7, 2007.
- 159 D. N. Kosterev, C. W. Taylor, and W. A. Mittelstadt, "Model Validation for the August 10, 1996 WSCC System Outage," *IEEE Trans. on Power Systems*, vol. 14, no. 3, pp. 967–979, 1999.
- 160 J. F. Hauer, C. J. Demeure, and L. L. Scharf, "Initial Results in PRONY Analysis of Power System Response Signals," *IEEE Trans. on Power Systems*, vol. PAS-93, vol. 2, pp. 676–684, 1974.
- 161 D. J. Trudnowski, J. W. Pierre, N. Zhou, J. F. Hauer, and M. Parashar, "Performance of Three Mode-Meter Block-Processing Algorithms for Automated Dynamic Stability Assessment," *IEEE Trans. on Power Systems*, vol. 23, no. 2, pp. 680–690, May 2008.
- 162 G. Liu, J. Ning, Z. Tashman, V. Venkatasubramanian, and P. Trachian, "Oscillation Monitoring System Using Synchrophasors," in *Proc. IEEE PES General Meeting*, 2012.
- 163 C. W. Taylor and D. C. Erickson, "Recording and Analyzing the July 2 Cascading Outage," *IEEE Computer Applications in Power*, pp. 26–30, January, 1997.
- 164 A. Abur and A. Gomez Exposito, *Power System State Estimation: Theory and Implementation*, New York, NY, USA: Marcel Dekker, 2004.
- 165 J. S. Thorp, A. G. Phadke, and K. J. Karimi, "Real Time Voltage-Phasor Measurements for Static State Estimation," *IEEE Trans. on Power Apparatus and Systems*, vol. 104, no. 11, pp. 3098–3106, 1985.
- 166 J. Chen and Ali Abur, "Placement of PMUs to Enable Bad Data Detection in State Estimation," *IEEE Trans. on Power Systems*, vol. 21, no. 4, pp. 1608–1615, 2006.
- 167 A. G. Phadke, J. S. Thorp, and K. J. Karimi, "State Estimation with Phasor Measurements," *IEEE Trans. on Power Systems*, vol. 1, no. 1, pp. 233–241, 1986.
- 168 K. D. Jones, *Three-Phase Linear State Estimation with Phasor Measurements*, MS Thesis, Virginia Polytechnic Institute and State University, 2011.
- 169 L. Vanfretti, J. H. Chow, S. Sarawgi, and B. Fardanesh, "A Phasor-Data-Based State Estimator Incorporating Phase Bias Correction," *IEEE Trans. on Power Systems*, vol. 26, no. 1, pp. 111–119, 2011.
- 170 E. R. Fernandes, S. G. Ghiocel, J. H. Chow, D. E. Ilse, D. R. Tran, Q. Zhang, D. B. Bertagnolli, X. Luo, G. Stefopoulos, B. Fardanesh, and R. Robertson, "Application of a Phasor-Only State Estimator to a Large Power System using Real PMU Data," *IEEE Trans. on Power Systems*, vol. 32, no. 1, pp. 411–420, 2017.
- 171 E. Ghahremani and I. Kamwa, "Dynamic State Estimation in Power System by Applying the Extended Kalman Filter With Unknown Inputs to Phasor Measurements," *IEEE Trans. on Power Systems*, vol. 26, no. 4, pp. 2556–2566, 2011.

- 172 D. Trudnowski, J. Johnson, and J. Hauer, "Making Prony Analysis More Accurate using Multiple Signals," *IEEE Trans. on Power Systems*, vol. 14, no. 1, pp. 226–231, 1999.
- 173 J. J. Sanchez-Gasca and J. H. Chow, "Computation of Power System Low-Order Models from Time Domain Simulations Using a Hankel Matrix," *IEEE Trans. on Power Systems*, vol. 12, no. 4, pp. 1461–1467, 1997.
- 174 M. L. Crow and A. Singh, "The Matrix Pencil for Power System Modal Extraction," *IEEE Trans. on Power Systems*, vol. 20, no. 1, pp. 501–502, 2005.
- 175 Z. Tashman, H. Khalilinia, and V. Venkatasubramanian, "Multi-Dimensional Fourier Ringdown Analysis for Power Systems Using Synchrophasors," *IEEE Trans. on Power Systems*, vol. 29, no. 2, pp. 731–741, 1997.
- 176 J. J. Sanchez-Gasca and J. H. Chow, "Performance Comparison of Three Identification Methods for the Analysis of Electromechanical Oscillations," *IEEE Trans. on Power Systems*, vol. 14, no. 3, pp. 995–1002, 1997.
- 177 D. J. Trudnowski and J. W. Pierre, "Overview of Algorithms for Estimating Swing Modes from Measured Responses," *Proc. IEEE PES General Meeting*, 2009.
- 178 L. Dosiek and J. W. Pierre, "Estimating Electromechanical Modes and Mode Shapes using the Multichannel ARMAX Model," *IEEE Trans. on Power Systems*, vol. 28, no. 2, pp. 1950–1959, May 2013.
- 179 J. H. Chow, A. Chakrabortty, M. Arcak, B. Bhargava, and A. Salazar, "Synchronized Phasor Data Based Energy Function Analysis of Dominant Power Transfer Paths in Large Power Systems," *IEEE Trans. on Power Systems*, vol. 22, pp. 727–734, 2007.
- 180 J. H. Chow, A. Chakrabortty, L. Vanfretti, and M. Arcak, "Estimation of Radial Power System Transfer Path Dynamic Parameters using Synchronized Phasor Data," *IEEE Trans. on Power Systems*, vol. 23, no. 2, pp. 564–571, 2008.
- 181 J. W. Stahlhut, T. J. Browne, G. T. Heydt, and V. Vittal, "Latency Viewed as a Stochastic Process and its Impact on Wide Area Power System Control Signals," *IEEE Trans. on Power Systems*, vol. 23, no. 1, pp. 84–91, 2008.
- 182 C. Cyr and I. Kamwa, "WACS design at Hydro-Quebec," in PMU Tutorial, IEEE PES General Meeting, Minneapolis, MN, July 2010.
- 183 G. F. Franklin, J. D. Powell, and A. Emami-Naeini, *Feedback Control of Dynamic Systems*, Sixth Edition, Prentice Hall, 2009.
- 184 J. H. Chow and S. Ghiocel, "An Adaptive Wide-Area Power System Damping Controller using Synchrophasor Data," in *Control and Optimization Theory for Electric Smart Grids*, A. Chakrabortty and M. Ilic, eds, Springer, 2012.
- 185 J. H. Chow and K. W. Cheung, "A Toolbox for Power System Dynamics and Control Engineering Education," *IEEE Transactions on Power Systems*, vol. 7, no. 4, pp. 1559–1564, 1992.
- 186 J. H. Chow and G. Rogers, "Power System Toolbox Manual: a Set of Coordinated m-files for Use with MATLAB," Cherry Tree Scientific Software, 1996. Available: <https://www.ecse.rpi.edu/chowj/>.
- 187 M. Crow, *Computational Methods for Electric Power Systems*, third edition, CRC Press, 2015.
- 188 A. Greenwood, *Electrical Transients in Power Systems*, 2nd Edition, Wiley-Interscience, 1991.
- 189 M. A. Pai, *Power Circuits and Electromechanics*, Stipes Publishing, 2012.
- 190 W. F. Tinney and J. W. Walker, "Direct Solutions of Sparse Network Equations by Optimally Ordered Triangular Factorization," *Proceedings of IEEE*, vol. 55, pp. 1801–1809, 1967.

- 191 B. Stott, "Review of Load-Flow Calculation Methods," *Proceedings of IEEE*, vol. 62, no. 7, pp. 916–929, 1974.
- 192 W. W. Price, *Power System Computations*, Course Notes, General Electric Power Engineering Course, 1980.
- 193 IEEE Standard 1110-2002, *IEEE Guide for Synchronous Generator Modeling Practices and Applications in Power System Stability Analyses*, Piscataway, NJ, 2002.
- 194 IEEE Committee Report, "Dynamic Models for Combined Cycle Plants in Power System Studies," *IEEE Transactions on Power Systems*, vol. 9, no. 3, pp. 1698–1708, Aug. 1994.
- 195 C. W. Gear, *Numerical Initial Value Problems in Ordinary Differential Equations*, Prentice-Hall, 1971.
- 196 NERC Report, *Reliability Assessment Guidebook*, Atlanta, August 2012. Available: nerc.com.
- 197 G. Rogers, *Power System Oscillations*, Springer, 2000.

A

Integral Manifolds for Model Reduction

A.1 Manifolds and Integral Manifolds

The term “manifold” in this chapter refers to a functional relationship between variables. For example, a manifold for z as a function of x is simply another term for the expression

$$z = h(x) \quad (\text{A.1})$$

When x is a scalar, the manifold is a line when plotted in the z, x space. When x is two-dimensional, the manifold is a surface that might appear as in Figure A.1.

To define an integral manifold, we have to introduce a multidimensional dynamic model of the form

$$\frac{dx}{dt} = f(x, z) \quad x(0) = x^o \quad (\text{A.2})$$

$$\frac{dz}{dt} = g(x, z) \quad z(0) = z^o. \quad (\text{A.3})$$

An integral manifold for z as a function of x is a manifold

$$z = h(x) \quad (\text{A.4})$$

which satisfies the differential equation for z . Thus, $h(x)$ is an integral manifold of (A.2)–(A.3) if it satisfies

$$\frac{\partial h}{\partial x} f(x, h) = g(x, h). \quad (\text{A.5})$$

If the initial conditions on x and z lie on the manifold ($z^o = h(x^o)$), then the integral manifold is an exact solution of the differential equation (A.3), and the following reduced-order model is exact:

$$\frac{dx}{dt} = f(x, h(x)) \quad x(0) = x^o. \quad (\text{A.6})$$

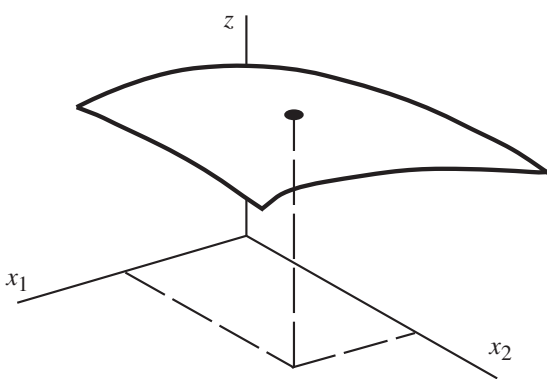


Figure A.1 Geometrical interpretation of a manifold.

A.2 Integral Manifolds for Linear Systems

The concept of integral manifolds is illustrated in this section through a series of examples. Consider the oversimplified system

$$\frac{dx}{dt} = -x + z \quad x(0) = x^o \quad (\text{A.7})$$

$$\frac{dz}{dt} = -10z + 10 \quad z(0) = z^o. \quad (\text{A.8})$$

We say that \$z\$ is predominantly *fast* because of the 10 multiplying the right side. We say that \$x\$ is predominantly *slow* because it has only 1 multiplying the right side. For comparison later, let's solve for the exact response. Because it is a linear time-invariant system, the solution will be of the form

$$x(t) = c_1 e^{\lambda_1 t} + c_2 e^{\lambda_2 t} + c_3 \quad (\text{A.9})$$

$$z(t) = c_4 e^{\lambda_1 t} + c_5 e^{\lambda_2 t} + c_6 \quad (\text{A.10})$$

where \$\lambda_1\$ and \$\lambda_2\$ are the two eigenvalues. These are found from the system-state matrix as follows:

$$\begin{bmatrix} \frac{dx}{dt} \\ \frac{dz}{dt} \end{bmatrix} = \underbrace{\begin{bmatrix} -1 & 1 \\ 0 & -10 \end{bmatrix}}_A \begin{bmatrix} x \\ z \end{bmatrix} + \begin{bmatrix} 0 \\ 10 \end{bmatrix}. \quad (\text{A.11})$$

The eigenvalues are the solutions of

$$\text{determinant } [\lambda I - A] = \begin{vmatrix} \lambda + 1 & -1 \\ 0 & \lambda + 10 \end{vmatrix} = 0 \quad (\text{A.12})$$

or \$(\lambda + 1)(\lambda + 10) - 0 = 0\$. The roots are \$\lambda_1 = -1, \lambda_2 = -10\$. The constants \$c_3\$ and \$c_6\$ are the steady-state solution

$$\left. \begin{aligned} 0 &= -x_{ss} + z_{ss} \\ 0 &= -10z_{ss} + 10 \end{aligned} \right\} z_{ss} = 1 \quad x_{ss} = 1 \quad (\text{A.13})$$

so

$$x = c_1 e^{-t} + c_2 e^{-10t} + 1 \quad (\text{A.14})$$

$$z = c_4 e^{-t} + c_5 e^{-10t} + 1. \quad (\text{A.15})$$

The other constants are found from the initial conditions:

$$x(0) = c_1 + c_2 + 1 = x^o \quad (\text{A.16})$$

$$\frac{dx}{dt} \Big|_0 = -c_1 - 10c_2 = -x^o + z^o \quad (\text{A.17})$$

$$z(0) = c_4 + c_5 + 1 = z^o \quad (\text{A.18})$$

$$\frac{dz}{dt} \Big|_0 = -c_4 - 10c_5 = -10z^o + 10. \quad (\text{A.19})$$

Solving

$$c_1 = -x^o + \frac{z^o - 10}{9} \quad c_2 = -\frac{z^o - 1}{9} \quad (\text{A.20})$$

$$c_3 = z^o - 1 \quad c_4 = 0 \quad (\text{A.21})$$

the exact solution is

$$x = \left(x^o - \frac{10}{9} + \underbrace{\frac{z^o}{9}}_{\substack{\text{small if } z^o \\ \text{is not large}}} \right) e^{-t} - \underbrace{\frac{z^o - 1}{9}}_{\substack{\text{small if } z^o \\ \text{is not large}}} e^{-10t} + 1. \quad (\text{A.22})$$

If z^o is not large, the major part of x is slow. The fast variation of z contributes only small amounts to x .

To see how we can develop a reduced-order model, look for an integral manifold of the form

$$z = hx + c \quad (\text{A.23})$$

where h and c are constants. Substituting into the z differential equation,

$$h \frac{dx}{dt} = -10(hx + c) + 10 \quad (\text{A.24})$$

or

$$h(-x + hx + c) = -10hx - 10c + 10. \quad (\text{A.25})$$

One solution is $h = 0, c = 1$. This means that $z = 1$ is an exact integral manifold for the z variable. That is, if $z = 1$ at any time, then z remains equal to one for all time. Or, more properly stated: "If the initial conditions start on the manifold, then the system remains on the manifold." If this integral manifold is substituted into the x differential equation, the reduced-order model (valid only for $z^o = 1$) is

$$\frac{dx}{dt} = -x + 1 \quad x(0) = x^o \quad (\text{A.26})$$

which clearly exhibits the exact slow eigenvalue and the following solution

$$x = (z^o - 1)e^{-t} + 1. \quad (\text{A.27})$$

Compare this to the exact solution of (A.22). If z^o is equal to 1.0, then (A.26) gives the exact response of x for any x^o . If z^o is not equal to 1.0, then (A.26) will not give the exact response of x . For this case, we define the off-manifold variable η as

$$\eta \stackrel{\Delta}{=} z - 1 \quad (\text{A.28})$$

which has the dynamics

$$\frac{d\eta}{dt} = -10\eta \quad \eta(0) = z^o - 1. \quad (\text{A.29})$$

Note that $\eta = 0$ is an exact integral manifold because if $\eta = 0$ at any time, $\eta = 0$ for all time. The exact solution, when $\eta(0) \neq 0$, is

$$\eta(t) = (z^o - 1)e^{-10t}. \quad (\text{A.30})$$

The integral manifold plus off-manifold solution for z as a function of x and t is

$$z = 1 + (z^o - 1)e^{-10t} \quad (\text{A.31})$$

This gives the exact reduced-order model (for any z^o)

$$\frac{dx}{dt} = -x + 1 + (z^o - 1)e^{-10t} \quad x(0) = x^o. \quad (\text{A.32})$$

While this may have been obvious from the beginning, the steps that led to this result are important for cases where it is not obvious.

The fast time-varying input into this slow subsystem is somewhat undesirable. An interesting approximation can be made to eliminate this term as follows. Since the time-varying term decays very rapidly (e^{-10t}), this term enters the slow differential equation almost as an impulse. It is $z^o - 1$ at time zero and essentially zero for $t > 0$. Using the following impulse identity,

$$\text{Imp}(t) \stackrel{\Delta}{=} \lim_{a \rightarrow o_a} \frac{1}{a} e^{-\frac{t}{a}}. \quad (\text{A.33})$$

Equation (A.32) can be approximated by

$$\frac{dx}{dt} \approx -x + 1 + \frac{(z^o - 1)}{10} \text{Imp}(t) \quad x(0) = x^o \quad (\text{A.34})$$

This impulse can be eliminated by recognizing that its integral can be included in the initial condition on x

$$x(t) = x^o + \int_o^t (-x + 1)d\hat{t} + \int_o^t \frac{(z^o - 1)}{10} \text{Imp}(\hat{t})d\hat{t} \quad (\text{A.35})$$

or

$$x(t) = x^o + \frac{z^o - 1}{10} + \int_o^t (-x + 1)d\hat{t}. \quad (\text{A.36})$$

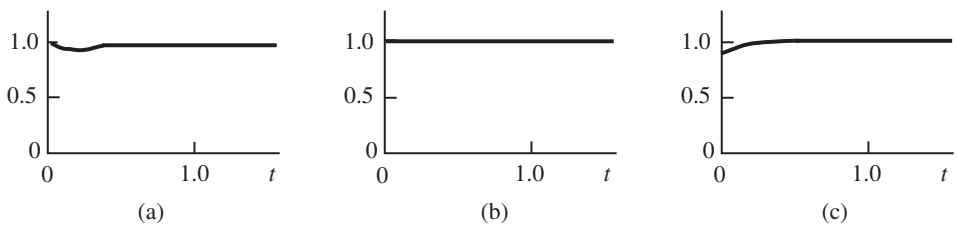


Figure A.2 Comparison of exact and approximate solutions.

This gives the approximate reduced-order model using the exact integral manifold for z and accounts for the z initial condition off-manifold dynamics through a revised initial condition on x :

$$\frac{dx}{dt} \approx -x + 1 \quad x(0) = x^o + \frac{(z^o - 1)}{10}. \quad (\text{A.37})$$

To see the impact of this approximation, consider the example in which $x^o = 1$ and $z^o = 0$. The exact response of x is the solution of

$$(a) \quad \frac{dx}{dt} = -x + 1 - e^{-10t} \quad x(0) = 1.0. \quad (\text{A.38})$$

The approximate response of x using only the exact integral manifold for z is the solution of

$$(b) \quad \frac{dx}{dt} \approx -x + 1 \quad x(0) = 1.0. \quad (\text{A.39})$$

The improved approximate response of x accounting for the off-manifold dynamics is the solution of

$$(c) \quad \frac{dx}{dt} \approx -x + 1 \quad x(0) = 0.9. \quad (\text{A.40})$$

A comparison of these solutions is given in Figure A.2. It is important to observe that the basic phenomenon was captured by the slow manifold of (b). The correction for the fast initial condition was a second-order effect approximated fairly well.

Before leaving this example, we return to (A.25) and observe that another integral manifold solution is

$$h = -9, \quad c = 10 \quad (\text{A.41})$$

which gives another exact integral manifold,

$$z = -9x + 10. \quad (\text{A.42})$$

If this solution is used in the original differential equation for x , the reduced-order model is

$$\frac{dx}{dt} = -10x + 10 \quad x(0) = x^o. \quad (\text{A.43})$$

The solution of this is

$$x = (x^o - 1)e^{-10t} + 1. \quad (\text{A.44})$$

Compare this to the exact solution of (A.22). It is exact if $z^o = -9x^o + 10$. This means it is exact for $x^o = 1, z^o = 1$. But, if $x^o = 0.5, z^o = 1$ (not significantly different), there will be a large error in this reduced-order model, which is good only for a very limited range of initial conditions.

We now extend this concept to the more general case with coupling in both equations as:

$$\frac{dx}{dt} = -x + z \quad (\text{A.45})$$

$$\frac{dz}{dt} = -10x - 10z. \quad (\text{A.46})$$

As before, we say that z is predominantly fast and x is predominantly slow. This is due to the 10 multiplying the right side of the z differential equation. The eigenvalues of this system are found from the state matrix

$$A = \begin{bmatrix} -1 & 1 \\ -10 & -10 \end{bmatrix} \quad (\text{A.47})$$

$$|\lambda I - A| = \begin{vmatrix} \lambda + 1 & -1 \\ 10 & \lambda + 10 \end{vmatrix} = (\lambda + 1)(\lambda + 10) + 10 = 0. \quad (\text{A.48})$$

The roots are

$$\lambda_1 = -2.3 \quad \lambda_2 = -8.7 \quad (\text{A.49})$$

so the exact solution is

$$x = c_1 e^{-2.3t} + c_2 e^{-8.7t} + c_3 \quad (\text{A.50})$$

$$z = c_4 e^{-2.3t} + c_5 e^{-8.7t} + c_6. \quad (\text{A.51})$$

The steady-state values of x and z are

$$x_{ss} = c_3 = 0 \quad z_{ss} = c_6 = 0. \quad (\text{A.52})$$

Focusing on x , let's solve for c_1 and c_2 .

$$x(o) = c_1 + c_2 = x^o \quad (\text{A.53})$$

$$\frac{dx}{dt} \Big|_o = -2.3c_1 - 8.7c_2 = -x^o + z^o. \quad (\text{A.54})$$

Solving

$$c_1 = \frac{7.7x^o + z^o}{6.4}, \quad c_2 = -\frac{1.3x^o + z^o}{6.4} \quad (\text{A.55})$$

so:

$$x = \left(\frac{7.7x^o}{6.4} + \underbrace{\frac{z^o}{6.4}}_{\substack{\text{small if } z^o \\ \text{is not large}}} \right) e^{-2.3t} - \left(\frac{1.3x^o}{6.4} + \underbrace{\frac{z^o}{6.4}}_{\substack{\text{small if } z^o \\ \text{is not large}}} \right) e^{-8.7t}. \quad (\text{A.56})$$

As before, if z^o is not large, the x response is dominated by the slow component. If we are interested only in capturing the mode with eigenvalue -2.3 , we propose that this mode is associated with the state x , and seek to eliminate z from (A.45)–(A.46) through an integral manifold of the general linear form

$$z = hx + c \quad (\text{A.57})$$

Substituting into (A.46) (and using (A.45)) gives

$$h(-x + hx + c) = -10x - 10hx - 10c. \quad (\text{A.58})$$

For arbitrary x , this has the solutions

$$c = 0 \quad h = -1.3 \quad (\text{A.59})$$

$$c = 0 \quad h = -7.7. \quad (\text{A.60})$$

Thus, there are two integral manifolds for z as before:

$$\text{IM 1 : } z = -1.3x \quad (\text{A.61})$$

$$\text{IM 2 : } z = -7.7x. \quad (\text{A.62})$$

Substitution of IM 1 into (A.45) gives

$$\frac{dx}{dt} = -2.3x \quad (\text{A.63})$$

and substitution of IM 2 into (A.45) gives the faster subsystem

$$\frac{dx}{dt} = -8.7x. \quad (\text{A.64})$$

This second result is somewhat disturbing, since we had originally proposed that the variable x was associated with the -2.3 mode. Several important points are illustrated here. First, integral manifolds can be used to decouple systems and find eigenvalues. Second, integral manifolds are not unique (one for each eigenvalue, it appears!). Third, the choice of the integral manifold determines the phenomena retained in the reduced-order model. To understand more about this technique, consider the same system with the introduction of the small parameter ϵ (1/10 in the above example), and the inclusion of initial conditions

$$\frac{dx}{dt} = -x + z \quad x(o) = x^o \quad (\text{A.65})$$

$$\epsilon \frac{dz}{dt} = -x - z \quad z(o) = z^o. \quad (\text{A.66})$$

Again we seek a linear manifold

$$z = h(\epsilon)x + c(\epsilon) \quad (\text{A.67})$$

where we presume that h and c would normally depend on the parameter ϵ . Substitution of (A.67) into (A.65)–(A.66) gives

$$\epsilon h(\epsilon)(-x + h(\epsilon)x + c(\epsilon)) = -x - h(\epsilon)x - c(\epsilon). \quad (\text{A.68})$$

Again, for arbitrary x , the solutions are

$$c(\epsilon) = 0, h(\epsilon) = -\frac{1-\epsilon}{2\epsilon} + \frac{1}{2\epsilon}\sqrt{(1-\epsilon)^2 - 4\epsilon}, \quad h(0) = -1 \quad (\text{A.69})$$

$$c(\epsilon) = 0, h(\epsilon) = -\frac{1-\epsilon}{2\epsilon} - \frac{1}{2\epsilon}\sqrt{(1-\epsilon)^2 - 4\epsilon}, \quad h(0) = -\infty. \quad (\text{A.70})$$

For positive $\epsilon < 1$, these solutions exist only for

$$0 \leq \epsilon \leq 0.1715. \quad (\text{A.71})$$

This makes sense, since the original system has complex eigenvalues for ϵ less than 1 but greater than 0.1715. It would be impossible to capture a complex mode from a single-state equation.

This simple example illustrates that integral manifolds may not exist and may not be unique. If we are interested in the “slow mode,” which we propose is associated with the variable x , we need a systematic way to compute the correct integral manifold. If z is infinitely fast ($\epsilon = 0$), the integral manifold of interest is $z = -x(h = -1)$. When ϵ is near zero, we propose that the integral manifold of interest should be near -1 . To systematically compute h for ϵ near zero, we expand $h(\epsilon)$ in a power series in ϵ as

$$h(\epsilon) = h_0 + \epsilon h_1 + \epsilon^2 h_2 + \dots \quad (\text{A.72})$$

and return to the example by substituting into (A.66) and (A.67) (using $c(\epsilon) = 0$)

$$\begin{aligned} \epsilon(h_0 + \epsilon h_1 + \epsilon^2 h_2 + \dots)(-x + (h_0 + \epsilon h_1 + \epsilon^2 h_2 + \dots)x) \\ = -x - (h_0 + \epsilon h_1 + \epsilon^2 h_2 + \dots)x. \end{aligned} \quad (\text{A.73})$$

For arbitrary x , we solve for h_0, h_1, h_2, \dots by equating coefficients of powers of ϵ :

$$\epsilon^0 : \quad 0 = -1 - h_0 \text{ or } h_0 = -1 \quad (\text{A.74})$$

$$\epsilon^1 : \quad h_0(-1 + h_0) = -h_1 \text{ or } h_1 = h_0 - h_0^2 = -2 \quad \text{etc.} \quad (\text{A.75})$$

Stopping with these terms,

$$h(\epsilon) \approx -1 - 2\epsilon. \quad (\text{A.76})$$

This approximates the exact integral manifold of (A.65)–(A.66) as

$$z \approx -(1 + 2\epsilon)x. \quad (\text{A.77})$$

Using this in (A.65) gives the approximate reduced-order model (valid when the initial conditions satisfy $z^0 = h(\epsilon)x^0$)

$$\frac{dx}{dt} \approx -(2 + 2\epsilon)x \quad x(0) = x^0. \quad (\text{A.78})$$

This model could be improved to any degree of accuracy by including additional terms of $h(\epsilon)$. Since these terms were computed from a power series near the integral manifold of interest (slow manifold), the correct mode has been captured. Note that it is necessary to consider only the off-manifold dynamics due to the initial conditions if the reduced order model is going to be used in a simulation. If only eigenvalues are of interest, the off-manifold dynamics due to initial conditions are not relevant. For $\epsilon = 0.1$, as in the previous example, the slow eigenvalue (-2.3) is approximated in (A.78) by -2.2 . As a warning, it is important to note that in this example the integral manifold always exists

when ϵ is actually zero. When ϵ is small but not zero, the infinite series of (A.72) can always be computed, but its convergence and, hence, its validity depend on the size of the actual ϵ . In this example, we would expect that this series converges only when ϵ is less than 0.1715. Thus, while terms of the integral manifold series can be computed for any ϵ , it should be used only when ϵ is less than 0.1715.

While computation of the integral manifold is the primary task in model reduction, it may not make sense to find a good approximation and then ignore the possibility that z does not start on the manifold ($z^o \neq h(\epsilon)x^o$). As in the earlier example, it is possible to approximate this impact on x by computing the off-manifold correction. To do this, we define the off-manifold variable as (with $c(\epsilon) = 0$)

$$\eta \stackrel{\Delta}{=} z - h(\epsilon)x \quad (\text{A.79})$$

which has dynamics (recalling (A.68) with $c(\epsilon) = 0$)

$$\epsilon \frac{d\eta}{dt} = -(1 + \epsilon h(\epsilon))\eta \quad \eta(o) = z^o - h(\epsilon)x^o. \quad (\text{A.80})$$

Clearly, $\eta = 0$ is also an integral manifold because if $\eta = 0$ at any time, then $\eta = 0$ for all time. The exact off-manifold dynamics are the solution of (A.80):

$$\eta(t) = (z^o - h(\epsilon)x^o)e^{(-\frac{1+\epsilon h(\epsilon)}{\epsilon})t}. \quad (\text{A.81})$$

If $h(\epsilon)$ is known exactly, then the exact slow subsystem is

$$\frac{dx}{dt} = -(1 - h(\epsilon))x + (z^o - h(\epsilon)x^o)e^{(\frac{1+\epsilon h(\epsilon)}{\epsilon})t} \quad x(o) = x^o. \quad (\text{A.82})$$

As before, this fast input can be approximated by an impulse and eliminated by modification of the initial condition to obtain

$$\begin{aligned} \frac{dx}{dt} &\approx -(1 - h(\epsilon))x \\ x(o) &= x^o + \left(\frac{\epsilon}{1 + \epsilon h(\epsilon)} \right) (z^o - h(\epsilon)x^o) \end{aligned} \quad (\text{A.83})$$

Clearly, if $z^o = h(\epsilon)x^o$ (on the slow manifold), this result is exact when $h(\epsilon)$ is exact. In our example, $h(\epsilon)$ was never found exactly. Using the approximation $h(\epsilon) \approx -1 - 2\epsilon$ with $\epsilon = 1/10$ gives the following slow subsystem approximate model (approximate for two reasons: $h(\epsilon)$ is not exact and the off-manifold dynamics are not exact):

$$\frac{dx}{dt} \approx -2.2x \quad x(o) = \frac{100}{88}x^o + \frac{10}{88}z^o. \quad (\text{A.84})$$

The basic result of all this is summarized as follows. Consider a linear system in standard two-time-scale form

$$\frac{dx}{dt} = Ax + Bz \quad (\text{A.85})$$

$$\epsilon \frac{dz}{dt} = Cx + Dz \quad (\text{A.86})$$

where A, B, C, D are of order 1 (not big) and D is nonsingular (D^{-1} exists).

A first-order approximation of the slow dynamics of x is obtained by simply setting $\epsilon = 0$.

$$\frac{dx}{dt} = Ax + Bz \quad (\text{A.87})$$

$$0 = Cx + Dz \quad (\text{A.88})$$

which gives the first approximation of the slow manifold (h_o)

$$z = -D^{-1}Cx \quad (\text{A.89})$$

and the first approximation of the slow dynamics of x

$$\frac{dx}{dt} = (A - BD^{-1}C)x. \quad (\text{A.90})$$

Using this approximate model will introduce two errors. One is due to the fact that the integral manifold is not exact (h_o is only the largest part of $h(\epsilon)$). The second error is due to the fact that the initial condition on z may not satisfy the integral manifold.

It can be shown that if the initial condition on z is not big, then the total error of these two approximations is small. The term “not big” means that z^o should be on the order of magnitude of 1 or less. The term “small” means on the order of magnitude of ϵ . References [69] and [70] discuss this in detail.

In most cases, the first-order approximation of the slow manifold coincides exactly with the steady-state relationship between z and x in the z differential equation, because the result of setting ϵ to zero is the same as the result of setting $\frac{dz}{dt}$ to zero. There is, however, a profound theoretical difference. Setting $\frac{dz}{dt} = 0$ implies $z = \text{constant}$. This would be contradicted by the change of z when x changes ($z = h_o x$). Setting $\epsilon = 0$ does not imply $z = \text{constant}$, and thus is not contradicted by the change of z when x changes.

A.3 Integral Manifolds for Nonlinear Systems

While there are many reduction techniques that can be applied to linear systems, the primary advantage of the integral manifold approach is its straightforward extension to nonlinear systems. We begin by considering the general form

$$\frac{dx}{dt} = f(x, z) \quad x(o) = x^o \quad (\text{A.91})$$

$$\frac{dz}{dt} = g(x, z) \quad z(o) = z^o \quad (\text{A.92})$$

To analyze the dynamics of x , it is necessary to also compute the dynamics of z . A reduced-order model involving only x requires the elimination of z from (A.91). An integral manifold for z as a function of x has the form

$$z = h(x) \quad (\text{A.93})$$

and must satisfy (A.92)

$$\frac{\partial h}{\partial x} f(x, h) = g(x, h). \quad (\text{A.94})$$

While, in general, it is very difficult to find such an integral manifold, there are several very important cases in which h can be either found exactly or approximated to any

degree of accuracy. We begin with a generic example, which closely resembles the single synchronous machine connected to an infinite bus with stator transients

$$\frac{dx_1}{dt} = x_2 - 1 \quad (\text{A.95})$$

$$\frac{dx_2}{dt} = f(x_1, x_2, z_1, z_2) \quad (\text{A.96})$$

$$\frac{dz_1}{dt} = -\sigma z_1 + x_2 z_2 + V \sin x_1 \quad (\text{A.97})$$

$$\frac{dz_2}{dt} = -\sigma z_2 - x_2 z_1 + V \cos x_1. \quad (\text{A.98})$$

We suppose that only x_1 and x_2 are of interest, and look for an integral manifold of the form

$$z_1 = h_1(x_1, x_2) \quad (\text{A.99})$$

$$z_2 = h_2(x_1, x_2). \quad (\text{A.100})$$

This two-dimensional integral manifold must satisfy

$$\frac{\partial h_1}{\partial x_1}(x_2 - 1) + \frac{\partial h_1}{\partial x_2}f(x_1, x_2, h_1, h_2) = -\sigma h_1 + x_2 h_2 + V \sin x_1 \quad (\text{A.101})$$

$$\frac{\partial h_2}{\partial x_1}(x_2 - 1) + \frac{\partial h_2}{\partial x_2}f(x_1, x_2, h_1, h_2) = -\sigma h_2 - x_2 h_1 + V \cos x_1. \quad (\text{A.102})$$

These partial differential equations can be solved by first assuming that h_1 and h_2 are independent of x_2 and then equating coefficients of x_2 to give

$$\frac{\partial h_1}{\partial x_1} = h_2, \quad \frac{\partial h_1}{\partial x_2} = \sigma h_1 - V \sin x_1 \quad (\text{A.103})$$

$$\frac{\partial h_2}{\partial x_1} = -h_1, \quad \frac{\partial h_2}{\partial x_2} = \sigma h_2 - V \cos x_1. \quad (\text{A.104})$$

Eliminating the partials gives the solution

$$h_1 = V \cos \alpha \cos(\alpha - x_1) \quad (\text{A.105})$$

$$h_2 = V \cos \alpha \sin(\alpha - x_1) \quad (\text{A.106})$$

where $\tan \alpha = \sigma$. Thus, if the initial conditions on z_1, z_2 , and x_1 satisfy (A.105)–(A.106), then substitution of (A.105)–(A.106) into (A.96) gives an exact reduced-order model. When the initial conditions on z_1, z_2 , and x_1 do not satisfy (A.105)–(A.106), it is necessary to introduce the “off-manifold” variables

$$\eta_1 \stackrel{\Delta}{=} z_1 - V \cos \alpha \cos(\alpha - x_1) \quad (\text{A.107})$$

$$\eta_2 \stackrel{\Delta}{=} z_2 - V \cos \alpha \sin(\alpha - x_1). \quad (\text{A.108})$$

These off-manifold variables have the following dynamics:

$$\frac{d\eta_1}{dt} = -\sigma\eta_1 + x_2\eta_2 \quad (\text{A.109})$$

$$\frac{d\eta_2}{dt} = -\sigma\eta_2 - x_2\eta_1. \quad (\text{A.110})$$

This system has the explicit solution

$$\eta_1 = c_1 e^{-\sigma t} \cos(t + x_1 - c_2) \quad (\text{A.111})$$

$$\eta_2 = -c_1 e^{-\sigma t} \sin(t + x_1 - c_2) \quad (\text{A.112})$$

where c_1 and c_2 are found from initial conditions by solving

$$z_1^o - V \cos \alpha \cos(\alpha - x_1^o) = c_1 \cos(x_1^o - c_2) \quad (\text{A.113})$$

$$z_2^o - V \cos \alpha \sin(\alpha - x_1^o) = -c_1 \sin(x_1^o - c_2). \quad (\text{A.114})$$

This result leads to an exact reduced-order model in x_1 and x_2 by using the following in (A.96):

$$z_1 = V \cos \alpha \cos(\alpha - x_1) + c_1 e^{-\sigma t} \cos(t + x_1 - c_2) \quad (\text{A.115})$$

$$z_2 = V \cos \alpha \sin(\alpha - x_1) - c_1 e^{-\sigma t} \sin(t + x_1 - c_2). \quad (\text{A.116})$$

Such exact integral manifolds and exact off-manifold solutions are rare in dynamic systems. The synchronous machine stands out as a unique device with this property [67].

A very broad class of systems in which integral manifolds can often be found or approximated to any degree of accuracy is the class of two-time-scale systems of the form

$$\frac{dx}{dt} = f(x, z)x(o) = x^o \quad (\text{A.117})$$

$$\epsilon \frac{dz}{dt} = g(x, z)z(o) = z^o. \quad (\text{A.118})$$

These systems are called two-time scales because when ϵ is small, the z variables are predominantly fast and the x variables are predominantly slow. This is clear because the derivative of z with respect to time is proportional to $1/\epsilon$, which is large for small ϵ . As in the linear case of the last section, we propose an integral manifold for z as a function of x and ϵ :

$$z = h(x, \epsilon). \quad (\text{A.119})$$

We assume that ϵ is sufficiently small so that the manifold can be expressed as a power series in ϵ :

$$h(x, \epsilon) = h_o(x) + \epsilon h_1(x) + \epsilon^2 h_2(x) + \dots \quad (\text{A.120})$$

Substitution into (A.119) and then (A.118) gives

$$\epsilon \left(\frac{\partial h_o}{\partial x} + \epsilon \frac{\partial h_1}{\partial x} + \dots \right) f(x, h) = g(x, h). \quad (\text{A.121})$$

Expanding f and g about $\epsilon = 0$,

$$f(x, h) = f(x, h_o) + \epsilon \frac{\partial f}{\partial z} \Big|_{z=h_o} h_1 + \dots \quad (\text{A.122})$$

$$g(x, h) = g(x, h_o) + \epsilon \frac{\partial g}{\partial z} \Big|_{z=h_o} h_1 + \dots \quad (\text{A.123})$$

the partial differential equation to be solved is

$$\begin{aligned} \epsilon \left(\frac{\partial h_o}{\partial x} + \epsilon \frac{\partial h_1}{\partial x} + \dots \right) \left(f(x, h_o) + \epsilon \frac{\partial f}{\partial z} \Big|_{z=h_o} h_1 + \dots \right) \\ = g(x, h_o) + \epsilon \frac{\partial g}{\partial z} \Big|_{z=h_o} h_1 + \dots \end{aligned} \quad (\text{A.124})$$

Equating coefficients of powers of ϵ produces a set of algebraic equations to be solved for $h_o, h_1, h_2 \dots$:

$$\epsilon^0 : \quad 0 = g(x, h_o) \quad (\text{A.125})$$

$$\epsilon^1 : \quad \frac{\partial h_o}{\partial x} f(x, h_o) = \frac{\partial g}{\partial z} \Big|_{z=h_o} h_1 \quad \text{etc.} \quad (\text{A.126})$$

Clearly, the most important equation is (A.125), which requires the solution of the nonlinear equation for h_o . Once this is found, the solution for h_1 simply requires nonsingular $\partial g / \partial z$. Normally, if (A.125) can be solved, the nonsingularity of $\partial g / \partial z$ follows.

As in the linear case, the use of an integral manifold in a reduced-order model can give exact results only if it is found exactly and if the initial conditions start on it. If the initial conditions do not start on the manifold (do not satisfy (A.119)), an error will be introduced. To eliminate this error, it is necessary to compute the off-manifold dynamics. This is done by introducing the off-manifold variables

$$\eta \stackrel{\Delta}{=} z - h(x, \epsilon) \quad (\text{A.127})$$

with the following dynamics

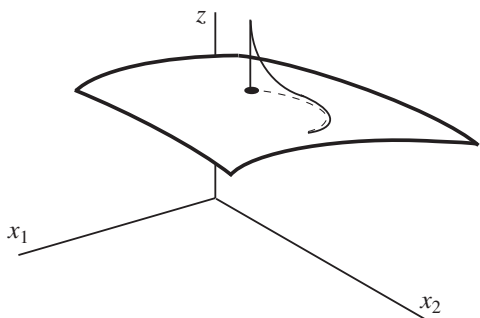
$$\epsilon \frac{d\eta}{dt} = g(x, \eta + h) - \epsilon \frac{\partial h}{\partial x} f(x, \eta + h) \quad (\text{A.128})$$

and the initial condition

$$\eta(o) = z^o - h(x^o, \epsilon). \quad (\text{A.129})$$

These off-manifold dynamics normally are difficult to compute because they require x . As a first approximation, (A.128) could be solved using x as a constant equal to its initial condition. This is a reasonably good approximation because the off-manifold dynamics should decay (if they are stable) before x changes significantly. A geometric illustration of the integral manifold and the off-manifold dynamics is shown in Figure A.3. If z starts off the surface $z = h(x, \epsilon)$, it should decay rapidly to the surface (if it is stable), as shown

Figure A.3 Off-manifold dynamics.



in the solid line. The dotted line shows the trajectory of z if off-manifold dynamics are neglected and z is forced to begin on the surface.

It can be shown that, if z is stable, using h_o as an approximation for h and neglecting off-manifold dynamics only introduces “order ϵ ” error into the slow variable x response. If further accuracy is desired and h is approximated by $h_o + \epsilon h_1$, there will still be “order ϵ ” error if the off-manifold dynamics are neglected. To reduce the error to “order ϵ^2 ”, it is necessary to include h_1 and approximate η to order ϵ^2 . This can be done by approximating the off-manifold dynamics as

$$\epsilon \frac{d\eta}{dt} \approx g(x^o, \eta + h_o + \epsilon h_1) - \epsilon \frac{\partial h_o}{\partial x} f(x^o, \eta + h_o) \quad (\text{A.130})$$

with

$$\eta(o) = z^o - h_o(x^o) - \epsilon h_1(x^o) \quad (\text{A.131})$$

and $h_o, h_1, \partial h_o / \partial x$ evaluated at $x = x^o$. Additional illustrations of integral manifolds and off-manifold dynamics are given in [66–72].

Index

a

- Adams-Bashforth method 317
- Admittance matrix 142
- Angle reference 127, 192
- Area control error 129, 132
- Auto-regressive equation 294
- Automatic generation control 70, 129
- Automatic voltage regulator 58

b

- Base point 130
- Bergeron's method 10, 17, 18
- Bias factor 130
- Bifurcation 200
 - Hopf 200, 203
 - saddle node 204
 - singularity-induced 200
- Boundary-controlling u.e.p method 235, 254
- Branch currents 107
- Branch voltages 105
- Branch-loop incidence matrix 105

c

- Center of inertia 128, 239
- Characteristic equation 218
- Characteristic impedance 9
- Classical model 84
 - multimachine 118
- Compensated voltage 60–62
- Conservative system 251
- Controlling u.e.p 235

Coupling field 23

- Critical clearing time 233, 234
- Critical energy 235

d

- D-axis 20
- Damper winding 20, 76
- Damper-winding 90
- Damping
 - electromechanical modes 215
 - negative 215, 221
 - positive 221
- Damping coefficient 225
- Damping ratio 224
- Damping torque 86, 90, 210, 215, 216, 220, 221, 225
 - multimachine 120
- DC steady-state error 226
- DeMello-Concordia constants 213
- Differential-algebraic equations
 - industry model 149
- Differential-algebraic model 135
- Directed graph 105
- Discrete Fourier transform (DFT) 264
 - recursive 265
- Disturbance propagation 280
- Disturbance signatures 285
- Disturbance triggering 285
- DQO transformation 21
- Droop 69, 129, 133
- Dynamic security assessment 233
- Dynamic simulation 311

e

- $E'q, E'd, Efd$ 32
 Eastern interconnection (EI) 279
 Economic dispatch 129
 Eigensystem realization algorithm (ERA)
 295
 Eigenvalue 194
 Eigenvectors 194
 Electromagnetic transients 7
 EMTP 7
 solution methods 12
 transmission line models 7
 Electromechanical modes 205, 219
 Electromechanical wave equation 281
 Energy
 kinetic 235, 236, 298, 320
 lowest u.e.p 235
 potential 235, 236, 320
 Energy function analysis 296
 Energy function methods 233, 238,
 246
 boundary-controlling u.e.p 254
 controlling u.e.p 235
 lowest-energy u.e.p 235
 potential energy boundary surface 235
 structure preserving 259
 EPRI 4, 142, 143, 165, 168
 Equal-area criteria 247
 Equilibrium points
 saddle type 245
 stable 236
 type 1, 245
 ETMSP 165, 168
 Euler full-step modification 316
 Euler's method 18
 Excess kinetic energy 245
 Excitation system 314
 Exciter 53
 IEEE-Type I 142
 saturation 57
 static 194
 Exit-point method 235
 Explicit integration 135

f

- Faulted trajectory 245
 Ferranti effect 307

Field current 33, 41

- Filter
 anti-aliasing 265
 three-point-average 269
 First-swing transient stability 177
 Florida event 284
 Flux linkages 29, 31, 35, 76
 Flux-decay model 83, 124, 171
 multimachine 116
 Frequency 126
 estimation 272
 response 278
 Frequency control 67
 Frequency response 44
 Frequency-domain analysis 215, 219

g

- Generator notation 20
 Governor 67
 model 69
 GPS 263
 Gradient system 256

h

- Heffron-Phillips constants 213
 Hessian matrix 246
 Hopf bifurcation 203
 HVDC 160
 Hydraulic speed governor 67
 Hydroturbines 62

i

- IEEE-Type I exciter 142, 183, 185
 Implicit integration 135
 Independent system operator (ISO)
 276
 Inductance 29
 Inertia constant 21, 26, 72
 Infinite bus 71, 127
 Initial conditions 158, 160, 172, 213
 classical model 179
 full model 158
 Initialization 313
 Instability
 monotonic 216
 torsional 223
 Integral manifolds 327

Integration schemes 12

Euler's forward 18

explicit 135

implicit 12

Internal-node model 177

j

Jacobian 170, 184, 192

algebraic equation 184

load flow 184, 308

k

K1-K6 constants 209, 324

l

Laplace domain 46

Latency 299

Lead-lag transfer function 222

Leakage reactance 31–33

Linear magnetic circuit 29, 33

Linear state estimator (LSE) 292

Linearization 184, 193, 211, 321

Load flow 158, 159, 306, 308

nonconvergent 311

Load frequency control 129

Load models 103, 110, 201

impedance 112, 115, 117, 119, 154

Low-frequency oscillations 209

Lowest-energy u.e.p method 235

Lumped parameter modeling 12

Lyapunov's method 235, 236, 246

m

Magnetic circuit 24, 29, 31

constraints 24

linear 29, 31

nonlinear 35

Magnetizing reactance 33

Manifolds

integral 327

Matrix pencil method 295

Modal analysis 293

Mode of instability 235, 250

Model reduction 327

Modeling 7

Bergeron's method 13

classical model 84, 118

exciter 53

flux-decay model 83, 116

governor 67, 69

loads 103, 110

multi-time-scale 74

Multimachine 101

one-axis model 83

synchronous machine 19

transmission line 7

turbine 62, 67

two-axis model 81, 113

voltage regulator 58

Motor notation 20

Multi-time-scale modeling 74

Multidimensional potential well 250

Multimachine models

classical model 118

flux-decay 171

internal node model 177

reduced order 171

structure preserving 173

two-axis model 123

Multimachine PEBS 249

n

Nadir 279

Natural frequency

undamped 219, 223

NERC 4, 129

Network equation

generator internal node 315

Network equations 140

current-balance form 142

power-balance form 140

Newton's method 165, 308

very dishonest 170

Nonlinear magnetic circuit 35, 37

Numerical solution

current-balance 168

power-balance 165

o

One-axis model 83

Open-circuit voltage 42

Operational impedance 44, 48

Optimal power flow 129

p

- Padé approximant 300
 Park's transformation 19, 21
 Participation factor 130, 194
 Partitioned-explicit 165
 Path-dependent integral 252
 PDC
 local 276
 TO 276
 PEBS 235
 Per-unit scaling 19, 25, 27, 30, 312
 Phase lag 223, 225
 Phase lead 224, 225
 Phase velocity 9
 Phasor
 computation 264
 data accuracy 274
 data communication 276
 data concentrator (PDC) 276
 off-nominal frequency 265
 Phasor estimation
 frequency compensation 266
 frequency tracking 266
 Phasors 28, 41
 PMU 263
 message format 276
 simulator 275
 Polar form 138
 Polarity 20
 Positive sequence 271
 Potential energy 298
 Potential energy boundary surface 235, 241, 246
 Potential energy well 245
 Power balance 22, 23
 Power System Simulation 305
 Power system stabilizer 209, 221
 design 221, 300
 frequency domain design 223
 gain 222, 223
 speed input 221
 stabilizing signals 221
 torsional instability 223
 washout stage 223
 Power System Toolbox (PST) 305
 Prime mover 67
 Prony analysis 294

q

- Q-axis 20, 161

r

- Rate of change of frequency (RoCoF) 278
 Reactive power 43
 Rectangular form 138
 Reduced-order modeling 171
 Reference angle 127, 207
 Reference frames
 center of inertia 128, 165
 machine 21
 synchronously rotating 101
 Reference node 105
 Region of attraction 235, 256
 Ring-down analysis 293
 Root locus 218, 224
 Rotor angle
 absolute 233
 relative 233
 Runge-Kutta method 316

s

- Saddle-node bifurcation 204
 Saturation 35, 37, 39, 40, 55, 121
 constraints 24
 exciter 57
 synchronous machine 94
 Second harmonic 267, 271
 Self-excited dc excitors 56
 Separately excited dc excitors 54
 Separatrix 92
 Shaft dynamics 63
 Shaft stiffness 63
 Simulation 135
 SIMULINKTM 275
 Simultaneous-implicit 165
 Single-machine infinite-bus system 90
 Single-machine steady state 40
 Singularity-induced bifurcation 203
 Speed governor 67
 Stability 183, 233
 small-signal 183
 transient 233
 Stability methods 236
 Stable equilibrium point (s.e.p) 235
 Standstill test 46

- State estimation (SE) 289
 phasor-only 289
 State-space analysis 215
 Static exciter 172, 194
 Stator algebraic equations 138, 139
 Stator/network transients 76, 105
 Steady state 40
 Steam turbine 64
 Structure-preserving model 173
 Structures 2
 physical 2
 political 4
 time-scale 3
 Sub-transient reactance 32, 33
 Synchronizing coefficient 219
 Synchronizing torque 210, 215, 216,
 219–221
 Synchronous machine 19, 313
 assumptions 28
 conventions and notation 19
 exciter 53
 inductance 29
 linear magnetic circuit model 33
 modeling 19
 nonlinear magnetic circuit model 37
 parameters 32
 Park's transformation 19, 21
 per-unit scaling 19, 25, 30
 power balance 22
 saturation 35, 37, 39, 40, 94
 schematic 20
 steady-state circuit 41
 terminal constraints 71
 three damper winding model 20
 transformations and scaling 21
 Synchronous phasor measurement 263
 Synchronously rotating reference frame 101, 233
 synchrophasor 263
- t**
- $T'_{do,T'qo}$ 32
 $T''_{do,T''qo}$ 32
 Tap-changing-under-load (TCUL)
 transformers 3, 160
 Terminal constraints 71
- Texas interconnection (ERCOT) 279
 Time constants 39, 44
 Topology 105
 Torque of electrical origin 24, 42, 81
 Torque-angle loop 216, 219, 226
 Torsional modes 223
 Total vector error 274
 Transfer conductances 207
 Transformations
 center of inertia 128
 machine–network 139
 Park's 19
 positive-sequence 271
 synchronously rotating 101
 Transformers 307
 phase-shifting 307
 Step-up 307
 Transient algebraic circuit 79, 82, 83, 85,
 113, 118
 Transient energy function 236
 Transient reactance 32, 33
 Transient stability 233, 319
 first-swing 177
 Lyapunov's method 236
 Transmission Control Protocol (TCP) 277
 Transmission line models 7, 307
 pi equivalent 12
 Transmission operator (TO) 276
 Trapezoidal rule 12, 166
 Turbine 62
 hydro 62
 model 67
 steam 64
 Two-axis model 81, 82, 123
 multimachine 113
- u**
- Uncompensated voltage 60–62
 Unstable equilibrium point (u.e.p) 235
 User Datagram Protocol (UDP) 277
- v**
- Voltage collapse 205
 Voltage regulator 58
 Voltage stability 183
 Voltage/current polarity 20

w

Washout filter 224, 225
WECC 3-machine system 143
Western Interconnection 287,
289
WECC 279

x

$X' d, X' q$ 32
 $X'' d, X'' q$ 32

X_d per-unit system 19
 X_d, X_q 31

y

Y_{bus} 137, 142, 156
 $Y_{reduced}$ 156

z

Zero eigenvalue 192
Zero sequence 40